Universidad Zaragoza
1542

# Tesis Doctoral

# CHEMICAL-LOOPING COMBUSTION OF COAL USING ILMENITE AS OXYGEN-CARRIER


Autor

Cuadrat Fernández, Ana

Director/es

Adánez Elorza, Juan
Abad Secades, Alberto

ESCUELA DE INGENIERIA Y ARQUITECTURA
Departamento de Ingeniería Química y Tecnologías del Medio Ambiente



2012

CONSEJO SUPERIOR DE INVESTIGACIONES CIENTÍFICAS

INSTITUTO DE CARBOQUÍMICA



# CHEMICAL-LOOPING COMBUSTION OF COAL USING ILMENITE AS OXYGEN-CARRIER

TESIS DOCTORAL - PhD

Ana Cuadrat Fernández

CONSEJO SUPERIOR DE INVESTIGACIONES CIENTÍFICAS

INSTITUTO DE CARBOQUÍMICA



# CHEMICAL-LOOPING COMBUSTION OF COAL USING ILMENITE AS OXYGEN-CARRIER

Thesis submitted to the University of Zaragoza
for the Degree of Doctor in Chemical Engineering

Ana Cuadrat Fernández

January 2012

Supervisors:

Juan Adánez Elorza

Alberto Abad Secades

# Chemical-Looping Combustion of coal using ilmenite as oxygen-carrier

Ana Cuadrat, Instituto de Carboquímica (ICB-CSIC)

## Abstract

Chemical-Looping Combustion, CLC, is a promising combustion technology with inherent capture of the greenhouse gas $CO_2$ at low cost for fossil-fuelled power units. In CLC the oxygen from air is transferred to the fuel by a solid oxygen-carrier that circulates between two interconnected fluidized-bed reactors: the fuel- and the air-reactor. Thus, the direct contact between air and the fuel is avoided and $CO_2$ is obtained in a separate stream from $N_2$ in air. In the application of CLC for solid fuels, the oxygen-carrier oxidizes the products of the fuel gasification, which can be carried out ex-situ or in-situ the CLC system. The process where coal gasification takes place in the fuel-reactor is here called in-situ gasification Chemical-Looping Combustion, iG-CLC. The spent oxygen-carrier is transported to the air-reactor where it is oxidized by air, being ready to start a new cycle. The $CO_2$ capture efficiency depends on the char conversion in the reactor.

This study is focused on the development and assessment of the feasibility of the CLC process for solid fuels, using ilmenite as oxygen-carrier. Ilmenite, a natural mineral composed of $FeTiO_3$, is a low cost and promising material for its use on a large scale in CLC.

The performance of ilmenite in the iG-CLC technology for solid fuels was studied from the smaller to the larger scale. The reactivity of ilmenite with $CH_4$, $H_2$ and CO as the main products of coal devolatilization and gasification under different operating conditions of temperature and gas concentration was analyzed in well-defined conditions in TGA and fluidized bed reactor in batch mode. Although initially ilmenite particles present a rather low reactivity, ilmenite was found to undergo an activation process in its reaction rate, whose final value is adequate for the use of ilmenite in iG-CLC. The reaction kinetics of ilmenite for the main reduction and oxidation reactions were determined. The chemical

and physical changes of ilmenite after many redox cycles, as well its fluid-dynamic behavior in fluidized beds were studied in batch fluidized bed reactor. No agglomeration problems and adequate attrition rates were found. The char gasification kinetics of El Cerrejón bituminous coal was determined, and furthermore the char gasification process in presence of ilmenite particles was evaluated in batch fluidized bed reactor at different temperatures and $H_2O$-$CO_2$ mixtures as gasification agents, since the gasification rate was found to increase in presence of the oxygen-carrier.

The process performance was studied in continuous testing with different coals from lignite to anthracite in a 500 $W_{th}$ and a 10 $kW_{th}$ facility. The effect of several operation parameters on the performance of iG-CLC process was analyzed. Thus, different experiments were carried out by varying the fuel-reactor temperature, the coal particle size, the solids recirculation rate, the coal feeding flow, and the flow and type of gasification agent. There are unburnt gases that get out of the system, which were found to come from the volatile matter, because they have poor contact with the oxygen-carrier bed. To get high carbon capture it is necessary to work at high fuel-reactor temperatures, desirably above 950ºC, and to have enough residence time to increase the extent of char gasification.

The feasibility of application of the iG-CLC technology with fuels of different rank was proven. Furthermore, the effect of the type and characteristics of the solid fuel was assessed. It was found that higher carbon captures are obtained with coals of lower rank which are more reactive and gasify faster. Using $H_2O$ as gasifying agent is desirable to enhance char conversion in case of most types of coals. The use of some using $CO_2$ is admissible, depending on the resulting gasification rate with $CO_2$ with the fuel used. Big differences in carbon capture were found depending on the coal. At 900ºC and with an average residence time of the solids of 14.4 minutes and steam as gasification agent, the carbon capture obtained were 90% for lignite, 48% for bituminous Colombian coal, 54% for bituminous South African coal and 29% for anthracite. The corresponding combustion efficiencies in the fuel-reactor were in all cases above 70% and at 950ºC with bituminous Colombian coal, a combustion efficiency as high as 95% was reached with an inventory of 3100 $kg/MW_{th}$. For all types of solid fuels the combustion efficiency can be increased when working at high temperatures and high inventories. The influence in the process of

limestone addition was also studied and a slight improvement in the gas conversion could be seen after limestone addition, which can be explained by limestone catalyzing the Water Gas Shift reaction.

To predict and optimize the iG-CLC process, a simplified model based on mass balances and kinetics of the reactions involved in the process was developed. The performance of the iG-CLC process considering El Cerrejón bituminous coal as fuel was analyzed as a function of the main operating parameters such as the fuel-reactor temperature, the solids inventory in the fuel-reactor, the oxygen-carrier-to-fuel ratio, or the gasification agent to fixed carbon ratio. It was found that it is highly beneficial to increase the solids inventory up to 1000-2000 kg/$MW_{th}$, but further increase gives no relevant improvement. Because of the low char gasification rate, to get high carbon capture efficiency, a carbon separation system should be implemented to separate unconverted char and recirculate it back to the fuel-reactor. To have a high efficient carbon separation system was found to be determining for the process and can lead to carbon capture values above 90%. The contact of the volatile matter with the oxygen-carrier should be improved with some design solutions. Besides, the implementation of a second fuel-reactor is proposed as a very promising option to fully burn the volatile matter and besides to avoid another oxygen polishing step.

On the whole, the good results confirm the feasibility of the iG-CLC technology with solid fuels and that ilmenite appears to be a suitable material to be used for solid fuel combustion, considering its chemical and physical properties, its lack of toxicity and low market cost.

**Keywords:** $CO_2$ Capture, Chemical-Looping Combustion, ilmenite, coal, oxygen-carrier.

## List of Papers

This thesis is based on these following papers that are referred by roman numbers:

I. Adánez J, Cuadrat A, Abad A, Gayán P, de Diego LF, García-Labiano F. Ilmenite Activation during Consecutive Redox Cycles in Chemical-Looping Combustion. Energy Fuels 2010;24:1402-13.

II. Abad A, Adánez J, Cuadrat A, García-Labiano F, Gayán P, de Diego LF. Reaction kinetics of ilmenite for Chemical-Looping Combustion. Chem Eng Sci 2011;66(4):689-702.

III. Cuadrat A, Abad A, Adánez J, de Diego LF, García-Labiano F, Gayán P. Behavior of Ilmenite as Oxygen-carrier in Chemical-Looping Combustion. Fuel Proc Tech 2012;94(1):101-112.

IV. Cuadrat A, Abad A, Adánez J, de Diego LF, García-Labiano F, Gayán P. Prompt Considerations on the Design of Chemical-Looping Combustion of Coal from Experimental Tests. *Accepted to publish in Fuel.*

V. Cuadrat A, Abad A, García-Labiano F, Gayán P, de Diego LF, Adánez J. The use of ilmenite as oxygen-carrier in a 500 Wth Chemical-Looping Coal Combustion unit. Int J Greenhouse Gas Control 2011;5:1630–42.

VI. Cuadrat A, Abad A, García-Labiano F, Gayán P, de Diego LF, Adánez J. Effect of operating conditions in Chemical-Looping Combustion of coal in a 500 Wth unit. Int J Greenhouse Gas Control. doi:10.1016/j.ijggc.2011.10.013

VII. Cuadrat A, Linderholm, C, Abad A, Lyngfelt A, Adánez J. Influence of limestone addition in a 10 kWth Chemical-Looping Combustion unit operated with pet coke. Energy Fuels 2011;25(10):4818-28.

VIII. Cuadrat A, Abad A, Gayán P, de Diego LF, García-Labiano F, Adánez J. Theoretical approach on the CLC performance with solid fuels: optimizing the solids inventory. *Accepted to publish in Fuel.*

IX. Cuadrat A, Abad A, Gayán P, de Diego LF, García-Labiano F, Adánez J. Effect of the coal rank in the performance of in-situ Gasification Chemical-Looping Combustion. *Submitted to publish in Chemical Engineering Journal.*

Others:

X. Linderholm C, Lyngfelt A, Cuadrat A, Jerndal E. Chemical-Looping combustion of solid fuels – operation in 10 kW unit with two fuels, above-bed and in-bed feed and two oxygen-carriers, manganese ore and ilmenite. *Submitted to publish in Fuel.*

**Contribution report**

I, III, IV, V, VI, VII and IX. Principal author, responsible for experimental work, data evaluation and writing.
VIII. Principal author, responsible for model developing, data evaluation and writing.
II: Co-author, responsible for experimental work, data evaluation and writing.
X: Co-author, responsible for part of the experimental work, data evaluation and revision of writing.

## Congress contributions

1. Cuadrat A, Abad A, Adánez J. Comportamiento de la ilmenita como transportador de Oxígeno en Chemical-Looping Combustion. 3 Jornadas de Jóvenes Investigadores (Física y Química) de Zaragoza (Spain). November 2008.
2. Cuadrat A, Abad A, Adánez J, de Diego LF, García-Labiano F, Gayán P. Behaviour Of Ilmenite As Oxygen-carrier In Chemical-Looping Combustion. Fourth European Combustion Meeting. Vienna (Austria), April 2009.
3. Cuadrat A, Abad A, Adánez J, de Diego LF, García-Labiano F, Gayán P. Activation of ilmenite as Oxygen-carrier in Chemical-Looping Combustion with Coal. Fourth International Conference on Clean Coal Technologies. Dresden (Germany), May 2009.

4. Cuadrat A, Abad A, Adánez J, de Diego LF, García-Labiano F, Gayán P. Performance of ilmenite as Oxygen-carrier for Chemical-Looping Combustion using coal as fuel. First International Conference on Chemical-Looping. Lyon (France), March 2010.

5. Cuadrat A, Abad A, Adánez J. Ilmenita como transportador de Oxígeno en Chemical-Looping Combustion con carbón. 10 Reunión del Grupo Español del Carbón. Gerona (Spain), May 2010.

6. Cuadrat A, Abad A, García-Labiano F, Gayán P, de Diego LF, Adánez J. Ilmenite as Oxygen-carrier in a 500Wth Chemical-Looping Combustion system with coal. 10th Conference on Greenhouse Gas Technologies. Amsterdam (Holland), September 2010.

7. Linderholm C, Cuadrat A, Lyngfelt A. Chemical-Looping combustion of solid fuels in a 10 kWth pilot – batch tests with five fuels. 10th Conference on Greenhouse Gas Technologies. Amsterdam (Holland), September 2010.

8. Cuadrat A, Abad A, Adánez J. Ilmenita como transportador de Oxígeno en Chemical-Looping Combustion con carbón. 4. Jornada de Jóvenes Investigadores (Física y Química) de Zaragoza (Spain). November 2010.

9. Cuadrat A, Abad A, García-Labiano F, Gayán P, de Diego LF, Adánez J. $CO_2$ capture by Chemical-Looping Coal Combustion using ilmenite as oxygen-carrier in a 500 Wth unit. Fifth International Conference on Clean Coal Technologies. Zaragoza (Spain), May 2011.

10. Abad A, Gayán P, Cuadrat A, Adánez-Rubio I, de Diego LF, García-Labiano F, Adánez J. Evaluation of direct coal CLC processes. 3rd High Temperature Solid Looping Network Meeting. Vienna (Austria), August 2011.

11. Cuadrat A, Abad A, Gayán P, de Diego LF, García-Labiano F, Adánez J. Modeling and optimization of Chemical-Looping Combustion for solid fuels with ilmenite as oxygen-carrier. International Conference on Coal Science & Technology. Oviedo (Spain), October 2011.

**Juan Adánez Elorza**, Profesor de Investigación del CSIC, y

**Alberto Abad Secades**, Científico Titular del CSIC,

**CERTIFICAN:**

que la presente memoria, titulada: **"Chemical-Looping Combustion of coal using ilmenite as oxygen-carrier"**, ha sido realizada bajo nuestra dirección en el Instituto de Carboquímica (ICB-CSIC) por Dña. Ana Cuadrat Fernández, autorizando su presentación como compendio de publicaciones.

Y para que así conste, firmamos el presente certificado en Zaragoza a 26 de enero de 2012.

Fdo: Dr. Juan Adánez Elorza

Fdo: Dr. Alberto Abad Secades

## Acknowledgments

The development of this PhD was carried out during 2008-2012 at the Instituto de Carboquímica (ICB-CSIC), which belongs to the Spanish National Research Council. Part of the research and experimental work was done during a three-month stay at Chalmers University of Technology in Göteborg (Sweden).

This work was partially supported by the European Commission, under the RFCS program (ECLAIR Project, Contract RFCP-CT-2008-0008), from Alstom Power Boilers and by the Spanish Ministry of Science and Innovation (Project ENE2010-19550). The aim of these projects was to study the $CO_2$ capture in a chemical-looping combustion process for solid fuels. I thank these institutions for providing economic support and CSIC for the JAE Pre. fellowship received.

Me gustaría expresar mi gratitud a la Dr. María Jesús Lázaro y Dr. Juan Adánez como directores del Instituto de Carboquímica, así como al Dr. Juan Adánez como director de esta tesis por su confianza y su respaldo, por aceptarme en su grupo de Gasificación y Combustión y por su consejo y las mejoras que añade en mi trabajo. Quiero expresar mi agradecimiento particular a mi director Dr. Alberto Abad por su paciencia, serenidad, guía y conocimiento inagotables y sobre todo, por su ejemplo. Por supuesto, mis gracias al resto del equipo de los 5 magníficos: Pili, Paco y Luis.

También estoy muy agradecida con el Dr. Anders Lyngfelt y el resto del Departamento de Energía y Medioambiente de Chalmers por la oportunidad de trabajar en su grupo y utilizar sus instalaciones. Gracias a mi compañero de equipo sueco Calle, con quien pasé tantas horas delante de la planta, entre dificultades de operación y charlas geniales. Y a todos los buenos amigos que hice en Suecia, como Marta, Erika, Patrick y Pedro. Porque me hicisteis estar como en casa.

Gracias a mis compañeros y personal del ICB, por haberme acogido en el Instituto y me habéis hecho como una más. Y en especial a los compañeros del despacho y de los mundos

de la nave: MA, Iñaki, Jose, María, Arancha, Marga y Javi. Por todos esos ratos, bromas y charlas juntos y su ayuda. Y a María como la nueva adquisición de la nave y Arturo como novedad del grupo. Gracias a Teresa, con la que no solo comparto trabajo, sino también afinidad, aficiones y amistad. Además quiero mencionar a los compañeros de la cafetería y desconexión, y particularmente a las chicas del Hidrógeno: Cinthia, Elena, Sonia, Sara, David y Dani, quienes son capaces de alegrarte el día en un minuto.

Tienen mi gratitud para siempre mis amigos, porque sois gente en la que se puede confiar, porque cada rato con vosotros es genial y, en definitiva, porque sois extraordinarios. María, Silvia, Irene, Cristina, Alex, Jose, Pablo, Edu, los amigos del Erasmus de Viena, y mis queridas Químicas: Sara, Rakel, Ainhoa, Mapi, Silvia, Luci, Javi, Pedro, Nacho y las del CPS que me acompañáis a diario y en muchos sentidos: Sus, Isa y Carlos.

Gracias a mi familia y en especial a mi hermano Javi y mis padres Pilar y Chema. Por vuestros valores, por todo lo que me habéis dado y porque sois un valor seguro.

Y gracias a Jorge. Por todo lo que significas para mí y por lo grande que eres.

TABLE OF CONTENTS

# 1 Introduction

## 1.1 Greenhouse effect and $CO_2$ mitigation

According to the IPCC (IPCC, 2007), "warming of the climate system is unequivocal", considering that eleven of the recent years (1995-2006) rank among the twelve warmest years in the instrumental record of global surface temperature since 1850. It is also clear that climate change can strongly modify the earth biodiversity (IPCC, 2002). Among the possible causes, it seems that most of the warming observed over the past 50 years is attributable to human activities, as a consequence of the gases emitted to the atmosphere, the so-called greenhouse gases (GHG) (IPCC, 2001). Among them, $CO_2$ is considered the gas making the largest contribution to the global warming, because $CO_2$ represents the largest emissions of all the global anthropogenic GHG emissions, with percentage values as high as 75% (Archer, 2005), and due to its high residence time in the atmosphere.

The $CO_2$ concentration in the atmosphere has increased strongly over the few past decades as a result of the dependency on fossil fuels for energy production. The global atmospheric $CO_2$ concentration increased from a pre-industrial value of about 280 ppm to 390 ppm in 2010 (NOAA-ESRL, 2010). To assure the increase in average temperatures was lower than 2 °C –which it is considered as the limit to prevent the most catastrophic changes in earth– the $CO_2$ concentrations must not exceed 450 ppm. Therefore, it is generally accepted that a reduction in emissions of greenhouse gases is necessary as soon as possible. In 1997, the nations participating in the United Nations Framework Convention on Climate Change drafted the historic agreement known as the Kyoto Protocol (United Nations, 1998). After ratification in 2005, its provisions include a mean reduction in the GHG emissions of the developed countries of 5.2% over the period 2008-2012 compared to 1990 levels.

As for the IPCC, the largest growth in global GHG emissions in the last years has come from the energy supply sector. Energy from fossil sources -gas, oil and coal-, which cause $CO_2$ emissions, will still satisfy over 80% of the demand during the first part of the 21st century. Furthermore, IEA predicts 57% increase of energy demand from 2004 to 2030 (IEA, 2007). Fossil-fueled power units are responsible for roughly 40% of total $CO_2$

emissions, coal-fired units being the main contributor (Carapellucci and Milazzo, 2003). Unfortunately these energy sources will not yet be ready to be substituted massively in the near future (IEA, 2007).

The abatement of GHG emissions can be achieved through a wide portfolio of measures in the energy, industry, agriculture and forest sectors. Up to now, the technological options for reducing net $CO_2$ emissions to the atmosphere have been focused on (IPCC, 2005): 1) increasing the efficiency of energy conversion and/or utilization; 2) switching to less carbon intensive fuels, e.g. natural gas; 3) increasing the use of renewable energy sources (biofuel, wind power, etc.) or nuclear energy, and 4) the use of technologies of $CO_2$ Capture and Storage (CCS) also appears as a relevant option to reduce the emissions of GHG, see Figure 1. It is clear that no single technology option will provide all of the emissions reductions needed.

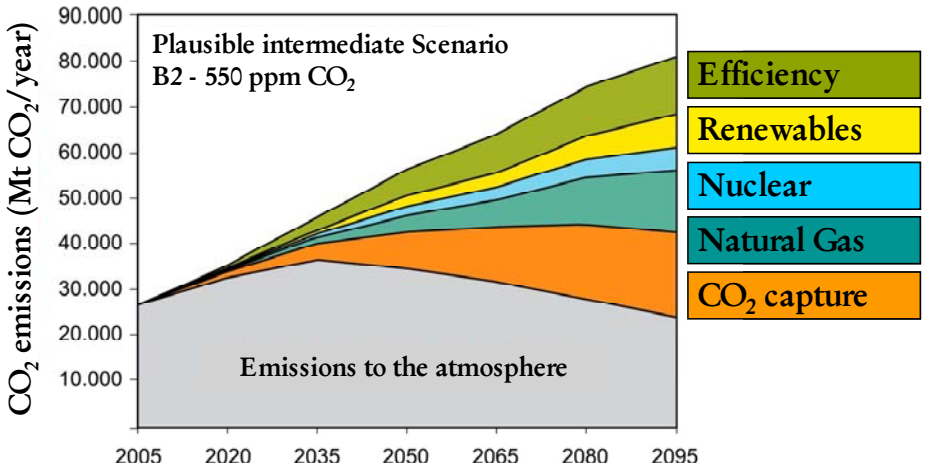


Figure 1. Illustrative example of the global potential contribution of CCS as part of a mitigation portfolio. Global $CO_2$ emissions in grey and corresponding contributions of main emissions reduction measures in color (IPCC, 2007).

According to the analysis made by the IPCC and IEA (IPCC, 2005; IEA, 2006), CCS could contribute 15–55% to the cumulative mitigation effort worldwide until 2100, averaged over a range of baseline scenarios (see Figure 1), to stabilize climate change at a reasonable cost. It is likely that there is enough technical potential for geological storage. CCS must provide 20% of the global $CO_2$ cuts required by 2050, according to the IEA (IEA, 2006).

## 1.2 $CO_2$ Capture and Storage

The purpose of CCS technology is to produce a concentrated stream of $CO_2$ from industrial and energy-related sources, transport it to a suitable storage location, and then store it away from the atmosphere for a long period of time. Thus, if $CO_2$ is transported and stored appropriately, it will not further contribute to the greenhouse effect. The IPCC Special Report on Carbon Dioxide Capture and Storage (IPCC, 2005) gives an overview of the different options available both for the capture, transport and storage processes. Figure 2 shows sources for which CCS might be relevant and $CO_2$ transport and storage options.

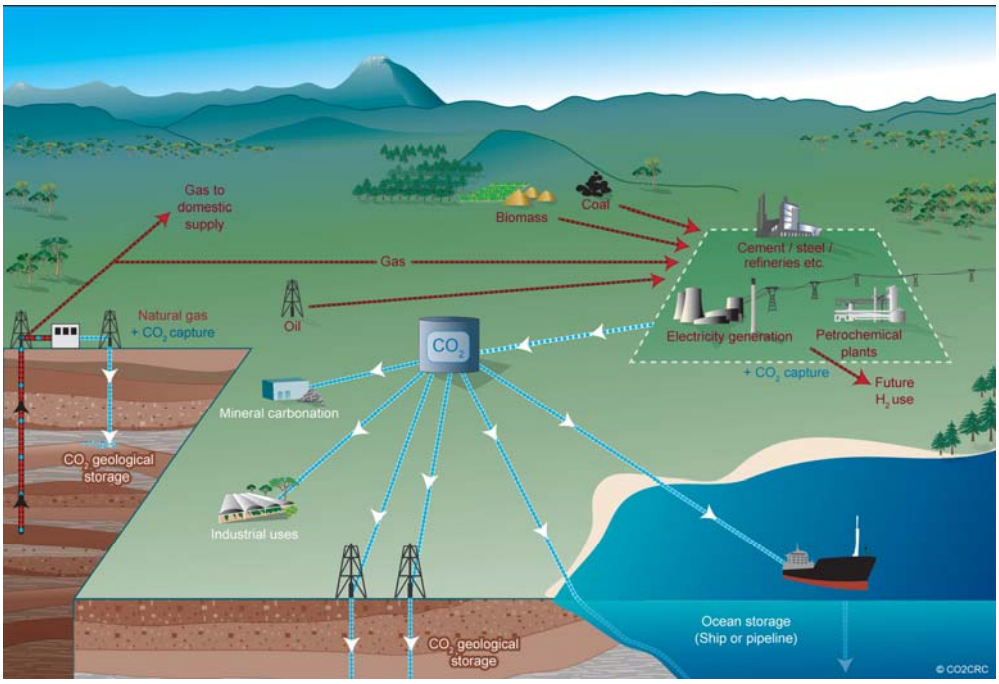


Figure 2. Schematic diagram of possible CCS options.

For CCS to achieve the estimated economic potential, several hundreds to thousands of $CO_2$ capture systems would need to be installed over the coming century, each capturing 1–5 $MtCO_2$ per year. One aspect of the cost competitiveness of CCS systems is that CCS technologies are compatible with most current energy infrastructures, being the implementation of these technologies more feasible and readily achievable in stationary power units. Thus, CCS is an essential component of a portfolio of technologies and measures to reduce global emissions and help to avoid the most serious impacts of climate

change (IPCC, 2005; IEA, 2010). Costs for $CO_2$ capture include the capture process, plus the conditioning and compression/liquefaction of the captured $CO_2$ required for transport. Implementing CCS will of course have an impact on the cost for the electricity production. Estimations on using commercially available technologies indicate an increase in the cost of produced electricity by 37-85% in natural gas combined cycle power units and 43-91% in pulverized coal power units (IPCC, 2005).

Among the three steps involving CCS (capture, transport and sequestration), $CO_2$ capture is the most costly. The development of $CO_2$ capture systems with low economic and energetic penalty has the mayor potential to reduce the global cost of the CCS process. Three main approaches were considered for $CO_2$ capture in industrial and power generation applications: post-combustion systems, oxy-fuel combustion, and pre-combustion systems. A brief overview of the current situation of these technologies can be found in the work of Toftegaard et al. (2010). However, most of the technologies that reduce $CO_2$ emissions have high energy penalty using commercial technologies available. This leads to a lower overall energetic efficiency and an increase in the energy price.

The Zero Emissions Platform (ZEP) report about the costs of CCS on existing pilot and planned demonstration projects concluded that for hard coal-fired power units, the addition of $CO_2$ capture and the processing of $CO_2$ for transport is equivalent to $CO_2$ avoidance costs of 30-40€/t (Zero Emissions Platform, 2011). They found no clear difference between any of the analyzed capture technologies and all could be competitive in the future if successfully demonstrated. The conclusion of the study was that, following the European Union's CCS demonstration program, CCS will be cost-competitive with other sources of low-carbon power, including on-/offshore wind, solar power and nuclear. Further decrease in the CCS cost will be possible by developing $CO_2$ capture technologies with low energetic and economical penalty.

### *1.2.1 Post-combustion capture*

It consists in separating the $CO_2$ from the flue gas after the combustion step. Amine absorption/desorption is often used for this purpose. With this method, the flue gas is led

to a scrubber where the liquid solvent absorbs the $CO_2$ and the rest of the flue gas is released to the atmosphere. Solvent regeneration is obtained by temperature changes which release $CO_2$. The separation is not inherent to the combustion step and since this method requires extra energy consumption, the process efficiency is affected. It has been estimated that $CO_2$ capture by post-combustion in coal power units would reduce their efficiency from 8 to 16% and for a natural gas combined cycle from 5 to 10% (Ghoniem, 2011). To decrease costs, there are several technologies in development, such as the chilled ammonia process by ALSTOM or the calcination-carbonation cycle.

### *1.2.2 Pre-combustion capture*

In a first step, the fuel is converted to a mixture of CO, $CO_2$, $H_2$ and $H_2O$ using $O_2$ and/or $H_2O$ by reforming natural gas or gasifying coal. The next step is to shift CO and $H_2O$ producing $CO_2$ and $H_2$. Removing $CO_2$ from the mixture, using e.g. physical absorption with solvents, yields almost pure $H_2$ which can be used as a carbon-free fuel in a combined gas and steam turbine cycle. As a result, no carbon containing gases are released. However, as for the post-combustion technology, this method is energy consuming. The technology required for pre-combustion capture is widely applied in fertilizer manufacturing and in hydrogen production. Although the initial fuel conversion steps of pre-combustion are more elaborate and costly, the higher concentrations of $CO_2$ in the gas stream and the higher pressure make the separation easier. The estimated efficiency reduction in a coal gasification unit is about 7 to 13% and in a natural gas reforming unit is 4-11% (Ghoniem, 2011). The integration of this process with a combined cycle can be beneficial, reaching high energetic efficiencies. Besides, membrane technologies are in development.

### *1.2.3 Oxy-fuel or $O_2/CO_2$ combustion*

In this method, the combustion step is achieved using a mixture of oxygen and recirculated flue gases, i.e. carbon dioxide, instead of air. In the flue gases, almost only $CO_2$ and $H_2O$ are present. By condensing steam, almost pure $CO_2$ is obtained. The carbon capture efficiency, nearly 100%, is thus considerably higher than the efficiency of the post-combustion treatment. However, an Air Separation Unit is required for the oxygen

production, which induces to extra cost and energy penalties. The estimated efficiency reduction in a coal gasification unit is 6-9% and in a natural gas unit is 5-12% (Ghoniem, 2011). Membrane technologies are also in development.

### *1.2.4 CCS demonstration projects*

As for projects in the bigger scale focused on storage in CCS, the first application started in 1996 within the Sleipner $CO_2$ storage project from the former Norwegian company Statoil, now StatoilHydro. The $CO_2$ contained in the natural gas from the Sleipner gas field is injected into a deep saline aquifer called the Utsira formation located in the North Sea between Norway and Scotland, at a depth of around 1000 meters. Around 1 million tones $CO_2$ is annually injected in the sand stone formation since the project start (IPCC, 2005).

There are several projects on CCS worldwide in operation to date. The most important are the following: The Weyburn Project since 2000 from US and Canada on $CO_2$ geological storage; the In Salah gas project in South Algeria on $CO_2$ post-combustion and storage in an underground aquifer; the Snøhvit project in the Norwegian Sea on $CO_2$ storage in a sandstone; the Callide 'A' Power Station project in Australia on oxy-fuel capture and storage on a gas field; the project at Schwarze Pumpe, Germany, which has a $30MW_{th}$ oxyfuel coal boiler and the CIUDEN foundation which accounts with a 30 $MW_{th}$ circulating fluidized bed and a 20 $MW_{th}$ pulverized oxyfuel coal boilers in El Bierzo, Spain.

## 1.3 Chemical-Looping Combustion

The previous technologies involve expensive and energy demanding gas separation processes. Thus, new processes and further research are being developed to reduce the energy penalty of these technologies. To address this issue and since the main cost comes from the separation of $CO_2$ from $N_2$, an alternative is to use a process where the combustion air and the fuel are never mixed, so that no nitrogen is present in the combustion exhaust gases. The $CO_2$ separation is then inherent to the combustion step.

This principle could be called unmixed combustion and requires a way to transfer oxygen from air to fuel. The process on which this thesis is based, Chemical-Looping Combustion (CLC), also belongs to this category.

The $CO_2$ Capture Project (CCP) –Phase I– decided at the beginning of 2000 to collaborate with governments, industry, academic institutions and environmental interest groups to develop technologies that greatly reduce the cost of $CO_2$ capture (Thomas and Benson, 2005). The objective was to identify the most promising technologies that had the potential to deliver performance and efficiency improvements resulting in close to a 50% reduction in the cost of $CO_2$ capture. Among them, the Chemical-Looping Combustion (CLC) process was suggested among the best alternatives to reduce the economic cost of $CO_2$ capture (Kerr, 2005). If the environmental impact is also considered, CLC is preferred against other $CO_2$ capture options (Petrakopoulou et al., 2011). Moreover, the IPCC in their special report on Carbon Dioxide Capture and Storage made a comparative economic evaluation of the different technologies (Thambimuthu et al., 2005). The CLC process, with a cost of 14 US$ per ton of $CO_2$ avoided, was one of the cheapest technologies. The main drawback attributed to CLC was a very low confidence level as a consequence of the lack of maturity of the technology. This is an emerging technology although during the last 10 years has undergone a great development.

Chemical-Looping Combustion (CLC) is based on the transfer of the oxygen from air to the fuel by means of a solid oxygen-carrier, avoiding direct contact between fuel and air. Lyngfelt et al. (2001) proposed the use of two interconnected fluidized beds for a CLC system with the oxygen-carrier circulating between them. Ideally, the stream of combustion gases from the fuel-reactor contains primarily $CO_2$ and $H_2O$, although some unburnt compounds can also appear (e.g. CO, $H_2$, $CH_4$). In this case, an oxygen polishing step can be necessary for complete combustion to $CO_2$ and $H_2O$. After that, water can be easily separated by condensation and a highly concentrated stream of $CO_2$ ready for compression and sequestration is achieved. The $CO_2$ capture is inherent to this process, as the air does not get mixed with the fuel, and no additional costs or energy penalties for gas separation are required. The gas stream from the air-reactor is oxygen-depleted and consists in $N_2$ and some unreacted $O_2$.

Important progress has been made in CLC for gaseous fuels, i.e., natural gas and syngas, to date. Most of the oxygen-carriers proposed in the literature are synthetic materials. In general, the oxygen-carrier is based on a transition state metal oxide, e.g. CuO, NiO, $Co_3O_4$, $Fe_2O_3$ or $Mn_3O_4$, which is supported on different inert materials, as $Al_2O_3$, $SiO_2$, $TiO_2$ or $ZrO_2$. A selection of oxygen-carrier materials for natural gas and syngas combustion has been summarized by Hossain and de Lasa (2008) and Lyngfelt et al. (2008) and recently by Adánez et al. (2011).

The feasibility of this process has been successfully demonstrated in different CLC prototypes in the 10-140 $kW_{th}$ range using oxygen-carriers based on nickel, copper and cobalt oxides (Ryu et al., 2005; Lyngfelt and Thunman, 2005; Adánez et al., 2006; Linderholm et al., 2008 and 2009; Kolbitsch et al., 2009). Regarding the intensive use of coal for energy generation, there is an increasing interest for CLC using this fuel.

### *1.3.1 CLC with solid fuels*

There are three options for the use of the CLC technology with coal. The first one is to carry out previous coal gasification and subsequently to introduce the produced gas in the CLC system. This option needs pure $O_2$ for the gasification step and thus an air separation unit and an external gasifier are required. Simulations performed by Jin and Ishida (2004) and Wolf et al. (2001) showed that this process has the potential to achieve an efficiency of about 5-10% points higher than a similar combined cycle with conventional $CO_2$ capture technology working under pressure. Several oxygen-carriers based on Ni, Cu, Fe and Mn oxides have shown good reactivity with syngas components, i.e. $H_2$ and CO (Mattisson et al., 2007; Abad et al., 2007a), and the use of syngas in a CLC system has been successfully accomplished in 300-500 $W_{th}$ continuous CLC units (Johansson et al., 2006a; Abad et al., 2006, 2007b; Dueso et al. 2009; Forero et al., 2009). The second possibility for the use of coal in CLC is the direct feeding in the CLC process, that is, avoiding the need of an external gasifier and the corresponding gaseous oxygen requirement (Cao and Pan, 2006; Dennis et al., 2006). The reactor scheme for this CLC configuration is shown in Figure 3. In this option coal is physically mixed with the oxygen-carrier in the fuel-reactor which is

fluidized by a gasification agent. As the gasification of coal happens inside the fuel-reactor, this process has been referred as the in-situ gasification CLC (Adánez et al., 2011).

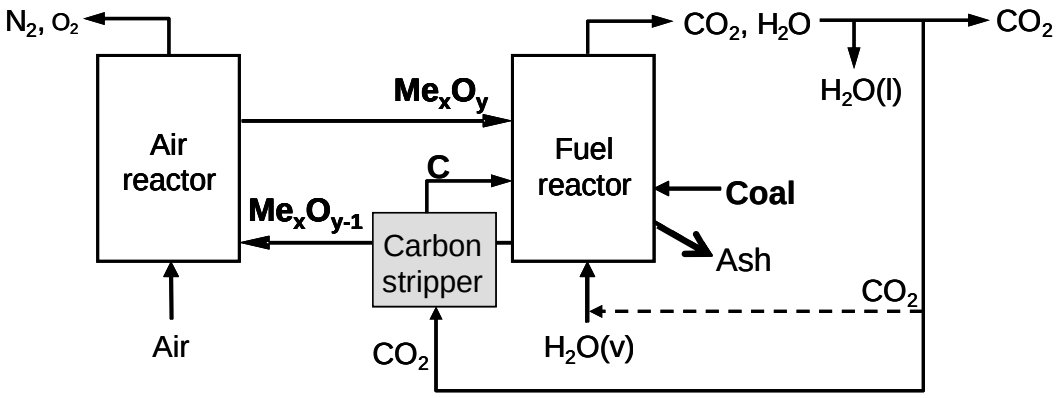


Figure 3. Reactor scheme of the iG-CLC process for solid fuels (_ _ _ optional stream).

The in-situ gasification of the solid fuel is carried out in the fuel-reactor and the carrier reacts with the gas products from steam coal gasification, where $H_2$ and CO are main components. Thus, the volatiles release and the solid fuel gasification proceed in the fuel-reactor according to reactions (1-3) and the resulting gases are oxidized through reduction of the oxidized oxygen-carrier, $Me_xO_y$, by reaction (4). The oxygen-carrier reduced in the fuel-reactor, $Me_xO_{y-1}$, is transferred to the air-reactor where reaction (5) with oxygen from air takes place. Thus the oxygen-carrier is regenerated to start a new cycle. The net chemical reaction is the same as usual combustion with the same combustion enthalpy.

$$\text{Coal} \rightarrow \text{Volatile matter} + \text{Char} \quad (1)$$

$$\text{Char} + H_2O \rightarrow H_2 + CO \quad (2)$$

$$\text{Char} + CO_2 \rightarrow 2\,CO \quad (3)$$

$$H_2, CO, \text{Volatile matter} + n\,Me_xO_y \rightarrow CO_2 + H_2O + n\,Me_xO_{y-1} \quad (4)$$

$$Me_xO_{y-1} + \tfrac{1}{2}\,O_2 \rightarrow Me_xO_y \quad (5)$$

It is expected that the gasification process was the limiting step in the fuel-reactor, so the stream of solids that exits from the fuel-reactor contains some unconverted char together with the oxygen-carrier. To increase the mean residence time of char and to avoid ungasified char to enter the air-reactor, the char particles can be separated from the oxygen-carrier in a carbon separation system and re-introduced to the fuel-reactor, as shown in

Figure 3. It is necessary to point out that the transference of char to the air-reactor does not reduce the energetic efficiency of the process but it decreases the carbon capture efficiency of the system because some $CO_2$ will exit with the exhaust gas from the air-reactor.

Moreover, as a consequence of the ash present in the solid fuel it is necessary to drain ashes from the system to avoid its accumulation in the reactors. The drain stream will also contain some oxygen-carrier. Thus, the lifetime of this material is expected to be limited by the losses together the drain stream rather than for its degradation.

For direct CLC with solid fuels, there are three particular aspects to be taken into account: (1) high combustion efficiencies in the fuel-reactor should be reached, (2) the system must be optimized to get maximum ash separation and minimum carrier losses, and (3) the carbon separation system should be optimized. Thus, the efficiency of char conversion in the fuel-reactor and the separation of ashes from the oxygen-carrier seem to be key factors for the development of this process.

Recently, a third option has been proposed: the Chemical-Looping with Oxygen Uncoupling process (CLOU) (Mattisson et al., 2009). In the CLOU process the oxygen-carrier releases oxygen in gas phase, and this gaseous oxygen reacts with the fuel. CLOU allows solid fuels to be burnt in gas-phase oxygen without the need for an energy-intensive air separation unit. A key issue for the development of the CLOU process is to develop suitable materials with oxygen uncoupling properties.

### *1.3.2 Oxygen-carriers for iG-CLC*

The selection of the oxygen-carrier is a key factor for the CLC technology development. Suitable oxygen-carriers must show high reaction rates and oxygen transport capacity, complete fuel conversion to $CO_2$ and $H_2O$, negligible carbon deposition, avoidance of agglomeration, and sufficient durability as well as good chemical performance. These properties must be maintained during many reduction and oxidation cycles. In addition, the cost of the oxygen-carrier, environmental characteristics and health aspects are also

important for its use with coal, as it is predictable a partial loss together with the coal ashes when removing them from the reactor to avoid their accumulation in the system.

Synthetic materials have been proposed as oxygen-carriers in CLC for solid fuels, e.g. coal, petroleum coke, biomass or solid wastes (Cao et al., 2006; Scott et al., 2006; Leion et al., 2007; Yang et al., 2007; Chuang et al., 2008; Shen et al., 2009a;b;c; Siriwardane et al., 2009). There are studies made on the reactivity of synthetic oxygen-carriers mainly based on CuO (Cao et al., 2006), $Fe_2O_3$ (Scott et al., 2006; Leion et al., 2007; Wu et al., 2010) and NiO (Zhao et al., 2008) for in-situ gasification of the solid fuel. However, for CLC with solid fuels, the use of low-cost natural minerals or industrial waste products seems to be more suitable, as it is predictable a partial loss of the oxygen-carrier together with the coal ashes.

At the beginning of this thesis in 2008, there were only a few studies about this technology. There were some studies on the suitability of using low cost minerals such as ilmenite, an iron based natural ore. Leion et al. (2008a,b) analyzed the reactivity of ilmenite in a batch fluidized bed for solid fuels combustion. Ilmenite gave high conversion of CO and $H_2$ but moderate conversion of $CH_4$. They observed a gain in ilmenite reactivity as increasing redox cycles, and eventually reactivity as high as for a synthetic $Fe_2O_3$-based oxygen-carrier was reached. Ilmenite showed high stability in its reactivity after repeated redox cycles. They also saw that defluidization occurred only when the ilmenite particles were in a highly reduced state (Leion et al., 2008b), which is not expected at CLC operation. These were first approaches of the ilmenite performance as oxygen-carrier in iG-CLC. In order to advance in this technology, a more comprehensive analysis of the properties of ilmenite as oxygen-carrier is needed. An assessment of the conditions in which the gain in reactivity occurs as well as the reactivity and properties of ilmenite after a high number of redox cycles, the evaluation of the intrinsic kinetics in the oxidation and reduction reactions and a study on the gasification reaction under iG-CLC conditions are required. A deeper study on the behavior in fluidized bed of the oxygen-carrier material is also essential.

The proof of the concept of the iG-CLC process in a continuously operated prototype was carried out by Berguerand and Lyngfelt (2008a; b) using ilmenite as oxygen-carrier. Due to the characteristics of this facility with over-bed coal feeding, the volatiles do not get in

good contact with oxygen-carrier particles. Thus, only the conversion of gases from steam gasification (CO and $H_2$) was analyzed. A $CO_2$ capture within the range 65-82% was obtained for South African coal as fuel at 900-950°C. Petcoke was also used as a fuel with low volatile content, for which $CO_2$ capture was 60-75% at 900-950°C, with an oxygen demand around 25%. The performance of this prototype could be improved by increasing the residence time of the particles in the fuel-reactor to get higher $CO_2$ capture and by increasing the separation efficiency of the cyclone after the fuel-reactor. Also, the incomplete gas conversion resulted into the presence of unconverted gases in the fuel-reactor outlet stream that demanded 29-30% of the total oxygen needed to fully burn coal to $H_2O$ and $CO_2$. The gas conversion could be improved by a polishing step with $O_2$ after the fuel-reactor. Due to the promising good behavior observed for ilmenite, in this work the iG-CLC process for solid fuels using ilmenite as oxygen-carrier was evaluated. Since to date only the effect of the temperature had been analyzed by doing experiments at two temperatures. To evaluate the influence of different operating variables in the system is necessary for the progress of this technology, as well as to try other types of fuels with different ranks. Besides, the combustion of the devolatilization products should be analyzed. While this thesis was developed, more studies about ilmenite and other possible oxygen-carriers –natural ores and industrial products, most of all- for iG-CLC in different scales were done concurrently, where different types of fuels were used. The main results obtained in other later studies will be commented along this thesis.

## 1.4 Objective

The aim of this work was to study the feasibility and performance of the Chemical-Looping Combustion technology for solid fuels and to evaluate the conditions and key parameters that improve the efficiency of the process, in order to get a technically and economically competitive combustion technology with $CO_2$ capture.

This was investigated by performing tests in a thermogravimetric analyzer, a batch fluidized bed reactor for gaseous fuels, a batch fluidized bed reactor for solid fuels and a continuous CLC unit for solid fuels, all these devices are placed at the Instituto de

Carboquímica (ICB-CSIC) in Zaragoza (Spain). Tests in a 10 $kW_{th}$ continuous CLC unit for solid fuels built at Chalmers in Göteborg (Sweden) were also done. Focus was made on analyzing the behavior and suitability of ilmenite as oxygen-carrier in CLC with solid fuels by in-situ gasification CLC (iG-CLC), on assessing the operation performance using different solid fuels and evaluating the effect of operational parameters on carbon capture and combustion efficiency. Furthermore, with the experimental information gathered, a theoretical simplified model for the fuel-reactor was developed to analyze the effect of the main operating variables in the CLC process performance.

This thesis is based on nine papers. Paper I analyzes the behavior of ilmenite as oxygen-carrier in CLC and its activation process. Changes in its properties through redox cycles in a thermogravimetric analyzer were also assessed. In Paper II the kinetics of ilmenite as oxygen-carrier for the reduction and oxidation reactions taking place in CLC with the main gas products of coal devolatilization and gasification were determined. In Paper III the reactivities with different mixtures of reducing agents and the variation of chemical and physical characteristics of ilmenite particles during high number of consecutive redox cycles in fluidized-bed was assessed. In Paper IV the char gasification step and subsequent conversion of the gasification products was studied in a fluidized bed using a bituminous coal char as fuel at different temperatures and using various $H_2O$-$CO_2$ mixtures as gasification agent and ilmenite as oxygen-carrier. Papers V, VI and IX explain results obtained in a continuous facility fuelled with coal. In Paper V the effect of temperature and coal particle size of a bituminous coal on the process performance was assessed. Char gasification and combustion of both gasification products and volatile matter were also evaluated. In Paper VI the effect of operating conditions such as the solids circulation rate and oxygen-carrier residence time, the coal flow feed and the gasification agent flow and type were investigated. In Paper IX the variation in the system performance and feasibility of the technology when using different types of coals is investigated. In Paper VII the influence of limestone addition to ilmenite as oxygen-carrier was tested in a continuous 10 $kW_{th}$ CLC pilot using petroleum coke as fuel at different temperatures and solids circulation rates. Based on experimental results, in Paper VIII a simplified model that describes the fuel-reactor of an iG-CLC system was developed. The model includes the possibility of using a carbon separation system.

# 2 Experimental

## 2.1 Oxygen-carrier

Ilmenite is a common mineral found in metamorphic and igneous rocks. Ilmenite is mainly composed of $FeTiO_3$ ($FeO \cdot TiO_2$), where iron oxide is the active phase that behaves as an oxygen-carrier.

The ilmenite used in this study is a concentrate from a Norwegian natural ore and it has a purity of 94.3%. The particle size used was 150-300 μm. Fresh ilmenite and calcined ilmenite particles were initially used in this work. Calcined ilmenite was obtained after a thermal treatment of fresh ilmenite at 950 °C in air during 24 hours.

Ilmenite particles were physically and chemically characterized by several techniques. Table 1 shows the main physical and chemical properties of the Norwegian ilmenite used as oxygen-carrier in the experiments of this research. Both fresh and calcined ilmenite are characterized. As it is later explained, the oxygen-carrier undergoes an activation process with the number of cycles. Therefore, the properties of the here called "activated ilmenite" are also analyzed. As an example of an activated ilmenite, the properties of the activated ilmenite after 20 redox cycles in fluidized bed with 25 vol.% $CH_4$ + 10 vol.% $H_2O$ as reducing agent at 900 °C are also given in Table 1. Both calcined and activated ilmenite were used for the determination of ilmenite reaction kinetics. The true density of the particles was measured with a Micromeritics AccuPyc II 1340 Helium picnometer. The force needed to fracture a particle was determined using a Shimpo FGN-5X crushing strength apparatus. The mechanical strength was taken as the average value of at least 15 measurements undertaken on different particles of each sample randomly chosen. Particle porosity was measured by Hg intrusion in a Quantachrome PoreMaster 33. The identification of crystalline chemical species was carried out by powder X-ray diffraction (XRD) patterns acquired in an X-ray diffractometer Bruker AXS D8ADVANCE using Ni-filtered Cu Ka radiation equipped with a graphite monochromator. Semi-quantitative percentages of the different components in each sample were obtained through normalization by means of a ratio between the intensity peaks of the main component and a substance of reference.

Table 1. Composition (%wt.) and physical properties of fresh, calcined and activated ilmenite after 20 redox cycles in fluidized bed (Reducing agent: 25 vol.%$CH_4$+10 vol.%$H_2O$).

| | Fresh ilmenite | Calcined ilmenite | Activated ilmenite |
|---|---|---|---|
| True density (kg/m$^3$) | 4580 | 4100 | 4250 |
| $R_{O,ilm}$ (%) | | 4.0 | 3.3 |
| Grain radius (μm) | 0.5 | 0.5 | 1.25 |
| Porosity (%) | 0 | 1.2 | 12.7 |
| BET Surface (m$^2$/g) | 0.6 | 0.8 | 0.4 |
| Crushing strength(N) | 2.4 | 2.2 | 2.0 |
| XRD (main species) | $FeTiO_3$, $Fe_2O_3$, $TiO_2$ | $Fe_2TiO_5$, $Fe_2O_3$, $TiO_2$ | $Fe_2TiO_5$, $Fe_2O_3$, $TiO_2$ |
| $Fe_2O_3$ (%wt.) | 14.8 | 11.2 | 22.0 |
| $Fe_2TiO_5$ (%wt.) | - | 54.7 | 38.5 |
| $TiO_2$ (%wt.) | 14.0 | 28.6 | 34.0 |
| $FeTiO_3$ (%wt.) | 65.5 | - | - |
| Inert (%wt.) | 5.7 | 5.5 | 5.5 |

The XRD analysis revealed ilmenite ($FeTiO_3$), hematite ($Fe_2O_3$) and rutile ($TiO_2$) as major components of fresh ilmenite. Besides, SEM-EDX analyses revealed a Fe:Ti molar ratio around 1:1. During the thermal treatment ilmenite ($FeTiO_3$) was fully oxidized to pseudobrookite ($Fe_2TiO_5$). Calcined ilmenite consists of a mixture of ferric pseudobrookite ($Fe_2TiO_5$), rutile ($TiO_2$) and some free hematite ($Fe_2O_3$), which confirms the literature data indicating that iron compounds in ilmenite are in the most oxidized state after calcination at 950°C (Rao and Prototypeaud, 1975). Minor amounts of oxides and silicates can be found, mainly $MgSiO_3$ and $MnO_2$.

The oxygen transport capacity of ilmenite $R_{O,ilm}$ corresponds to the reduction of the $Fe_2TiO_5$ and $Fe_2O_3$ present in ilmenite, being the reduced species $FeTiO_3$ and $Fe_3O_4$, respectively. Although the oxidized species can get further reduced, the thermodynamic equilibriums indicate that $Fe_2TiO_5$ and $Fe_2O_3$ should be only reduced up to $FeTiO_3$ and $Fe_3O_4$ respectively in order to reach full conversion to $CO_2$ and $H_2O$ of the reducing gases,

which is the objective of a CLC process. Low values of BET surface area were measured, but a slight increase was observed after calcination. Mercury porosimetry of both fresh and calcined ilmenite exhibit low porosity development. This ilmenite has shown good reactivity and properties from batch fluidized bed testing (Leion et al., 2008a,b; 2009a,b; Bidwe et al., 2011). It has also been tested with solid fuels in a 10 kW unit at Chalmers University of Technology (Berguerand and Lyngfelt, 2008a; b; 2009a; b) and with gaseous fuels in a 10 $kW_{th}$ unit (Bidwe et al., 2011) and a 120 $kW_{th}$ unit (Pröll et al., 2009).

## 2.2 Fuels

In this thesis both gaseous and solid fuels were used. As gaseous fuels, pure gases such as $CH_4$, $H_2$ or CO were used, considered as main products of coal devolatilization and gasification. A range of coals with different behavior was used as fuels: a Spanish anthracite, a Spanish lignite and two bituminous coals from Colombia and South Africa. Following the ASTM characterization, South African coal is a medium volatile (MV) bituminous coal, whereas Colombian coal is a high volatile (HV) bituminous coal. Mexican petcoke was also used. The properties of all these solid fuels are gathered in Table 2. Three different particle sizes of Colombian coal were used: +74-125, +125-200 and +200-300 μm. The particle size used for lignite, South African coal and anthracite was +200-300 μm and for petcoke was +90-200 μm.

The HV bituminous Colombian coal was subjected to a thermal pre-treatment for pre-oxidation to reduce its swelling properties. Thus, coal was placed in trays in layers of about 3 mm height and exposed to heating at 180 °C in air atmosphere for 28 hours. The use of pre-treated coal eliminates the swelling properties and avoids the pipe clogging and coal particles agglomeration showed when fresh coal was used. Pre-oxidation causes an increase in oxygen content and a decrease in the heating value.

Char of bituminous South African and pre-treated Colombian bituminous coal were produced and used. They were done by devolatilizing batches of 500 g of coal particles in a

fluidized-bed reactor. The reactor was fluidized by $N_2$ and it was heated up from room temperature to 900 °C with a temperature ramp of 20 °C/min and afterwards cooled down. The $N_2$ flow was correspondingly reduced as the temperature increased to ensure bubbling bed conditions and to avoid elutriation of particles. The particle size for South African coal char used was +100-200 μm and for bituminous Colombian coal it was +125-200 μm.

Table 2. Proximate and ultimate analysis and low heating value of solid fuels used.

| | Lignite | Fresh Bit. Colomb. | Pret. Bit. Colomb. | MV Bit. S.African | Anthracite | Petcoke |
|---|---|---|---|---|---|---|
| Moisture,%wt. | 12.5 | 6.2 | 2.3 | 4.2 | 1 | 8 |
| Volatile matter,%wt. | 28.7 | 33.4 | 33 | 25.5 | 7.6 | 9.9 |
| Fixed carbon,%wt. | 33.6 | 48.5 | 55.9 | 56 | 59.9 | 81.6 |
| Ash,%wt. | 25.2 | 11.9 | 8.8 | 14.3 | 31.5 | 0.5 |
| LHV,kJ/kg | 16252 | 25878 | 21899 | 26434 | 21878 | 31750 |
| C,%wt. | 45.4 | 68 | 65.8 | 69.3 | 60.7 | 81.3 |
| H,%wt. | 2.5 | 4.2 | 3.3 | 4 | 2.2 | 2.9 |
| N,%wt. | 0.5 | 1.6 | 1.6 | 2 | 0.9 | 0.9 |
| S,%wt. | 5.2 | 0.6 | 0.6 | 1 | 1.3 | 6 |
| O,%wt. | 8.6 | 7.5 | 17.6 | 5.2 | 2.4 | 0.4 |

Table 3. Composition of the chars used in this work.

| | C(%wt.) | H(%wt.) | N(%wt.) | S(%wt.) | O(%wt.) | Ash(%wt.) |
|---|---|---|---|---|---|---|
| Pret. Bit.Colomb | 79.8 | 0.7 | 1.3 | 0.6 | 4.0 | 13.6 |
| South African | 75.2 | 0.9 | 1.6 | 0.7 | 2.3 | 19.3 |

## 2.3 Thermogravimetric analyzer

The oxidation and reduction reaction rates of the different samples analyzed during this thesis, as well as the kinetics of the reduction and oxidation reactions for the calcined and activated ilmenite were determined through thermogravimetric analysis in a CI Electronics thermobalance, see Figure 4.

TGA experiments allowed analyzing the reactivity of the oxygen-carriers under well-defined conditions, by means of measuring the weight variation versus time or temperature during reaction with gases. The reactor consists of two concentric quartz tubes (24 mm i.d. and 10 mm i.d.) placed in an oven. The sample-holder was a wire mesh platinum basket (14 mm diameter and 8 mm height) designed to reduce mass-transfer resistance around the solid sample. The temperature and sample weight were continuously collected and recorded in a computer. The reacting gas mixture (25 $L_N$/h) was measured and controlled by electronic mass flow controllers.

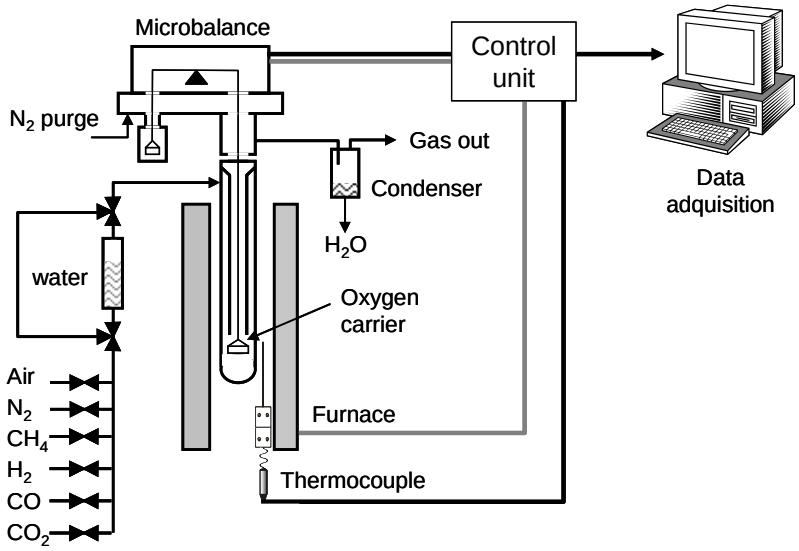


Figure 4. CI thermobalance layout.

For the measurement of the reaction rates, the ilmenite particles were loaded in a platinum wire basket. The sample weight used for the experiments was about 50 mg. The oxygen-carrier particles were heated up to the desired temperature in an air atmosphere. Once the set temperature was reached, the experiment started by exposing the oxygen-carrier to the

desired conditions for the reduction step. When a subsequent oxidation was made to measure the oxidation rate, in order to avoid the mixing of combustible gas and air, nitrogen was introduced for 2 min between the oxidizing and the reducing period. A mass value of 100% is assumed to be the sample in its most oxidized state and the mass loss is considered to be exclusively due to oxygen transfer.

In this thesis, the reactivity with the main reacting gases considered present in a CLC system, i.e. $CH_4$, CO and $H_2$ was analyzed for a wide variety of samples. If steam was used, before entering the reactor the reacting gases were directed through a water deposit which was heated at a set temperature so that the generated steam had the desired partial pressure.

*Data evaluation*

The conversion for the reduction, $X_r$, and the oxidation, $X_o$, reactions with time for consecutive cycles of ilmenite are calculated from the mass variations registered in TGA as:

$$X_r = \frac{m_o - m}{m_o - m_r} \tag{6}$$

$$X_o = 1 - X_r \tag{7}$$

The difference between the fully oxidized and reduced form of the oxygen-carrier defines its oxygen transport capacity, $R_{OC}$, which is the mass fraction of the oxygen-carrier that is used in the oxygen transfer:

$$R_{OC} = \frac{m_o - m_r}{m_o} \tag{8}$$

For the specific case of ilmenite as oxygen-carrier, the oxygen transport capacity of ilmenite is this thesis is designated as $R_{O,ilm}$. The mass based conversion of ilmenite, ω, indicates only the oxygen transfer and is independent of the oxygen transport capacity of the oxygen-carrier. It is expressed as:

$$\omega = \frac{m}{m_o} = 1 + R_{O,ilm}\left(X_o - 1\right) = 1 - R_{O,ilm}X_r \tag{9}$$

To facilitate a comparison of reactivity between different oxygen-carriers a rate index is often used as a normalized rate at a fuel gas concentration of 15% (Johansson et al., 2006b). The rate index, expressed in %/min is calculated as:

$$Rate\ index\ (\%) = 100 \cdot 60 \cdot \left(\left|\frac{d\omega}{dt}\right|\right)_{norm} = 100 \cdot 60 \cdot R_{O,ilm}\left(\frac{dX_i}{dt}\right)_{norm} \tag{10}$$

The normalized reactivity is calculated as:

$$\left(\frac{dX_i}{dt}\right)_{norm} = \frac{p_{ref}}{p_{TGA}}\left(\frac{dX_i}{dt}\right) \tag{11}$$

$P_{ref}$ is a reference partial pressure that has been used in previous studies and it is 0.15 atm for reduction and $p_{ref} = 0.10$ atm for oxidation (Johansson et al., 2006b). $p_{TGA}$ is the partial pressure of the fuel gas used in the TGA experiments.

## 2.4 Batch fluidized bed reactor for gaseous fuels

Several reduction-oxidation cycles with different reducing gases were performed in a batch fluidized-bed to investigate the gas product distribution and the variation of the chemical and physical properties of ilmenite particles with the number of cycles.

Figure 5 shows the experimental setup. It consists of a system for gas feeding, a fluidized-bed reactor (55 mm i.d.) made of Kanthal, two filters that recover the solids elutriated from the fluidized-bed working alternatively, and the gas analysis system. The whole fluidized-bed reactor is inside an electrically heated furnace. The gas feeding system allowed the feeding of the fuel gas (mixtures of $CH_4$, CO, $CO_2$, $H_2$, $H_2O$ and $N_2$) during the reducing

period and a mixture of air or $N_2$ for oxidation of ilmenite. $N_2$ was introduced between the two periods during 2 min to purge and avoid the contact between the gas fuel and air. For the supplying of the steam there is a liquid flow controller for water which is subsequently heated up and evaporated with a resistance heater and swept away by the rest of the reducing gas. Changes of gases during reduction, oxidation or purge were done by a three-way valve.

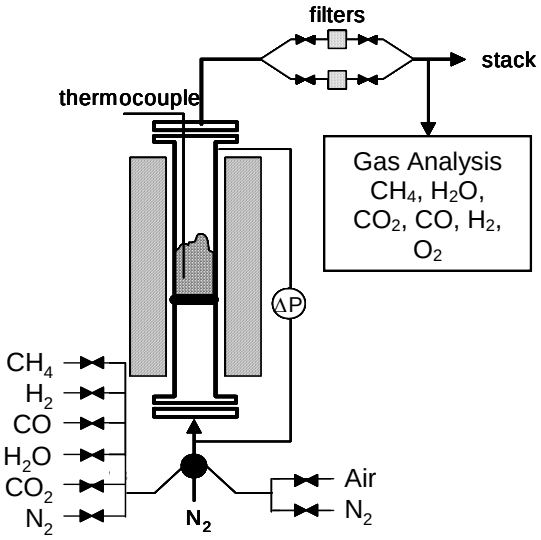


Figure 5. Experimental setup used for multicycle tests in a fluidized-bed reactor.

The differential pressure drop in the bed is measured by means of two pressure taps connected to the bottom and top of the reactor, and are used to detect possible agglomeration problems in the bed. The reaction progress is determined from gas analysis at the reactor outlet. The gas analysis system consists of several online gas analyzers. $CH_4$, CO and $CO_2$, dry basis concentrations are measured using non-dispersive infrared analysis (NDIR) and $H_2$ by thermal conductivity. $O_2$ concentration is determined using a paramagnetic analyzer. Water content is measured via Fourier Transform Infrared (FTIR Gasmet Cx-4000) analyzer. All data were collected by means of a data logger connected to a computer. The gas concentration was corrected considering the flow dispersion through the sampling line and the analyzers. Thus, the actual concentration of the gases at the bed exit was obtained by a deconvolution method similar to that found in Abad et al. (2006).

To measure the attrition rate, particles elutriated from the fluidized-bed reactor were retained in a filter, and were taken every 10 cycles.

*Data evaluation*

From the gas product distribution, it is possible to know the rate of oxygen transferred, $r_O(t)$, from ilmenite to the fuel gas in case of the reduction reaction, and from the oxygen in the air to ilmenite in case of the oxidation reaction, as a function of reaction time:

For $CH_4$, CO and $H_2$: $$r_O(t) = (y_{CO} + 2y_{CO_2} + y_{H_2O})_{out} \cdot F_{out} - (y_{H_2O} + 2y_{CO_2})_{in} \cdot F_{in} \quad (12)$$

For $O_2$: $$r_O(t) = 2 \cdot (y_{O_2})_{out} \cdot F_{out} - 2 \cdot (y_{O_2})_{in} \cdot F_{in} \quad (13)$$

where $F_{in}$ and $F_{out}$ are the molar flows of the respectively inlet and outlet gas streams and $y_i$ the molar fraction of the gas i.

The mass based conversion, ω, can be calculated as follows, where $\omega_{red}$ and $\omega_{ox}$ are the reduced and oxidized conversions reached in the previous period, correspondingly.

For reduction: $$\omega(t) = \omega_{ox} - \frac{M_O}{m_{ox}} \int_{t_{r,0}}^{t} r_0(t)dt \quad (14)$$

For oxidation: $$\omega(t) = \omega_{red} - \frac{M_O}{m_{ox}} \int_{t_{r,0}}^{t} r_0(t)dt \quad (15)$$

A normalized rate index was used to evaluate the reaction rates of all the gaseous fuels tested with ilmenite before and after the activation period, and also for comparison purposes. It is very similarly defined as for the TGA analysis section, and in this case the normalized rate was calculated from the experimental rate considering plug flow and that the reaction order is 1:

$$Rate\,index(\%/\min) = 60 \cdot 100 \left( \frac{d\omega}{dt} \right)_{norm} = 60 \cdot 100 \left( \frac{d\omega}{dt} \right)_{exp} \frac{P_{ref}}{P_m} \quad (16)$$

being $P_m$ the mean partial pressure of the gaseous fuel in the reactor, which is calculated with the coefficient of expansion of the gas mixture $\varepsilon_g$, and the partial pressures of the gaseous fuel at the reactor inlet and outlet.

$$P_m = \frac{(P_{in} - P_{out}) \Big/ (P_{in} + \varepsilon_g \cdot P_{out})}{\frac{(P_{out} - P_{in}) \cdot \varepsilon_g}{(P_{in} + \varepsilon_g \cdot P_{out})} + (1 + \varepsilon_g) \ln\left(\frac{P_{in} + \varepsilon_g \cdot P_{out}}{(1 + \varepsilon_g) P_{out}}\right)} \tag{17}$$

For comparison purposes among different experiments, the oxygen yield parameter is proposed, which gives the idea to what extend the fuel has been oxidized at each instant of the reducing period. The oxygen yield, $\gamma_O$, is defined as the oxygen gained in the fuel for its oxidation divided by the oxygen needed to fully oxidize the fuel, as follows:

$$\gamma_O(t) = \frac{r_O(t)}{(4y_{CH_4} + y_{CO} + y_{H_2})_{in} \cdot F_{in}} \tag{18}$$

## 2.5 Batch reactor fluidized bed for solid fuels

The experimental work has been carried out in a setup consisting of a system for gas feeding, a solid fuel feeding system, a fluidized-bed (FB) reactor and the gas analysis system. A schematic layout of the laboratory setup is presented in Figure 6. The fluidized-bed reactor (55 mm i.d. and 700 mm height) is electrically heated by a furnace, and had a preheating zone just under the distributor plate. The temperature inside the bed was measured and used to control the reaction temperature. The reactor had pressure taps in order to measure the absolute pressure in the bed and pressure drop. Possible agglomeration and defluidization problems could be detected by a sharp decrease in the bed pressure drop during operation. The pressure tap was also useful to detect possible blocking in the downstream pipes due to elutriated particles or tar condensation in cold points.

The reactor was loaded with 400 g of ilmenite with a particle size of +150-300 μm. In some tests silica sand (200-400 μm) was used instead of ilmenite. The feeding of the solid fuel was done by means of a fuel chute which ends 3 cm above the distributor plate and about 5-6 cm below the upper level of the fluidizing particles, so that char particles are fed inside the fluidized bed. The upper part of the chute has a valve system that creates a reservoir in which the fuel is placed and later pressurized by nitrogen to ensure quick char feeding.

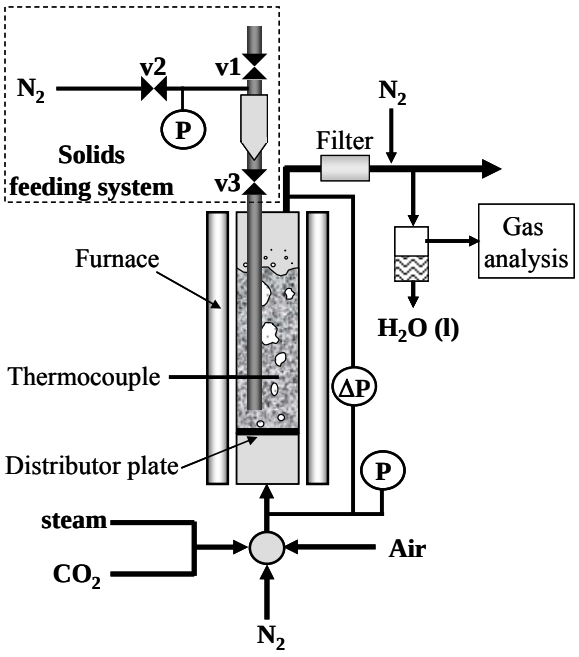


Figure 6. Schematic layout of the laboratory setup.

The gas feeding system had different mass flow controllers connected to an automatic three-way valve. This way it was possible to feed alternatively air, $N_2$ or a mixture of steam/$CO_2$. Steam was obtained by evaporation with a resistance heater of a known water flow supplied by a peristaltic pump. Different gas analyzers continuously measured the gas composition at the reactor exit after water condensation. As in most of cases gas is mainly composed by steam, a downstream $N_2$ flow of 90 $L_N$/h is introduced to ensure a continuous dry gas flow feeding the analyzers. This $N_2$ is also used to calculate the outlet gas flow by a balance to $N_2$.

*Data evaluation*

The evolution of char conversion, $X_{char}$, with time is calculated by integrating the rate of char conversion, $r_C(t)$, which is obtained from a mass balance to carbon in gaseous form in the reactor.

$$X_{char}(t) = \frac{1}{N_{C,char}} \int_0^t r_C(t)dt \tag{19}$$

$$r_C(t) = (y_{CO_2} + y_{CO})F_{out} - F_{CO_2,in} \tag{20}$$

$N_{C,char}$ being the mol number of carbon fed into the reactor. The instantaneous rate of conversion of the char, $r_{C,inst}$, is calculated as the rate of gasification per amount of non-gasified carbon that is still in the reactor.

$$r_{C,inst}(t) = \frac{r_C(t)}{N_{C,char} - \int_0^t r_C(t)dt} \tag{21}$$

The conversion of ilmenite in the fluidized bed for reduction reaction, $X_r$, can be calculated from the integration of $r_O(t)$ with time:

$$X_r(t) = \frac{1}{N_{O,ilm}} \int_0^t r_O(t)dt \tag{22}$$

$r_O(t)$ is the rate of oxygen transferred from ilmenite to the fuel gas, and is calculated by means of the oxygen balance:

$$r_O(t) = \left[ F_{out}(2y_{CO_2} + y_{CO}) - 2F_{CO_2,in} \right] + \left[ F_{H_2O,out} - F_{H_2O,in} \right] \tag{23}$$

$N_{0,ilm}$ is the molar amount of oxygen in ilmenite active for CLC process, calculated as:

$$N_{O,ilm} = \frac{m_o R_{O,ilm}}{M_O} \quad (24)$$

The conversion of gasification products, i.e. CO and $H_2$, to $CO_2$ and $H_2O$ by reaction with ilmenite particles was evaluated by the combustion efficiency, $\eta_c$. It is defined as the oxygen gained by the fuel for its oxidation divided per the oxygen needed to fully oxidize the fuel. Here, $\eta_c$ is calculated with Eq. (25).

$$\eta_c(t) = \frac{r_O(t)}{2r_C(t)} \quad (25)$$

## 2.6 Continuous ICB-CSIC-s1 unit for solid fuels

A schematic view of the continuous ICB-CSIC-s1 facility for solid fuels used in this thesis is shown in Figure 7. The CLC system was basically composed of two interconnected fluidized-bed reactors, the fuel-reactor (FR) (1) and the air-reactor (AR) (3) joined by a loop seal (2), a riser (4) for solids transport from the air- to the fuel-reactor, a cyclone to recover the entrained solids (5) and a solids valve (7) to control the flow rate of solids fed to the fuel-reactor.

The fuel-reactor consisted of a bubbling fluidized bed with 5 cm of inner diameter and 20 cm bed height. Coal (8) is fed by a screw feeder at the bottom of the bed above the fuel-reactor distributor plate in order to maximize the time that volatile matter is in contact with the bed material. The screw feeder (9) has two steps: the first one with variable speed to control the coal flow rate, and the second one has high rotating velocity to avoid coal pyrolysis inside the screw. A small $N_2$ flow of 18 $L_N$/h is fed at the beginning of the screw to avoid possible volatile reverse flow or entrance of steam. The coal flow was varied from 33 to 100 g/h. The thermal power reached in the unit was between 200 and 580 $W_{th}$ in the experiments done in this PhD. The fuel-reactor was fluidized by steam-$CO_2$ mixtures, which act also as a gasifying agent. In the fuel-reactor a gasification agent flow range from 110 to 190 $L_N$/h was introduced (corresponding to gas velocities of 0.07-0.12 m/s at 900

°C). In the fuel-reactor the oxygen-carrier is reduced by the volatile matter and gasification products of coal. Reduced oxygen-carrier particles overflowed into the air-reactor through a U-shaped fluidized bed loop seal with an inner diameter of 5 cm, to avoid gas mixing between fuel and air. It was fluidized with 75 $L_N$/h $N_2$. Since this prototype has no carbon separation system, unconverted char from the fuel-reactor goes to the air-reactor and is fully burnt there, releasing the $CO_2$ that is measured in the air-reactor.

The oxidation of the carrier took place in the air-reactor, consisting of a bubbling fluidized bed with 8 cm of inner diameter and 10 cm bed height that uses air as fluidizing gas. In this reactor air was used to oxidize the oxygen-carrier coming from the fuel-reactor. The gas flows introduced in the air-reactor were 2100 $L_N$/h as primary air and 400 $L_N$/h as secondary air at the top of the bubbling bed to help particle entrainment into the riser and later to the cyclone. That corresponded to gas velocity in the air-reactor of 0.1 m/s and a total gas velocity in the riser of 4.2 m/s at 900 °C. $N_2$ and unreacted $O_2$ leaving the cyclone passed through a filter before the stack. The oxidized solid particles were recovered by the cyclone and sent to a solids reservoir, setting the oxygen-carrier ready to start a new cycle. These particles act as a loop seal avoiding the leakage of gas between the fuel-reactor and riser. The regenerated oxygen-carrier particles returned to the fuel-reactor by gravity from the solids reservoir through a solids valve which controlled the flow rates of solids entering the fuel-reactor. A diverting solids valve located below the cyclone allowed the measurement of the solids flow rates at any time. The circulation flow rate was varied and controlled from 1.0 to 11.6 kg/h. The total ilmenite bed mass in the system was 3.5 kg and the solids bed mass in the fuel-reactor was 0.8 kg ilmenite, as the solids level in the fuel-reactor is fixed and the exceeding overflows and is directed to the air-reactor.

Because of its small size, the system is not auto-thermal and is heated up with various ovens to get independent temperature control of the air-reactor, fuel-reactor, and fuel-reactor freeboard. The temperature in the air-reactor was maintained at around 940 °C and the fuel-reactor temperature was varied from 820 °C to 950 °C. The fuel-reactor freeboard is kept constant at about 900 °C in all the experiments. The pressure drops in important locations of the system, such as the fuel-reactor bed, the air-reactor bed and the loop seal were monitored.

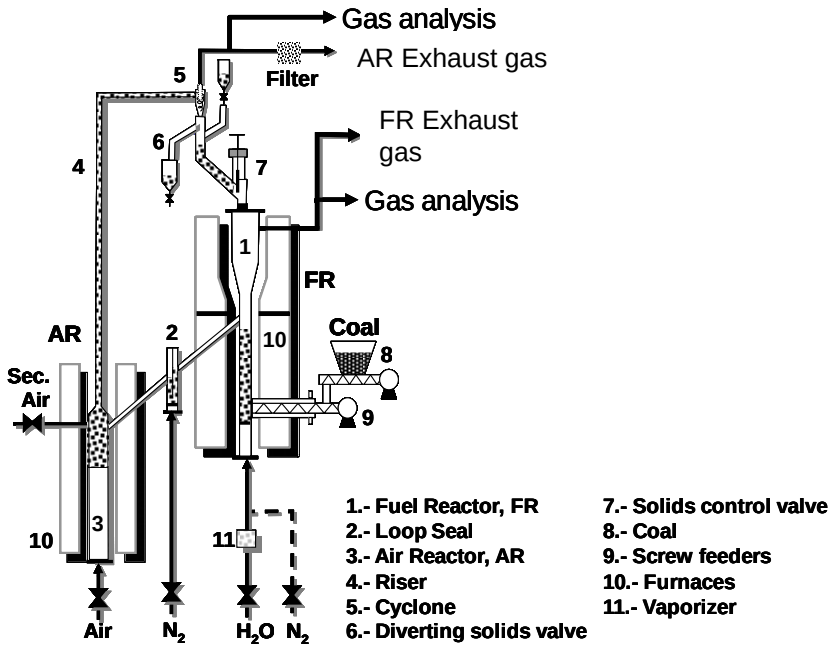


Figure 7. Schematic diagram of the coal-fuelled CLC facility.

CO, $CO_2$, $H_2$, $CH_4$, and $O_2$ were continuously analyzed in the exit streams from the fuel- and air-reactors. All data were collected by means of a data logger connected to a computer. In some selected experiments the tar amount present in fuel-reactor product gases was determined following a tar protocol (Simell et al., 2000). Collection of moisture and tar was performed in a series of eight impinger bottles by absorption in isopropanol and later cooling in external baths. Two different cooling baths were used. The first was an ice bath, where the first two impingers were located. The first was empty and the second contains isopropanol. In addition, the second bath contains six impingers at -18 °C. These impingers recover the majority of moisture and aromatic tar compounds (styrene, indene, benzene, etc.) and light Polycyclic aromatic hydrocarbons (PAHs). Several gaseous samples from the fuel-reactor stream were also taken in bags in order to measure the components through gas chromatography analysis.

*Data evaluation*

The parameters that indicate the performance of the process are the carbon capture and the combustion efficiency. The carbon capture is the removal of carbon dioxide that would

otherwise be emitted into the atmosphere. Getting high carbon capture during energy generation is the motivation of this technology. The carbon capture efficiency, $\eta_{CC}$, is here defined as the fraction of the carbon fed in that is converted to gas in the fuel-reactor.

$$\eta_{CC} = \frac{[F_{CO2,FR} + F_{CO,FR} + F_{CH4,FR}]_{out} - [F_{CO2,FR}]_{in}}{[F_{CO2,FR} + F_{CO,FR} + F_{CH4,FR}]_{out} + F_{CO2,AR} - [F_{CO2,FR}]_{in}} \quad (26)$$

The carbon captured in the system is the carbon contained in the volatiles plus the carbon in the char that is gasified. Thus, the carbon capture efficiency depends on the fraction of char that has been gasified.

The carbon measured in the gases coming from the fuel-reactor and the air-reactor is less than the carbon present in the introduced coal because there is elutriation of char during some experiments. The elutriated char flow was calculated as the difference between the coal carbon fed and the measured carbon in the fuel-reactor and air-reactor outlet gas flows. The effective char was calculated as the fed char that had not been elutriated from the fuel-reactor, and it was used as the char fed to the fuel-reactor in the calculations. Note that in case of an industrial unit the possible elutriated char will be collected in a cyclone and reintroduced to the fuel-reactor.

To do a deeper study of the system behavior on the carbon capture, the gasification step should be assessed. The char conversion, $X_{char}$, is defined as the fraction of carbon in the char which is gasified and released to the fuel-reactor outgoing gas stream:

$$X_{char} = \frac{F_{C,char\ eff} - F_{CO2,AR}}{F_{C,char\ eff}} = \frac{[F_{CO2,FR} + F_{CO,FR} + F_{CH4,FR} - F_{C,vol}]_{out} - [F_{CO2,FR}]_{in}}{[F_{CO2,FR} + F_{CO,FR} + F_{CH4,FR} + F_{CO2,AR} - F_{C,vol}]_{out} - [F_{CO2,FR}]_{in}} \quad (27)$$

$F_{C,char\ eff}$ is the carbon in the effective char flow introduced in the CLC system. The gasified char in the fuel-reactor was calculated as difference of the carbon in gases in the fuel-reactor outgoing flow, and the carbon flow coming from the volatile matter. The carbon content of the volatiles is directly calculated using the analysis of coal.

An approximation to the char gasification rates can be obtained, if a simplified model is used. The fuel-reactor is considered to follow a continuous stirred-tank reactor (CSTR) model. The char is assumed to be in perfect mixing of the solids in the fuel-reactor and to react at a mean rate ($-r_C$) which is proportional to the mass. With these considerations, ($-r_C$) is calculated from a carbon balance in the fuel-reactor:

$$(-r_C) = \frac{1}{m_{char}} \frac{dm_{char}}{dt} = k \quad \Rightarrow \quad (-r_C) = \frac{X_{char} \cdot F_{C,char\,eff}}{m_{char,FR}} \tag{28}$$

being $m_{char,FR}$ the mass of carbon in char in the fuel-reactor, which can be calculated with the mass of ilmenite in the fuel-reactor $m_{ilm,FR}$, the solids circulation rate $F_{ilm}$:

$$\frac{m_{char,FR}}{m_{ilm,FR}} = \frac{F_{CO2,AR}}{F_{ilm}} \tag{29}$$

Connected to the char conversion, the mean residence time of char, $t_{m,char}$, is calculated as:

$$t_{m,char} = \frac{m_{char,FR}}{F_{C,char\,eff}} = \frac{X_{char}}{(-r_C)} \tag{30}$$

Besides, the mean residence time of ilmenite, $t_{m,ilm}$, is calculated by Eq. (31).

$$t_{m,ilm} = \frac{m_{ilm,FR}}{F_{ilm}} \tag{31}$$

The fuel-reactor combustion efficiency, $\eta_{comb\ FR}$, is a measure of the gas conversion in the fuel-reactor and represents the extent of oxidation of volatiles and gasification products by the oxygen-carrier. It is defined as the fraction of the oxygen demanded by the volatile matter and gasification products that is supplied by the oxygen-carrier in the fuel-reactor. It is therefore dependent on the reaction rate of ilmenite with the gaseous fuels and on the amount of gases generated in the fuel-reactor from coal. The oxygen supplied by ilmenite in the fuel-reactor is calculated through the oxygen containing species in the fuel-reactor

product gas. The sum of volatile matter and gasified char is calculated as the effective coal introduced minus the char flowing towards the air-reactor. $\eta_{comb\ FR}$ was calculated as:

$$\eta_{comb\ FR} = \frac{[0.5 \cdot F_{H2O,FR} + F_{CO2,FR} + 0.5 \cdot F_{CO,FR}]_{out} - [0.5 \cdot F_{H2O,FR} + F_{CO2,FR} + 0.5 \cdot O_{coal,eff}]_{in}}{O_{2\ demand\ coal,eff} - F_{CO2,AR}} \quad (32)$$

$O_{coal,eff}$ is the oxygen contained in the effective coal flow. $O_{2\ demand\ coal,eff}$ or the oxygen demand of the effective coal flow is the oxygen flow needed to fully burn the fuel.

An oxygen demand $\Omega_{OD}$ can be defined as the fraction of oxygen lacking to achieve full combustion to $CO_2$ and $H_2O$ of the fuel-reactor product gas in comparison to the oxygen demand of the devolatilization and gasification products. It is the only fraction of oxygen required in the iG-CLC process to reach full combustion of the fuel that must be supplied in a subsequent polishing step as pure $O_2$. However in this thesis $\eta_{comb\ FR}$ is usually used because it is conceptually a simpler parameter.

$$\Omega_{OD} = 1 - \eta_{comb\ FR} \quad (33)$$

The rate of oxygen transferred by ilmenite, $(-r_O)$, measures the oxygen transfer rate from ilmenite to the fuel. $(-r_O)$ is calculated as the increased flow of oxygen in the oxygen-containing gases (CO, $CO_2$ and $H_2O$), divided by the ilmenite hold-up:

$$(-r_O) = \frac{([F_{H2O,FR} + 2F_{CO2,FR} + F_{CO,FR}]_{out} - [F_{H2O,FR} + 2F_{CO2,FR} + O_{coal,eff}]_{in}) \cdot M_O}{m_{ilm,FR}} \quad (34)$$

The oxygen-carrier to fuel ratio, $\phi$, is a measure of how much oxygen is available in the circulating oxygen-carrier compared to the oxygen needed to burn the fuel fed. In stoichiometric conditions the ratio $\phi$ is equal to one. It is defined as follows:

$$\phi = \frac{F_{ilm} \cdot R_{O,ilm}}{2 \cdot M_O \cdot O_{2\ demand\ coal,eff}} \quad (35)$$

## 2.7 Continuous 10 $kW_{th}$ CLC unit for solid fuels

The 10 $kW_{th}$ unit used is designed for CLC with solid fuels and located at Chalmers University of Technology. Figure 8 shows a scheme of the whole pilot unit. The reactor system consists of two interconnected fluidized beds: (a) the fuel-reactor (FR), where the fuel is gasified with steam and gasification products are oxidized by the oxygen-carrier, and (b) the air-reactor (AR), where the oxygen-carrier particles are oxidized. The regenerated oxidized particles are led through (c) a riser above the air-reactor, which ends up in (d) a cyclone that brings the solids flow back to the fuel-reactor. There are also two loop-seals fluidized by nitrogen placed after the cyclone (d) and in the connection leading from fuel- to air-reactor. The role of these upper and lower loop-seals is to eliminate gas leakages between the reactors. Represented in Figure 8 are also the particle filters, as well as the fuel feeding, steam production unit and a water seal used to collect condensates and to balance the pressure in the fuel-reactor. The system is not self-supporting in energy and it is therefore enclosed in an oven that keeps and controls the temperature.

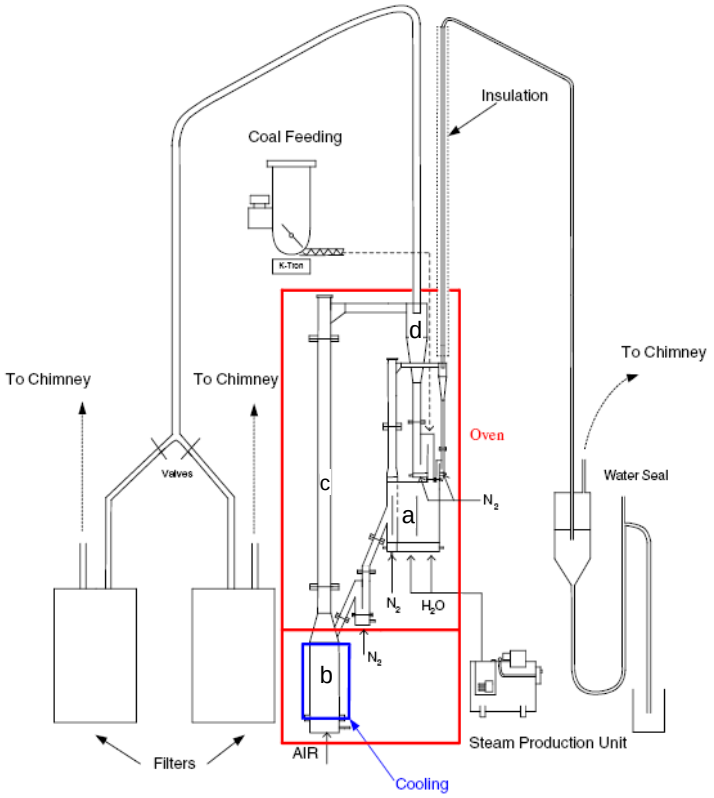


Figure 8. Pilot unit system: a. Fuel-reactor, b. Air-reactor, c. Riser, and d. Cyclone.

The fuel-reactor has three main sections: (1) a low-velocity section, which is operated as a bubbling bed. This chamber is divided into two parts separated by a wall with an opening at the bottom, through which the particles are conducted; (2) a carbon-stripper with the purpose to separate char particles from the solids flow going from the fuel-reactor to the air-reactor; and (3) a high velocity section that gives the opportunity to increase the flow in the internal loop by increasing the entrainment of the oxygen-carrier from the fuel-reactor. This option was however not used in the tests enclosed in this thesis. The low-velocity section is fluidized with steam and in this bed all reactions related to char are expected to take place, that is, fuel gasification and reaction of the gasification products with the oxygen-carrier.

The fuel is fed by a vertical fuel chute that ends above the reactor bed. Thereby, most of the volatiles are released above the bed and have little contact with the oxygen-carrier. Thus, this unit is useful to know the behavior towards char gasification with different solid fuels, but does not give information about the conversion of volatile matter. A detailed description of the 10 kW pilot is given elsewhere (Berguerand and Lyngfelt, 2008a; b). The solids inventory in the low-velocity section was around 6 kg and the total ilmenite hold-up in the unit was 15 kg of ilmenite with bulk density of about 2100 kg/m$^3$ and particle size of +90-250 μm. To assess the effect of limestone in the process, 4 kg of a Mexican limestone used in the Tamuin Power Unit were added. Its density was about 1900 kg/m$^3$ and the particle size +90-200 μm.

The pilot is equipped with 40 pressure transducers to monitor the pressures. The temperatures in the air-reactor, fuel-reactor and the air-reactor cyclone are also measured. Gas sampling outlets are located on both chimneys. At the air-reactor outlet concentrations of CO, $CO_2$, and $O_2$ are measured online and at the fuel-reactor outlet concentrations of CO, $CO_2$, $O_2$ and $CH_4$ are measured online with Sick Maihak Sidor analyzers and registered. The $H_2$ concentration could also be measured online with a Rosemount NGA2000 analyzer. Bag samples of the product gas flow from the fuel-reactor were also taken and analyzed with a gas chromatograph Varian Micro-GC CP4900; this was used to confirm the results from the other analyzers.

The flows for the fuel-reactor and the loops seals were kept constant during all experiments and are shown in The fluidizing gas flows are controlled and monitored by mass flow controllers. The steam flow to the low-velocity section is controlled by a steam generator. FLOVEL is the steam flow in the low-velocity section in the fuel-reactor, FCS is the N2 flow in the carbon-stripper, FHIVEL is the N2 flow in the high-velocity section in the fuel-reactor, FHILS is the N2 flow in the higher loop-seal, FLOLS is the N2 flow in the lower loop-seal and FFRLS is the N2 flow in the small fuel-reactor loop-seal.

Table 4. The fluidizing gas flows are controlled and monitored by mass flow controllers. The steam flow to the low-velocity section is controlled by a steam generator. $F_{LOVEL}$ is the steam flow in the low-velocity section in the fuel-reactor, $F_{CS}$ is the $N_2$ flow in the carbon-stripper, $F_{HIVEL}$ is the $N_2$ flow in the high-velocity section in the fuel-reactor, $F_{HILS}$ is the $N_2$ flow in the higher loop-seal, $F_{LOLS}$ is the $N_2$ flow in the lower loop-seal and $F_{FRLS}$ is the $N_2$ flow in the small fuel-reactor loop-seal.

Table 4. Flows for the fuel-reactor and the loop-seals, in $L_N$/min.

| $F_{LOVEL}(H_2O)$ | $F_{CS}(N_2)$ | $F_{HIVEL}(N_2)$ | $F_{HILS}(N_2)$ | $F_{LOLS}(N_2)$ | $F_{FRLS}(N_2)$ |
|---|---|---|---|---|---|
| 21 | 6 | 2 | 4 | 4 | 2 |

The data evaluation in this facility is the same as for the ICB-CSIC-s1 unit.

# 3 Results and discussion

## 3.1 Properties of ilmenite as oxygen-carrier

The aim of this section (studies published in Papers I and III) is to analyze the main characteristics of ilmenite as oxygen-carrier in CLC and the changes in its properties through redox cycles under well-defined conditions. Before this thesis started, there was little work done about ilmenite in its use in CLC. Leion et al. (2008a,b) proved the feasibility of using ilmenite as oxygen-carrier to oxidize gaseous fuels. They saw that the reaction rate of ilmenite increases after several redox cycles, but this activation process was not analyzed. They also observed that ilmenite is more reactive with CO and $H_2$ than with $CH_4$, but this study was done in batch fluidized bed and not in TGA, where the reactivity can be analyzed under well-defined conditions and without diffusional limitations. To assess the properties of ilmenite as oxygen-carrier, experiments consisting of reduction-oxidation cycles in a thermogravimetric analyzer (TGA) and in batch fluidized bed were carried out using the main products of coal devolatilization and gasification, that is, $CH_4$, $H_2$ and CO, as reducing gases. The reaction rates of ilmenite with these fuels were assessed, as well as the change on reactivity after hundred of redox cycles. Tests with different $H_2$:CO ratios were also made in order to see the reciprocal influence of both reducing gases in the reaction rate. The oxidation of ilmenite was also studied.

Both fresh and previously calcined at 950 °C ilmenite were used as initial oxygen-carriers in TGA but only calcined ilmenite was used as initial material for the experiments in the batch reactor. The properties of fresh, calcined and samples of ilmenite after different number of redox cycles and using different reacting gases were determined. The structural changes of ilmenite, as well as the variations in its behavior with a high number of cycles were also evaluated with a 100 cycle test in batch reactor. The attrition rates and fluidization performance of ilmenite in fluidized bed operation was also assessed.

In its use in iG-CLC, the components of ilmenite that can be used for the oxygen transfer are, considering the components in their oxidized form, $Fe_2TiO_5$ and $Fe_2O_3$. Table 5 shows the maximum oxygen yields at equilibrium conditions for every step in the reduction reaction. Thermodynamic calculations show that by reducing $Fe_2TiO_5$ with $CH_4$, $H_2$ or CO it is possible to reach very near full combustion of fuel gas into $H_2O$ and $CO_2$ when it

is reduced $FeTiO_3$, i.e. $\gamma_O$ can be considered 1 for practical purposes. Further reduction is prevented in a CLC system to avoid low fuel gas conversion. Besides, there is risk of agglomeration in the FeO or Fe oxidation (Cho et al.,2006).

Table 5. Oxygen yields at equilibrium conditions for different reducing gases in presence of $Fe_2TiO_5$ and $Fe_2O_3$ at 900°C.

| | | Oxygen yield ($\gamma_O$); | | |
|---|---|---|---|---|
| Oxidized | Reduced | $CH_4$ | CO | $H_2$ |
| $Fe_2TiO_5$ | $FeO{\cdot}TiO_2$ | 0.998 | 0.997 | 0.998 |
| $FeO{\cdot}TiO_2$ | $Fe+TiO_2$ | 0.308 | 0.085 | 0.067 |
| $Fe_2O_3$ | $Fe_3O_4$ | 1 | 1 | 1 |
| $Fe_3O_4$ | $Fe_{0.947}O$ | 0.741 | 0.615 | 0.675 |
| $Fe_{0.947}O$ | Fe | 0.523 | 0.325 | 0.385 |

Thus, both components that carry out the oxygen transfer would react with $H_2$ as an example of reduction reaction according to reactions (36-37) and the subsequent oxidation as for the reactions (38-39).

$$Fe_2TiO_5 + TiO_2 + H_2 \leftrightarrow 2\,FeTiO_3 + H_2O \quad (36)$$

$$3\,Fe_2O_3 + H_2 \leftrightarrow 2\,Fe_3O_4 + H_2O \quad (37)$$

$$4\,FeTiO_3 + O_2 \leftrightarrow 2\,Fe_2TiO_5 + 2\,TiO_2 \quad (38)$$

$$4\,Fe_3O_4 + O_2 \leftrightarrow 6\,Fe_2O_3 \quad (39)$$

### 3.1.1 Ilmenite reactivity: Activation

*Activation with $CH_4$, CO and $H_2$ in TGA*

The investigation of the conditions in which the activation process of ilmenite occurs, how fast and whether the improved reaction rate is maintained after many redox cycles was carried out. Several reduction-oxidation cycles were carried out in TGA to analyze the reactivity of fresh and calcined ilmenite. Reducing and oxidizing times for each cycle were

set to 30 minutes. The reducing agents used were 15% $CH_4$+20% $H_2O$, 15% $H_2$+20% $H_2O$ or 15% CO+20% $CO_2$. In these conditions all the $Fe^{3+}$ of ilmenite was reduced to $Fe^{2+}$, that is, the main final species were $FeTiO_3$ and FeO. Figure 9 shows the mass variations undergone by fresh ilmenite in this TGA experiment using $CH_4$ as reducing gas and subsequent oxidation with air. At the beginning, ilmenite was not completely reduced or oxidized after the fixed reacting time. However, there is an increase in both the reduction and oxidation extension during the repeated redox cycles. The mass loss is considered to be exclusively due to oxygen transfer and stabilized after 4 cycles.

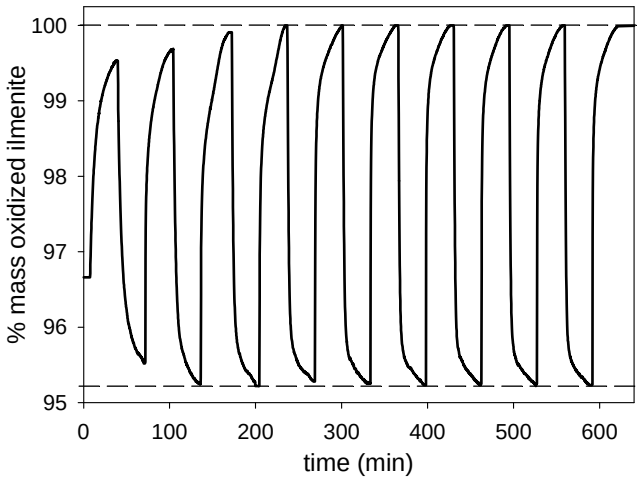


Figure 9. Mass variations during redox cycles in TGA starting from fresh ilmenite. Reduction and oxidation time: 30 min. Reducing gas: 15%$CH_4$+20%$H_2O$. T=900°C.

In this study a normalized conversion is used to analyze the changes in ilmenite reactivity. It is calculated considering that normalized conversion is 1 when the $Fe^{3+}$ present in ilmenite was reduced to $Fe^{2+}$. In this condition, the mass loss due to the oxygen transferred is 4.8%, as it can be seen in Figure 9. Figure 10 show the normalized conversion for the reduction, $X_{N,r}$, and the oxidation, $X_{N,o}$, reactions with time for consecutive cycles of fresh ilmenite. The reducing gas was 15% $CH_4$+20% $H_2O$ and the oxidations were done in air.

Although ilmenite presents initially a rather low reactivity, the oxygen-carrier has a gradual gain in its reduction reaction rate as well as in oxidation rate. The reactivity increases up to a maximum value after 4 cycles and stabilizes. This increase is more pronounced in the reduction reaction than in the oxidation reaction, because the initial

reactivity for the oxidation of ilmenite for the first oxidation step is relatively high, with $X_{N,o}$=0.25 in less than 9 seconds for fresh ilmenite. After 4 cycles carried out in TGA a value for the normalized conversion of 0.8 is reached in 120 s for reduction and 180 s for oxidation reaction. At this point, it can be considered that ilmenite had achieved maximum conversion rate in both reduction and oxidation reactions. Therefore, an activation process was observed which made the reactivity increase during the initial redox cycles. Also, it can be seen that the oxidation rate decreases gradually at high conversion values ($X_{N,o}$>0.8), and full conversion is reached in 30 min. This fact indicates that a change in the resistance control has happened or the oxidation reaction proceeds via two consecutive steps.

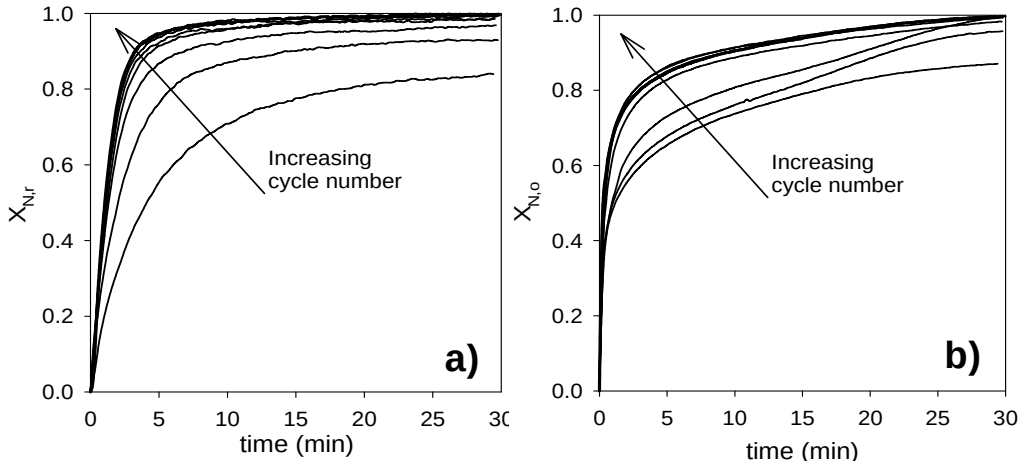


Figure 10. Normalized conversion during a) reduction and b) oxidation periods in TGA of fresh ilmenite vs. time through several cycles. Reducing gas:15%$CH_4$+20%$H_2O$. T=900°C.

Similar behavior was observed for redox cycles using $H_2$ and CO as reducing gases. The main consequence of ilmenite being more reactive with the number of cycles in the activation period is that fewer inventories of oxygen-carrier in the reactors are necessary.

*Effect of pre-oxidation on activation*

Samples of fresh and calcined ilmenite were subjected to alternating reduction-oxidation cycles using $CH_4$, $H_2$ or CO as reducing gases in TGA. Hundred cycles were performed and the reducing and oxidizing periods were one minute. Both fresh and calcined ilmenite achieve the same conversion variation after activation, but calcined ilmenite reached earlier

the activated state. When using $CH_4$ as reducing gas, 40 cycles were necessary for the activation and stabilization for fresh ilmenite, whereas about 30 cycles were enough to activate calcined ilmenite. Therefore, a previous calcination has a positive effect on both the reactivity of the oxygen-carrier and the activation rate during the activation period. Similar behavior was found when the activation was carried out using 15 vol.% $H_2$ or 15 vol.% CO as reducing gases, but in these cases calcined ilmenite activated in 9 cycles with $H_2$ and in 20 cycles with CO.

*Activation with $CH_4$, CO, $H_2$ and syngas in fluidized bed*

The activation of ilmenite was also analyzed in batch fluidized bed with the main gases involved in the process, because the reactions occur in conditions similar to the real process. The effect of the activation process of ilmenite, through consecutives redox cycles on the gas product distribution, was analyzed in a fluidized-bed reactor. $CH_4$, $H_2$ or CO were used as reducing gases. The total solids hold-up in the reactor was 500 g of calcined ilmenite. The oxygen-carrier was exposed to alternating reducing and oxidizing conditions at a temperature of 900 °C. The reducing conditions of the experiments performed are shown in Table 6. All reducing gaseous flows have the same oxygen demand. Thus, the resulting gas velocity for tests with $CH_4$ was 0.15 m/s and for all other tests it was 0.3 m/s.

Table 6. Experimental conditions during reduction period in the batch fluidized-bed reactor for experiments 1 to 4. $N_2$ to balance. T=900 °C.

| Exp. | Composition (vol.%) | | | | | $H_2$:CO | Reducing time (s) | Number of cycles | Solids inventory ($kg/MW_{th}$) |
|---|---|---|---|---|---|---|---|---|---|
| | $CH_4$ | $H_2$ | CO | $H_2O$ | $CO_2$ | | | | |
| 1 | 25 | - | - | 10 | - | - | 300 | 23 | 670 |
| 2 | - | - | 50 | - | 20 | 0:100 | 240 | 20 | 480 |
| 3 | - | 50 | - | 20 | - | 100:0 | 180 | 20 | 560 |
| 4 | - | 21.5 | 28.5 | 8 | 8.2 | 43:57 | 240 | 100 | 250 |

Figure 11 shows the $CO_2$ concentration in dry basis or $H_2O$ concentration during consecutive reduction periods when using $CH_4$, CO and $H_2$ as reducing gases. The

corresponding maximum $CO_2$ or $H_2O$ fractions if full combustion was reached are also represented. For every tested reducing gas, there was an increase in the percentage of $CO_2$ and/or $H_2O$ in the product gas with the cycles because ilmenite had a gradual gain in its reaction rate. After several redox cycles, ilmenite reactivity stabilized and the $CO_2$ and/or $H_2O$ concentrations achieved the highest values. Thus, an activation process is seen during the initial redox cycles.

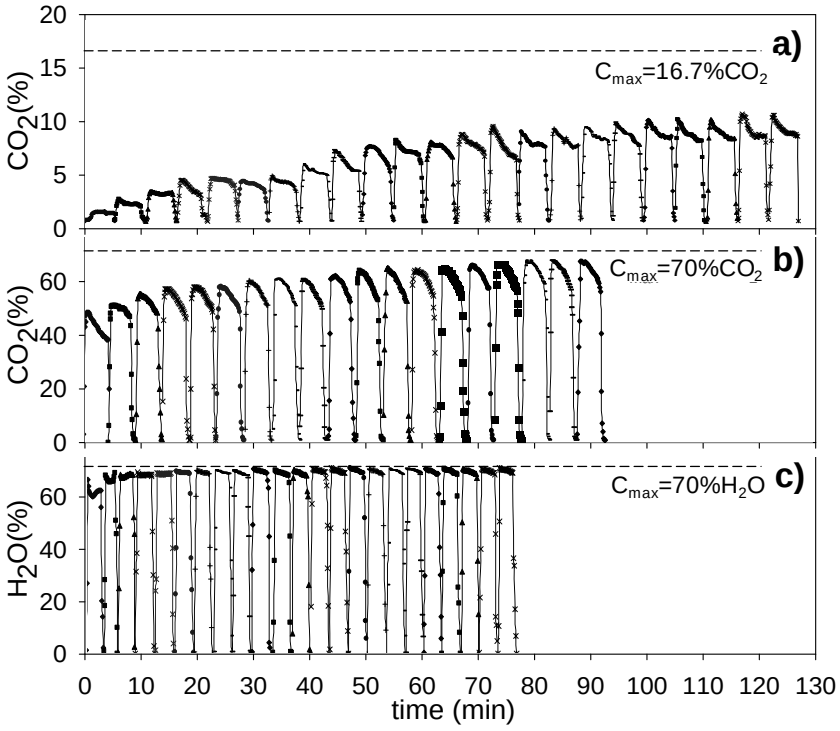


Figure 11. $CO_2$ or $H_2O$ fractions in the product gas (wet basis) during consecutive reduction periods in batch FB, for a) $CH_4$, b) CO and c) $H_2$ as reducing gases. The intervals between reducing periods are removed. $C_{max}$: maximum $CO_2$ or $H_2O$ fraction if full combustion was reached. Experimental conditions in Table 6. T=900ºC.

Reaction with $H_2$ is faster than with CO, and near full $H_2$ conversion was obtained in the fluidized-bed reactor. Lower reactivity was found for $CH_4$, being $CH_4$ the most unconverted gas. In this case, negligible amounts of $H_2$ or CO were observed during $CH_4$ combustion. Ilmenite activation process depended on the gas used as fuel, i.e., $CH_4$, $H_2$ or CO. Thus, when using $CH_4$ it activated after about 20 cycles, for CO after about 10 cycles and it was faster for $H_2$, as it took 3-4 cycles. The more reactive is the fuel gas, the lower is the number of cycles to activate ilmenite particles.

A long test in fluidized bed was done: 100 redox cycles with syngas as reducing gas was performed (see conditions in Table 6). The syngas composition is in Water-Gas Shift equilibrium. Very little $H_2$ in the outlet gas was seen at the beginning of the reducing cycles: about 1-2%. The CO content was about 2.4%. Figure 12 shows the variation of the oxygen yield, $\gamma_O$, with the solids conversion for various reducing periods from the 100 redox cycles. The oxygen yield is a parameter that gives the idea to what extent the fuel has been oxidized at each instant of the reducing period. $\gamma_O = 1$ corresponds to complete conversion of fuel gas to $CO_2$ and $H_2O$. When focusing only in the first 1.5 minutes of each reducing period, it can be seen that the oxygen yield increases within the first 10 cycles approximately and reach a maximum value of 98%, which is due to the activation of ilmenite. This maximum value is kept throughout the cycles, which indicates that ilmenite maintains its reaction rate and does not deactivate. This corresponded to a $\omega$ about 0.99.

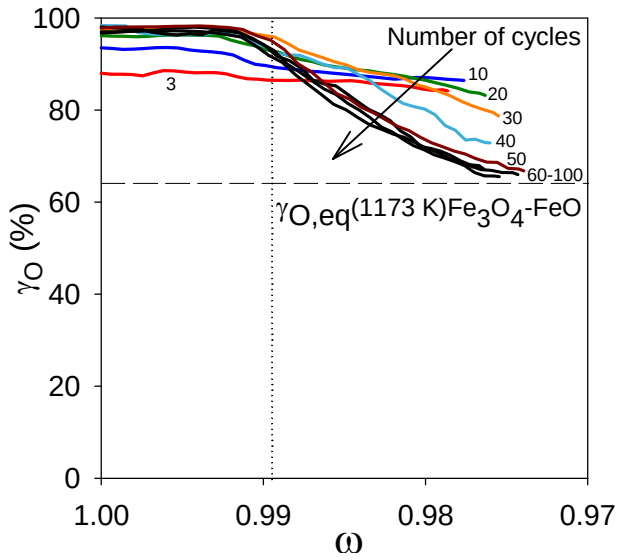


Figure 12. Oxygen yield variation vs. ilmenite mass based conversion for several reduction periods in a 100 redox cycle test in batch FB with syngas as reducing agent. T = 900°C.

On the other hand, after about 1.5 minutes and mass based conversions $\omega$ further than 0.99, there was a decrease in the oxygen yield from the cycle 20. In Figure 12 it can be seen that the $\gamma_O$ reached after many cycles was close to the corresponding $\gamma_O$ for the $Fe_3O_4 \leftrightarrow FeO$ equilibrium. This means that the oxygen transport capacity decreased with

the number of cycles, because reduction of $Fe_3O_4$ to FeO is not suitable in a CLC system in order to get complete combustion to $CO_2$ and $H_2O$.

*Activation of ilmenite with coal char*

Since this process is really applied to solid fuels, the activation process of ilmenite was also studied using solid fuels in batch fluidized bed. 16 consecutive redox cycles in batch fluidized bed were carried out using calcined ilmenite as starting material. Steam was used as fluidizing gas. Every reduction period consisted of two consecutive loads of 1.5 g of char. The second load in the same period was fed to get further reduction of the oxygen-carrier. After the reduction period, the bed material was oxidized by air. As in experiments with gaseous fuels (TGA and batch fluidized bed) an activation process was also seen using char as fuel. Effectively, there was a decrease in the unconverted gasification product CO (see Figure 13), which was similar for $H_2$, with the number of cycles accompanied by an increase in the production of $CO_2$. After several redox cycles no further substantial decrease on CO or $H_2$ concentration or increase on $CO_2$ concentration were observed and the $CO_2$ concentration achieved the highest value. This proved that ilmenite undergoes an activation process in its reactivity using char as fuel during the initial 6 or 7 cycles.

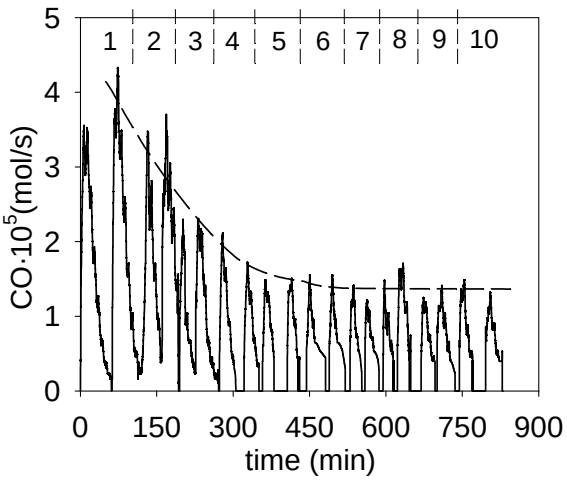


Figure 13. Molar flow evolution with time of CO in the gas product during the initial 10 reduction cycles. Every cycle consisted of 2 loads of char, 1.5 g each one, in batch FB. The intervals between reducing periods are removed. Gasification agent: steam. T = 900 °C.

*Activation for oxidation*

The activation in the oxidation reaction was also studied in the 100 cycle test performed in fluidized bed and using a syngas mixture as reducing agent (21.5% $H_2$+28.5% CO+8% $H_2O$+8.2% $CO_2$), with reducing periods of 4 minutes. After every reducing period, the ilmenite bed was fully re-oxidized with diluted air (10% $O_2$) in the oxidation period with a gas velocity of 0.23 m/s. At the beginning of the oxidation period no oxygen could be seen in the produced gas, since it reacted with the reduced ilmenite. After this period, the breakthrough curve of oxygen appeared. This curve is different depending on the reactivity of the bed material (Adánez et al., 2005). For higher number of cycles this second step of reaction appeared later and at higher oxidizing conversions (see Figure 14.a)) until roughly equal breakthrough curve is obtained, this being the activation period. This behavior was also in line with TGA results. For a mass based conversion of 0.975 in the previous reduction periods, the activation in the oxidation reaction took about 8 cycles. The oxidation reaction was fast and fully oxidized ilmenite was reached in every cycle. Oxidation seems to happen in two steps. From Figure 14.b) it could be seen that if the area under the $O_2$ curve was integrated, the oxygen amount taken by ilmenite with the number of cycles was slight but gradually decreasing. That is because in the previous reducing period ilmenite was less reduced, as the oxygen transfer capacity was gradually decreasing.

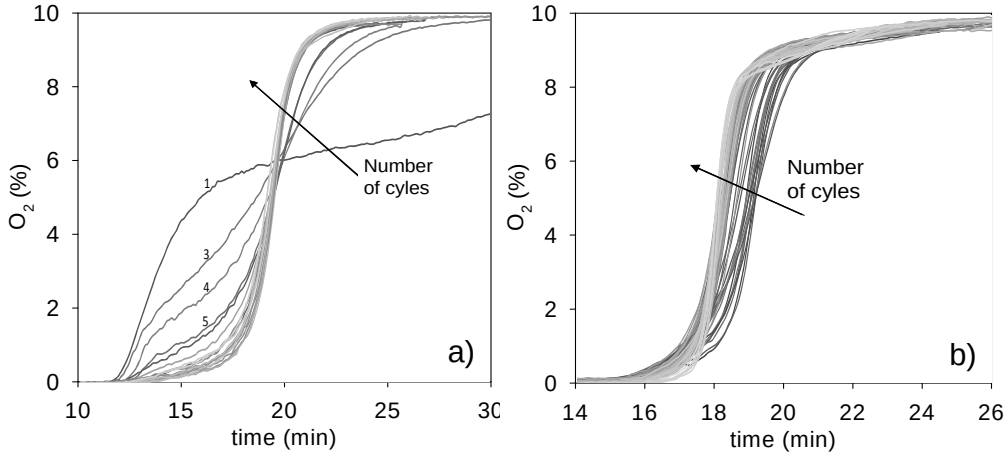


Figure 14. $O_2$ profiles in the product gas for a) the first 20 oxidation periods and b) subsequent oxidations in batch FB from cycle 20 to cycle 100. Previous reductions with syngas up to conversion $\omega \sim 0.975$. Oxidations with 10% $O_2$. T = 900 °C.

### 3.1.2 Characterization of ilmenite

Table 1 shows the main physical and chemical properties of the fresh, calcined and activated Norwegian ilmenite used as oxygen-carrier in the experiments of this research.

The major change with respect to the initial ilmenite was that porosity increased substantially with the redox cycles. For the 100 cycle test using syngas as reducing agent in batch fluidized bed, the initial porosity of calcined ilmenite was 1.2%, after 20 cycles it was 27.5% and after 100 cycles it reached the value of 38%. The pore distribution shown in Figure 15 confirms that the minimum pore size is about 30 nm, but as porosity increases, the pore size distribution locates at higher pore diameters and the average pore diameter gradually increases with the number of cycles and higher size pores are formed.

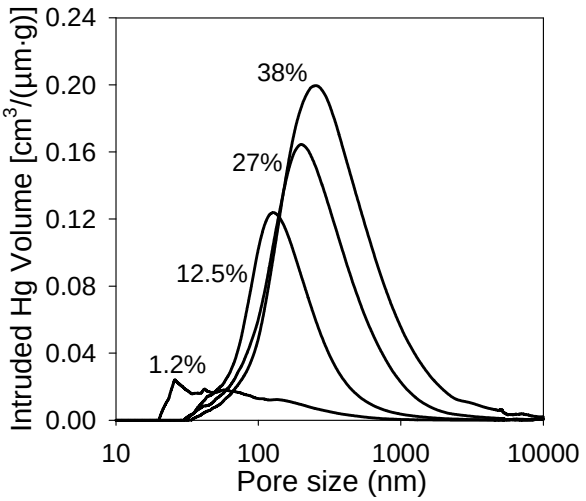


Figure 15. Pore distribution of different samples of ilmenite samples taken after several redox cycles in Batch FB using syngas as fuel (conditions in Table 6): Calcined, after 8 cycles, after 18 cycles and after 100 cycles.

Figure 16 shows SEM microphotographs of the general overview and external surface of several particles that confirm the low pore development for fresh and calcined ilmenite and the gain of granular shape on the surface and porosity after several redox cycles.

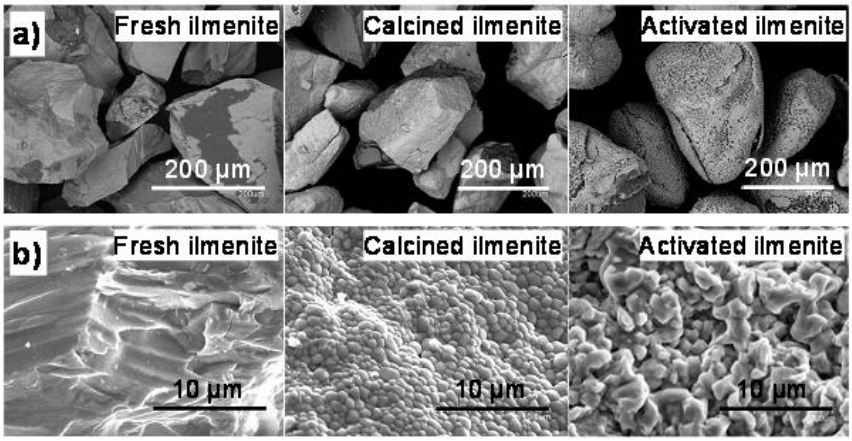


Figure 16. SEM images of a) a general overview of several particles, b) the external surface of particles of fresh, calcined ilmenite and ilmenite after undergoing several redox cycles.

Figure 17 shows the evolution of porosity by SEM photographs of cross-cut particles of different samples taken from the 100 cycle experiment done using syngas as reducing agent in batch fluidized bed. Throughout the reduction-oxidation cycles, there is a continuous appearance of porosity, since the final porosity after 100 redox cycles was measured to be 38%. Moreover, a gradual generation of an external layer slightly separated from the rest of the particle which grows with the number of cycles could be clearly observed. This space between the layer and the core also enhances the porosity measured for the particle.

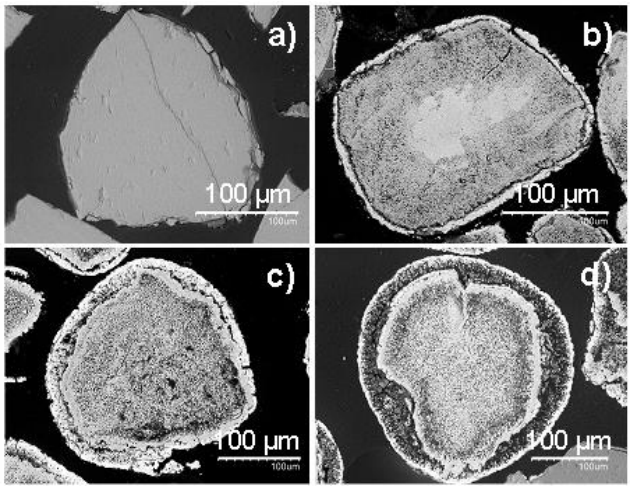


Figure 17. SEM-EDX images of cross-cut ilmenite particles a) calcined and after b) 16, c) 50 and d) 100 redox cycles, using syngas as reducing agent in batch FB.

EDX analyses were done to determine Fe and Ti distributions throughout the particles, see Figure 18. In fresh and calcined ilmenite distributions of both elements were uniform,

which agrees with the XRD analysis that reveals $Fe_2TiO_5$ as main component. For activated ilmenite the particle core is titanium enriched, whereas the external part is iron enriched. XRD analyses to the external part found that this region is composed only by iron oxide, whereas XRD to the internal core revealed the existence of $TiO_2$ and $Fe_2TiO_5$. Thus, the external shell formed during activation period was Fe enriched, likely due to a physical segregation of $Fe_2TiO_5$ and subsequent migration phenomenon of $Fe_2O_3$ towards the external part of the particle, where there is no $TiO_2$ to form iron titanates. The diffusion of iron –or titanium, depending on the conditions- within the ilmenite particles was already reported by Rao and Prototypeaud (1975). However, this iron migration or layer formation did not appear in other ilmenite samples that were activated in a different way, for example in case of the samples activated in batch fluidized bed using char as fuel, or even in case of ilmenite that was used for about 100 hours of operation using coal as fuel (see Figure 19). This is because in those tests the reduction degree of ilmenite was low, compared to the higher conversion reached in the experiments done using syngas as fuel.

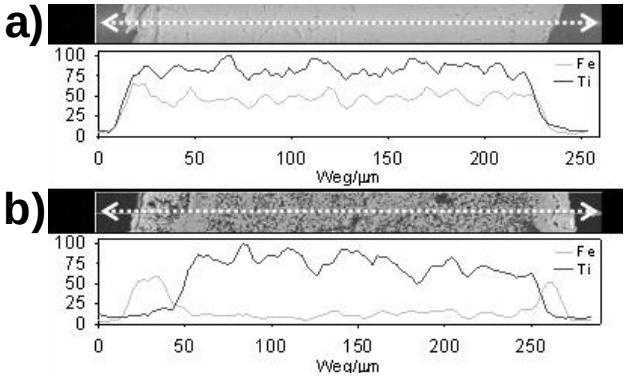


Figure 18. EDX line profiles of Fe and Ti in a) calcined and b) activated ilmenite particle.

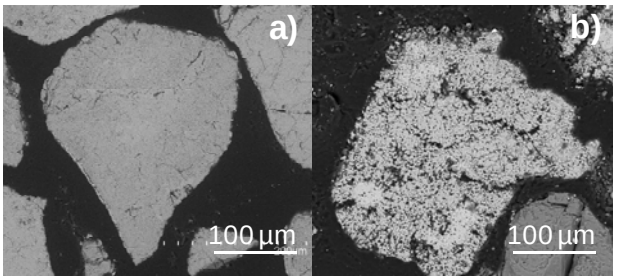


Figure 19. SEM-EDX images of cross-cut ilmenite particles a) activated ilmenite in batch FB using char as fuel after 16 cycles, b) activated ilmenite used for about 100 hours of operation using coal as fuel in the 10 $kW_{th}$ CLC facility.

To evaluate the fraction of Fe as $Fe_2TiO_5$ or $Fe_2O_3$ as a function of the number of redox cycles, particles subjected to different numbers of redox cycles (up to 100 cycles) in TGA with 15 vol.% $H_2$, CO or $CH_4$ as fuel gas during the reduction period were analyzed by XRD. Figure 20 shows the semi-quantitative mass fractions of $Fe_2TiO_5$ and $Fe_2O_3$ in the oxidized ilmenite particles as a function of the number of cycles when $H_2$ was used as reducing gas. It can be seen that the $Fe_2TiO_5$ fraction decreases with the number of cycles whereas the $Fe_2O_3$ fraction increases.

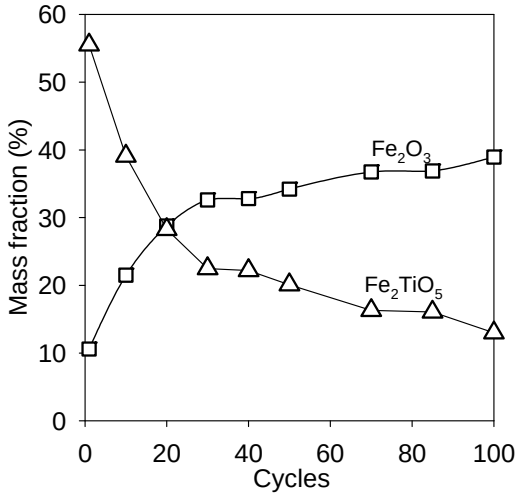


Figure 20. Mass fraction of $Fe_2O_3$ and $Fe_2TiO_5$ in ilmenite after several redox cycles in TGA up to 100 cycles. Oxidation and reduction periods: 1 min. Reducing gas used: 15% $H_2$ + 20% $H_2O$. T=900 °C.

Initial and activated ilmenite particles after 20 cycles in batch fluidized bed using syngas as fuel had relatively high values of crushing strength; because it varied from 2.2 N to 2.9 N. The values of crushing strength obtained are similar to other Fe-based oxygen-carriers and they are acceptable for the use of these particles in circulating fluidized bed (Johansson et al., 2006b). However, particles after 50 and 100 cycles in fluidized bed show a decrease in the crushing strength down to a value of 1 N after 100 cycles (see Figure 21).

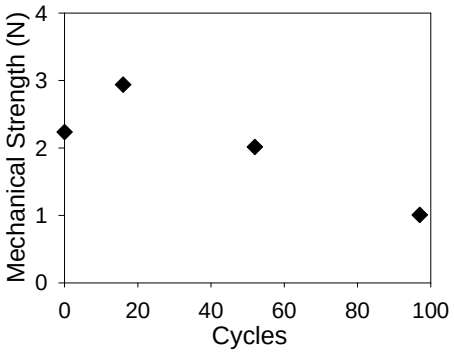


Figure 21. Mechanical strength evolution with the number of cycles. T = 900 ºC.

1 N is considered to be the minimum value for the use of a material in interconnected fluidized-beds (Johansson et al., 2004). Nevertheless, since in these particles there was formation of an external layer, the normal strength under which the particles are subjected could break this layer and not the whole particles.

**Variation of the oxygen transport capacity, $R_{O,ilm}$**

The oxygen transport capacity is a fundamental property of the oxygen-carrier since it determines the recirculation rate and solids inventory in the system, and therewith the suitability of ilmenite as oxygen-carrier in CLC. The oxygen transport capacity is the oxygen fraction of the total oxygen-carrier mass that can be used in the oxygen transfer (Eq. 8). However, free $Fe_2O_3$ is only capable to fully convert CO and $H_2$ into $CO_2$ and $H_2O$ when it is reduced to $Fe_3O_4$. On the other hand, $Fe_2TiO_5$ can be reduced to $FeTiO_3$.

Therefore, $R_{O,ilm}$ depends on the relative abundance of free $Fe_2O_3$ and iron titanates, which varies with the number of redox cycles. As the number of cycles increases, the fraction of free $Fe_2O_3$ rises at expenses of $Fe_2TiO_5$. With these percentages the $R_{O,ilm}$ can be calculated:

$$R_{o,ilm} = R_{o,Fe_2O_3} \cdot f_{Fe_2O_3} + R_{o,Fe_2TiO_5} \cdot f_{Fe_2TiO_5} \quad (40)$$

$R_{o,Fe_2O_3}$ is the oxygen transport capacity of $Fe_2O_3$ when converted to $Fe_3O_4$ ($R_{o,Fe_2O_3} = 3.3\%$) and $R_{o,Fe_2TiO_5}$ is the oxygen transport capacity of $Fe_2TiO_5$ when converted to $FeTiO_3$ ($R_{o,Fe_2TiO_5} = 6.7\%$). $f_{Fe_2O_3}$ and $f_{Fe_2TiO_5}$ are the $Fe_2O_3$ and $Fe_2TiO_5$ mass fractions, respectively

The initial $R_{O,ilm}$ value for calcined ilmenite was 4.0 %wt. However, the fraction of free $Fe_2O_3$ increases with the number of cycles due to the mentioned $Fe_2TiO_5$ segregation. As a consequence, the oxygen transport capacity decreases because free $Fe_2O_3$ reduction to $Fe_3O_4$ transfers less oxygen than its reduction to $Fe^{2+}$. This decrease of $R_{O,ilm}$ was starker for the first cycles and after several cycles the decrease was slight and continuous. After 100 redox cycles in TGA with $H_2$ as reducing gas $R_{O,ilm}$ had decreased down to 2.1 %wt.

The values of $R_{O,ilm}$ were also measured by TGA when reducing the samples with 5%$H_2$ + 40%$H_2O$ to ensure that the final reduced species are $FeTiO_3$ + $Fe_3O_4$. Figure 22 shows the $R_{O,ilm}$ value obtained for samples extracted from experiments in batch fluidized bed, as well as the values calculated from the measured fraction of $Fe_2TiO_5$ and $Fe_2O_3$ in the solids (in Figure 20). The results indicate a similar variation of oxygen transport capacity during cycles in TGA or batch fluidized bed. The disadvantage of having a decrease in $R_{O,ilm}$ is that higher solid circulating flows between reactors are needed.

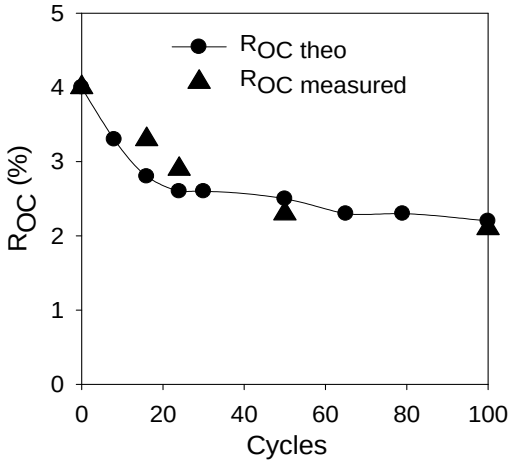


Figure 22. Measured in TGA and theoretical $R_{OC}$. $R_{OC}$ variation with the number of cycles reduction periods in a 100 redox cycle test using syngas as reducing agent (see conditions in Table 6). T=900 ºC.

From all the experiments performed in TGA and batch fluidized bed, the decrease in the oxygen transport capacity was not influenced by the reducing agent used. For the different gases used, if the reduction degree of ilmenite in every cycle was the same, the final $R_{O,ilm}$ had the same value. It depended only on the extent of conversion reached in every cycle.

Higher conversions led to a greater extent of segregation of $Fe_2TiO_5$ to $Fe_2O_3 + TiO_2$ and therefore stronger decrease in $R_{O,ilm}$. This correlation between $R_{O,ilm}$ and the extent of conversion can be seen in Figure 23, which shows the decrease in the oxygen transport capacity after around 20 cycles in the experiments in batch fluidized bed with the different gaseous fuels tested, i.e., $CH_4$, CO, $H_2$ and the $CO + H_2$ mixture, as a function of the ilmenite conversion reached in every reducing cycle. Figure 23 also includes the $R_{O,ilm}$ of ilmenite particles after 35 h of continuous operation in a CLC unit fuelled with coal. The oxygen transport capacity decreased only to 3.9% and the reduction conversion in the continuous tests was about 0.23. The same occurred with the ilmenite sample that was used in the 10 $kW_{th}$ prototype: it had been used for about 100 hours of operation, where $R_{O,ilm}$ was also measured to be 3.9%. Thus, working with low values of ΔX allows to maintain the initial $R_{O,ilm}$ roughly constant during long time.

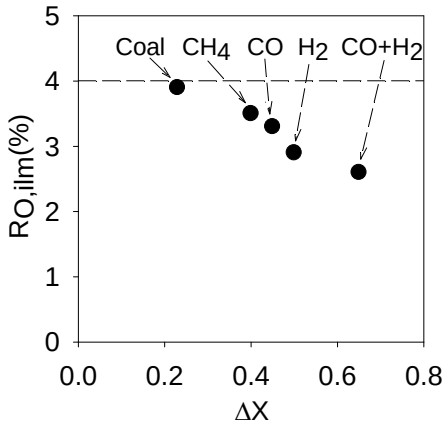


Figure 23. Decrease in the oxygen transport capacity after 20 cycles as a function of the ilmenite conversion reached in every reducing cycle in the experiments in batch fluidized bed using $CH_4$, CO, $H_2$ and syngas as fuel and in continuous test with coal as fuel.

### 3.1.3 Analysis of the reactivity

The reactivity of calcined and activated ilmenite was investigated using $H_2$, CO or $CH_4$ as reducing gas, in TGA as well as in batch fluidized bed. Figure 24 represents the conversion curves obtained in TGA during reductions using $H_2$, CO and $CH_4$ as reducing agents and during oxidations with air for a) calcined and b) activated ilmenite. It demonstrates that for the different reducing gases, calcined and activated ilmenite react faster with $H_2$ than with

CO and $CH_4$. After the activation, for $H_2$ and CO the reactivity increased around 5 times, while for $CH_4$ this increase was about 15 times.

To analyze the reactivity of the oxidation reaction, it was necessary to reduce the sample first until the particles were composed of $Fe_3O_4$ and $FeTiO_3$, so simulating the behavior expected in a CLC system. Tests carried out by TGA showed that the oxidation rate was the same independently of the gas previously used for the reduction. The reactivity of the oxidation reaction is higher than the reactivity for the reduction with $H_2$, CO, and $CH_4$, except for the oxidation of calcined ilmenite for solid conversions higher than $\approx 0.25$. After this value, the reaction rate sharply decreased for calcined ilmenite. Nevertheless, complete oxidation of calcined particles was reached after a long enough oxidizing period.

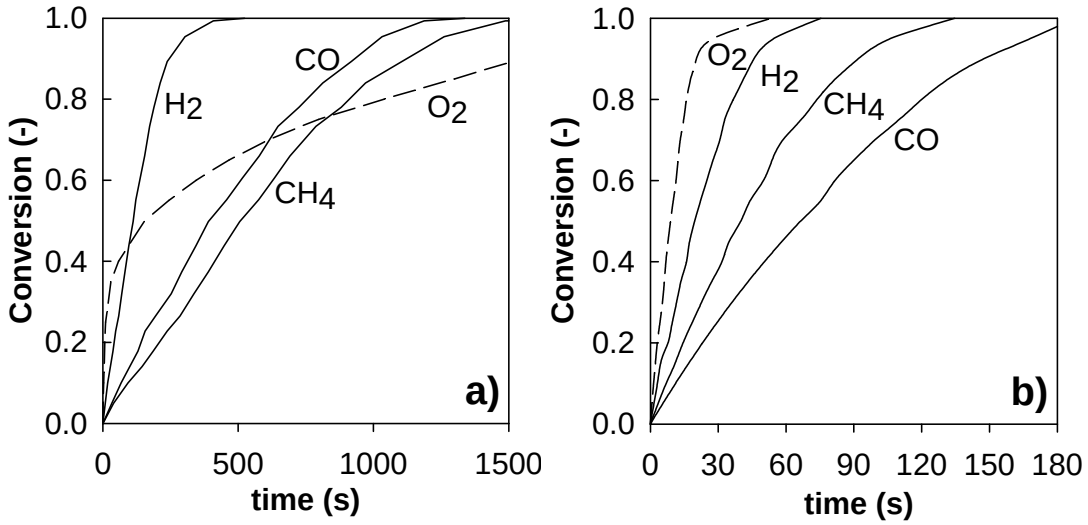


Figure 24. Conversion vs. time curves obtained in TGA during reduction period using $H_2$, CO or $CH_4$ as reducing agent (continuous lines). Oxidation by air is showed for the reduced ilmenite (dotted lines): a) calcined and b) activated ilmenite. Reducing gas mixtures: 15% $H_2$ + 20% $H_2O$ or 15% CO + 20% $CO_2$ or 15% $CH_4$ + 20% $H_2O$. T = 900 °C.

In order to assess whether ilmenite has adequate values of reactivity and oxygen transport capacity for its use in the CLC technology, the rate index is calculated for $H_2$, CO, $CH_4$ and $O_2$. The rate index (see Eq.10) can be used to compare ilmenite with other oxygen-carriers that have been proposed for CLC. Figure 25 shows the rate index obtained in TGA for every reacting gas as a function of the number of cycles. The rate index increased

during the activation period and eventually reached a maximum and stable value that was kept constant during the cycles. The maximum value of the rate index was around 5.1%/min for $H_2$, 1.6%/min for CO, 3.1%/min for $CH_4$ and 8.1%/min for $O_2$. Other iron-based oxygen-carriers previously tested by Johansson et al. (2006b) had normalized rate index values with $CH_4$ within the range of 0.4 to 4%/min. This fact agrees with the results showed by Leion et al. (2008a), where it was concluded that ilmenite reacts just as well as a synthetic $Fe_2O_3/MgAl_2O_4$ oxygen-carrier. Nevertheless, it is necessary to remark that ilmenite is a natural mineral and a considerably cheaper material than a synthetic material and it has adequate values of reactivity and oxygen transport capacity for its use in the CLC technology with solid fuels.

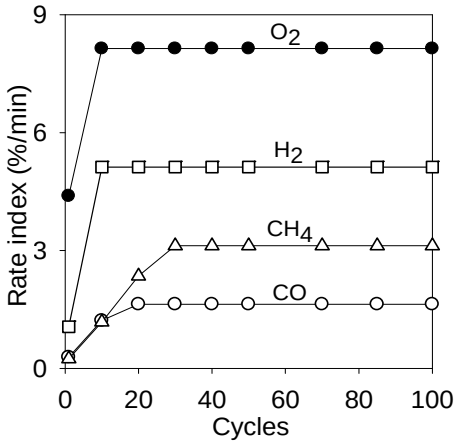


Figure 25. Variation of the rate index with the number of redox cycles in TGA. Oxidation and reduction periods: 1 min. Reacting gases: 15% $H_2$, 15% CO, 15% $CH_4$ and 10% $O_2$.

The reduction reactivity of ilmenite in fluidized bed was also assessed. Figure 26 plots the normalized rate index as a function of the mass based conversion in the reduction reaction for calcined and activated ilmenite for the gases tested and shows that the reaction rate of ilmenite increased after activation. In case of $CH_4$ the increase in the reaction rate is greater than with the other gaseous fuels, as the rate index raised here in batch fluidized-bed 5 times after activation. The increase in the rate index for CO and for $H_2$ was lower and it was about 2 times. The resulting rate index calculated from these experiments (Eq. 16) were lower compared to the values obtained in TGA because in fluidized bed there is resistance to mass transfer between the bubble and the emulsion that makes the effective concentration lower to the concentration of the gas main flow.

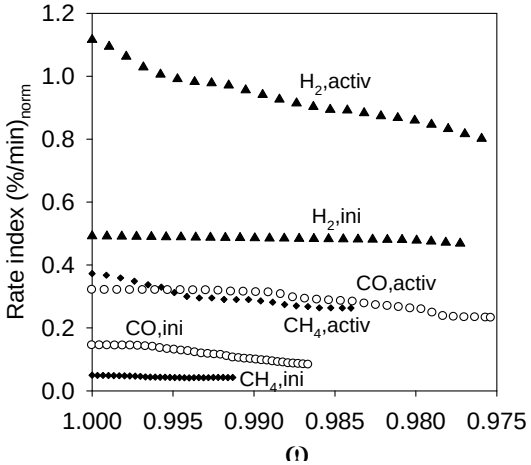


Figure 26. Normalized rate index as a function of the ilmenite mass based conversion, ω, for the reduction reactions with $CH_4$, CO and $H_2$ with calcined and activated ilmenite in batch FB. $P_{ref}$=0.15. T=900 ºC.

*Reactivity with syngas*

Additional redox cycles with different $H_2$:CO ratios in fluidized bed were also done with the same activated ilmenite after the 100 cycles with syngas. The reducing periods lasted 240 seconds and the gas velocity of the reducing flow was 0.3 m/s. The solids inventory in these tests was 250 kg/$MW_{th}$. Figure 27 plots the average rate index as a function of the fraction of $H_2$ in the reducing agent. It can be seen that the reaction rate was higher for the experiments carried out with $H_2$ and the lower values were obtained when using only CO. The dotted line is a theoretical rate index calculated as sum of the rate index of $H_2$ and CO multiplied per their corresponding fractions. It can be seen that the resulting reaction rates for all syngas mixtures tested matches with the theoretical line. Therefore, the reaction rate for a syngas mixture can be actually calculated as the sum of both reducing agents reaction rates. As it has been observed with other Fe oxygen-carriers (Abad et al., 2007a). In addition, no significant displacement of the Water-Gas Shift (WGS) equilibrium towards CO or $H_2$ formation can be deduced. If WGS reaction was relevant, more $H_2$ could be produced by reaction of CO with $H_2O$ in excess. As $H_2$ is more reactive than CO, the WGS would cause an increase in the rate index compared to the theoretical rate calculated as the sum of the rates with $H_2$ and CO.

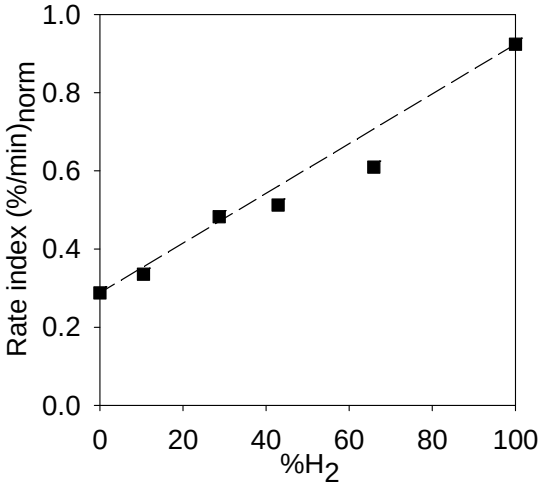


Figure 27. Average normalized rate index as function of the fraction of $H_2$ in the reducing gas for different $H_2$:CO mixtures. T = 900 °C.

In this study, ilmenite was seen to undergo an activation process. The achieved maximum reaction rate is maintained throughout the cycles for all gaseous fuels tested. The activation is faster if ilmenite is pre-oxidized. Besides, it is also quicker if the conversion degree reached in the reducing periods of the redox cycles is higher.

### 3.1.4 Carbon formation and fluidizing behavior

*Carbon formation*

The deposition of carbon from carbon containing gases is a concern because it can deactivate the oxygen-carrier. It can also cause defluidization problems. Besides, if carbon is formed, it can be further directed to the air-reactor where it will be burnt, being therewith the carbon capture efficiency decreased. The conditions for which carbon formation is thermodynamically possible in the CLC process depend on the amount of oxygen added with the oxygen-carrier as well as the temperature and pressure. Nevertheless, there was no CO or $CO_2$ observed any time during inert or oxidation periods when using carbon-containing fuel gases, i.e. $CH_4$ and CO, indicating that there was not accumulation of carbon during reduction periods.

*Particle integrity and attrition*

The attrition rate of the carriers is an important parameter to be accounted as a criterion for using a specific oxygen-carrier in a fluidized-bed reactor. High attrition rates will decrease the lifetime of the particles increasing the reposition of the oxygen-carrier in the CLC system. 100 redox cycles were done in 56 hours of operation in fluidizing conditions. Figure 28 shows the attrition rate as a function of fluidization time. The loss of fines was considered as the recovered particles with a diameter under 40 $\mu$m. The initial value of attrition at the beginning is due to the rounding off of angular initial ilmenite particles. With the number of cycles, an external layer was formed, and that this layer is mainly composed by iron oxides. After 40 hours of operation the attrition rate stabilized to a low value: 0.076%/hour. Furthermore, XRD analysis of fines showed that they are formed only by iron oxide. This fact suggests that fines are produced by an attrition process in the particle surface, and not by the fragmentation of particles. There is particle rounding and detachment of part of the external layer, but no particle fragmentation. The resulting average lifetime of the particles was 1310 hours. This is an acceptable value. Furthermore, ilmenite particles are expected to be lost together with coal ash removal in this technology, so the continuous feeding of new oxygen-carrier will be also determined by this loss.

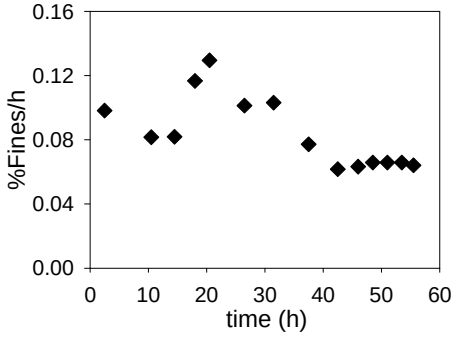


Figure 28. Fine attrition rate in batch FB as a function of fluidization time. T = 900 ºC.

*Defluidization*

The behavior of ilmenite with respect to particle agglomeration in the fluidized-bed has been also analyzed in this work. Particle agglomeration must be avoided because it can lead

to bed defluidization that causes solids circulation disturbances and channeling of the gas stream through the bed, which turns the contact between gas and particles less efficient. During the experimental tests, defluidization problems were never observed. Moreover, particles extracted from the fluidized-bed at the end of the tests did not show agglomeration evidences.

## 3.2 Gasification in CLC with solid fuels

Char gasification is one of the crucial steps to take into account, since in this technology char must be previously gasified to react with the oxygen-carrier and get oxidized to $CO_2$. Leion et al. (2007) reported an enhancement of the gasification rate of a petcoke due to the presence of a Fe-based oxygen-carrier. Leion et al. (2008a) saw that the gasification rate is influenced by the temperature and the amount of gasification agent introduced. They also observed that ilmenite showed similar results than a synthetic Fe-based oxygen-carrier with different fuels. Besides, $CO_2$ was used as gasification agent by Leion et al. (2009c) with a bituminous Colombian coal as fuel. Their evaluation was focused on the general fuel conversion comparing both gasification agents, which was 5 times faster with steam as compared to $CO_2$.

To have a comprehensive knowledge of char conversion within the frame and conditions of CLC with solid fuels, the parameters that influence both the gasification rate and the later combustion of the gasification products must be deeply studied to improve the performance of the process. The study was done in a batch fluidized bed reactor as valuable information can be obtained in this device under defined conditions and as a previous facility before doing tests in a continuous prototype. The aim of this section, a study that constitutes Paper IV, is to analyze the performance of ilmenite as oxygen-carrier for iG-CLC regarding the char conversion and the conversion of gasification products. The effect of ilmenite itself and the gasification agent, i.e. $H_2O$, $CO_2$ or $H_2O/CO_2$ mixtures at different temperatures, on the gasification rate and on the combustion of the gasification products were evaluated. Successive redox cycles were carried out in a batch fluidized bed

using char from a South African MV bituminous coal as reducing agent. Every reduction period consisted of two consecutive loads of 1.5 g of char. After the reduction period, the bed material was oxidized by air. In some tests, a second load of char was fed in the same reduction period to get further reduction of the oxygen-carrier.

### 3.2.1 Role of ilmenite in char gasification

The effect of ilmenite as oxygen-carrier in the gasification process was evaluated by comparing the gas product distribution obtained using ilmenite or silica sand as bed material. Lower concentrations of CO and $H_2$ were obtained when using ilmenite as bed material compared to sand. No $CH_4$ was observed during any test, since the volatile matter content in the char is negligible and no methane was generated at these conditions, e.g. by methanation of hydrogasification reactions. From the concentrations obtained, an instantaneous rate of char conversion is calculated with Eq. (21), which is shown in Figure 29. Average values of char conversion rate of 10.9%/min for ilmenite and of 6.5%/min for sand were obtained at 950 °C using steam. Thus, the use of ilmenite improves the char gasification rate because it has an effect on the gas distribution, as it reacts with CO and $H_2$, which are well known to be inhibitors for the char gasification reaction.

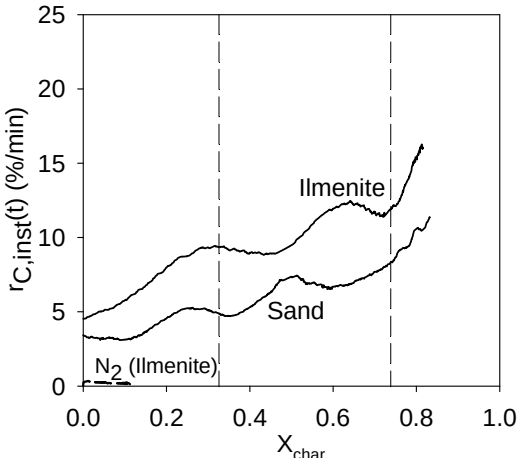


Figure 29. Instantaneous rate of char conversion, $r_{C,inst}(t)$, as a function of the char conversion with activated ilmenite and sand as bed materials. Loads of 1.5 g char in batch FB. Gasification agent: steam. T = 900 °C.

Solid-solid reaction between char and oxygen-carrier particles has been reported to happen at relevante rate in TGA (Siriwardane et al., 2009). T check this possible solid-solid reaction in a fluidized bed, tests were performed using $N_2$ as fluidizing gas and ilmenite or sand as bed material. In both cases almost negligible $CO_2$ or CO concentrations were generated. This means, that the possible solid-solid reaction among char and the oxygen-carrier happened at a negligible rate. A substantial increase in the rate of char gasification could be observed when a gasification agent ($H_2O$) was used as fluidizing gas. Therefore, the conversion of the solid fuel when is fluidized with $H_2O$ was mainly happening through gasification as an intermediate step, with CO and $H_2$ as intermediate products.

### 3.2.2 Effect of the fluidizing gas composition

$H_2O$ and $CO_2$ can be used as fluidizing gases because both can act as gasifying agent. $CO_2$ can be fed by recirculating a fraction of the product gas stream. Thus, the steam requirements for the gasification would be decreased in some extension if a mixture of $CO_2$ and $H_2O$ was used, or even avoided if a pure stream of $CO_2$ was used as fluidizing gas.

Here, the effect of using a gas mixture of $CO_2$ and $H_2O$ on the gasification of char particles from the South African bituminous coal was analyzed. Figure 30.a) shows the instantaneous rate of char gasification, $r_{C,inst}(t)$, as a function of the char conversion when the reactor was fluidized by different $H_2O$:$CO_2$ mixtures, and Figure 30.b) shows the evolution with time of the char conversion working with different $H_2O$:$CO_2$ ratios. The instantaneous rate of char conversion increased significantly as higher was the $H_2O$ percentage in the gasification gas. Thus, the average gasification rate of char from South African bituminous coal dropped from 10.9%/min for steam to a value of 3.4%/min for gasification with $CO_2$. For 100% steam, most of the char is gasified the first 30 minutes, whereas only 60% char conversion was reached after 30 minutes with $CO_2$. From these results it can be concluded that steam seems to be the more adequate fluidizing gas for bituminous South African coal to reach high char gasification conversion. This fact will depend on the type of coal used, as it will be later explained with experiments done in continuous operation with different types of fuels.

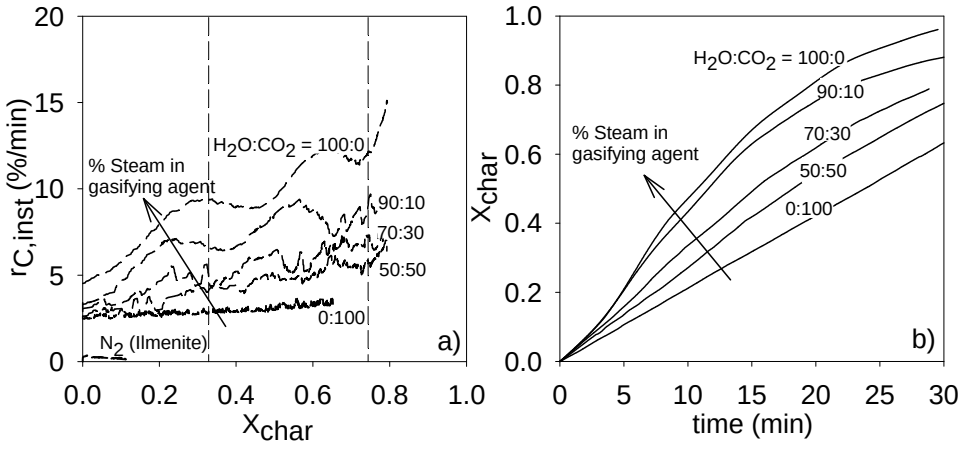


Figure 30. a) Instantaneous rate of char conversion, $r_{C,inst}(t)$, as a function of the char conversion and b) Char conversion vs. time curves with activated ilmenite as bed material with different $H_2O$:$CO_2$ ratios. Loads of 1.5 g char in batch FB. T=900 ºC.

In this technology, the gasification products, mainly composed of CO+$H_2$, must react with the oxygen-carrier getting oxidized. Figure 31 shows the evolution of combustion efficiency, $\eta_c$, with the char conversion for different $H_2O$:$CO_2$ ratios. The combustion efficiency decreases as the $CO_2$ content in the fluidizing gas increases. Although the flow of reacting gases is lower with $CO_2$, they are enriched in CO. That is, the use of $CO_2$ as gasification agent leads to a worse combustion, since ilmenite reacts slower with CO than with $H_2$.

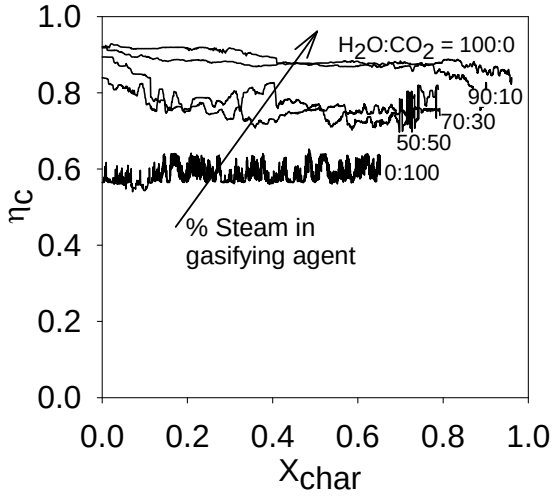


Figure 31. Combustion efficiency vs. char conversion for several $H_2O$:$CO_2$ ratios. Bed material: Activated ilmenite. Loads of 1.5 g char in batch FB. T=900 ºC.

### 3.2.3. Effect of reacting temperature

The effect of the reacting temperature on the gasification rate and the subsequent conversion of gasification products by reaction with ilmenite particles were studied in the batch fluidized bed. Figure 32 shows the instantaneous rate of char conversion, $r_{C,inst}(t)$, as a function of the char conversion when the reactor temperature was 900, 950 or 1000 °C and fluidizing gas was steam or $CO_2$. It can be seen an important increase in the rate of char conversion with temperature when steam is used as gasifying agent. The average $r_{C,inst}$ value increases from 10.9%/min at 900 °C up to 37.3%/min at 1000 °C. Gasification rate with $CO_2$ also increased: the average $r_{C,inst}$ value increases from 3.4%/min at 900 °C up to 6.9%/min at 1000 °C. The apparent activation energy, $E_a$, can be calculated from these values assuming an Arrhenius type dependence with the temperature, thus $E_a$=162 kJ/mol for steam gasification and $E_a$=88 kJ/mol for gasification with $CO_2$. The residence time that would be needed to convert 95% of char fed to the reactor is 7.8 min at 1000 °C for the char particles when using steam, whereas 43.4 min should be necessary using $CO_2$.

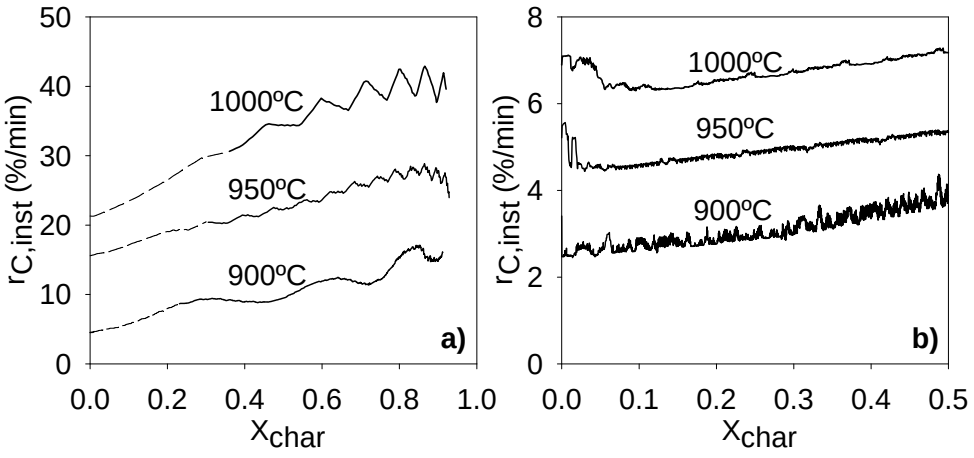


Figure 32. Instantaneous rate of char conversion, $r_{C,inst}(t)$, as a function of the char conversion at 900, 950 and 1000 °C in batch FB. Fluidizing agent: a) $H_2O$; b) $CO_2$. Activated ilmenite as bed material. Loads of 1.5 g char.

As for the combustion efficiency, for both gasification agents the combustion efficiencies are promoted with the temperature, as ilmenite reacts faster at higher temperatures. However, the dependence of $\eta_c$ with temperature was of lower relevance that those showed for char gasification, see Figure 33. The combustion efficiency for steam is very

high and increases from about 89% at 900 °C to 95% at 1000 °C. Note that although the resulting $\eta_c$ at 950°C and 1000°C is almost the same, the amount of oxidized gases is higher due to an enhanced extent of gasification. When using $CO_2$ as gasification agent $\eta_c$ rises from about 59% at 900 °C to 65% at 1000 °C.

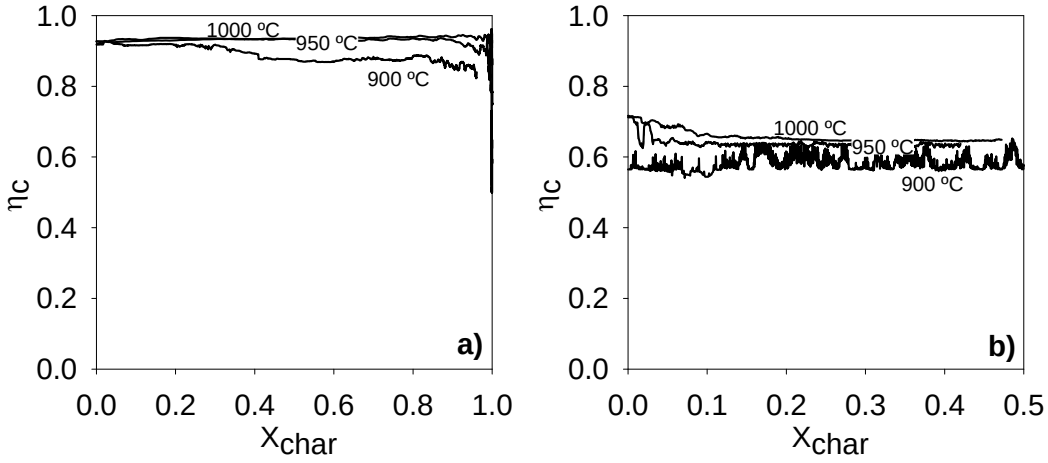


Figure 33. Combustion efficiency as a function of $X_{char}$ at 900, 950 and 1000 °C in batch FB. Fluidizing gas: a) $H_2O$; b) $CO_2$. Bed material: activated ilmenite. Loads of 1.5 g char.

In conclusion, a relevant increase in the gasification rate was seen when ilmenite was used compared to an inert bed material, because ilmenite reacts with $H_2$ and CO which are gasification inhibitors. Steam is preferred as gasification agent to $CO_2$, since with this coal the gasification rate with steam is higher. High temperature enhanced steam gasification substantially: the residence time to convert 95% South African bituminous coal char decreased from 27.5 min at 900°C to 7.8 min at 1000°C.

## 3.3 Continuous operation of CLC with solid fuels

Up to 2011, there have been only several studies done in continuous CLC units fuelled with solid fuels. Berguerand and Lyngfelt (Berguerand and Lyngfelt, 2008a; b; 2009 a; b) used a 10 $kW_{th}$ chemical-looping combustor with ilmenite as oxygen-carrier and South African coal and petroleum coke as solid fuels. They analyzed the combustion process focusing on char conversion. They analyzed mainly the temperature as one of the main

parameters of influence in the system performance, being higher efficiencies reached at high temperatures. Temperatures above 1000 ºC were tested in some cases (Berguerand and Lyngfelt, 2009a). Combustion efficiencies from 85 to 95 % and average carbon capture efficiencies of 80% were obtained in all the experimental works at high temperatures with fuels of low volatile content. Biomass as solid fuel was evaluated by Shen et al. (Shen et al., 2009a) in a continuous 10 $kW_{th}$ CLC combustor using an oxygen-carrier prepared from iron oxide and $CO_2$ as gasification medium. Gu et al. (Gu et al., 2011) also proved the feasibility of using CLC for both biomass and a biomass/coal mixture as solid fuels in a continuous 1 $kW_{th}$ CLC facility using an Australian iron ore as oxygen-carrier. In order to get more knowledge about the iG-CLC process, in this thesis various series of experiments were performed in two continuous CLC units for solid fuels.

The first one is the ICB-CSIC-s1 unit placed at the Instituto de Carboquímica-CSIC, Zaragoza, Spain. The maximum thermal power reached in these experiments was 580 $W_{th}$. The two main advantages of this facility are that it allows the control and measurement of the solids circulation flow rate and that the fuel is fed at the bottom of the reactor, so the volatiles get in contact with the oxygen-carrier bed. This facility has no carbon separation system, which facilitates the evaluation of the effect of the solids mean residence time. The experiments were done with several fuels ranging from lignite to anthracite. Nevertheless, most experiments were carried out with HV bituminous Colombian coal El Cerrejón as fuel. A total of 98 hours of continuous operation feeding fuel and 122 hours of continuous fluidization were made in this prototype, where the carbon capture and combustion efficiency of the CLC process with coal was analyzed. The effect on the process of several variables of operation was assessed. Results obtained from the experiments performed in this unit are presented in Papers V, VI and IX. In Paper V the different behavior and conversion of the char and the volatile matter is analyzed, as well as the fuel-reactor temperature and the coal particle size on the system performance. Besides, the property variation of ilmenite along the operating time could be analyzed. In Paper VI the effect of variables of operation such as solids recirculation rate, coal feeding flow, and flow and type of gasification agent is studied. Paper IX evaluates the feasibility of using different types of coals, as well as the effect of the coal rank on this technology.

The second unit has a thermal power of 10 $kW_{th}$ and is placed at Chalmers University of Technology, Göteborg, Sweden. Since in this facility the volatiles are not efficiently mixed with the oxygen-carrier bed because of its above-bed feeding system, petcoke was used as fuel due to its low content in volatiles. A total of 4 hours of continuous operation feeding fuel and 8 hours of fluidization were made in this unit, where the influence of limestone addition to ilmenite in the CLC process with solid fuels was evaluated. Results obtained were presented in Paper VII. Both CLC prototypes were easy to operate and control, and the steady state for each operating condition was maintained stable for at least 30 min.

Table 7 shows the conditions for the series of experiments carried out with Colombian coal in the ICB-CSIC-s1 facility. One further test was done with sand as bed material with a feed flow of 75 g/h of coal and steam as fluidizing agent at 915 °C. The total sand bed mass in the system was 1.8 kg and the solid bed mass in the fuel-reactor was 0.38 kg sand.

Table 7. Conditions for the experiments with bituminous Colombian coal as fuel. A) Fuel-reactor temperature variation for different coal particle sizes; B) Variation of coal flow rate; C) Solids circulation flow rate variation for different coal particle sizes; D) Variation of the gasification agent flow; E) Variation of the gasification agent type ($H_2O$:$CO_2$ mixtures).

| Exp. | Coal particle size(μm) | $T_{FR}$ (°C) | Coal feed (g/h) | Solids circ. Flow(kg/h) | Gasif.agent flow($L_N$/h) | $H_2O$:$CO_2$ (%:%) |
|---|---|---|---|---|---|---|
| A1 | 74-125 | 820-950 | 42 | 3.5 | 180 | 100:0 |
| A2 | 125-200 | 820-950 | 42 | 3.5 | 180 | 100:0 |
| A3 | 200-300 | 820-950 | 42 | 3.5 | 180 | 100:0 |
| B | 74-125 | 890 | 33-83 | 8.4 | 190 | 100:0 |
| C1 | 74-125 | | 41.1 | 1.2–11.6 | | |
| C2 | 125-200 | 890 | 46.7 | 1.0–3.6 | 190 | 100:0 |
| C3 | 200-300 | | 38.5 | 1.6–11.3 | | |
| D | 125-200 | 940 | 161 | 2.5 | 110-190 | 100:0 |
| E | 125-200 | 935 | 72 | 3.3 | 190 | 100:0-0:100 |

The activation process on ilmenite reactivity was observed in the continuous ICB-CSIC-s1 unit, as ilmenite samples were extracted after several hours of operation and the reactivity

was measured by TGA. It could be considered that ilmenite was already active after 3 hours for the reduction reaction. However, ilmenite was not completely activated for oxidation reaction after 35 hours operation yet and it was almost fully activated after 98 hours. This was attributed to the fact that it had not developed enough porosity. This was because in the continuous tests the ilmenite conversion variation was low.

As an example, in Figure 34 the obtained gas distributions (dry and $N_2$ free basis) in fuel- and air-reactor for tests with increasing fuel-reactor temperature in the ICB-CSIC-s1 unit are represented. The outlet of the fuel-reactor was mainly composed of oxidized $CO_2$, and $H_2$ and CO as not fully oxidized products. In case of this series of experiments, it can be observed that an increase in the fuel-reactor temperature led to an increase in the generated $CO_2$ and to a decrease in the unburnt gases in the fuel-reactor, that is, CO, $H_2$ and $CH_4$, and to a decrease in the $CO_2$ in the air-reactor, which was ungasified char coming from the fuel-reactor that was burnt in the air-reactor.

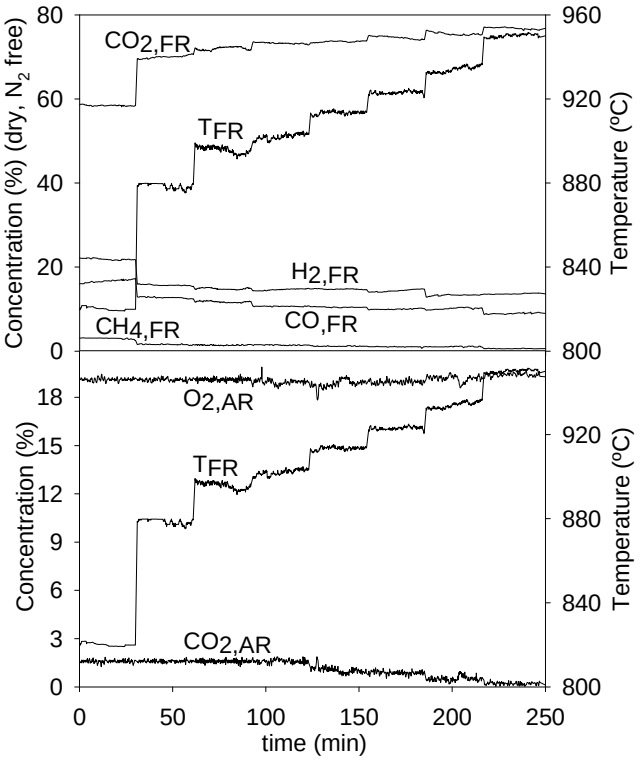


Figure 34. Gas distributions in fuel-reactor (dry basis and $N_2$ free) and air-reactor for increasing fuel-reactor temperature in continuous test. Solids circulation flow: 3.5 kg/h. Fuel: pre-treated bituminous Colombian coal. Coal particle size: +125-200 μm.

A key aspect of the process is the oxidation of the gasification products by ilmenite, as well as the released volatile matter, and possible tars formed. Experiments with char showed complete combustion of gasification products to $CO_2$ and $H_2O$. Therefore, unconverted gases should come from incomplete combustion of volatile matter.

In order to evaluate to what extent ilmenite oxidizes the volatile matter, an experiment with sand as inert bed material was done with coal as fuel at 915 °C and steam as gasification agent in the fuel-reactor. Therefore, from the comparison between the tests with ilmenite and sand as be materials, at 915 °C the combustion efficiency of the released volatiles by the oxidation with ilmenite was 38.3% for $CH_4$, 35.3% for CO and 79.0% for $H_2$. The reaction differences between gases are due to the reaction rates of ilmenite, since it reacts faster with $H_2$ and slower $CH_4$. In addition, more oxygen transfer is needed to oxidize $CH_4$. Thus, the combustion efficiency of the volatile matter was 63.0%.

For sand as bed material, the GC measurement showed that the fuel-reactor product gas had compositions of 0.13% $C_2H_6$ and 0.04% $C_3H_8$. Besides, the tar content in the fuel-reactor outlet was measured to be 0.895 g/Nm$^3$ dry gas. Although the quantities measured of both tars and higher hydrocarbons for this fuel were quite low in absence of an oxygen-carrier, ilmenite showed to promote the decomposition and later oxidation of those species, since no tars either hydrocarbons heavier than $CH_4$ were formed when using ilmenite.

Char gasification increased from 5.2% with sand to 48.1% with ilmenite as bed material. This can be explained through the inhibitory effect that causes the presence of high amounts of $H_2$ and CO in the fuel-reactor, as they do not react with the oxygen-carrier.

### 3.3.1 Effect of fuel-reactor temperature

The influence of the fuel-reactor temperature on the main parameters of the CLC process for 3 different coal particle sizes, i.e., +74-125 μm, +125-200 μm and +200-300 μm, was studied. Temperatures from 820 to 950 °C were used in this study. Figure 35 represents the efficiencies of carbon capture, char conversion and combustion as a function of the reactor

temperature for different coal particle sizes. As it was presumable, the results show that there is a continuous increase of all efficiencies with the temperature for all coal particle sizes. In this prototype carbon capture presented low values below 920 ºC. This was because the gasification rate at these temperatures is slow and thus a relatively high amount of char went to the air-reactor. The carbon capture at 870 ºC had a value of 35% and increased up to 86% at 950 ºC. The increase in the carbon capture efficiency with the temperature is due to more carbon in char is being gasified in the reactor. The char conversion changed from 15% at 870 ºC to 82% at 950 ºC as extreme cases. If the trends are extrapolated, it could be expected that all efficiencies would reach a value close to 100% at 1000 ºC, which means that most of carbon in the coal would exit with the fuel-reactor flue gases. This unit has no carbon separation system, so the ungasified char from the fuel-reactor is directed to the air-reactor where it is burnt with air. Nevertheless, the absence of a carbon stripper facilitates the interpretation of the effect of the operational conditions on the char conversion, specially the effect of the mean residence time.

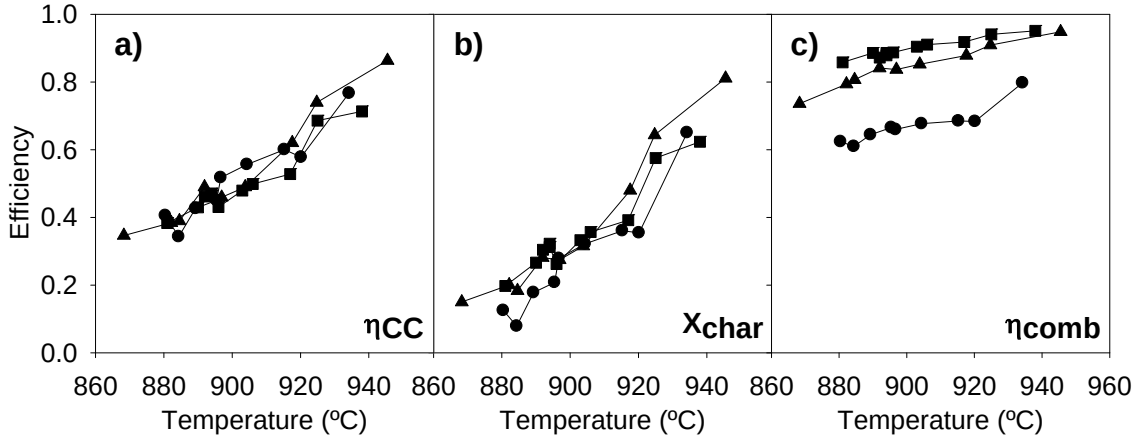


Figure 35. a) Carbon capture, b) char conversion and c) combustion efficiency variation with fuel-reactor temperature for various coal particle sizes. Particle size: —●— 74-125 μm; —▲— 125-200 μm; —■— 200-300 μm.

The combustion efficiency varied from 70% at 870 ºC to 95% at 950 ºC for the middle and bigger particle sizes. It is likely that the combustion efficiencies observed for the smaller particle size were lower because relevant fraction of char was gasified in the upper part of the reactor, where gasification products are not in contact with the oxygen-carrier. Full oxidation of the outlet fuel-reactor stream was not achieved in any of the previous CLC

experiments with solid fuels performed to date (Berguerand and Lyngfelt, 2008a; b; 2009a; b; Wu et al., 2010; Shen et al., 2009a;b;c;2010). Furthermore, the extent of unburt gases was similar as if a highly Ni-based oxygen-carrier was used (Shen et al., 2009b;2009c;2010).

### 3.3.2 Effect of coal particle size

The effect of the coal particle size on the process performance was investigated because it is a key parameter in the operation of fluidized-bed reactors. Three different coal particle sizes were assessed: +74-125, +125-200 and +200-300 μm. Differences on combustion efficiency with the smaller particle sizes can be explained because elutriated char particles could be gasified to some extent in the reactor freeboard. There the gasification products did not get in contact with the oxygen-carrier and could not be therefore oxidized. However, the char from the smaller size could still get gasified in the freeboard. The resulting char conversions and carbon captures are similar at different particle sizes. The slight differences can be explained because smaller particles are more easily elutriated than bigger ones. For particle sizes of +74-125 μm about 35% of the introduced char was elutriated, whereas lower values than 5% were found in most cases for bigger particles. At about 900 °C the residence time of char was 9 min for +200-300 μm, 8 min for +125-200 μm and decreased to 5 min for +74-125 μm. Figure 36 shows the calculated char gasification rates at different temperatures and for the three particle sizes used.

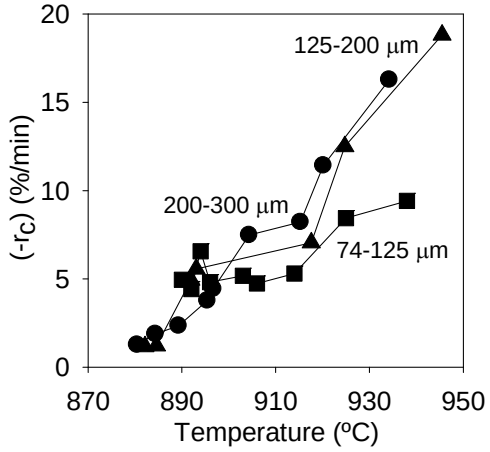


Figure 36. Calculated gasification rate considering the fuel-reactor as a CSTR for different fuel-reactor temperatures. Coal particle size:—●—74-125 μm;—▲—125-200 μm;—■—200-300 μm.

It can be observed that the char gasification rate increased with the temperature for every particle size.

### 3.3.3 Effect of solids recirculation rate

The effect of the solids circulation rate on the process performance was studied. Solids circulation flow rates from 1.0 to 11.6 kg/h for three coal particle sizes at an average fuel-reactor temperature of 890 °C were used. This range corresponded to an ilmenite residence time range from 4.2 to 48 minutes and the oxygen-carrier to fuel ratio $\phi$ was varied from 0.5 to 8.4. Thus, there were cases where the solids recirculation rate was lowered so much that $\phi$ reached values under the unity, which meant that there was not enough oxygen-carrier available to fully oxidize the fuel.

Figure 37.a) shows the carbon capture efficiency obtained as a function of the oxygen to fuel ratio for the different coal particle sizes tested. The carbon capture efficiency decreases for increasing oxygen-carrier to fuel ratio, that is, when the recirculation rate increases. This trend is clear for $\phi$ closer to the unity, and when $\phi$ has higher values the influence is smaller. This follows the tendency of the solids residence time, that is, the decrease in $\eta_{CC}$ can be explained because coal was less gasified, due to a lower residence time of the solids in the fuel-reactor.

The combustion efficiencies were less influenced by the solids circulation rate. This indicates that the process is actually controlled by char gasification, although the amount or reactivity of the oxygen-carrier has also some influence in the system. Figure 37.b) shows that the combustion efficiency had some increase when $\phi$ decreases: from 75% with $\phi=8$ to 86% with $\phi=1.1$. With lower $\phi$ the char conversion increased, and since the gasification products had almost full conversion, the percentage of unconverted gases -mainly coming from volatiles- decreased, as the relative importance of the gasification products in the reacting gases increased. Thus, higher char conversions will lead to enhanced combustion efficiencies. The lower combustion efficiencies obtained for the +74-

125 μm particles are due to the higher fraction of char in the freeboard with smaller particles.

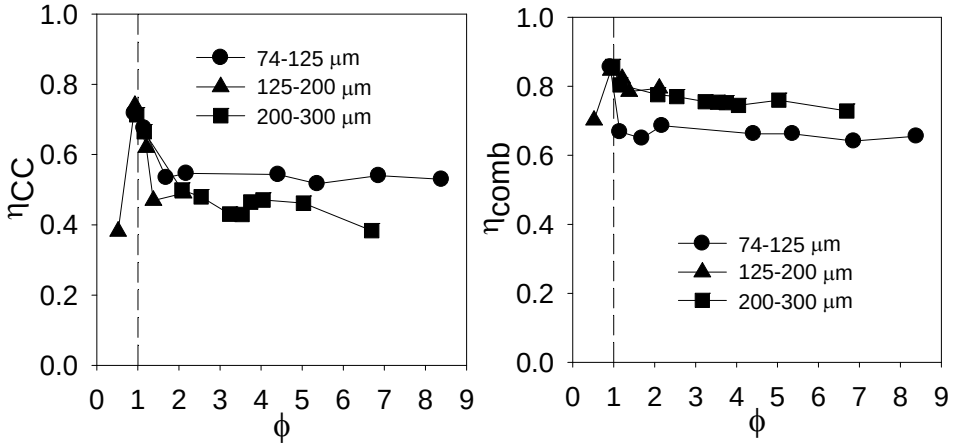


Figure 37. a) Carbon capture and b) Combustion efficiencies with different oxygen-carrier to fuel ratios for different coal particle sizes. $T_{FR}$ = 890 °C. El Cerrejón coal.

When oxygen-carrier to fuel ratios lower than 1 were used, the performance of the system dropped substantially although the residence time was very high. When ϕ decreased to 0.5 the combustion efficiency decreased because there was not enough oxygen available to burn the fuel fed and as a consequence the char conversion also dropped because the reactor got enriched in the generated $H_2$ and CO, which are inhibitors for the char gasification rate.

### 3.3.4 Effect of coal feeding flow

The effect of the coal feeding rate on the process performance was also studied. Coal feeding flow rate was changed from 33 to 83 g/h, corresponding to a thermal power of 200 $W_{th}$ to 505 $W_{th}$. In these experiments the fuel-reactor temperature was maintained constant at about 890 °C and the solids circulation rate at 8.4 kg/h. This study was carried out using coal with particle size +74-125 μm.

When higher coal feeding flow was introduced, the corresponding flows from all products increased because there was more fuel to devolatilize, gasify and burn. However, the char

conversion was not really influenced by an increase in the coal feed because there was no major increase in the residence time, as can be seen in Fig. 4 from Paper VI.

The resulting combustion efficiency was not influenced by the coal feeding rate, as the oxygen-carrier to fuel ratio was above one. When more coal was introduced in the system, the variation of ilmenite conversion and therefore the oxygen transferred increased proportionally to the coal feeding rate increase (see Fig. 6 from Paper VI). This confirms the statement made that in this system the combustion efficiency is not limited by the reaction rate of ilmenite, but for the gasification step.

### 3.3.5 Effect of gasification agent: flow and type

The flow of steam feed was varied from 110 to 190 $L_N$/h, corresponding to a gas velocity variation in the fuel-reactor from 0.07 to 0.12 m/s at 900 °C. The steam to fixed carbon ratio changed from 0.7 to 1.1. When the gasification products are burnt by ilmenite, $H_2O$ and $CO_2$ are formed which can further gasify the fuel, so $H_2O$ is being regenerated in the process. The increase in the steam flow fed had some beneficial effect on the char conversion. For conditions of steam excess, there was no major effect on the char conversion, so it would not be necessary to have $H_2O$/C over the unity. The change in the gasification agent flow did not influence the combustion efficiency.

The steam requirements for the gasification would be decreased in some extension, or even avoided if a pure $CO_2$ stream was used as fluidizing gas. The motivation of this is that $CO_2$ can be fed by recirculating a fraction of the product gas stream. The effect of using a gas mixture of $CO_2$:$H_2O$ on the gasification step and the whole performance of the process was evaluated in a continuous system. The average fuel-reactor temperature was 935 °C. The total gasification agent flow was 190 $L_N$/h. The solids circulation rate was 3.3 kg/h.

The results showed that the char conversion increased for higher fraction of steam in the gasification agent, as it was previously found in batch FB experiments. With this type of fuel, gasification with steam is faster than with $CO_2$. However, the combustion efficiency was not really influenced by the gasification agent used. When gasifying with $CO_2$, more

CO is generated as when gasifying with steam, where $H_2$ is also generated. This result is opposite to that found in batch FB done with bituminous South African coal. This is because in this plant the combustion efficiency was limited by the combustion of volatiles which is not influenced by the fluidizing gas.

Limited use of $CO_2$ in the fluidizing gas would be desirable to maintain high gasification rates for this fuel. This was also seen in the previous tests in batch FB with Colombian South African coal. On the other hand, the implementation of a carbon separation system that increased the char residence time would offset any possible poorer system performance caused by the slower gasification rate.

### 3.3.6 Effect of limestone addition

The influence of limestone addition to ilmenite as oxygen-carrier was tested in a continuous 10 $kW_{th}$ CLC pilot for solid fuels. The results of it comprise Paper VII. This study was motivated by previous tests where calcined limestone addition in a batch fluidized bed had some beneficial effect on the char conversion rate and led to an enhancement on the gas conversion (Teyssié et al., 2011). Tests with an ilmenite-limestone mixture as bed material were performed, and also tests using only ilmenite as bed material were carried out in that unit for comparison. Global solids circulation was varied as it is an important operational parameter, which determines the solid fuel residence time. The tests were performed at two temperatures of the fuel-reactor: 950 °C and 1000 °C. The fuel flow was 479 g/h, which is a fuel power of 4.2 $kW_{th}$. The particle recirculation between reactors was controlled by the air flow to the air-reactor: it was varied from 155 to 190 $L_N$/min. The fuel was petcoke, which has relative low fraction of volatile matter, 9.9%. Thus, only the gasification process and oxidation of gasification products are really the scope of evaluation in this study.

As an example of the most important results, Figure 38 shows the comparison between the obtained oxygen demand, $\Omega_{OD}$, and carbon capture $\eta_{CC}$ from the experimental conditions used, for experiments done at 950 and 1000 °C; and using only ilmenite as bed material and

after limestone addition. The limestone fraction in the fuel-reactor bed at the end of the experiments was weighed to be about 12 %wt.

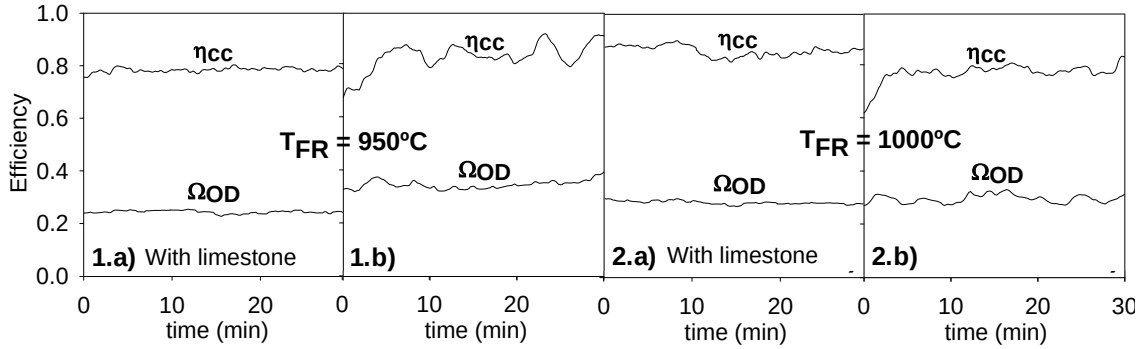


Figure 38. Comparison between $\Omega_{OD}$ and $\eta_{CC}$ for tests at $T_{FR}$ = 1) 950 °C and 2) 1000 °C using a) mixture ilmenite-limestone and b) ilmenite as bed material. Fuel flow = 479 g/h.

Table 8 shows a summary of the average values for the main experiments performed: the carbon capture efficiency, $\eta_{CC}$, the oxygen demand, $\Omega_{OD}$, the oxygen-carrier to fuel ratio, $\phi$, and the oxygen-carrier average residence time in the fuel-reactor, $t_{r,ilm}$.

The conversion of gasification products after limestone addition was higher at 950 °C, as $\Omega_{OD}$ decreased from 0.33 to 0.24. For a mean residence time of 10.7 minutes, $\eta_{CC}$ was 0.79. In order to compare tests with the same residence time, an interpolated value of $\eta_{CC}$ of 0.76 was obtained for ilmenite only, for a mean value of $t_{r,ilm}$ of 10.7 minutes. Thus, $\eta_{CC}$ was somewhat lower for ilmenite only, as compared to ilmenite + limestone. At 1000 °C there was no significant difference in the gas conversion, as $\Omega_{OD}$ was quite similar after limestone addition. However, the efficiencies related to char conversion improved by the presence of limestone: $\eta_{CC}$ increased from 0.77 to 0.86, as can be seen in

Table 8. As for the influence of adding limestone to the CLC process with ilmenite, at 950°C, there is a reduction in the oxygen demand, whereas no clear difference is seen at 1000°C. In all the cases char was faster converted in presence of limestone.

Table 8. Summary of the mean values obtained in the continuous experiments with petcoke as fuel and with ilmenite or a limestone-ilmenite mixture as bed material.

| $T_{FR}$ = 950 °C | | | |
|---|---|---|---|
| Bed material | $\eta_{CC}$ | $\Omega_{OD}$ | $t_{r,ilm}$(min) |
| Ilmenite + Lime | 0.79 | 0.24 | 10.7 |
| Ilmenite | 0.7 | 0.33 | 8.1 |
| Ilmenite | 0.83 | 0.33 | 13.5 |
| $T_{FR}$ = 1000 °C | | | |
| Bed material | $\eta_{CC}$ | $\Omega_{OD}$ | $t_{r,ilm}$(min) |
| Ilmenite + Lime | 0.86 | 0.28 | 10.8 |
| Ilmenite | 0.58 | 0.28 | 4.9 |
| Ilmenite | 0.77 | 0.29 | 9.2 |

The addition of some limestone was somewhat advantageous for the efficiency improvement, for gasification as well as for gas conversion due to its effect in the water-gas shift equilibrium. Figure 39 shows the fraction $(F_{H2,FR} \cdot F_{CO2,FR})/(F_{H2O,FR\ out} \cdot F_{CO,FR})$ obtained for experiments with ilmenite-limestone and for tests done with ilmenite only at 950 °C and 1000 °C. The equilibrium constant $k_{WGS}$ at the temperature considered is also represented. At both temperatures the exiting gaseous flows with limestone addition were closer to the WGS equilibrium, i.e. to higher $H_2 + CO_2$ formation, although the difference was much more pronounced at 950 °C.

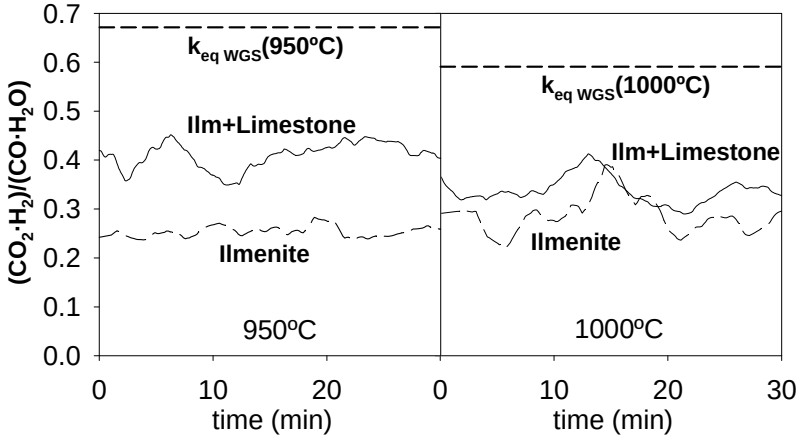


Figure 39. Fraction $(F_{H2,FR} \cdot F_{CO2,FR})/(F_{H2O,FR\ out} \cdot F_{CO,FR})$ for experiments with ilmenite-limestone mixture and with ilmenite as bed material at 950 °C and 1000 °C.

Thus, limestone addition causes CO and $H_2O$ to react to give $CO_2$ and $H_2$, i.e. Ca-based compounds could act as a catalyst for the WGS reaction (Teyssié et al., 2011). This happens in the presence of an oxygen-carrier, ilmenite, which reacts faster with $H_2$ than with CO. Consequently, the oxidation of the gas should proceed faster, giving higher gas conversion and lower oxygen demand. This effect is clearly seen at 950 °C (see Figure 38.a)), although at a temperature of 1000 °C the improvement regarding the gas conversion was residual when CaO was present in the solids mixture (see Figure 38.b)). From results showed in Figure 39 it seems that the WGS reaction itself is fast enough at 1000 °C to happen at similar extension with and without limestone addition.

### 3.3.7 Effect of the coal rank

The carbon capture and combustion efficiencies as representative of the process performance were studied in continuous testing with different coals from lignite to anthracite, in order to prove the feasibility of the technology with coals of different ranks and to assess the performance of the process as a function of the solid fuel properties. Previous research studies in batch FB concluded that the char conversion is related to the reactivity of solid fuel particles (Linderholm et al. 2011), being the nature of the oxygen-carrier of lower relevance (Leion et al., 2008a; 2009d). This study is gathered in Paper IX.

Table 9 shows the conditions for the series of experiments carried out, where the fuel-reactor temperature and of the gasification agent type ($H_2O$:$CO_2$ mixtures) were varied. The average solids circulation flow rate was 3.0 kg/h and the resulting oxygen-carrier to fuel ratio for all fuels tested was about 1.0-1.1. The gasification agent flow was 190 $L_N$/h, corresponding to a gas velocity of 0.12 m/s at 900°C. The flows introduced are the same as in the tests done with the HV bituminous Colombian coal. An experiment previously performed with this coal, which had similar solids residence time and solids inventory, is included in the discussion of results.

Table 9. Conditions for the series of experiments with the different types of coals tested, i.e, lignite, Colombian and South African bituminous coals and anthracite.

| Effect of the temperature | | | | | |
|---|---|---|---|---|---|
| Coal type | $T_{FR}$,°C | Coal feed, g/h | Gasif.agent / Fixed C | Gasification mixture,%$H_2O$ | Thermal output, $W_{th}$ |
| Lignite | 870-920 | 100 | 3.0 | 100 | 450 |
| MV Bit. S.African | 850-915 | 79 | 2.3 | 100 | 580 |
| Anthracite | 870-930 | 94 | 1.8 | 100 | 570 |
| Effect of the gasification mixture $H_2O$:$CO_2$ | | | | | |
| Coal type | $T_{FR}$,°C | Coal feed, g/h | Gasif.agent / Fixed C | Gasification mixture,%$H_2O$ | Thermal output, $W_{th}$ |
| Lignite | 920 | 100 | 3.0 | 100;60;0 | 450 |
| MV Bit. S.African | 910 | 79 | 2.3 | 100;58;0 | 580 |
| Anthracite | 925 | 94 | 1.8 | 100;48;0 | 570 |

Continuous tests were done at different temperatures. Figure 40.a) shows the carbon capture obtained for different temperatures for the coals tested, as well as the values that were obtained for HV bituminous Colombian coal in the previous study. $\eta_{CC}$ was highly dependent on coal rank because of the gasification reactivity of the coal chars. Lignite reached the highest values of $\eta_{CC}$, followed by HV bituminous Colombian, MV bituminous South African coal and it was lower for anthracite. As an example, at 900°C $\eta_{CC}$ was 0.90 for lignite, 0.55 for Colombian coal (at 890°C), 0.54 for South African coal and 0.29 for anthracite. The carbon capture depended on the char conversion and on the ratio $F_{C,vol}/F_{C,char\ eff}$ of the coal considered.

Figure 40.b) shows the char conversions reached at different temperatures for the coals studied. Lignite had much higher char conversion than the other coals. The char conversion obtained for the other coals are closer, indicating that they have more similar gasification rates, but lower that the gasification rate of lignite.

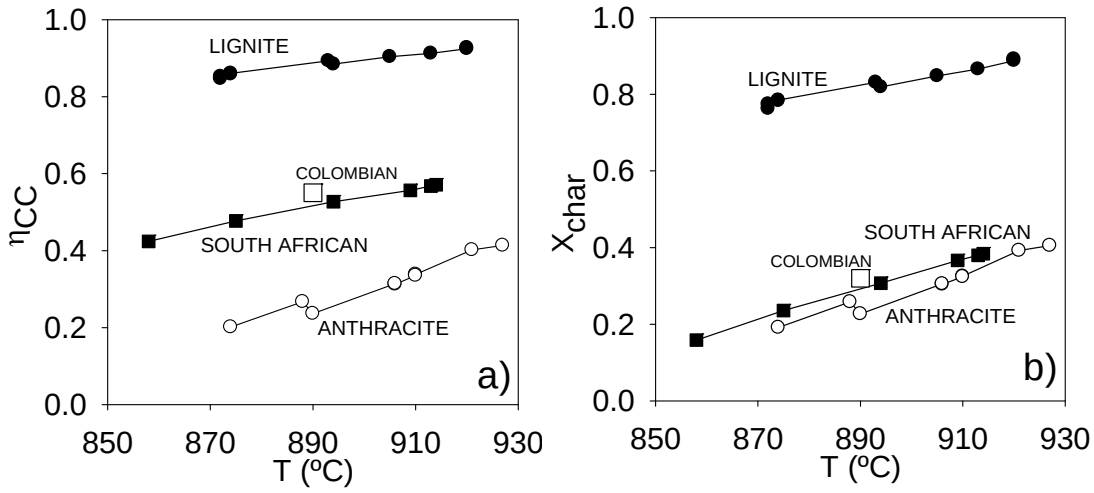


Figure 40. a) Carbon Capture and b) char conversion variation with the fuel-reactor temperature for –●– lignite, –□– HV bituminous Colombian coal, –■– MV bituminous South African coal, –○– anthracite. Coal particle size: +200-300 μm.

The residence time of solids was similar for all fuels tested, that is, the char from all fuels had similar time to gasifiy. It was around 14 minutes. From these results, it can be concluded that the gasification rates follow the order expected from the rank of the different coals: it is much faster for lignite, then HV bituminous coal, MV bituminous coal and it is slower for anthracite. The gasification rates in all experiments were also calculated and confirmed this statement at all temperatures tested. This was also in line with the trend of the char gasification rates expected from the rank of the coals used (Johnson, 1981).

Both char conversion and carbon capture for anthracite were similar because the volatile matter fraction is low, whereas for the other coals the values of carbon capture were higher. For lignite the differences between $X_{char}$ and $\eta_{CC}$ are not big either because $X_{char}$ is already quite high. HV bituminous Colombian and MV bituminous South African coal have similar fractions of volatiles and fixed carbon and char conversions reached, so their increase in $\eta_{CC}$ compared to $X_{char}$ is similar.

Figure 41.a) shows that for the fuels tested in this work, the fuel-reactor combustion efficiencies obtained have a slow growth with the temperature because of the increase in the reaction rate of ilmenite. Besides, for all the temperatures tested, $\eta_{comb\ FR}$ was higher for

anthracite, followed by lignite and MV bituminous South African coal, which was similar to HV bituminous Colombian coal. As it was concluded from the experiments with the bituminous Colombian coal, the released volatiles have worse contact with the oxygen-carrier particles and are therefore less converted. On the contrary, gasification products are highly oxidized. This explains the higher $\eta_{comb\ FR}$ for anthracite, since the volatile fraction is lower. Although lignite has a higher fraction of volatile matter compared to South African coal, the resulting $\eta_{comb\ FR}$ for lignite was slightly higher because the relative fraction of gasification products compared to volatiles was higher due to the fast char gasification rate of lignite. As an example, at 900ºC $\eta_{comb\ FR}$ was 0.73 for Colombian coal (at 890ºC), 0.84 for anthracite 0.75 for lignite and 0.73 for South African coal. Solid residence times are similar for all coals used, around 14 minutes, although the solids inventories have some differences that also affect the results: it was 1770 kg/$MW_{th}$ for lignite, 1580 kg/$MW_{th}$ for Colombian coal, 1380 kg/$MW_{th}$ for South African coal and 1400 kg/$MW_{th}$ for anthracite.

If complete combustion of the gasification products is assumed, a combustion efficiency of the volatile matter, $\eta_{comb\ vol}$, can be defined, as for Eq. (41). This parameter can give an idea of how much the volatiles of each type of fuel are oxidized.

$$\eta_{comb\ vol} = \frac{O_{2\ demand\ gases\ FR}}{O_{2\ demand\ volatiles}} = \frac{2 \cdot F_{CH4,FR} + 0.5 \cdot F_{H2,FR} + 0.5 \cdot F_{CO,FR}}{O_{2\ demand\ coal} - O_{2\ demand\ char}} \quad (41)$$

As it can be seen in Figure 41.b), the volatile combustion efficiency was lower for anthracite and higher for lignite and very similar for both bituminous coals. This could be explained by means of the composition of volatiles of each type of fuel: the oxygen demanded by the volatiles of anthracite is higher than for lignite, then for South African and bituminous Colombian coal. The average combustion efficiency of volatiles was around 52% for lignite, 61% for HV bituminous Colombian coal, 58% for MV bituminous South African coal, 42% for anthracite.

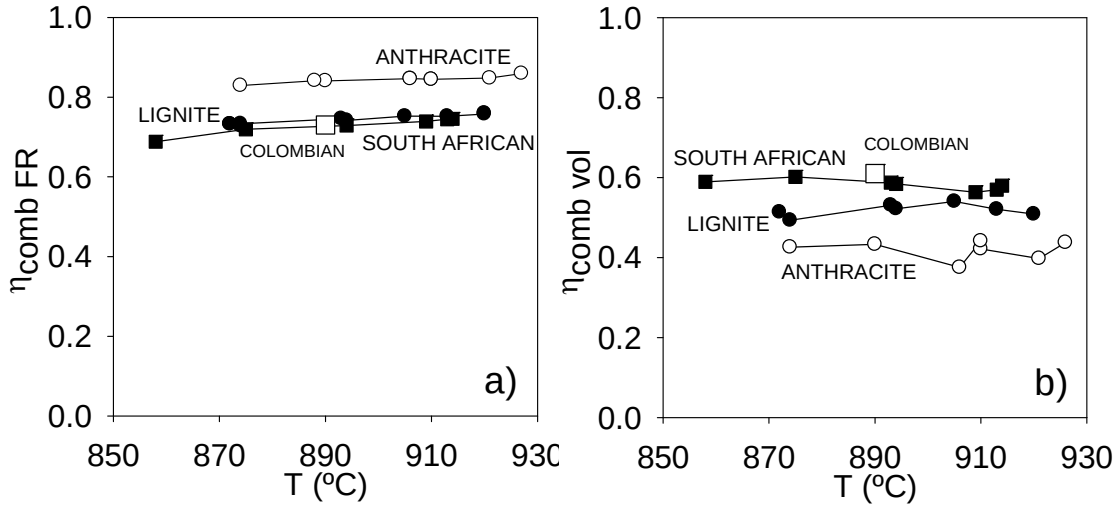


Figure 41. a) Fuel-reactor combustion efficiency and b) volatile combustion efficiency variation with the fuel-reactor temperature for –●–lignite, –□–HV bituminous Colombian coal, –■–MV bituminous South African coal, –○–anthracite.

Since the rate of gasification of the fuel in this process is a determining factor, the effect of using a gas mixture of $CO_2$ and $H_2O$ on the gasification step and the whole performance of the process with the fuels used in this work was evaluated. In case of lignite there is no change in the process performance when gasifying with $CO_2$, as it can be seen in Figure 42.

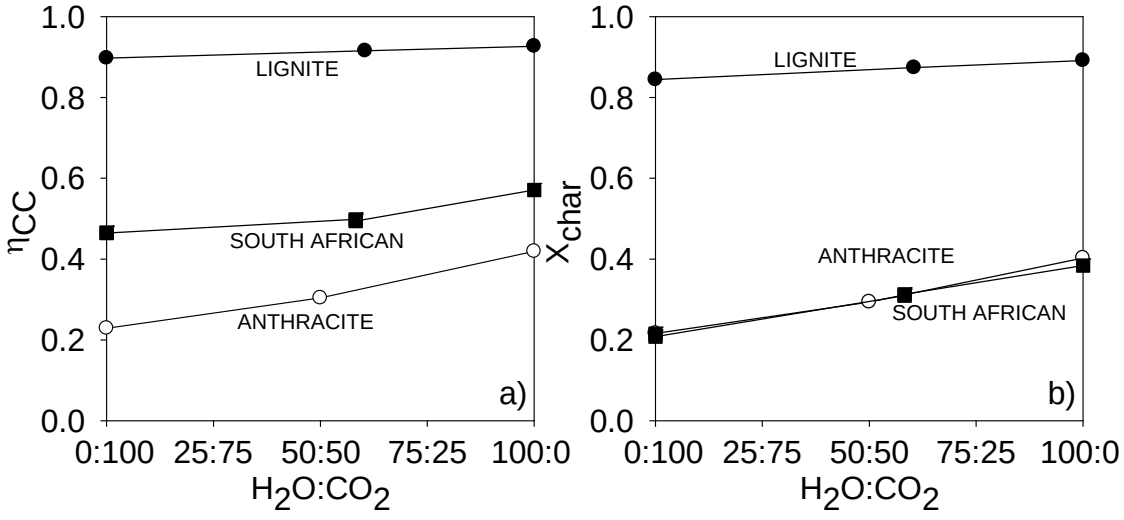


Figure 42. a) Carbon capture efficiency and b) Char conversion variation for different $H_2O$:$CO_2$ mixtures as gasification agent for –●– lignite, –■– bituminous South African coal, –○– anthracite.

On the other hand, for anthracite the lower gasification rate of char with $CO_2$ leads to a substantial drop in the performance. The combustion efficiency is not affected by the gasification agent used. Thus, depending on the type of fuel, $CO_2$ recirculated from the outlet fuel-reactor flow can replaced some of the steam as gasification agent, getting similar system performance and thereby saving energy derived from steam generation.

In this study it has been concluded that the outgoing unburnt gases in the fuel-reactor seem to come from volatile matter that had not been fully oxidized. At higher fuel-reactor temperatures, gasification and combustion reactions are faster and promoted for all types of solid fuels. The carbon capture is higher for the solid fuels with faster char gasification rates and also when the volatile content in the fuel is higher. High values of carbon capture can be obtained, but it is essential to have a highly efficient carbon separation system that reintroduced unconverted char particles back to the fuel-reactor, especially for solid fuels with slow gasification rates such as anthracites. The combustion efficiency in the fuel-reactor is higher for higher temperature, higher solids inventory and for solid fuels with lower volatile content and with faster gasification rate. Furthermore, depending on the type of fuel, some of the steam as gasification agent can be replaced by $CO_2$.

# 4 Simplified model of a CLC system with solid fuels and optimization

A theoretical model is a useful tool to understand the operation of the system in a general way, as well as to predict the influence of the different variables and optimize their values. A validated model can be also used for the design of an industrial unit. In this section a theoretical simplified model for the fuel-reactor of an iG-CLC process using ilmenite as oxygen-carrier has been developed based on a simple reacting scheme. The model calculations were made considering the HV bituminous Colombian coal "El Cerrejón" as solid fuel. For the development of the simplified model of iG-CLC, it was necessary to know: (1) the reaction scheme to be considered in the mass balance; (2) the content and composition of the volatile matter in coal; (3) kinetics of char gasification with the gasification agents used; and (4) kinetics of the subsequent reaction of the gaseous compounds (CO, $H_2$, $CH_4$) with the oxygen-carrier are also required.

## 4.1 Gasification kinetics

For char gasification the most common gasification agents are steam and $CO_2$, through which $H_2$ and CO are generated as for the following reactions:

$$C + H_2O \rightarrow CO + H_2 \quad (42)$$

$$C + CO_2 \rightarrow 2\,CO \quad (43)$$

Kinetics of the gasification reactions for the bituminous Colombian coal were obtained by TGA analysis, in order to implement the kinetics in the model of the iG-CLC system. Conversion vs. time curves at different temperatures (900-1050ºC), gasification agent concentrations (i.e. 20-80 vol.% $H_2O$ or $CO_2$) and gas product concentrations (i.e. 0-40 vol.% $H_2$ or CO) were obtained. A similar procedure was used to those found in (Adánez et al., 1985). Char was assumed to gasify according to the homogeneous reaction model with control by chemical reaction. The surface reaction follows a Langmuir-Hinshelwood reaction model and the reaction rate is constant with the char conversion. The gasification rate $(-r_C)$ is defined by Eq. (44).

$$(-r_C) = \frac{1}{(1-X_{char})}\frac{dX_{char}}{dt} = \frac{k_1 p_{react}}{1 + k_2 p_{react} + k_3 p_{prod}} \quad (44)$$

where $X_{char}$ is the char conversion, $p_{react}$ is the partial pressure of the gaseous reactants, i.e. $H_2O$ or $CO_2$, $p_{prod}$ is the partial pressure of the gasification products, i.e. $H_2$ or CO, and $k_1$, $k_2$ and $k_3$ are the kinetic constants. Thereby, the gasification kinetic parameters were obtained when using $H_2O$ and $CO_2$ as gasification agents and taking into account the inhibitory effect of $H_2$ and CO.

As an example, Figure 43 shows the char conversion versus time curves for the gasification reactions with $H_2O$ of El Cerrejón coal at different temperatures and different $H_2$ fractions as inhibitory agent obtained by TGA. In the TGA tests, the coal sample is heated up immediately in $N_2$ and pyrolysis takes place until constant weight is reached at the temperature of reaction. Later, the gas mixture for char gasification is introduced.

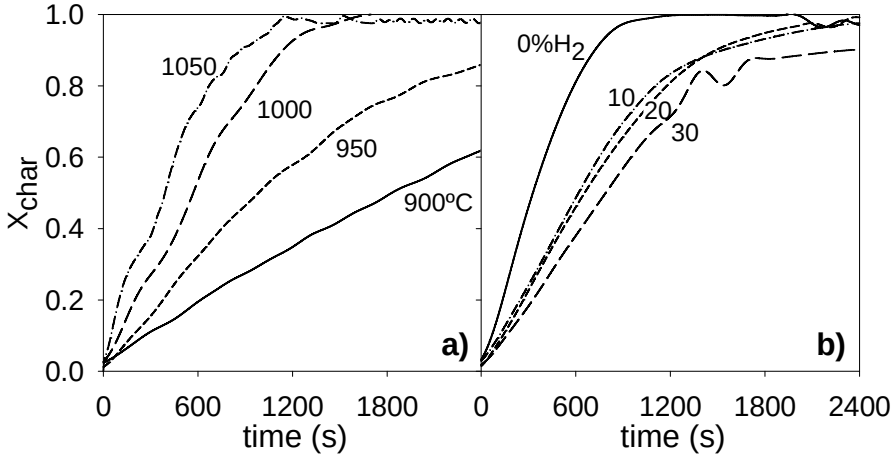


Figure 43. Char conversion versus time curves for the gasification reactions with $H_2O$ of El Cerrejón coal obtained by TGA a) at different temperatures, using 20% $H_2O$ + 0% $H_2$; and b) with 40% $H_2O$ and different $H_2$ fractions at 1000°C.

The gasification kinetic parameters were obtained when using $H_2O$ and $CO_2$ as gasification agents and taking into account the inhibitory effect of $H_2$ and CO. The gasification kinetic constants obtained are gathered in Table 10.

Table 10. Gasification kinetic constants for char from pre-treated El Cerrejón coal. Gasification agents: $H_2O/H_2$ and $CO_2/CO$.

| | $H_2O$ | | | $CO_2$ | | |
|---|---|---|---|---|---|---|
| | $k_{1,H2O}$ ($s^{-1}bar^{-1}$) | $k_{2,H2O}$ ($s^{-1}bar^{-1}$) | $k_{3,H2O}$ ($s^{-1}$) | $k_{1,CO2}$ ($s^{-1}bar^{-1}$) | $k_{2,CO2}$ ($s^{-1}bar^{-1}$) | $k_{3,CO2}$ ($s^{-1}$) |
| $k_o$ | 52.6 | $2.81 \cdot 10^{-6}$ | $8.1 \cdot 10^{-9}$ | $4.53 \cdot 10^{3}$ | $3.28 \cdot 10^{-7}$ | $1.84 \cdot 10^{-6}$ |
| $E_a$ (kJ/mol) | 95.1 | -135.1 | -218.5 | 160.1 | -158.5 | -157.6 |

## 4.2 Reaction kinetics of ilmenite

To design a CLC system it is necessary to determine the reactivity under different operating conditions of temperature and gas concentration. Thus, the objective of this section, a study published in Paper II, was to establish the kinetic of both reduction and oxidation reactions taking place in the CLC process using ilmenite as oxygen-carrier. Because of the beneficial of the use of calcined ilmenite against fresh ilmenite and the activation of the ilmenite during the redox cycles, both the reactivity of calcined and activated ilmenite was analyzed. The reaction studied was the reduction of the components in oxidized ilmenite, $Fe_2TiO_5$ and $Fe_2O_3$ to $FeTiO_3$ and $Fe_3O_4$, and vice versa for the oxidation. The experimental tests were carried out in a thermogravimetric analyzer (TGA), using $H_2$, CO and $CH_4$ as reducing gases at different temperatures (800, 850, 900 and 950 °C) and gas concentrations (5%, 15%, 30%, 50%) to analyze the reactivity of the reduction reaction. Preliminary results showed that the reaction products, i.e, $H_2O$ or $CO_2$, had no effect on the reaction rate. To analyze the reactivity of the oxidation reaction, $O_2$ was used as reacting gas at different temperatures (800, 850, 900 and 950 °C) and gas concentrations from 5 to 21 vol.%. For the study of the oxidation, the sample was first reduced at a reference temperature of 900 °C in an atmosphere composed of 5 vol.% $H_2$ and 40 vol.% $H_2O$. The starting particles ready for oxidation were composed of $Fe_3O_4$ and $FeTiO_3$, so simulating the behavior expected in a CLC system.

The oxygen transport capacity $R_{O,ilm}$ of calcined ilmenite was 4% and $R_{O,ilm}$ was 3.3% for the activated ilmenite analyzed. However, although activated particles had other $R_{O,ilm}$

values, it was found that the oxygen transference rate $R_{O,ilm} \cdot (dX_i/dt)$ is constant. A discussion about the use of kinetics when $R_{O,ilm}$ changes during the activation process can be found in Paper II. For the kinetic determination, the data used corresponded to the first reduction or oxidation period, because the reactivity of ilmenite varies during the first cycles using calcined ilmenite. Fully activated samples had no change in the reaction rates.

*Kinetics determination*

By using a particle reaction model, the kinetic parameters of the different reactions can be determined for the oxygen-carrier. The model used to determine the kinetic parameters is the grain model with uniform reaction in the particle with changing grain size model (CGSM) and with control of chemical reaction in the grain. The model assumes that the particle consists of a number of nonporous spherical grains of uniform initial radius, $r_g$. Considering that the reaction is controlled by the chemical reaction in the grain and considering spherical grains, the equations that describe this model are:

$$\frac{t}{\tau_{chr}} = 1-(1-X_i)^{1/3} \qquad \tau_{chr} = \frac{\rho_m r_g}{b k_s C_g^n} \tag{45}$$

This model describes the reduction kinetics of calcined and activated ilmenite, as well as the oxidation reaction for activated ilmenite. Nevertheless, the oxidation mechanism of calcined ilmenite was slightly different: it was a two-step mechanism that changed from a chemical reaction control to a diffusional control in the particle due to the loss of porosity inside the particle as oxidation proceeds. Thus, a mixed resistance between chemical reaction and diffusion in the solid product was needed. In this case, it was assumed that the reaction rate was controlled by chemical reaction in the grain, whereas the porosity of particles decreases because the volume of the solid products ($Fe_2TiO_5 + TiO_2$ and $Fe_2O_3$) is higher than those for the solid reactants ($FeTiO_3$ and $Fe_3O_4$). This chemically controlled step proceeds until the porosity collapses at a determined conversion value, $X_{chr}$, which will be determined from the conversion-time curves. From this point, it was assumed that the oxidation proceeds following a shrinking core model in the particle, and it is controlled by

the diffusion in the solid product layer. Furthermore, it was found that the oxygen concentration do not affect the oxidation rate when the reaction is controlled by diffusion through the product layer. The equations that describe this oxidation step are:

$$\frac{t}{\tau_{dif}} = 3\left[1-(1-X_0')^{2/3} + \frac{1-Z+(1-Z)(1-X_0')^{2/3}}{Z-1}\right] \qquad \tau_{dif} = \frac{\rho_m\, r_p^2}{6\,\bar{b}\,D_e} \tag{46}$$

The reaction order, *n*, with respect to each reacting gas was obtained from the calculus of $X_{chr}$ by fitting the experimental curves conversion-time to the model equations for different gas concentrations.

From experiments done at different temperatures, values for the chemical reaction kinetic constant, $k_s$, as a function of the temperature were obtained. The dependence on the temperature of the kinetic constant was assumed to be Arrhenius type. More details about the parameter calculations and kinetic model can be found in Paper II.

As example, Figure 44 shows plots of the effect of $H_2$ concentration on the conversion-time curves, and Figure 45 represents plots of the effect of $O_2$, together with the corresponding model predictions of conversion-time for calcined and activated ilmenite.

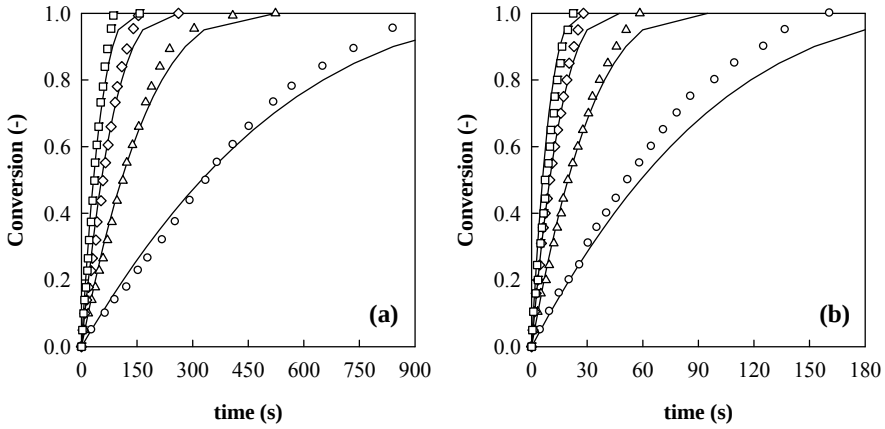


Figure 44. Effect of $H_2$ concentration on the reduction reaction for (a) calcined and (b) activated ilmenite. T=900 °C. $H_2$ concentration: ○ 5 vol.%; △ 15 vol.%; ◇ 30 vol.%; □ 50 vol.%. 20 vol.% $H_2O$; $N_2$ to balance. Continuous line: model predictions.

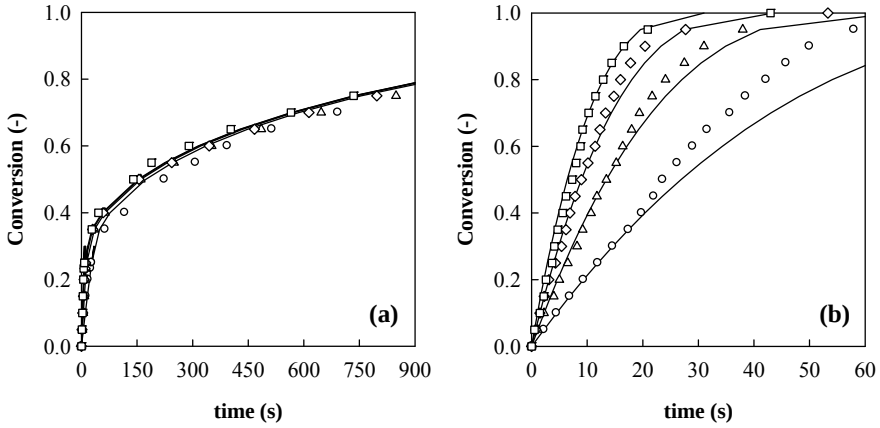


Figure 45. Effect of $O_2$ concentration on the oxidation reaction for (a) calcined and (b) activated ilmenite. T=900 ºC. $O_2$ concentration: ° 5 vol.%; ▵ 10 vol.%; ◇ 15 vol.%; ▫ 21 vol.%. $N_2$ to balance. Continuous line: model predictions.

It can be seen that the reaction models proposed predicted adequately the experimental results in all range of operating conditions studied for both calcined and activated ilmenite. Table 11 gathers the obtained kinetic parameters for ilmenite reduction with $H_2$, CO and $CH_4$, and oxidation with $O_2$ for both calcined and activated ilmenite.

Table 11. Kinetic parameters for ilmenite reduction with $H_2$, CO and $CH_4$, and oxidation with air.

| | Calcined | | | | Activated | | | |
|---|---|---|---|---|---|---|---|---|
| | $H_2$ | CO | $CH_4$ | $O_2$ | $H_2$ | CO | $CH_4$ | $O_2$ |
| $\rho_m$ (mol/m$^3$) | 13590 | 13590 | 13590 | 31100 | 13590 | 13590 | 13590 | 31100 |
| $r_g$ (m) | $0.5\ 10^{-6}$ | $0.5\ 10^{-6}$ | $0.5\ 10^{-6}$ | $0.48\ 10^{-6}$ | $1.25\ 10^{-6}$ | $1.25\ 10^{-6}$ | $1.25\ 10^{-6}$ | $1.20\ 10^{-6}$ |
| $\bar{b}$ | 1.19 | 1.19 | 4.74 | 4 | 1.45 | 1.45 | 5.78 | 4 |
| $k_{s0}$(mol$^{1-n}$ m$^{3n-2}$ s$^{-1}$) | $5.1\ 10^{-1}$ | $2.1\ 10^{-1}$ | 8.8 | $8.0{\cdot}10^{-5}$ | $6.2{\cdot}10^{-2}$ | $1.0{\cdot}10^{-1}$ | 10.5 | $1.9{\cdot}10^{-3}$ |
| $E_{cbr}$ (kJ/mol) | 109 | 113 | 165 | 12 | 65 | 81 | 136 | 25 |
| $n$ | 1 | 1 | 1 | 1 | 1 | 0.8 | 1 | 1 |
| $D_{e0}$ (mol m$^{-2}$ s$^{-1}$) | | | | $1.37{\cdot}10^{-5}$ | | | | |
| $E_{dif}$ (kJ/mol) | | | | 77 | | | | |

*Analysis of the reactivity from the kinetic data*

To analyze the reactivity of ilmenite and to compare it with other oxygen-carriers, a preliminary estimation of the solids inventory needed for the gaseous fuels $H_2$, CO and $CH_4$ is calculated. To do that, the reaction kinetics of ilmenite were introduced in the model proposed by Abad et al. (2007a). The simplified model considers perfect mixing of solids, no restriction for the gas-solid contact and the solid reaction following the shrinking core model. This model considers the effect of residence time distribution of ilmenite on its reactivity. The kinetic parameters can be introduced in this model describing the reactors of a CLC system with gaseous fuels.

Minimum solid inventories showed in

Table 12 can be compared to the solids inventory calculated for several synthetic oxygen-carriers (Abad et al.,2007a; Zafar et al.,2007a,b). For comparison purposes with other oxygen-carriers, only the minimum solids inventory for activated particles is considered, as activation is expected to occur quickly in the CLC system. The solids inventories calculated for the air-reactor (30-47 kg/$MW_{th}$) are in the range of those calculated for other Ni-, Cu-, Mn- and Fe-based oxygen-carriers, which were in the range 10-60 kg/$MW_{th}$. On the contrary, the calculated solids inventories in the fuel-reactor for ilmenite were usually higher than those obtained for other oxygen-carriers. For ilmenite the solids inventories were in the range 42-66 kg/$MW_{th}$ for $H_2$, 105-189 kg/$MW_{th}$ for CO and 167-461 kg/$MW_{th}$ for $CH_4$. For a highly reactive synthetic Fe-based oxygen-carrier the solids inventory obtained for $H_2$ and CO were 12 kg/$MW_{th}$ and 29 kg/$MW_{th}$, respectively; whereas the solids inventory for $CH_4$ was 950 kg/$MW_{th}$. Nevertheless, lower solids inventories were calculated for methane using other oxygen-carriers, e.g. in the range 10-20 kg/$MW_{th}$ for Ni-based oxygen-carriers, 52 kg/$MW_{th}$ for a Cu-based oxygen-carrier or 85 kg/$MW_{th}$ for a Mn-based oxygen-carrier (Abad et al., 2007a; Zafar et al., 2007a,b). Note that these values were obtained without considering bubble-emulsion resistance, but are useful for comparison purposes.

Table 12. Minimum solid inventory data for calcined and activated ilmenite (kg of solids per $MW_{th}$ of fuel), calculated for $\Delta X = 0.5$.

| | Calcined | | | Activated | | |
|---|---|---|---|---|---|---|
| Fuel-Reactor | $H_2$ | CO | $CH_4$ | $H_2$ | CO | $CH_4$ |
| $\overline{C}_g$ (% of fuel) | 14.5 | 14.5 | 5.3 | 14.5 | 19.2 | 5.3 |
| T | | | | | | |
| 900°C | 299 | 955 | 4481 | 66 | 189 | 461 |
| 950°C | 197 | 619 | 2337 | 52 | 139 | 272 |
| 1000°C | 135 | 416 | 1285 | 42 | 105 | 167 |
| Air-Reactor | $H_2$ | CO | $CH_4$ | $H_2$ | CO | $CH_4$ |
| 900°C | 75 | 64 | 90 | 39 | 33 | 47 |
| 950°C | 74 | 63 | 89 | 37 | 31 | 44 |
| 1000°C | 74 | 63 | 89 | 35 | 30 | 42 |

The use of ilmenite for the combustion of methane is not adequate, but the use of ilmenite for syngas combustion could be interesting. Thus, the first approach for solid inventories needed for ilmenite take acceptable values for the main products of coal devolatilization and gasification, in the same range as the values observed for synthetic oxygen-carriers with proven suitability for CLC (Zafar et al., 2007a). Thus, the use of ilmenite for coal it is highly recommended because ilmenite is harmless for the environment and a considerably cheaper material than a synthetic material.

## 4.3 Theoretical approach on the CLC performance with solid fuels

The objective of this section, which constitutes Paper VIII, was to optimize the operating conditions for direct CLC with solid fuels using ilmenite as oxygen-carrier. Two of the key parameters in the design of a CLC system are the solids circulation rate and the solids inventory. This section approaches the design of an iG-CLC system using HV bituminous Colombian coal El Cerrejón as fuel.

### 4.3.1 Calculation of the solids circulation rate

Figure 46 shows the solids circulation rate calculated as a function of the solid conversion variation between air- and fuel-reactors, ΔX, considering "El Cerrejón" coal as fuel. A solids circulation rate value of $\dot{m}_{OC}$ = 16 kg/s per $MW_{th}$ is considered to be the maximum circulation rate feasible in a CLC unit without increased costs according to commercial experience on CFB systems (Abad et al., 2007c). That is, the solids circulation rate that can be used with el Cerrejón coal is between 2.04 and 16 kg/s per $MW_{th}$. The result is that ΔX can be within the range 0.13-1.

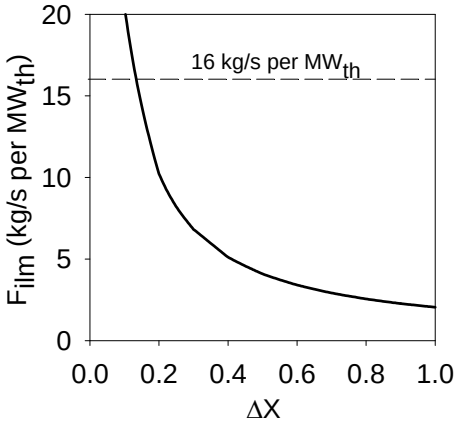


Figure 46. Solids circulation rate as a function of the solid conversion variation between air- and fuel-reactors, ΔX. Fuel: "El Cerrejón" coal.

### 4.3.2 Calculation of the solids inventory in the fuel-reactor

In this section a theoretical model for the fuel-reactor has been developed based on a simple reacting scheme for the flow patterns of gas and solids, but describing the complex chemical processes happening in the fuel-reactor. The gasification kinetics of El Cerrejón coal for both $H_2O$ and $CO_2$ as gasification agents and the kinetics of the reduction reaction of ilmenite with $H_2$, CO and $CH_4$ are incorporated to the model. The model also includes the possibility of using a carbon separation system to recirculate unreacted char particles that exit from the fuel-reactor. The simulated results have been first compared to experimental results from tests performed in the ICB-CSIC-s1 unit. Simulations were done

afterwards to study the effect of the main operating variables of the fuel-reactor (e.g. temperature, solids inventory, efficiency of the carbon separation system, oxygen-carrier to fuel ratio, or flow and type of gasification agent) on the combustion and carbon capture efficiencies. The effect of the main operating variables in the iG-CLC process can be analyzed in a simpler way than using a detailed model.

*Differential mass balances in the fuel-reactor*

The differential mass balances are defined according to Eqs. (47)-(49), which are the scheme of ilmenite reduction reactions happening simultaneously in the fuel-reactor:

$$Me_xO_y + CH_4 \rightarrow Me_xO_{y-1} + CO + 2\,H_2 \quad (47)$$

$$Me_xO_y + H_2 \rightarrow Me_xO_{y-1} + H_2O \quad (48)$$

$$Me_xO_y + CO \rightarrow Me_xO_{y-1} + CO_2 \quad (49)$$

The pattern of gas and solids here assumed were based on the previous results obtained in the ICB-CSIC-s1 unit fuelled with the bituminous Colombian coal "El Cerrejón". In these experiments, it was found that unconverted $CH_4$, CO and $H_2$ from the fuel-reactor were mainly coming from unconverted volatile matter. However, neither tars nor other hydrocarbons than $CH_4$ were found. Also, gasification products were highly converted to $CO_2$ and $H_2O$. A bad contact between volatile matter and oxygen-carrier particles was proposed as the main reason for incomplete combustion.

Based on these results, a model of the system was developed to predict and optimize the combustion and carbon capture efficiencies of the CLC process as a function of various operational parameters. The oxygen-carrier bed in the fuel-reactor was considered to be divided into two separated zones: one zone is in contact with the volatiles, with reducing species CO, $H_2$ and $CH_4$; and the other zone reacts with the generated gasification products, CO and $H_2$. Both gaseous flows are assumed to be independent and in plug flow. The gas flow inside the reactor is simplified and the bubble-emulsion two-phase theory is not considered. In order to solve the whole system, the reactor was considered to be divided into compartments with differential bed mass. Figure 47 shows a scheme of this assumed flow pattern. The gasification products generated in the dense bed have good

contact with the oxygen-carrier particles. The volatiles are released in a plume and they have poorer contact with the oxygen-carrier. To take this into account, the parameter $\chi_{OC,v}$ is introduced as the fraction of the oxygen-carrier bed that is in contact with the volatiles. It is considered that there is perfect mixing of the solids and no constrictions for the gas-solid reactions. This model assumes that there is no gas exchange between the flow of gasification products in the dense bed and volatile plume. Also, the model assumes that the only reducing species in the dense bed are $H_2$ and CO, whereas $CH_4$ also appears in the flow coming from the volatile plume.

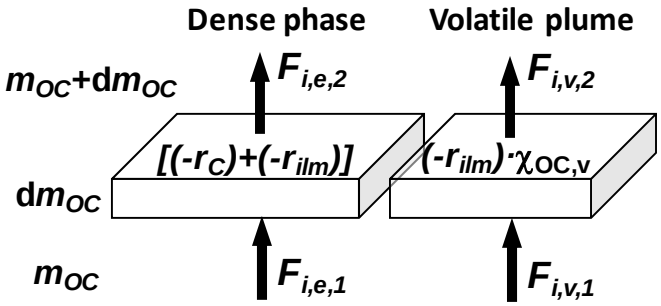


Figure 47. Mass flows changes of the gases involved in the process –products of gasification and devolatilization- for a fuel-reactor element of differential mass, $dm_{OC}$.

The changes of the mass flow in a differential mass of the reactor have been considered in the model. The reaction of the oxygen-carrier with the volatile matter species and char gasification products is considered separately, to take into account that they are generated in a different location and have different contact with the oxygen-carrier. Therefore, the mass balances for the $H_2$ and CO generated from char gasification are expressed by Eq. (50) and (51), respectively. For the volatile matter released reducing species, i.e., $CH_4$, $H_2$ and CO, the mass balances are Eqs. (52-54). These equations show the variation of the molar flows of $H_2$, CO and $CH_4$ -$F_{H_2}$, $F_{CO}$ and $F_{CH_4}$, respectively-, for the gasification and devolatilization products in a differential bed with mass inventory $dm_{OC}$. Neither sulfur nor nitrogen present in the fuel were considered in this simple model.

Mass balances in dense bed:

$$\frac{\partial F_{H_2}}{\partial m_{OC}} + \left[ \frac{1}{2d \cdot M_O} (-r_{ilm,H_2}) - \frac{f_C}{1-f_C} (-r_C)_{H_2O} \frac{1}{M_C} \right] = 0 \qquad (50)$$

$$\frac{\partial F_{CO}}{\partial m_{OC}} + \left[ \frac{1}{2d \cdot M_O}(-r_{ilm,CO}) - \frac{f_C}{1-f_C}(-r_C)_{H_2O}\frac{1}{M_C} - 2\frac{f_C}{1-f_C}(-r_C)_{CO_2}\frac{1}{M_C} \right] = 0 \quad (51)$$

Mass balances in volatile plume:

$$\frac{\partial F_{CH_4}}{\partial m_{OC}} + \frac{1}{2d \cdot M_O}(-r_{ilm,CH_4}) \cdot \chi_{OC,v} = 0 \quad (52)$$

$$\frac{\partial F_{H_2}}{\partial m_{OC}} + \frac{1}{2d \cdot M_O}(-r_{ilm,H_2}) \cdot \chi_{OC,v} + 2\frac{\partial F_{CH_4}}{\partial m_{OC}} = 0 \quad (53)$$

$$\frac{\partial F_{CO}}{\partial m_{OC}} + \frac{1}{2d \cdot M_O}(-r_{ilm,CO}) \cdot \chi_{OC,v} + \frac{\partial F_{CH_4}}{\partial m_{OC}} = 0 \quad (54)$$

$(-r_C)_{H_2O}$ and $(-r_C)_{CO_2}$ are the char gasification rates with $H_2O$ and $CO_2$, respectively. $f_C$ is the carbon fraction in the fuel-reactor bed. Char is supposed to have constant concentration throughout the reactor and it is uniformly distributed in the bed in perfect mixing. The gasification takes place simultaneously with the reaction of the released volatile matter and gasification products with ilmenite. $(-r_{ilm,H_2})$, $(-r_{ilm,CO})$ and $(-r_{ilm,CH_4})$ are the reaction rates of ilmenite with $H_2$, CO and $CH_4$, respectively.

To solve the mathematical model it was assumed that the coal devolatilization takes place instantaneously at the coal feeding level. The composition of the released volatiles from El Cerrejón coal was obtained experimentally by devolatilization in a fluidized bed using silica sand as bed material and $H_2O$ or $CO_2$ as fluidizing gas, see Table 13.

Table 13. Mass (g) of the different gaseous species generated from the release of the volatile matter of 100 g of El Cerrejón coal after $CH_4$ reforming, for different $H_2O$-$CO_2$ mixtures as gasification agent.

| Gasification agent | CO | $CO_2$ | $CH_4$ | $H_2O$ | $H_2$ |
|---|---|---|---|---|---|
| 100% $H_2O$ | 5.7 | 42.8 | 7.1 | -27.8 | 5.5 |
| 50% $H_2O$ + 50% $CO_2$ | 23.1 | 12.7 | 8.8 | -14.7 | 3.4 |
| 100% $CO_2$ | 46.5 | -29.1 | 9.9 | 4.8 | 1.2 |

The difference between the released devolatilized species for different $H_2O$:$CO_2$ composition is because there is some $CH_4$ reforming taking place with. In some cases of the compositions given the values of $H_2O$ or $CO_2$ have negative values, because some $H_2O$ and $CO_2$ was taken from the gasification agent flow for the partial $CH_4$ reforming.

The implementation of a carbon separation system to obtain high carbon capture was also assessed. The use of a highly efficient carbon separation system with high efficiency, $\eta_{CS}$, ensures high extent of gasification, and thereby high carbon capture, by increasing char residence time in the fuel-reactor. $\eta_{CS}$ is defined as the fraction of carbon in char that is separated and recirculated back to the fuel-reactor with respect to the carbon in the char that exits the fuel-reactor together the flow of oxygen-carrier particles. Figure 48 represents a scheme of the carbon flows involved in the fuel-reactor and carbon separation system.

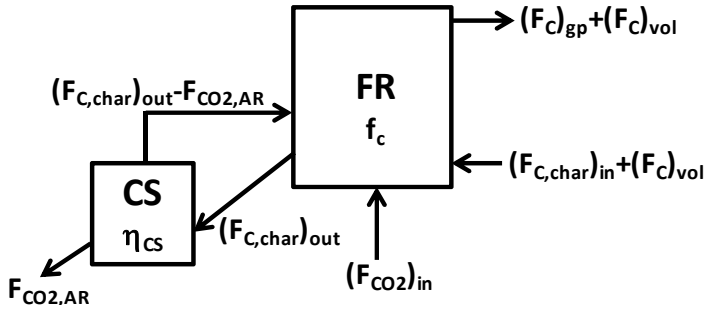


Figure 48. Scheme of carbon flows in the fuel-reactor and carbon separation system.

$(F_{C,char})_{in}$ is the carbon flow of char in the coal feed; $(F_{C,char})_{out}$ is the carbon flow of ungasified char that exits the fuel-reactor; $(F_C)_{gp}$ is the flow of carbon contained in the products of char gasification; and $(F_C)_{vol}$ is the flow of carbon in volatiles. $(F_{C,char})_{out}$ depends on the solids recirculation rate, $\dot{m}_{OC}$, which is the oxygen-carrier circulation rate. Thus, the carbon capture depends on the solids circulation rate.

The global balance to the whole reactor is done by integrating the differential equations over the total bed mass inventory. To solve the system of simultaneous differential equations, the Runge–Kutta–Merson method was used. To find the solution of the system, a value of ilmenite conversion variation $\Delta X$ and of carbon fraction in the bed $f_C$ are

initially assumed and the system is solved in two interconnected loops. In the internal loop, with the assumed value of $f_C$ the system of differential equations is integrated and with these data the outlet gaseous flows are obtained, as well as the carbon flow that returns from the carbon separation system and that leaves the fuel-reactor. With the last carbon flow $f_C$ is recalculated, until the convergence is reached after successive approaches. Once the carbon balance has converged, the oxygen balance that would give the value of $\Delta X$ for the fixed ilmenite circulation rate must be accomplished. With this new value the calculations are repeated until the simultaneous convergence for both $f_C$ and $\Delta X$ is reached.

Initially, a value of the oxygen-carrier conversion variation $\Delta X$ is assumed. Thus, considering an initial value of carbon fraction in the fuel-reactor bed $f_C$, the values of the flows of $H_2$, CO, $CH_4$, $CO_2$ and $H_2O$ outgoing the reactor are obtained. To solve the whole equation system, the flow of carbon that exits the fuel-reactor must fulfill the carbon mass balance in the system, as shown in Figure 48. This carbon flow depends on $f_C$ and the total outlet flow of the fuel-reactor is determined by the ilmenite circulation rate. Iterations on $f_C$ must be done until the carbon mass balance is fulfilled. From the final outlet gaseous flows a new value of $\Delta X$ is obtained. And the iterative method must be used again until both parameters converged to obtain the solution to the mathematical model.

The model was developed and applied to the natural mineral ilmenite as oxygen-carrier and El Cerrejón bituminous Colombian coal as fuel. More details about the model are found in Paper VIII. Predictions of the coal conversion in the ICB-CSIC-s1 unit used in the experimental work were carried out with the model.

The direct application of the model predicted the experimental values of char conversion and carbon capture, see Figure 49.a), but it predicted full combustion. The fraction of oxygen-carrier in contact with the volatile matter $\chi_{OC,v}$ that predicts the combustion efficiencies obtained experimentally at different temperatures is 0.53%, see Figure 49.b). $\chi_{OC,v}$ =0.53% is a rather low value, that is, the volatile matter released in the plume in the experimental facility had indeed bad contact with the oxygen-carrier.

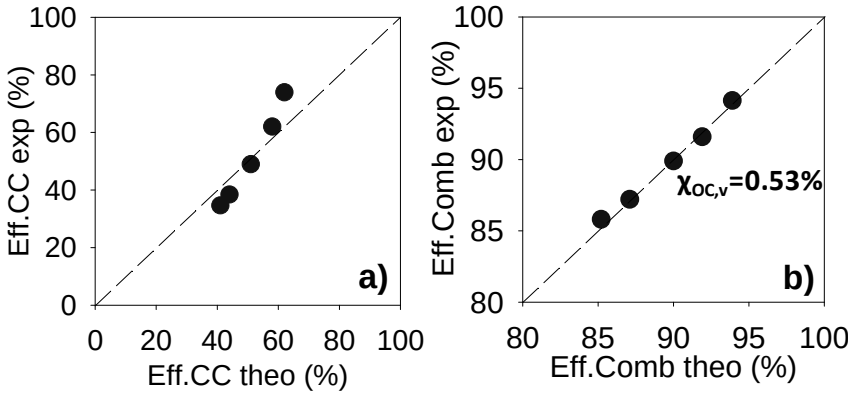


Figure 49. Experimental values obtained for a) Carbon capture and b) Combustion efficiency compared to the theoretical with the model simulated values at different temperatures ($T_{FR}$: 880-925°C). Inventory: 3100 kg/$MW_{th}$. $\eta_{CS}=0$.

As an example of the model predictions, Figure 50 represents the evolution of $CH_4$, $H_2$, CO, $CO_2$ and $H_2O$ molar flows within the fuel-reactor bed, expressed as mass fraction of the bed, $m_{OC}/m_{OC,tot}$, for a solids inventory of 3100 kg/$MW_{th}$, as used in the experimental work. Figure 50Figure 51.a) shows the flows in the dense bed, that is, derived from the gasification; Figure 50.b) represents the evolution of the volatile matter species released in the plume; and the total sum of the flows of both phases is shown in Figure 50.c).

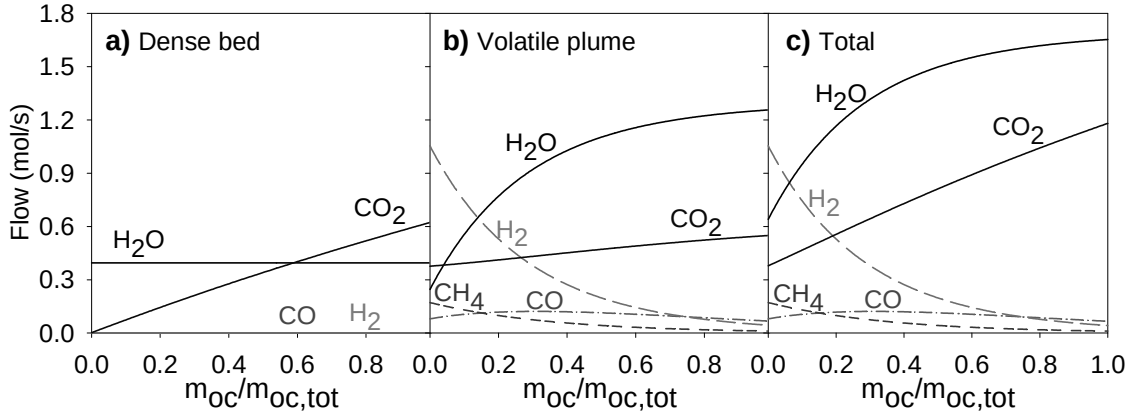


Figure 50. Evolution of the a) in the dense bed b) in the plume and c) total $CH_4$, $H_2$, CO, $CO_2$ and $H_2O$ molar flows within the fuel-reactor bed, for a solids inventory of 3100 kg/$MW_{th}$. $T_{FR}=900$ °C. $H_2O/C=0.7$. $\phi=2$. $\eta_{CS}=0$. $X_{o,in}=0$. $\chi_{OC,v}=0.53\%$.

In the dense bed all the gasification products, i.e., $H_2$ and CO, are fully oxidized by the oxygen-carrier and the dense bed is only composed by increasing $CO_2$ from char oxidation

and the $H_2O$ as gasification agent. In the plume both $CH_4$ and $H_2$ decrease when the reactor mass increases. $CH_4$ comes only as part of the released volatile matter species and is gradually consumed by its oxidation with the oxygen-carrier. $H_2$ and CO come from volatile matter release and as intermediates of $CH_4$ oxidation. $H_2$ disappears along the bed mass as it is quickly oxidized by ilmenite, while the CO profile has a smooth maximum because there is competition between the CO generation in the $CH_4$ conversion and its slower reaction with ilmenite.

After seeing that there is a good agreement between the values predicted by the model and the experimental results with a determined $\chi_{OC,v}$, simulation and process optimization can be performed. The effect of the main variables in CLC with solid fuels was analyzed, taking the solids inventory as independent variable.

***Influence of the fuel-reactor temperature, solids inventory and implementation of a carbon separation system***

The following calculations were made on the basis of 1 $MW_{th}$ fuel power (see coal analysis in Table 2). Simulations showed that $\eta_{CC}$, $X_{char}$ and $\eta_{comb\ FR}$ increase with increasing solids inventory in the fuel-reactor for all temperatures simulated. For all the temperatures simulated and up to a solids inventory of 2000 kg/$MW_{th}$ all efficiencies increased substantially. For higher inventories the beneficial effect was not so intense. Gasification and combustion reactions are promoted with the temperature, and thus $X_{char}$, $\eta_{CC}$ and $\eta_{comb\ FR}$, increased at higher temperatures.

If the inventory is doubled from 1000 to 2000 kg/$MW_{th}$, $\eta_{comb\ FR}$ increases from 73.1% to 89.0%. If the inventory is again doubled to 4000 kg/$MW_{th}$, the increase is less substantial, $\eta_{comb\ FR}$ is 97.2%, so it is not worth it to increase so much the solids inventory, as well as the increased pressure drop and operational cost, size and investment of such big facility. At 950ºC as reference temperature, and with an inventory of 2000 kg/$MW_{th}$, values obtained for char conversion and carbon capture efficiency were $X_{char}=0.334$ and $\eta_{CC}=0.525$.

The first simulations were done considering that there was no carbon separation system. In order to get higher extent of gasification, it was proposed to implement one. Figure 51 shows the simulated char conversion, carbon capture and combustion efficiencies with a wide range of oxygen-carrier inventories for a carbon separation system of efficiency 0%, 80%, 90% and 100%. Higher $\eta_{CS}$ leads to higher $\eta_{CC}$, which is essential in this process. Note the important increase in $\eta_{CC}$ and $X_{char}$ when using the carbon separation system. This points out the importance of implementing a carbon separation system in iG-CLC.

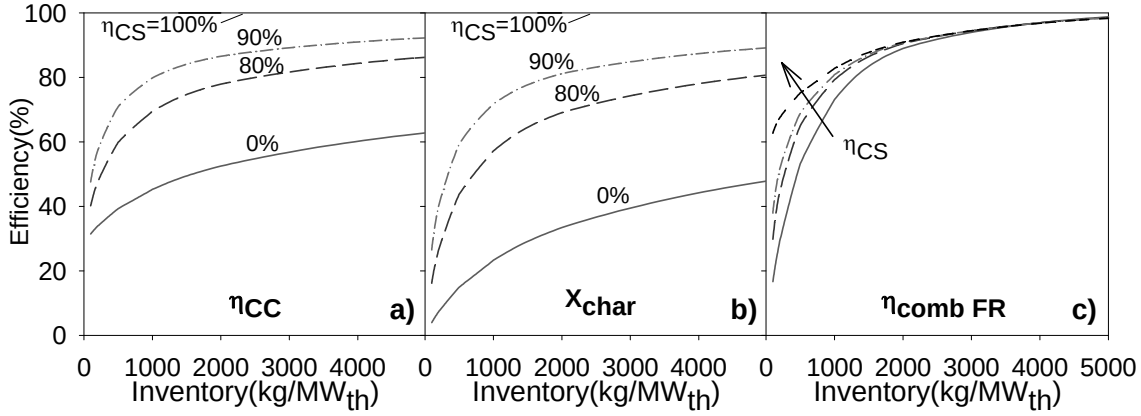


Figure 51. Variation of a) carbon capture, b) char conversion and c) combustion efficiency with increasing solids inventory for $\eta_{CS}$=0, 80%, 90% and 100%. $T_{FR}$=950°C. $H_2O/C$=0.7. $\phi$=2. $\eta_{CS}$=0. $X_{o,in}$= 0. $\chi_{OC,v}$ =0.53%.

Considering an iG-CLC system with a carbon separation system of $\eta_{CS}$=90%, the effect of the temperature and inventory is assessed. Figure 52.a) and b) represents the carbon capture and char conversion in the process, where it can be seen that to get high performance, an inventory between 1000 and 2000 kg/$MW_{th}$ seem to be necessary and reasonable. To get high gasification and oxidation rates, it is necessary to work at high temperatures. As an example, with an inventory of 2000 kg/$MW_{th}$ and $\eta_{CS}$=90%, predictions of $\eta_{CC}$ of 79.3% at 900°C and 90.7% at 1000°C were obtained.

The simulated performance of the process regarding the oxidation of volatiles and gasification products is shown in Figure 52.c), where it can be seen that the fuel-reactor combustion efficiency grows with the temperature because of the increase in the oxidation rat of ilmenite. Above 900°C, the minimum solids inventory needed to obtain $\eta_{comb\ FR}$

above 85% is 1000 kg/$MW_{th}$. As an example, with a solids inventory of 2000 kg/$MW_{th}$, the simulated resulting $\eta_{comb\ FR}$ was 86.0% at 900°C and 94.2% at 1000°C. For an optimum performance of the iG-CLC system, it would be best to have a carbon separation system with high $\eta_{CS}$ and to operate at temperatures above 950°C. However, simulations showed that although the temperature of operation was high, with high oxygen-carrier inventory and high $\eta_{CS}$, there would be still some unburnt volatile matter and a subsequent oxygen polishing step would be necessary to fully oxidize the unburnt gases in the outlet stream from the fuel-reactor.

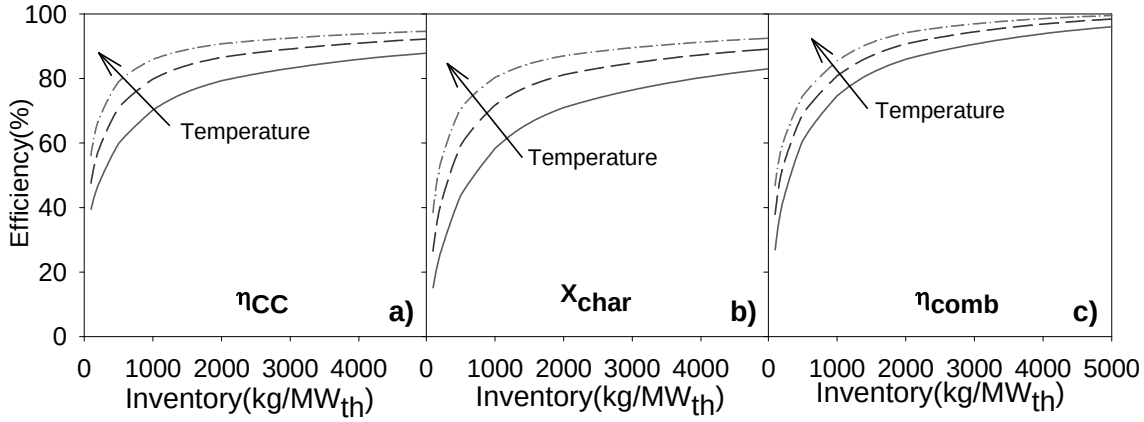


Figure 52. Variation of a) carbon capture and b) char conversion with increasing solids inventory for several fuel-reactor temperatures. ——900°C, ----950°C and ·····1000°C. $H_2O/C=0.7$. $\phi=2$. $\eta_{CS}=90\%$. $X_{o,in}=0$. $\chi_{OC,v}=0.53\%$.

*Influence of other operational parameters*

Although the main parameters that turned out to determine the efficiency of the iG-CLC process are the temperature of operation, the solids inventory and the efficiency of the carbon separation system, other operational parameters also influence on the efficiency of the process, although to a lower extent.

The system was evaluated for variation the steam to fixed carbon ratio, $H_2O/C$, considering steam as gasification agent. It turned out that the $H_2O/C$ ratio has no influence on the combustion efficiency and little influence on the gasification step. Although a $H_2O/C$ ratio of 0.4 could be insufficient to ensure high gasification extent, it would be

reasonable to work with a $H_2O/C$ ratio of 0.7-1, since there is no major benefit on working with higher $H_2O/C$ ratios.

The influence of the gasification agent type was simulated with various $H_2O$:$CO_2$ mixtures. The gasification agent type has minor effect on the combustion efficiency. When gasifying with higher fraction of $CO_2$ only CO is produced, whereas when gasifying with $H_2O$, $H_2$ is also generated. But although ilmenite reacts faster with $H_2$ than with CO, the reaction rate of ilmenite is fast if there is enough inventory and $\eta_{comb\ FR}$ has no substantial change. The carbon capture increase when there is higher steam fraction in the gasification agent, being this less noticeable for higher $\eta_{CS}$. This is because for this fuel the gasification rate with steam is faster than with $CO_2$.

The carbon capture efficiency decreases for higher oxygen-carrier to fuel ratio. High oxygen-carrier to fuel ratio means high solids recirculation rate and thereby low residence time, which entails a decrease in the char conversion in the bed. The lower residence time leads to lower extent of gasification and thereby lower $\eta_{CC}$.

The effect of the reactivity of the oxygen-carrier was also evaluated. The simulations showed that $\eta_{comb\ FR}$ increases with higher oxygen-carrier reaction rate, but the influence in $X_{char}$ and $\eta_{CC}$ is negligible. Thus, the use of an oxygen-carrier with high reactivity is important to reach high $\eta_{comb\ FR}$, but is not the key factor in iG-CLC to get high $\eta_{CC}$. The major limitation to reach high $\eta_{comb\ FR}$ was the poor contact of the volatiles with the dense bed, and not the reactivity of the oxygen-carrier.

The fraction of oxygen-carrier in contact with the volatile matter, $\chi_{OC,v}$, resulted to be quite poor. Some design solutions can be applied in order to increase $\chi_{OC,v}$. Figure 53 shows that there is a big effect of $\chi_{OC,v\ s}$ on the combustion efficiency and $\eta_{comb\ FR}$ increases from 80.8% to 99% if $\chi_{OC,v}$ increased from 0.53% to 3% with an inventory of 1000 kg/$MW_{th}$. The char conversion and carbon capture are not affected.

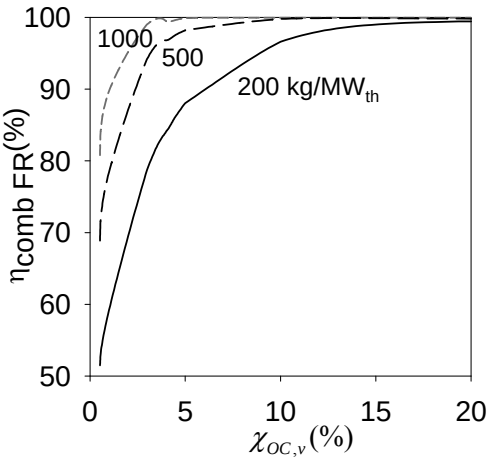


Figure 53. Combustion efficiency variation with increasing $\chi_{OC,v}$ for: ── 200 kg/$MW_{th}$, ---- 500 kg/$MW_{th}$ and ····· 1000 kg/$MW_{th}$. $T_{FR}$=950°C. $H_2O/C$=0.7. $\phi$=2. $\eta_{CS}$=90%. $X_{s,in}$= 0.

A second option to fully burn the volatile matter is to implement a second step in the fuel-reactor (FR2), whose fuel would be the outlet gaseous stream of the solid fuelled fuel-reactor (FR1). It is also an alternative to the oxygen polishing step. As the fuel is gaseous, this second reactor would not be limited by the gasification step and the contact efficiency would be much higher, since the fuel would be introduced at the bottom of the reactor and not released in a plume. The simulated values obtained for the second step fuel-reactor FR2 are about 44 kg/$MW_{th}$ to fully oxidize the fuel for FR1 1000-2000 kg/$MW_{th}$, see Figure 54.

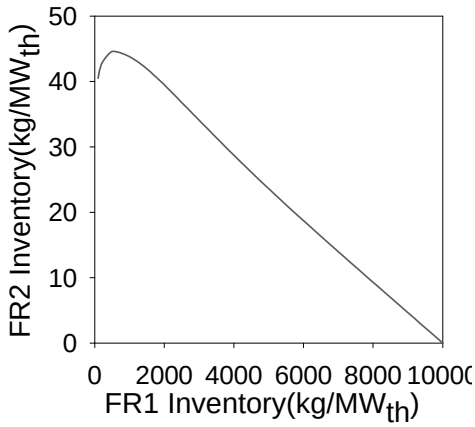


Figure 54. Minimum ilmenite inventory in the second fuel-reactor to completely oxidize the fuel for different inventories in the first fuel-reactor. $T_{FR}$=950°C. Conditions in the first fuel-reactor: $H_2O/C$=0.7. $\phi$=2. $\eta_{CS}$=90%. $X_{s,in}$= 0. $\chi_{OC,v}$=0.53%.

This second step could be made by using a two-step reactor if the fuel-reactor works with bubbling bed conditions. However, if the reactor is a circulating bed, it would be necessary to install a second reactor or it would be also feasible to improve the solid-gas contact by means of internals in the diluted region.

The simulations done with the simplified model for the iG-CLC process showed that an optimized CLC system for solid fuels with ilmenite as oxygen-carrier should have a carbon separation system with high efficiency above 90%, work at a high fuel-reactor temperature -desirably above 950ºC- and would need 1000-2000 kg/$MW_{th}$ of inventory. These parameters would lead to high carbon captures above 90%. The contact efficiency of the volatile matter with the oxygen-carrier should be increased with some design solutions. The implementation of a second fuel-reactor whose inventory was calculated to be around 44 kg/$MW_{th}$ is proposed as a very promising option to fully burn the volatile matter and avoid an extra oxygen polishing step.

# 5 Conclusions

The feasibility and performance of the Chemical-Looping Combustion technology for solid fuels was studied. The natural mineral ilmenite was used as oxygen-carrier regarding its properties, low cost and because it is environmentally friendly. The conditions and key parameters that improve the process efficiency were evaluated, in order to get a competitive combustion technology with low cost $CO_2$ capture. This was studied by doing tests in a thermogravimetric analyzer (TGA), a batch fluidized bed reactor for gaseous fuels, a batch fluidized bed reactor for solid fuels and a continuous CLC unit for solid fuels, the ICB-CSIC-s1, all these devices are placed at the Instituto de Carboquímica (ICB-CSIC) in Zaragoza (Spain). Tests in a 10 $kW_{th}$ continuous CLC unit for solid fuels at Chalmers University of Technology in Göteborg (Sweden) were also done.

Focus was made on analyzing the behavior and suitability of ilmenite as oxygen-carrier in CLC with solid fuels by in-situ gasification CLC (iG-CLC). Ilmenite was seen to undergo an activation process, since it increases its reactivity with the number of redox cycles. After several cycles, reduction and oxidation rate of ilmenite reaches a maximum value which is maintained after many hours of operation. The higher is the conversion variation reached in the redox cycles, the faster is the activation. Previous calcination of ilmenite has a positive effect on the activation process. After activation, the reactivity for $H_2$ and CO rises around 5 times, while for $CH_4$ this increase is about 15 times. The activated ilmenite exhibited high reactivity in both reduction and oxidation reactions. Reaction with $H_2$ is faster than with CO and $CH_4$. Times for complete conversion at 950 °C lower than 120 s using 15% of $H_2$, CO or $CH_4$, and 30 s using 21% of $O_2$ in TGA.

Structural changes on ilmenite particles after activation were observed. The most remarkable is the porosity increase in the particles: for calcined particles it was 1.2% and it increased up to 38% after 100 cycles in batch fluidized bed with a conversion of 65%. It was observed the appearance of cracks and an external shell in the particle, which is Fe enriched. As activation proceeds the reactivity increases, but the oxygen transport capacity of ilmenite decreases due to the physical segregation of $Fe_2TiO_5$ in the oxidized ilmenite and the appearance of an external shell which is enriched in free $Fe_2O_3$. The higher is the conversion variation reached in the redox cycles, the faster is the segregation of $Fe_2TiO_5$

and the decrease in the oxygen transport capacity. The initial oxygen transport capacity value is 4.0% and it decreased until 2.1% after 100 redox cycles in batch fluidized bed with a conversion of 65%. However, in continuous testing with an average conversion of 30%, the oxygen transport capacity after almost 100 hours of operation only decreased to 3.9%.

In comparison to other oxygen-carriers and in particular to iron-based carriers, the oxygen transport capacity and reactivity showed for ilmenite have high enough values to transfer the required oxygen from air to fuel in a CLC system. As for its fluidization properties, low attrition values were found for ilmenite during fluidized-bed operation, and no defluidization was seen for typical CLC operating conditions.

98 hours of continuous operation with coal feed and 122 hours of fluidization were made in the ICB-CSIC-s1 CLC facility. The operation performance was assessed in these tests using different solid fuels ranging from lignite to anthracite and evaluating the effect of operational parameters on carbon capture and combustion efficiency.

In all cases, unburnt compounds were found in the gas stream from the fuel-reactor. The outgoing unburnt gases in the fuel-reactor were measured when using coal as fuel, that is, $CH_4$, CO and $H_2$, which came from volatile matter that had not been fully oxidized. Gasification products were fully oxidized.

The combustion efficiency in the fuel-reactor is higher for higher temperature, higher solids inventory and for solid fuels with lower volatile content and with faster gasification rate. The combustion efficiency was not limited by the reaction rate of ilmenite, but it is limited by the low conversion of volatile matter. The combustion efficiency of the volatiles seems to depend on the composition of the released volatiles of each fuel. The average of combustion efficiency of volatiles was around 52% for lignite, 61% for HV bituminous Colombian coal, 58% for MV bituminous South African coal and 42% for anthracite. Combustion efficiencies had values higher than 75% at 910°C with an average inventory of 1200 kg/$MW_{th}$ for all the fuels tested, and for bituminous Colombian coal at 950°C the combustion efficiency was 95% with 3100 kg/$MW_{th}$ inventory. Thus, the oxygen polishing need is quite low.

The carbon capture efficiency was increased by increasing the char gasification rate. A relevant growth in the gasification rate was seen when ilmenite was used compared to an inert bed material, because ilmenite reacts with $H_2$ and CO which are gasification inhibitors. The temperature is one of the most influencing parameters. At higher fuel-reactor temperatures, gasification is faster and promoted for all types of solid fuels. The carbon capture is higher for the solid fuels with faster char gasification rates and also when the volatile content in the fuel is higher. High values of carbon capture can be obtained, but it is essential to have a highly efficient carbon separation system that reintroduced unconverted char particles back to the fuel-reactor, especially for solid fuels with slow gasification rates such as anthracites. Carbon capture as high as 93% at 920°C was obtained even without a carbon separation system with lignite, which has fast char gasification rate. In addition, lower recirculation rates and thereby lower oxygen-carrier to fuel ratios led to enhanced $CO_2$ capture efficiencies. That was because the increase in char residence time led to an increase in the char conversion.

Several $CO_2$:$H_2O$ mixtures as gasification agent were tested. Depending on the type of fuel, some of the steam as gasification agent can be replaced by $CO_2$ recirculated from the outlet fuel-reactor flow, getting similar system performance and thereby saving energy derived from steam generation. In case of lignite there is no change in the process performance when gasifying with $CO_2$ and for bituminous coals the use of some $CO_2$ would be admissible. On the other hand, for anthracite the lower gasification rate of char with $CO_2$ leads to a substantial drop in the performance.

Continuous tests carried out in a 10 $kW_{th}$ CLC facility fuelled with petcoke found that the addition of some limestone to a bed of ilmenite led to some improvement in the process performance. This beneficial effect could be explained by lime catalyzing the water-gas shift equilibrium, and subsequent faster reaction of $H_2$ with ilmenite.

With all the experimental information gathered, a theoretical simplified model for the fuel-reactor was developed, based on the differential mass balances with reaction in the fuel-

reactor. The model includes the kinetics of coal char gasification and reaction of the gasification and devolatilization products with the oxygen-carrier.

The kinetic parameters of calcined and activated particles were obtained by determining the reactivities of the reduction reaction with $H_2$, CO or $CH_4$, as main gases of coal devolatilization and gasification, and the oxidation reaction by oxygen were determined by thermogravimetric analysis. The grain model with uniform reaction in the particle and reaction in the grains following a changing grain size model with chemical reaction control was used to determine the kinetic parameters. In addition, to predict the behavior of the oxidation of calcined ilmenite, a mixed resistance between chemical reaction and diffusion in the solid product was needed.

The model results were compared and validated with results from tests done in the ICB-CSIC-s1 facility fuelled with bituminous Colombian coal and ilmenite as oxygen-carrier. The limitation to obtain full combustion in the fuel-reactor was assigned to poor contact of the volatile matter with the oxygen-carrier. The fraction of fuel-reactor bed in contact with the volatiles in that facility was calculated to be 0.53%. After that, the most relevant operating conditions for iG-CLC were optimized by analyzing their effect on the performance of the system.

The carbon capture was directly related to the gasification extent, which is promoted by increasing the temperature or the residence time of char in the fuel-reactor, which agrees with experimental results. It is highly beneficial to increase the solids inventory to 1000-2000 kg/$MW_{th}$, but further increase leads to no relevant improvements. To further enhance the carbon capture, the implementation of a carbon separation system was proposed, whose separation efficiency was found to be a key factor to reach high values of char conversion. With 1000 kg/$MW_{th}$ inventory at 900°C, the simulated carbon capture increased from 45.2% with 0% separation efficiency to 79.8% with 90% separation efficiency.

High oxygen-carrier to fuel ratio means high solids recirculation rate and thereby lower residence time, which leads to a decrease in carbon capture efficiency. The negative

influence of the gasification step as the oxygen-carrier to fuel ratio increases had lower relevance as the efficiency of the carbon separation system increased.

To have a high reactive oxygen-carrier is important to reach high combustion efficiencies, but is not the key factor to get high performance of the process. Lower influence was observed for the gasification agent to fixed carbon ratio or the type of gasification agent (for different $H_2O$:$CO_2$ mixtures).

The experience from the smaller to the larger lab-scale experiments and the simulation with a wide range of conditions showed that an optimized CLC system for solid fuels with ilmenite as oxygen-carrier should have a carbon separation system with high efficiency above 90%, work at a high fuel-reactor temperature -desirably above 950°C- and would need 1000-2000 kg/$MW_{th}$ of inventory. The contact efficiency of the volatile matter with the oxygen-carrier should be increased with some design solutions or the implementation of a second fuel-reactor is proposed as an option to fully burn the volatile matter and avoid an extra oxygen polishing step. With these measures and parameter values, carbon capture efficiency higher than 90% and full combustion can be reached with a wide range of solid fuels.

# 6 Acronyms, notations and symbols

AR air-reactor

$C_{max}$ maximum $CO_2$ or $H_2O$ fraction if there is full combustion (%)

$\overline{C}_g$ average concentration of fuel gas in the reactor (%)

CLC Chemical-Looping Combustion

Ea activation energy (kJ/mol)

*exp* experimental

FB fluidized bed

$f_C$ carbon concentration from char in the fuel-reactor (kg/kg)

$F_{C,char\ eff}$ flow of effective carbon char introduced (mol/s)

$(F_C)_{gp}$ flow of carbon contained in the products of char gasification (mol/s)

$F_{C,vol}$ carbon flow coming from the volatile matter (mol/s)

$F_{CO2,AR}$ $CO_2$ flow in the air-reactor outlet (mol/s)

$F_{CO2,FR}$, $F_{H2O,FR}$, $F_{H2,FR}$, $F_{CH4,FR}$, $F_{CO,FR}$ flows of $CO_2$, $H_2O$, $H_2$, $CH_4$, and CO in the fuel-reactor, respectively (mol/s)

$F_{CS}$ flow in the carbon-stripper (mol/s)

$f_{Fe_2O_3}$ y $f_{Fe_2TiO_5}$ mass fractions of $Fe_2O_3$ and $Fe_2TiO_5$ in ilmenite, respectively (%wt.)

$F_{FRLS}$ flow in the small fuel-reactor loop-seal (mol/s)

$F_{HILS}$ flow in the higher loop-seal (mol/s)

$F_{HIVEL}$ flow in the high-velocity section in the fuel-reactor (mol/s)

$F_{ilm}$ solids circulation rate (kg/s)

$F_{in}$ and $F_{out}$ molar flows of the respectively inlet and outlet gas streams (mol/s)

$F_{LOLS}$ flow in the lower loop-seal (mol/s)

$F_{LOVEL}$ steam flow in the low-velocity section in the fuel-reactor (mol/s)

FR fuel-reactor

FR1 first fuel-reactor

FR2 second fuel-reactor

$H_2O/C$ steam to fixed carbon ratio (mol/mol)

HV high volatile

i.d. internal diameter (m)

iG-CLC in-situ Gasification Chemical-Looping Combustion

k constant value of char gasification rate ($s^{-1}$)

$k_s$ chemical reaction kinetic constant ($mol^{1-n}\ m^{3n-2}\ s^{-1}$)

$k_1$ y $k_2$ kinetic constants of the char gasification model ($s^{-1}bar^{-1}$)

$k_3$ kinetic constant of the char gasification model ($s^{-1}$)

LHV low heating value (kJ/kg)

*m* oxygen-carrier instantaneous mass (kg)

$Me_xO_y$ oxidized oxygen-carrier

$Me_xO_{y-1}$ reduced oxygen-carrier

$m_{char,FR}$ mass of char in the fuel-reactor (kg)

$m_{ilm,FR}$ ilmenite mass in the fuel-reactor (kg)

$M_C$ atomic weight of carbon (kg/mol)

$M_O$ atomic weight of oxygen (kg/mol)

$m_{OC}$ mass inventory of the oxygen-carrier in the fuel-reactor (kg)

$m_o$ mass of fully oxidized oxygen-carrier(kg)

$m_r$ mass of fully reduced oxygen-carrier (kg)

$\dot{m}_{OC}$ solids circulation rate (kg/s per $MW_{th}$)

MV medium volatile

*n* reaction order

$N_{0,ilm}$ molar amount of oxygen in ilmenite active for CLC process (mol O)

$N_{C,char}$ mol number of carbon fed into the reactor (mol C)

OC oxygen-carrier

$O_{2\ dem\ coal,eff}$ oxygen demand of the effective coal fed (mol $O_2$/s)

$O_{coal,eff}$ flow of oxygen contained in the effective coal introduced (mol O/s)

$P_{in}$ and $P_{out}$ partial pressures of the gas at the reactor inlet and outlet, respectively

$P_m$ mean partial pressure of the gaseous fuel in the reactor

$p_{prod}$ partial pressure of the gaseous products

$p_{react}$ partial pressure of the gaseous reactants

$P_{ref}$ reference partial pressure

$p_{TGA}$ partial pressure of the fuel gas used in the TGA experiments

$r_C$ char gasification rate ($s^{-1}$)

$r_{C,inst}$ char conversion instantaneous rate ($s^{-1}$)

$r_g$ grain radius (m)

$(-r_{ilm,i})$ reaction rate of ilmenite with the gas i ($s^{-1}$)

(-$r_O$) rate of oxygen transferred by ilmenite (kg $O_2$/s kg oxygen-carrier)

$R_{o,Fe_2O_3}$ oxygen transport capacity of $Fe_2O_3$ when it is reduced to $Fe_3O_4$ (kg/kg)

$R_{o,Fe_2TiO_5}$ oxygen transport capacity of $Fe_2TiO_5$ when it is reduced to $Fe_2TiO_5$ (kg/kg)

$R_{O,ilm}$ oxygen transport capacity of ilmenite (kg/kg)

$R_{OC}$ transport capacity of an oxygen-carrier

t time (s)

T temperature (ºC)

$T_{FR}$ fuel-reactor temperature (ºC)

TGA thermogravimetric analyzer

$t_{m,char}$ char mean residence time (s)

$t_{r,0}$ is the initial time when the considered reaction begins (s)

WGS Water-Gas Shift

$X_{char}$ char conversion

$X_{chr}$ conversion value for which porosity collapses in ilmenite oxidation

$X_o$ conversion for the oxidation reaction

$X_r$ conversion for the reduction reaction

$\Delta X$ oxygen-carrier conversion variation

$y_i$ molar fraction of the gas i

$\varepsilon_g$ coefficient of expansion of the gas mixture

$\Omega_{OD}$ oxygen demand

$\phi$ oxygen-carrier to fuel ratio

$\chi_{OC,v}$ fraction of the oxygen-carrier bed that is in contact with the volatile matter

$\gamma_O$ oxygen yield

$\eta_c$ combustion efficiency

$\eta_{CC}$ carbon capture efficiency

$\eta_{comb\ FR}$ combustion efficiency in the fuel-reactor

$\eta_{CS}$ efficiency of the carbon separation system

$\rho_m$ molar density ($mol/m^3$)

$\omega$ mass based conversion (kg/kg)

$\omega_{red}$ and $\omega_{ox}$ reduced and oxidized mass based conversions of ilmenite reached in the previous period, correspondingly

# 7 References

Abad et al., 2006. Abad A, Mattisson T, Lyngfelt A, Rydén M. Chemical-Looping combustion in a 300 W continuously operating reactor system using a manganese-based oxygen-carrier. Fuel 2006;85:1174-85.

Abad et al., 2007a. Abad A, García-Labiano F, de Diego LF, Gayán P, Adánez J. Reduction kinetics of Cu-, Ni-, and Fe-based oxygen-carriers using syngas (CO + $H_2$) for chemical-looping combustion. Energy Fuels 2007;21:1843-53.

Abad et al., 2007b. Abad A, Mattisson T, Lyngfelt A, Johansson M. The use of iron oxide as oxygen-carrier in a chemical-looping reactor. Fuel 2007;86:1021-35.

Abad et al., 2007c. Abad A, Adánez J, García-Labiano F, de Diego LF, Gayán P, Celaya J.. Mapping of the range of operational conditions for Cu-, Fe-and Ni-based oxygen-carriers in chemical-looping combustion. Chem Eng Sci 2007;62(1-2):533-549.

Adánez et al., 1985. Adánez J, Miranda JL, Gavilán JM. Kinetics of a lignite-char gasification by $CO_2$. Fuel 1985;64(6):801-804.

Adánez et al., 2005. Adánez J, Abad A, García-Labiano F, de Diego LF, Gayán P. $H_2S$ retention with Ca-based sorbents in a pressurized fixed-bed reactor: Application to moving-bed design. Fuel 2005;84(5):533-542.

Adánez et al., 2006. Adánez J, Gayán P, Celaya J, de Diego LF, García-Labiano F, Abad A. Chemical looping combustion in a 10 kW prototype using a $CuO/Al_2O_3$ oxygen-carrier: effect of operating conditions on methane combustion. Ind Eng Chem Res 2006;45:6075-80.

Adánez et al., 2011. Adánez J, Abad A, Garcia-Labiano F, Gayán P, de Diego LF. Progress in Chemical-Looping Combustion and Reforming technologies. Prog Energy Comb Sci. doi:10.1016/j.pecs.2011.09.001.

Archer, 2005. Archer D. Fate of fossil fuel $CO_2$ in geologic time. J Geophys Res 2005;110, C09S05, doi:10.1029/2004JC002625.

Barin, 1989. Barin, I. Thermochemical Data of Pure Substances. 1989. VCH, Weinhein, Germany.

Berguerand and Lyngfelt, 2008a. Berguerand N, Lyngfelt A. The use of petroleum coke as fuel in a 10 kWth chemical-looping combustor. Int J Greenhouse Gas Control 2008;2:169-179.

Berguerand and Lyngfelt, 2008b. Berguerand N, Lyngfelt A. Design and operation of a 10 kWth chemical-looping combustor for solid fuels – Testing with South African coal. Fuel 2008;87:2713-2726.

Berguerand and Lyngfelt, 2009a. Berguerand N, Lyngfelt A. Chemical-Looping combustion of petroleum coke using ilmenite in a 10 kWth unit-high-temperature operation. Energy Fuels 2009;23(10):5257-68.

Berguerand and Lyngfelt, 2009b. Berguerand N, Lyngfelt A. Operation in a 10 kWth chemical-looping combustor for solid fuel—Testing with a Mexican petroleum coke. GHGT-9. Energy Procedia 2009;1(1):407-414.

Bidwe et al., 2011. Bidwe AR, Mayer F, Hawthorne C, Charitos A, Schuster A, Scheffknecht G. Use of ilmenite as an oxygen-carrier in Chemical-Looping Combustion – Batch and continuous dual fluidized bed investigation. Energy Procedia 2011;4:433-440.

Cao and Pan, 2006. Cao Y, Pan W-P. Investigation of chemical looping combustion by solid fuels. 1. Process analysis. Energy Fuels 2006;20:1836-44.

Cao et al., 2006. Cao Y, Casenas B, Pan W-P. Investigation of Chemical-Looping Combustion by Solid Fuels. 2. Redox Reaction Kinetics and Product Characterization with Coal, Biomass, and Solid Waste as Solid Fuels and CuO as an Oxygen-carrier. Energy Fuels 2006;20:1845-54.

Carapellucci and Milazzo, 2003. Carapellucci R, Milazzo A. Membrane systems for $CO_2$ capture and their integration with gas turbine units. Proceedings of the Institution of Mechanical Engineers Part A: Journal of Power and Energy 2003;217:505-517.

Cho et al., 2006. Cho P, Mattisson T, Lyngfelt A. Defluidization Conditions for a Fluidized Bed of Iron Oxide-, Nickel Oxide-, and Manganese Oxide-Containing Oxygen-carriers for Chemical-Looping Combustion. Ind Eng Chem Res 2006;45:968-977.

Chuang et al., 2008. Chuang SY, Dennis JS, Hayhurst AN, Scott SA. Development and performance of Cu-based oxygen-carriers for chemical-looping combustion. Combust Flame 2008;154:109-121.

Dennis et al., 2006. Dennis JS, Scott SA, Hayhurst AN. In situ gasification of coal using steam with chemical looping: a technique for isolating $CO_2$ from burning a solid fuel. Journal of the Energy Institute 2006;79(3):187-190.

Dueso et al., 2009. Dueso C, García-Labiano F, Adánez J, de Diego LF, Gayán P, Abad A. Syngas combustion in a chemical-looping combustion system using an impregnated Ni based oxygen-carrier. Fuel 2009;88:2357-64.

Forero et al., 2009. Forero CR, Gayán P, de Diego LF, Abad A, García-Labiano F, Adánez J. Syngas combustion in a 500 Wth chemical-looping combustion system using an impregnated Cu-based oxygen-carrier. Fuel Proc Technol 2009;90:1471-9.

Ghoniem, 2011. Ghoniem AF. Needs, resources and climate change: Clean and efficient conversion technologies. Progress in Energy and Combustion Science 2011;37(1):15-51.

Gu et al., 2011. Gu H, Shen L, Xiao J, Zhang S, Song T. Chemical Looping Combustion of Biomass/Coal with Natural Iron Ore as Oxygen-carrier in a Continuous Reactor. Energy Fuels 2011;25(1):446–455.

Hossain and de Lasa, 2008. Hossain MM, de Lasa HI. Chemical-Looping combustion (CLC) for inherent $CO_2$ separations—a review. Chem Eng Sci 2008;63:4433-51.

IEA, 2006. International Energy Agency (IEA). Energy technology perspectives: Scenarios and strategies to 2050. Paris, France: OECD/IEA; 2006.

IEA, 2007. International Energy Agency (IEA). World energy outlook 2007. IEA Publications; 2007.

IEA, 2010. International Energy Agency (IEA). Energy Technology Perspectives 2010, OECD/IEA, Paris.

IPCC, 2001. Climate Change 2001. The third Assesment Report of the Intergovernmental Panel on Climate Change (IPCC). Cambridge, UK: Cambridge University Press; 2001.

IPCC, 2002. Climate change and biodiversity. IPCC technical paper V. IPCC; 2002.

IPCC, 2005. IPCC special report on carbon dioxide capture and storage, Cambridge, UK: Cambridge University Press; 2005.

IPCC, 2007. IPCC. Climate Change 2007: Synthesis Report.

Jin and Ishida, 2004. Jin H, Ishida M. A new type of coal gas fuelled chemical-looping combustion. Fuel 2004;83:2411-7.

Johansson et al., 2004. Johansson M, Mattisson T, Lyngfelt A. Investigation of Fe2O3 with MgAl2O4 for Chemical-Looping Combustion. Ind Eng Chem Res 2004;43(22):6978-87.

Johansson et al., 2006a. Johansson E, Mattisson T, Lyngfelt A, Thunman H. Combustion of Syngas and Natural Gas in a 300 W Chemical-Looping Combustor. Chem Eng Res Des 2006;84:819-27.

Johansson et al., 2006b. Johansson M, Mattisson T, Lyngfelt A. Comparison of oxygen-carriers for chemical-looping combustion. Thermal Sci 2006;10:93-107.

Johnson, 1981. Johnson J L. Fundamentals of Coal Gasification. In Chemistry of coal utilization. 2nd supplementary volume. Chapter 23. Ed. M.A. Elliott. Wiley-Interscience Publication, New York, 1981.

Kerr, 2005. Kerr HR. Capture and separation technology gaps and priority research needs. In: Thomas DC, Benson SM, editors. Carbon dioxide capture for storage in deep geologic formations– Results from the $CO_2$ capture project, Oxford, UK: Elsevier; 2005, vol. 1, Chapter 38.

Kolbitsch et al., 2009. Kolbitsch P, Bolhàr-Nordenkampf J, Pröll T, Hofbauer H. Comparison of two Ni based oxygen-carriers for chemical looping combustion of natural gas in 140 kW continuous looping operation. Ind Eng Chem Res 2009;48:5542-7.

Leion et al., 2007. Leion H, Mattisson T, Lyngfelt A. The use of petroleum coke as fuel in chemical-looping combustion. Fuel 2007;86:1947-58.

Leion et al., 2008a. Leion H, Mattisson T, Lyngfelt A. Solid fuels in chemical-looping combustion. Int. J. Greenhouse Gas Control 2008;2:180-93.

Leion et al., 2008b. Leion H, Lyngfelt A, Johansson M, Jerndal E, Mattisson T. The use of ilmenite as an oxygen-carrier in chemical-looping combustion. Chem Eng Res Des 2008;86:1017-26.

Leion et al., 2009a. Leion H, Mattissson T, Lyngfelt A. Use of ores and industrial products as oxygen-carriers in chemical-looping combustion. Energy Fuels 2009;23:2307-15.

Leion et al., 2009b. Leion H, Jerndal E, Steenari B-M, Hermansson S, Israelsson M, Jansson E, Johnsson M, Thunberg R, Vadenbo A, Mattisson T, Lyngfelt A. Solid fuels in chemical–looping combustion using oxide scale and unprocessed iron ore as oxygen-carriers. Fuel 2009;88:1945-54.

Leion et al., 2009c. Leion H, Mattisson T, Lyngfelt A. Effects of steam and $CO_2$ in the fluidizing gas when using bituminous coal in chemical-looping combustion. Proceedings of the 20th International Conference on Fluidized Bed Combustion, Xian (China), 2009, 608-11.

Leion et al., 2009d. Leion H, Lyngfelt A, Mattisson T. Solid fuels in chemical-looping combustion using a NiO-based oxygen-carrier. Chem Eng Res Des 2009;87:1543-50.

Linderholm et al., 2008. Linderholm C, Abad A, Mattisson T, Lyngfelt A. 160 h of chemical-looping combustion in a 10 kW reactor system with a NiO-based oxygen-carrier. Int J Greenhouse Gas Control 2008;2:520-30.

Linderholm et al., 2009. Linderholm C, Mattisson T, Lyngfelt A. Long-term integrity testing of spray dried particles in a 10 kW chemical-looping combustor using natural gas as fuel. Fuel 2009;88:2083-96.

Linderholm et al., 2011. Linderholm C, Cuadrat A, Lyngfelt A. Chemical-Looping combustion of solid fuels in a 10 kWth pilot – batch tests with five fuels. Energy Procedia 2011;4:385-92.

Lyngfelt et al., 2001. Lyngfelt A, Leckner B, Mattisson T. A fluidized-bed combustion process with inherent $CO_2$ separation, application of chemical-looping combustion. Chem Eng Sci 2001;56:3101-13.

Lyngfelt and Thunman, 2005. Lyngfelt A, Thunman H. Construction and 100 h of operational experience of a 10 kW chemical-looping combustor. In: Thomas DC, Benson SM, editors. Carbon dioxide capture for storage in deep geologic formations–Results from the $CO_2$ capture project, Oxford, UK: Elsevier; 2005, vol. 1, Chapter 36.

Lyngfelt et al., 2008. Lyngfelt A, Johansson M, Mattisson T. Chemical-Looping Combustion – Status of Development. Proceedings of the 9th International Conference on Circulating Fluidized Beds (CFB-9), Hamburg, Germany, 2008.

Mattisson et al., 2007. Mattisson T, García-Labiano F, Kronberger B, Lyngfelt A, Adánez J, Hofbauer H. Chemical-Looping combustion using syngas as fuel. Int J Greenhouse Gas Control 2007;1:158-69.

Mattisson et al., 2009. Mattisson T, Lyngfelt A, Leion H. Chemical-looping with oxygen uncoupling for combustion of solid fuels. Int J Greenhouse Gas Control 2009;3(1):11-19.

NOAA-ESRL, 2010. National Oceanic and Atmospheric Administration in the US. Average concentration of $CO_2$ in the atmosphere (Mauna Loa Observatory) for 2010 was posted September 8, 2011

Petrakopoulou et al., 2011. Petrakopoulou F, Boyano A, Cabrera M, Tsatsaronis G. Exergoeconomic and exergoenvironmental analyses of a combined cycle power unit with chemical looping technology. Int J of Greenhouse Gas Control 2011;5(3):475-482.

Pröll et al., 2009. Pröll T, Mayer K, Bolhàr-Nordenkampf J, Kolbitsch P, Mattisson T, Lyngfelt A, Hofbauer H. Natural minerals as oxygen-carriers for chemical-looping combustion in a dual circulating fluidized bed system. Energy Procedia 2009;1:27-34.

Rao and Prototypeaud, 1975. Rao DB and Prototypeaud M. Kinetics of the oxidation of ilmenite. Oxidation of Metals 1975;9(1):99-116.

Ryu et al., 2005. Ryu HJ, Jin G-T, Yi C-K. Demonstration of inherent $CO_2$ separation and no NOx emission in a 50 kW chemical-looping combustor: Continuous reduction and oxidation experiment. Proc 7th Int Conf Greenhouse Gas Control Technology (GHGT-7). Vancouver, Canada, 2004.

Scott et al., 2006. Scott SA, Dennis JS, Hayhurst AN, Brown T. In situ gasification of a solid fuel and $CO_2$ separation using chemical looping. AIChE J 2006;52:3325-8.

Shen et al., 2009a. Shen L, Wu J, Xiao J, Song Q, Xiao R. Chemical-Looping Combustion of Biomass in a 10 kWth Reactor with Iron Oxide as an Oxygen-carrier. Energy Fuels 2009;23:2498-2505.

Shen et al., 2009b. Shen L, Wu J, Xiao J. Experiments on chemical looping combustion of coal with a NiO based oxygen-carrier. Combust Flame 2009;156:721-8.

Shen et al., 2009c. Shen L, Wu J, Gao Z, Xiao J. Reactivity deterioration of $NiO/Al_2O_3$ oxygen-carrier for chemical looping combustion of coal in a 10 kWth reactor. Combust Flame 2009;156:1377-85.

Shen et al., 2010. Shen L, Wu J, Gao Z, Xiao J. Characterization of chemical looping combustion of coal in a 1 kWth reactor with a nickel-based oxygen-carrier. Combust Flame 2010;157:934-42.

Simell et al., 2000. Simell P, Stahlberg P, Kurkela E, Albrecht J, Deutsch S and Sjöström K. Provisional protocol for the sampling and analysis of tar and particulates in the gas from large-scale biomass gasifiers. Version 1998. Biomass Bioenergy 2000;18(1):19-38.

Siriwardane et al., 2009. Siriwardane R, Tian H, Richards G, Simonyi T, Poston J. Chemical-Looping Combustion of Coal with Metal Oxide Oxygen-carriers. Energy Fuels 2009;23:3885-92.

Teyssié et al., 2011. Teyssié G, Leion H, Schwebel GL, Lyngfelt A, Mattisson T. Influence of lime addition to ilmenite in chemical-looping combustion (CLC) with solid fuels. Energy Fuels 2011;25(8):3843-53.

Thambimuthu et al., 2005. Thambimuthu K, Soltanieh M, Abanades JC. Capture of $CO_2$. In: Metz B, Davidson O, de Coninck HC, Loos M, Meyer LA, editors. IPCC special report on carbon dioxide capture and storage, Cambridge. UK: Cambridge University Press; 2005, chapter 3.

Thomas and Benson, 2005. Thomas DC, Benson SM. Carbon dioxide capture for storage in deep geologic formations– Results from the $CO_2$ capture project, Oxford, UK: Elsevier; 2005. Vol 1 and 2.

Toftegaard et al., 2010. Toftegaard MB, Brix J, Jensen PA, Glarborg P, Jensen AD. Oxy-fuel combustion of solid fuels. Prog Energy Combust Sci 2010;36:581-625.

United Nations, 1998. Kyoto protocol to the United Nations framework convention on climate change. United Nations; 1998.

Wu et al., 2010. Wu J, Shen L, Hao J, Gu H. Chemical looping combustion of coal in a 1 kWth reactor with iron ore as an oxygen-carrier. Proc 1st Int Conf on Chemical Looping. Lyon, France; 2010.

Wolf et al., 2001. Wolf J, Anheden M, Yan J. Performance Analysis of Combined Cycles with Chemical-Looping Combustion for $CO_2$ Capture. In International Pittsburg Coal Conference, Newcastle, New South Wales, Australia, Dec 3-7, 2001.

Yang et al., 2007. Yang J-B, Cai N-S, Li Z-S. Reduction of iron oxide as an oxygen-carrier by coal pyrolysis and steam char gasification intermediate products. Energy Fuels 2007;21:3360-8.

Zafar et al., 2007a. Zafar Q, Abad A, Mattisson T, Gevert B, Strand M. Reduction and oxidation kinetics of $Mn_3O_4$/Mg-$ZrO_2$ oxygen-carrier particles for chemical-looping combustion. Chem Eng Sci 2007;62:6556-67.

Zafar et al., 2007b. Zafar Q, Abad A, Mattisson T, Gevert B. Reaction kinetics of freeze-granulated NiO/$MgAl_2O_4$ oxygen-carrier particles for chemical-looping combustion. Energy Fuels 2007;21:610-8.

Zero Emissions Platform, 2011. European Technology Platform for Zero Emission Fossil Fuel Power Units. The Costs of $CO_2$ Capture, Transport and Storage. 2011.

Zhao et al., 2008. Zhao H, Liu L, Wang B, Xu D, Jiang L, Zheng C. Sol-gel-derived NiO/$NiAl_2O_4$ oxygen-carriers for chemical-looping combustion by coal char. Energy Fuels 2008;22:898-905.

# Appendix – Papers

# Paper I

*Energy Fuels* **2010,** *24,* 1402–1413 · DOI:10.1021/ef900856d
Published on Web 01/07/2010

energy&fuels
article

# Ilmenite Activation during Consecutive Redox Cycles in Chemical-Looping Combustion

Juan Adánez,* Ana Cuadrat, Alberto Abad, Pilar Gayán, Luis F. de Diego, and Francisco García-Labiano

*Department of Energy and Environment, Instituto de Carboquímica, Consejo Superior de Investigaciones Científicas (CSIC), Miguel Luesma Castán 4, 50018 Zaragoza, Spain*

*Received August 5, 2009. Revised Manuscript Received December 14, 2009*

Ilmenite, a natural mineral composed of $FeTiO_3$, is a low-cost and promising oxygen carrier (OC) for solid fuels combustion in a chemical-looping combustion (CLC) system. The aim of this study is to analyze the behavior of ilmenite as an OC in CLC and the changes in its properties through redox cycles. Experiments consisting of reduction−oxidation cycles in a thermogravimetric analyzer were carried out using the main products of coal pyrolysis and gasification, that is, $CH_4$, $H_2$, and CO, as reducing gases. Characterizations of ilmenite through scanning electron microscopy−energy-dispersive X-ray (SEM−EDX), X-ray diffraction (XRD), Hg porosimetry, $N_2$ fisisorption, He pycnometry, and hardness measures have been performed. Both fresh and previously calcined at 1223 K ilmenite have been used as initial OCs. Fresh ilmenite reacts slowly; nevertheless, there is a gain in reactivity in reduction as well as in oxidation with the number of cycles. This activation occurs for all tested fuel gases and is faster if ilmenite has been previously calcined. The initial oxygen transport capacity was measured to be 4%, and it decreases with the number of cycles up to 2.1% after 100 redox cycles. Nevertheless, ilmenite shows adequate values of reactivity and oxygen transport capacity for its use in CLC technology with solid fuels. The trade-off between the increase in reactivity and decrease in oxygen transport capacity on ilmenite performance in a CLC system has been evaluated through the estimation of the solids inventory needed in the fuel reactor. If fresh or calcined ilmenite is fed into the CLC system, the activation process could happen in the CLC itself. Also, a previous step for activation can be designed.

## Introduction

At present, there is a general consensus on the need of reducing the emissions of greenhouse gas $CO_2$ to restrain climate change. Anthropogenic $CO_2$ is mainly generated in combustion of fossil fuels, which are foreseen to provide about 80% of the overall world consumption of energy for the next several decades. With regard to the energy-related $CO_2$ emissions by fuel type, coal use generated 39% of the emissions in 2004, and it is estimated that the percentage in 2030 will rise to 43%.[1,2] Among the different opportunities to reduce the anthropogenic $CO_2$ emissions, carbon capture and sequestration (CCS) has been identified as a relevant option in stationary power plants using fossil fuels. In this context, chemical-looping combustion (CLC) is one of the most promising technologies to carry out $CO_2$ capture at a low cost.[3−5]

CLC is based on the transfer of the oxygen from air to the fuel by means of a solid oxygen carrier (OC) that circulates between two interconnected fluidized beds (FBs), avoiding direct contact between fuel and air.[6] Important progress has been made in CLC for gaseous fuels (natural gas and syngas) to date. Several authors have successfully demonstrated the feasibility of this process in different CLC prototypes in the 10−140 $kW_{th}$ range using OCs based on nickel and cobalt oxides,[7] NiO,[8−11] and CuO.[12] Also, there is an increasing interest for the application of CLC using coal, regarding the intensive use of this fuel for energy generation. There are two possibilities for the use of the CLC technology with coal. The first one is to carry out previous coal gasification and, subsequently, to introduce the produced gas in the CLC system. Simulations performed by Jin and Ishida[13] and Wolf et al.[14]

*To whom correspondence should be addressed. Telephone: +34-976-733977. Fax: +34-976-733318. E-mail: jadanez@icb.csic.es.

(1) Intergovernmental Panel on Climate Change (IPCC). Climate Change 2007. Synthesis Report. Contribution of Working Groups I, II, and III to the Fourth Assessment Report of the Intergovernmental Panel on Climate Change, Geneva, Switzerland, 2007 (www.ipcc.ch).

(2) Industrial Environmental Association (IEA). International Energy Outlook 2008. IEA, Washington, D.C., 2008.

(3) Eide, L. I.; Anheden, M.; Lyngfelt, A.; Abanades, C.; Younes, M.; Clodic, D. *Oil Gas Sci. Technol.* **2005**, *60*, 497–508.

(4) Kerr, H. R. Capture and separation technologies gaps and priority research needs. In *Carbon Dioxide Capture for Storage in Deep Geologic Formations—Results from the $CO_2$ Capture Project*; Thomas, D., Benson, S., Eds.; Elsevier Ltd.: Amsterdam, The Netherlands, 2005; Vol. 1, Chapter 38.

(5) Hossain, M. M.; de Lasa, H. I. *Chem. Eng. Sci.* **2008**, *63*, 4433–4451.

(6) Lyngfelt, A.; Leckner, B.; Mattisson, T. *Chem. Eng. Sci.* **2001**, *56*, 3101–3113.

(7) Ryu, H. J.; Jin, G. T.; Yi, C. K. Demonstration of inherent $CO_2$ separation and no $NO_x$ emission in a 50 kW chemical-looping combustor: Continuous reduction and oxidation experiment. In *Proceedings of the Seventh International Conference of Greenhouse Gas Control Technologies*; Wilson, M., Morris, T., Gale, J., Thambibutu, K., Eds.; Elsevier Ltd.: Amsterdam, The Netherlands, 2005; Vol. 2, p 1907.

(8) Lyngfelt, A.; Thunman, H. In *Carbon Dioxide Capture for Storage in Deep Geologic Formations—Results from the $CO_2$ Capture Project*; Thomas, D., Benson, S., Eds.; Elsevier Ltd.: Amsterdam, Netherlands, 2005; Vol. 1, Chapter 36.

(9) Linderholm, C.; Abad, A.; Mattisson, T.; Lyngfelt, A. *Int. J. Greenhouse Gas Control* **2008**, *2*, 520–530.

(10) Linderholm, C.; Mattisson, T.; Lyngfelt, A. *Fuel* **2009**, *88*, 2083–2096.

(11) Kolbitsch, P.; Pröll, T.; Bolhar-Nordenkampf, J.; Hofbauer, H. *Energy Procedia* **2009**, *1*, 1465–1472.

(12) Adánez, J.; Gayán, P.; Celaya, J.; de Diego, L. F.; García-Labiano, F.; Abad, A. *Ind. Eng. Chem. Res.* **2006**, *45*, 6075–6080.

(13) Jin, H.; Ishida, M. *Fuel* **2004**, *83*, 2411–2417.

(14) Wolf, J.; Anheden, M.; Yan, J. Performance analysis of combined cycles with chemical looping combustion for $CO_2$ capture. In Proceedings of the International Pittsburgh Coal Conference, Newcastle, New South Wales, Australia, Dec 3−7, 2001.

 

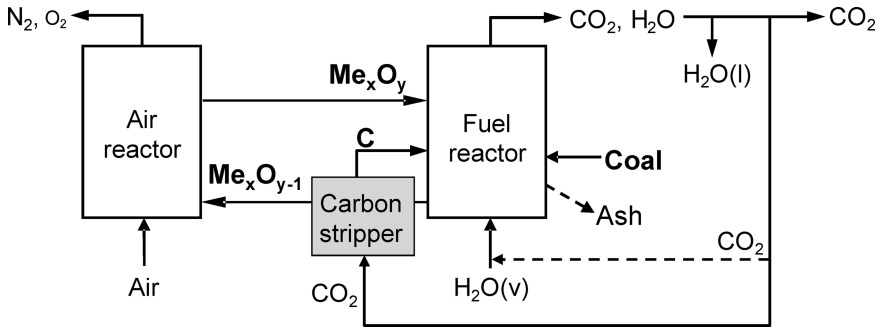


**Figure 1.** Reactor scheme of the CLC process using solid fuels (- - -, optional stream).

showed that this process has the potential to achieve an efficiency of about 5−10% points higher than a similar combined cycle with conventional $CO_2$-capture technology. Several OCs based on Ni, Cu, Fe, and Mn oxides have shown good reactivity with syngas components, i.e., $H_2$ and CO,[15,16] and the use of syngas in a CLC system has been successfully accomplished in 300−500 $W_{th}$ continuous CLC units.[17−21]

The second possibility for the use of coal in CLC is the direct combustion in the CLC process, that is, avoiding the need of coal gasification and the corresponding gaseous oxygen requirement.[22,23] The reactor scheme for this CLC configuration is shown in Figure 1. In this option, coal is physically mixed with the OC in the fuel reactor (FR) and the carrier reacts with the gas products from steam coal gasification, where $H_2$ and CO are main components. Thus, the solid fuel gasification proceeds in the FR first according to reactions 1−3 and the resulting gases and volatiles are oxidized through reduction of the oxidized OC, $Me_xO_y$, by means of reaction 4. The OC reduced in the FR, $Me_xO_{y-1}$, is transferred to the air reactor (AR), where reaction 5 with oxygen from air takes place. Thus, the OC is regenerated to start a new cycle. The net chemical reaction is the same as usual combustion with the same combustion enthalpy.

$$\text{coal} \rightarrow \text{volatile matter} + \text{char} \quad (1)$$

$$\text{char} + H_2O \rightarrow H_2 + CO \quad (2)$$

$$\text{char} + CO_2 \rightarrow 2CO \quad (3)$$

$$H_2, CO, \text{volatile matter } (CH_4) + nMe_xO_y \rightarrow CO_2 + H_2O + nMe_xO_{y-1} \quad (4)$$

$$Me_xO_{y-1} + 1/2O_2 \rightarrow Me_xO_y \quad (5)$$

Ideally, the stream of combustion gases from the FR contains primarily $CO_2$ and $H_2O$, although some unburnt compounds can also appear (CO, $H_2$, $CH_4$, and volatiles). In this case, an oxygen-polishing step can be necessary for complete combustion to $CO_2$ and $H_2O$. After that, water can be easily separated by condensation, and a highly concentrated stream of $CO_2$ ready for compression and sequestration is achieved. The $CO_2$ capture is inherent to this process, because the air does not become mixed with the fuel and no additional costs or energy penalties for gas separation are required. The gas stream from the AR is oxygen-depleted and consists of $N_2$ and some unreacted $O_2$.

It is expected that the gasification process was the limiting step in the FR; therefore, the stream of solids exiting from the FR could contain some unconverted char together with the OC. Thus, for solid fuels, an additional carbon stripper is necessary to separate char particles from OC particles and, therefore, reduce the amount of carbon transferred from the FR to the AR. It is necessary to point out that the transference of char to the AR does not reduce the energetic efficiency of the process but decreases the carbon-capture efficiency of the system because some $CO_2$ will exit together with the exhaust gas from the AR. Moreover, as a consequence of the ash present in the solid fuel, it is necessary to drain ashes from the system to avoid its accumulation in the reactors. The drain stream will also contain some amount of OC. Thus, it is expected that the active life of this material would be limited by the losses together the drain stream rather than for its degradation. The efficiency of char combustion in the FR and the separation of ash from the OC seem to be key factors for the development of this process.

As for gaseous fuels, suitable OCs for solid fuels in the CLC process must have high selectivity toward $CO_2$ and $H_2O$, enough oxygen transport capacity, high reactivity, high mechanical strength, attrition resistance, and agglomeration absence. All of these characteristics must be maintained during many reduction and oxidation cycles. There are studies made on the reactivity of synthetic OCs based on CuO,[24] $Fe_2O_3$,[25,26] and NiO[27] for *in situ* gasification of the solid fuel. However, the low cost of the carrier is rather desirable for its use with coal, because a partial loss together with the coal ashes is predictable when removing them from the reactor to avoid their accumulation in the system. The use of natural minerals for this option seems to be very interesting, with ilmenite being an appropriate material.[28] Ilmenite is mainly

(15) Mattisson, T.; García-Labiano, F.; Kronberger, B.; Lyngfelt, A.; Adánez, J.; Hofbauer, H. *Int. J. Greenhouse Gas Control* **2007**, *1*, 158–169.
(16) Abad, A.; García-Labiano, F.; de Diego, L. F.; Gayán, P.; Adánez, J. *Energy Fuels* **2007**, *21*, 1843–1853.
(17) Johansson, E.; Mattisson, T.; Lyngfelt, A.; Thunman, H. *Chem. Eng. Res. Des.* **2006**, *84*, 819–827.
(18) Abad, A.; Mattisson, T.; Lyngfelt, A.; Rydén, M. *Fuel* **2006**, *85*, 1174–1185.
(19) Abad, A.; Mattisson, T.; Lyngfelt, A.; Johansson, M. *Fuel* **2007**, *86*, 1021–1035.
(20) Dueso, C.; García-Labiano, F.; Adánez, J.; de Diego, L. F.; Gayán, P.; Abad, A. *Fuel* **2009**, *88*, 2357–2364.
(21) Forero, C. R.; Gayán, P.; de Diego, L. F.; Abad, A.; García-Labiano, F.; Adánez, J. *Fuel Process. Technol.* **2009**, *90*, 1471–1479.
(22) Cao, Y.; Pan, W.-P. *Energy Fuels* **2006**, *20*, 1836–1844.
(23) Dennis, J. S.; Scott, S. A.; Hayhurst, A. N. *J. Energy Inst.* **2006**, *79*, 187–190.
(24) Cao, Y.; Casenas, B.; Pan, W.-P. *Energy Fuels* **2006**, *20*, 1845–1854.
(25) Scott, S. A.; Dennis, J. S.; Hayhurst, A. N.; Brown, T. *AIChE J.* **2006**, *52*, 3325–3328.
(26) Leion, H.; Mattisson, T.; Lyngfelt, A. *Fuel* **2007**, *86*, 1947–1958.
(27) Zhao, H.; Liu, L.; Wang, B.; Xu, D.; Jiang, L.; Zheng, C. *Energy Fuels* **2008**, *22*, 898–905.
(28) Leion, H.; Lyngfelt, A.; Johansson, M.; Jerndal, E.; Mattisson, T. *Chem. Eng. Res. Des.* **2008**, *86*, 1017–1026.

composed of $FeTiO_3$ ($FeO \cdot TiO_2$), where iron oxide is the active phase that behaves as an OC. There are a few recent studies showing an acceptable performance of ilmenite as an OC in CLC at different scales. Leion et al.[28,29] analyzed the reactivity of ilmenite in a batch FB for solid fuels combustion. Ilmenite gave high conversion of CO and $H_2$ but moderate conversion of $CH_4$. They observed a gain in ilmenite reactivity as increasing redox cycles, and eventually, reactivity as high as for a synthetic $Fe_2O_3$-based OC was reached. Berguerand et al.[30,31] operated a 10 $kW_{th}$ chemical-looping combustor using South African coal and petroleum coke as solid fuels. They concluded that ilmenite appeared to be a suitable material to be used for solid fuel combustion in a CLC system. The encouraging results obtained to date indicate that there is still further research to be carried out.

The aim of this work is to study the performance and activation of ilmenite as an OC in a CLC system with the main gases from coal gasification, that is, $H_2$, CO, and $CH_4$. To do this, consecutive reduction−oxidation cycles were carried out in a thermogravimetric analyzer (TGA), and to analyze the activation process, a characterization of the initial and reacted samples of the OC was performed.

## Experimental Section

The behavior of ilmenite as an OC to be used in a CLC system has been analyzed by consecutive redox cycles in a TGA system.

**Oxygen Carrier.** Ilmenite is a common mineral found in metamorphic and igneous rocks, mainly composed of $FeTiO_3$. In principle, when using ilmenite as an OC in a CLC process, the reduced form consists of $FeTiO_3$ ($FeO + TiO_2$) and the most oxidized level is $Fe_2TiO_5$, which corresponds to $Fe_2O_3 + TiO_2$. The ilmenite used in this study is a concentrate from a natural ore. Fresh ilmenite and ilmenite particles after a thermal treatment were used in this work. The calcination of fresh ilmenite was made at 1223 K in air during 24 h. The calcination was considered to improve properties and initial reaction rates[32] and to obtain ilmenite in its most oxidized state, as already performed by Leion et al.[29] Moreover, a pre-oxidation of ilmenite was also beneficial to avoid defluidization problems.[33]

Ilmenite particles were physically and chemically characterized by several techniques. The real density of the particles was measured with a Micromeritics AccuPyc II 1340 helium picnometer. The force needed to fracture a particle was determined using a Shimpo FGN-5X crushing strength apparatus. The mechanical strength was taken as the average value of at least 15 measurements undertaken on different particles of each sample randomly chosen. Particle porosity was measured by Hg intrusion in a Quantachrome PoreMaster 33. The identification of crystalline chemical species was carried out by powder X-ray diffraction (XRD) patterns acquired in an X-ray diffractometer Bruker AXS D8ADVANCE using Ni-filtered Cu Ka radiation equipped with a graphite monochromator.

**Thermogravimetric Analysis.** The effect of consecutive reduction−oxidation cycles on the reactivity of fresh and precalcined ilmenite using various reducing gas compositions was tested in a TGA, CI Electronics type. A detailed description of the apparatus and procedure can be found elsewhere.[34]

For the experiments, about 50 mg of ilmenite particles was loaded on the platinum basket. The system was heated to 1173 K in a $N_2$ atmosphere. After the set temperature was reached, the experiment was started by exposing the OC to alternating reducing and oxidizing conditions. To prevent reducing gas and air as an oxidizing agent from mixing, a nitrogen flow was passed for 2 min after the oxidizing and reducing processes. The composition of the gas during the reduction period was 15% $H_2$ + 20% $H_2O$, 15% CO + 20% $CO_2$, or 15% $CH_4$ + 20% $H_2O$, depending upon the reducing gas used, and $N_2$ to balance. The addition of steam to the reducing gas flow was made by bubbling the gas flow through a saturator containing water at the temperature of saturation at the desired steam concentration. Subsequent oxidation was carried out by air.

## Results and Discussion

**Characterization of Ilmenite Particles.** Table 1 shows the main properties for fresh and calcined ilmenite. The fresh ilmenite used in this study was the same one used by Leion et al.[28] and has a purity of 94.3%. The inert part is a mixture of oxides containing $MgSiO_3$ as the main compound. Through scanning electron microscopy (SEM) analysis, it could be observed that the inert part is clearly distinguishable as a separated phase from the active part formed by iron and titanium compounds. The XRD analysis revealed ilmenite ($FeTiO_3$), hematite ($Fe_2O_3$), and rutile ($TiO_2$) as major components of fresh ilmenite. Besides, SEM−energy-dispersive X-ray (EDX) analyses revealed a Fe/Ti molar relation around 1:1.

Calcined ilmenite consists of a mixture of ferric pseudobrookite ($Fe_2TiO_5$), rutile ($TiO_2$), and some free hematite ($Fe_2O_3$), which confirms the literature data indicating that iron compounds in ilmenite are in the most oxidized state after calcination at 1223 K.[32,35] To analyze the effect of the calcination time, samples were calcined during 1, 2, 6, and 24 h. For 2, 6, and 24 h, the same XRD profiles are obtained; therefore, it would be necessary that the pretreatment lasted only 2 h.

Mercury porosimetry of both fresh and calcined ilmenite exhibit low porosity development. Low values of Brunauer−Emmett−Teller (BET) surface area were measured, but a slight increase was observed after calcination. The values of crushing strength obtained are similar to other Fe-based OCs, and they are acceptable for the use of these particles in a circulating fluidized bed (CFB).[36] Table 1 also includes the main properties of activated particles after several redox cycles, and they will be discussed later.

Ilmenite composition was calculated through weight variations during oxidation or reduction of fresh ilmenite. Fresh ilmenite is mainly composed by $FeTiO_3$, $Fe_2O_3$, and $TiO_2$. When ilmenite is calcined, a gain of 3.5 wt % is observed because of the oxidation of $FeTiO_3$ ($Fe^{2+}$) to $Fe_2TiO_5$ ($Fe^{3+}$). This means that the fraction of $FeTiO_3$ in the raw material should be 65.5% considering the stoichiometric oxidation of $Fe^{2+}$ to $Fe^{3+}$. In addition, Table 2 shows the results from experiments carried out with calcined ilmenite in a thermobalance at 1173 K and varying the $H_2O/H_2$ ratio. Dependent upon the $H_2O/H_2$ ratio, the reduction of free $Fe_2O_3$ can finish in $Fe_3O_4$, FeO, or Fe because of thermodynamic equilibrium.[16] At 1173 K, for $H_2O/H_2 < 0.6$, free $Fe_2O_3$ can be reduced to metallic $Fe^0$, whereas for $H_2O/H_2 > 2.7$,

(29) Leion, H.; Mattisson, T.; Lyngfelt, A. *Int. J. Greenhouse Gas Control* **2008**, *2*, 180–193.
(30) Berguerand, N.; Lyngfelt, A. *Int. J. Greenhouse Gas Control* **2008**, *2*, 169–179.
(31) Berguerand, N.; Lyngfelt, A. *Fuel* **2008**, *87*, 2713–2726.
(32) Zhang, G.; Ostrovski, O. *Int. J. Miner. Process.* **2002**, *64*, 201–218.
(33) Pröll, T.; Mayer, K.; Bolhàr-Nordenkampf, J.; Kolbitsch, P.; Mattisson, T.; Lyngfelt, A.; Hofbauer, H. *Energy Procedia* **2009**, *1*, 27–34.
(34) Adánez, J.; de Diego, L. F.; García-Labiano, F.; Gayán, P.; Abad, A.; Palacios, J. M. *Energy Fuels* **2004**, *18*, 371–377.
(35) Bhogeswara Rao, D.; Rigaud, M. *Oxid. Met.* **1975**, *9*, 99–116.
(36) Johansson, M.; Mattisson, T.; Lyngfelt, A. *Therm. Sci.* **2006**, *10*, 93–107.

**Table 1. Characterization of Fresh, Calcined, and Activated Ilmenite**

| | fresh | calcined | activated |
|---|---|---|---|
| XRD (main species) | $FeTiO_3$, $Fe_2O_3$, $TiO_2$ | $Fe_2TiO_5$, $Fe_2O_3$, $TiO_2$ | $Fe_2TiO_5$, $Fe_2O_3$, $Fe_3O_4$, $TiO_2$ |
| true density (kg/m$^3$) | 4580 | 4100 | 4250 |
| porosity (%) | 0 | 1.2 | 35 |
| particle diameter ($\mu$m) | 150−300 | 150−300 | na |
| BET surface (m$^2$/g) | 0.6 | 0.8 | 0.4 |
| crushing strength (N) | 2.4 | 2.2 | 1.0 |

**Table 2. Mass Variations of Ilmenite When Reduced to Various Oxidation States at 1173 K and Iron-Containing Species Determined by XRD**

| $H_2O/H_2$ | mass loss (%) | final state of reduced $Fe_2O_3$ | final state of reduced $Fe_2TiO_5$ |
|---|---|---|---|
| 50 | 4.0 | $Fe_3O_4$ | $FeTiO_3$, $Fe_2TiO_4$ |
| 1.34 | 4.8 | FeO | $FeTiO_3$, $Fe_2TiO_4$ |

the reaction proceeds only until the formation of $Fe_3O_4$.[16] At $H_2O/H_2$ ratios between these values, free $Fe_2O_3$ is reduced to FeO. However, in all cases, $Fe_2TiO_5$ is reduced to $FeTiO_3$ or $Fe_2TiO_4$, corresponding to $Fe^{2+}$.[28] Consequently, the mass loss observed in each case should be different depending upon the final oxidation state of Fe from the reduction of free $Fe_2O_3$. Considering these mass variations, the resulting ilmenite composition is shown in Table 3. The Fe/Ti molar ratio thus obtained was 1:1.

**Ilmenite Reactivity.** Several reduction−oxidation cycles were carried out in TGA to analyze the reactivity of fresh and activated ilmenite. Oxidizing as well as reducing times for each cycle were set to 30 min. Figure 2 represents the sample mass variation during 10 cycles for fresh ilmenite. A mass value of 100% is assumed to be the sample in its most oxidized state. The initial mass is 3.5% lower, i.e., 96.5%, corresponding to the composition of fresh ilmenite. At the beginning, it can be observed that ilmenite is not completely reduced or oxidized after the fixed reacting time. However, there is an increase in both the reduction and oxidation extension during the repeated redox cycles. The mass loss is considered to be exclusively due to oxygen transfer and is stabilized at a value of 4.8% after 4 cycles, which is the maximum mass loss expected from the ilmenite composition estimation (see Table 2). Therefore, an activation process was observed that made the reactivity increase during the first redox cycles.

Figures 3 and 4 show the normalized conversion for the reduction, $X_{N,r}$, and oxidation, $X_{N,o}$, reactions with time for consecutive cycles of fresh ilmenite calculated from the mass variations registered in TGA as

$$X_{N,r} = \frac{m_o - m}{m_o - m_r} = \frac{m_o - m}{R_o m_o} \quad (6)$$

$$X_{N,o} = 1 - X_{N,r} = \frac{m - m_r}{R_o m_o} \quad (7)$$

where $m$ is the instantaneous mass and $m_o$ and $m_r$ are the mass of fully oxidized and reduced ilmenite at the reacting condition, respectively. The oxygen transport capacity, $R_o$, was defined as the mass fraction of the OC that is used in the oxygen transfer, calculated as

$$R_o = \frac{m_o - m_r}{m_o} \quad (8)$$

For the calculation of the normalized conversion, a value of $R_o = 4.8\%$ was considered in all cases.

**Table 3. Calculated Ilmenite Composition (wt %)**

| | fresh ilmenite | calcined ilmenite |
|---|---|---|
| $Fe_2O_3$ | 14.8 | 11.2 |
| $FeTiO_3$ | 65.5 | |
| $Fe_2TiO_5$ | | 54.7 |
| $TiO_2$ | 14.0 | 28.6 |
| inerts | 5.7 | 5.5 |

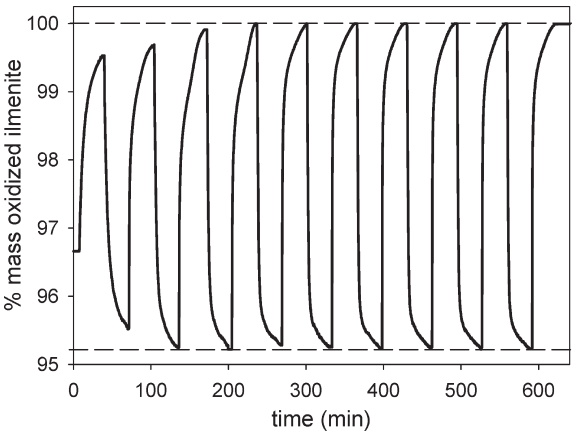


**Figure 2.** Mass variations during reduction−oxidation cycles in TGA starting from fresh ilmenite. Reduction and oxidation times = 30 min. Reducing gas = 15% $CH_4$ + 20% $H_2O$. Oxidation by air. $T$ = 1173 K.

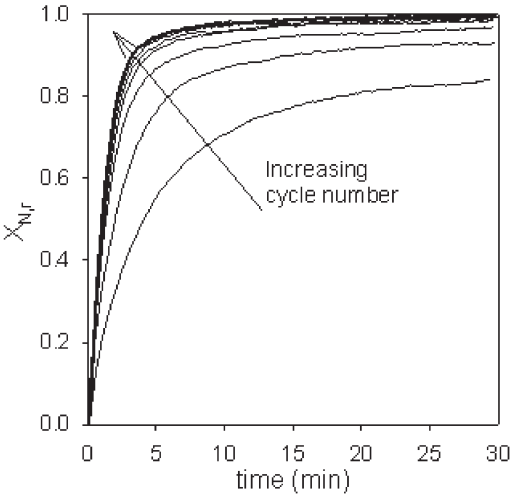


**Figure 3.** Normalized conversion during the reduction period of fresh ilmenite versus time through several cycles. Reducing gas = 15% $CH_4$ + 20% $H_2O$. Nitrogen to balance. $T$ = 1173 K.

Although ilmenite presents initially a rather low reactivity, the OC has a gradual gain in its reduction reaction rate as well as in its oxidation rate. The reactivity increases up to a maximum value after several cycles and stabilizes. This increase is more pronounced in the reduction reaction than in the oxidation reaction, because the initial reactivity for the

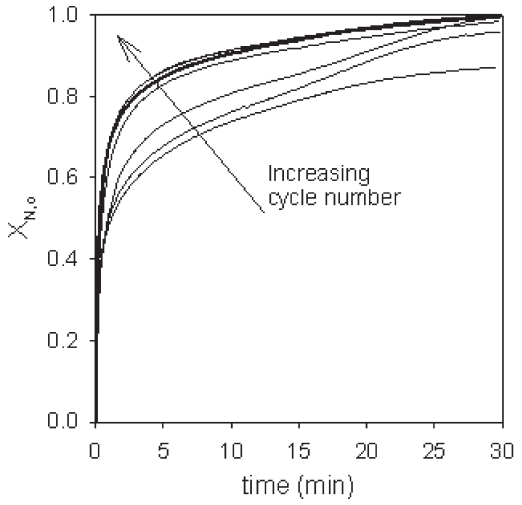


**Figure 4.** Normalized conversion during the oxidation period in air of fresh ilmenite versus time through several cycles. $T$ = 1173 K.

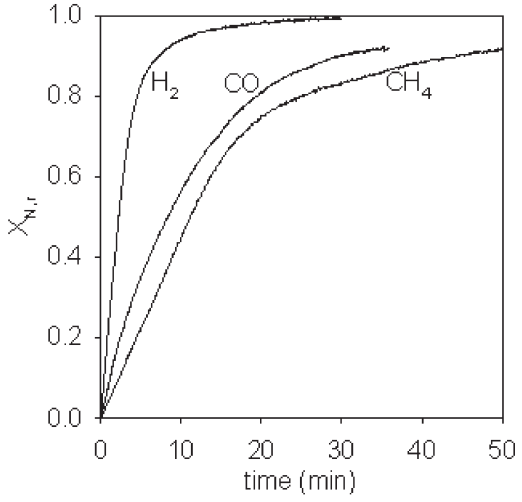


**Figure 5.** Normalized conversion during the reduction period of calcined ilmenite versus time for different reducing gases: 15% $H_2$ + 20% $H_2O$, 15% CO + 20% $CO_2$, and 15% $CH_4$ + 20% $H_2O$. Nitrogen to balance. $T$ = 1173 K.

oxidation of ilmenite for the first oxidation step is relatively high, with $X_{N,o}$ = 0.25 in less than 9 s for fresh ilmenite. After 4 cycles carried out in TGA, a value for the normalized conversion of 0.8 is reached in 120 s for reduction and 180 s for oxidation reactions. At this point, it can be considered that ilmenite had achieved the maximum conversion rate in both reduction and oxidation reactions. Also, it can be observed that the oxidation rate decreases gradually at high conversion values ($X_{N,o}$ > 0.8), reaching full conversion in 30 min. This fact indicates that a change in the resistance control has happen or the oxidation reaction proceeds via two consecutive steps.

Similar behavior was observed for redox cycles using $H_2$ and CO as reducing gases. For the different reducing gases, fresh, calcined, and activated ilmenite react faster with $H_2$ than with CO and $CH_4$. Figures 5 and 6 show the conversion versus time curves for the different reducing gases for calcined and activated ilmenite, respectively. Observe that the time scales are different in these figures. Calcined ilmenite reacts faster with CO than with $CH_4$, unlike activated

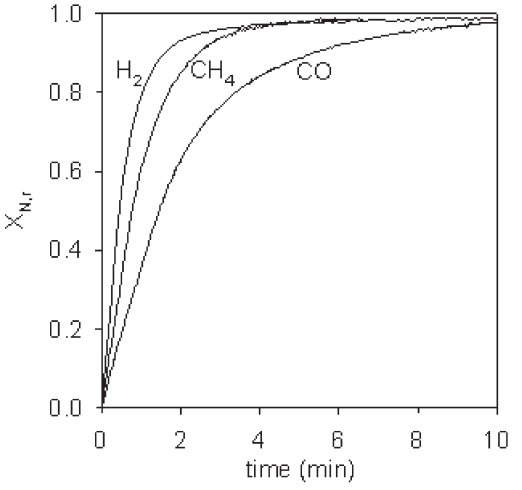


**Figure 6.** Normalized conversion during the reduction period of activated ilmenite versus time for different reducing gases: 15% $H_2$ + 20% $H_2O$, 15% CO + 20% $CO_2$, and 15% $CH_4$ + 20% $H_2O$. Nitrogen to balance. $T$ = 1173 K.

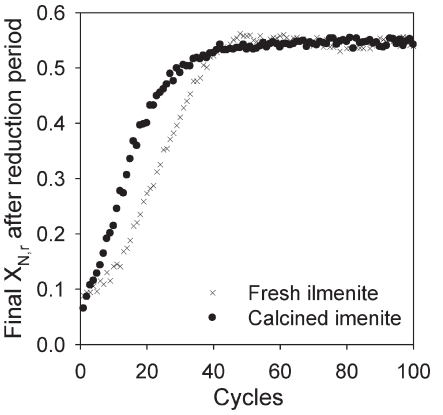


**Figure 7.** Comparison of the evolution of the final normalized conversion reached after the reduction period of fresh and calcined ilmenite through several cycles. Reduction and oxidation time = 1 min. Reducing gas = 15% $CH_4$ + 20% $H_2O$. Nitrogen to balance. $T$ = 1173 K.

ilmenite. For $H_2$ and CO, the reactivity increases around 5 times after the activation, while for $CH_4$, this increase is about 15 times. The reactivity increase observed for all of these fuel gases can be explained through the structural changes undergoing the solid during consecutives redox cycles, which will be discussed later.

**Effect of Precalcination on Ilmenite Activation.** Samples of fresh and calcined ilmenite were subjected to alternating reduction−oxidation cycles using $CH_4$, $H_2$, or CO as reducing gases. A total of 100 cycles were performed, and the reducing and oxidizing periods were 1 min. Thus, the effect of the extension of reduction can also be analyzed comparing the results to that shown in Figure 2. Figure 7 represents the final normalized conversion, $X_{N,r}$, reached after each reducing period using $CH_4$ as the reducing gas. Both samples showed an increase in the $X_{N,r}$ reached with the cycles up to a constant value. This was related to the fact that the reaction rate was higher in each cycle during the activation period before stabilizing. After that, no gain in the reaction rate was observed.

Both fresh and calcined ilmenite achieve the same conversion level after activation, but it can be observed however

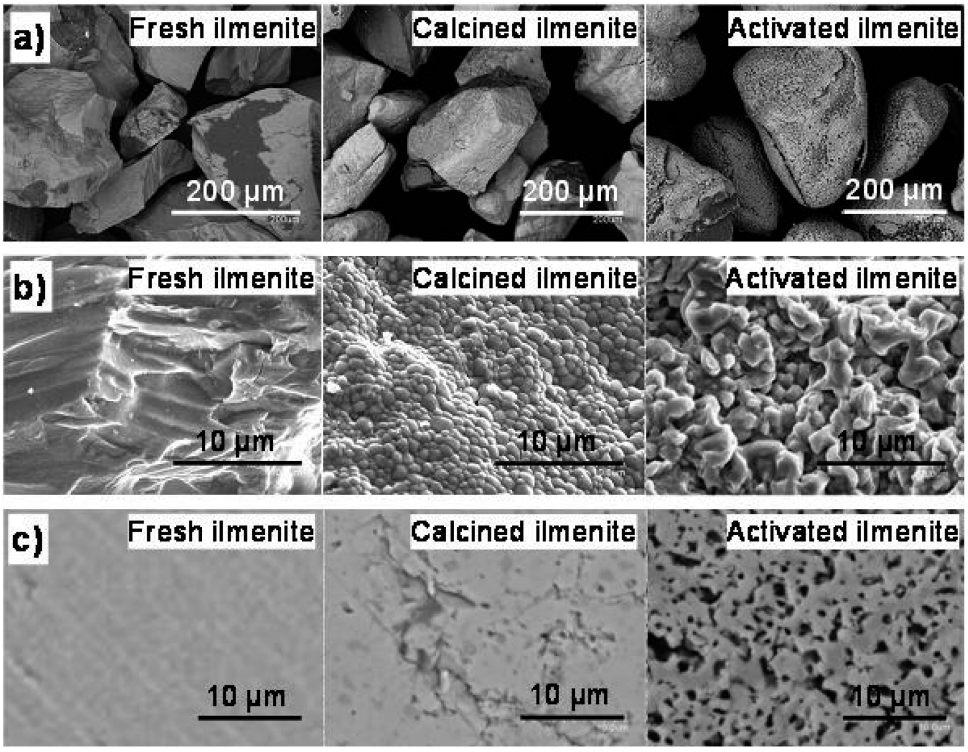


**Figure 8.** SEM images of (a) a general overview of several particles, (b) the external surface of the particles, and (c) a detail of the cross-section inside the particles for the fresh, calcined, and activated ilmenite.

that calcined ilmenite reached the activated state earlier. Whereas 40 cycles were necessary for the activation and stabilization for fresh ilmenite, about 30 cycles were enough to activate calcined ilmenite. Therefore, a previous calcination has a positive effect on both the reactivity of the OC and the activation rate during the activation period. A similar behavior was found when the activation was carried out using 15 vol % $H_2$ or 15 vol % CO as reducing gases, but in these cases calcined ilmenite activates in 9 cycles with $H_2$ and in 20 cycles with CO.

**Effect of the Extension of Reduction on Ilmenite Activation.** Experimental results where the reducing and oxidizing periods were 30 and 1 min are shown in Figures 2 and 7, respectively. The activation took only 4 cycles when the reacting periods were 30 min, whereas about 30−40 cycles were necessary when the reacting periods were 1 min. Thus, the activation state was clearly reached in a lower number of redox cycles when the redox periods were 30 min than when the redox periods were 1 min. This fact was because the reduction conversion reached in each cycle was higher as the reducing period was longer. The reduction conversion for 30 min was higher than 90%, but the conversion for 1 min was in the range of 10−50%. Leion et al.[28] also observed the activation of ilmenite during about 20 cycles before stabilizing, when the conversion reached in each cycle was around 50%. Therefore, the reduction conversion reached in each cycle has an important effect on the number of cycles needed to activate the ilmenite: the higher the reduction conversion, the less number of cycles are needed to activate ilmenite. Nevertheless, the total time used during reducing periods for activation of fresh ilmenite was 40 min for reducing periods of 1 min and 120 min for reducing periods of 30 min.

The activation period shown for the different reducing gases can also be explained for the diverse conversion reached in every redox cycle. The reactivity initially followed the order $H_2 > CO > CH_4$ (see Figure 5). Therefore, the conversion reached during the reduction period, 1 min in all cases, followed the same order, which explains that the number of redox cycles necessary for the ilmenite activation was in the reverse order $CH_4 > CO > H_2$.

The activation process has a beneficial and strong influence on the reactivity in both the oxidation and reduction reactions. To accelerate the activation process, calcined ilmenite should be preferred to fresh ilmenite. The activation of ilmenite particles is a process that can happen in the CLC system itself. Thus, the activation process should be considered during the startup period. At steady state, most of the particles in the CLC system should be activated ilmenite. Only a small fraction could be non-activated particles, corresponding to the makeup flow to maintain the solids holdup in the FR. Thus, the feeding of non-activated particles in the CLC system should not have a big effect on the CLC performance. In this case, the activation rate will depend upon the operating conditions, e.g., the residence time in the FR that affect the extension of reduction.

Nevertheless, in view of the relatively fast activation process, it could be advantageous for starting the operation to activate ilmenite particles previously to introduce them to the CLC system. Moreover, it can be beneficial for the economy of the process to carry out the activation in multiple short cycles instead of a few long cycles because a lower time is spent.

**Structural Changes during Activation.** To explain the activation observed by ilmenite during the calcination and redox cycles, a morphological characterization of each sample was performed by SEM. Figure 8 shows SEM microphotographs that confirm the lack of pores in fresh ilmenite and a slight gain in porosity after calcination. Throughout the reduction−oxidation cycles, there is a continuous appearance of macropores or cracks, which generate a rise in

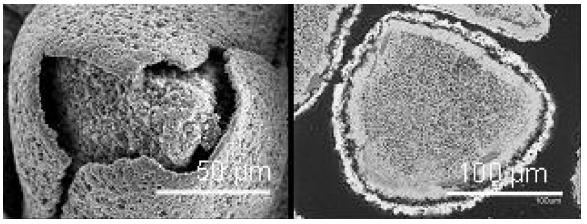


**Figure 9.** SEM micrograph of a particle and image of a cross-section of a particle of activated ilmenite.

porosity up to values of 35% for completely activated ilmenite. In Figure 8, a quite sharp-edged surface in fresh ilmenite can be observed and the active-phase surface begins to conform to a granular shape after calcination. The granulation is enhanced during redox cycles, as observed for activated ilmenite. This appearance of grains leads to a higher reaction surface, and likely this fact would be the reason for the reactivity increase with the cycle number. Similar results are found in the literature when natural minerals based on iron are used as OCs. Mattisson et al.[37] found the reactivity of an iron ore increased with redox cycles, likely because of the development of cracks and fissures in the particle. According to the work by Leion et al.,[28] the porosity development is also important for ilmenite with redox cycles.

Figure 9 shows the SEM image of a particle activated after repeated redox cycles. An external shell slightly separated from the rest of the particle was observed. The space between the shell and the core also enhances the porosity measured for the particle. This shell is gradually generated and grows with the number of cycles. EDX analyses were performed to determine Fe and Ti distributions throughout the particles (see Figure 10). In fresh and calcined ilmenite, distributions of both elements were uniform, which agrees with the XRD analysis that reveals $Fe_2TiO_5$ as the main component. For activated ilmenite, the particle core is titanium-enriched, whereas the external part is iron-enriched. XRD analyses to the external part found that this region is composed only by iron oxide, whereas XRD to the internal core revealed the existence of $TiO_2$ and $Fe_2TiO_5$. Thus, the external shell formed during the activation period was Fe-enriched, likely because of a migration phenomenon of iron oxide toward the external part of the particle, where there is not $TiO_2$ to form iron titanates. The segregation of $Fe_2O_3$ from the titanium-rich phase also has been reported in the literature because of the migration of $Fe^{2+}$ or $Fe^{3+}$ ions through the solid lattice toward the grain boundary during the oxidation step.[38,39]

**Oxygen Transport Capacity, $R_{o,ilm}$.** In addition to the OC reactivity, the oxygen transport capacity is a fundamental property of the OC because it determines the recirculation rate and solids inventory in the system and, thus, the suitability of ilmenite as an OC in CLC. The oxygen transport capacity of ilmenite can be obtained from eq 8 as the mass fraction of oxygen that can be used in the oxygen transfer. For CLC application, the oxygen transport capacity was defined as the oxygen that the OC can supply to reach full conversion to $CO_2$ and $H_2O$ at thermodynamic equilibrium. Initially, eq 8 was used to obtain a value of $R_o = 4.8\%$, which was used to calculate the normalized conversions, $X_{N,r}$ and $X_{N,o}$.

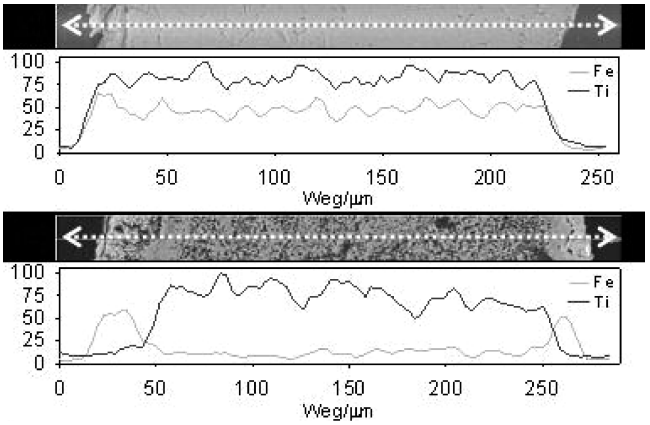


**Figure 10.** EDX line profiles of Fe and Ti in (a) calcined and (b) activated ilmenite particles.

This value corresponded to the oxygen transport observed during TGA experiments using 15% $H_2$ + 20% $H_2O$, 15% CO + 20% $CO_2$, or 15% $CH_4$ + 20% $H_2O$ in the reacting gases (see Figure 2). At these conditions, $Fe_2TiO_5$ reduces to $FeTiO_3$ and $Fe_2TiO_4$[28] and free $Fe_2O_3$ reduces to FeO.[16] However, free $Fe_2O_3$ is only capable to fully convert CO and $H_2$ into $CO_2$ and $H_2O$ when it is reduced to $Fe_3O_4$. Further reduction to FeO prevents full conversion of CO and $H_2$ toward $CO_2$ and $H_2O$ because of thermodynamic limitations.[16] Thus, the oxygen transport capacity for ilmenite, $R_{o,ilm}$, must be obtained considering that in the reduced state Fe is present as $FeTiO_3$ or $Fe_3O_4$. Therefore, $R_{o,ilm}$ depends upon the relative abundance of free $Fe_2O_3$ and iron titanates, which varies with the number of redox cycles.

To evaluate the fraction of Fe as $Fe_2TiO_5$ or $Fe_2O_3$ as a function of the number of redox cycles, different samples of calcined ilmenite were exposed at 10, 20, 30, 40, 50, 70, 85, and 100 redox cycles with 15 vol % $H_2$, CO, or $CH_4$ as fuel gas during the reduction period. The oxidation and reduction periods were 1 min. Particles subjected to different numbers of redox cycles had different activation degrees, and they were analyzed by XRD. Semi-quantitative percentages of $Fe_2O_3$ and $Fe_2TiO_5$ in each sample were obtained through normalization by means of a ratio between the intensity peaks of the main species and a substance of reference. Figure 11 shows the mass fraction of $Fe_2TiO_5$ and $Fe_2O_3$ in the ilmenite particles as a function of the number of cycles when $H_2$ was used as a reducing gas.

As the number of cycles increases, the fraction of free $Fe_2O_3$ rises at the expense of $Fe_2TiO_5$. With these percentages, the $R_{o,ilm}$ can be calculated, according to the formula

$$R_{o,\,ilm} = R_{o,\,Fe_2O_3} x_{Fe_2O_3} + R_{o,\,Fe_2TiO_5} x_{Fe_2TiO_5} \qquad (9)$$

$R_{o,Fe_2O_3}$ is the oxygen transport capacity of $Fe_2O_3$ when converted to $Fe_3O_4$ ($R_{o,Fe_2O_3} = 3.3\%$), and $R_{o,Fe_2TiO_5}$ is the oxygen transport capacity of $Fe_2TiO_5$ when converted to $FeTiO_3$ ($R_{o,Fe_2TiO_5} = 6.7\%$). $x_{Fe_2O_3}$ and $x_{Fe_2TiO_5}$ are the mass fractions of $Fe_2O_3$ and $Fe_2TiO_5$, respectively.

Figure 12a shows the evolution with the number of redox cycles of the oxygen transport capacity obtained from eq 9, $R_{o,ilm}$, for the different gases used. These values were confirmed by reduction of the different activated ilmenite samples in TGA using a $H_2O/H_2$ ratio of 50. At this ratio, it is ensured that free $Fe_2O_3$ is unable to become reduced further than $Fe_3O_4$, while $Fe_2TiO_5$ is reduced to $FeTiO_3 + Fe_2TiO_4$. The mass variation thus obtained gave similar values of

(37) Mattisson, T.; Lyngfelt, A.; Cho, P. *Fuel* **2001**, *80*, 1953–1962.
(38) Rao, D. B.; Rigaud, M. *Oxid. Met.* **1975**, *9*, 99–116.
(39) Nell, J. *Heavy Miner.* **1999**, 137–145.

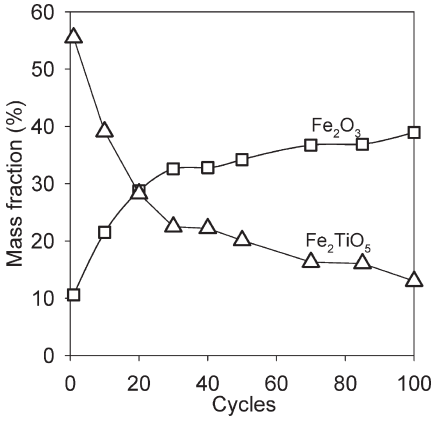


**Figure 11.** Mass fraction of $Fe_2O_3$ and $Fe_2TiO_5$ in ilmenite after 10, 20, 30, 40, 50, 70, 85, and 100 redox cycles. Oxidation and reduction periods were 1 min. Reducing gas = 15% $H_2$ + 20% $H_2O$. Nitrogen to balance. $T$ = 1173 K.

$R_{o,ilm}$ than those obtained using eq 9. The initial $R_{o,ilm}$ value for calcined ilmenite was 4 wt %. However, the fraction of free $Fe_2O_3$ increases with the number of cycles. As a consequence, the oxygen transport capacity decreases because free $Fe_2O_3$ reduction to $Fe_3O_4$ transfers less oxygen than reduction to $Fe^{2+}$. This decrease of $R_{o,ilm}$ is starker for the first cycles, and after the activation period, it decreases slight and continuously. The differences observed among the gases used were because of the different ilmenite conversion reached during the redox cycles, which affect the activation process, as previously stated. After 100 redox cycles, $R_{o,ilm}$ has a value of 2.1 wt %, but still a stable value was not reached.

**Evaluation of the Feasibility of Ilmenite as an Oxygen Carrier.** The use of a specific OC has important implications for a CLC system.[40] The reduction and oxidation reactivity of solids determines the solids inventory in the FR and AR, respectively, to reach full conversion of fuel gas. Moreover, the oxygen transport capacity is a fundamental property of the OC because it determines the recirculation rate and solids inventory in the system.

To facilitate a comparison of reactivity between different OCs, a rate index is often used as a normalized rate at a fuel gas concentration of 15%.[36] The rate index, expressed in %/min, is calculated as

$$\text{rate index} = 100 \cdot 60 \cdot \left( \left| \frac{d\omega}{dt} \right| \right)_{norm} = 100 \cdot 60 \cdot R_{o,ilm} \left( \frac{dX_i}{dt} \right)_{norm} \quad (10)$$

The mass-based conversion, $\omega$, was defined as

$$\omega = \frac{m}{m_o} = 1 + R_{o,ilm}(X_o - 1) = 1 - R_{o,ilm} X_r \quad (11)$$

Ilmenite conversion $X_i$ of the oxidation or reduction reaction was obtained using eqs 6 and 7 and considering that free $Fe_2O_3$ and $Fe_2TiO_5$ in ilmenite are reduced to $Fe_3O_4$ and $FeTiO_3$, respectively. Now the actual oxygen transport capacity, $R_{o,ilm}$, is used instead of the initial value $R_o$. The normalized reactivity is calculated as

$$\left( \frac{dX_i}{dt} \right)_{norm} = \frac{p_{ref}}{p_{TGA}} \left( \frac{dX_i}{dt} \right) \quad (12)$$

where $p_{ref}$ is the reference partial pressure of the fuel gas, here, equal to 0.15 atm, and $p_{TGA}$ is the partial pressure of the fuel gas used in the TGA experiments. For the reduction reaction, the fuel gas concentration used in the TGA experiments was 15% in all cases ($CH_4$, CO, and $H_2$). However, for the oxidation reaction, air was used as a reacting gas. In this case, $p_{TGA}$ = 0.21 atm and $p_{ref}$ = 0.10 atm. The reactivity, $dX_i/dt$, is defined here as the variation of conversion with time at zero conversion. For the reduction cases, this value is maintained roughly constant until conversion values as high as 60−80% (see Figures 3−6).

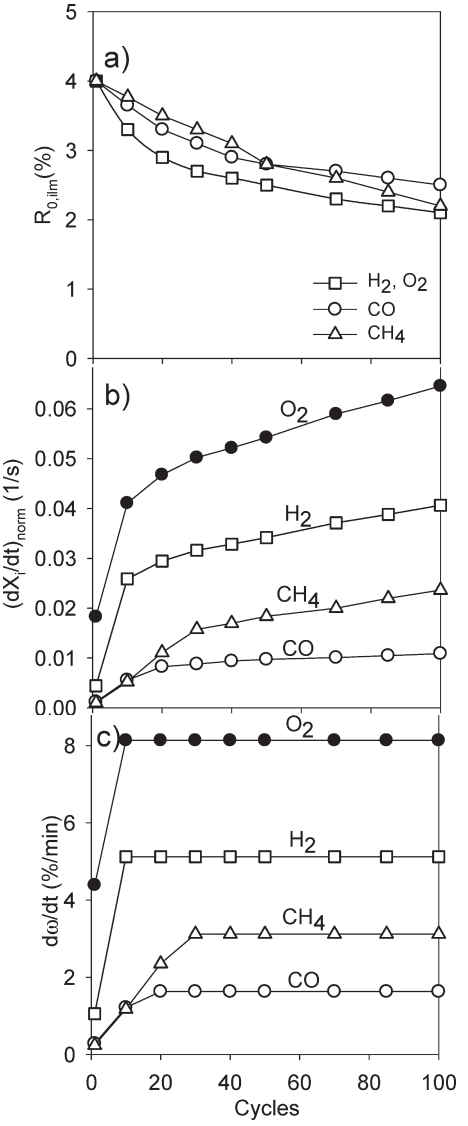


**Figure 12.** Variation of (a) the oxygen transport capacity, (b) the normalized reactivity, and (c) the rate index with the number of redox cycles. Oxidation and reduction periods were 1 min. Reacting gases = 15% $H_2$, 15% CO, 15% $CH_4$, and 10% $O_2$. Nitrogen to balance. $T$ = 1173 K.

Figure 12b shows the variation of the reactivity of ilmenite with the number of cycles. During the activation period, which was previously determined to be 9 cycles with $H_2$,

(40) Abad, A.; Adánez, J.; García-Labiano, F.; de Diego, L. F.; Gayán, P.; Celaya, J. *Chem. Eng. Sci.* **2007**, *62*, 533–549.

20 cycles with CO, and 30 cycles with $CH_4$, there is a considerable increase in the reaction rate. The slower reaction rate increase observed after this period was due to a concomitant effect of the variation of the oxygen transport capacity, $R_{o,ilm}$, on the conversion values. As previously shown, the oxygen transport capacity decreased with the cycle number. Therefore, the effect of ilmenite activation on the performance of a CLC system has a trade-off between the increase in reactivity and the decrease in oxygen transport capacity.

Figure 12c shows the rate index for every reacting gas as a function of the number of cycles. In this case, the reactivity is expressed as the rate of transference of oxygen by means of a mass fraction with respect to the ilmenite mass. It is observed that the rate index increased during the activation period and eventually reached a maximum and stable value that was kept constant during the cycles. This fact was expected from the normalized conversion curves shown in Figure 7, where the normalized conversion was calculated using a constant value of $R_o$ = 4.8 wt %.

The maximum value of the rate index was around 5.1%/min for $H_2$, 1.6%/min for CO, 3.1%/min for $CH_4$, and 8.1%/min for $O_2$. The rate index obtained for $CH_4$ is comparable to the rate index of 4.3%/min obtained from TGA experiments for a synthetic $Fe_2O_3/Al_2O_3$ OC.[40] A lower value of 2.8%/min was obtained by Johansson[41] for the same OC from FB experiments. This lower value could be due to gas-transfer limitations between bubble and emulsion phases that affect the reactivity obtained in the FB. Also from FB experiments, Johansson[36,41] showed that the rate index for several synthetic iron-based carriers was in the range of 0.5−4%/min for $CH_4$ combustion, which is in line with the rate index shown for activated ilmenite. This fact agrees with the results shown by Leion et al.,[29] where it was concluded that ilmenite reacts just as well as a synthetic $Fe_2O_3/MgAl_2O_4$ OC. However, higher reactivities were found for the $Fe_2O_3/Al_2O_3$ OC with $H_2$, CO, and $O_2$ from TGA experiments.[16] The calculated rate index from results shown by Abad et al.[16,40] were 9%/min for 15 vol % CO, 21%/min for 15 vol % $H_2$, and 14%/min for 10% $O_2$, which are considerably higher than the rate index shown by activated ilmenite. Nevertheless, it is necessary to remark that ilmenite is a natural mineral and a considerably cheaper material than a synthetic material.

**Applications to Design.** The important parameters in the design of a CLC system are the recirculation rate of particles and the solids inventory. These parameters will be determined in this section for the use of ilmenite as an OC following the methodology shown by Abad et al.[40] The CLC concept is based on the CFB configuration, and the circulation rate depends upon the operating conditions and configuration of the riser. Abad et al.[40] took a circulation rate value of $\dot{m}_{OC}$ = 16 kg $s^{-1}$ $MW_{th}{}^{-1}$ as the maximum circulation rate feasible in a CLC plant without increased costs according to commercial experience on CFB systems. Thus, in a real CLC system, the solids circulation may be fixed by the primary design of the AR, which acts as a riser to transport the solids to the FR. The recirculation rate between the AR and FR must be high enough to transport oxygen necessary for the fuel combustion, and it determines the solid conversion variation in the reactors. For combustion of gaseous fuels, e.g., $CH_4$ or syngas, the solid conversion variation in the reactors is calculated from a mass balance as a function of the solids circulation rate per $MW_{th}$ of fuel, $\dot{m}_{OC}$, as

$$\Delta X = \frac{2dM_o}{R_{o,ilm}\Delta H_c^o \dot{m}_{OC}} \quad (13)$$

The solid conversion variation, $\Delta X$, increases as the oxygen transport capacity, $R_{o,ilm}$, decreases, as seen in Figure 13a. Using the value $\dot{m}_{OC}$ = 16 kg $s^{-1}$ $MW_{th}{}^{-1}$, the solid conversion variation changes from $\Delta X$ = 0.09−0.12 when $R_{o,ilm}$ = 4.0% to $\Delta X_i$ = 0.14−0.23 for the $R_{o,ilm}$ corresponding to particles after 100 redox cycles, depending upon the fuel gas. For syngas combustion, the $\Delta X$ value should be between those values for $H_2$ and CO and will depend upon the syngas composition.

For combustion of solid fuels, e.g., coal, the solid conversion variation, $\Delta X$, depends upon the solids circulation rate

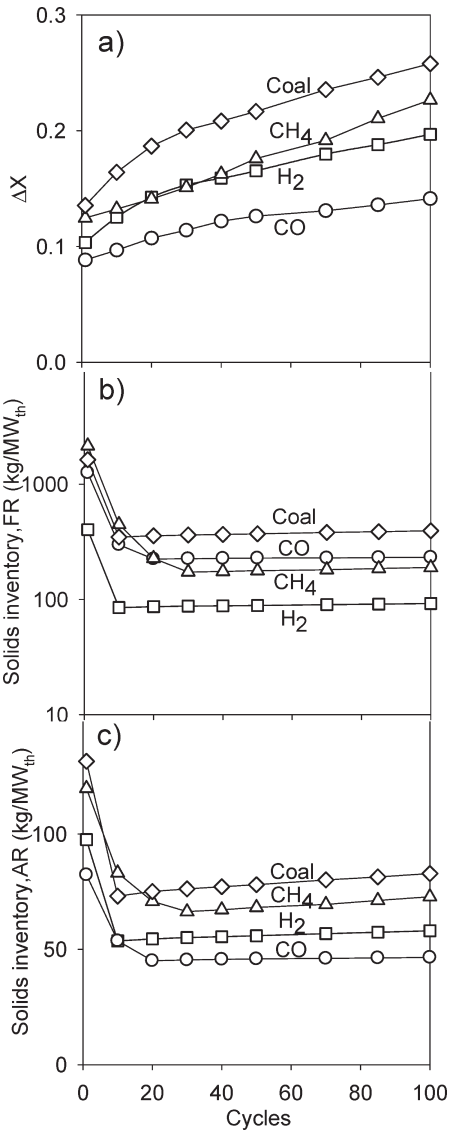


**Figure 13.** Calculated solid conversion variation (a) between AR and FR and solid inventories, $m_{OC}$, in the (b) FR and (c) AR for ilmenite reacted during several redox cycles. $T$ = 1173 K. $\dot{m}_{OC}$ = 16 kg $s^{-1}$ $MW_{th}{}^{-1}$. $X_{i,in} = 0.5 - \Delta X/2$.

(41) Johansson, M. Screening of oxygen-carrier particles based on iron, manganese, copper and nickel oxides for use in chemical-looping technologies. Ph.D. Dissertation, Department of Chemical and Biological Engineering, Environmental Inorganic Chemistry, Chalmers University of Technology, Göteborg, Sweden, 2007.

and the solid fuel type. In a similar way to eq 13, $\Delta X$ can be calculated as

$$\Delta X_i = \frac{10^3 m_O}{R_{o,ilm} LHV} \frac{1}{\dot{m}_{OC}} \quad (14)$$

with $m_O$ being the mass of oxygen required per kilogram of solid fuel to fully convert the solid fuel to $CO_2$ and $H_2O$ and LHV being the lower heating value of the solid fuel. It is necessary to point out that $m_O$ is the oxygen required for coal combustion, although the main reaction of coal particles in the FR is steam coal gasification. This is because the sum of reactions taking place in the FR, i.e., reactions 1−4, is the coal combustion. The steam fed into the FR does not supply oxygen for the coal combustion and only acts as a gasification agent.

In this work, a typical composition for coal of 70% carbon, 5% hydrogen, and 10% oxygen has been assumed, corresponding to a value of $m_O = 2.2$ kg of O/kg of coal. The LHV was assumed to be 25 000 kJ/kg, and the solids circulation rate per $MW_{th}$ of fuel equal to the value for gaseous fuels, i.e., $\dot{m}_{OC} = 16$ kg $s^{-1}$ $MW_{th}^{-1}$. The conversion variation, $\Delta X$, thus obtained is shown in Figure 13a. In this case, it was assumed that the activation process follows the behavior shown by the reduction using $H_2$. It can be seen that the $\Delta X$ values are somewhat higher than the values obtained for gaseous fuels because the oxygen demand for coal is higher than this for $CH_4$, $H_2$, and CO per $MW_{th}$ of fuel, which are 0.087, 0.08, 0.066, and 0.057 kg of oxygen per MJ for coal, $CH_4$, $H_2$, and CO, respectively. Moreover, $\Delta X$ also increases as the number of cycles increases because of the decrease of oxygen transport capacity. The low values obtained for $\Delta X$ indicate that ilmenite has enough oxygen transport capacity to be used as an OC in a CLC system, for gaseous and solid fuels.

The reactivity data obtained can be used to design the FR and AR in a CLC system, i.e., to obtain the solids inventory necessary to fully convert the gas fuel. In a CLC process, it is desirable to minimize the amount of bed material in the reactors because this will reduce the size and investment cost of the system and less power will be needed by the fans that supply the reacting gases to the reactors.

For combustion of gaseous fuels, e.g., $CH_4$ or syngas, a simplified model has been used to obtain an initial estimation of the solids inventory and for comparison purposes among different OCs.[16,40] This model considers perfect mixing of solids, no restriction for the gas−solid contact, and the solid reaction following the shrinking core model. In this case, the bed mass in the FR and AR per $MW_{th}$ of fuel, $m_{OC}$, can be calculated as[16,40]

$$m_{OC} = \eta_c \frac{2dM_o}{\Delta H_c^o} \frac{3}{\Phi R_{o,ilm} \left(\frac{dX_i}{dt}\right)_{av}} = \eta_c \frac{2dM_o}{\Delta H_c^o} \frac{3}{\Phi \left(\left|\frac{d\omega}{dt}\right|\right)_{av}} \quad (15)$$

The average reactivities, $(dX_i/dt)_{av}$ and $(d\omega/dt)_{av}$, are obtained at the average gas concentration in the reactor. In line with other works,[36,41] an average gas concentration of 15% for fuel gas and 10% for oxygen is considered. Thus, the average reactivity corresponds to the normalized values previously shown. The parameter $\Phi$ was defined as the characteristic reactivity of the particles in the reactor.[40] This parameter involves the effect of both the residence time distribution of the particles in the reactor and the fact that particles entering the reactor could have been not fully oxidized in the AR. Thus, the higher the average residence time or the lower the oxidation conversion in the AR, the lower the average reactivity in the reactor. With the assumption of perfect mixing of solid particles in the FR and AR, the parameter $\Phi$ can be expressed as a function of the solid conversion at the inlet of the reactor, $X_{i,in}$, and the conversion variation in the reactor, $\Delta X$

$$\Phi = 3\left[1 - X_{i,in}^{2/3} \exp\left(\frac{(1 - X_{i,in}^{1/3})}{\Delta X}\Phi\right)\right] - \frac{6\Delta X}{\Phi}\left[1 - X_{i,in}^{1/3} \exp\left(\frac{(1 - X_{i,in}^{1/3})}{\Delta X}\Phi\right)\right] + \frac{6\Delta X^2}{\Phi^2}\left[1 - \exp\left(\frac{(1 - X_{i,in}^{1/3})}{\Delta X}\Phi\right)\right] \quad (16)$$

For the shrinking-core model in spherical grains, the value of characteristic reactivity, $\Phi$, is limited between 3 and 0. The minimum solids inventory in every reactor is obtained considering that $\Phi = 3$, which is the case for $X_{i,in} = 0$ and $\Delta X \approx 0$. This condition could be reached when there were no limitations for solids circulation between FR and AR. However, as previously discussed, a limitation for $\dot{m}_{OC} = 16$ kg $s^{-1}$ $MW_{th}^{-1}$ can be expected, which gives values of $\Delta X$ in the range of 0.10−0.25 (see Figure 13a). The characteristic reactivity, $\Phi$, decreases as $\Delta X$ increases and the resulting solids inventory increases. This parameter can be obtained from eq 16 by an iterative calculation or more easily being estimated from Figure 7 in the work performed by Abad et al.[40]

From results obtained in previous works,[40,42−44] the minimum solids inventory in a CLC system, considering the sum of solids in both AR and FR, is obtained for an intermediate situation between the full OC reduction in the FR and the full OC oxidation in the AR. To minimize the solids inventory, the inlet conversion to each reactor was found to be around the value $X_{i,in} = 0.5 - \Delta X/2$.[40,42−44] For comparison purposes, the value for $X_{i,in}$ corresponding to every value of $\Delta X$ was used to obtain the solids inventory. Figure 13b shows the evolution of the solids inventory obtained from eq 15 with the number of cycles for $H_2$, CO, and $CH_4$. It can be seen that the solids inventory decreases initially because the ilmenite reactivity increases during the activation process. After this period, the solids inventory slightly increases as $R_{o,ilm}$ decreases with the number of cycles. Indeed, the lower oxygen available in ilmenite as the number of cycle increases is the reason for both the increase in $\Delta X$ and the solids inventory when the rate of oxygen transference, i.e., $d\omega/dt$, is constant, as is the case. The solids inventory thus obtained is about 85 kg/$MW_{th}$ for $H_2$, 225 kg/$MW_{th}$ for CO, and 175 kg/$MW_{th}$ for $CH_4$, after ilmenite activation. For a highly reactive

(42) Zafar, Q.; Abad, A.; Mattisson, T.; Gevert, B. *Energy Fuels* **2007**, *21*, 610–618.
(43) Zafar, Q.; Abad, A.; Mattisson, T.; Gevert, B.; Strand, M. *Chem. Eng. Sci.* **2007**, *62*, 6556–6567.
(44) García-Labiano, F.; de Diego, L. F.; Adánez, J.; Abad, A.; Gayán, P. *Ind. Eng. Chem. Res.* **2004**, *43*, 8168–8177.

synthethic Fe-based OC, a similar solids inventory was obtained for $CH_4$,[40] whereas for $H_2$ and CO, the solids inventory is lower than that for activated ilmenite, i.e., about 20 kg/$MW_{th}$ for $H_2$ and 40 kg/$MW_{th}$ for CO,[16,40] with all of them referred to an average gas concentration of 15%. Nevertheless, the solids inventory needed for ilmenite takes acceptable values and is in the same range as the values observed for synthetic OCs with proven suitability in a CLC process.[43]

For syngas, which is a gas mixture mainly composed of $H_2$, CO, $H_2O$, and $CO_2$, the reactivity and the solids inventory have been found to be close to those shown for only $H_2$, with the $H_2$ concentration the sum of both $H_2$ and CO concentrations.[16,44] This fact can be due to the synergic effect of the water−gas shift reaction that produces more $H_2$ from the less reactive CO.[20,21]

For solid fuels, the solids inventory can be calculated by analogy to eq 15 respecting eq 13 for gaseous fuels. Considering the oxygen demanded by the fuel calculated by eq 14, the solids inventory for solid fuels was obtained as

$$m_{OC} = \eta_c \frac{10^3 m_o}{LHV} \frac{3}{\Phi R_{o,ilm} \left(\frac{dX_i}{dt}\right)_{av}} = \eta_c \frac{10^3 m_o}{LHV} \frac{3}{\Phi \left(\left|\frac{d\omega}{dt}\right|\right)_{av}} \quad (17)$$

The reactivity parameters in this equation, i.e., $(dX_i/dt)_{av}$ or $(|d\omega/dt|)_{av}$, should be evaluated at an average gas concentration in the reactor. The main gases reacting with the OC during operation with solid fuel are $H_2$ and CO proceeding from the char gasification and gases proceeding from the coal devolatilization that can be initially assumed to be $CH_4$. However, other important issues for volatile compounds are the rate of mixing between the OC and coal particles and the injection point of coal inside the reactor,[30,31] with it being difficult at this stage to assign an average concentration for volatile compounds. For comparison purposes, an initial estimation of the solids inventory was calculated only considering $H_2$ and CO proceeding from coal gasification. The average concentration of $H_2$ and CO in the reactor will depend upon the dynamics of the reactions in the FR. It is likely that the concentration of these gases stabilizes at a value at which the generation rate from coal gasification is equal to the disappearance rate by the reaction with the OC. These concentration values can be as low as 2%, as found during CLC continuous operation using ilmenite as an OC[30,31] because the gasification reaction would be the limiting step in the process. Moreover, the $H_2$ and CO concentrations would be roughly constant in the whole reactor. Considering that the reactivity of a mixture of $H_2$ and CO is similar to the reactivity for $H_2$,[16,44] as stated above, the average reactivity was calculated for $H_2$. The $H_2$ concentration was considered to be 5%, as the sum of $H_2$ and CO concentrations, and the average reactivity was calculated from eq 12 with $p_{ref}$ = 0.05 atm $H_2$.

Figure 13b shows the solids inventory thus obtained from eq 17. Similar to gaseous fuels, the initial solids inventory value is high because the reduction rate is rather low and ilmenite is not yet activated. The minimum solids inventory is obtained after the activation period, when the oxygen transport capacity, $R_{o,ilm}$, still has high values. The solids inventory increases with the number of cycles because of the decrease in $R_{o,ilm}$. The solids inventory after ilmenite activation takes an average value of about 350 kg/$MW_{th}$.

The solids inventory in the AR can be obtained from eqs 15 and 17 for gaseous and solids fuels, respectively.[40] In this case, the average reactivity, i.e., $(dX_i/dt)_{av}$ or $(|d\omega/dt|)_{av}$, should be that corresponding to the oxidation reaction. Because the oxygen demanded by each fuel ($CH_4$, $H_2$, CO, or coal) is different per $MW_{th}$ of fuel, the solids inventory per $MW_{th}$ in the AR is also different for every fuel gas, even if the oxidation reactivity is the same in all cases. Therefore, a solids inventory in the AR can be calculated for each fuel gas, as shown in Figure 13c. Lower values of the solids inventory are found for the AR than for the FR because of the higher ilmenite reactivity for the oxidation reaction with respect to the reduction reactions.

It must be remarked that all of these values for solids inventory correspond to conditions where the resistance to the gas exchange between the bubble and emulsion phases are considered negligible. In real systems, if the resistance to the gas exchange between the bubble and emulsion phases is important, higher solids inventories would be necessary. Nevertheless, these values can be used for comparison purposes between different OCs and to give an easy and fast evaluation of the solids inventory in a CLC system. A FB model must be used to give a more accurate evaluation of the solids inventory needed in the FR.[45]

In any case, from results shown in this work, it can be concluded that ilmenite presents a competitive performance for its use in CLC against synthetic OCs when it is taken into account for the oxygen transport capacity, the moderated solids inventory, and the low cost of the material. This last issue can be determinant for the selection of an OC for solid fuels combustion in a CLC system.

## Conclusions

The activation process of ilmenite through consecutive redox cycles has been analyzed. Ilmenite increases its reactivity with the number of cycles. For reducing and oxidizing periods of 30 min, it can be considered that from cycle 4 the reaction rate has already become maximum and stable, reaching complete conversion in every cycle. For reducing periods of 1 min, the activation takes about 9 cycles with $H_2$, 20 cycles with CO, and 30 cycles with $CH_4$. The different activation behavior with different gases was attributed to the different reduction degree reached for each fuel gas in every cycle. A previous calcination of ilmenite has a positive effect on the activation process. After activation, the reactivity for $H_2$ and CO rises around 5 times, while for $CH_4$, this increase is about 15 times. Reduction and oxidation rates of activated ilmenite are relatively high, with a conversion of 80% in less than 5 min. The reaction with $H_2$ is faster than with CO and $CH_4$.

Structural changes on the ilmenite particles after calcination and activation have been observed. The surface texture changes from a quite sharp-edged surface in fresh ilmenite to a granular shape in calcined samples. The granular shape was enhanced during the activation process. The porosity slightly increases during calcination. After activation, the porosity of particles increases up to values of 35%. The appearance of

(45) Abad, A.; Adánez, J.; García-Labiano, F.; de Diego, L. F.; Gayán, P. *Combust. Flame* **2009**, doi: 10.1016/j.combustflame.2009.10.010.

cracks and an external shell in the particle, which is Fe-enriched, was observed. All of them can explain the increase of ilmenite reactivity with the redox cycles.

As activation proceeds, the reactivity increases but the oxygen transport capacity of ilmenite, $R_{o,ilm}$, decreases because of the appearance of free $Fe_2O_3$ in the external shell. Thus, the initial $R_{o,ilm}$ value is 4%, and it decreases until 2.1% after 100 redox cycles with hydrogen as fuel gas.

In comparison to other OCs and, in particular, to iron-based carriers, the $R_{o,ilm}$ and reactivity values shown for calcined and activated ilmenite have high enough values to transfer the required oxygen from air to fuel in a CLC system and to obtain acceptable values of minimum solids inventories in the system and good performance of ilmenite for a CLC purpose with solid fuels. A simplified method for the estimation of solids inventory in the AR and FR was proposed for solid fuels. The solids inventory in the FR thus obtained depended upon the activation progress, decreasing from 1600 to 350 kg/$MW_{th}$ for coal during the activation period. These values can be used for comparison purposes among OCs.

**Acknowledgment.** This work was partially supported by the European Commission, under the RFCS program (ECLAIR Project, Contract RFCP-CT-2008-0008), and from Alstom Power Boilers. A. Cuadrat thanks CSIC for the JAE Pre-fellowship.

## Nomenclature

$d$ = stoichiometric factor in the fuel combustion reaction with oxygen (mol of $O_2$/mol of fuel)
$\Delta H_c^0$ = standard combustion heat of the gas fuel (kJ $mol^{-1}$)
$m$ = instantaneous mass of the OC (kg)
$m_o$ = mass of fully oxidized OC (kg)
$m_r$ = mass of fully reduced OC at the reacting condition (kg)
$m_O$ = mass of oxygen required per kilogram of solid fuel to fully convert the solid fuel (kg of oxygen/kg of coal)
$m_{OC}$ = solids inventory (kg/$MW_{th}$)
$\dot{m}_{OC}$ = solids circulation rate per $MW_{th}$ of fuel (kg $s^{-1}$ $MW_{th}^{-1}$)
$M_O$ = molecular weight of oxygen (16 g $mol^{-1}$)
$p_{ref}$ = reference partial pressure of the fuel gas (atm)
$p_{TGA}$ = partial pressure of the fuel gas used in the TGA experiments (atm)
$R_o$ = oxygen transport capacity for the normalized case
$R_{o,ilm}$ = actual oxygen transport capacity of ilmenite
$R_{o,Fe_2O_3}$ = oxygen transport capacity of $Fe_2O_3$
$R_{o,Fe_2TiO_5}$ = oxygen transport capacity of $Fe_2TiO_5$
$t$ = time (s)
$T$ = temperature (K)
$x_{Fe_2O_3}$ = mass fraction of $Fe_2O_3$
$x_{Fe_2TiO_5}$ = mass fraction of $Fe_2TiO_5$
$X_i$ = ilmenite conversion for the reaction $i$
$X_{i,in}$ = solid conversion at the inlet of the reactor
$X_{N,i}$ = normalized conversion for the reaction $i$
$\Delta X$ = variation of the solids conversion

*Greek Symbols*

$\eta_c$ = combustion efficiency
$\omega$ = mass-based conversion
$\Phi$ = characteristic reactivity in the reactor

*Acronyms*

AR = air reactor
CLC = chemical-looping combustion
FB = fluidized bed
FR = fuel reactor
LHV = lower heating value of the solid fuel (kJ/kg)
OC = oxygen carrier

*Subscripts*

av = average condition
$i$ = oxidation (o) or reduction (r) reaction
ilm = ilmenite
norm = normalized gas concentration

# Paper II

Chemical Engineering Science 66 (2011) 689–702

Contents lists available at ScienceDirect

Chemical Engineering Science

journal homepage: www.elsevier.com/locate/ces

# Kinetics of redox reactions of ilmenite for chemical-looping combustion

Alberto Abad *, Juan Adánez, Ana Cuadrat, Francisco García-Labiano, Pilar Gayán, Luis F. de Diego

*Department of Energy and Environment, Instituto de Carboquímica (CSIC), Miguel Luesma Castán 4, 50018 Zaragoza, Spain*

ARTICLE INFO

*Article history:*
Received 13 January 2010
Received in revised form
27 September 2010
Accepted 11 November 2010
Available online 18 November 2010

*Keywords:*
Combustion
Energy
Fuel
Kinetics
Chemical-looping combustion
Ilmenite

ABSTRACT

The objective of this study was to establish the kinetic of both reduction and oxidation reactions taking place in the chemical-looping combustion (CLC) process using ilmenite as an oxygen carrier. Because of the benefits of using of pre-oxidized ilmenite and the activation of the ilmenite during the redox cycles, the reactivity of both the pre-oxidized and activated ilmenite was analyzed. The experimental tests were carried out in a thermogravimetric analyzer (TGA), using $H_2$, CO or $CH_4$ as reducing gases, and $O_2$ for the oxidation step. Thus, the reactivity with the main reacting gases was analyzed when natural gas, syngas or coal are used as fuels in a CLC system. The changing grain size model (CGSM) was used to predict the evolution with time of the solid conversion and to determine the kinetic parameters. In most cases, the reaction was controlled by chemical reaction in the grain boundary. In addition, to predict the behaviour of the oxidation during the first redox cycle of pre-oxidized ilmenite, a mixed resistance between chemical reaction and diffusion in the solid product was needed. The kinetic parameters of both reduction and oxidation reactions of the pre-oxidized and activated ilmenite were established. The reaction order for the main part of the reduction reactions of pre-oxidized and activated ilmenite with $H_2$, CO, $CH_4$ and $O_2$ was $n=1$, being different ($n=0.8$) for the reaction of activated ilmenite with CO. Activation energies from 109 to 165 kJ mol$^{-1}$ for pre-oxidized ilmenite and from 65 to 135 kJ mol$^{-1}$ for activated ilmenite were found for the different reactions with $H_2$, CO and $CH_4$. For the oxidation reaction activation energies found were lower, 11 kJ mol$^{-1}$ for pre-oxidized and 25 kJ mol$^{-1}$ for activated ilmenite.

Finally, simplified models of the fuel and air reactors were used to do an assessment of the use of ilmenite as an oxygen carrier in a CLC system. The reactor models use the reaction model in the particle and the kinetic parameters obtained in this work. Taking into account for its oxygen transport capacity, the moderated solids inventory and the low cost of the material, ilmenite presents a competitive performance against synthetic oxygen carriers when coal or syngas are used as fuel.



## 1. Introduction

Chemical-looping combustion (CLC) is one of the most promising technologies to carry out $CO_2$ capture at a low cost (Ekström et al., 2009; IPCC, 2005; Kerr, 2005). CLC is based on the transfer of the oxygen from air to the fuel by means of a solid oxygen carrier. In the most common configuration, the oxygen carrier circulates between two interconnected fluidized beds – the fuel reactor and the air reactor – avoiding direct contact between fuel and air. Fig. 1 shows a general scheme of this process. In the fuel reactor the oxygen carrier is reduced through oxidation of the fuel. If the composition of the fuel gas is expressed as $C_nH_mO_l$, the reduction reaction is

$$(2p+q/2-r)Me_xO_y+C_pH_qO_r\rightarrow(2p+q/2-r)Me_xO_{y-1}+pCO_2+q/2H_2O \quad (1)$$

where $Me_xO_y$ denotes a metal oxide and $Me_xO_{y-1}$ its reduced compound. The oxygen carrier reduced in the fuel reactor, $Me_xO_{y-1}$, is transferred to the air reactor where reaction (2) with oxygen from air takes place. Thus the oxygen carrier is regenerated to start a new cycle

$$2Me_xO_{y-1}+O_2\rightarrow2Me_xO_y \quad (2)$$

In a CLC system, the stream of combustion gases from the fuel reactor contains primarily $CO_2$ and $H_2O$. Water can be easily separated by condensation and a highly concentrated stream of $CO_2$ ready for sequestration is achieved. Thus, the $CO_2$ capture is inherent to this process, as the air does not get mixed with the fuel, and virtually a 100% of $CO_2$ capture can be reached in a CLC system without additional costs or energy penalties for gas separation. Moreover, the net chemical reaction is the same as at usual combustion with the same combustion enthalpy.

The fuel can be a gaseous, liquid or solid compound. On the one hand, natural gas and syngas have been widely proven as gaseous fuels (Lyngfelt, 2010). On the other hand, the in-situ gasification of

* Corresponding author. Tel.: +34 976 733977; fax: +34 976 733318.
*E-mail address:* abad@icb.csic.es (A. Abad).

0009-2509/$ - see front matter © 2010 Elsevier Ltd. All rights reserved.
doi:10.1016/j.ces.2010.11.010

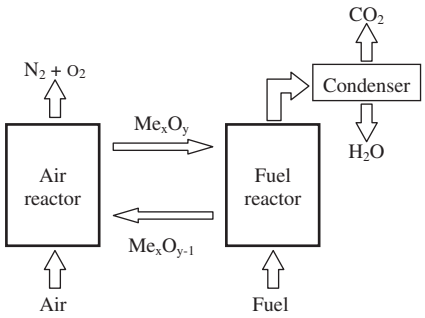


**Fig. 1.** General scheme of a chemical-looping combustion system.

solid fuels is a relevant option to process them in a CLC system (Leion et al., 2008a). Pyrolysis and gasification of the solid fuel take place in the fuel reactor, and the oxygen carrier, $Me_xO_y$, reacts with the gaseous products, where $H_2$, CO and volatile matter are the main components. Against the use of syngas from coal gasification as fuel gas in a CLC system, the direct use of coal in the CLC process has the benefit of avoiding the need of a gasifier and oxygen for coal gasification.

To design a CLC system it is necessary to define the reducing agents of the oxygen carrier. For gaseous fuels, the main reacting gases in the fuel reactor are $CH_4$, CO and $H_2$. When solid fuels are used, the direct reduction of the solid material with carbon also is possible (Siriwardane et al., 2009). However, in a CLC system the reduction by volatiles and the gasification gases, i.e. $H_2$ and CO, should have a higher relevance, and the effect of reduction by carbon should be negligible at temperatures lower than 1300 K (Dey et al., 1993; Donskoi et al., 2003; Sohn and Fruehan, 2005).

### 1.1. The oxygen carrier

Most of the oxygen carriers proposed in the literature are synthetic materials. In general, the oxygen carrier is based on a transition state metal oxide, e.g. CuO, NiO, CoO, $Fe_2O_3$ or $Mn_3O_4$, which is supported on different inert materials, as $Al_2O_3$, $SiO_2$, $TiO_2$ or $ZrO_2$. A selection of oxygen carrier materials for natural gas and syngas combustion has been summarized by Hossain and de Lasa (2008) and Lyngfelt et al. (2008). In addition, there is an increasing interest for the application of CLC regarding the intensive use of coal for energy generation. Since the ashes are present in the solid fuel the draining of ashes from the system is necessary so as to avoid their accumulation in the reactors, a partial loss of the oxygen carrier together with the coal ashes being predictable. Although synthetic materials – mainly based on Fe, Cu and Ni – have been proposed as oxygen carriers in CLC for solid fuels, e.g. coal, petroleum coke, biomass or solid wastes (Cao et al., 2006; Chuang et al., 2008; Leion et al., 2007; Scott et al., 2006; Shen et al., 2009; Siriwardane et al., 2009; Yang et al., 2007), low cost of the carrier is rather desirable for its use. The use of natural minerals or industrial waste products for this option seems to be very promising (Leion et al., 2009a). These authors analyzed the behaviour of several iron ores, and Fe and Mn industrial products during repeated redox cycles at fluidizing conditions. They concluded ilmenite – a natural mineral mainly composed of $FeTiO_3$ – meet all criteria to be considered as an oxygen carrier for CLC with solid fuels.

Comparing the performance of several natural iron ores and industrial products, ilmenite was ranged among the materials which showed higher reactivity (Leion et al., 2009a, 2009b). The gas conversion showed by ilmenite was even similar to the one manufactured $Fe_2O_3/MgAl_2O_4$ selected from previous works because of their good performance for CLC applications (Leion et al., 2008a). In addition, the use of ilmenite as an oxygen carrier has shown to have high conversion for syngas applications, where CO and $H_2$ are the main components. However, moderate conversion of $CH_4$ for the use of natural gas as fuel was obtained (Leion et al., 2008b). Ilmenite showed high stability in its reactivity after repeated redox cycles. Additionally, ilmenite showed good mechanical stability and good fluidizing properties (Leion et al., 2009a). Defluidization occurred only when the ilmenite particles were in a highly reduced state (Leion et al., 2008b), which is not expected at CLC operation. It should be mentioned that the same ilmenite particles have been used in a 10-kW CLC unit for long periods without difficulties of defluidization (Berguerand and Lyngfelt, 2008a, 2008b).

The effect of successive redox cycles on the ilmenite performance was analyzed in a previous work (Adánez et al., 2010). Ilmenite's reactivity has found to be increasing with the cycle number during first 5–20 cycles, so-called the activation period, and after this period its reactivity was maintained roughly constant. The number of cycles of the activation period depended on the reduction conversion reached in every cycle and the reducing gas used. The activation of ilmenite particles is a relatively fast process. Thus, the activation of ilmenite can be done in the CLC system itself, being not necessary the previous activation of ilmenite. Moreover, the fraction of hematite increased at the expense of pseudobrookite with the redox cycles. As a consequence, the oxygen transport capacity of ilmenite particles decreased with the redox cycles. Moreover, the pre-oxidation of ilmenite particles was considered in order to improve properties, the initial reaction rates and decrease the time for the activation period. Thus, a thermal pre-treatment before feeding ilmenite to the CLC system is appropriate.

### 1.2. Kinetics of reaction for CLC

A key parameter for the design of a CLC system is the solids inventory in the fuel and air reactors as well as the recirculation rate of oxygen carriers between the reactors. Both parameters are linked and depend on the reactivity of the materials and on the oxygen transport capacity of the oxygen carrier (Abad et al., 2007a). The oxygen carrier must have enough reactivity to fully convert the coal in the fuel reactor, and to be regenerated in the air reactor. Therefore to design a CLC system it is necessary to determine the reactivity under different operating conditions of temperature and gas concentration. It must be considered that the oxygen carrier will be found in different environments during their stage in the fluidized bed reactors. In addition, the modelling of the reactor would be helpful for the design, optimization, and scale-up of the process, in order to obtain high combustion efficiencies in a CLC system. To obtain theoretical results which could be validated against experimental data, the kinetics of reduction and oxidation of the oxygen carrier must be determined.

The kinetics of reaction for the reduction with the main reducing gases present in a CLC system, i.e. $CH_4$, CO and $H_2$, and the oxidation with oxygen have been determined for CuO-, NiO-, $Fe_2O_3$- and $Mn_3O_4$-based oxygen carriers, as it was reviewed by Hossain and de Lasa (2008). The shrinking core model, the changing grain size model and the nucleation model have been widely used to determine the kinetic parameters. However, most of these works give only limited information to apply the kinetics parameters in a mathematical model for the CLC system, because either the effect of the gas concentration or temperature has not been analyzed. Only a limited number of studies have focused on the kinetics of oxygen carriers considering the variation of gas concentration and reactor temperature that could happen in a CLC system, i.e. covering a wide range of gas concentration and temperature representative of the

appearing in the air and fuel reactors (Abad et al., 2007a, 2007b; Bohn et al., 2009; Chuang et al., 2009a, 2009b; García-Labiano et al., 2004, 2006; Ishida et al., 1996; Moghtaderi et al., 2010; Sedor et al., 2008; Zafar et al., 2007a, 2007b). Moreover, less are the studies focused on the kinetics of one certain oxygen carrier with all the reducing gases when natural gas, syngas or coal are used as fuel, mainly $CH_4$, CO and $H_2$ (Abad et al., 2007a; García-Labiano et al., 2004; Moghtaderi et al., 2010). It is necessary to point out that CO and $H_2$ appear during reaction of coal, and can be intermediate products during the reaction of $CH_4$, being necessary to know the reaction kinetic with CO and $H_2$ even if $CH_4$ are used as fuel (Abad et al., 2009).

No works about the reaction kinetics of natural minerals for CLC uses – such as ilmenite – were found. Ilmenite is a natural mineral mainly composed of $FeTiO_3$, being the principal source for the production of titanium dioxide, which is widely used in the metallurgy and pigment industries. One process used commonly to obtain titanium dioxide from ilmenite is the high-temperature (1300–1500 K) reduction of iron present in ilmenite to produce metallic iron and titanium dioxide, which subsequently may be separated by ore-dressing methods. As an alternative, it is possible also to oxidize at temperatures below 1300 K to produce a mixture of titanium dioxide and hematite (Itoh et al., 2006). Then, titanium dioxide is recovered by ore-dressing or aqueous leaching methods. Oxidation of ilmenite to pseudobrookite ($Fe_2TiO_5$) also has been suggested as a pre-treatment before subsequent reduction because it has been found that reduction of ilmenite is enhanced by the pre-oxidation of ilmenite (Park and Ostrovski, 2004; Sun et al., 1993; Zhang and Ostrovski, 2002).

Thus, an intensive work has been done in the past about the reactivity and kinetic determination of the reduction of ilmenite for metallurgical applications using $H_2$ (Bardi et al., 1987; Grey et al., 2007; Sun et al., 1992b, 1993; Vries and Grey, 2006; Zhao and Shadman, 1991), CO (Park and Ostrovski, 2003; Zhao and Shadman, 1990), $CH_4$ (Zhang and Ostrovski, 2001) or carbon (Wang and Yuan, 2006) as reducing agents.

Also the oxidation kinetics of ilmenite has been analyzed in the past because of its relevance on some processes of beneficiation of ilmenite to produce rutile (Jabloński and Przepiera, 2001; Rao and Rigaud, 1975; Sun et al., 1992a, 1993).

However, the application of the experience achieved for metallurgical applications, where high reducing potentials are used, cannot be directly applied to the reactions involved in the CLC process by several reasons. Firstly, most of the works done about the reduction of ilmenite are focused in the reduction of the iron present in $FeTiO_3$ to metallic iron. However, when ilmenite is used as an oxygen carrier, $FeTiO_3$ is the most reduced compound, while pseudobrookite ($Fe_2TiO_5$) is the oxidized form. Moreover, the thermal pre-treatment of ilmenite particles has beneficial effects on its reactivity, thus pre-oxidized ilmenite should be preferred to fresh ilmenite as an initial material. Only few works have dealt with the reduction of pre-oxidized ilmenite particles, i.e. the reduction of pseudobrookite (Sun et al., 1992b, 1993). In these works, the kinetic of reaction of pre-oxidized particles was analyzed according to a two-interface kinetic model, where the overall reduction is assumed to follow two steps: reaction (I) the reduction of $Fe^{3+}$ in pseudobrookite to $Fe^{2+}$ in ilmenite; and reaction (II) the reduction of $Fe^{2+}$ to metallic iron. Thus, the reduction reaction occurring in a CLC system corresponds to reaction (I).

Secondly, the analysis of the ilmenite reactivity in the past was limited to the oxidation and reduction of either fresh or pre-oxidized ilmenite particles, as it is necessary for metallurgical applications. On the contrary, in a CLC system the solid particles suffer from repeated reduction and oxidation cycles, which can affect their chemical and physical properties. Thus, even though the oxidation of ilmenite particles and the reduction step of pre-oxidized ilmenite have been analyzed for metallurgical applications, the reaction kinetics for the oxidation and reduction should be different among unused and activated ilmenite.

### 1.3. Objective

The objective of this work was to analyze the reactivity of pre-oxidized and activated ilmenite particles for CLC applications. The kinetic parameters of the oxidation with oxygen and the reduction with the main reducing gases – as much for gaseous fuels as for solid fuels – existing in a CLC system (CO, $H_2$ and $CH_4$) were established. As ilmenite increases its reactivity with the cycle number, the reactivity of pre-oxidized and activated ilmenite was analyzed. The kinetic parameters obtained will be useful for the design and optimization of a CLC system using ilmenite as an oxygen carrier for both gaseous and solids fuels.

## 2. Experimental section

The effect of the main operating variables (type of fuel, gas concentration and temperature) on the oxidation and reduction reaction rates of the selected ilmenite was determined. The experimental tests were carried out in a thermogravimetric analyzer (TGA), using CO, $H_2$ or $CH_4$ as reducing gases, and $O_2$ for the oxidation step. Thus, it was analyzed the reactivity with the main products gases from coal gasification in the fuel reactor, i.e. CO and $H_2$ from coal gasification, and $CH_4$ as a representative gas from coal devolatilization.

### 2.1. Ilmenite

A Norwegian ilmenite was used in this study. The raw material is a concentrate from a natural ore and it has a purity of 94.3%. This material is mainly composed of ilmenite ($FeTiO_3$), rutile ($TiO_2$) and some hematite ($Fe_2O_3$). SEM-EDX analyses revealed a Fe:Ti molar ratio around 1:1. Also minor amounts of oxides and silicates can be found, with $MgSiO_3$ and $MnO_2$ as main compounds. The particle size used for kinetics determination was 150–300 μm. This ilmenite has been showing good reactivity and excellent properties from both TGA and batch fluidized bed testing (Adánez et al., 2010; Leion et al., 2008a, 2008b, 2009a, 2009b). It has also been tested with solid fuel in a 10 kW unit at Chalmers University of Technology (Berguerand and Lyngfelt, 2008a, 2008b).

Pre-oxidized ilmenite and activated particles were used in this work. Pre-oxidized ilmenite was obtained after a thermal treatment of fresh ilmenite at 1223 K in air during 24 h. During the thermal treatment ilmenite ($FeTiO_3$) was fully oxidized to pseudobrookite ($Fe_2TiO_5$). In a previous work (Adánez et al., 2010), it was found that ilmenite activates through consecutive redox cycles. During the activation period the reactivity of ilmenite particles increases and the $Fe_2O_3$ content increases at expense of $Fe_2TiO_5$. After the activation period the reactivity was maintained roughly constant, although the $Fe_2O_3$ content was still increasing. Activated ilmenite used in this work was obtained after 30 redox cycles in a fluidized bed using 25 vol% $CH_4$+10 vol% $H_2O$ at 1173 K for the reduction period, guaranteeing the complete activation of the ilmenite particles. The solid conversion reached in the cycles was $\approx$ 50%, defined for the reduction reaction from $Fe^{3+}$ to $Fe^{2+}$, i.e. from $Fe_2TiO_5$ and $Fe_2O_3$ to $FeTiO_3$ and FeO, respectively.

Table 1 shows the chemical composition for pre-oxidized and activated ilmenite. The XRD analysis of pre-oxidized and activated particles revealed ferric pseudobrookite ($Fe_2TiO_5$), rutile ($TiO_2$) and some free hematite ($Fe_2O_3$) as major components. It can be seen that the fraction of hematite increases in the activated ilmenite regarding to pre-oxidized particles.

**Table 1**
Composition (wt%) and physical properties of pre-oxidized and activated ilmenite.

| | **Pre-oxidized ilmenite** | **Activated ilmenite** |
|---|---|---|
| XRD (main species) | $Fe_2TiO_5$, $Fe_2O_3$, $TiO_2$ | $Fe_2TiO_5$, $Fe_2O_3$, $TiO_2$ |
| $Fe_2O_3$ | 11.2 | 22.0 |
| $Fe_2TiO_5$ | 54.7 | 38.5 |
| $TiO_2$ | 28.6 | 34.0 |
| Inerts | 5.5 | 5.5 |
| True density (kg m$^{-3}$) | 4100 | 4250 |
| $R_{o,ilm}$ (%) | 4.0 | 3.3 |
| Grain radius, $r_g$ (μm) | 0.5 | 1.25 |
| Porosity (%) | 1.2 | 12.7 |
| BET surface (m$^2$ g$^{-1}$) | 0.8 | 0.4 |
| Crushing strength (N) | 2.2 | 2.0 |

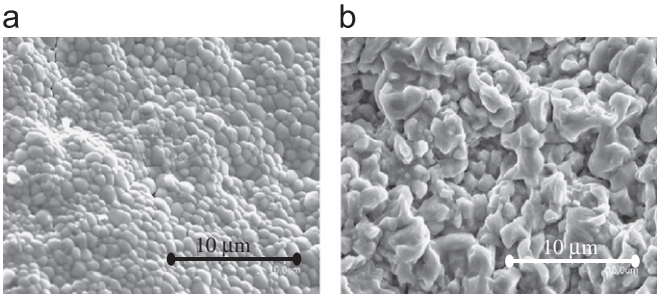


**Fig. 2.** SEM images of (a) pre-oxidized and (b) activated ilmenite particles.

The oxygen transport capacity of ilmenite $R_{o,ilm}$ was calculated as

$$R_{o,ilm} = \frac{m_o - m_r}{m_o} \quad (3)$$

where $m_o$ and $m_r$ are the mass of the most oxidized and reduced form of the oxygen carrier, respectively. In the CLC process, pseudobrookite ($Fe_2TiO_5$) and hematite ($Fe_2O_3$) are reduced to ilmenite ($FeTiO_3$) and magnetite ($Fe_3O_4$), respectively. Rutile is considered to be an inert. Higher reduction prevents the complete conversion of the fuel to $CO_2$ and $H_2O$ because thermodynamic constrictions (Leion et al., 2008b). Thus, $R_{o,ilm}$ was defined as the oxygen transport capacity useful for CLC, and took the values 4.0 wt% for pre-oxidized ilmenite and 3.3 wt% for activated ilmenite. This difference was due to the effect of the ilmenite composition on the mass in the reduced state, $m_r$. The mass corresponding to this reduced state is $m_r$ in Eq. (3), which increases as the hematite content increases giving a lower value of $R_{o,ilm}$.

SEM pictures of pre-oxidized and activated particles can be seen in Fig. 2. For pre-oxidized ilmenite a granular structure of the solid is observed, which is enhanced during the activation period, together with a gain in porosity. The porosity of pre-oxidized ilmenite was 1.2%, whereas for activated ilmenite the porosity value was as high as 12.7%. From SEM observation, the mean size of the grains was determined to be about 1 μm for pre-oxidized ilmenite and about 2.5 μm for activated ilmenite. More detail about the ilmenite composition and physical properties of ilmenite particles can be found elsewhere (Adánez et al., 2010).

### 2.2. Experimental setup

The kinetic of the reduction and oxidation reactions for the pre-oxidized and activated ilmenite has been carried out through thermogravimetric analysis in a CI thermobalance, see Fig. 3. TGA experiments allowed analyzing the reactivity of the oxygen carriers under well-defined conditions. The reactor consists of two concentric quartz tubes (24 mm i.d. and 10 mm i.d.) placed in an oven. The

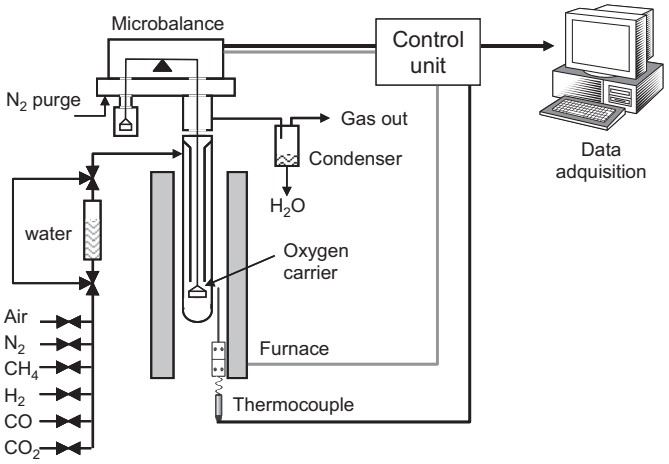


**Fig. 3.** CI thermobalance layout.

sample-holder was a wire mesh platinum basket (14 mm diameter and 8 mm height) designed to reduce mass-transfer resistance around the solid sample. The temperature and sample weight were continuously collected and recorded in a computer. $N_2$ (2.5 cm$^3$ s$^{-1}$ STP) flowed through the microbalance head to kept the electronic parts free of reactant gas. The reacting gas mixture (~7 cm$^3$ s$^{-1}$ STP) was measured and controlled by electronic mass flow controllers. The reacting gas mixture was introduced at the upper part of the reaction tube. The gas was heated at the desired temperature flowing down through the external annulus of the reactor before contacting with the sample, which was located at the bottom of the reactor. The gas left the reactor through an internal quartz tube after mixing with the gas coming from the head of the balance.

For the reactivity experiments, the ilmenite particles were loaded in the platinum basket. The sample weight used for the experiments was about 50 mg. The oxygen carrier particles were heated up to the desired temperature in an air atmosphere. Once the set temperature was reached, the experiment was started by exposing the oxygen carrier to the desired conditions for the reduction step. In order to avoid the mixing of combustible gas and air, nitrogen was introduced for 2 min between the oxidizing and the reducing period.

The reactivity with the main reacting gases considered being in a CLC system, i.e. $CH_4$, CO and $H_2$ was analyzed. The composition of the gas used to determine the kinetic of the reduction reactions was varied to cover a wide range of gas concentrations (fuel gas, 5–50 vol%; $H_2O$, 20 vol%; $CO_2$, 20 vol%; $O_2$, 5–21 vol%). The temperature was varied from 1073 to 1223 K. For the kinetic determination, the data used corresponded to the first reduction or oxidation period. Moreover, the same sample of solid particles was not used to obtain the reaction rate at different conditions, but for each experimental condition a new sample of solid particles was used. This procedure was necessary because the reactivity of ilmenite varies with the number of cycles, mainly during the first cycles using pre-oxidized ilmenite.

As much pre-oxidized as activated ilmenite were in its fully oxidized state. To analyze the reactivity of the oxidation reaction it was necessary to reduce the sample first until the particles were composed of $Fe_3O_4$ and $FeTiO_3$, so simulating the behaviour expected in a CLC system. The previous reduction step was carried out at 1173 K in an atmosphere composed of 5 vol% $H_2$ and 40 vol% $H_2O$ ($N_2$ to balance). At these conditions, the reduction of $Fe_2O_3$ was stopped in the $Fe_3O_4$ compound because thermodynamically is unfavourable the subsequent reduction to FeO. After that, ilmenite particles were ready to be oxidized. The oxygen concentration was varied from 5 to 21 vol%, and the reacting temperature was in the range 1073–1223 K. Studies carried out by TGA showed that the oxidation rate was the same independently of the gas previously used for the reduction.

Initially, to establish whether external film mass transfer and/or inter-particle diffusion were affecting the reaction rate, the gas flow rate and the sample weight were varied in the range 6–14 $cm^3\ s^{-1}$ STP and from 20 to 60 mg, respectively. It was observed that the reaction rate was not affected by the amount of sample used or the flow rate, indicating that external and inter-particle diffusion was not of importance. Moreover, several experiments showed that particle sizes in the range 90–500 μm did not affect the reaction rates, excepting for the oxidation of pre-oxidized particles. In this case, the particle size affected to the reactivity in some extension. In the other cases, the internal mass-transfer resistances were not important.

### 2.3. Data evaluation

The reduction of ilmenite components, i.e. pseudobrookite and hematite, by the different reducing gases are given by the following reactions:

*for reduction with $H_2$*

$$Fe_2TiO_5+TiO_2+H_2\rightarrow 2FeTiO_3+H_2O \quad (4)$$

$$3Fe_2O_3+H_2\rightarrow 2Fe_3O_4+H_2O \quad (5)$$

*for reduction with CO*

$$Fe_2TiO_5+TiO_2+CO\rightarrow 2FeTiO_3+CO_2 \quad (6)$$

$$3Fe_2O_3+CO\rightarrow 2Fe_3O_4+CO_2 \quad (7)$$

*for reduction with $CH_4$*

$$4Fe_2TiO_5+4TiO_2+CH_4\rightarrow 8FeTiO_3+CO_2+2H_2O \quad (8)$$

$$12Fe_2O_3+CH_4\rightarrow 8Fe_3O_4+CO_2+2H_2O \quad (9)$$

For the oxidation reaction, it can be expected that the reaction follows as

$$4FeTiO_3+O_2\rightarrow 2Fe_2TiO_5+2TiO \quad (10)$$

$$4Fe_3O_4+O_2\rightarrow 6Fe_2O_3 \quad (11)$$

However, the mechanism of oxidation can be some more complex. From thermodynamic calculations (Borowiec and Rosenqvist, 1981; Itoh et al., 2006), the end-product after the oxidation of ilmenite at temperatures higher than 853 K is pseudobrookite ($Fe_2TiO_5$) and rutile ($TiO_2$). However, the end-product experimentally observed when ilmenite is oxidized by air depends on the reacting time and temperature. Rao and Rigaud (1975) found three different oxidation products depending on the temperature of oxidation. Thus, hematite ($Fe_2O_3$) and titanium dioxide ($TiO_2$) were the final products in the temperature range 773–1023 K; hematite and pseudorutile ($Fe_2Ti_3O_9$) were the final products at 1043–1163 K; and pseudobrookite ($Fe_2TiO_5$) and rutile ($TiO_2$) were identified as oxidation products above 1173 K. Karkhanavala and Momin (1959) and Gupta et al. (1991) found that ilmenite oxidized at temperatures lower than 1123 K produced a mixture of hematite, pseudobrookite and rutile. The metastable compounds $Fe_2O_3 \bullet TiO_2$ and $Fe_2Ti_3O_9$ can appear as intermediate products at temperatures lower than 1273 K (Zhang and Ostrovski, 2002). In short, pseudobrookite was found to be the only end-product when the oxidation was carried out at high temperature ( $>1123$ K) and during long time ( $>24$ h), but a mixture of different compounds can be found at lower temperatures or lower oxidation time.

Following the above consideration, the oxidation of ilmenite ($FeTiO_3$) can be considered as

$$2FeTiO_3+1/2O_2\rightarrow Fe_2O_3\bullet TiO_2+TiO_2\rightarrow Fe_2O_3+2TiO_2 \quad (12)$$

$$3FeTiO_3+3/4O_2\rightarrow Fe_2Ti_3O_9+1/2Fe_2O_3\rightarrow 3/2Fe_2TiO_5+3/2TiO_2 \quad (13)$$

being the end-product a mixture of $Fe_2TiO_5$, $Fe_2O_3$ and $TiO_2$ in a ratio which depends on the reacting time and temperature. Besides, the segregation of $Fe_2O_3$ from the titanium-rich phase also has been reported at 973 K because of the migration of $Fe^{2+}$ and $Fe^{3+}$ ions through the solid lattice towards the grain boundary (Nell, 1999). Once iron is segregated from the titanium-rich phase, the formation of $Fe_2TiO_5$ product is prevented because there is not physical contact between them. Thus, the amount of free $Fe_2O_3$ can be increased after every redox cycle, as it was confirmed from experimental results in a previous work (Adánez et al., 2010). In addition, the oxidation of the $Fe_3O_4$ coming from the previous reduction of $Fe_2O_3$ also is described by reaction (11).

During the ilmenite reduction, the oxygen transferred to the fuel gas is the sum of the contribution of the reduction of $Fe_2TiO_5$ and $Fe_2O_3$. More complex is the interpretation of the oxygen gained during the oxidation step, as has been above showed, because new hematite appeared. Unfortunately, from the analysis of the thermogravimetric curves it was not possible to separate the contribution in the gaining or losing weight of each one of the reactions (4)–(13). Therefore, the "Integrated Rate of Reduction" (IRoR) was used, by which the total rate of reduction of a whole particle is used instead of the local rate of reduction (LRoR). The IRoR has been widely used for the analysis of the reduction of iron ores, as it was reviewed by Donskoi et al. (2003). In the IRoR model, the pseudobrookite was considered to be $Fe_2O_3+TiO_2$, ilmenite was $FeO+TiO_2$, and magnetite was $Fe_2O_3+FeO$. $TiO_2$ was considered to be an inert material. So, the reduction and oxidation sequence of ilmenite can be summarized and simply expressed as the following two reactions:

$$Fe_2O_3+H_2\rightarrow 2FeO+H_2O \quad (14)$$

$$Fe_2O_3+CO\rightarrow 2FeO+CO_2 \quad (15)$$

$$4Fe_2O_3+CH_4\rightarrow 8FeO+CO_2+2H_2O \quad (16)$$

$$4FeO+O_2\rightarrow 2Fe_2O_3 \quad (17)$$

where $Fe_2O_3$ includes all the ferric materials, and FeO the ferrous materials, as was used by Sun et al. (1992b). It is worth nothing that magnetite ($Fe_3O_4$) was considered as a mixture of $Fe_2O_3$ and FeO. Therefore, the reduction of hematite to magnetite is assumed to be due to the reduction of 1/3 of the hematite containing iron to FeO, being the remaining 2/3 of iron not reduced.

The conversion level of the oxygen carrier was calculated for the reduction ($X_r$) and oxidation ($X_o$) reactions as

$$X_r=\frac{m_o-m}{R_{o,ilm}m_o} \quad (18)$$

$$X_o=1-X_r=\frac{m-m_r}{R_{o,ilm}m_o} \quad (19)$$

The oxygen transport capacity of ilmenite, $R_{o,ilm}$, was 4.0 and 3.3 wt% for pre-oxidized and activated ilmenite, respectively, as previously discussed.

## 3. Results

### 3.1. Analysis of the reduction reaction

The reactivity of pre-oxidized and activated ilmenite was investigated using $H_2$, CO or $CH_4$ as reducing gas. To determine the kinetic parameters of the reduction reaction, several experiments at different temperatures (1073, 1123, 1173 and 1223 K) and gas concentrations (5%, 15%, 30%, 50%) were carried out.

*3.1.1. Effect of the gas products on the reduction reaction*

To analyze the effect of the gas product, i.e. $H_2O$ and $CO_2$, on the reaction rate of the ilmenite, experiments were done with $H_2$ or CO as reacting gases and varying the ratio $H_2O/H_2$ or $CO_2/CO$, respectively. Fig. 4 shows the thermograms obtained for activated ilmenite with 5 vol% $H_2$ and $H_2O$ content from 0 to 30 vol%. Similar curves were obtained for pre-oxidized ilmenite or with 5 vol% CO varying the $CO_2$ content.

When $H_2O$ was not present in the reaction gas mixture the mass loss was about 5% in 200 s. This value is higher than the oxygen transport capacity showed for activated ilmenite, i.e. $R_{o,ilm}=3.3\%$. The excess in the mass loss was due to the reduction of $Fe_3O_4$ to FeO, or even for longer times, to Fe. In addition, it can be seen two reaction zones. Until a decrease in the initial mass about 3.3% the reaction was fast, but later the reaction rate decreased with time. The mass loss observed during the first step was assigned to the reduction of $Fe_2TiO_5$ and $Fe_2O_3$ to $FeTiO_3$ and $Fe_3O_4$, respectively. In this case, the reaction rate was not affected by the $H_2O$ content because both reductions are allowed by thermodynamic considerations at all the experimental conditions used. However, the subsequent reaction – corresponding to the reduction of $Fe_3O_4$ – is clearly affected by the $H_2O$ content: a higher amount of $H_2O$ in the reacting gases leads to a lower reaction rate. This reaction was ceased with $H_2O$ content higher than 20 vol% when the mass loss was 3.3 wt% because the reduction of $Fe_3O_4$ was avoided due to thermodynamic reasons. The equilibrium constant for the reduction of $Fe_3O_4$ to FeO is 2.1 for $H_2$ and 1.6 for CO at 1173 K (Barin, 1989). This means that the reduction of $Fe_3O_4$ is prevented when $H_2O/H_2 > 2.7$ or $CO_2/CO > 2.1$, as it can be seen in Fig. 4. At these conditions, the final solid products are $FeTiO_3$ and $Fe_3O_4$.

Another consequence of the thermodynamic restrictions for the reduction of $Fe_3O_4$ is that ilmenite should be reduced at maximum to a mixture of $FeTiO_3$ and $Fe_3O_4$ to get complete conversion of gases to $CO_2$ and $H_2O$ in a CLC system. Thus, the corresponding value taking for $R_{o,ilm}$ was 3.3 wt%. Further losses in the mass were not considered to happen in a CLC system, i.e. the oxygen present in $Fe_3O_4$ was not accounted.

The following conversion vs. time curves were calculated from the mass loss showed in the thermograms at different conditions (gas composition and temperature) using Eq. (18). Conversions higher than 100% – which corresponds to the dotted line – could be obtained in experiments when the mass loss exceeded these values, i.e. for $H_2O/H_2 < 2.7$ or $CO_2/CO < 2.1$. As further reduction of $FeTiO_3$ to $Fe^0$ or $Fe_3O_4$ to wustite (FeO) must be prevented in a CLC system, only the part of the curve up to conversion of 100% was of interest for CLC applications, i.e. the reduction until $FeTiO_3$ and $Fe_3O_4$, which is scarcely affected by the product gas concentration.

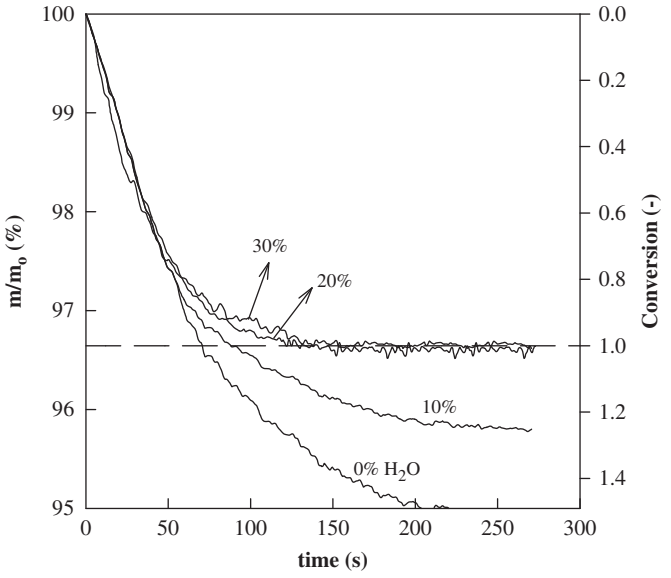


**Fig. 4.** Thermograms obtained during the reduction of activated ilmenite using different $H_2O/H_2$ ratios. $H_2=5\%$. $N_2$ to balance. $T=1173$ K.

*3.1.2. Effect of fuel type*

The study carried out about reactivity showed the different behaviour obtained for the three fuel gases considered in the fuel reactor, i.e. $H_2$, CO and $CH_4$. To compare ilmenite reactivity with these gases, Fig. 5(a) and (b) show the conversion vs. time curves for the different reducing gases for pre-oxidized and activated ilmenite, respectively. Observe that the time scales are different in these figures.

Although ilmenite presents initially a rather low reactivity, there is an important reactivity increase after the activation period. For the different reducing gases, pre-oxidized and activated ilmenite react faster with $H_2$ than with CO and $CH_4$, reaching a conversion value of 80% in 35 s. Pre-oxidized ilmenite reacts faster with CO than with $CH_4$, unlike activated ilmenite. For $H_2$ and CO the reactivity rises around 5 times after the activation, while for $CH_4$ this increase is about 15 times. The reactivity increase observed for all these fuel gases can

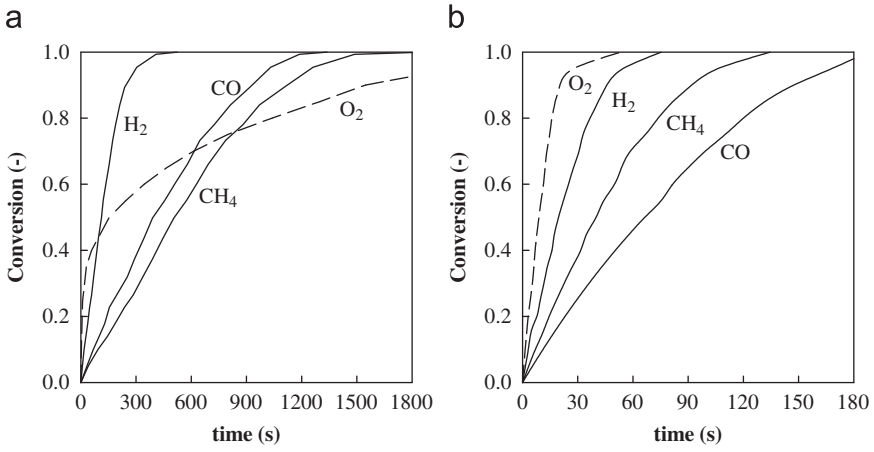


**Fig. 5.** Conversion vs. time curves during reduction period using $H_2$, CO or $CH_4$ as reducing agent (continuous lines). Also the oxidation by air is showed for the reduced ilmenite (broken lines): (a) pre-oxidized ilmenite and (b) activated ilmenite. Experimental conditions: $T=1173$ K; reducing gas mixtures: 15% $H_2$+20% $H_2O$ or 15% CO+20% $CO_2$ or 15% $CH_4$+20% $H_2O$. Nitrogen to balance.

be explained through the structural changes undergoing the solid during consecutives redox cycles (Adánez et al., 2010).

### 3.1.3. Effect of gas concentration

To determine the effect of the gas concentration on the kinetics of the reduction reaction, several experiments at 1173 K and gas concentrations (5%, 15%, 30% and 50%) were carried out. As an example, Fig. 6 shows plots of the effect of $H_2$ concentration on the conversion–time curves. Similar behaviour was observed for CO and $CH_4$. As expected, an increase in the fuel gas concentration produces an increase on the reaction rate.

### 3.1.4. Effect of temperature

The effect of temperature on the reaction rate of ilmenite was later investigated. Fig. 7 shows the conversion vs. time curves for the reduction with CO of pre-oxidized and activated ilmenite. Similar curves were obtained for $H_2$ and $CH_4$. In all cases, the reaction rate is quite affected by the temperature. An increase of temperature produces an increase on the reduction rate.

## 3.2. Analysis of the oxidation reaction

The CLC system is composed of two interconnected fluidized bed reactors. The reduced oxygen carrier from the fuel reactor is regenerated in the air reactor. Therefore, the regeneration of the oxygen carrier with air should be also analyzed. The oxidation reactivity of pre-oxidized and activated ilmenite was investigated. As the solid samples were completely oxidized, before the oxidation step they were fully reduced until $FeTiO_3$ and $Fe_3O_4$ using 5 vol% $H_2$ and 40 vol% $H_2O$. To determine the kinetic parameters of the oxidation reaction several experiments at different temperatures (1073, 1123, 1173 and 1223 K) and oxygen concentrations (5%, 10%, 15%, 21%) were carried out.

Fig. 5 shows the conversion vs. time curves obtained for pre-oxidized and activated ilmenite, together those obtained for the reduction with $H_2$, CO and $CH_4$. The reactivity of the oxidation reaction is higher than those for the reduction with $H_2$, CO, and $CH_4$, except for the oxidation of pre-oxidized ilmenite for solid conversions higher than $\approx 0.25$. After this value, the reaction rate sharply decreased for pre-oxidized ilmenite, being evident at conversions higher than 0.35. Nevertheless, the complete oxidation of pre-oxidized particles was obtained after a long enough oxidizing period. To analyze the reason for this strong decrease of the reactivity at a conversion $\approx 0.25$, different samples of pre-oxidized particles were fully reduced and later oxidized for different times. Thus, samples of ilmenite particles with different conversion of oxidation were obtained. SEM images of these particles are shown in Fig. 8. It can be seen that the fully reduced particle exhibits a granular and porous structure. This structure was still maintained when the particle was partially oxidized to $X_o=0.2$, but it can be seen some decrease in the porosity development. However, the porosity collapsed when particles were further oxidized

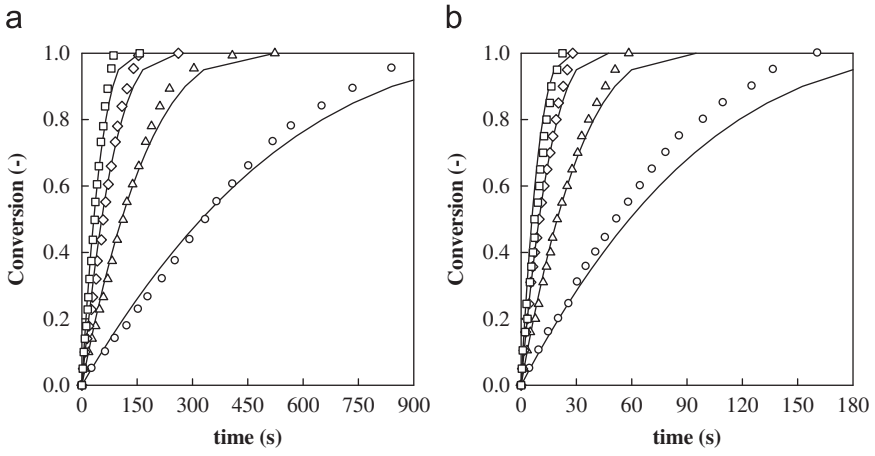


**Fig. 6.** Effect of $H_2$ concentration on the reduction reaction for (a) pre-oxidized and (b) activated ilmenite. $T=1173$ K. $H_2$ concentration: ○ 5 vol%; △ 15 vol%; ⋄ 30 vol%; □ 50 vol%. 20 vol% $H_2O$; $N_2$ to balance. Continuous line: model predictions.

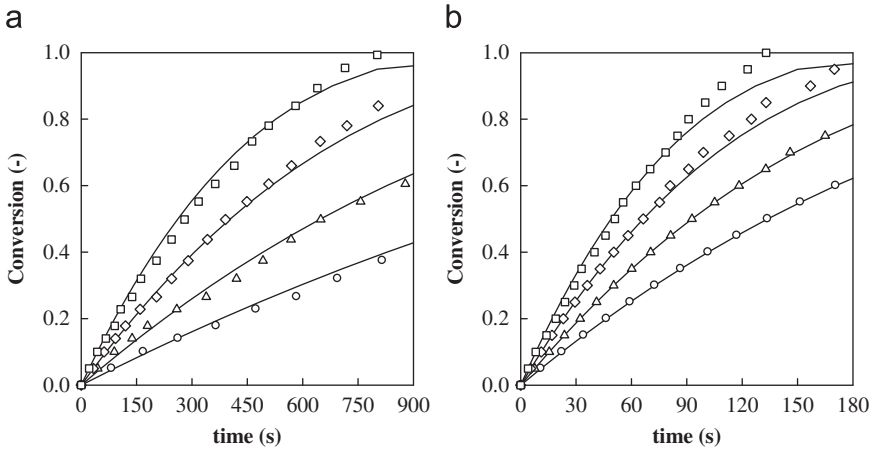


**Fig. 7.** Effect of CO concentration on the reduction reaction for (a) pre-oxidized and (b) activated ilmenite. Temperature: ○ 1073 K; △ 1123 K; ⋄ 1173 K; □ 1223 K. 15 vol% CO; 20 vol% $CO_2$; $N_2$ to balance. Continuous line: model predictions.

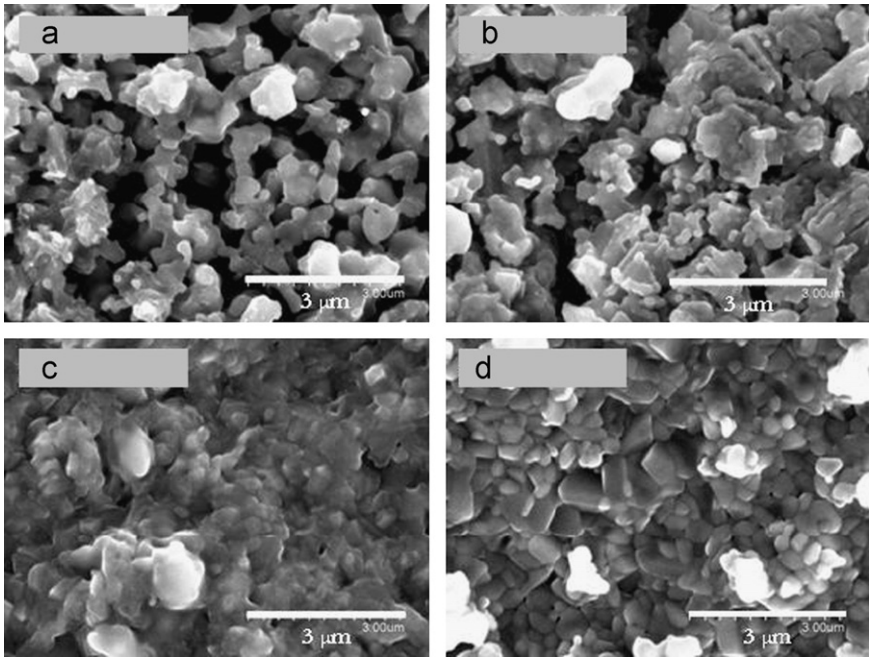


**Fig. 8.** SEM images of pre-oxidized ilmenite particles after one reduction step (a) and at different conversion of the following oxidation: (b) $X_o$=0.2; (c) $X_o$=0.5; (d) $X_o$=0.8.

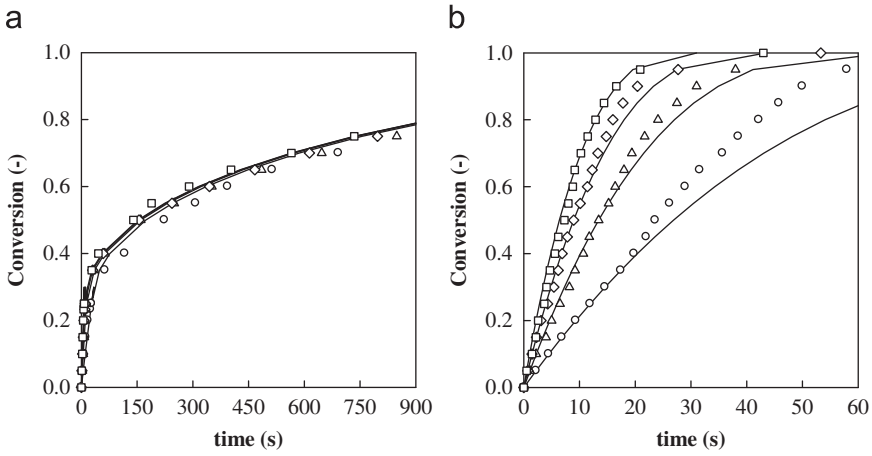


**Fig. 9.** Effect of $O_2$ concentration on the oxidation reaction for (a) pre-oxidized and (b) activated ilmenite. $T$=1173 K. $O_2$ concentration: ○ 5 vol%; △ 10 vol%; ⋄ 15 vol%; □ 21 vol%. $N_2$ to balance. Continuous line: model predictions.

at $X_o$=0.5 and 0.8. This fact suggests that the reaction mechanism probably changes from a chemical reaction control to a diffusional control in the particle due to the loss of porosity inside the particle as oxidation proceeds. This fact agrees to the results showed by other authors. Rao and Rigaud (1975) observed a quick decrease on the oxidation reaction rate at conversion varying from 0.3 to 0.75, which depended on the particle size. They suggested that this decrease was due to the formation of a thick adherent film around the particle. Sun et al. (1992a) determined that oxidation of ilmenite was mainly controlled by the intrinsic kinetic and diffusional effects in the product layer, being the diffusion more important as the oxidation proceeds.

After the activation period, it was found a considerable increase in the reaction rate, which is more pronounced for solid conversions higher than ≈0.25, see Fig. 5. On the contrary than for pre-oxidized ilmenite, for activated ilmenite the initial porosity is high enough to be conserved after the oxidation step, as can be seen in Table 1. Thus, the oxidation reaction of activated ilmenite is relatively fast and mainly controlled by the chemical reaction in the solid surface. A conversion value as high as 80% is obtained in 15 s.

### 3.2.1. *Effect of oxygen concentration*

Several experiments were carried out at 1173 K with different $O_2$ concentration (5%, 10%, 15% and 21%). Fig. 9 shows the conversion–time curves obtained for pre-oxidized and activated ilmenite. It can be observed that the reaction rate increases as the $O_2$ concentration increases when the reaction rate was controlled by the chemical reaction. However, the $O_2$ concentration scarcely affects the reaction rate when the reaction was controlled by diffusion in the particle, i.e. when the reaction rate was slow for pre-oxidized ilmenite.

### 3.2.2. *Effect of temperature*

Several experiments were carried out at different temperatures from 1073 to 1223 K with a constant oxygen concentration of 21 vol%, and following the procedure described in the experimental section. Fig. 10 shows the conversion vs. time curves obtained for pre-oxidized and activated ilmenite. Contrary to the effect showed for the reduction reaction, the oxidation rate scarcely increased when the temperature was increased, mainly when the reaction

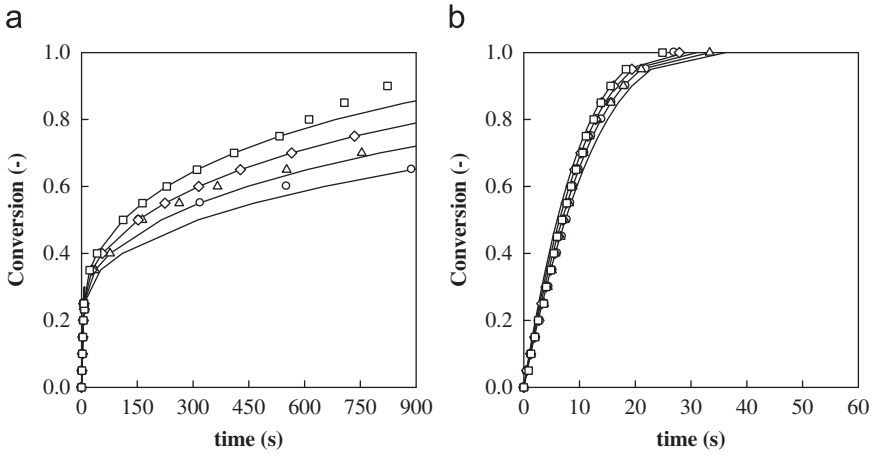


**Fig. 10.** Effect of temperature on the oxidation reaction for (a) pre-oxidized and (b) activated ilmenite. Temperature: ○ 1073 K; △ 1123 K; ◇ 1173 K; □ 1223 K. 21 vol% $O_2$; $N_2$ to balance. Continuous line: model predictions.

was controlled by the chemical reaction. Some higher effect of the temperature was observed when the reaction was controlled by diffusion in the particle, i.e. the oxidation of pre-oxidized particles for $X_o > 0.25$.

### 3.3. Determination of the kinetic parameters

By using a particle reaction model, the kinetic parameters of the different reactions can be determined for the oxygen carrier. Most of reaction models used for the oxidation of ilmenite (Jabloński and Przepiera, 2001; Rao and Rigaud, 1975; Sun et al., 1992a) and the reduction of pre-oxidized ilmenite (Sun et al., 1992b) were based on a mixed control of chemical reaction at the grain boundary and diffusion in the particle. Other reaction models, as nucleation models, have been refused in the past to describe the oxidation reaction of ilmenite (Rao and Rigaud, 1975).

The requirements that must fulfil a model are to be a representation as near as possible to the real process and that can be coupled without many difficulties with the fluidized bed reactor model. Several SEM images showed a granular structure inside the ilmenite particles (see Fig. 2). Moreover, previous studies showed that the particle size did not affect the reaction rates of ilmenite. Taking into account for these considerations and the results showed by other authors, the grain model with uniform reaction in the particle with changing grain size model in the grains, controlled by chemical reaction, was used to determine the kinetic parameters.

The model assumes that the particle consists of a number of nonporous spherical grains of uniform initial radius, $r_g$. The reaction proceeds in the grain following the changing grain size model. Considering that the reaction is controlled by the reaction in the grain which corresponds to negligible resistances to gas film mass transfer and diffusion inside the particle, the equations that describe this model are the following:

$$\frac{t}{\tau_{chr}} = 1-(1-X_i)^{1/3}, \quad \tau_{chr} = \frac{\rho_m r_g}{\overline{b} k_s C_g^n} \tag{20}$$

In addition, to predict the behaviour of the oxidation of pre-oxidized ilmenite a mixed resistance between chemical reaction and diffusion in the solid product was needed, as previously has been discussed. In this case, it was assumed that the reaction rate was controlled by chemical reaction in the grain up to a determined conversion value, $X_{chr}$, which will be determined from the conversion–time curves. During this period, the porosity of particles decreases because the volume of the solid products ($Fe_2TiO_5$+$TiO_2$ and $Fe_2O_3$) is higher than those for the solid reactants ($FeTiO_3$ and $Fe_3O_4$). This chemically controlled step proceeds until the porosity collapses. From this point, it was assumed that the oxidation proceeds following a shrinking core model in the particle, and it is controlled by the diffusion in the solid. Furthermore, it was found that the oxygen concentration do not affect the oxidation rate when the reaction is controlled by diffusion through the product layer. This fact was already showed by Rao and Rigaud (1975), suggesting that iron ions are mobile through the solid lattice, which agrees with the iron segregation observed during the activation process. The equations that describe this oxidation step are the following:

$$\frac{t}{\tau_{dif}} = 3\left[1-(1-X_o')^{2/3} + \frac{1-Z+(1-Z)(1-X_o')^{2/3}}{Z-1}\right], \quad \tau_{dif} = \frac{\rho_m r_p^2}{6\overline{b} D_e} \tag{21}$$

where $Z$ is the expansion ratio between the solid product and solid reactive

$$Z = \frac{V_{m,prod}}{V_{m,reac}} \tag{22}$$

and $X_o'$ is a modified conversion that takes into account that the diffusional control starts at the conversion $X_{chr}$, and it is calculated as

$$X_o' = \frac{X_o - X_{chr}}{1-X_{chr}} \tag{23}$$

being $X_o' = 0$ at $X_o = X_{chr}$, and $X_o' = 1$ at $X_o = 1$.

The time necessary to reach any conversion for values higher than $X_{chr}$ is given by

$$t = t_{dif} + t_{chr}|_{X_{chr}} \tag{24}$$

$t_{chr}|_{X_{chr}}$ is the time at which $X_{chr}$ is reached and it is calculated from Eq. (20).

As it has been discussed above, from the conversion vs. time curves it was not possible to differentiate the reduction of $Fe_2TiO_5$ from that of $Fe_2O_3$. Thus, a global kinetic rate constant was calculated for the sum of both reactions, i.e. the reduction of $Fe^{3+}$ to $Fe^{2+}$, as it was expressed by Eqs. (14)–(16). Similarly, a global kinetic rate constant was obtained for the oxidation reaction of $Fe^{2+}$ to $Fe^{3+}$, see Eq. (17). In this line, an average coefficient $\overline{b}$ was used in Eqs. (20) and (21) as a function of ilmenite composition, which is shown in Table 2.

This kinetic model was used to determine the kinetic parameters for the reduction of pre-oxidized and activated ilmenite with $H_2$, CO and $CH_4$, and the oxidation with $O_2$.

The reaction order, $n$, with respect to each reacting gas ($H_2$, CO, $CH_4$ or $O_2$) was obtained from the calculus of $\tau_{chr}$ by fitting the experimental curves conversion–time to the model equation.

**Table 2**
Kinetic parameters for ilmenite reduction with $H_2$, CO and $CH_4$, and oxidation with air.

| Kinetic parameters | Pre-oxidized | | | | Activated | | | |
|---|---|---|---|---|---|---|---|---|
| | $H_2$ | CO | $CH_4$ | $O_2$ | $H_2$ | CO | $CH_4$ | $O_2$ |
| $\rho_m$ (mol m$^{-3}$) | 13,590 | 13,590 | 13,590 | 31,100 | 13,590 | 13,590 | 13,590 | 31,100 |
| $r_g$ (m) | $0.5\times10^{-6}$ | $0.5\times10^{-6}$ | $0.5\times10^{-6}$ | $0.48\times10^{-6}$ | $1.25\times10^{-6}$ | $1.25\times10^{-6}$ | $1.25\times10^{-6}$ | $1.20\times10^{-6}$ |
| $\overline{b}$ | 1.19 | 1.19 | 4.74 | 4 | 1.45 | 1.45 | 5.78 | 4 |
| $k_{s0}$ (mol$^{1-n}$ m$^{3n-2}$ s$^{-1}$) | $5.1\times10^{-1}$ | $2.1\times10^{-1}$ | 8.8 | $8.0\times10^{-5}$ | $6.2\times10^{-2}$ | $1.0\times10^{-1}$ | 9.8 | $1.9\times10^{-3}$ |
| $E_{chr}$ (kJ mol$^{-1}$) | $109.2\pm2.3$ | $113.3\pm3.0$ | $165.2\pm12.4$ | $11.8\pm0.1$ | $65.0\pm2.7$ | $80.7\pm2.4$ | $135.2\pm6.6$ | $25.5\pm1.2$ |
| $n$ | 1 | 1 | 1 | 1 | 1 | 0.8 | 1 | 1 |
| $D_{e0}$ (mol m$^{-2}$ s$^{-1}$) | | | | $1.37\times10^{-5}$ | | | | |
| $E_{dif}$ (kJ mol$^{-1}$) | | | | $77.4\pm0.3$ | | | | |

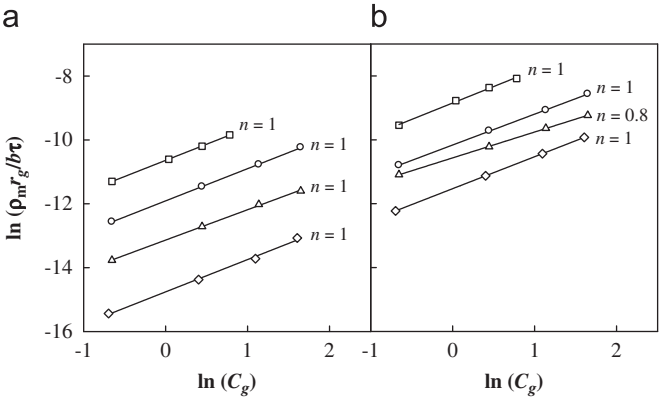


**Fig. 11.** Plot to obtain the reaction order with respect to $H_2$, CO and $CH_4$, and $O_2$ for (a) pre-oxidized and (b) activated ilmenite. $T$=1173 K. ○ $H_2$; △ CO; ⋄ $CH_4$; □ $O_2$.

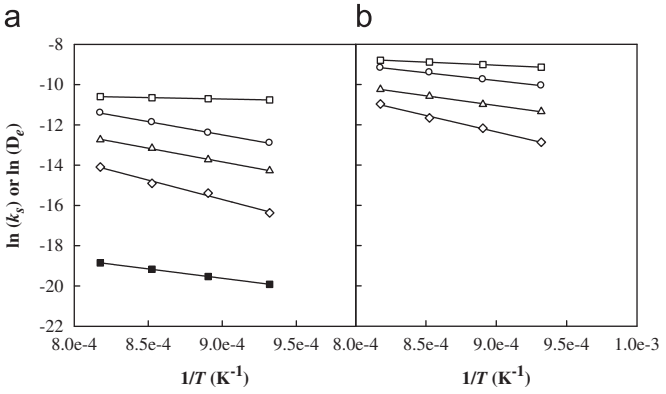


**Fig. 12.** Arrhenius plot for the kinetic constant $k_s$ for the reaction of $H_2$, CO, $CH_4$ and $O_2$ and the effective diffusivity, $D_e$, for the oxidation with (a) pre-oxidized and (b) activated ilmenite. $k_s$: ○ $H_2$; △ CO; ⋄ $CH_4$; □ $O_2$. $D_s$: ■ $O_2$.

Thereby, Eq. (20) can be expressed as follows:

$$\ln\left(\frac{\rho_m r_g}{\overline{b}\tau_{chr}}\right) = \ln(k_s) + n\ln(C_g) \tag{25}$$

From a plot of $\ln(\rho_m r_g/b\tau_{chr})$ vs. $\ln(C_g)$ the values of the reaction order, $n$, can be obtained from the slope of the figure, and the $\ln(k_s)$ at the reaction temperature. Fig. 11 shows this plot for each reacting gas. The calculated reaction order for each reaction is shown in Table 2.

From the experiments carried out at different temperatures, values for the chemical reaction kinetic constant, $k_s$, as a function of the temperature were obtained. The dependence on the temperature of the kinetic constant was assumed to be Arrhenius type, as follows:

$$k_s = k_{s0}e^{-E_{chr}/R_gT} \tag{26}$$

Fig. 12 shows the Arrhenius plot of the $k_s$ values as a function of $1/T$. The values of the kinetic parameters finally obtained for pre-oxidized and activated ilmenite are given in Table 2.

For the oxidation of pre-oxidized ilmenite, the diffusion in the product layer of the particle was also considered from a value of $X_{chr}$ = 0.25. By fitting the conversion curves obtained at different temperatures, the values of the effective diffusivity in the product layer, $D_e$, at each temperature were obtained. Fig. 12 shows the Arrhenius's plot for the dependence of $D_e$ with the temperature, and the values of the pre-exponential factor and the activation energy finally obtained are given in Table 2.

The theoretical curves calculated using the reaction model with the kinetic parameters showed in Table 2 predicted adequately the experimental results in all range of operating conditions studied for both pre-oxidized and activated ilmenite. As example, some conversion–time curves predicted by the reaction model are shown in Figs. 6, 7 and 9, 10.

For the reduction reactions, values for activation energies ranged from 109 to 165 kJ mol$^{-1}$ for pre-oxidized ilmenite, and lower values, from 65 to 136 kJ mol$^{-1}$ were obtained for activated ilmenite. These values are higher than those showed for other iron-based oxygen carriers (Son and Kim, 2006; Abad et al., 2007a, 2007b; Moghtaderi et al., 2010), except for that calculated by Bohn et al. (2009), who referred an activation energy of 75 kJ mol$^{-1}$ for the reduction with CO. In addition, the values of the activation energy are in the range of that obtained by Sun et al. (1992b) for different pre-oxidized materials at 1073 K, in which some hematite was found. Lower values of the activation energy were found for the oxidation of pre-oxidized and activated ilmenite (11.8 and 25.5 kJ mol$^{-1}$, respectively), but a higher value was found for the effective diffusivity for pre-oxidized ilmenite (77 kJ mol$^{-1}$). The activation energy for diffusion in the solids during the oxidation reaction was mainly found in the range 46–180 kJ mol$^{-1}$ (Rao and Rigaud, 1975; Sun et al., 1993) when the reaction was controlled by lattice diffusion. The lower limit of this range was found for the oxidation when there are a complete segregation among hematite and rutile, whereas the higher limit was found for complete oxidation to pseudobrookite. In this work it was found a value of the activation energy between them, which can be related to a partial segregation of hematite from the titanium-rich phase in every redox cycle. A lower value of the activation energy of 31 kJ mol$^{-1}$ was found by Jabloński and Przepiera (2001) when the chemical reaction was controlling the reaction, in line to the results obtained in this work.

## 4. Discussion

A key parameter for the design of a CLC system is the solids inventory in the fuel- and air-reactors as well as the recirculation rate of oxygen carriers between the reactors. Both parameters are linked and depend on the reactivity of the materials and on the

oxygen transport capacity of the oxygen carrier. In this section the use of the kinetic parameters determined in this work for design purposes is discussed.

### 4.1. Assessment of the use of ilmenite as an oxygen carrier

The important parameters in the design of a CLC system are the recirculation rate of particles and the solids inventory. Both the oxygen transport capacity and the reduction and oxidation reactivity of solids determine the solids inventory in the fuel and air reactors to reach full conversion of fuel gas. A simplified model has been used to get an initial estimation of the solids inventory (Abad et al., 2007a). Thus, the calculated solids inventory facilitates the comparison of the feasibility of different oxygen carriers in an adequate way. The simplified model considers perfect mixing of solids, no restriction for the gas–solid contact, and the solid reaction following the shrinking core model. Considering the mass balance to the reactor, the mass of solids in the fuel and air reactors per $MW_{th}$ of fuel, $m_{OC}$, can be calculated for gaseous fuels as (Abad et al., 2007a)

$$m_{OC} = \eta_c \frac{2dM_O}{\Delta H_c^0} \frac{3}{\Phi R_{o,ilm} \left(\frac{dX_i}{dt}\Big|_{X_i=0}\right)_{av}} = \eta_c \frac{2dM_O}{\Delta H_c^0} \frac{3}{\Phi \left(\left|\frac{d\omega}{dt}\right|_{X_i=0}\right)_{av}} \quad (27)$$

and for solid fuels, e.g. coal, as (Adánez et al., 2010)

$$m_{OC} = \eta_c \frac{10^3 m_O}{LHV} \frac{3}{\Phi R_{o,ilm} \left(\frac{dX_i}{dt}\Big|_{X_i=0}\right)_{av}} = \eta_c \frac{10^3 m_O}{LHV} \frac{3}{\Phi \left(\left|\frac{d\omega}{dt}\right|_{X_i=0}\right)_{av}} \quad (28)$$

being $m_O$ the mass of oxygen required per kg of solid fuel to fully convert the solid fuel to $CO_2$ and $H_2O$, as for the case of the conventional combustion with air. LHV is the lower heating value of the solid fuel. In this work a typical composition for coal of 70% carbon, 5% hydrogen and 10% oxygen has been assumed, corresponding to a value of $m_O$=2.2 kg O $kg^{-1}$ coal. The LHV was assumed to be 25,000 kJ $kg^{-1}$.

Often the rate of oxygen transference is expressed as a mass based conversion rate, $d\omega/dt$, where $\omega$ is the mass based conversion defined as

$$\omega = \frac{m}{m_o} = 1 + R_{o,ilm}(X_o - 1) = 1 - R_{o,ilm} X_r \quad (29)$$

The mass based conversion rate can be calculated as

$$\frac{d\omega}{dt} = R_{o,ilm}\left(\frac{dX_i}{dt}\right) \quad (30)$$

The average reactivities

$$\left(\frac{dX_i}{dt}\Big|_{X_i=0}\right)_{av} \quad \text{and} \quad \left(\left|\frac{d\omega}{dt}\right|_{X_i=0}\right)_{av}$$

are obtained at the average gas concentration in the reactor and at the conversion of ilmenite $X_i$=0. For gaseous fuels, the average concentration can be obtained from the following equation:

$$\overline{C}_g^n = \frac{\Delta X_g C_{g0}^n}{\int_{X_{g,in}}^{X_{g,out}} \left[\frac{1+\varepsilon_g X_g}{1-X_g}\right]^n dX_g} \quad (31)$$

where $\varepsilon_g$ considers the gas expansion as a consequence of the reaction, and it was calculated as

$$\varepsilon_g = \frac{V_{g,X_g=1} - V_{g,X_g=0}}{V_{g,X_g=0}} \quad (32)$$

The value of $\varepsilon_g$ was 2 for the reduction reaction with $CH_4$, 0 for the use of $H_2$ and CO, and −0.21 for the oxidation reaction. Table 3 shows the average concentration considering a gas conversion of $X_{g,out}$=99.9% in the fuel reactor, and an air excess of 20% in the air reactor. For solid fuels, an initial estimation of the solids inventory was calculated only considering $H_2$ and CO proceeding from coal gasification. $H_2$ and CO concentration values can be as low as 2%, as found during CLC continuous operation (Berguerand and Lyngfelt, 2008a, 2008b). Considering that the reactivity of a mixture of $H_2$ and CO is similar to the reactivity for $H_2$ (Abad et al., 2007b), the average reactivity in Eq. (28) was calculated for 5% $H_2$, as the sum of $H_2$ and CO concentrations (Adánez et al., 2010).

**Table 3**
Minimum solid inventory data for pre-oxidized and activated ilmenite (kg of solids per $MW_{th}$ of fuel).

| | Pre-oxidized | | | | Activated | | | |
|---|---|---|---|---|---|---|---|---|
| $C_g$ (% of fuel) | $H_2$ 14.5 | CO 14.5 | $CH_4$ 5.3 | Coal[a] 5 | $H_2$ 14.5 | CO 19.2 | $CH_4$ 5.3 | Coal[a] 5 |
| *Fuel reactor* | | | | | | | | |
| $T$=1173 K | 299 | 955 | 4481 | 1152 | 66 | 189 | 461 | 253 |
| $T$=1223 K | 197 | 619 | 2337 | 760 | 52 | 139 | 272 | 201 |
| $T$=1273 K | 135 | 416 | 1285 | 519 | 42 | 105 | 167 | 163 |
| *Air reactor*[b] | | | | | | | | |
| $T$=1173 K | 75 | 64 | 90 | 99 | 39 | 33 | 47 | 52 |
| $T$=1223 K | 74 | 63 | 89 | 99 | 37 | 31 | 44 | 49 |
| $T$=1273 K | 74 | 63 | 89 | 98 | 35 | 30 | 42 | 46 |

[a] It was used 5 vol% $H_2$ for coal as fuel.
[b] The reaction rate was calculated using 11.1 vol% $O_2$.

The parameter $\Phi$ is the characteristic reactivity in the reactor, and it can be easily obtained from Fig. 7 in the work done by Abad et al. (2007a) as a function of the variation of the solids conversion in the reactor, $\Delta X_i$, and the conversion of solids at the reactor inlet. Nevertheless, assuming spherical grains in the kinetic model the value of characteristic reactivity, $\Phi$, is limited between 3 and 0. The minimum solids inventory in every reactor is obtained considering that $\Phi$=3, which is the case for $X_{i,in}$=0 and $\Delta X_i \approx 0$. This condition has been chosen to calculate the solids inventory and it could be reached when there were not limitations for solids circulation between fuel reactor and air reactor. The solids inventories so obtained for pre-oxidized and activated ilmenite are shown in Table 3.

The solids inventory in the air reactor can be also obtained from Eqs. (27) and (28) for gaseous and solid fuels, respectively. In this case, the average reactivity, i.e.

$$\left(\frac{dX_i}{dt}\Big|_{X_i=0}\right)_{av} \quad \text{or} \quad \left(\left|\frac{d\omega}{dt}\right|_{X_i=0}\right)_{av}$$

should be the corresponding to the oxidation reaction. As the oxygen demanded by each fuel ($CH_4$, $H_2$, CO or coal) is different per $MW_{th}$ of fuel, the solids inventory per $MW_{th}$ in the air reactor is also different for every fuel gas, even if the oxidation reactivity is the same in all cases. Therefore, a solids inventory in the air reactor can be calculated for each fuel gas, as it is shown in Table 3.

Higher solids inventories were found for pre-oxidized ilmenite than for activated ilmenite because the increase of the reactivity during the activation period. Also lower values of the solids inventory are found for the air reactor than for the fuel reactor because of the higher ilmenite reactivity for the oxidation reaction with respect to the reduction reactions. In the same way, higher solids inventories are required for the use of methane as fuel gas than for the syngas components, i.e. $H_2$ and CO. The solids inventory in the fuel reactor is highly dependent on the reactor temperature because the considerable increase of the reactivity with the temperature. However, minor differences in the solids inventory of the air reactor with the temperature were found because the low activation energy of the oxidation reaction, see Table 2.

The numbers showed in Table 3 can be compared to the solids inventory calculated for several synthetic oxygen carriers (Abad et al., 2007a; Zafar et al., 2007a, 2007b). Activation is expected to

occur quickly in the CLC system and it can be considered that most of particles in the CLC system are activated. Thus, only the minimum solids inventory for activated particles will be used for comparison purposes with other oxygen carriers. The solids inventories calculated for the air reactor (30–52 kg/$MW_{th}$) are in the range of those calculated for other Ni-, Cu-, Mn- and Fe-based oxygen carriers, which were in the range 10–60 kg/$MW_{th}$. On the contrary, the calculated solids inventories in the fuel reactor for ilmenite were usually higher than the obtained for others oxygen carriers. For ilmenite the solids inventories were in the range 42–66 kg/$MW_{th}$ for $H_2$, 105–189 kg/$MW_{th}$ for CO and 167–461 kg/$MW_{th}$ for $CH_4$. For a highly reactive synthetic Fe-based oxygen carrier the solids inventory obtained for $H_2$ and CO were 12 and 29 kg/$MW_{th}$, respectively, whereas that the solids inventory for $CH_4$ was 950 kg/$MW_{th}$. Nevertheless, lower solids inventories were calculated for methane using other oxygen carriers, e.g. in the range 10–20 kg/$MW_{th}$ for Ni-based oxygen carriers, 52 kg/$MW_{th}$ for a Cu-based oxygen carrier or 85 kg/$MW_{th}$ for a Mn-based oxygen carrier (Abad et al., 2007a; Zafar et al., 2007a, 2007b).

Regarding the values obtained for the solids inventory and comparing these values with those calculated for synthetic oxygen carriers with proven suitability in a CLC process, the assessment of the use of ilmenite as an oxygen carrier can be done. Thus, the use of ilmenite for the combustion of methane is not adequate, but there could be interesting the use of ilmenite for syngas combustion. Also, the solids inventory needed for ilmenite takes also acceptable values for coal combustion and the use of ilmenite for coal it is highly recommended because ilmenite is harmless for the environment and a considerably cheaper material than a synthetic material.

### 4.2. Application of the kinetic data to a reactor model

To predict satisfactorily the experimental results of a CLC plant with the mathematical model, it is necessary to know the actual reactivity of the oxygen carrier in the air and fuel reactors, which should be an average reactivity of all particles inside the reactors. For this purpose, it is necessary to consider how the reactivity of a particle changes during successive redox cycles, and the lifetime of every particle in a CLC system until they are elutriated or drained together the coal ashes. Every particle in a CLC has a different lifetime. For example, the number of cycles and the reacting time in each reactor has not to be the same for all particles existing in a CLC system. Thus, the reactivity of every particle would be different.

In a previous work (Adánez et al., 2010) it was found that pre-oxidized ilmenite particles increase their reactivity – here defined as the variation of conversion with time ($dX_i/dt$) – with the number of cycles. Ilmenite conversion $X_i$ of the reduction or oxidation reaction was obtained using Eqs. (18) or (19) and considering that free $Fe_2O_3$ and $Fe_2TiO_5$ in ilmenite are reduced up to $Fe_3O_4$ and $FeTiO_3$, respectively. However, the oxygen transport capacity, $R_{o,ilm}$, decreased with the redox cycles because the amount of hematite in the particles increased. From this complex situation, it seems that to know the average reactivity of particles which had different degree of activation – as it is the case in a CLC system – could be a hard task. That is, the reactivity of newly introduced particles, i.e. pre-oxidized, and particles with different degree of activation should be determined, and then to calculate an average reactivity of the particles in the air and fuel reactors.

To solve this problem and for preliminary estimations, it was assumed that the fraction of non-activated particles in the CLC system is low compared to the activated ones and it can be considered that most of particles in the CLC system are activated. This assumption can be realistic if the activation process was shorter than the lifetime of the particles in the CLC system. This can be the case because the activation of ilmenite particles is a fast process, which happens in a few redox cycles. Moreover, it is necessary to consider that the rate of oxygen transference remains constant after the activation period (Adánez et al., 2010). Thus, the mass based conversion rate, $d\omega/dt$, is maintained constant, and the same value can be obtained from two activated particles with different oxygen transport capacity, i.e.

$$\frac{d\omega}{dt} = R_{o,1}\left(\frac{dX_i}{dt}\right)_1 = R_{o,2}\left(\frac{dX_i}{dt}\right)_2 \tag{33}$$

The reactivity $(dX_i/dt)_1$ of activated particles with an oxygen transport capacity $R_{o,1}=3.3$ wt% can be determined from the kinetics parameters obtained in this work. Thus, the reactivity $(dX_i/dt)_2$ of any other particles with an oxygen transport capacity $R_{o,2}$ can be easily determined from Eq. (33). Similarly, the average reactivity, $(\overline{dX_i}/dt)_2$, of a mixture of activated particles with an average oxygen transport capacity $\overline{R}_{o,2}$ can be calculated using the kinetic parameters obtained in this work for activated ilmenite.

As an example, Fig. 13 shows the solids inventory in the fuel reactor as a function of the oxygen transport capacity for activated ilmenite and using coal as fuel. As it was shown in a previous work (Abad et al., 2007a), the solids inventory depends on the solids circulation flow rate, $\dot{m}_{OC}$. Thus, the solids inventory calculated for different values of $\dot{m}_{OC}$ are shown in Fig. 13. It can be seen that the solids inventory decreases as the solids circulation flow rate increases or the oxygen transport capacity increases. Both parameters, $\dot{m}_{OC}$ and $R_{o,ilm}$, are linked to the variation of solids conversion in the reactor, $\Delta X_i$, by Eq. (34) for gaseous fuels and Eq. (35) for solids fuels, which is the parameter affecting the solids inventory through the parameter $\Phi$, see Eqs. (27) and (28)

$$\Delta X_i = \frac{2dM_O}{R_{o,ilm}\Delta H_c^0}\frac{1}{\dot{m}_{OC}} \tag{34}$$

$$\Delta X_i = \frac{10^3 m_O}{R_{o,ilm}LHV}\frac{1}{\dot{m}_{OC}} \tag{35}$$

Therefore, as $\dot{m}_{OC}$ or $R_{o,ilm}$ increases, $\Delta X_i$ decreases. Thus, as $\Delta X_i$ decreases the residence time of particles in the reactor should be lower, and the solids inventory decreases. Here, it is useful to remember that the rate of oxygen transference is maintained constant for activated particles with different values of $R_{o,ilm}$, as it was stated in Eq. (33). At this condition, the parameter affecting

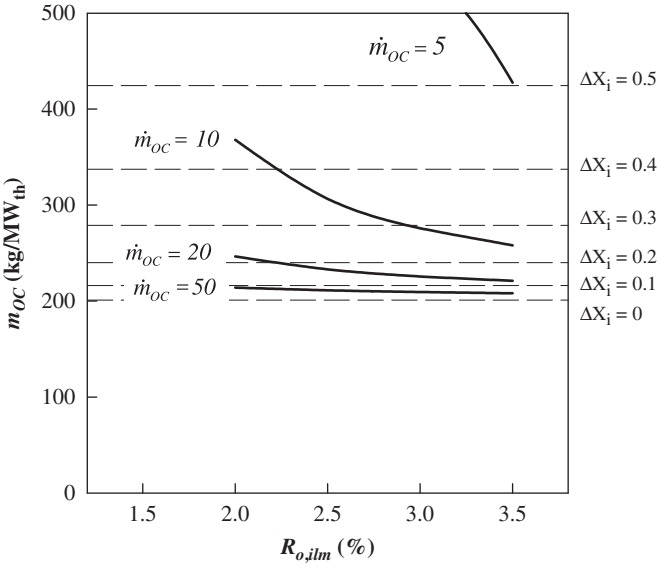


**Fig. 13.** Solids inventory for activated ilmenite (kg of solids per $MW_{th}$ of fuel) as a function of the oxygen transport capacity for several solids circulation flow rate, $\dot{m}_{OC}$ (kg $s^{-1}$ per $MW_{th}$). $T=1223$ K; $X_{i,in}=0.5-\Delta X_i/2$. Fuel: coal.

the solids inventory is $\Delta X_i$, i.e. the same solids inventory value will be obtained for a constant value of $\Delta X_i$ corresponding to the same value for the product of $\dot{m}_{OC}$ and $R_{o,ilm}$. In Fig. 13 some reference lines corresponding to various values of $\Delta X_i$ are plotted.

Also it can be observed in Fig. 13 that the effect of the oxygen transport capacity on the solids inventory is less noticeable as the solids circulation rate increases, i.e. when $\Delta X_i$ decreases. This fact is an effect of considering perfect mixing of solids in the reactor. When $\Delta X_i \to 0$, the fraction of reacting oxygen is much lower than the total available oxygen in particles. Thus, the total available oxygen in the particles, i.e. the oxygen transport capacity, has low relevance on the average reactivity of particles in the reactor and hence in the solids inventory. At the condition $\Delta X_i \to 0$ the minimum solids inventory is reached, as it was showed in Table 3.

Under these considerations, the kinetic parameters determined in this work can be introduced in a mathematical model describing the reactors of a CLC system when gaseous or solids fuels are used. In a future work, the mathematical model of the CLC system will be used to simulate and optimize the process for industrial operation under different operating conditions.

## 5. Conclusions

The reactivities of the reduction and oxidation reactions for pre-oxidized and activated ilmenite were determined by thermogravimetric analysis using methane, hydrogen, carbon monoxide or oxygen as reacting gases. The activated ilmenite exhibited high reactivity in both reduction and oxidation reactions, with times for complete conversion at 1223 K lower than 120 s using 15% of $H_2$, CO or $CH_4$, and 30 s using 21% of $O_2$.

The kinetic parameters of the reduction reaction with $H_2$, CO or $CH_4$ and the oxidation by oxygen of pre-oxidized and activated particles were obtained. The grain model with uniform reaction in the particle and reaction in the grains following a changing grain size model with chemical reaction control in the grains was used to determine the kinetic parameters. In addition, to predict the behaviour of the oxidation of pre-oxidized ilmenite, a mixed resistance between chemical reaction and diffusion in the solid product was needed.

The reaction order in the main part of the reactions of pre-oxidized and activated ilmenite with $H_2$, CO, $CH_4$ and $O_2$ was $n=1$, being different ($n=0.8$) for the reaction of activated ilmenite with CO. Activation energies from 109 to 165 kJ mol$^{-1}$ for pre-oxidized ilmenite and from 65 to 135 kJ mol$^{-1}$ for activated ilmenite were found for the different reactions with $CH_4$, CO and $H_2$. For the oxidation reaction activation energies found were lower: 11 kJ mol$^{-1}$ for pre-oxidized and 25 kJ mol$^{-1}$ for activated ilmenite.

The activation process has a beneficial and strong influence on the solids inventory needed in both the air and fuel reactor. An analysis of the performance of ilmenite depending on the activation degree has been done. From results showed in this work, it can be concluded that ilmenite presents a competitive performance for its use in CLC against synthetic oxygen carriers when it is taken into account for the oxygen transport capacity, the moderated solids inventory and the low cost of the material. This last issue can be determinant for the selection of an oxygen carrier for solid fuels combustion in a CLC system.

## Nomenclature

| | |
|---|---|
| $\overline{b}$ | average stoichiometric coefficient for reaction of solid with reacting gas, mol metal oxide per mol of gas |
| $d$ | stoichiometric factor in the fuel combustion reaction with oxygen, mol $O_2$ per mol of fuel |
| $C_g$ | reacting gas concentration, mol m$^{-3}$ |
| $C_{g0}$ | gas concentration at the reactor inlet, mol m$^{-3}$ |
| $\overline{C}_g$ | average gas concentration in the reactor, mol m$^{-3}$ |
| $D_e$ | effective diffusivity in the product layer, mol m$^{-2}$ s$^{-1}$ |
| $D_{e0}$ | pre-exponential factor for effective diffusivity, mol m$^{-2}$ s$^{-1}$ |
| $E_j$ | activation energy of the reacting mechanism $j$, kJ mol$^{-1}$ |
| $k_s$ | chemical kinetic constant, mol$^{1-n}$ m$^{3n-2}$ s$^{-1}$ |
| $k_{s0}$ | pre-exponential factor for chemical kinetic constant, mol$^{1-n}$ m$^{3n-2}$ s$^{-1}$ |
| $m$ | instantaneous mass of the oxygen carrier, kg |
| $m_r$ | mass of the reduced form of the oxygen carrier, kg |
| $m_o$ | mass of the oxidized form of the oxygen carrier, kg |
| $m_O$ | mass of oxygen required per kg of solid fuel to full convert the solid fuel, kg oxygen kg$^{-1}$ coal |
| $m_{OC}$ | solids inventory, kg per $MW_{th}$ |
| $\dot{m}_{OC}$ | solids circulation rate per $MW_{th}$ of fuel, kg s$^{-1}$ per $MW_{th}$ |
| $M_O$ | molecular weight of oxygen = 16 g mol$^{-1}$ |
| $n$ | reaction order |
| $r_g$ | grain radius, m |
| $r_p$ | particle radius, m |
| $R_g$ | ideal gas constant = 8.314 J mol$^{-1}$ K$^{-1}$ |
| $R_{0,ilm}$ | oxygen transport capacity of ilmenite |
| $t$ | time, s |
| $t_j$ | reacting time while the mechanism j controlling the reaction is fulfilled, s |
| $T$ | temperature, K |
| $V_{g,X_g=0}$ | volume of the gas mixture at $X_g=0$, m$^3$ |
| $V_{g,X_g=1}$ | volume of the gas mixture at $X_g=1$, m$^3$ |
| $V_{m,prod}$ | molar volume of reacting product, m$^3$ mol$^{-1}$ |
| $V_{m,reac}$ | molar volume of reacting solid, m$^3$ mol$^{-1}$ |
| $X_g$ | gas conversion |
| $X_i$ | conversion of solids of the reaction $i$ |
| $X_{chr}$ | particle conversion until chemical reaction control is fulfilled |
| $X'_o$ | modified conversion, defined by Eq. (23) |
| $Z$ | expansion ratio between the solid product and solid reactive |

*Greek letters*

| | |
|---|---|
| $\Delta H_c^0$ | standard combustion heat of the gas fuel, kJ mol$^{-1}$ |
| $\Delta X_g$ | variation of the gas conversion in the reactor |
| $\Delta X_i$ | variation of the solid conversion in the reactor for the reaction $i$ |
| $\varepsilon_g$ | coefficient of expansion of the gas mixture |
| $\Phi$ | characteristic reactivity in the reactor |
| $\rho_m$ | molar density, mol m$^{-3}$ |
| $\tau_j$ | time for complete conversion by controlling the mechanism $j$, s |
| $\omega$ | mass based conversion |

*Subscripts*

| | |
|---|---|
| *av* | average condition |
| *chr* | control by chemical reaction at the solid surface |
| *dif* | control by diffusion through the product layer around the particle |
| *in* | inlet |
| *o* | oxidation reaction |
| *out* | outlet |
| *r* | reduction reaction |

*Abbreviation*

| | |
|---|---|
| LHV | lower heating value of the solid fuel, kJ kg$^{-1}$ |

## Acknowledgments

This work was partially supported by the European Commission, under the RFCS program (ECLAIR Project, Contract RFCP-CT-2008-0008) and from Alstom Power Boilers. A. Cuadrat thanks CSIC for the JAE Pre-fellowship. Alberto Abad thanks to the Ministerio de Ciencia e Innovación for the financial support in the course of the I3 Program.

## References

Abad, A., Adánez, J., García-Labiano, F., de Diego, L.F., Gayán, P., Celaya, J., 2007a. Mapping of the range of operational conditions for Cu-, Fe-, and Ni-based oxygen carriers in chemical-looping combustion. Chemical Engineering Science 62, 533–549.

Abad, A., García-Labiano, F., de Diego, L.F., Gayán, P., Adánez, J., 2007b. Reduction kinetics of Cu-, Ni-, and Fe-based oxygen carriers using syngas ($CO+H_2$) for chemical-looping combustion. Energy & Fuels 21, 1843–1853.

Abad, A., Adánez, J., García-Labiano, F., de Diego, L.F., Gayán, P, 2009. Modeling of the chemical-looping combustion of methane using a Cu-based oxygen carrier. Energy Procedia 1, 391–398.

Adánez, J., Cuadrat, A., Abad, A., Gayán, P., de Diego, L.F., García-Labiano, F., 2010. Ilmenite activation during consecutive redox cycles in chemical-looping combustion. Energy & Fuel 24, 1402–1413.

Bardi, G., Gozzi, D., Stranges, S., 1987. High temperature reduction kinetics of ilmenite by hydrogen. Materials Chemistry and Physics 17, 325–341.

Barin, I., 1989. Thermochemical Data of Pure Substances. VCH Publishers, Cambridge.

Berguerand, N., Lyngfelt, A., 2008a. Design and operation of a 10 kWth chemical-looping combustor for solid fuels—testing with South African coal. Fuel 87, 2713–2726.

Berguerand, N., Lyngfelt, A., 2008b. The use of petroleum coke as fuel in a 10 kWth chemical-looping combustor. International Journal of Greenhouse Gas Control 2, 169–179.

Bohn, C.D., Cleeton, J.P., Müller, C.M., Scott, S.A., Dennis, J.S., 2009. Mesuring the kinetics of the reduction of iron oxide with carbon monoxide in a fluidized bed. In: Proceedings of the 20th International Conference on Fluidized Bed Combustion, Xian, China, pp. 555–561.

Borowiec, K., Rosenqvist, T., 1981. Phase Relations and Oxidation Studies in the System $Fe–Fe_2O_3–TiO_2$ at 700–1100 °C. Scandinavian Journal of Metallurgy 10, 217–224.

Cao, Y., Casenas, B., Pan, W.-P., 2006. Investigation of chemical looping combustion by solid fuels. 2. Redox reaction kinetics and product characterization with coal, biomass, and solid waste as solid fuels and CuO as an oxygen carrier. Energy & Fuels 20, 1845–1854.

Chuang, S.Y., Dennis, J.S., Hayhurst, A.N., Scott, S.A., 2008. Development and performance of Cu-based oxygen carriers for chemical-looping combustion. Combustion and Flame 154, 109–121.

Chuang, S.Y., Dennis, J.S., Hayhurst, A.N., Scott, S.A., 2009a. Kinetics of the chemical looping oxidation of CO by a co-precipitated mixture of CuO and $Al_2O_3$. Proceedings of the Combustion Institute 32, 2633–2640.

Chuang, S.Y., Dennis, J.S., Hayhurst, A.N., Scott, S.A., 2009b. Kinetics of oxidation of a reduced form of the Cu-based oxygen-carrier for use in Chemical-Looping Combustion. In: Proceedings of the 20th International Conference on Fluidized Bed Combustion, Xian, China, pp. 512–518.

Dey, S.K., Jana, B., Basumallick, A., 1993. Kinetics and reduction characteristics of hematite-noncoking coal mixed pellets under nitrogen gas atmosphere. ISIJ International 33 (7), 735–739.

Donskoi, E., McElwain, D.L.S., Wibberley, L.J., 2003. Estimation and modeling of parameters for direct reduction in iron ore/coal composites: Part II. Kinetic parameters. Metallurgical and Materials Transactions B 34B, 255–266.

Ekström, C., Schwendig, F., Biede, O., Franco, F., Haupt, G., de Koeijer, G., Papapavlou, C., Røkke, P.E., 2009. Techno-economic evaluations and benchmarking of pre-combustion $CO_2$ capture and oxy-fuel processes developed in the European ENCAP Project. Energy Procedia 1, 4233–4240.

García-Labiano, F., de Diego, L.F., Adánez, J., Abad, A., Gayán, P., 2004. Reduction and oxidation kinetics of a copper-based oxygen carrier prepared by impregnation for chemical-looping combustion. Industrial & Engineering Chemistry Research 43, 8168–8177.

García-Labiano, F., Adánez, J., de Diego, L.F., Gayán, P., Abad, A., 2006. Effect of pressure on the behavior of copper-, iron-, and nickel-based oxygen carriers for chemical-looping combustion. Energy & Fuels 20, 26–33.

Grey, I., McDonald, K., Fisher-White, M., de Vries, M., 2007. Hydrogen reduction of peroxidised ilmenite in fluidised bed and packed bed reactors. Mineral Processing and Extractive Metallurgy 116 (4), 209–216.

Gupta, S.K., Rajakumar, V., Grievenson, P., 1991. Phase transformations during heating of ilmenite concentrates. Metallurgical and Materials Transactions B 22B (5), 711–716.

Hossain, M.M., de Lasa, H.I., 2008. Chemical-looping combustion (CLC) for inherent $CO_2$ separations—a review. Chemical Engineering Science 63, 4433–4451.

IPCC Special Report on Carbon Dioxide Capture and Storage, 2005. Available at: 〈http://ipcc.ch〉 (Chapter 3. Capture).

Ishida, M., Jin, H., Okamoto, T., 1996. A fundamental study of a new kind of medium material for chemical-looping combustion. Energy & Fuels 10, 958–963.

Itoh, S., Sato, S., Ono, J., Okada, H., Nagasaka, T., 2006. Feasibility study of the new rutile extraction process from natural ilmenite ore based on the oxidation reaction. Metallurgical and Materials Transactions B 37B, 979–985.

Jabloński, M., Przepiera, A., 2001. Estimation of kinetic parameters of thermal oxidation of ilmenite. Journal of Thermal Analysis and Calorimetry 66, 617–622.

Karkhanavala, M.D., Momin, A.C., 1959. The alteration of ilmenite. Economic Geology 54, 1095–1102.

Kerr, H.R., 2005. Capture and separation technologies gaps and priority research needs. In: Thomas, D., Benson, S. (Eds.), Carbon Dioxide Capture for Storage in Deep Geologic Formations—Results from the $CO_2$ Capture Project, vol. 1. Elsevier Ltd., Oxford, UK (Chapter 38).

Leion, H., Mattisson, T., Lyngfelt, A., 2007. The use of petroleum coke as fuel in chemical-looping combustion. Fuel 86, 1947–1958.

Leion, H., Mattisson, T., Lyngfelt, A., 2008a. Solid fuels in chemical-looping combustion. International Journal of Greenhouse Gas Control 2, 180–193.

Leion, H., Lyngfelt, A., Johansson, M., Jerndal, E., Mattisson, T., 2008b. The use of ilmenite as an oxygen carrier in chemical-looping combustion. Chemical Engineering Research and Design 86, 1017–1026.

Leion, H., Mattisson, T., Lyngfelt, A., 2009a. Use of ores and industrial products as oxygen carriers in chemical-looping combustion. Energy & Fuels 23, 2307–2315.

Leion, H., Jerndal, E., Steenari, B.-M., Hermansson, S., Israelsson, M., Jansson, E., Johnsson, M., Thunberg, R., Vadenbo, A., Mattisson, T., Lyngfelt, A., 2009b. Solid fuels in chemical-looping combustion using oxide scale and unprocessed iron ore as oxygen carriers. Fuel 88, 1945–1954.

Lyngfelt, A., Johansson, M., Mattisson, T., 2008. Chemical-looping combustion—status of development. In: Proceedings of the Ninth International Conference on Circulating Fluidized Beds (CFB-9), Hamburg, Germany.

Lyngfelt, A., 2010. Oxygen carriers for chemical-looping combustion—operational experience. In: Proceedings of the First International Conference on Chemical Looping, IFP-Lyon, France.

Moghtaderi, B., Song, H., Doroodchi, E., Wall, T., 2010. Reactivity analysis of mixed metal oxides. In: Proceedings of the First International Conference on Chemical Looping, IFP-Lyon, France.

Nell, J., 1999. An overview of the phase-chemistry involved in the production of high-titanium slag from ilmenite feedstock. Heavy Minerals, 137–145.

Park, E., Ostrovski, O., 2003. Reduction of titania-ferrous ore by carbon monoxide. ISIJ International 43 (9), 1316–1325.

Park, E., Ostrovski, O., 2004. Effect of preoxidation of titania-ferrous ore on the ore structure and reduction behavior. ISIJ International 44 (1), 74–81.

Rao, D.B., Rigaud, M., 1975. Kinetics of the oxidation of ilmenite. Oxidation of Metals 9 (1), 99–116.

Scott, S.A., Dennis, J.S., Hayhurst, A.N., Brown, T., 2006. Situ gasification of a solid fuel and $CO_2$ separation using chemical looping. AIChE Journal 52, 3325–3328.

Sedor, K.E., Hossain, M.M., de Lasa, H.I., 2008. Reduction kinetics of a fluidizable nickel-alumina oxygen carrier for chemical-looping combustion. The Canadian Journal of Chemical Engineering 86, 323–334.

Shen, L., Wu, J., Xiao, J., Song, Q., Xiao, R., 2009. Chemical-looping combustion of biomass in a 10 kWth reactor with iron oxide as an oxygen carrier. Energy & Fuels 23, 2498–2505.

Siriwardane, R., Tian, H., Richards, G., Simonyi, T., Poston, J., 2009. Chemical-looping combustion of coal with metal oxide oxygen carriers. Energy & Fuels, 10.1021/ef9001605.

Sohn, I., Fruehan, R.J., 2005. The reduction of iron oxides by volatiles in a rotary hearth furnace process: Part I. The role and kinetics of volatile reduction. Metallurgical and Materials Transactions B 36B, 605–612.

Son, S.R., Kim, S.D., 2006. Chemical-looping combustion with NiO and $Fe_2O_3$ in a thermobalance and circulating fluidized bed reactor with double loops. Industrial & Engineering Chemistry Research 45, 2689–2696.

Sun, K., Ishii, M., Takahashi, R., Yagi, J.-I., 1992a. Oxidation kinetics of cement-bonded natural ilmenite pellets. ISIJ International 32 (4), 489–495.

Sun, K., Ishii, M., Takahashi, R., Yagi, J.-I., 1992b. Reduction kinetics of cement-bonded natural ilmenite pellets with hydrogen. ISIJ International 32 (4), 496–504.

Sun, K., Takahashi, R., Yagi, J.-I., 1993. Kinetics of the oxidation and reduction of synthetic ilmenite. ISIJ International 33 (5), 523–528.

Vries, M.L., Grey, I.E., 2006. Influence of pressure on the kinetics of synthetic ilmenite reduction in hydrogen. Metallurgical and Materials Transactions B 37B, 199–208.

Wang, Y., Yuan, Z., 2006. Reductive kinetics of the reaction between a natural ilmenite and carbon. International Journal of Mineral Processing 81, 133–140.

Yang, J.-b., Cai, N.-s., Li, Z.-S., 2007. Reduction of iron oxide as an oxygen carrier by coal pyrolysis and steam char gasification intermediate products. Energy & Fuels 21, 3360–3368.

Zafar, Q., Abad, A., Mattisson, T., Gevert, B., 2007a. Reaction kinetics of freeze-granulated $NiO/MgAl_2O_4$ oxygen carrier particles for chemical-looping combustion. Energy & Fuels 21, 610–618.

Zafar, Q., Abad, A., Mattisson, T., Gevert, B., Strand, M., 2007b. Reduction and oxidation kinetics of $Mn_3O_4$/Mg-$ZrO_2$ oxygen carrier particles for chemical-looping combustion. Chemical Engineering Science 62, 6556–6567.

Zhang, G., Ostrovski, O., 2001. Reduction of ilmenite concentrates by methane containing gas, Part II: Effects of preoxidation and sintering. Canadian Metallurgical Quarterly 40 (4), 489–497.

Zhang, G., Ostrovski, O., 2002. Effect of preoxidation and sintering on properties of ilmenite concentrates. International Journal of Mineral Processing 64, 201–218.

Zhao, Y., Shadman, F., 1990. Kinetics and mechanism of ilmenite reduction with carbon monoxide. AIChE Journal 36, 1433–1438.

Zhao, Y., Shadman, F., 1991. Reduction of ilmenite with hydrogen. Industrial & Engineering Chemistry Research 30, 2080–2087.

# Paper III

Fuel Processing Technology 94 (2012) 101–112

Contents lists available at SciVerse ScienceDirect

Fuel Processing Technology

journal homepage: www.elsevier.com/locate/fuproc

# Behavior of ilmenite as oxygen carrier in chemical-looping combustion

A. Cuadrat, A. Abad *, J. Adánez, L.F. de Diego, F. García-Labiano, P. Gayán

*Instituto de Carboquímica (C.S.I.C.), Dept. of Energy & Environment, Miguel Luesma Castán, 4, Zaragoza, 50018, Spain*

ARTICLE INFO

*Article history:*
Received 7 June 2011
Received in revised form 24 October 2011
Accepted 24 October 2011
Available online 29 November 2011

*Keywords:*
$CO_2$ capture
Chemical-looping combustion
Oxygen-carrier
Ilmenite
Fuel

ABSTRACT

For a future scenery where will exist limitation for $CO_2$ emissions, chemical-looping combustion (CLC) has been identified as a promising technology to reduce the cost related to $CO_2$ capture from power plants. In CLC a solid oxygen-carrier transfers oxygen from the air to the fuel in a cyclic manner, avoiding direct contact between them. $CO_2$ is inherently obtained in a separate stream. For this process the oxygen-carrier circulates between two interconnected fluidized-bed reactors. To adapt CLC for solid fuels the oxygen-carrier reacts with the gas proceeding from the solid fuel gasification, which is carried out right in the fuel-reactor. Ilmenite, a natural mineral composed of $FeTiO_3$, is a low cost and promising material for its use on a large scale in CLC.
The aim of this study is to analyze the behavior of ilmenite as oxygen-carrier in CLC. Particular attention was put on the variation of chemical and physical characteristics of ilmenite particles during consecutive redox cycles in a batch fluidized-bed reactor using $CH_4$, $H_2$ and CO as reducing gases. Reaction with $H_2$ was faster than with CO, and near full $H_2$ conversion was obtained in the fluidized-bed. Lower reactivity was found for $CH_4$. Ilmenite increased its reactivity with the number of cycles, especially for $CH_4$. The structural changes of ilmenite, as well as the variations in its behavior with a high number of cycles were also evaluated with a 100 cycle test using a $CO + H_2$ syngas mixture. Tests with different $H_2$:CO ratios were also made in order to see the reciprocal influence of both reducing gases and it turned out that the reaction rate is the sum of the individual reaction rates of $H_2$ and CO. The oxidation reaction of ilmenite was also investigated. An activation process for the oxidation reaction was observed and two steps for the reaction development were differenced. The oxidation reaction was fast and complete oxidation could be reached after every cycle. Low attrition values were found and no defluidization was observed during fluidized-bed operation. During activation process, the porosity of particles increased from low porosity values up to values of 27.5%. The appearance of an external shell in the particle was observed, which is Fe enriched. The segregation of Fe from $TiO_2$ causes that the oxygen transport capacity, $R_{OC}$, decreases from the initial $R_{OC} = 4.0\%$ to 2.1% after 100 redox cycles.



## 1. Introduction

At present there is a general assent on the need of reducing the emissions of the greenhouse gas $CO_2$ in order to restrain climate change. Anthropogenic $CO_2$ is mainly generated in combustion of fossil fuels, which are foreseen to provide about 80% of the overall world consumption of energy for the next several decades. For the power generation and heat supply sector, emissions were 12.7 Gt $CO_2$-eq in 2004, which is 26% of total $CO_2$-eq emissions. When regarding the energy-related $CO_2$ emissions by fuel type, coal use generated 39% of the emissions in 2004 and it is estimated that the percentage in 2030 will rise up to 43% [1,2]. Among the different opportunities to reduce the anthropogenic $CO_2$ emissions, the development of technologies to capture $CO_2$ from fossil fuel uses and to store it permanently has been identified as a relevant option in the future, being the implementation of these technologies more feasible and readily in stationary power plants.

In this context, chemical-looping combustion (CLC) is one of the most promising technologies to carry out the $CO_2$ capture at a low cost [3–5]. CLC is based on the transfer of the oxygen from air to the fuel by means of a solid oxygen-carrier that circulates between two interconnected fluidized-beds: the fuel- and the air-reactor [6]. In the fuel-reactor the oxygen-carrier is reduced through oxidation of the fuel. Afterwards the oxygen-carrier is directed to the air-reactor, where it is again regenerated, as the inlet air flow reacts with the solid. The net chemical reaction is the same as at usual combustion with the same combustion heat released.

Important progress has been made in CLC with natural gas to date. Several authors have successfully demonstrated the feasibility of this process in different CLC prototypes in the 10–140 $kW_{th}$ range using oxygen-carriers based on NiO [7–10] and CuO [11].

But increasing interest is found about the application of CLC using coal as fuel, regarding the intensive use of this fuel. There are two possibilities for the use of the CLC technology with coal. The first one is to carry out previous coal gasification and subsequently to

* Corresponding author.
*E-mail address:* abad@icb.csic.es (A. Abad).

0378-3820/$ – see front matter © 2011 Elsevier B.V. All rights reserved.
doi:10.1016/j.fuproc.2011.10.020

introduce the produced gas in the CLC system [12]. In this option pure oxygen is needed to carry out the gasification to produce syngas with no $N_2$. Thus, the extra gasifier and the production of pure oxygen would entail an additional energetic cost. Simulations performed by Jin and Ishida [13] and Wolf et al. [14] showed that this process has the potential to achieve an efficiency of about 5–10% points higher than a similar combined cycle that uses conventional $CO_2$ capture technology. Several oxygen-carriers based on Ni, Cu, Fe and Mn oxides have shown good reactivity with syngas components, i.e. $H_2$ and CO [15,16], and the use of syngas in a CLC system has been successfully accomplished in 300–500 $W_{th}$ continuously operated reactors [17–21].

The second possibility for the use of coal in a CLC is the direct combustion in the CLC process [22,23]. The reactor scheme of the direct CLC process with solid fuels is shown in Fig. 1. In this option coal is physically mixed with the oxygen-carrier in the fuel-reactor and the carrier reacts with volatiles and the gas product of coal gasification, where $H_2$ and CO are main components. Eqs. (1) to (5) express generally the reactions that take place in the fuel-reactor, being (3) to (5) the oxygen-carrier reduction reactions with the main products of coal devolatilization and gasification. The oxygen-carrier is subsequently introduced in the air-reactor where it is re-oxidized following reaction (6). $Me_xO_y$ and $Me_xO_{y-1}$ are the oxidized and reduced form, respectively, of the oxygen-carrier.

$$\text{Coal} \rightarrow \text{Volatiles} + \text{Char} \quad (1)$$

$$\text{Char} + H_2O \rightarrow CO + H_2 \quad (2)$$

$$CH_4 + 4Me_xO_y \rightarrow CO_2 + 2H_2O + 4Me_xO_{y-1} \quad (3)$$

$$H_2 + Me_xO_y \rightarrow H_2O + Me_xO_{y-1} \quad (4)$$

$$CO + Me_xO_y \rightarrow CO_2 + Me_xO_{y-1} \quad (5)$$

$$2Me_xO_{y-1} + O_2 \rightarrow 2Me_xO_y \quad (6)$$

The stream of combustion gases from the fuel-reactor contains primarily $CO_2$ and $H_2O$. Water can be easily separated by condensation and a highly concentrated stream of $CO_2$ ready for sequestration is achieved. The gas stream from the air-reactor is oxygen-depleted and consists in $N_2$ and some unreacted $O_2$. The $CO_2$ capture is inherent to this process, as the air does not get mixed with the fuel, and no additional costs or energy penalties for gas separation are required.

The gasification process is expected to be the limiting step in the fuel-reactor, so the stream of solids exiting the fuel-reactor could contain some unconverted char together with the oxygen-carrier. Thus, an additional carbon stripper is necessary to separate char particles from oxygen-carrier particles, reducing the carbon transferred from the fuel- to the air-reactor. As a consequence of the ashes present in the solid fuel, the draining of ashes from the system is necessary to avoid its accumulation in the reactors. This drain stream will also contain some oxygen-carrier. It is therefore expected that the active life of this material would be limited by the losses with the drain stream rather than by its degradation.

Low cost of the carrier is rather desirable for its use with coal, as it is predictable a partial loss together with the coal ashes when removing them from the reactor to avoid their accumulation in the system. The use of natural minerals for this option seems to be very interesting, being ilmenite an appropriate material [24–28].

As for gaseous fuels, suitable oxygen-carriers for solid fuels in the CLC process must have high selectivity towards $CO_2$ and $H_2O$, enough oxygen transport capacity, high reactivity, high mechanical strength, attrition resistance and agglomeration absence. All these properties must be maintained during many reduction and oxidation cycles. Ilmenite has shown to be a low cost suitable material to be used for solid fuel combustion in a CLC system. Leion et al. [29,30] analyzed the reactivity of ilmenite in a batch fluidized-bed and ilmenite gave high conversion of $H_2$ and CO but moderate conversion of $CH_4$. This carrier has been already used in both gaseous and solid fuels [24–27,31]. Ilmenite is mainly composed of $FeTiO_3$ ($FeO{\cdot}TiO_2$), where iron oxide is the active phase that behaves as the oxygen-carrier. There are a few recent studies made and a good performance of ilmenite at different levels as oxygen-carrier in CLC has been observed. For solid fuels combustion, the ilmenite reacted just as well as a synthetic $Fe_2O_3$-based oxygen-carrier. They also observed a gain in the ilmenite reactivity as increasing the redox cycles until a maximum reaction rate was reached and maintained with the cycles, which has been also seen and proven after 100 redox cycles in TGA for various gaseous fuels by Adánez et al. [32], as well as when using solid fuels in batch testing [33]. Berguerand et al. [24,25] operated a 10 $kW_{th}$ chemical-looping combustor using South African coal and petroleum coke as solid fuels. They used the same batch of ilmenite particles for about 100 h under different conditions and the oxygen-carrier maintained its good properties throughout operation. This was confirmed by Cuadrat et al. [27] in their study of the fuel reactor and the effect of operational variables in the efficiency of the process. The encouraging results to date obtained indicate that there is still further research to be carried out. Besides, all research to date about ilmenite performance as oxygen-carrier has analyzed only the reduction step.

The aim of this work is to investigate ilmenite as oxygen-carrier in a CLC system and the effect of the number of cycles on its reactivity with the main gases from coal pyrolysis and gasification, that is, $CH_4$, CO and $H_2$. In addition, this study includes an assessment on the oxidation step and its changes after many redox cycles. Consecutive reduction–oxidation cycles were carried out in a batch fluidized-bed reactor using $CH_4$, CO and $H_2$ as reducing agents. To analyze the activation process a characterization of the initial and reacted samples of oxygen-carrier was also done. Further fluidized-bed tests were carried out using syngas as fuel. The structural changes of ilmenite, as well as the variations in its behavior with a high number of cycles were also evaluated with a 100 cycle test using a $H_2 + CO$ syngas mixture. Tests with different $H_2$:CO ratios were also made in order to see the reciprocal influence of both reducing gases in the reaction rate.

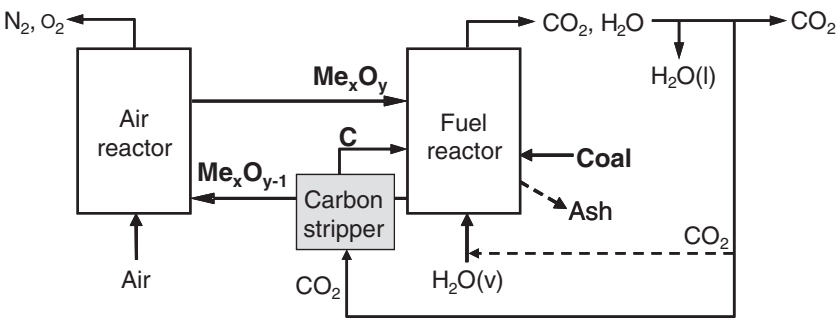


**Fig. 1.** Reactor scheme of the CLC process with solid fuels.

## 2. Experimental section

### 2.1. Oxygen-carrier material

Ilmenite is a common mineral found in metamorphic and igneous rocks. The ilmenite used is a concentrate from a natural ore. Fresh particles have been exposed to thermal pre-treatment at 950 °C in air during 24 h, since it improves its performance as oxygen-carrier [30,31]. Table 1 shows the main properties for calcined ilmenite. The XRD analysis of calcined ilmenite revealed that $Fe_2TiO_5$ and $TiO_2$ were the major components, with minor amount of $Fe_2O_3$. The composition of calcined ilmenite was 55.5 wt.% $Fe_2TiO_5$, 10.6 wt.% $Fe_2O_3$, 28.4 wt.% $TiO_2$ and 5.5 wt.% of other inert compounds. The crushing strength was measured by using a Shimpo FGN-5 crushing strength apparatus. The final measure was obtained from the average of at least 20 different measurements. The values of crushing strength obtained for the initial ilmenite are similar to other Fe-based oxygen-carriers [34]. Mercury porosimetry of initial ilmenite exhibits low porosity development. Table 1 also shows the main properties of the so-called activated ilmenite. They are reacted particles after several redox cycles and undergo an increase in the reaction rate which will be discussed later.

### 2.2. Batch fluidized-bed reactor

Several reduction–oxidation cycles with different reducing gases were performed in a batch fluidized-bed to investigate the gas product distribution and the variation of chemical and physical properties of the ilmenite particles with the number of cycles.

Fig. 2 shows the experimental setup. It consists of a system for gas feeding, a fluidized-bed reactor (55 mm I.D.), two filters that recovers the solids elutriated from the fluidized-bed working alternatively, and the gas analysis system. The whole fluidized-bed reactor is inside an electrically heated furnace. A detailed description of the apparatus and procedure can be found elsewhere [35]. The gas feeding system had different mass flow controllers connected to an automatic three-way valve. This allowed the feeding of the fuel gas (mixtures of $CH_4$, CO, $CO_2$, $H_2$, $H_2O$ and $N_2$) during the reducing period and a mixture of air and $N_2$ for oxidation of ilmenite. Nitrogen was introduced between the two periods during 2 min to purge and avoid the contact between the fuel and the oxygen. For the supplying of the steam there is a liquid flow controller for water which is subsequently heated up and evaporated with a resistance heater and swept away by the rest of the reducing gas.

The differential pressure drop in the bed is measured by means of two pressure taps connected to the bottom and top of the reactor, and are used to detect possible agglomeration problems in the bed. The gas analysis system consists of several online gas analyzers. $CH_4$, CO and $CO_2$, dry basis concentrations are measured using non-dispersive infrared analysis (NDIR) and $H_2$ by thermal conductivity. $O_2$ concentration is determined using a paramagnetic analyzer. Water content, on wet basis is measured via Fourier Transform Infrared (FTIR Gasmet Cx-4000) analyzer. All data were collected by means of a data logger connected to a computer. The gas flow dispersion through the sampling line and the analyzers was corrected for all the measured gas concentrations in order to obtain the actual concentration of the gases at the bed exit by a deconvolution method [19].

**Table 1**
Characterization of calcined and activated ilmenite after 20 redox cycles with CO as reducing agent.

| | Calcined | Activated |
|---|---|---|
| Composition by XRD | $Fe_2TiO_5$, $Fe_2O_3$, $TiO_2$ | $Fe_2TiO_5$, $Fe_2O_3$, $Fe_3O_4$, $TiO_2$ |
| Particle diameter (μm) | 150–300 | 150–300 |
| True density (kg/m$^3$) | 4100 | 4220 |
| Crushing strength (N) | 2.2 | 2.9 |
| Porosity (%) | 1.2 | 27.5 |
| BET surface (m$^2$/g) | 0.8 | 0.6 |

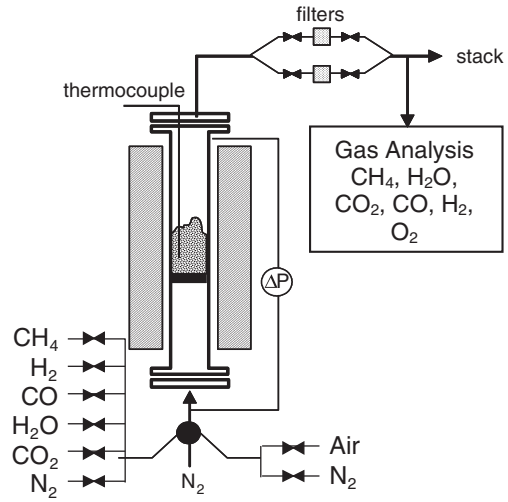


**Fig. 2.** Experimental setup used for multicycle tests in a fluidized-bed reactor.

The total solids hold-up in the reactor was 500 g of precalcined ilmenite. The oxygen-carrier was exposed to alternating reducing and oxidizing conditions at a temperature of 1173 K. The reducing conditions of each experiment are shown in Table 2. 20–23 redox cycles with $CH_4$, CO and $H_2$ as reducing agents were performed to see the reaction and activation process of ilmenite with the main gases involved in the CLC process with coal. The behavior of the oxygen-carrier upon different syngas mixtures was also assessed. Together with $H_2$ and CO, both $H_2O$ and $CO_2$ were introduced to accomplish the water–gas shift equilibrium at 1173 K. The reducing time in these tests was 240 s. A long 100 redox cycle test was performed with one of the syngas mixtures as reducing agent. All tests, except the $CH_4$ tests, accomplished that 50% of the inlet flow is a gaseous fuel mixture and the total inlet gas velocity was 0.30 m/s.

The reducing gas flows were chosen to have the same oxygen consumption. This condition was obtained by doubling the gas concentrations and fluidizing gas velocity for CO and $H_2$ in reference to what was used for $CH_4$. The flow for CO, $H_2$ and the syngas mixtures was 300 $L_N$/h, which was four times the flow of the introduced $CH_4$, 75 $L_N$/h. Considering a mean particle diameter of 212 μm, the minimum fluidization velocity for the calcined ilmenite particles at this temperature is 2.7 cm/s and the terminal velocity is 1.7 m/s. The gas velocities were 5 and 10 times the minimum fluidization velocity, respectively.

$H_2O$ or $CO_2$ were added to the reducing gases because in the continuous real process the fuel-reactor will be at a steam and $CO_2$ enriched atmosphere, and also to prevent carbon formation. The thermodynamic equilibriums indicate that with the gas mixtures of these experiments the ilmenite particles can get reduced further than $Fe_3O_4 + FeTiO_3$. $Fe_2TiO_5$ in ilmenite should be reduced to $FeTiO_3$ and $Fe_2O_3$ should be only reduced up to $Fe_3O_4$ to reach full conversion of the reducing gases [32].The reducing times are however short and ilmenite was not in any case converted further than the wanted species, i.e., no further reduction of $Fe_3O_4$ to FeO or Fe.

The subsequent oxidations were carried out with diluted air (10% $O_2$) to avoid a high temperature increase in the reactor because the heat released during the exothermic oxidation. The oxidation period lasted until full oxidation of the oxygen-carrier.

## 3. Data evaluation

The oxygen transport capacity of the ilmenite, $R_{OC}$, is defined as the mass fraction of oxygen that can be used in the oxygen transfer and calculated as $R_{OC} = (m_{ox} - m_{red})/m_{ox}$, where $m_{ox}$ and $m_{red}$ are

**Table 2**
Experimental conditions during reduction period in the batch fluidized-bed reactor for experiments 1 to 7. Nitrogen to balance. T = 1173 K.

| Exp | Composition (vol.%) | Gas velocity (m/s) | Reducing time (s) | Number of cycles | Solids inventory (kg/$MW_{th}$) |
|---|---|---|---|---|---|
| 1 | 25% $CH_4$ + 10% $H_2O$ | 0.15 | 300 | 23 | 670 |
| 2 | 50% CO + 20% $CO_2$ | 0.3 | 240 | 20 | 480 |
| 3 | 50% $H_2$ + 20% $H_2O$ | 0.3 | 180 | 20 | 560 |
| Exp | Composition (vol.%) | | $H_2O$:$CO_2$ | Number of cycles | Solids inventory (kg/$MW_{th}$) |
| 4 | 33% $H_2$ + 17% CO + 13.1% $H_2O$ + 5.2% $CO_2$ | | 66:34 | 1 | 260 |
| 5 | 21.5% $H_2$ + 28.5% CO + 8% $H_2O$ + 8.2% $CO_2$ | | 43:57 | 100 | 250 |
| 6 | 14.4% $H_2$ + 35.6% CO + 10.5% $H_2O$ + 20% $CO_2$ | | 28.8:71.2 | 1 | 250 |
| 7 | 5.3% $H_2$ + 44.7% CO + 3.2% $H_2O$ + 20.8% $CO_2$ | | 10.6:89.4 | 1 | 240 |

the mass of the most oxidized and reduced form of the oxygen-carrier, respectively. The oxygen transport capacity, for ilmenite is the oxygen transferred in its reduction from $Fe_2TiO_5 + Fe_2O_3$ to $FeTiO_3 + Fe_3O_4$, as later will be discussed.

From the gas product distribution, it is possible to know the rate of oxygen transferred, $r_0(t)$, from ilmenite to the fuel gas in case of the reduction reaction, and from the oxygen in the air to ilmenite in case of the oxidation reaction, as a function of reaction time using Eqs. (7) to (10):

$$\text{For } CH_4 : r_0(t) = \left(x_{CO} + 2x_{CO_2} + x_{H_2O}\right)_{out} \cdot F_{out} - \left(x_{H_2O}\right)_{in} \cdot F_{in} \quad (7)$$

$$\text{For CO} : r_0(t) = \left(x_{CO_2}\right)_{out} \cdot F_{out} - \left(x_{CO_2}\right)_{in} \cdot F_{in} \quad (8)$$

$$\text{For } H_2 : r_0(t) = \left(x_{H_2O}\right)_{out} \cdot F_{out} - \left(x_{H_2O}\right)_{in} \cdot F_{in} \quad (9)$$

$$\text{For } O_2 : r_0(t) = 2 \cdot \left(x_{O_2}\right)_{out} \cdot F_{out} - 2 \cdot \left(x_{O_2}\right)_{in} \cdot F_{in} \quad (10)$$

where $F_{in}$ and $F_{out}$ are the molar flows of the respectively inlet and outlet gas streams and $x_i$ the molar fraction of the gas i.

The mass based conversion of ilmenite in the fluidized-bed, $\omega$, indicates only the oxygen transfer and is independent of the oxygen transport capacity of the oxygen-carrier. It can be calculated for the reduction and oxidation reactions as:

$$\text{For reduction} : \omega(t) = 1 - \frac{M_O}{m_{ox}} \int_{t_{r,0}}^{t} r_0(t)dt \quad (11)$$

$$\text{For oxidation} : \omega(t) = \omega_{f,red} - \frac{M_O}{m_{ox}} \int_{t_{r,0}}^{t} r_0(t)dt \quad (12)$$

where $M_O$ is the molecular mass of oxygen, $t_{r,0}$ is the initial time when the considered reaction begins and $\omega_{f,red}$ is the final conversion of ilmenite reached in the previous reduction. The experimental rate of conversion, $(d\omega/dt)_{exp}$, is therefore obtained by means of Eq. (13):

$$\left(\frac{d\omega}{dt}\right)_{exp} = \frac{M_O}{m_{ox}} r_0(t). \quad (13)$$

For comparison purposes among different experiments, the oxygen yield parameter is proposed, which gives the idea to what extend the fuel has been oxidized at each instant of the reducing period. The oxygen yield, $\gamma_O$, is defined as the oxygen gained in the fuel for its oxidation divided by the oxygen needed to fully oxidize the fuel, according to Eq. (14):

$$\gamma_O(t) = \frac{r_0(t)}{\left(4x_{CH_4} + x_{CO} + x_{H_2}\right)_{in} \cdot F_{in}}. \quad (14)$$

A normalized rate index expressed in %/min was used in this study to evaluate the reaction rates of all the gaseous fuels tested with ilmenite before and after the activation period, and also as a comparison parameter that has been previously used with other oxygen-carriers for CLC. It is defined as follows [34]:

$$Rate\,index(\%/\min) = 60 \cdot 100 \left(\frac{d\omega}{dt}\right)_{norm}. \quad (15)$$

The normalized rate was calculated from the experimental rate considering that the order of reaction is 1 by the use of Eq. (16):

$$\left(\frac{d\omega}{dt}\right)_{norm} = \left(\frac{d\omega}{dt}\right)_{exp} \frac{P_{ref}}{P_m} \quad (16)$$

being $P_m$ the mean partial pressure of the gaseous fuel in the reactor, which is calculated with the coefficient of expansion of the gas mixture $\varepsilon_g$, and the partial pressures of the gaseous fuel at the reactor inlet and outlet, $P_{in}$ and $P_{out}$, respectively, see Eq. (17) [36]. $P_{ref}$ is a reference partial pressure that has been used in previous studies and it is 0.15 [34] and is here used to be able to compare ilmenite to other previously oxygen-carriers used.

$$P_m = \frac{\left(P_{in} - P_{out}\right) \Big/ \left(P_{in} + \varepsilon_g \cdot P_{out}\right)}{\frac{\left(P_{out} - P_{in}\right) \cdot \varepsilon_g}{\left(P_{in} + \varepsilon_g \cdot P_{out}\right)} + \left(1 + \varepsilon_g\right) \ln\left(\frac{P_{in} + \varepsilon_g \cdot P_{out}}{\left(1 + \varepsilon_g\right) P_{out}}\right)} \quad (17)$$

## 4. Results and discussion

### 4.1. Activation and reactivity with gaseous fuels: $CH_4$, CO and $H_2$

The experiments carried out in the fluidized-bed reactor allow the knowledge of the behavior of the ilmenite to oxidize $CH_4$, CO or $H_2$ during successive reduction–oxidation cycles. Fig. 3 shows the $CO_2$ concentration in dry basis or $H_2O$ concentration during consecutive reduction periods for experiments 1, 2 and 3, that is, tests using $CH_4$, CO and $H_2$ as reducing gases, respectively. The experimental conditions are gathered in Table 2. The corresponding maximum $CO_2$ or $H_2O$ fractions if full combustion was reached are also represented. It can be seen that, for every tested reducing gas, there is an increase in the percentage of $CO_2$ and/or $H_2O$ in the product gas with the cycles because ilmenite has a gradual gain in its reaction rate. After several redox cycles, ilmenite reactivity stabilizes and the $CO_2$ and/or $H_2O$ concentrations achieve the highest values. After that, the outlet gas profiles could be considered rather the same from cycle to cycle and thus no further substantial activation of ilmenite was taking place. Therefore, there is a progressive activation process with the redox cycle number. It is noticeable the strong increase of the ilmenite reactivity with $CH_4$. These results are similar than those showed by Leion et al. during redox cycles of ilmenite in a fluidized-bed using $CH_4$ and 50% $H_2$ + 50% CO as reducing gases [29]. This was also observed by Abad et al.

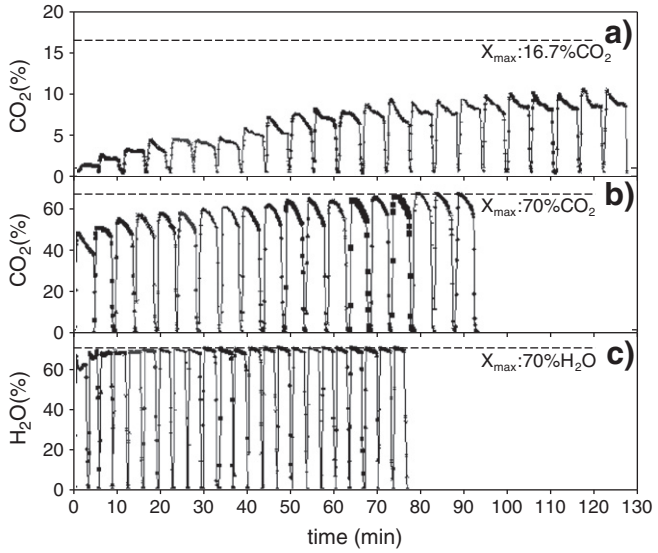


**Fig. 3.** Profiles of $CO_2$ or $H_2O$ fractions in the product gas (wet basis) during consecutive reduction periods, for a) $CH_4$, b) CO and c) $H_2$ as reducing gases. The intervals between reducing periods have been removed. $X_{max}$ is the maximum $CO_2$ or $H_2O$ corresponding fraction if full combustion was reached. Experimental conditions are shown in Table 2. T = 1173 K.

[36], for which reaction rate of ilmenite with $CH_4$ rises about 15 times after several redox cycles and activating.

An increase of the generated $H_2O$ can be also seen when using $H_2$ as reducing agent (see Fig. 3c), but the activation of ilmenite can be slightly seen, since it oxidizes almost all the fuel fed in the reactor. Thus, the reaction rate of ilmenite in the bed was limited by the $H_2$ supply.

The product gas distribution of the gases at the reactor exit was obtained to evaluate the performance of ilmenite on the conversion of $CH_4$, $H_2$ and CO, and its evolution with the cycle number.

As an example, Fig. 4 shows the outlet product gas distribution for the 20th cycle for experiment 1 using $CH_4$ as reducing agent. $CO_2$ and $H_2O$ were formed just immediately after the introduction of the reducing gas to the reactor, but full conversion of the reducing gas was not obtained. The ilmenite mass based conversion, $\omega$, as a function of the reaction time is also displayed. The unconverted fuel gas increased as the conversion increased, because the rate of oxygen transference decreased as there was continuous oxygen depletion in ilmenite. For $CH_4$ combustion is noticeable that most of unconverted gas is the selfsame $CH_4$ and almost no CO or $H_2$ were observed. This fact suggests that the reforming reaction of $CH_4$ with $H_2O$ or $CO_2$ has low relevance in this system using ilmenite as oxygen-carrier. Furthermore, in previous studies with Fe-based oxygen-carriers, the majority of $CH_4$

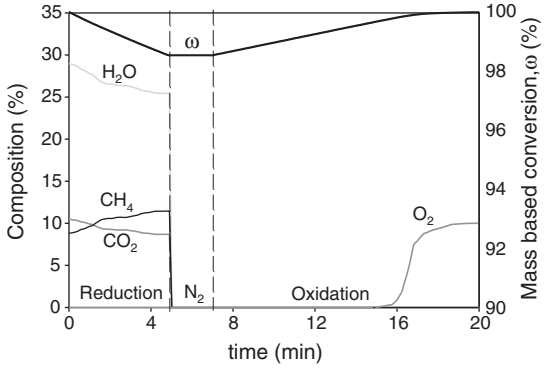


**Fig. 4.** Product gas distribution in wet basis during reduction with $CH_4$ and subsequent oxidation for the 20th cycle. Reducing gas: 25% $CH_4$ + 20% $H_2O$. T = 1173 K. $N_2$ to balance. Oxidation: 10% $O_2$.

converted goes to $CO_2$ and $H_2O$, but CO and $H_2$ also appear in variable amounts [20,31]. Thus, it can be assumed that reaction of $CH_4$ takes place with $H_2$ and CO as intermediate products. However in this case there was no $H_2$ or CO at the outlet because the possible generated $H_2$ and CO react faster with ilmenite than $CH_4$ and they were therefore consumed. The appearance of unconverted gases during the experimental tests did not mean that fuel gas could not be fully converted to $CO_2$ and $H_2O$ using ilmenite as oxygen-carrier, but a higher amount of ilmenite in the fluidized-bed reactor would be needed to fully convert the fuel gas at the experimental conditions, i.e. temperature and gas velocity. However, experiments with incomplete fuel conversion are required to analyze the reactivity of an oxygen-carrier in fluidized-bed experiments, so that the gas conversion is not limited by the fuel gas supply.

After reduction, ilmenite was regenerated by oxidation with diluted air until full oxidation of ilmenite was reached. During most of ilmenite oxidation period, the $O_2$ outlet concentration was zero because the oxygen was consumed by the oxidation reaction. Thus, ilmenite oxidation was limited by the supply of $O_2$ to the reactor. At the end of the oxidation period, the oxygen concentration rapidly increased until the inlet concentration.

Similar gas profiles were found with all redox cycles, except for differences on the fuel gas conversion with the cycle number. With CO as reducing agent, relevant amount of unreacted CO was found during the reducing periods. Ilmenite reacted faster with CO than with $CH_4$, but not as fast as with $H_2$. The conversion after 4 min of the 20th reducing period was 0.982. That conversion meant that the oxygen-carrier was partially reduced, as the corresponding value for completely reduced ilmenite to $FeTiO_3 + Fe_3O_4$ was lower: it was 0.965. XRD of completely reduced samples confirmed that the final species were $FeTiO_3$, $Fe_2TiO_4$ and $Fe_3O_4$.

The reactivity of the oxygen-carrier can be seen by means of the oxygen yield, $\gamma_O$. It shows the percentage of the fuel that has been oxidized at each instant of the reducing period. Thus, Fig. 5 represents the oxygen yield vs. ilmenite mass based conversion for selected cycles during the activating period using $CH_4$, CO and $H_2$ as reducing agents. As expected, the oxygen yield and the ilmenite mass based conversion reached in every cycle increases with the first number of cycles, as there is reactivity rise, and when ilmenite is active, $\gamma_O$ stabilized in a maximum value. It can be seen, in the $CO_2$ and $H_2O$ profiles as well as in the oxygen yield, that ilmenite undergoes an activation process.

The decrease seen in the oxygen yield for higher ilmenite conversions is due to its gradual oxygen depletion. The oxygen yield at the beginning of the first cycle was 10% and rose up to 56% in the twentieth cycle for $CH_4$ as reducing agent. $\gamma_O$ for CO is lower than for $H_2$ because of the lower reactivity of ilmenite with CO, but it was higher than for $CH_4$, and reached values of 78%.

When using $H_2$ as reducing agent, a very low amount of unconverted $H_2$ was observed throughout the reducing period. Only for the first 3–4 cycles before the activation of the oxygen-carrier, the reaction was limited by the $H_2$ flow introduced in the system from the beginning of the reducing period. For later cycles ilmenite oxidizes almost all the $H_2$ at the beginning of the reductions, and further activation of ilmenite could not be seen, if happened. $\gamma_O$ was as high as 98% at the beginning of the reducing period when ilmenite was activated. Ilmenite is very reactive with this gas, as it has already been proven in several studies. The conversion at the end of the reducing cycle was higher than with methane even after only 3 minute reduction and went up to $\omega = 0.98$.

When using $CH_4$ it activated after about 20 cycles and for CO it was faster, as it took about 10 cycles. This is in accordance with previous work carried out by Adánez et al. [32], which found that the activation of ilmenite particles is a relatively fast process, and that the number of cycles needed to reach a roughly constant reactivity during TGA experiments did not depend on the reducing gas used, but on the conversion of the oxygen-carrier reached in each reducing cycle.

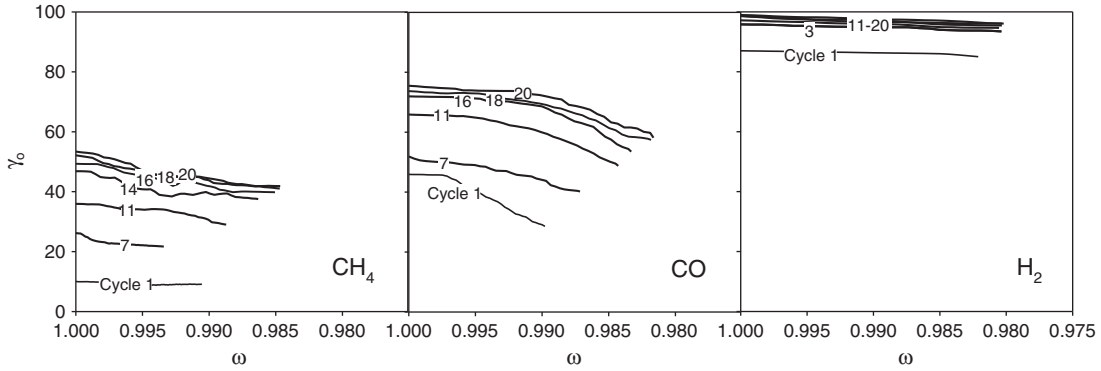


**Fig. 5.** Oxygen yield, $\gamma_O$, as a function of the ilmenite mass based conversion, $\omega$, for the reduction period after 20 redox cycles for reduction with $CH_4$ (reducing gas: 25% $CH_4$ + 20% $H_2O$), CO (reducing gas: 50% CO + 20% $CO_2$) and $H_2$ (reducing gas: 50% $H_2$ + 20% $H_2O$). T = 1173 K.

Ilmenite had a faster activation with CO because ilmenite was further converted in every reduction.

The reduction reactivity of ilmenite during consecutive redox periods was assessed. The representation of the normalized rate index of ilmenite reaction before and after the activation process and for the gases tested (see Fig. 6) showed that the reaction rate of ilmenite increased after activation. In case of $CH_4$ the increase in the reaction rate is greater than with the other gaseous fuels, as the rate index raised here in batch fluidized-bed 5 times after activation. The increase in the rate index for CO and for $H_2$ was lower as shown by previous studies and it was about 2 times. In the rate index showed not only the oxygen-carrier reactivity is included, but it is also influenced by diffusional limitations in the fluidized bed. The intrinsic kinetics of ilmenite was evaluated in TGA in a previous work [35]. These data obtained in fluidized bed reactor can be easier comparable to data obtained for other oxygen-carriers in similar experiments. For example, other iron-based oxygen-carriers previously tested in batch fluidized-bed by Johansson et al. [34] had normalized rate index values with $CH_4$ within the range of 0.4 to 4%/min. This oxygen-carrier had a rate index slightly lower than 0.4%/min with $CH_4$, that is, in the lower range of other synthetic Fe-based oxygen-carriers. Nevertheless, the rate index for $H_2$ was calculated to be above 1.1%/min at the start of the reduction period, which is adequate for the use in CLC with solid fuels [33].

### 4.2. Reactivity with syngas

Batch experiments were also performed using syngas as fuel, since it is actually the coal gasification product, primarily composed by $H_2$ and CO. Thus, in CLC with solid fuels syngas is the main gaseous fuel that reacts with the oxygen-carrier, when coal is previously externally gasified and the product gas is later introduced into the CLC system. A mixture CO + $H_2$ is also the main reacting gas flow when coal is directly introduced in the fuel-reactor and is in situ-gasified.

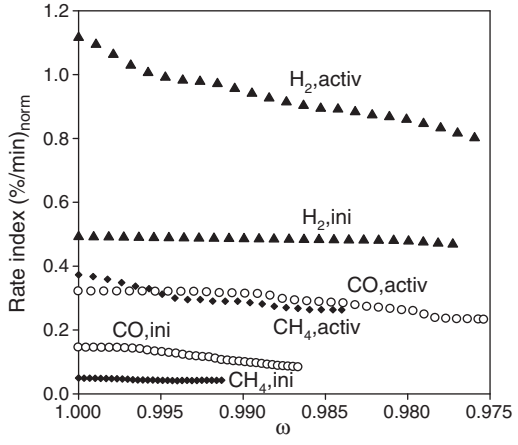


**Fig. 6.** Normalized rate index as a function of the ilmenite mass based conversion, $\omega$, for the reduction reactions with $CH_4$, CO and $H_2$ with calcined and activated ilmenite. $P_{ref}$ = 0.15. T = 1173 K.

100 redox cycles with syngas of composition 21.5% $H_2$ + 28.5% CO + 8% $H_2O$ + 8.2% $CO_2$ were performed. Very little $H_2$ in the outlet gas was seen at the beginning of the reducing cycles: about 1–2%. Likewise, the CO content was about 2.4%. Fig. 7a represents the $CO_2$ concentration profiles obtained and Fig. 7b shows the variation of the oxygen yield with the solids conversion for various reducing periods from the 100 redox cycles.

When focusing only in the first 1.5 min of each reducing period, it can be seen that the $CO_2$ and the oxygen yield increase within the first 10 cycles approximately and reach a maximum value, which is due to the activation of ilmenite. This maximum value is maintained throughout the cycles, which indicates that ilmenite maintains its reaction rate and does not deactivate. This corresponded to a $\omega$ of about 0.99. Besides, the oxygen yield obtained was as high as 98%.

On the other hand, after about 1.5 min and $\omega$ further than 0.99, there was a decrease in the produced $CO_2$ and in the oxygen yield. This was not due to a deactivation of ilmenite, but to a decrease in the oxygen transport capacity. In previous work, Adánez et al. [32] found that the $Fe_2TiO_5$ present in the ilmenite undergoes a physical segregation with the number of cycles and separated $Fe_2O_3$ and $TiO_2$ are formed, which reduce the oxygen transport capacity, $R_{OC}$, of ilmenite. This fact will be deeply discussed later. Fig. 7b shows that the oxygen yield reached after many cycles was close to the corresponding $\gamma_O$ for the $Fe_3O_4 \leftrightarrow FeO$ equilibrium.

#### 4.2.1. Various syngas ratios

Additional redox cycles with different $H_2$:CO ratios were also done with the same activated ilmenite after the 100 cycles with syngas. Different $H_2$:CO ratios from 100:0 to 0:100 have been tested. As well as in the previous tests with syngas, $H_2O$ and $CO_2$ were introduced to accomplish the water–gas shift equilibrium at 1173 K for every mixture.

In Fig. 8a the variation along the reducing cycle of the calculated normalized rate index for $H_2$, CO and the syngas mixtures as a function of ilmenite mass based conversion are shown. It can be seen that the reaction rate was higher for the experiments carried out with $H_2$ and the lower values were obtained when using only CO. A dotted line is drawn at $\omega$ of 0.99 because it was previously seen that until that conversion the reaction rate and oxygen yield were maintained constant and had maximum values that decreased when ilmenite was further converted.

Fig. 8b represents the average rate index as a function of the fraction of $H_2$ in the reducing agent, together with a dotted line, which is a theoretical rate index calculated as sum of the rate index of $H_2$ and CO multiplied per their corresponding fractions. It can be seen that

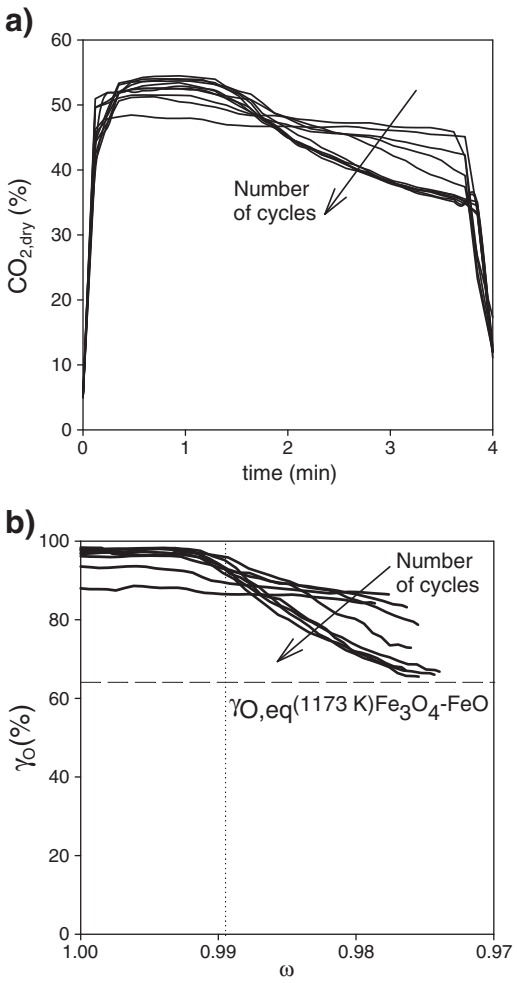


**Fig. 7.** a) $CO_{2\ dry\ basis}$ profiles in the product gas for various reduction periods and b) oxygen yield, $\gamma_o$, variation with the ilmenite mass based conversion for the reduction periods 3, 10, 20, 40, 50, 70, 85, and 100 for a 100 redox cycle test using syngas as reducing agent. Reducing gas: 21.5% $H_2$ + 28.5% CO + 8% $H_2O$ + 8.2% $CO_2$. T = 1173 K.

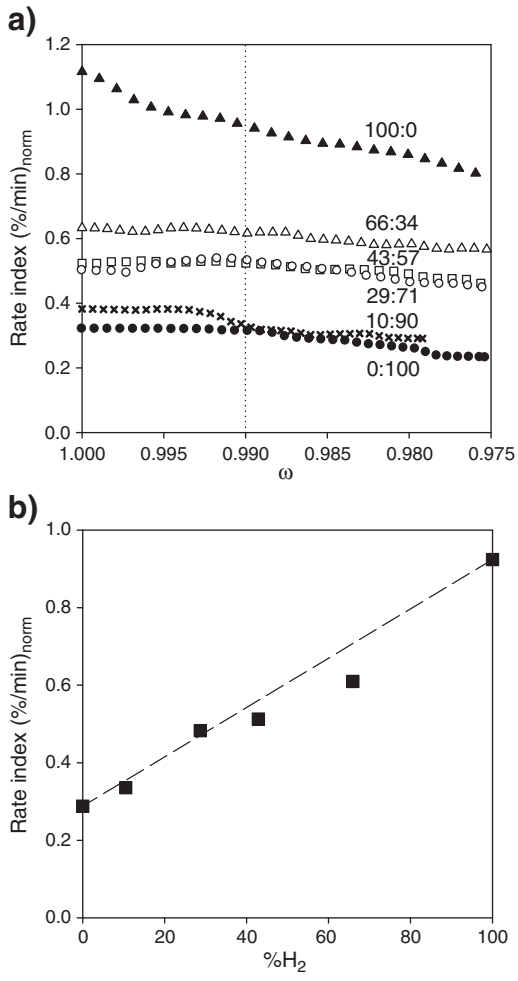


**Fig. 8.** a) Normalized rate index variation along the reducing cycle as a function of ilmenite mass based conversion and b) average normalized rate index as function of the fraction of $H_2$ in the reducing gas for different $H_2$:CO mixtures tested (see conditions in Table 2). T = 1173 K.

the resulting reaction rates for all syngas mixtures tested matches with the theoretical line. It can be thereby concluded that the reaction rate for a syngas mixture can be actually calculated as the sum of both reducing agents reaction rates.

### 4.3. Reactivity in oxidation

Ilmenite had undergone an activation process for the reduction reaction after a low number of cycles and depending on the conversion variation reached in each cycle. The oxidation reaction is a two step reaction [35]: the first step is controlled by chemical reaction and the second is controlled by the diffusion. The first step of the reaction was also fast activated after a low number of redox cycles. Fig. 9 represents the $O_2$ profiles obtained during the first oxidation periods in the above mentioned 100 redox cycle test performed in the batch fluidized-bed. The oxidation gas is diluted air in $N_2$ with 10% $O_2$. At the beginning of the oxidation period no oxygen could be seen in the produced gas, since it reacted with ilmenite, re-oxidizing it. After this period, the breakthrough curve of oxygen appeared, which is different depending on the reactivity of the bed material [37]. The profiles show that the slope increased significantly with the number of cycles, which was due to the activation process and increase in the reaction rate that was later proven with TGA analysis. The activation took about 8 cycles.

Fig. 10 shows the $O_2$ profiles for the oxidation periods, from cycles 20 to 100. The slope rose slightly with the number of cycles and it took longer for oxygen to appear. The second step of reaction, controlled by diffusion, appeared later for higher oxidizing conversions. This was because of the increase in the porosity of the oxygen-carrier. When ilmenite was completely activated for the oxidation reaction, the diffusion did not control the reaction anymore.

It could be also observed that if the surface under the $O_2$ curve was integrated, the oxygen amount taken by ilmenite with the number of cycles was slight but gradually decreasing. That is because the ilmenite was in the previous reducing period less reduced, as the oxygen transfer capacity was gradually decreasing, as will be later discussed.

### 4.4. Physical and chemical changes in ilmenite particles throughout the redox cycles

The major change with respect to the initial ilmenite was that porosity increased substantially with the redox cycles. For the 100 cycle test using syngas as reducing agent, the initial porosity of calcined ilmenite was measured to be 1.2%, after 8 cycles it increased to 12.5%, after 20 cycles it was 27.5% and after 100 cycles it reached the value of 38%.

Final BET measurements for activated ilmenite: with $CH_4$, after 23 cycles: 0.4 $m^2/g$; with CO, after 20 cycles: 0.6 $m^2/g$, and with CO + $H_2$ mixture: 0.4 $m^2/g$. The initial calcined ilmenite had a BET surface of 0.8 $m^2/g$. The BET surface in ilmenite in all cases and thus the

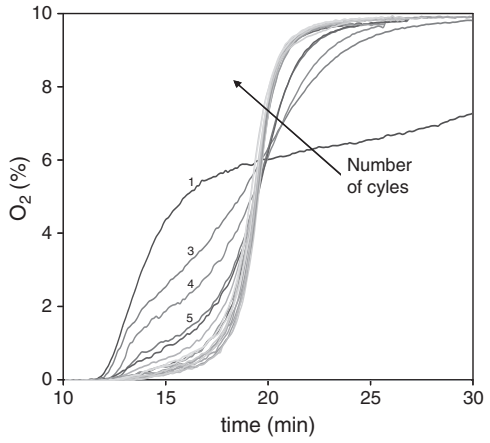


**Fig. 9.** $O_2$ profiles in the product gas for the first subsequent 20 oxidation periods in a 100 redox cycle test. Previous reducing period of 4 min (reducing gas: 21.5% $H_2$ + 28.5% CO + 8% $H_2O$ + 8.2% $CO_2$) and purge with $N_2$ of 2 min. Oxidation with 10% $O_2$ and gas velocity: 23 cm/s. T = 1173 K. The initial solid mass based conversion of the partially reduced ilmenite was about 0.975.

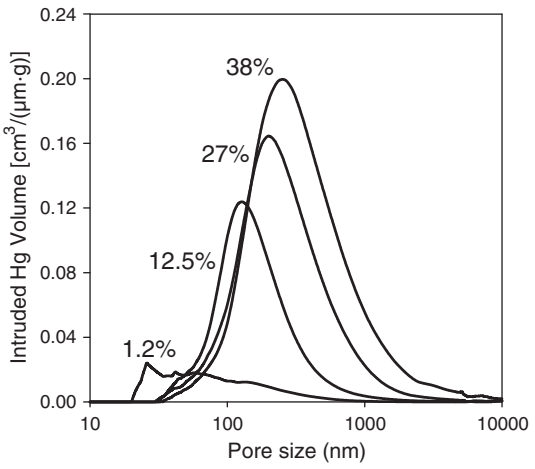


**Fig. 11.** Pore distribution of different samples of ilmenite: calcined with porosity of 1.2%, after 8 cycles, with porosity of 12.5%, after 18 cycles with porosity of 27% and after 100 cycles with porosity of 38%. Ilmenite samples taken after several redox cycles in batch fluidized bed. Reductions with syngas as fuel (see conditions in Table 2). T = 1173 K.

microporosity is negligible in this material. Macropores are considered to be bigger than 50 nm and the pore distribution shown in Fig. 11 confirms that the minimum pore size is about 30 nm, but as porosity increases, the pore distribution locates in higher pore diameters and the average pore diameter gradually increases with the number of cycles and higher pores are formed. In order to explain this gradual increase in porosity, a morphological characterization of samples taken from the 100 redox cycle experiment was done by SEM.

Fig. 12 shows SEM microphotographs that confirm the low pore development for calcined ilmenite. The final porosity after 100 redox cycles was 38%. Throughout the reduction–oxidation cycles, there is continuous appearance of cracks, which generate the mentioned rise in porosity. Moreover, a gradual generation of an external layer slightly separated from the rest of the particle which grows with the number of cycles could be clearly observed. This space between the layer and the core also enhances the porosity measured for the particle.

EDX analyses were done to determine Fe and Ti distributions throughout the particles. In calcined ilmenite both distributions were uniform, what agrees with the XRD analysis that reveals $Fe_2TiO_5$ as main component. However with the number of cycles $Fe_2TiO_5$ has been seen to undergo a physical segregation and the particle core gets titanium enriched, whereas the external part gets iron enriched. XRD analyses to the external layer found that this region is composed only by iron oxide, whereas XRD to the internal core revealed the existence of $TiO_2$ and $Fe_2TiO_5$. After each cycle there is more free $TiO_2$ in the core and iron oxide in the external shell, together with a decrease of iron titanates. That means that there is a migration phenomenon of iron oxide towards the external part of the particle, where there is not $TiO_2$ to form iron titanates. Since the active phase for a CLC application is the iron oxide, the fact that iron oxide is at the outer part of the solid facilitates the reaction.

Initial and activated ilmenite after 20 cycles particles have relatively high values of crushing strength, it varied from 2.2 N to 2.9 N. These values for the crushing strength would be acceptable for the use of these particles in circulating fluidized-bed [34]. Crushing strength measures were made for fully oxidized as well as fully reduced samples of ilmenite activated with CO. Both samples have a similar value for crushing strength around 2.9. However, particles after 50 and 100 cycles show a decreased crushing strength down to a value of 1 N after 100 cycles (Fig. 13). 1 N is a border value for the use of a material in fluidized-bed. Nevertheless, as it was previously stated, since there is formation of an external layer, the normal strength under which the particles are subjected could break this layer and not the whole particle.

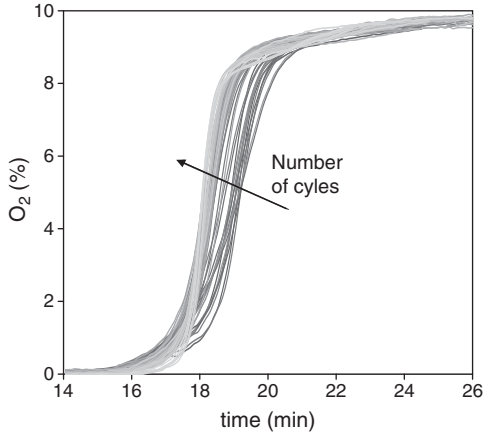


**Fig. 10.** $O_2$ profile evolution in the product gas for the oxidation period from cycle 20 to cycle 100. Previous reducing period of 4 min (reducing gas: 21.5% $H_2$ + 28.5% CO + 8% $H_2O$ + 8.2% $CO_2$) and purge with $N_2$ of 2 min. Oxidation with 10% $O_2$ and gas velocity: 23 cm/s. T = 1173 K. The initial conversion $\omega$ of the partially reduced ilmenite was about 0.975.

*4.4.1. Maximum oxygen yields and oxygen transport capacity, $R_{OC}$*

Several thermodynamic calculations were carried out to evaluate the maximum oxygen yield, $\gamma_O$, at equilibrium conditions. Ilmenite needs special attention due to their composition and the final oxidation states during reduction reaction to reach full conversion of fuel gases towards $H_2O$ and $CO_2$. In the fully oxidized ilmenite, the iron was found to be as $Fe^{III}$, either in the $Fe_2TiO_5$ compound or as free $Fe_2O_3$. Both compounds have different thermodynamic properties for the reduction reaction. $Fe^{III}$ in $Fe_2TiO_5$ can be reduced to $Fe^{II}$ in $FeTiO_3$ via the compound $Fe_3Ti_3O_{10}$ [29], which corresponds to $Fe_3O_4 \cdot 3TiO_2$. Table 3 shows the maximum oxygen yields at equilibrium conditions for every step in the reduction reaction mechanism. Thermodynamic calculations show that by reducing $Fe_2TiO_5$ with $CH_4$, $H_2$ or CO it is possible to reach very near full combustion of fuel gas into $H_2O$ and $CO_2$ when it is reduced into $Fe_3O_4 \cdot 3TiO_2$ and $FeTiO_3$, i.e. $\gamma_O$ can be considered 1 for practical purposes. Further reduction to $Fe^0$ is prevented in a CLC system to avoid low fuel gas conversion. However, the reduction of free $Fe_2O_3$ must be limited to $Fe_3O_4$ because further reduction to FeO or Fe would produce low values of oxygen yield, $\gamma_O$, and therefore, a high increase in the equilibrium concentrations of $H_2$ and CO exiting

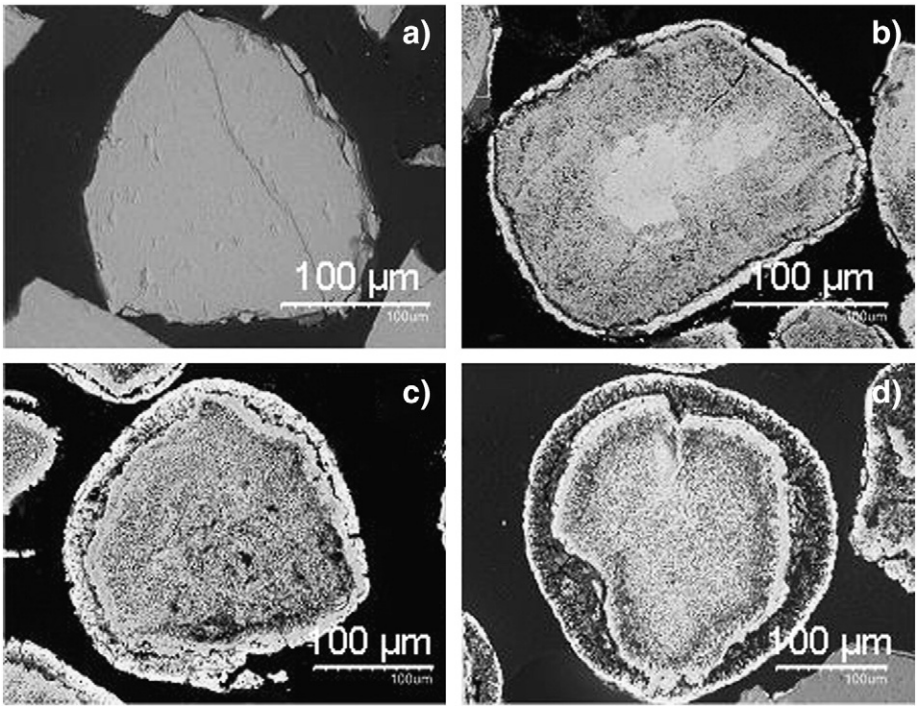


**Fig. 12.** SEM-EDX images of cross-cut ilmenite particles a) calcined and after b) 16, c) 50 and d) 100 redox cycles.

from the fuel-reactor. Therefore, $Fe^{III}$ should be reduced as maximum to a mixture of $FeTiO_3$ and $Fe_3O_4$ in order to get full fuel gas combustion in a CLC system. This condition corresponds to a value for $R_{OC}$ of 4.0% for calcined ilmenite. That means, if more oxygen was transferred and therefore further conversion than $\omega = 0.96$ was reached for that sample, significant amounts of $Fe^{II}$ as FeO would be formed.

Adánez et al. [32] saw that ilmenite undergoes a segregation process with the redox cycles that generates more free $Fe_2O_3$ and less $Fe_2TiO_5$. As the oxygen transport capacity for free $Fe_2O_3$ is lower ($R_{o,Fe2O3} = 3.3\%$) than the oxygen transport capacity for $Fe_2O_3$ as iron titanate ($R_{o,Fe2TiO5} = 6.7\%$), the gradual separation of $Fe_2O_3$ from $TiO_2$ causes a slight and gradual decrease of the oxygen transport capacity of ilmenite with the cycle number.

This decrease in $R_{OC}$ could be clearly seen in the 100 cycle test. Fig. 14 is a representation of the $R_{OC}$ measured by TGA of several samples after different number of cycles. The mass variations of the samples were measured when reducing them with $5\%H_2 + 40\%H_2O$. In these conditions it is ensured that the final reduced species are $FeTiO_3 + Fe_3O_4$. XRD analyses of the samples were also done and semi-quantitative analyses measured the free $Fe_2O_3$ and $Fe_2TiO_5$ content in the samples. The here called "theoretical $R_{OC}$" is defined as the oxygen transport capacity that would have the ilmenite sample if the measured free $Fe_2O_3$ got reduced to $Fe_3O_4$ and the $Fe_2TiO_5$ got reduced to $FeTiO_3$. Fig. 14 also includes the calculated values of $R_{OC\ theo}$, which are in concordance with the measured $R_{OC}$. The oxygen transfer capacity, $R_{OC}$, decreased with the number of cycles. The initial $R_{OC}$ is 4.0% and after 100 redox cycles it was measured to be 2.1%. The main consequence of ilmenite being more reactive with the number of cycles is that with the time fewer inventories are necessary. On the other hand, the decrease in $R_{OC}$ causes the need of higher solid circulating flows between reactors.

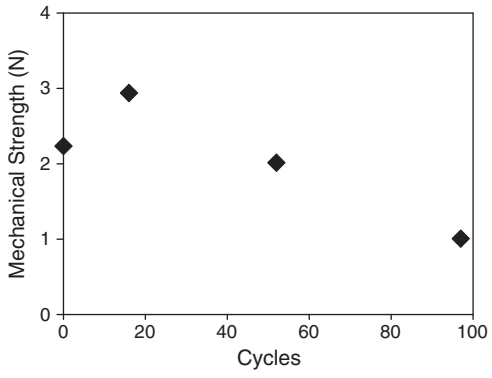


**Fig. 13.** Mechanical strength evolution with the number of cycles.

However, the decrease in the oxygen transport capacity is not influenced by the reducing agent used, but it depends on the extent of conversion reached in every cycle [32]. Table 4 shows the measured oxygen transport capacity after 20 cycles for the experiments with the gaseous fuels tested, i.e., $CH_4$, CO and $H_2$, as well as the average conversion $\omega$ reached after every reducing cycle. In all cases ilmenite had undergone the activation period.

If a simplified linear regression is established, the $R_{OC}$ in the 20th cycle could be calculated as $R_{OC}(20th) = (37.5 \cdot \omega - 36.017) \cdot R_{OC,ini}$, being $R_{OC,ini}$ the initial oxygen transport capacity, which for this ilmenite was 4.0%.

The effect of ilmenite activation on the performance of a CLC system was already investigated by Adánez et al. [32] because there is a trade-off between the increase in reactivity and the decrease in the oxygen transport capacity. However, the $R_{OC}$ values showed for initial, activated ilmenite and after a high number of redox cycles are high enough values to transfer the required oxygen from air to fuel in a CLC system [36].

**Table 3**
Maximum oxygen yields at equilibrium conditions for different reducing gases in presence of $Fe_2TiO_5$ and $Fe_2O_3$ at 1173 K.

| | | Oxygen yield ($\gamma_O$); | | |
|---|---|---|---|---|
| Oxidized | Reduced | $CH_4$ | CO | $H_2$ |
| $Fe_2TiO_5$ | $FeO \cdot TiO_2$ | 0.9984 | 0.9975 | 0.9981 |
| $FeO \cdot TiO_2$ | $Fe + TiO_2$ | 0.3083 | 0.0849 | 0.0666 |
| $Fe_2O_3$ | $Fe_3O_4$ | 1 | 1 | 1 |
| $Fe_3O_4$ | $Fe_{0.947}O$ | 0.7411 | 0.6146 | 0.6748 |
| $Fe_{0.947}O$ | Fe | 0.5235 | 0.3246 | 0.3848 |

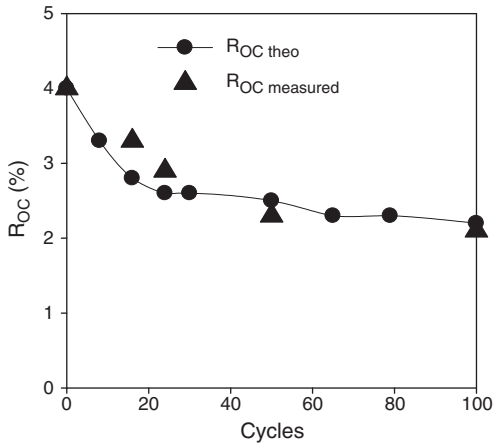


**Fig. 14.** Measured and theoretical $R_{OC}$. $R_{OC}$ variation with the number of cycles reduction periods 3, 10, 20, 40, 50, 70, 85, and 100 in a 100 redox cycle test using $H_2 + CO$ syngas as reducing agent. Reducing gas: 21.5% $H_2$ + 28.5% CO + 8% $H_2O$ + 8.2% $CO_2$. T = 1173 K.

Furthermore, the performance in continuous testing showed that the oxygen transport capacity of ilmenite decreased very little, because the extent of conversion reached in the fuel-reactor was not high [27].

### 4.5. Carbon formation and fluidizing behavior

#### 4.5.1. Carbon formation

The deposition of carbon from carbon containing gases is a concern because it can deactivate the oxygen-carrier or diminish its oxygen transfer. It can also cause defluidization problems. Besides, if carbon is formed, it can be further directed to the air-reactor where it will be burnt, being therewith the carbon capture efficiency decreased. Carbon formations in CLC processes have been already seen and studied with different oxygen-carriers [38,39]. There are two possible ways of carbon formation: through methane decomposition or through Boudouard reaction. The conditions for which carbon formation is thermodynamically possible in the CLC process depend on the amount of oxygen added with the oxygen-carrier as well as the temperature and pressure.

If there was carbon formation when using carbon-containing fuel gases, i.e. $CH_4$ and CO, there would be some CO or $CO_2$ release during the oxidizing periods due to the oxidation of the carbon. However, no CO and $CO_2$ were observed any time during inert or oxidation periods, indicating that there was not accumulation of carbon during reduction periods in any of the experiments carried out.

#### 4.5.2. Particle integrity and attrition

The attrition rate of the carriers is an important parameter to be accounted as a criterion for using a specific oxygen-carrier in a fluidized-bed reactor. High attrition rates will decrease the lifetime of the particles increasing the reposition of the oxygen-carrier in the CLC system. Particles elutriated from the fluidized-bed reactor were retained in a filter, and were taken every 10 cycles. The loss of fines was considered as the particles with a diameter under 40 μm, because they are the particles that could only be recovered in cyclones with separation efficiency higher than 99% [40]. Ilmenite showed low attrition rates. 100 redox cycles were done in 56 h of performance in fluidizing conditions. Fig. 15 shows the fine attrition rate (particle size below 40 μm) as a function of fluidization time. The initial value of attrition at the beginning is due to the rounding off of angular initial ilmenite particles. With the number of cycles, an external layer was seen to be formed, as it can be seen in Fig. 12, and that this layer is mainly composed by iron oxides. After 40 h of operation the attrition rate stabilized to a value of 0.076%/h. Furthermore, XRD analysis of fines showed that they are formed only by iron oxide, and titanium oxide or iron titanates were not observed. This fact suggests that fines are produced by an attrition process in the particle surface, and not by the breakage of particles. There is particle rounding and detachment of part of the external layer, but no particle fragmentation.

**Table 4**
Measured oxygen transport capacity after 20 cycles and corresponding average conversion $\omega$ reached after the reducing cycles for the tests with $CH_4$, CO and $H_2$ as reducing agents.

| Reducing agent | $R_{OC}$ (%) | $\omega$ |
|---|---|---|
| $CH_4$ | 3.5 | 0.984 |
| CO | 3.3 | 0.982 |
| $H_2$ | 2.9 | 0.98 |

#### 4.5.3. Defluidization

The behavior of ilmenite with respect to particle agglomeration in the fluidized-bed has been also analyzed in this work. Particle agglomeration must be avoided because it can lead to bed defluidization that causes solids circulation disturbances and channeling of the gas stream through the bed, which turns the contact between gas and particles less efficient. During the experimental tests, defluidization problems were never observed. Moreover, particles extracted from the fluidized-bed at the end of the tests did not show agglomeration evidences. However, the extent of reduction during the experiments was limited to $\omega = 0.98$. To check if agglomeration problems could appear at higher conversion levels, ilmenite was reduced during longer periods. The particles used were the just activated with $H_2$ from experiment 3. Reduction time was gradually increased in successive redox cycles. Defluidization appeared during the oxidation period and when the mass based conversion was about 0.97. For such conversions some free $Fe_2O_3$ would get reduced up to FeO, regarding the thermodynamics. The appearance of defluidization problems by oxidation of FeO was previously found by Cho et al. [38] for iron-based oxygen-carriers supported on alumina. This also agrees with the fact found by Leion et al. [29] that ilmenite presents an agglomeration risk at high conversions. However, FeO formation in a CLC system should be avoided because thermodynamic limitations. Furthermore, Abad et al. [36] concluded that for the optimization of the CLC process it is necessary to get to a compromise between the solids circulation and the solids inventory. The optimum values of the conversion variation in the fuel-reactor to get low circulation rates and low solids inventory could be about 0.2–0.4 because higher values highly increase the solid inventories. Therefore, agglomeration of ilmenite particles is not expected at these conditions if ilmenite reaches a high oxidation degree in the air-reactor.

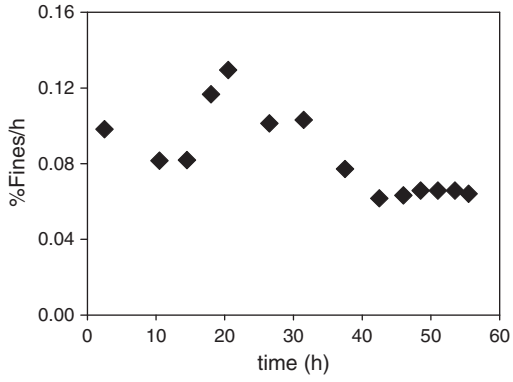


**Fig. 15.** Fine attrition rate (particle size below 40 μm) as a function of fluidization time.

## 5. Conclusions

The activation process of ilmenite through consecutives redox cycles in a fluidized-bed reactor has been analyzed. $CH_4$, $H_2$ or CO was used as reducing gases. Ilmenite increased its reactivity with the number of cycles, especially for $CH_4$. Ilmenite activation process depended on the reduction conversion reached in every cycle, being faster activated when the conversion was higher. Reaction with $H_2$ is faster than with CO, and near full $H_2$ conversion was obtained in the fluidized-bed reactor. Lower reactivity was found for $CH_4$, being $CH_4$ the most unconverted gas. In this case, negligible amounts of $H_2$ or CO were observed, indicating that $CH_4$ reforming reaction has low relevance in this system.

For all gaseous fuels tested the reaction rate was maximum and constant at the beginning of the reducing period until an ilmenite mass conversion of about 0.99 and that this value did not decrease for a high number of redox cycles, i.e., 100 cycles. For a conversion further than 0.99, there was a decrease in the oxygen yield that was not due to a deactivation of ilmenite, but to a decrease in the oxygen transport capacity with the redox cycles. The oxygen yield reached after many cycles was close to the corresponding for the $Fe_3O_4 \leftrightarrow FeO$ equilibrium.

For mixtures with different $H_2$:CO ratios it was seen that reaction rate for a syngas mixture can be calculated as the sum of both reducing agents reaction rates.

The oxidation reaction was also studied. For a conversion of 0.975 in the previous reduction periods, the activation in the oxidation reaction took about 8 cycles. The second step of reaction, controlled by diffusion, appeared later and for higher oxidizing conversions for higher number of cycles and when ilmenite was completely activated for the oxidation reaction, the diffusion did not control the reaction anymore. This was because of the increase in the porosity of the oxygen-carrier. The oxidation reaction was fast and fully oxidized ilmenite was reached in every cycle. With the number of cycles the oxygen amount taken by ilmenite was slight but gradually decreasing because of the decrease in the oxygen transfer capacity.

Structural changes on the ilmenite particles after activation were observed. Initial ilmenite particles had low porosity of 1.2% and the porosity of the particles after 100 cycles increased up to 38%. The appearance of an external shell in the particle was observed, which is Fe enriched. As activation proceeds the reactivity increased, but the oxygen transport capacity decreased due to the appearance of free $Fe_2O_3$ in the external shell. Thus, the initial $R_{OC}$ value is 4.0% and it decreased until 2.1% after 100 redox cycles. A relation between the oxygen transport capacity decrease and the extension of reduction was calculated.

Low attrition values were found during fluidized-bed operation, and no defluidization was observed for typical operating conditions in a CLC process.

*Nomenclature*

| | |
|---|---|
| CLC | chemical-looping combustion |
| $F_{in}$ | molar flow of the inlet gas stream (mol/s) |
| $F_{out}$ | molar flow of the outlet gas stream (mol/s) |
| $Me_xO_y$ | oxidized form of the oxygen-carrier |
| $Me_xO_{y-1}$ | reduced form of the oxygen-carrier |
| $M_O$ | molecular mass of oxygen (kg/mol) |
| $m_{ox}$ | mass of the most oxidized form of the oxygen-carrier (kg) |
| $m_{red}$ | mass of the reduced form of the oxygen-carrier (kg) |
| $P_{in}$, $P_{out}$ | partial pressures of the gaseous fuel at the reactor inlet and outlet, respectively |
| $P_m$ | mean partial pressure of the gaseous fuel in the reactor |
| $P_{ref}$ | reference partial pressure |
| $r_0(t)$ | rate of oxygen transferred (mol O/s) |
| $R_{OC}$ | oxygen transport capacity of the oxygen-carrier |
| $R_{OC\ theo}$ | theoretical oxygen transport capacity of the oxygen-carrier |
| T | temperature (K) |
| $t_{r,0}$ | initial time when the considered reaction begins (s) |
| $x_i$ | molar fraction of the gas i |
| $X_{max}$ | maximum $CO_2$ or $H_2O$ corresponding fraction if full combustion was reached |
| $\varepsilon_g$ | coefficient of expansion of the gas mixture |
| $\gamma_O$ | oxygen yield |
| $\omega$ | mass based conversion of ilmenite in the fluidized-bed |
| $\omega_{f,red}$ | final conversion of ilmenite reached in the previous reduction |
| $(d\omega/dt)_{exp}$ | experimental rate of conversion (kg O/(s·kg oxygen-carrier)) |

## Acknowledgments

This work was partially supported by the European Commission, under the RFCS program (ECLAIR Project, Contract RFCP-CT-2008-0008), from Alstom Power Boilers and by the Spanish Ministry of Science and Innovation (Project ENE2010-19550). A. Cuadrat thanks CSIC for the JAE Pre. fellowship. Alberto Abad thanks to the Ministerio de Ciencia e Innovación for the financial support in the course of the I3 Program.

## References

[1] Climate Change 2007: Synthesis Report. Contribution of Working Groups I, II and III to the Fourth Assessment Report of the Intergovernmental Panel on Climate Change, in: R.K. Pachauri, A. Reisinger (Eds.), IPCC, Geneva, CH, 2008.
[2] IEA, International Energy Outlook, 2008, www.eia.doe.gov/iea.
[3] L.I. Eide, M. Anheden, A. Lyngfelt, C. Abanades, M. Younes, D. Clodic, Novel capture processes, Oil & Gas Science and Technology 60 (2005) 497–508.
[4] H.R. Kerr, Capture and separation technologies gaps and priority research need, in: D. Thomas, S. Benson (Eds.), Carbon Dioxide Capture for Storage in Deep Geologic Formations — Results from the $CO_2$ Capture Project, Elsevier Science, Oxford, 2005, (vol. 1, Chapter 38).
[5] M.M. Hossain, H.I. de Lasa, Chemical-looping combustion (CLC) for inherent CO2 separation—a review, Chemical Engineering Science 63 (18) (2008) 4433–4451.
[6] A. Lyngfelt, B. Leckner, T. Mattisson, A fluidized-bed combustion process with inherent $CO_2$ separation; application of chemical-looping combustion, Chemical Engineering Science 56 (2001) 3101–3113.
[7] H.J. Ryu, G.T. Jin, C.K. Yi, Demonstration of inherent $CO_2$ separation and no $NO_x$ emission in a 50 kW chemical-looping combustor: continuous reduction and oxidation experiment, in: M. Wilson, T. Morris, J. Gale, K. Thambibutu (Eds.), Proceedings of the Seventh International Conference of Greenhouse Gas Control Technologies, Elsevier Ltd, Amsterdam, The Netherlands, 2005, p. 1907, (vol. 2).
[8] P. Kolbitsch, J. Bolhàr-Nordenkampf, T. Pröll, H. Hofbauer, Operating experience with chemical looping combustion in a 120 kW dual circulating fluidized bed (DCFB) unit, International Journal of Greenhouse Gas Control 4 (2) (2010) 180–185.
[9] C. Linderholm, A. Abad, T. Mattisson, A. Lyngfelt, 160 hours of chemical-looping combustion in a 10 kW reactor system with a NiO-based oxygen carrier, International Journal of Greenhouse Gas Control 2 (2008) 520–530.
[10] C. Linderholm, T. Mattisson, A. Lyngfelt, Long-term integrity testing of spray-dried particles in a 10 kW chemical-looping combustor using natural gas as fuel, Fuel 88 (2009) 2083–2096.
[11] L.F. de Diego, F. Garcia-Labiano, P. Gayan, J. Celaya, J.M. Palacios, J. Adanez, Operation of a 10 kWth chemical-looping combustor during 200 h with a $CuO–Al_2O_3$ oxygen carrier, Fuel 86 (7–8) (2007) 1036–1045.
[12] T. Mattisson, F. García-Labiano, B. Kronberger, A. Lyngfelt, J. Adánez, H. Hofbauer, Chemical-looping combustion using syngas as fuel, International Journal of Greenhouse Gas Control 1 (2) (2007) 158–169.
[13] H. Jin, M. Ishida, A new type of coal gas fueled chemical-looping combustion, Fuel 83 (17–18) (2004) 2411–2417.
[14] J. Wolf, M. Anheden, J. Yan, Performance analysis of combined cycles with chemical looping combustion for $CO_2$ capture, International Pittsburg Coal Conference, Newcastle, New South Wales, Australia, Dec 3–7, 2001.
[15] T. Mattisson, F. Garcia-Labiano, B. Kronberger, A. Lyngfelt, J. Adanez, H. Hofbauer, Chemical-looping combustion using syngas as fuel, International Journal of Greenhouse Gas Control 1 (2007) 158–169.
[16] A. Abad, F. García-Labiano, L.F. de Diego, P. Gayán, J. Adánez, Reduction kinetics of Cu-, Ni-, and Fe-based oxygen carriers using syngas ($CO + H_2$) for chemical-looping combustion, Energy & Fuels 21 (2007) 1843–1853.
[17] C.R. Forero, P. Gayán, L.F. de Diego, A. Abad, F. Garcia-Labiano, J. Adánez, Syngas combustion in a 500 Wth chemical-looping combustion system using an impregnated Cu-based oxygen carrier, Fuel Processing Technology 90 (2009) 1471–1479.
[18] E. Johansson, T. Mattisson, A. Lyngfelt, H. Thunman, Combustion of syngas and natural gas in a 300 W chemical-looping combustor, Chemical Engineering Research and Design 84 (2006) 819–827.

[19] A. Abad, T. Mattisson, A. Lyngfelt, M. Rydén, Chemical-looping combustion in a 300 W continuously operating reactor system using a manganese-based oxygen carrier, Fuel 85 (2006) 1174–1185.
[20] A. Abad, T. Mattisson, A. Lyngfelt, M. Johansson, The use of iron oxide as oxygen carrier in a chemical-looping reactor, Fuel 86 (2007) 1021–1035.
[21] C. Dueso, F. García-Labiano, J. Adánez, L.F. de Diego, P. Gayán, A. Abad, Syngas combustion in a chemical-looping combustion system using an impregnated Ni-based oxygen carrier, Fuel 88 (12) (2009) 2357–2364.
[22] Y. Cao, W.P. Pan, Investigation of chemical looping combustion by solid fuels. 1. Process analysis, Energy & Fuels 20 (5) (2006) 1836–1844.
[23] J.S. Dennis, S.A. Scott, A.N. Hayhurst, In situ gasification of coal using steam with chemical looping: a technique for isolating $CO_2$ from burning a solid fuel, Journal of the Energy Institute 79 (3) (2006) 187–190.
[24] N. Berguerand, A. Lyngfelt, Chemical-looping combustion of petroleum coke using ilmenite in a 10 kWth unit-high-temperature operation, Energy & Fuels 23 (10) (2009) 5257–5268.
[25] N. Berguerand, A. Lyngfelt, The use of petroleum coke as fuel in a 10 kWth chemical-looping combustor, International Journal of Greenhouse Gas Control 2 (2008) 169–179.
[26] N. Berguerand, A. Lyngfelt, Design and operation of a 10 kWth chemical-looping combustor for solid fuels — testing with South African coal, Fuel 87 (2008) 2713–2726.
[27] A. Cuadrat, A. Abad, F. García-Labiano, P. Gayán, L.F. de Diego, J. Adánez, The use of ilmenite as oxygen-carrier in a 500 Wth chemical looping coal combustion unit. doi:10.1016/j.ijggc.2011.09.010.
[28] A. Bidwe, C. Hawthorne, F. Mayer, A. Charitos, A. Schuster, G. Scheffknecht, Use of ilmenite as oxygen-carrier in chemical looping combustion-batch and continuous dual fluidized bed investigation, Energy Procedia 4 (2011) 433–440.
[29] H. Leion, A. Lyngfelt, M. Johansson, E. Jerndal, T. Mattisson, The use of ilmenite as an oxygen carrier in chemical-looping combustion, Chemical Engineering Research and Design 86 (2008) 1017–1026.
[30] H. Leion, T. Mattisson, A. Lyngfelt, Solid fuels in chemical-looping combustion, International Journal of Greenhouse Gas Control 2 (2008) 180–193.
[31] T. Pröll, K. Mayer, J. Bolhàr-Nordenkampf, P. Kolbitsch, T. Mattisson, A. Lyngfelt, Natural minerals as oxygen carriers for chemical looping combustion in a dual circulating fluidized bed system, GHGT-9: 9th International Conference on Greenhouse Gas Control Technologies, 16–20 November, 2008.
[32] J. Adánez, A. Cuadrat, A. Abad, P. Gayán, L.F. de Diego, F. García-Labiano, Ilmenite activation during consecutive redox cycles in chemical-looping combustion, Energy & Fuels 24 (2010) 1402–1413.
[33] A. Cuadrat, A. Abad, J. Adánez, L.F. de Diego, F. García-Labiano, P. Gayán, Design Considerations for chemical-looping combustion of coal — Part 1. Experimental tests, Submitted article.
[34] M. Johansson, T. Mattisson, A. Lyngfelt, Comparison of oxygen carriers for chemical-looping combustion, Thermal Science 10 (2006) 93–107.
[35] A. Abad, J. Adánez, A. Cuadrat, F. García-Labiano, P. Gayán, L.F. de Diego, Reaction kinetics of ilmenite for chemical-looping combustion, Chemical Engineering Science 66 (4) (2011) 689–702.
[36] A. Abad, J. Adánez, F. García-Labiano, L.F. de Diego, P. Gayán, J. Celaya, Mapping of the range of operational conditions for Cu-, Fe-, and Ni-based oxygen carriers in chemical-looping combustion, Chemical Engineering Science 62 (2007) 533–549.
[37] J. Adánez, A. Abad, F. García-Labiano, L.F. de Diego, P. Gayán, $H_2S$ retention with Ca-based sorbents in a pressurized fixed-bed reactor: application to moving-bed design, Fuel 84 (5) (2005) 533–542.
[38] P. Cho, T. Mattisson, A. Lyngfelt, Carbon formation on nickel and iron oxide-containing oxygen carriers for chemical-looping combustion, Industrial and Engineering Chemistry Research 44 (4) (2005) 668–676.
[39] M. Ishida, H. Jin, T. Okamoto, Kinetic behavior of solid particle in chemical-looping combustion: suppressing carbon deposition in reduction, Energy & Fuels 12 (2) (1998) 223–229.
[40] J.M. Coulson, J.F. Richardson, R.K. Sinnott, Chemical engineering: Vol. VI, Chemical Engineering Design, Butterworth-Heinemann, Oxford, 1997.

# Paper IV

# Prompt Considerations on the Design of Chemical-Looping Combustion of Coal from Experimental Tests

Ana Cuadrat, Alberto Abad*, Luis F. de Diego, Francisco García-Labiano, Pilar Gayán, Juan Adánez

Instituto de Carboquímica (C.S.I.C.), Department of Energy and Environment, Miguel Luesma Castán 4, 50018, Zaragoza, Spain
*Corresponding author. Tel.: +34 976 733977; fax: +34 976 733318.
Email address: abad@icb.csic.es (Alberto Abad).

## Abstract

The Chemical-Looping Combustion of coal in the reactor system has been proposed as an interesting option to process a solid fuel in a CLC system. In this process, a solid fuel is directly fed to the fuel reactor in a CLC system. Solid fuel pyrolysis, char gasification and oxidation of gaseous products by reaction with the oxygen-carrier are the main chemical processes happening in the fuel reactor. The aim of this study is to analyze the performance of ilmenite as oxygen-carrier for CLC of coal regarding to the conversion of gaseous products from char gasification. Successive reduction-oxidation cycles were carried out in a fluidized bed using bituminous coal char as reducing agent. The changes on chemical and physical properties of ilmenite particles were determined. An activation process of ilmenite through the redox cycles was evidenced which was justified by an increase of porosity. The results showed that the activation for ilmenite reduction reaction was completed after 7 redox cycles. However, the oxidation reaction rate was increasing still after 16 redox cycles because the porosity was not fully developed. The gasification reaction rate and the ilmenite reactivity were analyzed. The effect of ilmenite itself and the influence of the gasification agent, i.e. $H_2O$, $CO_2$ or $H_2O/CO_2$ mixtures, and temperature on the gasification rate were evaluated. Limited use of $CO_2$ in the fluidizing gas was identified in order to maintain high gasification rates. Higher temperature improved the char gasification rate, mainly using steam as gasification agent, and the combustion efficiency of the gasification products. Nevertheless, the effect of temperature on the combustion efficiency was of lower relevance than that on the gasification rate. Finally, a theoretical approach was developed to easily evaluate the conversion of char in the fuel-reactor by gasification.

Keywords: $CO_2$ capture, Chemical-Looping Combustion, Oxygen-carrier, Ilmenite, Coal, Gasification

## 1. Introduction

According to the Intergovernmental Panel on Climate Change (IPCC) [1], "most of the observed increase in global average temperatures since the mid-20$^{th}$ century is very likely due to the observed increase in anthropogenic greenhouse gas concentrations". There is therefore a broad acceptance by scientists of the link between greenhouse-gas emissions and global climate change. As the use of fossil fuels in energy generation represents about 65% of global anthropogenic greenhouse-gas emissions [2], actions geared to reduce emissions from fossil fuel combustion are necessary. The intensified use of coal would substantially increase the emissions of $CO_2$ unless there was very widespread deployment of carbon capture and storage [3]. Carbon dioxide capture is generally estimated to represent three-fourths of the total cost of a carbon capture, transport and sequestration system. Among the different capture concepts, Chemical-Looping Combustion (CLC) is one of the most promising technologies to carry out the $CO_2$ capture with low cost and small efficiency loss.

CLC is based on the transfer of the oxygen from air to the fuel by means of a solid oxygen-carrier. CLC technology has been widely proven using two interconnected fluidized beds: the fuel reactor and the air reactor [4]. In the fuel reactor the fuel is oxidized through reduction of the oxygen-carrier. The oxygen-carrier is transported to the air reactor where is regenerated by oxidation with air. The stream of combustion gases from the fuel reactor contains primarily $CO_2$ and $H_2O$. Water can be easily separated by condensation and a highly concentrated stream of $CO_2$ ready for compression, transport and sequestration is achieved. The gas stream from the air reactor is oxygen-depleted and consists only in $N_2$ and some unreacted $O_2$. Thus, $N_2$ in air is not mixed with the combustion gases and inherent separation of $CO_2$ from other gases is performed with no costs or energy penalty for gas separation.

Chemical Looping Combustion (CLC) with gaseous fuels has been developed in the last few years, but using CLC with solid fuels has shown to have recently a great interest [5]. The use of coal in CLC is very attractive in future sceneries with restriction in $CO_2$

emissions, since coal will keep on being a main energy source in the medium-term. One option for CLC with solid fuels is directly to introduce coal in the fuel-reactor, which is fluidized by a gasification agent [6-9]. The reactor scheme of Chemical-Looping Combustion of solid fuels is shown in Fig. 1. In this technology coal is physically mixed with the oxygen-carrier in the fuel reactor where $H_2O$ and/or $CO_2$ are used as fluidizing gas and gasifying agent. Thus, different processes are happening simultaneously in the reactor: (i) the pyrolysis and gasification of coal, where CO and $H_2$ are the main product, proceed according reactions (1-3); and (ii) the reaction of volatiles and gasification products with the oxygen-carrier to give $CO_2$ and $H_2O$, according reaction (4). The oxygen-carrier reduced in the fuel reactor, $Me_xO_{y-1}$, is transferred to the air reactor where reaction (5) with oxygen from air takes place. Thus the oxygen-carrier is regenerated to start a new cycle. The net chemical reaction is the same as usual combustion with the same combustion enthalpy.

$$\text{Coal} \rightarrow \text{Volatile matter} + \text{Char} \quad (1)$$

$$\text{Char} + H_2O \rightarrow H_2 + CO \quad (2)$$

$$\text{Char} + CO_2 \rightarrow 2\,CO \quad (3)$$

$$n\,Me_xO_y + H_2, CO, \text{Volatile matter (e.g. } CH_4) \rightarrow n\,Me_xO_{y-1} + CO_2 + H_2O \quad (4)$$

$$Me_xO_{y-1} + \tfrac{1}{2}\,O_2 \rightarrow Me_xO_y \quad (5)$$

The gasification process is expected to be the slower step in the fuel reactor, thus the mean residence time for char particles in the fuel reactor should be higher than for oxygen-carrier particles. To increase the mean residence time of char and to avoid unreacted carbon entering the air reactor, the char particles can be separated from the oxygen-carrier in a so-called carbon stripper and re-introduced to the fuel reactor.

The possibility of using the CLC technology for solid fuels has been showed at laboratory scale using different oxygen-carrier materials –e.g. Cu- or Fe-based particles–, and different solid fuels –e.g. coal, biomass, solid wastes, pet-coke– [7-10]. After the encouraging results obtained at laboratory scale, the feasibility of the CLC process for solid fuels in a continuously operated prototype was proven by Berguerand and Lyngfelt [11-12] using ilmenite as oxygen-carrier. A carbon stripper was designed between the fuel reactor and the air reactor to increase the residence time of char particles in the fuel reactor. Due to the characteristics of this facility, the volatiles do not

get in contact with oxygen-carrier particles. Thus, only the conversion of gases from steam gasification (CO and $H_2$) was analyzed. The importance of using high temperatures in this process was acknowledged [13] in order to have high conversion of the solid fuel to gases into the reactor. Also the effect of the mean residence time of char particles –determined by the solids circulation flow-rate– on its conversion in the fuel reactor was analyzed [14]. A higher circulation of solids reduced the mean residence time in the reactor and thus a lower efficiency of gasification was obtained. In general, high carbon capture efficiencies can be reached (82-96%) [11]. However, some fraction of unconverted gases (CO and $H_2$) were obtained in the outlet stream, which demanded about 5-7% of the total oxygen necessary to burn coal to $CO_2$ and $H_2O$ when the fuel reactor temperature was 1000ºC [13]. Furthermore, Cuadrat et al. [15] investigated the effect of operating conditions such as temperature and coal particle size on the combustion efficiency as well as on the extent of gasification in a continuous CLC rig. In this case, volatiles were generated inside the bed. Values for the oxygen demand of gases from 5% to 15% were found in all the experimental work, mainly due to unconverted CO and $H_2$ coming from devolatilization process. Nevertheless, the char gasification and combustion reactions are faster and promoted at higher temperatures. They concluded that high carbon capture efficiencies are expected to be obtained, as well as high combustion efficiencies, especially at temperatures higher than 950ºC.

Most of the works involving CLC with solid fuels indicate that gasification is probably the rate-limiting step. Thus, in order to analyze the efficiency of carbon capture in a CLC system with solid fuels, the attention has been usually put on the reactivity of char gasification [10-19]. Some works have related the solids inventory in the fuel reactor to the reactivity of solid fuel. Thus, the residence time will be larger if a less reactive coal is used, and higher the needed solids inventory [20]. However, this fact is only true when the mean residence time of oxygen-carrier particles was the same order of magnitude than those for char particles. If a carbon stripper is used –as it was showed in Figure 1– the residence time of char particles in the fuel reactor can be increased without the need for increasing the oxygen-carrier inventory.

Nevertheless, to evaluate the performance of the fuel reactor in the CLC process with solid fuels, the reactivity of the oxygen-carrier must be also considered in addition to the gasification reactivity. Thus, the gasification kinetics and the reaction kinetics of

oxygen-carrier particles with reducing gases were considered by Brown et al. when they modelled the gasification and chemical-looping combustion of a lignite char in a fluidized bed of iron oxide particles [18]. The fraction of gases from coal gasification being converted to $CO_2$ and $H_2O$ by the oxygen-carrier greatly depended on the oxygen-carrier reactivity. A more reactive oxygen-carrier gives higher conversion of gases to $CO_2$ and $H_2O$ [21]. Nevertheless, unconverted CO, $H_2$, and $CH_4$ were found in the outlet gas even though highly reactive Ni-based materials were used. Unconverted gases come from both volatiles and gasification products [22,23]. Unconverted gases from gasification products are believed to be due to the characteristics of the char–oxygen-carrier mixing. Char gasification takes place throughout the fluidized-bed reactor. The gasification taking place in the upper part of the bed generates CO and $H_2$ which have not enough time to react with oxygen-carrier particles. So, some unconverted gases are expected to exit from the fuel reactor. This behaviour is fully different from the conversion of a fuel gas introduced at the bottom of the fluidized-bed reactor, where the fuel is gradually converted in the bed [24].Thus, to evaluate the conversion of a solid fuel in a CLC system for solid fuels, both the reactivity of char gasification and oxygen-carrier material must be considered, in addition to the particular char–oxygen-carrier mixing pattern in the reactor.

A key factor for the CLC technology development is the oxygen-carrier material. Suitable oxygen-carriers for a CLC process must have high reactivity during reduction and oxidation, high attrition resistance and agglomeration absence. Low cost of the material is rather desirable for its use with coal, as it is predictable a partial loss together with the coal ashes when removing them from the reactor. Natural minerals are therefore very interesting materials for this purpose. In this context, ilmenite was identified by Leion et al. [25] as oxygen-carrier for solid fuels, proving to be an appropriate material for this scope. Ilmenite showed good fluidizing properties and only agglomeration problems were observed if ilmenite particles were reduced to a high extent, which is not expected at the CLC process. They also show a thermodynamic analysis showing that $Fe^{3+}$ and $Fe^{2+}$ can be involved during the redox cycles in a CLC system whereas the fuel gas can be fully oxidized into $CO_2$ and $H_2O$. Thus, $Fe_2TiO_5$ (i.e. $Fe_2O_3{\cdot}TiO_2$) is the oxidized form, whereas $FeTiO_3$ (i.e. $FeO{\cdot}TiO_2$) is the reduced form when ilmenite is used in CLC. Thus, the main reduction reactions, i.e. with $H_2$, CO or

$CH_4$ as reducing agents, proceed according reactions (6-8) and subsequent oxidation as reaction (9).

$$Fe_2TiO_5 + TiO_2 + H_2 \rightarrow 2\,FeTiO_3 + H_2O \quad (6)$$

$$Fe_2TiO_5 + TiO_2 + CO \rightarrow 2\,FeTiO_3 + CO_2 \quad (7)$$

$$4\,Fe_2TiO_5 + 4\,TiO_2 + CH_4 \rightarrow 8\,FeTiO_3 + CO_2 + 2\,H_2O \quad (8)$$

$$4\,FeTiO_3 + O_2 \rightarrow 2\,Fe_2TiO_5 + 2\,TiO_2 \quad (9)$$

As for the reactivity, the reaction rate is quite high with syngas, and moderate with $CH_4$ [19,25,26]. Although ilmenite has initially a rather low reactivity to be used as oxygen-carrier, it undergoes an activation process after several redox cycles, being its reactivity remarkably increased for $H_2$, CO and $CH_4$ as reacting gases [26]. From a comparison among different iron oxide based minerals as well as oxide scale residues from the steel industry [27], ilmenite looks as a material highly reactive and adequate for its use as oxygen-carrier for CLC with solid fuels. In addition, natural ilmenite showed comparable reactivity with synthetic $Fe_2O_3/MgAl_2O_4$ particles with different solid fuels [17,21].

Ilmenite has been tested with solid fuels in batch tests and in continuously operated prototypes. In a batch fluidized-bed reactor, Leion et al. [20] found that ilmenite enhances the gasification rate of coal because the presence of oxygen-carrier particles reduces the fraction of $H_2$ in the bed, which has an inhibitory effect on the gasification. This fact has been observed as much for steam gasification as for $CO_2$ gasification using different oxygen-carrier materials [10,18]. Thus, the char gasification rate is increased as the inhibitor gas ($H_2$ or CO) decreases its concentration in the reactor because of the reaction with the oxygen-carrier. The char conversion is related to the reactivity of solid fuel particles [28], being the nature of the oxygen-carrier of lower relevance [20,21]. In addition, the type of fluidizing gas –which acts also as gasifying agent– and reacting temperature have a great influence on the char gasification. Thus, the fuel conversion was reduced when $H_2O$ was replaced by $CO_2$ [29], but it was increased with the temperature [12,19,20]. The ilmenite material was also tested in continuous CLC systems. The good conversion of syngas using ilmenite has been showed in dual fluidized bed CLC systems [19,30]. The performance of ilmenite in the 10 $kW_{th}$ continuous CLC system was analyzed with various solid fuels [11-13]. They concluded

that the low tendency for attrition or agglomeration of this material and its low market price make it an interesting option for use in CLC with solid fuels.

$H_2$ and CO from char gasification can account for a relevant oxygen demand in unconverted gases. Moreover, non-gasified char can pass to the air reactor, so losing carbon capture efficiency. Thus, the char gasification process and subsequent oxidation of $H_2$ and CO by the oxygen-carrier is an important issue to be considered in the CLC process. This work investigated the performance of ilmenite as oxygen-carrier in CLC for solid fuels through the reduction-oxidation cycles when using coal as fuel. Specifically, the conversion of char particles and the subsequent oxidation of gasification products with ilmenite were analyzed. Coal char was used as reducing agent, thus avoiding complex interpretation of the results due to volatiles conversion when coal is fed to the reactor.

The activation process of ilmenite particles was investigated when repeated redox cycles using coal char as reducing agent were carried out. Ilmenite activation with a solid fuel was compared to previous activation carried out by gaseous fuels. In addition, the effect of operating conditions (temperature, gas composition) on the char conversion and combustion efficiency of gasification gases were analyzed. Results here obtained will be later used to describe the effect of the char–oxygen-carrier mixing on the combustion efficiency by using a simplified reactor model, and to propose a way to optimize the solids inventory in a CLC system for solid fuels.

## 2. Experimental

### *2.1. Oxygen-carrier: ilmenite*

Ilmenite is a common mineral found in metamorphic and igneous rocks. The ilmenite used in this work is a concentrate from a natural ore from Norway with a purity of 94.3%. Ilmenite particles are mainly composed of $FeTiO_3$, $TiO_2$ and $Fe_2O_3$. This ilmenite has shown good reactivity and excellent properties from both TGA and batch fluidized bed testing [17,20,25,26]. It has also been tested with solid fuels in continuously operated facilities [11-15].

As starting material, pre-oxidized ilmenite particles were used in this work. They were obtained by exposing fresh particles to a thermal pre-treatment at 950ºC in air during 24 hours. The pre-oxidation was considered in order to get ilmenite in its most oxidized state [25], to improve properties and initial reaction rates [26], and to avoid defluidization problems [30]. The main properties for pre-oxidized ilmenite are showed in Table 1. The composition of pre-oxidized ilmenite was 54.7 wt.% $Fe_2TiO_5$, 11.2 wt.% $Fe_2O_3$, 28.6% $TiO_2$ and 5.5 wt.% of other inert compounds, mainly $MgSiO_3$. Thus, the Fe:Ti molar ratio was around 1:1. In the fully oxidized ilmenite, the iron was found to be as $Fe^{3+}$, either in the $Fe_2TiO_5$ compound or as free $Fe_2O_3$. However, in the CLC process pseudobrookite ($Fe_2TiO_5$) and hematite ($Fe_2O_3$) are reduced to ilmenite ($FeTiO_3$) and magnetite ($Fe_3O_4$), respectively. Rutile is considered to be an inert. Higher reduction prevents the complete conversion of the fuel to $CO_2$ and $H_2O$ because thermodynamic constrictions (Leion et al., 2008b). Thus, the oxygen transport capacity of ilmenite, $R_{O,ilm}$, was defined as the oxygen transport capacity useful for CLC, being calculated as

$$R_{O,ilm} = \frac{m_o - m_r}{m_o} \tag{10}$$

being $m_o$ the mass of the most oxidized form of the oxygen carrier, and $m_r$ the mass in the reduced form, i.e. a mixture of $FeTiO_3$ and $Fe_3O_4$.

*2.2 Solid fuel: coal char*

The fuel used was char coming from a devolatilized South African coal, which is, as for the ASTM, classified as medium volatile bituminous coal. To produce the char, batch of 500 g of coal particles were devolatilizated in a fluidized-bed reactor. The reactor was fluidized by $N_2$ and it was heated up from room temperature to 900ºC with a temperature ramp of 20ºC/min and afterwards cooled down. Since the gas velocity increases with the temperature, the $N_2$ flow was correspondingly reduced as the temperature increased to ensure bubbling bed conditions and to avoid elutration of particles. The proximate and ultimate analysis of the obtained char is shown in Table 2. The particle size of char was in the range 100-200 μm, and the density of the particles was about 1000 kg/m$^3$.

*2.3 Experimental setup: fluidized-bed reactor*

The experimental work has been carried out in a setup consisting of a system for gas feeding, a solid fuel feeding system, a fluidized-bed reactor and the gas analysis system. A schematic layout of the laboratory setup is presented in Fig. 2. The fluidized-bed reactor –55 mm D.I. and 700 mm height– is electrically heated by a furnace, and had a preheating zone just under the distributor plate. The temperature inside the bed was measured and used to control the reaction temperature. The reactor had pressure taps in order to measure the absolute pressure in the bed and pressure drop. Agglomeration and defluidization problems could be detected by a sharp decrease in the bed pressure drop during operation. The pressure tap was also useful to detect possible blocking in the downstream pipes due to elutriated particles or tar condensation in cold points.

The reactor was loaded with 400 g of ilmenite with a particle size of +150-300 μm. In some tests silica sand (200-400 μm) was used instead of ilmenite. The feeding of the solid fuel was done by means of a fuel chute which ends 3 cm above the distributor plate and about 5-6 cm below the upper level of the fluidizing particles. So, char particles are fed inside the fluidized bed. The upper part of the chute has a valve system that creates a reservoir in which the fuel is placed and later pressurized by nitrogen to ensure quick char feeding.

The gas feeding system had different mass flow controllers connected to an automatic three-way valve. In this way, it was possible to feed alternatively air, nitrogen or a mixture of steam/$CO_2$. The steam was obtained by evaporation with a resistance heater of a known water flow supplied by a peristaltic pump. Different gas analyzers continuously measured the gas composition at the reactor exit after water condensation. CO, $CO_2$ and $CH_4$ dry basis concentrations were determined using non-dispersive infrared analysis (NDIR) and $H_2$ by thermal gas conductivity. The $O_2$ concentration was determined in a paramagnetic analyzer. As in most of cases gas is mainly composed by steam, a downstream $N_2$ flow of 90 $L_N$/h is introduced to ensure a continuous dry gas flow feeding the analyzers. This nitrogen is also later used to calculate the total outlet gas flow by a nitrogen balance.

*2.4. Experimental procedure*

The experimental work has been carried out in the fluidized-bed reactor above described at temperatures between 900 and 1000ºC. The reactor was loaded with 400 g of ilmenite particles and they were exposed sequentially to reducing and oxidizing conditions. During reduction periods, char was used as fuel whereas the reactor was fluidized with steam, $CO_2$ or steam/$CO_2$ mixtures, which also acted as gasification agent. After every reducing period, ilmenite particles were fully re-oxidized with air before starting a new cycle. Between the reducing and oxidizing periods a $N_2$ flow was also introduced during 2 min to purge the system. The total fluidizing flow was 200 $L_N$/h, which corresponds to a gas velocity of 0.1 m/s at 900ºC in the reactor.

During the reducing periods, batch loads of South African coal char were fed to the reactor through the solids feeding system. Char particles were fed by valve v1 to a small reservoir placed in the upper part of the fuel chute, see Fig. 2. After that, the deposit was over-pressurized 1 bar with $N_2$ by valve v2. Once the reservoir was pressurized, valve v2 was closed and v3 was opened and quickly closed. Then, char particles fall to the fluidized bed through the fuel chute as the reservoir is unpressurized. Thus, it was ensured that char particles were forced to enter to the fluidized bed, whereas a continuous flow of nitrogen through the fuel chute is avoided.

Two series of experiments were performed. The first tests were done to evaluate the evolution of the reaction rate of ilmenite particles with the cycle number. In this case, the reducing periods consisted in introducing 2 loads of char –1.5 g each load– using steam as fluidization gas at 900ºC. A previous series of tests were done introducing char loads with different weight of fuel. The loads of 1.5 g resulted to be the loads with highest char quantity that could be fed with no major fuel entrainment. Every load was left till char gasification was complete. Thus, the evolution in the ilmenite reactivity was evaluated in successive redox cycles. Reduction-oxidation cycles were made until it could be considered that ilmenite had reached a constant reaction rate. Once ilmenite was activated and for the second series of experiments, a load of 1.5 g of South African coal char was introduced in the reactor in every reduction period. The reduction periods were 1800 s. The oxidation periods necessary for complete oxidation varied between 600 and 1800 s. The effect of temperature and gas composition on the reaction rates of

gasification and subsequent combustion of gasification products was analyzed, as well as the role of ilmenite during char gasification. The oxygen carriers were exposed to a total number of 50 reduction/oxidation cycles.

SEM pictures of the different samples, XRD analysis, as well as Hg porosimetry were carried out to see the changes undergone in the physical properties of ilmenite after various cycles when using a solid fuel as reducing agent. In addition, the reactivity of ilmenite particles during the activation period was analyzed by TGA experiments using 5 vol.% $H_2$ at 900ºC.

## 3. Data evaluation

To analyze the performance of ilmenite during char gasification and combustion of gasification products, a mass balance to carbon, hydrogen and oxygen was done from the concentration of $CO_2$, CO, $H_2$ and $CH_4$ analyzed in every experimental condition. The molar gas flow of each component exiting the fuel reactor, $F_i$, is calculated as:

$$F_i = F_{out} \cdot y_i \tag{11}$$

$y_i$ being the molar fraction of the component *i* ($CO_2$, CO, $H_2$ or $CH_4$) in the product gas. The total dry basis outlet flow, $F_{out}$, can be calculated by using the downstream introduced $N_2$ flow, $F_{N_2}$.

$$F_{out} = \frac{F_{N_2}}{(1-\sum_i y_i)} \tag{12}$$

The rate of char conversion, $r_C(t)$, was calculated from a mass balance to carbon in gaseous form in the reactor.

$$r_C(t) = (y_{CO_2} + y_{CO})F_{out} - F_{CO_2,in} \tag{13}$$

Methane was not considered in the carbon balance because it was not detected in any case. The evolution of char conversion, $X_{char}$, with time can be calculated by integrating Eq. (13).

$$X_{char}(t) = \frac{1}{N_{C,char}} \int_0^t r_C(t)dt \tag{14}$$

$N_{C,char}$ being the mol number of carbon fed into the reactor.

The instantaneous rate of conversion of the char, $r_{C,inst}$, is calculated as the rate of gasification per the amount of non-gasified carbon that is still in the reactor.

$$r_{C,inst}(t) = \frac{r_C(t)}{N_{C,char} - \int_0^t r_C(t)dt} \tag{15}$$

In addition, from the gas product distribution, it is possible to know the rate of oxygen transferred from ilmenite to the fuel gas, $r_O(t)$, which can be calculated by means of the following oxygen balance:

$$r_O(t) = F_{O_2,out} - F_{O_2,in} = \left[ F_{out}(2y_{CO_2} + y_{CO}) - 2F_{CO_2,in} \right] + \left[ F_{H_2O,out} - F_{H_2O,in} \right] \tag{16}$$

Note that in the experiments where $CO_2$ is fed to the reactor, the amount of $CO_2$ generated is represented and calculated by subtracting the inlet flow of $CO_2$. Regarding the ultimate analysis it can be seen that the hydrogen and oxygen in the fuel used is negligible, and it was not considered in the mass balances, see Table 2. The flow of water at the reactor exit was calculated considering that the flow of hydrogen either in $H_2$ or $H_2O$ comes only from introduced steam, $F_{H_2O,in}$. The hydrogen coming from char moisture was considered to be negligible.

$$F_{H_2O,out} = F_{H_2O,in} - F_{out} y_{H_2} \tag{17}$$

Thus, equation 13 can be reduced to:

$$r_O(t) = F_{out}(2y_{CO_2} + y_{CO} - y_{H_2}) - 2F_{CO_2,in} \quad (18)$$

The conversion of ilmenite, $X_{red}$, in the fluidized bed for reduction reaction can be calculated from the integration of $r_O(t)$ with time:

$$X_{red}(t) = \frac{1}{N_{O,ilm}} \int_0^t r_O(t)dt \quad (19)$$

$N_{0,ilm}$ being the molar amount of oxygen in ilmenite active for CLC process, calculated as

$$N_{O,ilm} = \frac{m_o R_{O,ilm}}{M_O} \quad (20)$$

Finally, the conversion of gasification products, i.e. CO and $H_2$, to $CO_2$ and $H_2O$ by reaction with ilmenite particles was evaluated using the combustion efficiency, $\eta_c$. The combustion efficiency is defined as the oxygen gained by the fuel for its oxidation divided per the oxygen needed to fully oxidize the fuel. Here, the combustion efficiency, $\eta_c$, is calculated with Eq. (21).

$$\eta_c(t) = \frac{r_O(t)}{2r_C(t)} \quad (21)$$

## 4. Results and discussion

In a previous work, an activation process of the ilmenite was observed when using gaseous fuels as reducing agents [26]. The activation process happened during ilmenite exposition to consecutive redox cycles. As activation proceeds, the reactivity increases but the oxygen transport capacity of ilmenite, $R_{O,ilm}$, decreases because of the appearance of free $Fe_2O_3$. After the activation period, reactivity of ilmenite was maintained roughly constant. Thus, prior to analyze the performance of ilmenite on gasification of char and subsequent combustion of gasification products, the activation

of ilmenite was carried out by doing consecutives redox cycles using char as fuel in the reduction period. After that, tests were carried out using the previously activated ilmenite varying the reaction temperature and the composition of the fluidizing gas.

*4.1. Activation of ilmenite with coal char*

In the first series of experiments, 16 consecutive redox cycles in batch fluidized bed were carried out using pre-oxidized ilmenite as starting material. Steam was used as fluidizing gas. Every reduction period consisted of two consecutive loads of 1.5 g of char. After the reduction period, the bed material was oxidized by air. The second load in the same period was fed to get further reduction of the oxygen carrier.

Figs. 3a), 3b) and 3c) show the evolution in the flow of $CO_2$, CO and $H_2$ corresponding to the initial 10 redox cycles. No $CH_4$ was observed during any test, since the volatile matter content in the fuel is negligible and no methane was generated at these conditions, e.g. by methanation of hydrogasification reactions. Just after introducing the char load, the concentration of $CO_2$, CO and $H_2$ had their maximum values and then decreased over time. This fact is evident as there was less remaining char in the reactor. In addition, the second loads showed similar profiles than the first ones. Differences can be attributed to experimental error. The final conversion of ilmenite after the reducing period was lower than 12 % in all cases, which are quite low and therefore no oxygen depletion effect in the ilmenite was seen. When the effect of consecutives redox cycles on the concentration of gases is analyzed, it can be seen that there is an increase in the production of $CO_2$ and a decrease in the gasification products ($H_2$ and CO) in the product gas with the cycles. After several redox cycles the $CO_2$ concentration achieves the highest value and no further substantial increase on $CO_2$ concentration or decrease on CO or $H_2$ concentration was observed. It seems that an activation process was happening, where the reactivity of ilmenite was increased, and the gas conversion of CO and $H_2$ to $CO_2$ and $H_2O$ was increased during the initial 6 or 7 cycles. After that, ilmenite reactivity stabilizes and no further substantial increase in gas conversion was taking place.

To confirm the activation process, reactivity of ilmenite samples withdrew from the reactor after 1, 3, 7, 10, 13 and 16 cycles was determined by thermogravimetric

analysis. The conversion vs. time curves obtained from TGA experiments are shown in Fig. 4. For comparison purposes, the conversion curves for pre-oxidized and fully activated ilmenite are also shown. The conversion curve for fully activated ilmenite was taken from activated ilmenite after 20 cycles using $H_2$ as reducing gas, as it was shown in a previous work [26]. The conversion during reduction reaction, $X_{red}$, and oxidation reaction, $X_{ox}$, were determined from the mass variation of solid samples in TGA by using Eqs (22) and (23), respectively.

$$X_{red} = \frac{m_o - m}{R_{O,ilm} m_o} \tag{22}$$

$$X_{ox} = \frac{m - m_r}{R_{O,ilm} m_o} \tag{23}$$

*m* being the instantaneous mass of the solid sample as the reaction proceeds.

For the reduction reaction, it can be seen in Fig. 4a) that the reaction rate mostly increases during the initial redox cycles. After one cycle, the reactivity increase is very important, and ilmenite can be considered activated after 7 cycles. On the contrary, for oxidation the activation process is slower than for reduction, see Fig. 4b). Indeed, ilmenite is not completely activated after 16 redox cycles for the oxidation reaction. In a previous work [31] it was determined that oxidation reaction proceeds in two consecutives steps: the first one controlled by chemical reaction and the second one controlled by diffusion of gases in the product layer. The second step is influenced by the porosity of the solid, and the conversion which the product layer diffusion begins to control the reaction rate increases with the particle porosity. Thus, porosity of the ilmenite samples were determined by mercury porosimetry. Samples for ilmenite after 1, 3, 7, 10, 13 and 16 cycles have, respectively, porosities of 2, 3.8, 5.9, 8.5 and 12.6%. However, the porosity for a fully activated particle was 27.5%.

The two steps above described in the oxidation reaction can be clearly seen in Fig. 4b). The reactivity of the first step was maintained roughly constant in all cases, but the conversion at which the controlling mechanism is shifted increases with the cycle number, i.e. as the porosity of ilmenite particles increases.

To observe changes in the solid structure throughout consecutives redox cycles, a morphological characterization of several samples was performed by SEM. Fig. 5 shows SEM images of pre-oxidized particles and after 3 and 13 cycles. Pre-oxidized ilmenite shows a granular structure with little porosity development. There is a continuous development of porosity as well as the granulation is enhanced during redox cycles. The development of the granular structure and porosity leads to a reactivity increase with the cycle number. These observations follow the same pattern as when using gaseous fuels [26].

Furthermore, the possible variation in the oxygen transport capacity of ilmenite, $R_{O,ilm}$, with the cycle number has been analyzed. The oxygen transport capacity of several samples withdrew from the reactor after 1, 3, 7, 10, 13 and 16 cycles was measured with TGA at 900ºC using 5 vol.% $H_2$ and 40% $H_2O$ in the reacting gases. At this condition, iron compounds in the fully reduced sample appear as $FeTiO_3$ or $Fe_3O_4$, i.e. the oxygen transport capacity useful for CLC is directly measured from the mass variation between the oxidized and reduced form. The oxygen transport capacity barely decreased with the cycle number. After 16 redox cycles with char there was only a very slight decrease in the measured $R_{O,ilm}$ value from 4 % to 3.9 %.

Previous work [26] showed that the oxygen transport capacity of ilmenite, $R_{O,ilm}$, got reduced gradually with the number of cycles. The reason for that was the migration of iron towards the outer surface of the particle creating an external shell of free $Fe_2O_3$. The initial $R_{O,ilm}$ value was 4%, and it decreased until 2.1% after 100 redox cycles because the $Fe_2O_3$ fraction increased with the cycle number at expenses of decreasing the fraction of $Fe_2TiO_5$.

SEM images show that in this work, the outer shell observed in the previous work is not formed. In addition, XRD analysis showed that the share of iron compounds between $Fe_2TiO_5$ and $Fe_2O_3$ was not affected by the cycle number in the fully oxidized samples. Thus, the composition described in Section 2.1 for pre-oxidized ilmenite was maintained roughly constant during the activation period. This fact confirms that the oxygen transport capacity –which depends on the share of iron– was barely affected by the number of cycles.

Thus, during the activation period showed in this work, the migration of iron was not observed as in previous work using gaseous fuels [26]. The difference between both cases can be found in the extent of ilmenite reduction happening in every redox cycle because the iron migration was enhanced as the reduction conversion increased [26]. In experiments showed in this work, ilmenite conversion was as low as 8 % in the first cycle and increased to 12 % after the activation period, i.e. $6^{th}$-$7^{th}$ cycle. These values were lower than the final conversion reached in previous tests with gaseous fuels. Thus, the migration of iron was not promoted at low ilmenite conversion values as in experiments carried out in this work, and it seemed not be affected by the fact that the initial fuel is gaseous or solid. Iron migration would be expected with higher conversion values or more redox cycles.

The effect of the activation process on the char gasification was analyzed by considering the rate of char conversion, $r_C(t)$, as the total flow of $CO_2$ and CO exiting from the reactor, as it is shown in Fig. 6. When the evolution of carbon in the gases is analyzed with the cycle number, it was observed a slight increase in the rate of char conversion during the initial 6-7 cycles and then it was maintained roughly constant. Thus, the char gasification is being affected in some mode by the increase of reactivity of ilmenite. Likely, the lower concentrations of $H_2$ and CO –which present an inhibitory effect on the char gasification– as ilmenite is being activated increased the gasification rate with the initial 6-7 cycles.

Regarding the differences in the density and particle size used for char and ilmenite particles, some char particles could be segregated to the top of the fluidized bed. Thus, some unconverted $H_2$ and CO could not have been in contact with the oxygen-carrier if they came from the gasification of segregated char particles. However, in that case the increase in ilmenite reactivity would have a lower effect on the $H_2$ and CO concentrations. Therefore, the effect of the possible segregation of the char particles on the gas distribution would be of low relevance.

All the following tests were performed with the so-called activated ilmenite, which has constant reactivity in the reducing reaction. Thus, the effect of the variation in ilmenite reactivity on the evaluation of the results can be ignored.

*4.2. Role of ilmenite in char gasification*

The effect of ilmenite as oxygen-carrier in the gasification process was evaluated by comparing the gas product distribution obtained using ilmenite or silica sand as bed material, see Fig. 7. Obviously, ilmenite has an effect on the gas distribution. It reacts with CO and $H_2$ and gives $CO_2$ and $H_2O$. Furthermore, the selectivity of ilmenite towards the reaction with $H_2$ or CO also can be observed. Thus, the ratio $CO/H_2$ in the product gas for sand is about 0.7, whereas is 2.8 for ilmenite because the reaction with $H_2$ is faster than with CO [31].

Fig. 8 shows the instantaneous rate of char conversion, $r_{C,ins}(t)$, when ilmenite or sand is used as bed material. The $r_{C,ins}$ values were higher for ilmenite that for sand. The positive effect of the oxygen-carrier in the gasification process has already been proven in several studies [10,18,20]. The use of ilmenite improves the gasification since the concentrations of $H_2$ and CO decreased, which are well known to be inhibitors for gasification. In both cases, a slight tendency towards the increase in the instantaneous rate of char gasification with char conversion is observed. Average values of char conversion rate of 10.9 %/min for ilmenite and of 6.5%/min for sand were obtained at 950ºC using steam. Only average rates for char conversion between 0.35 and 0.75 were considered as representative of the process. So, it was avoided any possible effect of the back-mixing at the beginning or mathematical errors introduced at the end of the period when the concentrations or remaining char are too low.

Usually, the gasification process is explained by the homogeneous model or the random pore model [32]. If a random pore model was fulfilled the instantaneous rate goes through a maximum, which was not observed. If gasification followed a homogeneous model, the instantaneous rate of char conversion should be constant with the char conversion. From these batch tests and the resulting gas profiles (see Fig. 7), no conclusive statement about what the gasification model is for this fuel can be drawn up. However, a study made by TGA analysis on char gasification of this fuel showed that it follows a homogeneous model [33]. The slight increase in the rate of char gasification observed in these batch tests could be explained by an increase in the gasification rate because there was lower concentration of $H_2$ –which inhibits steam gasification–in the reacting gas as the char was being converted.

In addition, for comparison purposes tests were performed using $N_2$ as fluidizing gas and ilmenite or sand as bed material. Here, the rate of char gasification represents the flow of carbon species ($CO_2$ and CO) exiting in the gas stream. In this case, the evolution of carbon species to the gas stream was low when ilmenite was used, whereas no $CO_2$ or CO was detected when sand was used. Thus, fuel oxidation is exclusively performed by the solid-solid reaction among char and oxygen-carrier [34], which depends on the surface of contact between solids and the type of contact [35]. However, it can be observed a substantial increase in the rate of char gasification when a gasification agent ($H_2O$) is used as fluidizing gas. Therefore, the conversion of the solid fuel when is fluidized with $H_2O$ is mainly happening through gasification as an intermediate step, with CO and $H_2$ as intermediate products, see Eqs. (1-4). In this case, solid-solid reaction between char and ilmenite particles would be negligible, which agreed to results previously obtained by other authors [10,18].

*4.3. Effect of the fluidizing gas composition*

As much $H_2O$ as $CO_2$ has been proposed as fluidizing gas because both of them can act as gasifying agent. Indeed, several works have analyzed the gasification in the CLC process for solid fuels using either $H_2O$ [10,20,25,27] or $CO_2$ [7,18,29]. $CO_2$ can be fed by recirculating a fraction of the product gas stream, as it was indicated in Fig. 1. Thus, the steam requirements for the gasification would be decreased in some extension if a mixture of $CO_2$ and $H_2O$ was used, or even avoided if a pure stream of $CO_2$ was used as fluidizing gas.

Here, the effect of using a gas mixture of $CO_2$ and $H_2O$ on the gasification of char particles from the South African bituminous coal was analyzed. Fig. 9 shows the instantaneous rate of char gasification, $r_{C,inst}(t)$, as a function of the char conversion when the reactor was fluidized by different $H_2O$:$CO_2$ mixtures, and Fig. 10 shows the char conversion reached throughout the time obtained from the gas distribution products by using Eq. (14). The instantaneous rate of char conversion increased significantly as higher was the $H_2O$ percentage in the gasification gas. Thus, the average gasification rate of char from South African bituminous coal dropped from 10.9 %/min for steam to a value of 3.4 %/min for gasification with $CO_2$. For 100% steam, most of the char is

gasified the first 30 minutes, whereas only 60% char conversion was reached after 30 minutes with $CO_2$.

To make comparisons about the use of $H_2O$:$CO_2$ mixtures as fluidizing gas it was considered the use of the half-life time, $t_{50}$, defined as the reacting time necessary to reach 50% of char conversion. In addition, the time to convert 95% char, $t_{95}$, which has been taken in other works [10,20] as a reference value to determine the residence time to mostly convert the char in the reactor, has been considered. Values of $t_{50}$ and $t_{95}$ were calculated from the following equations assuming the gasification reaction follows the homogeneous model.

$$\frac{1}{1-X_{char}}\frac{dX_{char}}{dt} = r_{C,inst} \Rightarrow \; r_{C,inst} \cdot t = -ln(1-X_{char}) \tag{24}$$

Thus, the residence time to reach a conversion $X_t$, i.e. $t_X$, was obtained as:

$$t_X = -\frac{1}{r_{C,inst}} ln(1-X_t) \tag{25}$$

Table 3 shows the $t_{50}$ values for different $H_2O$:$CO_2$ ratios, that is when $X_t$ = 0.5. The half-life of char particles when fluidizing with 30% $CO_2$ is two times in comparison to 100% $H_2O$, whereas is three times when fluidizing with 100% $CO_2$. Furthermore, Table 3 also shows the $t_{95}$ values for different $H_2O$:$CO_2$ ratios. Thus, the residence time of char particles in the fuel reactor should be 27.5 min when $H_2O$ is used as gasifying agent, being increased up to 88.1 min if $CO_2$ was used. In addition, the introduction of 10 vol.% $CO_2$ in the fluidizing gases gives an increase of nearly 50% in the residence time necessary to convert char particles. From these results it can be concluded that steam seems to be the more adequate fluidizing gas for the South African coal used in this work. The case could be different for other type of coal, as lignite, which shows high reactivity for gasification with $CO_2$ [18,36].

In this technology, the gasification products, mainly composed of CO+$H_2$, must react with the oxygen-carrier getting oxidized. Thus, the reactivity of the oxygen-carrier with the gasification products will affect the combustion efficiency in the fuel reactor, and

also must be analyzed in order to fully understand the performance of the fuel reactor [18]. Fig. 11 shows the evolution of combustion efficiency, $\eta_c$, with the char conversion for different $H_2O$:$CO_2$ ratios. The combustion efficiency decreases as the $CO_2$ content in the fluidizing gas increases, in spite of the flow of gasification products which must react with a constant amount of ilmenite decreases as it was discussed above (see Fig. 9). Nevertheless, although of flow of reacting gases is lower, they are enriched in CO by reaction (3). That is, the outgoing $H_2$ flow decreases when using $CO_2$ as gasification agent, which leads to a worse combustion, since ilmenite reacts slower with CO than with $H_2$ [31]. Thus, not only the gasification step, but the oxidation is proven to be also influenced by the gasification agent.

Besides, when gasifying with 100% steam some $H_2$ was measured, but for the $H_2O$:$CO_2$ mixtures no $H_2$ was measured in the product gas. Here, the water-gas shift (WGS) reaction, see Eq. (26), it is believed to have low relevance in the CO generation because the gas composition is far away from WGS equilibrium. This is confirmed by the small amounts of $H_2$ obtained in the reactor outlet.

$$H_2O + CO \leftrightarrow H_2 + CO_2 \quad (26)$$

In addition, it can be seen in Fig. 11 that the combustion efficiency is maintained roughly constant with the char conversion, although the flow of gasification products, i.e. $H_2$ and CO, decreased as char is being converted. Thus, a constant amount of ilmenite (that existing in the reactor) is not able to better oxidize a lower flow of reacting gas (that is $H_2$ and CO). This means that the rate of oxygen transferred from ilmenite to the fuel, $r_O$, decreases as the amount of char remaining in the bed decreases. This decrease in the reaction rate of ilmenite is due to a lower concentration of $H_2$ and CO in the reacting gas mixture.

### *4.4. Effect of the reacting temperature*

The effect of the reacting temperature on the gasification rate and the subsequent conversion of gasification products by reaction with ilmenite particles were studied in the batch fluidized bed. Fig. 13 shows the instantaneous rate of char conversion, $r_{C,inst}(t)$, as a function of the char conversion when the reactor temperature was 900, 950

or 1000ºC and fluidizing gas was steam or $CO_2$. It can be seen an important increase in the rate of char conversion with temperature when steam is used as gasifying agent. Thus, the average $r_{C,inst}$ value increases from 10.9 %/min at 900ºC up to 37.3 %/min at 1000ºC. The values here obtained are in concordance with the previous results and evidence the great influence of the temperature in the gasification process [10,20]. On the contrary, the gasification rate with $CO_2$ is not increased in the same proportion. Thus, the average $r_{C,inst}$ value increases from 3.4 %/min at 900ºC up to 6.9 %/min at 1000ºC. Table 4 resumes the average $r_{C,inst}$ values for the different temperatures. The apparent activation energy, $E_a$, can be calculated from these values assuming an Arrhenius type dependence with the temperature, thus calculating that $E_a$ = 162 kJ/mol for steam gasification and $E_a$ = 88 kJ/mol for gasification with $CO_2$.

Table 4 shows the $t_{50}$ and $t_{95}$ values for the different tests performed at various temperatures with steam and $CO_2$ as gasification agents. It can be seen that high temperature using steam as gasification agent is preferred in order to reduce the residence time of char particles to be gasified. So, the residence time to convert 95 % of char fed to the reactor is 7.8 min at 1000ºC for char particles used (+100-200 μm) using steam, whereas 43.4 min should be necessary using $CO_2$.

Regarding the oxidation of gasification products by reaction with ilmenite, Fig. 14 shows the combustion efficiency, $\eta_c$, at different temperatures when the fluidization gas was steam or $CO_2$. For both gasification agents the combustion efficiencies are promoted with the temperature, as ilmenite reacts faster at higher temperatures. However, the dependence of $\eta_c$ with temperature was of lower relevance that those showed for char gasification, see Fig. 13. The combustion efficiency for steam is very high and increases from about 89% at 900ºC to 95% at 1000ºC. For $CO_2$ $\eta_c$ rises from about 59% at 900ºC to 65% at 1000ºC. $H_2$ is generated as a gasification product when $H_2O$ is present in the fluidizing gas, whereas CO is the only gasification product when using $CO_2$. In a previous study on ilmenite kinetics, $H_2$ was proved to have higher reaction rate ilmenite than CO [31]. The differences seen in the combustion efficiencies when using $H_2O$ or $CO_2$ as fluidizing agents lie in the generation of the more reactive gas $H_2$ when gasifying with $H_2O$.

*4.5. Theoretical approach*

The conversion of char in the fuel-reactor will determine the carbon capture efficiency of the CLC system with coal. A theoretical study in the fuel-reactor was done to get further valuable information about the char conversion in the CLC system. Considering the fuel-reactor as control volume, the simplified mass balance for carbon in char can be expressed with Eq. (27).

$$F_{C,in} + F_{C,r} = F_{C,out} + F_{C,g} \tag{27}$$

The carbon inlet flows to the fuel-reactor are: (1) the incoming carbon flow in char with the coal feed, $F_{C,in}$, and (2) the carbon flow that is separated by the carbon stripper and recirculated back to the fuel-reactor, $F_{C,r}$. The carbon outlet flows from the fuel-reactor are: (1) the remaining carbon in char exiting the fuel-reactor, $F_{C,out}$, and (2) the gasified carbon, exiting as part of the product gas, $F_{C,g}$. The following carbon balance was done to the carbon stripper:

$$F_{C,out} = F_{C,AR} + F_{C,r} = \frac{F_{C,AR}}{1-\eta_{CS}} = \frac{F_{C,r}}{\eta_{CS}} \tag{28}$$

$F_{C,AR}$ being the carbon flow passing to the air-reactor and $\eta_{CS}$ the efficiency of separation in the carbon stripper. The flow of gasified carbon was calculated as

$$F_{C,g} = r_{C,inst} \cdot m_C \tag{29}$$

$r_{C,inst}$ being the instantaneous char gasification rate, as defined in Eq. (15), and $m_C$ the mass of carbon in the fuel-reactor. $m_C$ was calculated assuming that a perfect mixing of solids in the fuel-reactor and a constant reaction rate for the char particles. Thus, the carbon concentration in the fuel-reactor, $C_C$, is equal to that in the outlet stream of solids.

$$C_C = \frac{F_{C,out}}{F_{ilm} + F_{C,out}} = \frac{m_C}{m_{ilm} + m_C} \tag{30}$$

$F_{ilm}$ being the circulation flow of ilmenite and $m_{ilm}$ the mass of ilmenite in the fuel-reactor. After some algebra arrangements with Eqs. (27-30), char conversion, $X_C$, is calculated as:

$$X_C = \frac{F_{C,in} - F_{C,AR}}{F_{C,in}} = 1 - \frac{F_{ilm}(1-\eta_{CS})}{r_{C,inst} \cdot m_{ilm} + F_{ilm}(1-\eta_{CS})} \quad (31)$$

Char conversion was defined as the fraction of carbon introduced with the char feed that exits as gaseous product from the fuel-reactor. Thus, char conversion can be easily calculated knowing the char gasification rate, $r_{C,inst}$, and giving some design and operational parameters, i.e. the circulation flow rate of ilmenite, $F_{ilm}$, the ilmenite inventory in the fuel-reactor, $m_{ilm}$, and the carbon stripper efficiency, $\eta_{CS}$.

The reactivity data showed in this work for char from a South African coal were used to calculate the char conversion at different operating conditions, see $r_{C,inst}$ in Tables 3 and 4. Table 5 shows the proximate and ultimate analysis of this coal. Taking 1 $MW_{th}$ as reference value and considering $R_{O,ilm}$=4.0 wt%, the stoichiometric circulation flow rate of ilmenite to fully convert coal to $CO_2$ and $H_2O$ was 2.1 kg/s, i.e. with an oxygen-carrier to fuel ratio $\phi$ = 1. Abad et al. [24] showed that the optimum oxygen-carrier to fuel ratio was in the range 2.5 to 5. Thus, a $\phi$ value of 3 was here chosen for simulations. In addition, 200 kg/$MW_{th}$ was considered as ilmenite inventory during first approach. In a previous work, it was estimated that 200 kg/$MW_{th}$ would be enough to burn 95% of the gasification products [31].

Firstly, it was considered that the system had no carbon stripper, i.e. $\eta_{CS}$ = 0. Fig. 15a) shows the effect of temperature in the calculated char conversion using steam or $CO_2$ as gasification agents. It can be seen that the char conversion reached a very low value even at 1000ºC with steam as gasification agent, for which only 17% of char is gasified. Lower values were obtained at lower temperatures or using $CO_2$ as gasification agent because of the lower gasification reactivity. This fact evidences the need of a carbon stripper unit in order to separate a fraction of the non-gasified char and re-introduce it to the fuel-reactor. Thus, the residence time of char particles in the fuel-reactor will be

increased. Fig. 15b) shows the char conversion with steam at 1000ºC as a function of the carbon stripper efficiency, $\eta_{CS}$. The char conversion is correspondingly increased with the carbon stripper efficiency. If 90% of char conversion is desired, the carbon stripper efficiency must be about 95%. Obviously, if the carbon separation efficiency is $\eta_{CS}$ = 1, all carbon is gasified and no carbon is passing to the air-reactor. Fig. 15b) also shows the carbon concentration in the fuel-reactor. Thus, the carbon concentration increases with the carbon stripper efficiency. This fact will be relevant for the carbon stripper design.

Considering a reasonable carbon stripper efficiency of 90%, in order to ensure high char conversion efficiencies, higher ilmenite inventories are needed. Fig. 15c) displays the char conversion with steam at 1000ºC calculated for increasing ilmenite inventory ($\eta_{CS}$ = 90%). The char conversion rapidly increases until a solids inventory about 500-1000 kg/$MW_{th}$. Thus, the char conversion increased from 67% with 200 kg/$MW_{th}$ to 91% with 1000 kg/$MW_{th}$. Further increase in the solids inventory has a minor effect on the char conversion. To increase the solids inventory above 1000 kg/$MW_{th}$ would not be therefore recommended.

These results show the reliability of the process using ilmenite as oxygen-carrier. High carbon capture efficiency can be obtained or by optimizing the carbon stripper design or by increasing the solids inventory. The following question is to know the fraction of gasification products that will be converted to $CO_2$ and $H_2O$ by reaction with ilmenite particles. This task needs to consider simultaneously the reaction kinetics of the gaseous products with ilmenite and the gas flow throughout the reactor.

## 5. Conclusions

An analysis of the char gasification in presence of ilmenite particles –which act as oxygen-carrier– was carried out to determine key parameters in Chemical-Looping Combustion of coal. Both, char gasification and ilmenite reactivity were evaluated through consecutive redox cycles using char particles coming from devolatilization of South African bituminous coal. The activation process of ilmenite particles as well as the effects of the fluidization gas and temperature were studied.

For the reduction reaction, ilmenite increases its reactivity relatively fast during the initial redox cycles. Seven redox cycles are enough to fully activate ilmenite particles when coal char was used as fuel. However, ilmenite was not activated yet for the oxidation reaction even after 16 redox cycles, because of the low variation of the ilmenite conversion in every cycle. At this condition, porosity was not developed at enough extension to overcome diffusion restrictions in the oxidation reaction. Besides, the oxygen transport capacity of the ilmenite particles barely changed with the redox cycles.

Regarding the char conversion, lower concentration of $H_2$ and CO enhanced the gasification reaction. Thus, a relevant increase in the gasification rate was observed when ilmenite instead of an inert substance was used as bed material. Moreover, the gasification rate itself raises slightly by the increase of ilmenite reaction rate during activation period, and gasification is improved as the generated $H_2$ and CO decreases with the char conversion.

Steam is preferred as gasification agent as $CO_2$, since gasification rate is higher. Even if low fraction of $CO_2$ was present in the feeding gas stream, the gasification rate was appreciably decreased. In addition, high temperature enhanced in high extent the steam gasification. Thus, the residence time to convert 95 % of char fed was decreased from 27.5 min at 900ºC to 7.8 min at 1000ºC using char from South African bituminous coal (+100-200 μm).

The later combustion of the gasification products with ilmenite is also influenced by the gasifying agent, as gasification with $H_2O$ generates more $H_2$ that is more reactive with ilmenite and on the other hand gasification with $CO_2$ produces more CO. The resulting combustion efficiency is therefore higher when gasifying with increasing $H_2O/CO_2$ ratio. Moreover, the combustion efficiencies have turned out to be quite constant as char is further converted. A rise in the operation temperature also causes an increase in the combustion efficiencies, since ilmenite reaction rates are promoted.

A mass balance to the fuel-reactor and carbon stripper was done in order to know the conversion of char in the system. The use of a carbon stripper was found to be essential in order to reach high values of char conversion by gasification in the fuel-reactor. The

optimal range of solids inventory in the fuel-reactor that leads to high char conversions (around 90%) was found in the range 500-1000 kg/$MW_{th}$.

**Notation**

$C_C$ = char concentration in the fuel reactor bed

$F_{CO_2,in}$ = $CO_2$ flow introduced in the fuel reactor (mol/s)

$F_{C,AR}$ = carbon flow in char that enters the air reactor (mol/s)

$F_{C,g}$ = gasified carbon flow exiting as part of the product gas (mol/s)

$F_{C,in}$ = carbon flow in char fed with the fuel flow (mol/s)

$F_{C,out}$ = carbon flow in char leaving the fuel reactor (mol/s)

$F_{C,r}$ = carbon flow in char recirculated back to the fuel reactor (mol/s)

$F_{H_2O,in}$ = $H_2O$ flow introduced in the fuel reactor (mol/s)

$F_{H_2O,out}$ = molar gas flow of $H_2O$ in the product gas (mol/s)

$F_i$ = molar gas flow of each component $i$ ($CO_2$, CO, $H_2$ or $CH_4$) in the product gas (mol/s)

$F_{ilm}$ = ilmenite flow between reactors (mol/s)

$F_{N_2}$ = downstream introduced $N_2$ flow (mol/s)

$F_{O_2,in}$ = total introduced oxygen flow in the fuel reactor (mol $O_2$/s)

$F_{O_2,out}$ = total oxygen flow exiting the fuel reactor (mol $O_2$/s)

$F_{out}$ = total dry basis outlet gas flow (mol/s)

$m$ = instantaneous mass of the ilmenite sample (kg)

$m_C$ = mass of char in the fuel reactor bed (kg)

$Me_xO_y$ = oxidized form of the oxygen carrier

$Me_xO_{y-1}$ = reduced form of the oxygen carrier

$m_{ilm}$ = ilmenite inventory in the fuel reactor (kg/$MW_{th}$)

$m_o$ = mass of the oxidized form of the oxygen carrier (kg)

$m_r$ = mass of the reduced form of the oxygen carrier (kg)

$N_{0,ilm}$ = molar amount of oxygen in ilmenite active for CLC process (mol)

$N_{C,char}$ = mol number of carbon fed into the reactor (mol)

$R_{0,ilm}$ = oxygen transport capacity of ilmenite

$r_C(t)$ = rate of char conversion (mol/s)

$r_{C,inst}$ = instantaneous rate of char conversion ($s^{-1}$)

$r_O(t)$ = rate of oxygen transferred from ilmenite to the fuel gas (mol/s)

t = time (s)

$t_{50}$ = time to convert 50% char (s)

$t_{95}$ = time to convert 95% char (s)

$t_X$ = residence time to reach a conversion $X_t$

$X_{char}$ = char conversion

$X_{ox}$ = conversion of ilmenite for the oxidation reaction

$X_{red}$ = conversion of ilmenite for the reduction reaction

$X_t$ = char conversion reached with a residence time $t_X$

$y_i$ = being the molar fraction of the component $i$ ($CO_2$, CO, $H_2$ or $CH_4$) in the product gas

$\eta_{CS}$ = carbon stripper efficiency

$\eta_C$ = combustion efficiency

**Acknowledgments**

This work was partially supported by the European Commission, under the RFCS program (ECLAIR Project, Contract RFCP-CT-2008-0008), from Alstom Power Boilers and by the Spanish Ministry of Science and Innovation (Project ENE2010-19550). A. Cuadrat thanks CSIC for the JAE Pre. fellowship. Alberto Abad thanks to the Ministerio de Ciencia e Innovación for the financial support in the course of the I3 Program.

**References**

[1] IPCC Fourth Assessment Report – Climate Change 2007. Summary for Policymakers. Available at http://www.ipcc.ch.

[2] IEA Statistics. CO2 emissions from fuel combustion – Highlights. 2010 edition. Available at http://www.iea.org/co2highlights/co2highlights.pdf

[3] Energy Technology Perspectives 2008: Scenarios and strategies to 2050. Executive Summary. IEA.

[4] Lyngfelt A. Oxygen carriers for chemical-looping combustion – operational experience. Proceedings of the 1st International Conference on Chemical Looping, Lyon (France), 2010.

[5] Fan L-S, Li F. Chemical Looping Technology and Its Fossil Energy Conversion Applications. Ind Eng Chem Res 2010; 49 (21):10200–10211.

[6] Cao Y, Pan WP. Investigation of Chemical Looping Combustion by Solid Fuels. 1.Process Analysis. Energy Fuels 2006;20:1836-1844.

[7] Cao Y, Casenas B, Pan WP. Investigation of Chemical Looping Combustion by Solid Fuels. 2. Redox Reaction Kinetics and Product Characterization with Coal, Biomass, and Solid Waste as Solid Fuels and CuO as an Oxygen Carrier. Energy Fuels 2006;20:1845-1854.

[8] Dennis JS, Scott SA, Hayhurst AN. In situ gasification of coal using steam with chemical looping: a technique for isolating CO2 from burning a solid fuel. J Energy Inst 2006;79:187-190.

[9] Scott SA, Dennis JS, Hayhurst AN, Brown T. In Situ Gasification of a Solid Fuel and CO2 Separation using Chemical Looping. AIChE J 2006;52:3325-3328.

[10] Leion H, Mattisson T, Lyngfelt A. The use of petroleum coke as fuel in chemical-looping combustion. Fuel 2007;86:1947-1958.

[11] Berguerand N, Lyngfelt A. Design and operation of a 10 kWth chemical-looping combustor for solid fuels – Testing with South African coal. Fuel 2008;87:2713-2726.

[12] Berguerand N, Lyngfelt A. The use of petroleum coke as fuel in a 10 kWth chemical-looping combustor. Int J Greenhouse Gas Control 2008;2:169-179.

[13] Berguerand N, Lyngfelt A. Chemical-Looping Combustion of Petroleum Coke Using Ilmenite in a 10 kWth Unit – High-Temperature Operation. Energy Fuels 2009;23:5257-5268.

[14] Markström P, Berguerand N, Lyngfelt A. The application of a multistage-bed model for residence-time analysis in chemical-looping combustion of solid fuel. Chem Eng Sci 2010;65:5055-66.
[15] Cuadrat A, Abad A, García-Labiano F, Gayán P, de Diego LF, Adánez J. The use of ilmenite as oxygen-carrier in a 500 Wth Chemical Looping Coal Combustion unit. Submitted to publish.
[16] Berguerand N, Lyngfelt A. Batch testing of solid fuels with ilmenite in a 10 kWth chemical-looping combustor. Fuel 2010;89:1749-62.
[17] Azis MM, Jerndal E, Leion H, Mattisson T, Lyngfelt A. On the evaluation of synthetic and natural ilmenite using syngas as fuel in chemical-looping combustion (CLC). Chem Eng Res Des 2010; 88(11):1505-1514.
[18] Brown TA, Dennis JS, Scott SA, Davidson JF, Hayhurst AN. Gasification and Chemical-Looping Combustion of a Lignite Char in a Fluidized Bed of Iron Oxide. Energy & Fuels 2010;24:3034-48.
[19] Bidwe AR, Mayer F, Hawthorne C, Charitos A, Schuster A, Scheffknecht G. Use of ilmenite as an oxygen carrier in Chemical Looping Combustion – Batch and continuous dual fluidized bed investigation. Energy Procedia 2010, in press.
[20] Leion H, Mattisson T, Lyngfelt A. Solid fuels in chemical-looping combustion. Int J Greenhouse Gas Control 2008;2:180-193.
[21] Leion H, Lyngfet A, Mattisson T. Solid fuels in chemical-looping combustion using a NiO-based oxygen carrier. Chem Eng Res Des 2009;87:1543-1550.
[22] Gao Z, Shen L, Xiao J, Qing C, Song Q. Use of Coal as Fuel for Chemical-Looping Combustion with Ni-Based Oxygen Carrier. Ind Eng Chem Res 2008;47:9279-9287.
[23] Shen L, Wu J, Xiao J. Experiments on chemical looping combustion of coal with a NiO based oxygen carrier. Combustion and Flame 2009;156:721-728.
[24] Abad A, Adánez J, García-Labiano F, de Diego LF, Gayán P, Celaya J. Mapping of the range of operational conditions for Cu-, Fe-, and Ni-based oxygen carriers in chemical-looping combustion. Chem Eng Sci 2007;62:533-549.
[25] Leion H, Lyngfelt A, Johansson M, Jerndal E, Mattisson T. The use of ilmenite as an oxygen carrier in chemical-looping combustion. Chem Eng Res Des 2008;86:1017-26.

[26] Adánez J, Cuadrat A, Abad A, Gayán P, de Diego L.F, García-Labiano F. Ilmenite Activation during Consecutive Redox Cycles in Chemical-Looping Combustion. Energy & Fuel 2010;24:1402-1413.
[27] Leion H, Jerndal E, Steenari B-M, Hermansson S, Israelsson M, Jansson E, Johnsson M, Thunberg R, Vadenbo A, Mattisson T, Lyngfelt A. Solid fuels in chemical-looping combustion using oxide scale and unprocessed iron ore as oxygen carriers. Fuel 2009;88:1945-1954.
[28] Linderholm C, Cuadrat A, Lyngfelt A. Chemical-looping combustion of solid fuels in a 10 kWth pilot – batch tests with five fuels. Energy Procedia 2010, in press.
[29] Leion H, Mattisson T, Lyngfelt A. Effects of steam and CO2 in the fluidizing gas when using bituminous coal in chemical-looping combustion. Proceedings of the 20th International Conference on Fluidized Bed Combustion, Xian (China), 2009, 608-611.
[30] Pröll T, Mayer K, Bolhàr-Nordenkampf J, Kolbitsch P, Mattisson T, Lyngfelt A, Hofbauer H. Natural minerals as oxygen carrier for chemical looping combustion in a dual circulating fluidized bed system. GHGT-9. Energy Procedia 2009;1:27-34.
[31] Abad A, Adánez J, Cuadrat A, García-Labiano F, Gayán P, de Diego LF. Kinetics of redox reactions of ilmenite for Chemical-Looping Combustion. . Chem Eng Sci 2011;66(4):689-702.
[32] Johnson JL. Fundamentals of coal gasification. In: (2nd ed.) Elliot MA, editor. Chemistry of Coal Utilization (second supplementary volume), New York: John Wiley and Sons; 1981. 1491-1598.
[33] Cuadrat A, Abad A, Gayán P, de Diego LF, García-Labiano F, Adánez J. Modeling and optimization of Chemical Looping Combustion for solid fuels with ilmenite as oxygen carrier. International Conference on Coal Science & Technology (ICCS&T), October 2011.
[34] Siriwardane R, Tian H, Richards G, Simonyi T, Poston J. Chemical-Looping Combustion of Coal with Metal Oxide Oxygen Carriers. Energy & Fuels 2009;23:3885-92.
[35] Siriwardane R, Tian H, Miller D, Richards G, Simonyi T, Poston J. Investigation on Reaction Mechanism of Chemical-Looping Combustion of Coal Utilizing Oxygen Carriers. Proceedings of the 1st International Conference on Chemical Looping, Lyon, 2010.
[36] Adánez J, Miranda JL, Gavilán JM. Kinetics of a lignite-char gasification by CO2. Fuel 1985;64:801-4.

Design Considerations for Chemical-Looping Combustion of coal – Part 1. Experimental Tests.

Ana Cuadrat*, Alberto Abad, Juan Adánez, Luis F. de Diego, Francisco García-Labiano, Pilar Gayán.

**Tables**

**Table 1.** Chemical and physical properties of pre-oxidized ilmenite.

**Table 2.** Proximate and ultimate analysis (% weight) of char from devolatizing South African coal.

**Table 3.** Average values of the instantaneous rate of char conversion, $r_{C,inst}(t)$, half-life time, $t_{50}$ and residence time to convert 95% of char, $t_{95}$, at different $H_2O$:$CO_2$ ratios. $T$ = 900ºC.

**Table 4.** Average values of the instantaneous rate of char conversion, $r_{C,inst}(t)$, half-life time, $t_{50}$ and residence time to convert 95% of char, $t_{95}$, at different temperatures for $H_2O$ or $CO_2$ as gasification agent.

**Table 5.** Proximate and ultimate analysis (% weight) of South African coal.

Design Considerations for Chemical-Looping Combustion of coal – Part 1. Experimental Tests.

Ana Cuadrat*, Alberto Abad, Juan Adánez, Luis F. de Diego, Francisco García-Labiano, Pilar Gayán.

**Table 1.** Chemical and physical properties of pre-oxidized ilmenite.

| | |
|---|---|
| XRD (main species) | $Fe_2TiO_5$, $Fe_2O_3$, $TiO_2$ |
| Oxygen transport capacity, $R_{O,ilm}$ (%) | 4.0 |
| Particle diameter (μm) | 150-300 |
| True density (kg/m$^3$) | 4100 |
| Porosity (%) | 1.2 |
| BET Surface (m$^2$/g) | 0.8 |
| Crushing strength (N) | 2.2 |

**Table 2.** Proximate and ultimate analysis (% weight) of char from devolatizing South African coal.

| Proximate analysis | |
|---|---|
| Water content | 0.9 |
| Ash | 20.0 |
| Volatile matter | 1.1 |
| Fixed carbon | 78.0 |
| Ultimate analysis | |
| Carbon | 76.5 |
| Hydrogen | 0.2 |
| Nitrogen | 1.6 |
| Sulfur | 0.8 |

**Table 3.** Average values of the instantaneous rate of char conversion, $r_{C,inst}(t)$, half-life time, $t_{50}$ and residence time to convert 95% of char, $t_{95}$, at different $H_2O$:$CO_2$ ratios. $T$ = 900ºC.

| $H_2O$:$CO_2$ | 100:0 | 90:10 | 70:30 | 50:50 | 0:100 |
|---|---|---|---|---|---|
| $r_{C,inst}$ (%/min) | 10.9 | 8.1 | 5.7 | 4.8 | 3.4 |
| $t_{50}$ (min) | 6.4 | 8.6 | 12.2 | 14.4 | 20.4 |
| $t_{95}$ (min) | 27.5 | 37.0 | 52.6 | 62.4 | 88.1 |

Design Considerations for Chemical-Looping Combustion of coal – Part 1. Experimental Tests.

Ana Cuadrat*, Alberto Abad, Juan Adánez, Luis F. de Diego, Francisco García-Labiano, Pilar Gayán.

**Table 4.** Average values of the instantaneous rate of char conversion, $r_{C,inst}(t)$, half-life time, $t_{50}$ and residence time to convert 95% of char, $t_{95}$, at different temperatures for $H_2O$ or $CO_2$ as gasification agent.

| Gasification agent | $H_2O$ | | | $CO_2$ | | |
|---|---|---|---|---|---|---|
| Temperature (ºC) | 900 | 950 | 1000 | 900 | 950 | 1000 |
| $r_{C,inst}$ (%/min) | 10.9 | 24.0 | 37.3 | 3.4 | 5.2 | 6.9 |
| $t_{50}$ (min) | 6.4 | 2.9 | 1.8 | 20.4 | 13.3 | 10.0 |
| $t_{95}$ (min) | 27.5 | 12.5 | 7.8 | 88.1 | 57.6 | 43.4 |

**Table 5.** Proximate and ultimate analysis (% weight) of South African coal.

| Proximate analysis | |
|---|---|
| Water content | 4.2 |
| Ash | 14.3 |
| Volatile matter | 25.5 |
| Fixed carbon | 56.0 |
| Ultimate analysis | |
| Carbon | 69.3 |
| Hydrogen | 4.0 |
| Nitrogen | 2.0 |
| Sulfur | 1.0 |
| LHV (kJ/kg) | 25500 |

Design Considerations for Chemical-Looping Combustion of coal – Part 1. Experimental Tests.

Ana Cuadrat*, Alberto Abad, Juan Adánez, Luis F. de Diego, Francisco García-Labiano, Pilar Gayán.

**Captions of figures**

**Fig. 1.** Reactor scheme of Chemical-Looping Combustion using solid fuels (- - - optional stream).

**Fig. 2.** Schematic layout of the laboratory setup.

**Fig. 3.** Molar flow evolution with time of a) $CO_2$, b) CO and c) $H_2$ in the gas product during the initial 10 reduction cycles. The intervals between reducing periods have been removed. Every cycle consisted of 2 loads of char, 1.5 g each one. Gasification agent: steam. $T$ = 900ºC.

**Fig. 4.** Conversion of (a) reduction, Xred, and (b) oxidation, Xox, with time of ilmenite after 1, 3, 7, 10, 13 and 16 redox cycles using char as fuel and steam as fluidizing gas. The corresponding curves for pre-oxidized ilmenite and fully activated ilmenite are also showed. Reducing gas: 5% $H_2$ + 40% $H_2O$. Nitrogen to balance. Oxidation gas: air. $T$ = 900ºC.

**Fig. 5.** SEM images of (a) detail of the external surface, (b) detail of the cross section inside the particles and (c) cross section of a particle for pre-oxidized ilmenite, after 3 cycles and after 13 cycles using coal char as fuel.

**Fig. 6.** Evolution of the rate of char conversion with time during the initial 10 reduction cycles. Every cycle consisted of 2 loads of char, 1.5 g each one. Gasification agent: steam. $T$ = 900ºC.

**Fig. 7.** Gas flow evolution with char conversion of a) $CO_2$, b) CO and c) $H_2$ in the gas product during char conversion using activated ilmenite (——) or sand (– – –) as bed material. Loads of 1.5 g char. Gasification agent: steam. $T$ = 900ºC.

**Fig. 8.** Instantaneous rate of char conversion, $r_{C,inst}(t)$, as a function of the char conversion with activated ilmenite and sand as bed materials. Loads of 1.5 g char. Gasification agent: steam. $T$ = 900ºC.

**Fig. 9.** Instantaneous rate of char conversion, $r_{C,inst}(t)$, as a function of the char conversion with activated ilmenite as bed material when different $H_2O$:$CO_2$ ratios was used, corresponding to that showed in Table 3. Loads of 1.5 g char. $T$ = 900ºC.

**Fig. 10.** Char conversion vs. time curves for different $H_2O$:$CO_2$ ratios. Activated ilmenite as bed material. Loads of 1.5 g char. $T$ = 900ºC.

**Fig. 11.** Combustion efficiency as a function of the char conversion for several $H_2O$:$CO_2$ ratios. Activated ilmenite as bed material. Loads of 1.5 g char. $T$ = 900ºC.

**Fig. 12.** Evolution with time of the flow of CO exiting from the reactor for different $H_2O$:$CO_2$ ratios. Activated ilmenite as bed material. Loads of 1.5 g char. $T$ = 900ºC.

**Fig. 13.** Instantaneous rate of char conversion, $r_{C,inst}(t)$, as a function of the char conversion at 900, 950 and 1000ºC. Fluidizing agent: (a) $H_2O$; (b) $CO_2$. Activated ilmenite as bed material. Loads of 1.5 g char.

**Fig. 14.** Combustion efficiency as a function of the char conversion at 900, 950 and 1000ºC. Fluidizing gas: a) $H_2O$; b) $CO_2$. Activated ilmenite as bed material. Loads of 1.5 g char.

**Fig. 15.** Conversion of char by gasification in the fuel-reactor as a function of a) temperature with steam or $CO_2$ as gasification agents and without carbon stripper; b) carbon stripper efficiency; and c) ilmenite inventory in the fuel-reactor with a carbon stripper efficiency of $\eta_{CS}$ = 90%. In Figs. a) and b) the solids inventory was 200 kg/$MW_{th}$. In Figs. b) and c) steam was the gasification agent and the temperature 1000ºC.

Design Considerations for Chemical-Looping Combustion of coal – Part 1. Experimental Tests.

Ana Cuadrat*, Alberto Abad, Juan Adánez, Luis F. de Diego, Francisco García-Labiano, Pilar Gayán.

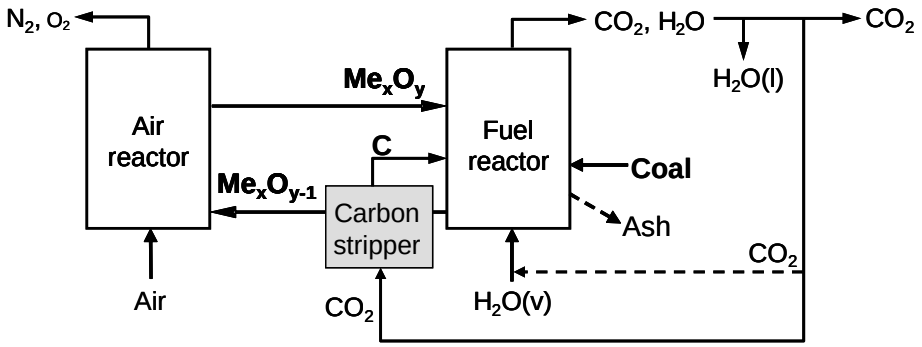


**Fig. 1.** Reactor scheme of Chemical-Looping Combustion using solid fuels (- - - optional stream).

Design Considerations for Chemical-Looping Combustion of coal – Part 1. Experimental Tests.

Ana Cuadrat*, Alberto Abad, Juan Adánez, Luis F. de Diego, Francisco García-Labiano, Pilar Gayán.

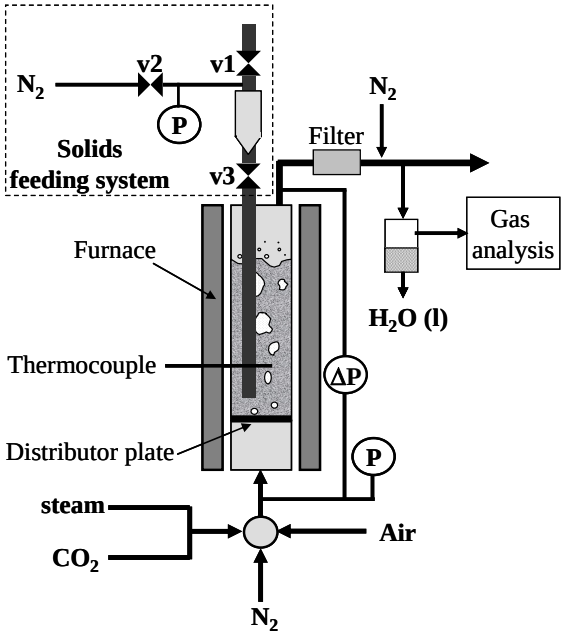


**Fig. 2.** Schematic layout of the laboratory setup.

Design Considerations for Chemical-Looping Combustion of coal – Part 1. Experimental Tests.

Ana Cuadrat*, Alberto Abad, Juan Adánez, Luis F. de Diego, Francisco García-Labiano, Pilar Gayán.

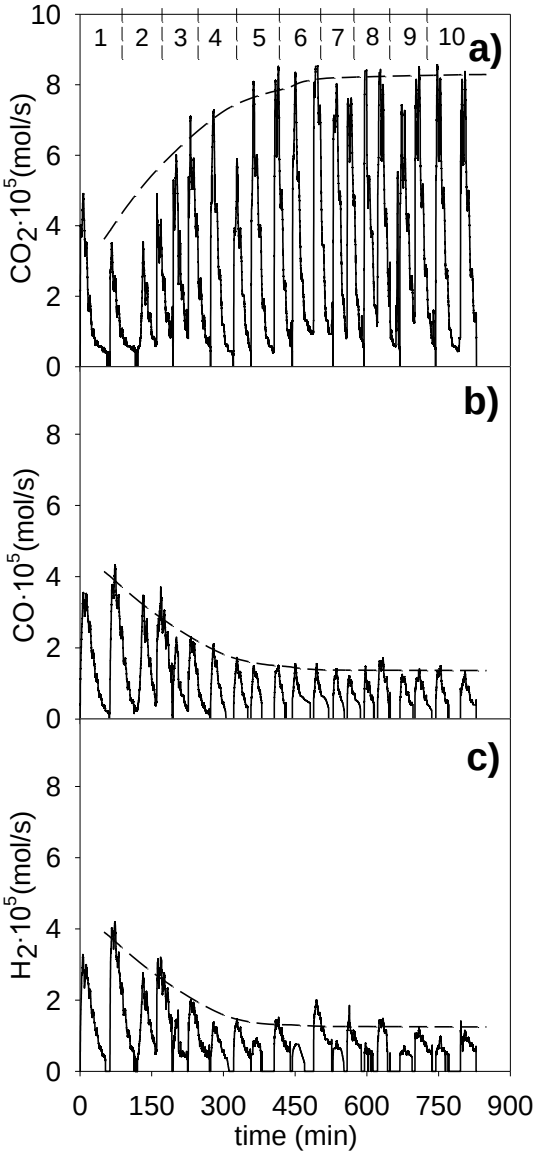


**Fig. 3.** Molar flow evolution with time of a) $CO_2$, b) CO and c) $H_2$ in the gas product during the initial 10 reduction cycles. The intervals between reducing periods have been removed. Every cycle consisted of 2 loads of char, 1.5 g each one. Gasification agent: steam. $T$ = 900ºC.

Design Considerations for Chemical-Looping Combustion of coal – Part 1. Experimental Tests.

Ana Cuadrat*, Alberto Abad, Juan Adánez, Luis F. de Diego, Francisco García-Labiano, Pilar Gayán.

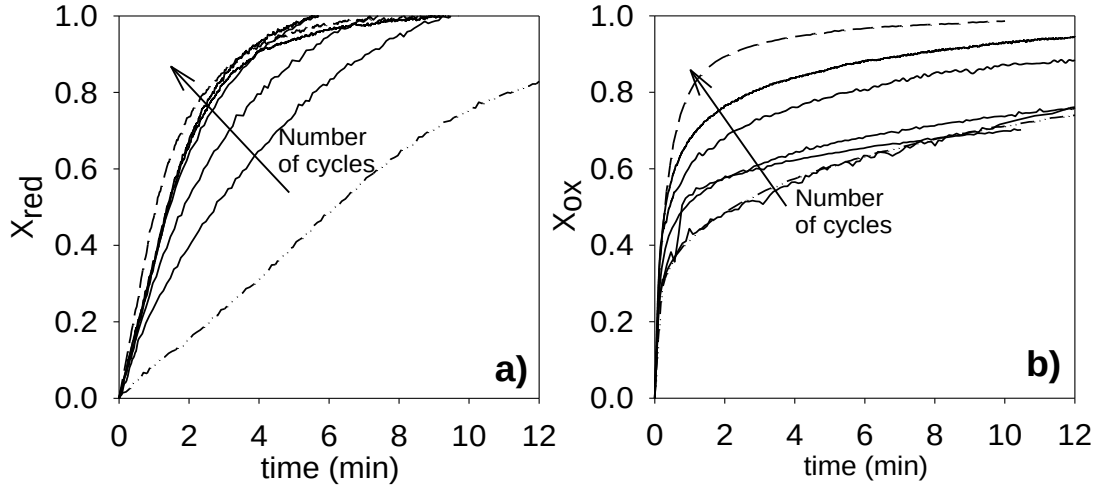


**Fig. 4.** Conversion of (a) reduction, $X_{red}$, and (b) oxidation, $X_{ox}$, with time of ilmenite after 1, 3, 7, 10, 13 and 16 redox cycles using char as fuel and steam as fluidizing gas. The corresponding curves for pre-oxidized ilmenite (–···–) and fully activated ilmenite (– – –) are also showed. Reducing gas: 5% $H_2$ + 40% $H_2O$. Nitrogen to balance. Oxidation gas: air. $T$ = 900ºC.

Design Considerations for Chemical-Looping Combustion of coal – Part 1. Experimental Tests.

Ana Cuadrat*, Alberto Abad, Juan Adánez, Luis F. de Diego, Francisco García-Labiano, Pilar Gayán.

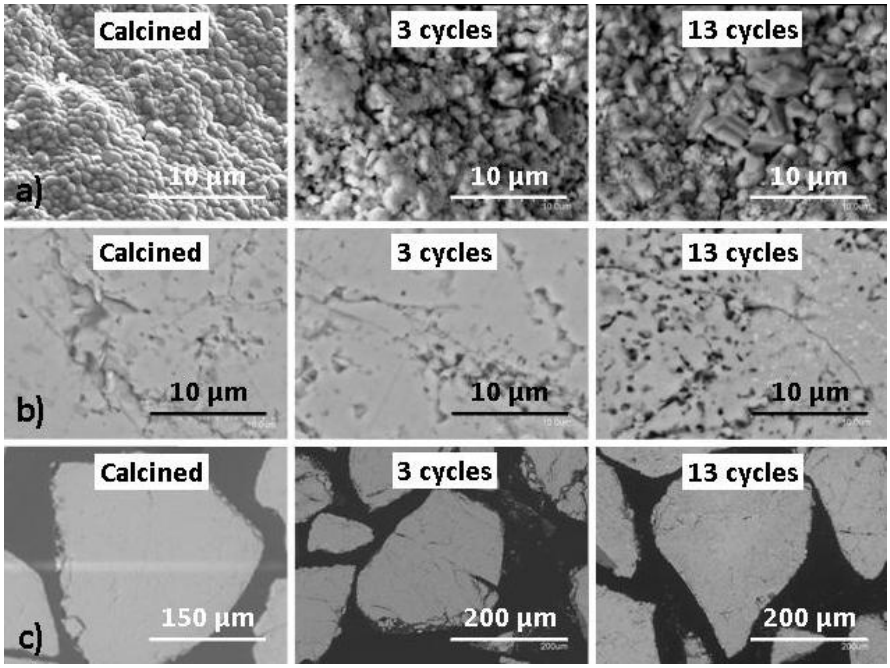


**Fig. 5.** SEM images of (a) detail of the external surface, (b) detail of the cross section inside the particles and (c) cross section of a particle for pre-oxidized ilmenite, after 3 cycles and after 13 cycles using coal char as fuel.

Design Considerations for Chemical-Looping Combustion of coal – Part 1. Experimental Tests.

Ana Cuadrat*, Alberto Abad, Juan Adánez, Luis F. de Diego, Francisco García-Labiano, Pilar Gayán.

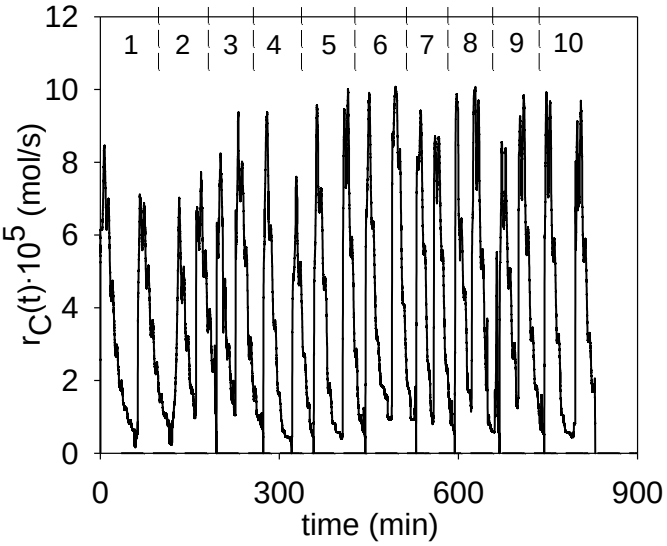


**Fig. 6.** Evolution of the rate of char conversion with time during the initial 10 reduction cycles. Every cycle consisted of 2 loads of char, 1.5 g each one. Gasification agent: steam. $T$ = 900ºC.

Design Considerations for Chemical-Looping Combustion of coal – Part 1. Experimental Tests.

Ana Cuadrat*, Alberto Abad, Juan Adánez, Luis F. de Diego, Francisco García-Labiano, Pilar Gayán.

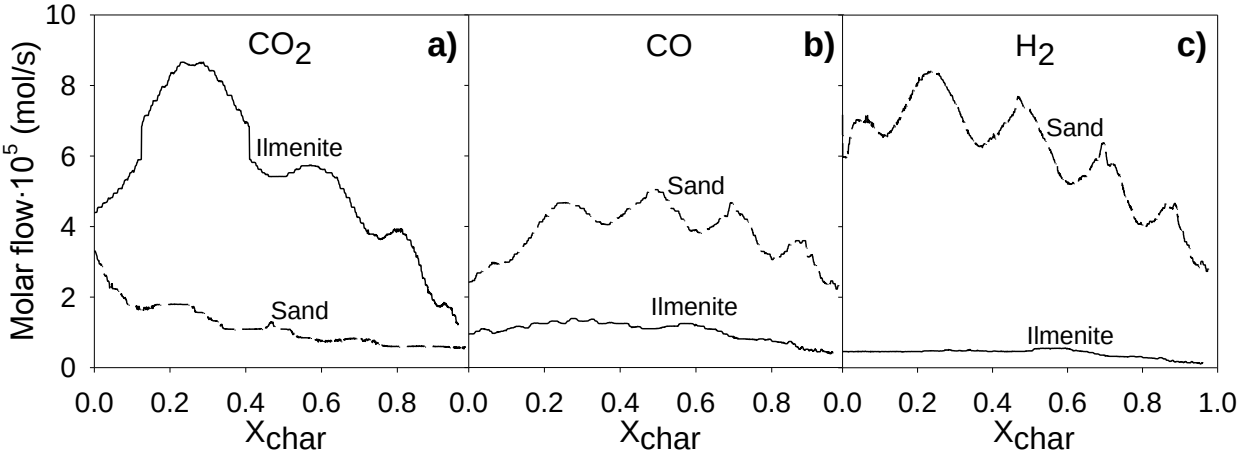


**Fig. 7.** Gas flow evolution with char conversion of a) $CO_2$, b) CO and c) $H_2$ in the gas product during char conversion using activated ilmenite (——) or sand (– – –) as bed material. Loads of 1.5 g char. Gasification agent: steam. $T$ = 900ºC.

Design Considerations for Chemical-Looping Combustion of coal – Part 1. Experimental Tests.

Ana Cuadrat*, Alberto Abad, Juan Adánez, Luis F. de Diego, Francisco García-Labiano, Pilar Gayán.

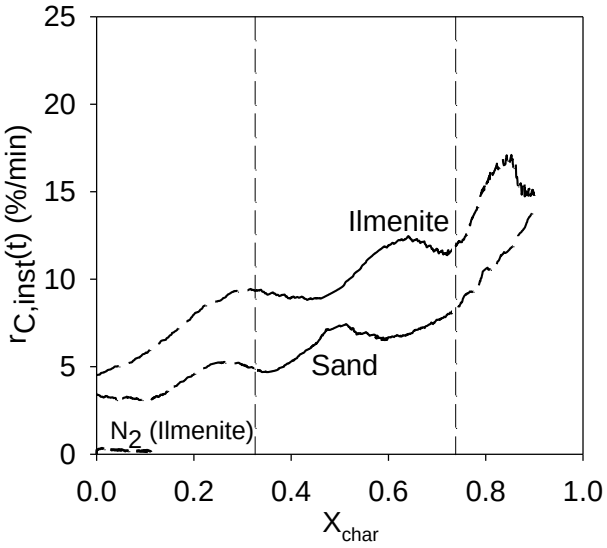


**Fig. 8.** Instantaneous rate of char conversion, $r_{C,inst}(t)$, as a function of the char conversion with activated ilmenite and sand as bed materials. Loads of 1.5 g char. Gasification agent: steam. $T$ = 900ºC.

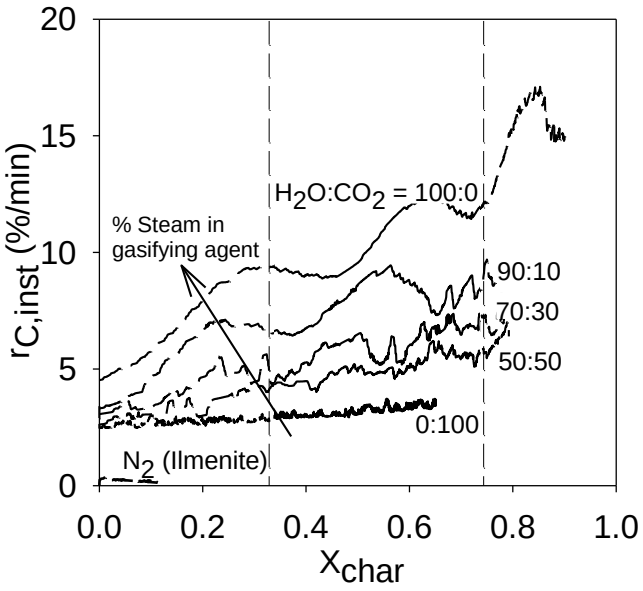


**Fig. 9.** Instantaneous rate of char conversion, $r_{C,inst}(t)$, as a function of the char conversion with activated ilmenite as bed material when different $H_2O:CO_2$ ratios was used, corresponding to that showed in Table 3. Loads of 1.5 g char. $T$ = 900ºC.

Design Considerations for Chemical-Looping Combustion of coal – Part 1. Experimental Tests.

Ana Cuadrat*, Alberto Abad, Juan Adánez, Luis F. de Diego, Francisco García-Labiano, Pilar Gayán.

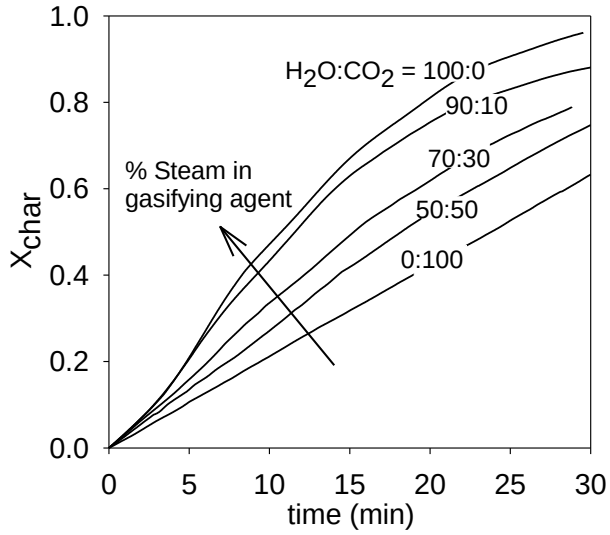


**Fig. 10.** Char conversion vs. time curves for different $H_2O:CO_2$ ratios. Activated ilmenite as bed material. Loads of 1.5 g char. $T$ = 900ºC.

Design Considerations for Chemical-Looping Combustion of coal – Part 1. Experimental Tests.

Ana Cuadrat*, Alberto Abad, Juan Adánez, Luis F. de Diego, Francisco García-Labiano, Pilar Gayán.

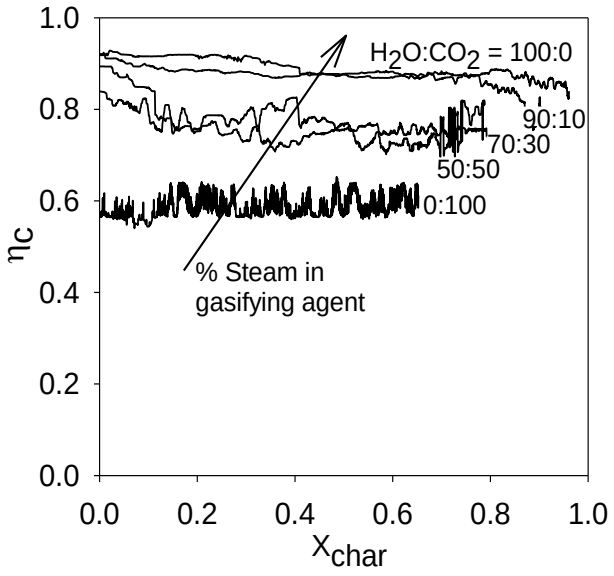


**Fig. 11.** Combustion efficiency as a function of the char conversion for several $H_2O$:$CO_2$ ratios. Activated ilmenite as bed material. Loads of 1.5 g char. $T$ = 900ºC.

Design Considerations for Chemical-Looping Combustion of coal – Part 1. Experimental Tests.

Ana Cuadrat*, Alberto Abad, Juan Adánez, Luis F. de Diego, Francisco García-Labiano, Pilar Gayán.

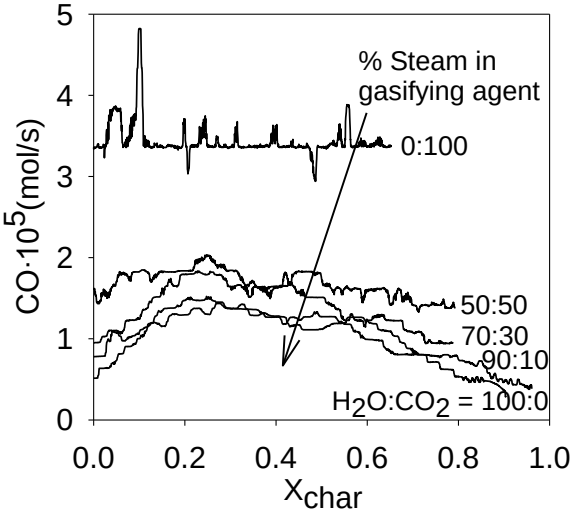


**Fig. 12.** Evolution with time of the flow of CO exiting from the reactor for different $H_2O$:$CO_2$ ratios. Activated ilmenite as bed material. Loads of 1.5 g char. $T$ = 900ºC.

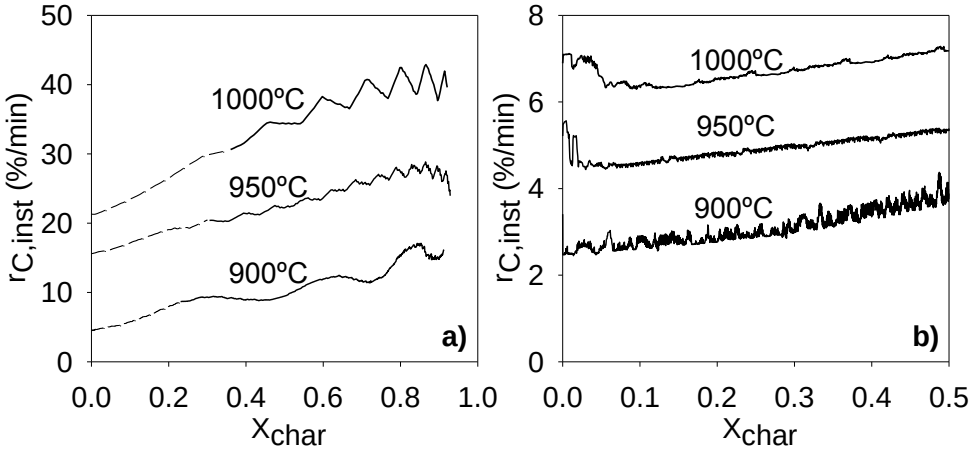


**Fig. 13.** Instantaneous rate of char conversion, $r_{C,inst}(t)$, as a function of the char conversion at 900, 950 and 1000ºC. Fluidizing agent: (a) $H_2O$; (b) $CO_2$. Activated ilmenite as bed material. Loads of 1.5 g char.

Design Considerations for Chemical-Looping Combustion of coal – Part 1. Experimental Tests.

Ana Cuadrat*, Alberto Abad, Juan Adánez, Luis F. de Diego, Francisco García-Labiano, Pilar Gayán.

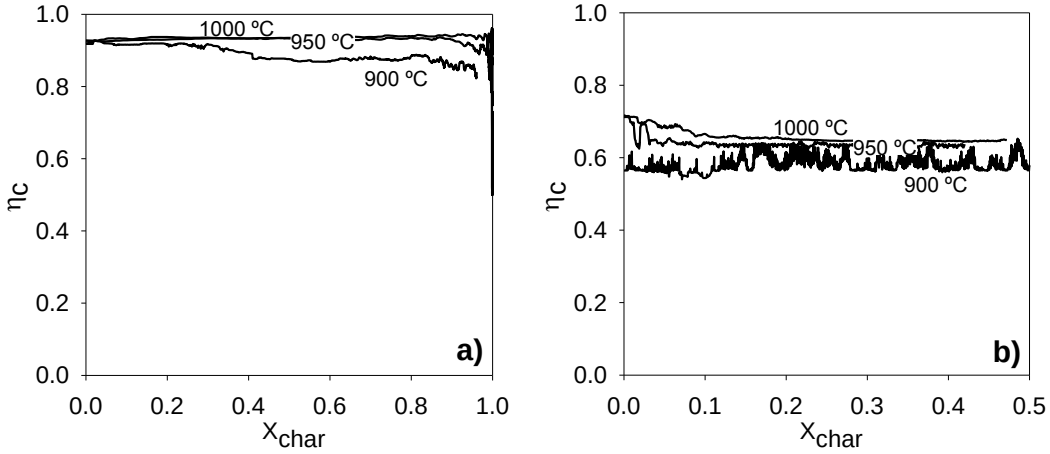


**Fig. 14.** Combustion efficiency as a function of the char conversion at 900, 950 and 1000ºC. Fluidizing gas: a) $H_2O$; b) $CO_2$. Activated ilmenite as bed material. Loads of 1.5 g char.

Design Considerations for Chemical-Looping Combustion of coal – Part 1. Experimental Tests.

Ana Cuadrat*, Alberto Abad, Juan Adánez, Luis F. de Diego, Francisco García-Labiano, Pilar Gayán.

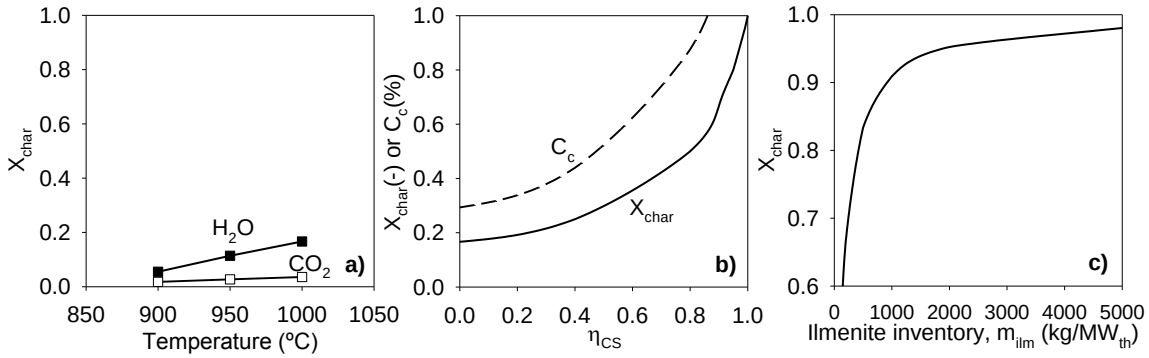


**Fig. 15.** Conversion of char by gasification in the fuel-reactor as a function of a) temperature with steam or $CO_2$ as gasification agents and without carbon stripper; b) carbon stripper efficiency; and c) ilmenite inventory in the fuel-reactor with a carbon stripper efficiency of $\eta_{CS}$ = 90%. In Figs. a) and b) the solids inventory was 200 kg/$MW_{th}$. In Figs. b) and c) steam was the gasification agent and the temperature 1000ºC.

# Paper V

International Journal of Greenhouse Gas Control 5 (2011) 1630–1642

Contents lists available at SciVerse ScienceDirect

International Journal of Greenhouse Gas Control

journal homepage: www.elsevier.com/locate/ijggc

# The use of ilmenite as oxygen-carrier in a 500 $W_{th}$ Chemical-Looping Coal Combustion unit

A. Cuadrat, A. Abad*, F. García-Labiano, P. Gayán, L.F. de Diego, J. Adánez

*Instituto de Carboquímica (ICB-CSIC), Department of Energy & Environment, Miguel Luesma Castán 4, 50018-Zaragoza, Spain*

ARTICLE INFO

*Article history:*
Received 16 May 2011
Received in revised form 6 September 2011
Accepted 29 September 2011
Available online 4 November 2011

*Keywords:*
Chemical-Looping Combustion
Oxygen-carrier
Ilmenite
$CO_2$ capture
Coal

ABSTRACT

Chemical-Looping Combustion, CLC, is a promising technology to capture $CO_2$ at low cost in fossil-fuelled power plants. In CLC the oxygen from air is transferred to the fuel by a solid oxygen-carrier that circulates between two interconnected fluidized-bed reactors: the fuel- and the air-reactor.

This work studies the CLC technology in a 500 $W_{th}$ facility fuelled with bituminous coal with ilmenite as oxygen-carrier. The effect of temperature and coal particle size on coal conversion and combustion efficiency was assessed. Char gasification and combustion of both gasification products and volatile matter were evaluated. At higher temperatures, gasification and combustion reactions are promoted. Carbon capture and combustion efficiencies grow with the temperature, with faster increase at temperatures higher than 910 °C. The outgoing unburnt gases come from volatile matter that was not fully oxidized by ilmenite. Little $CH_4$ was measured and there were neither hydrocarbons heavier than $CH_4$ nor tars in the fuel-reactor outlet. At 870 °C the char conversion was 15% and reached 82% at 950 °C. The combustion efficiency in the fuel-reactor increased from 70% at 870 °C to 95% at 950 °C. The results show that ilmenite has good behavior as oxygen-carrier and that optimizing CLC with coal can lead to energy production with high $CO_2$ capture.



## 1. Introduction

Anthropogenic carbon dioxide emissions, which mainly come from the combustion of fossil fuels for power generation, transport and industry, significantly contribute to global warming (IPCC, 2007). Therefore, there is a need to decrease $CO_2$ emissions in order to stabilize its concentration in the atmosphere. Since fossil fuels are still the dominant energy source worldwide and the transition to more sustainable energy system is a slow process, $CO_2$ capture and sequestration (CCS) has been proposed as an important option to reduce $CO_2$ emissions from power production. Current CCS technologies, available or under development, have the disadvantage of high costs and energy penalties, associated mainly to the $CO_2$ capture process, recovering the gas from flue streams.

Chemical-Looping Combustion (CLC) is one of the most promising technologies to carry out $CO_2$ capture in power plants at a low cost (IPCC, 2005; Eide et al., 2005; Kerr, 2005). In this process the $CO_2$ separation from the other flue gas components is inherent to the process and thus no energy is expended for the capture. The CLC concept is based on the transfer of oxygen from the combustion air to fuel by means of an oxygen-carrier in the form of a metal oxide, which takes place in two separate reactors. In CLC systems, the conventional combustion reaction is replaced by two successive reactions forming a chemical loop. The oxygen-carrier particles circulate between two interconnected reactors, the fuel-reactor and the air-reactor. In the fuel-reactor, the metal oxide reacts with the gaseous fuel to produce $CO_2$ and $H_2O$. Pure $CO_2$, ready to compression and storage, will be readily recovered by condensing the steam. It could be advantageous if the CLC process could be adapted to the use of solid fuels. In the Chemical Looping Combustion with coal the solid fuel is directly introduced to the fuel-reactor, where is converted to $CO_2$ and $H_2O$ by the oxygen transferred from the oxygen-carrier. In this case the gasification of the solid fuel is carried out in the fuel-reactor simultaneously as the oxygen-carrier reacts with the products of the fuel devolatilization and gasification (Adánez et al., 2011). In this process the fuel-reactor is fluidized by a gasifying agent, e.g., $H_2O$ or $CO_2$, as proposed by Cao and Pan (2006). Thereby, the solid fuel gasification takes place in the same reactor first according to reactions (1–3) and the resulting gases and volatiles are oxidized through reduction of the oxidized oxygen-carrier, $Me_xO_y$, by means of reaction (4). The oxygen-carrier reduced in the fuel-reactor, $Me_xO_{y-1}$, is later led to the air-reactor where it is oxidized with air by reaction (5), and it is ready to start a new cycle. The net chemical reaction as well as the

* Corresponding author. Tel.: +34 976 733 977; fax: +34 976 733 318.
*E-mail address:* abad@icb.csic.es (A. Abad).

1750-5836/$ – see front matter © 2011 Elsevier Ltd. All rights reserved.
doi:10.1016/j.ijggc.2011.09.010

**Nomenclature**

| | |
|---|---|
| AR | air-reactor |
| CLC | Chemical-Looping Combustion |
| $C_{\text{char AR}}$ | carbon flow from the char that goes to the air-reactor (mol/s) |
| $C_{\text{char FR}}$ | carbon flow from the gasified char in the fuel-reactor (mol/s) |
| $C_{\text{char eff}}$ | carbon flow from the effective char introduced (mol/s) |
| $C_{\text{char elutr}}$ | carbon flow from the elutriated char (mol/s) |
| $C_{\text{FR}}$ | outlet carbon flow from the fuel-reactor (mol/s) |
| $C_{\text{vol}}$ | carbon flow coming from the volatile matter fed (mol/s) |
| $\%C_{\text{char,FR}}$ | char concentration in the fuel-reactor (%) |
| FR | fuel-reactor |
| $F_{\text{AR}}$ | outlet air-reactor gas flow (mol/s) |
| $F_{\text{CH}_4,\text{FR}}, F_{\text{H}_2,\text{FR}}, F_{\text{CO,FR}}, F_{\text{CO}_2,\text{FR}}, F_{\text{H}_2\text{O,FR out}}$ | outlet flows in the fuel-reactor of $CH_4$, $H_2$, CO, $CO_2$ and $H_2O$, respectively (mol/s) |
| $F_{\text{CO}_2,\text{AR}}$ | outlet flow in the air-reactor of $CO_2$ (mol/s) |
| $F_{\text{FR}}$ | dry basis product gas flow (mol/s) |
| $F_{\text{H}_2\text{O,in}}$ | water steam inlet flow in the fuel-reactor (mol/s) |
| $F_{\text{ilm}}$ | solids circulation rate (kg/s) |
| $F_{\text{N}_2,\text{AR}}$ | $N_2$ inlet flow in the fuel-reactor (mol/s) |
| $F_{\text{N}_2,\text{FR}}$ | $N_2$ inlet flow in the fuel-reactor (mol/s) |
| $M_C$ | atomic weight of carbon (kg/mol) |
| $\text{Me}_x\text{O}_y$ | oxidized oxygen-carrier |
| $\text{Me}_x\text{O}_{y-1}$ | reduced oxygen-carrier |
| $m_{\text{char,FR}}$ | mass of char in the fuel-reactor (kg) |
| $m_{\text{ilm,FR}}$ | fuel-reactor bed mass or solid hold-up in the fuel-reactor (kg) |
| $m$ | instantaneous mass of the oxygen-carrier (kg) |
| $m_{\text{r}}$ | mass of the reduced form of the oxygen-carrier (kg) |
| $m_{\text{o}}$ | mass of the oxidized form of the oxygen-carrier (kg) |
| $O_{\text{coal,eff}}$ | flow of oxygen contained in the effective coal introduced (mol/s) |
| $O_{2\ \text{demand coal,eff}}$ | oxygen demand of the effective coal fed (moles $O_2$/s) |
| $(-r_C)$ | rate of char coal conversion ($s^{-1}$) |
| $R_{\text{O,ilm}}$ | oxygen transport capacity of ilmenite |
| $T_{\text{FR}}$ | temperature in the fuel-reactor (°C) |
| $X_{\text{char}}$ | char conversion |
| $X_{\text{ilm}}$ | reaction conversion of ilmenite |
| $y_{\text{O}_2,\text{AR}}, y_{\text{CO}_2,\text{AR}}$ | fractions in the air-reactor outlet flow of $O_2$ and $CO_2$ |
| $y_{\text{CH}_4,\text{FR}}, y_{\text{CO}_2,\text{FR}}, y_{\text{CO,FR}}, y_{\text{H}_2,\text{FR}}$ | dry basis fractions in the fuel-reactor product gas of $CH_4$, $CO_2$, CO, $H_2$, respectively |
| $\Delta X_{\text{ilm}}$ | variation of reaction conversion of ilmenite |
| $t_{\text{m,char}}$ | mean residence time of char (s) |
| $t_{\text{m,ilm}}$ | mean residence time of ilmenite (s) |

*Greek letters*

| | |
|---|---|
| $\eta_{\text{CC}}$ | carbon capture efficiency |
| $\eta_{\text{comb}}$ | combustion efficiency |
| $\Omega_{\text{T}}$ | total oxygen demand of fuel-reactor product gas |

heat involved in the global process is the same as for normal fuel gas combustion.

$$\text{Coal} \rightarrow \text{Volatile matter} + \text{Char} \quad (1)$$

$$\text{Char} + H_2O \rightarrow H_2 + CO \quad (2)$$

$$\text{Char} + CO_2 \rightarrow 2CO \quad (3)$$

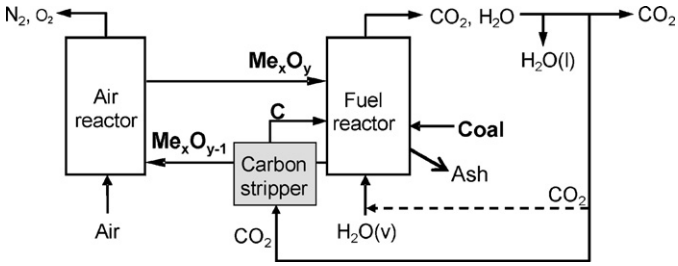


**Fig. 1.** Reactor scheme of the CLC with solid fuels process (- - - optional stream).

$$\text{H}_2,\ \text{CO},\ \text{Volatile matter} + n\text{Me}_x\text{O}_y \rightarrow\ \text{CO}_2 + \text{H}_2\text{O} + n\text{Me}_x\text{O}_{y-1} \quad (4)$$

$$\text{Me}_x\text{O}_{y-1} + \tfrac{1}{2}\text{O}_2 \rightarrow\ \text{Me}_x\text{O}_y \quad (5)$$

Fig. 1 shows the simplified reactor scheme of the CLC process with direct introduction of solid fuels, which counts with the air- and fuel- reactors, the circulating oxygen-carrier. As the gasification process is expected to be the limiting step in the fuel-reactor, the solids stream going out from the fuel-reactor can contain certain fraction of unconverted char. Thus, a carbon stripper step is proposed to separate char from the oxygen-carrier (Cao and Pan, 2006; Berguerand and Lyngfelt, 2008a).

For direct CLC with solid fuels, there are 3 particular aspects to be taken into account: (1) to reach high combustion efficiencies it is necessary to have good contact between the oxygen-carrier particles and the volatile matter and gasification products, (2) the system must be optimized to get maximum ash separation and minimum carrier extraction, since part of the carrier will be removed together with the draining of ashes present in the solid fuel, and (3) the carbon stripper should be optimized for the carbon separation; otherwise, the $CO_2$ capture efficiency will be reduced because of $CO_2$ exiting together with the depleted air stream.

The research on CLC with solid fuels concludes that gasification is probably the rate-limiting step (Leion et al., 2008a,b; Bidwe et al., 2011). Linderholm et al. (2011) studied the gasification rates for a wide variety of coal chars, showing the feasibility of using the CLC technology with different type of coals with the appropriate design modifications or high efficiency carbon stripper implementation. Cuadrat et al. (submitted for publication-a) studied the fuel-reactor performance regarding the gasification rate and later reaction of ilmenite with the gasification products in batch fluidized bed with South African coal char feed. They calculated an optimal range of solids inventory in the fuel-reactor of 500–1000 kg/$MW_{th}$ to get char conversions as high as 90–95%, which is feasible and adequate for this technology.

A key factor for the CLC technology development is the selection of the oxygen-carrier. Solid particles based on Fe, Ni and Cu have been extensively investigated as feasible oxygen-carriers to be used in CLC systems, as reviewed by Adánez et al. (2011) Suitable oxygen-carriers for a CLC process must have high reactivity during reduction and oxidation, high attrition resistance and agglomeration absence.

To evaluate the performance of CLC with solid fuels, several works have been done in continuously operated coal fuelled CLC prototypes. Shen et al. (2009a,b, 2010) used a synthetic $NiO/Al_2O_3$ oxygen-carrier in two continuous facilities with different particle recirculation system design of thermal power of 10 $kW_{th}$ and 1 $kW_{th}$. Although they had some CO and $CH_4$ in the fuel-reactor product gas, high coal conversions to $CO_2$ were reached. For the 10 $kW_{th}$ rig, they found that coal gasification controlled the CO and $CH_4$ concentrations in the fuel-reactor product gas, as well as the carbon capture efficiency. They obtained a carbon conversion efficiency of 92.8% at a fuel-reactor temperature of 970 °C. The 1 $kW_{th}$ rig had an improved external particle recirculation configuration

that reduced the char particles escaping to the air-reactor. A $CO_2$ capture of 95% at 985 °C was then reached. Although no major operational problems occurred and good results were obtained, the use of NiO based oxygen-carriers at industrial-scale presents some disadvantages due to its higher cost and environmental issues.

Low cost of the material is rather desirable for its use with coal, as a partial loss together with the coal ashes is predictable when removing them from the reactor to avoid their accumulation in the system. Recently, interest on the use of $CaSO_4$ as oxygen-carrier has been showed by several research groups. For instance, $CaSO_4$ from natural anhydrite is a low cost material with much higher oxygen transport capacity than other proposed materials but lower reactivity with reducing gases ($H_2$, CO and $CH_4$) (Wang and Anthony, 2008; Song et al., 2008).

Furthermore, there are some studies on the suitability of using some minerals as iron ore, ilmenite, manganese ore or waste materials coming from steel industry and alumina production. Leion et al. (2009) and Fossdal et al. (2011) analyzed the behavior of several iron and manganese ores, as well as iron and manganese industrial products, during repeated redox cycles at fluidizing conditions using syngas or methane as fuel gases. Regarding the reactivity, Fossdal et al. (2011) found a Mn ore as the most promising for CLC applications. However, Leion et al. (2009) concluded that manganese ores showed poor mechanical stability and poor fluidizing properties making them unsuitable as oxygen-carriers. They found adequate materials based on manganese and iron industrial products. In addition, iron based minerals, exhibited high reactivity with mixtures of $H_2$ and CO being suitable for both solid fuelled CLC and syngas combustion. An Australian natural mineral based in hematite as oxygen-carrier was used by Gu et al. (2010). They successfully tested the CLC process during 30 h in a 1 $kW_{th}$ facility with coal as fuel. Combustion efficiencies of 82–87% were obtained at a fuel-reactor temperature of 950 °C. Besides, the adequate behavior of an iron waste material as oxygen-carrier with respect to gas combustion was proved in a continuous 500 $W_{th}$ CLC prototype by Ortiz et al. (2011) using a simulated PSA off-gas stream, methane and syngas as fuel. Among all these low cost materials, ilmenite is a natural mineral which is promising for its large scale industrial use as oxygen-carrier with solid fuels. It is mainly composed of $FeTiO_3$ ($FeO{\cdot}TiO_2$), where iron oxide is the active phase that behaves as the oxygen-carrier.

Performance of ilmenite has been proved to be acceptable as oxygen-carrier for CLC in recent studies made at different scales. Reactivity of ilmenite in a batch fluidized bed for solid fuels combustion was studied by Leion et al. (2008a). Ilmenite gave high conversion of CO and $H_2$ but moderate conversion of $CH_4$. Fresh ilmenite reacts slowly, but there is a gain in reactivity in reduction as well as in oxidation with the number of cycles (Adánez et al., 2010), and eventually reactivities as high as for a synthetic $Fe_2O_3$-based oxygen-carrier were reached (Leion et al., 2008b). The reaction kinetics of ilmenite for both reduction and oxidation reactions taking place in the CLC process was studied by Abad et al. (2011). This activation occurred for $H_2$, CO as well as $CH_4$ as fuel gases, and was faster if ilmenite had been previously calcined. The initial oxygen transport capacity was measured to be 4 wt.% and it decreased with the number of cycles. In continuous operation with natural gas and syngas as fuel, a Norwegian ilmenite was tested in a 120 kW CLC facility by Pröll et al. (2009). Although some conditions needed optimization, reasonable fuel conversion for CO and $H_2$ at 950 °C was obtained. Furthermore, syngas was combusted at 900 °C in a CLC dual fluidized bed system using an Australian ilmenite by Bidwe et al. (2011) resulting in a steady-state conversion of circa 90%.

For ilmenite as oxygen-carrier, the feasibility of the CLC process in the bigger scale and continuous operation was proved in a 10 $kW_{th}$ chemical-looping combustor using South African coal and petroleum coke as solid fuels by Berguerand and Lyngfelt (2008a,b). This rig counts with a carbon stripper to increase the residence time of char particles in the fuel-reactor. However, due to the feeding system, volatile matter exits the system without getting in contact with the oxygen-carrier bed and therefore the analysis was only made to the gas conversion of the gasification products, i.e., $H_2$ and CO. The combustion of a Mexican petroleum coke using ilmenite as oxygen-carrier was tested during 26 h (Berguerand and Lyngfelt, 2009a). A $CO_2$ capture within the range 65–82% was obtained, which are rather low values mainly because the fuel has low reactivity. The performance of this rig could be improved by increasing the residence time of the particles in the fuel-reactor to get higher $CO_2$ capture and by increasing the separation efficiency of the cyclone after the fuel-reactor. The solid fuel conversion was 65–70%, whereas the incomplete gas conversion resulted into the presence of unconverted gases, i.e., $CH_4$, CO, $H_2$ and $H_2S$, in the fuel-reactor outlet stream that demanded 29–30% of the total oxygen needed to fully burn coal to $H_2O$ and $CO_2$. The gas conversion could be improved by a polishing step after the fuel-reactor, or through a fuel-reactor design that got better contact between the gases released by the fuel and the oxygen-carrier bed. When a more reactive coal was used, it was confirmed that high carbon capture efficiencies can be obtained: 82–96% (Berguerand and Lyngfelt, 2008a). Although in all tests there was some fraction of unconverted gases, i.e., $H_2$ and CO, the importance of using high temperatures in this process to get both high fuel and gas conversions was proven, and the oxygen demand at a fuel-reactor temperature of 1000 °C was as low as 5–7% (Berguerand and Lyngfelt, 2009b). Furthermore, the effect that the mean residence time of char particles given by a determined solids circulation flowrate has on the char conversion was assessed (Markström et al., 2010).

On the whole, all studies to date confirm the feasibility of the CLC technology with solid fuels and that ilmenite appears to be a suitable material to be used for solid fuel combustion in a CLC system, considering its chemical and physical properties and low cost. Nevertheless, the good behavior of the fuel-reactor is fundamental for the reliability of a CLC system. On the one hand, it will determine the gas losses obtained at the exit of the reactor and the possible necessity to take additional actions, as to recirculate the unburned gases, e.g. CO, $H_2$ or $CH_4$, after removing $H_2O$ and $CO_2$ from the flue gas, or to add a final gas polishing step by $O_2$ addition. On the other hand, the gasification rate will affect the char concentration in the bed and the carbon stripper performance.

The aim of this work was to investigate the capability of ilmenite to process coal as fuel in a coal fuelled CLC reactor, when ilmenite is continuously circulated between the fuel- and air-reactor and coal is continuously fed to the fuel-reactor. The conversion of gasifying products and volatile matter to $CO_2$ and $H_2O$ by reaction with ilmenite was studied in a 500 $W_{th}$ unit, besides the gasification of char in the fuel-reactor. A Colombian bituminous coal was used as fuel. The experiments were carried out at 820–950 °C in the fuel-reactor, and the fluidizing gas was pure steam, which also acts as gasifying agent. The effect of fuel-reactor temperature and coal particle size on the extent of gasification in the fuel-reactor and oxygen polishing requirements was investigated. Special attention was done in the relevance of gasifying products and volatiles in the oxygen demand. Furthermore, the evolution of chemical and physical properties of ilmenite particles with the time in continuous operation was also evaluated. The results obtained are analyzed and discussed in order to be useful for the scale-up of the CLC with solids fuel process.

**Table 1**
Fresh and calcined ilmenite compositions (wt.%).

| | Fresh ilmenite | Calcined ilmenite |
|---|---|---|
| $Fe_2O_3$ | 14.8 | 11.2 |
| $FeTiO_3$ | 65.5 | – |
| $Fe_2TiO_5$ | – | 54.7 |
| $TiO_2$ | 14.0 | 28.6 |
| Inerts | 5.7 | 5.5 |

## 2. Experimental

### 2.1. Ilmenite and coal

The oxygen-carrier used in this work is an iron titanium oxide called ilmenite, which is extracted from a natural ore and provided by the Norwegian company Titania A/S and received in its reduced form $FeTiO_3$. The ilmenite used was pre-calcined at 950 °C. The pre-oxidation was carried out to get ilmenite to its most oxidized state and improve properties and initial reaction rates (Adánez et al., 2010; Leion et al., 2008b). Moreover, a pre-oxidation of ilmenite was also beneficial in order to avoid defluidization problems (Pröll et al., 2009). The same type of ilmenite has been already used in several studies in continuous testing (Bidwe et al., 2011; Berguerand and Lyngfelt, 2008a,b, 2009a,b). The oxidized species present in ilmenite are $Fe_2TiO_5$, $Fe_2O_3$ and $TiO_2$, and its reduced state for the CLC technology is mainly composed of $FeTiO_3$, $Fe_3O_4$ and $TiO_2$. The initial oxygen transport capacity was measured to be 4.0 wt.%. Table 1 shows the compositions of both fresh and calcined ilmenite. The true density of ilmenite particles was 3980 kg/m$^3$. The particle size used was +150–300 μm. More details about the composition, physical properties and reactivity of ilmenite particles can be found elsewhere (Adánez et al., 2010; Abad et al., 2011).

The fuel used was a bituminous Colombian coal "El Cerrejón". The coal was subjected to a thermal pre-treatment for pre-oxidation in order to reduce its swelling properties. Thus, coal was placed in trays in layers of about 3 mm height and exposed to heating at 180 °C in air atmosphere for 28 h. The use of pre-treated coal avoids the pipe clogging and coal particles agglomeration showed when fresh coal was used. Ultimate and proximate analyses of the fresh and pre-treated coal are shown in Table 2. The pre-oxidation causes an increase in oxygen content and a decrease in the heating value. The density of coal particles was 1600 kg/m$^3$. Three different coal particle sizes were used: +74–125, +125–200 and +200–300 μm.

Char of the used coal was produced and fed as fuel in the CLC system in order to evaluate separately the combustion of char and of volatile matter. Thus, part of the pre-treated coal was devolatilized by heating it up to 900 °C in a batch fluidized bed reactor, keeping the solids permanently in bubbling bed conditions fluidized with $N_2$ in inert atmosphere. The ultimate analysis of the resulting char is shown in Table 3. The char particle size was +125–200 μm.

**Table 2**
Properties of the fresh and pre-treated Colombian coal.

| | | | |
|---|---|---|---|
| *Fresh Colombian coal* | | | |
| C | 68.0% | Moisture | 6.2% |
| H | 4.2% | Volatile matter | 33.4% |
| N | 1.6% | Fixed carbon | 48.5% |
| S | 0.6% | Ash | 11.9% |
| O | 7.5% | | |
| Low heating value: 25,878 kJ/kg | | | |
| *Pre-treated Colombian coal* | | | |
| C | 65.8% | Moisture | 2.3% |
| H | 3.3% | Volatile matter | 33.0% |
| N | 1.6% | Fixed carbon | 55.9% |
| S | 0.6% | Ash | 8.8% |
| O | 17.6% | | |
| Low heating value: 21,899 kJ/kg | | | |

**Table 3**
Ultimate analysis of the used pre-treated Colombian char coal.

| | |
|---|---|
| C | 79.8% |
| H | 0.7% |
| N | 1.3% |
| S | 0.6% |
| O | 4.0% |

### 2.2. Oxygen-carrier characterization

Various samples of ilmenite were taken to evaluate the evolution and change of the particles properties during the continuous performance. The textural properties of the oxygen-carrier samples were determined by Hg intrusion in a Quantachrome PoreMaster 33; solid density was measured by a He Micromeritics AccuPyc II 1340 picnometer.

A thermogravimetric analyzer (TGA) was used for the determination of the reactivity and activation extent of ilmenite by means of its reaction rate in reduction and oxidation of every extracted sample. The TGA was also used to measure the oxygen transport capacity of the samples. The thermogravimetric analyzer is a CI Electronics type. More information about this set-up can be found elsewhere (Adánez et al., 2004). The experiments were performed at 900 °C with a 5% $H_2$ + 40% $H_2O$ mixture, and afterwards to oxidation conditions in air. The reductions were done with a reducing gas with a $H_2O$:$H_2$ ratio of 8:1 to ensure that the final oxygen-carrier reduced species are $FeTiO_3$ and $Fe_3O_4$. The reaction rates of the samples extracted during the continuous testing were compared to the initial calcined ilmenite and a fully activated sample.

### 2.3. 500 $W_{th}$ coal fuelled CLC reactor

In this work, the CLC technology with a Colombian bituminous coal was investigated in the ICB-CSIC-s1 continuous rig using ilmenite as oxygen-carrier. A schematic view of the experiment facility is shown in Fig. 2. The CLC system was basically composed of two interconnected fluidized-bed (FB) reactors, the fuel-reactor (FR) (1) and the air-reactor (AR) (3), joined by a loop seal (2), a riser (4) for solids transport from the air- to the fuel-reactor, a cyclone to recover the entrained solids (5) and a solids valve (7) to control the flow rate of solids fed to the fuel-reactor. The temperatures in the different sectors of the plant can be set, as it is heated up by various furnaces (10), i.e., in the air-reactor and bottom bed and freeboard of the fuel-reactor.

The fuel-reactor consisted of a bubbling fluidized bed with 5 cm of inner diameter and 20 cm bed height. Coal (8) is fed by a screw feeder at the bottom of the bed above the fuel-reactor distributor plate in order to maximize the time that volatile matter is in contact with the bed material. The screw feeder (9) has two steps: the first one with variable speed to control the coal flow rate, and the second has high rotating velocity to avoid coal pyrolysis inside the screw. A small $N_2$ flow is fed in the beginning of the screw to avoid possible volatile reverse flow or entrance of steam. The maximum thermal power capacity of the unit was 500 $W_{th}$ for the Colombian coal used in this work. In the fuel-reactor the oxygen-carrier is reduced by the volatile matter and gasification products of coal, where $H_2$ and CO are the main components. The fuel-reactor is fluidized by steam, which acts also as a gasifying agent. The solid fuel devolatilization proceeds in the fuel-reactor first and the resulting gases and gasification products are oxidized through reduction of the oxidized ilmenite. Reduced oxygen-carrier particles overflowed into the air-reactor through a U-shaped fluidized bed loop seal with

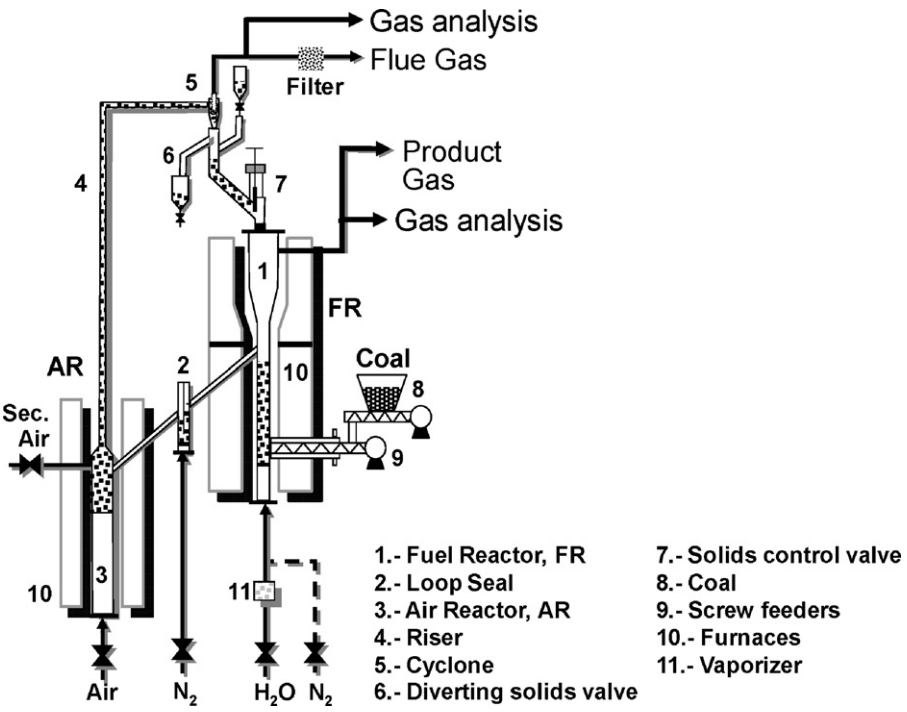


**Fig. 2.** Schematic diagram of the ICB-CSIC-s1 facility for coal-fuelled CLC.

an inner diameter of 5 cm, to avoid gas mixing between fuel and air. Since this rig has no carbon stripper, unconverted char from the fuel-reactor goes to the air-reactor and is fully burnt there, releasing the $CO_2$ that is measured in the air-reactor. The implementation of a carbon stripper would decrease the $CO_2$ flow in the air-reactor and thereby the carbon capture efficiency would increase. However, the absence of a carbon stripper facilitates the interpretation of the effect of these operational conditions on the results obtained.

The oxidation of the carrier took place in the air-reactor, consisting of a bubbling FB fluidized with air with 8 cm of inner diameter and 10 cm bed height, and followed by a riser. Secondary air was introduced at the top of the bubbling bed to help particle entrainment. $N_2$ and unreacted $O_2$ left the air-reactor and went through a high-efficiency cyclone and a filter before the stack. The oxidized solid particles recovered by the cyclone were sent to a solids reservoir, setting the oxygen-carrier ready to start a new cycle. These particles act as a loop seal avoiding the leakage of gas between the fuel-reactor and riser. Previous testing in the ICB-CSIC-s1 continuous rig confirmed that there was no gas leakage between reactors and that the pressure balance was adequate. The regenerated oxygen-carrier particles returned to the fuel-reactor by gravity from the solids reservoir through a solids valve which controlled the flow rates of solids entering the fuel-reactor. The solid valve consists of a hole which can be partially closed by a sliding sheet. A diverting solids valve located below the cyclone allowed the measurement of the solids flow rates at any time. The total ilmenite bed mass in the system was 3.5 kg and the solids bed mass in the fuel-reactor was 0.8 kg ilmenite, as the solids level in the fuel-reactor is fixed and the exceeding overflows and heads for the air-reactor.

In the fuel-reactor a steam flow of 180 $L_N$/h was introduced (corresponding to a velocity of 0.11 m/s at 900 °C) and in the air-reactor the total stream of primary plus secondary air flow was 2500 $L_N$/h (corresponding to a velocity of 0.6 m/s at 900 °C). The circulation flow rate was measured and controlled to be about 2.1 kg/h and the coal flow was about 42 g/h, corresponding to a thermal power of 255 $W_{th}$. That is, the solids hold-up in the fuel-reactor was 3140 kg/$MW_{th}$.

During operation, temperatures in the bed and freeboard of the fuel-reactor, air-reactor bed and riser were monitored as well as the pressure drops in important locations of the system, such as the fuel-reactor bed, the air-reactor bed and the loop seal. Because of its small size, the system is not auto-thermal and is heated up with various ovens to get independent temperature control of the air-reactor, fuel-reactor, and fuel-reactor freeboard. The temperature in the air-reactor was maintained at around 950 °C and the fuel-reactor temperature was varied from 820 °C to 950 °C. The fuel-reactor freeboard is kept constant at about 900 °C in all the experiments. Different experiments were carried out varying the temperature and using different particle size of coal. 40 different stable conditions were reached with ilmenite as bed material: in 30 of them coal was fed and 10 with char. One further experiment was done with coal as fuel, but silica sand as inert bed material. At least every condition was maintained stable during 30 min. A total of 35 h of continuous operation feeding fuel and 42 h of continuous fluidization were made.

CO, $CO_2$, $H_2$, $CH_4$, and $O_2$ were continuously analyzed in the exit streams from the fuel-reactor and from the air-reactor. Nondispersive infrared (NDIR) analyzers (Maihak S710/UNOR) were used for CO, $CO_2$, and $CH_4$ concentration determination; a paramagnetic analyzer (Maihak S710/OXOR-P) was used for $O_2$ concentration determination; and a thermal conductivity detector (Maihak S710/THERMOR) was used for $H_2$ concentration determination. All data were collected by means of a data logger connected to a computer. In some selected experiments the tar amount present in fuel-reactor product gases was determined following the tar protocol (Simell et al., 2000). Collection of moisture and tar was performed in a series of 8 impinger bottles by absorption in isopropanol and later cooling in external baths. Two different cooling baths were used. The first was an ice bath, where the first 2 impingers were located. The first was empty and the second contains isopropanol. These impingers recover the majority of moisture and aromatic tar compounds (styrene, indene, benzene, etc.) and light Polycyclic aromatic hydrocarbons (PAHs), mainly naphthalene. The second bath contains 6 impingers at −18 °C. Several gaseous

samples from the fuel-reactor stream were also taken in bags in order to measure the components through gas chromatography analysis.

## 3. Data evaluation

The evaluation of the fuel-reactor performance is carried out by the analysis of two main parameters: the carbon capture and the combustion efficiency. The oxygen demand is also calculated in order to know the oxygen requirements in the oxygen polishing step, if required. The purpose of the data evaluation is to assess the performance of the process in the different experiments done, using the measured values of the variables.

The efficiencies that indicate the performance of the process are defined as follows. The carbon capture efficiency, $\eta_{CC}$, is the fraction of the carbon introduced that is converted to gas in the fuel-reactor. As it will be later explained, as carbon containing species in the fuel-reactor product gas only $CH_4$, CO and $CO_2$ were taken into account, as the measured tars and hydrocarbons heavier than $CH_4$ were negligible. The carbon measured in the gases coming from the fuel-reactor and the air-reactor is less than the carbon present in the introduced coal, because there is elutriation of char. However, in case of an industrial plant the possible elutriated char will be collected in a cyclone and reintroduced in the fuel-reactor. The elutriated char flow was calculated as the difference between the fed coal carbon and the measured carbon in the fuel-reactor and air-reactor outlet gas flows. Thus, only the effective coal fed was considered to evaluate the performance of the plant. The carbon of the effective coal is the sum of all carbon containing species measured in the outlet streams of both fuel- and air-reactor. The calculations for the technology assessment were therefore done following these considerations. Thus, the carbon capture efficiency was calculated as:

$$\eta_{CC} = \frac{F_{CO_2,FR} + F_{CO,FR} + F_{CH_4,FR}}{F_{CO_2,FR} + F_{CO,FR} + F_{CH_4,FR} + F_{CO_2,AR}} \quad (6)$$

$F_{CH_4,FR}$, $F_{H_2,FR}$ and $F_{CO,FR}$ being the flows in the fuel-reactor of $CH_4$, $H_2$ and CO. These flows were calculated from the $CH_4$, $H_2$ and CO concentrations at the fuel-reactor exit which were on-line analyzed. The carbon of the unreacted char flowing towards the air-reactor is the $CO_2$ gas flow in the air-reactor, $F_{CO_2,AR}$.

The gas flows of every gas were calculated by multiplying the corresponding gas fraction and the outlet gas flow, i.e., $F_{FR}$ in the case of the fuel-reactor, and $F_{AR}$ for the air-reactor. The dry basis product gas flow, $F_{FR}$, was calculated by using the $N_2$ flow $F_{N_2,FR}$ that is introduced in the fuel-reactor coming from the Loop Seal. Preliminary results showed that about 65% of the $N_2$ introduced to fluidize the Loop Seal went to the fuel-reactor and the rest to the air-reactor. The outlet air-reactor gas flow, $F_{AR}$, was calculated though the introduced $N_2$, $F_{N_2,AR}$, which is sum of the $N_2$ present in the air introduced in the air-reactor and the $N_2$ coming from the Loop Seal.

$$F_{FR} = \frac{F_{N_2,FR}}{1 - (y_{CH_4,FR} + y_{CO_2,FR} + y_{CO,FR} + y_{H_2,FR})} \quad (7)$$

$$F_{AR} = \frac{F_{N_2,AR}}{1 - (y_{CO_2,AR} + y_{O_2,AR})} \quad (8)$$

$y_{CH_4,FR}$, $y_{CO_2,FR}$, $y_{CO,FR}$ and $y_{H_2,FR}$ are the dry basis fractions in the fuel-reactor product gas of $CH_4$, $CO_2$, CO and $H_2$, respectively. $y_{O_2,AR}$, $y_{CO_2,AR}$ are the fractions in the air-reactor outlet flow of $O_2$ and $CO_2$, respectively. The char conversion, $X_{char}$, is defined as the fraction of carbon in the effective char fed to the fuel-reactor which is released to the fuel-reactor outgoing gas stream:

$$X_{char} = \frac{C_{char\,FR}}{C_{char\,eff}} = \frac{F_{CO_2,FR} + F_{CO,FR} + F_{CH_4,FR} - C_{vol}}{F_{CO_2,FR} + F_{CO,FR} + F_{CH_4,FR} + F_{CO_2,AR} - C_{vol}} \quad (9)$$

The flow of carbon in char converted in the fuel-reactor, $C_{char\,FR}$, was calculated as difference of the carbon in gases in the fuel-reactor outgoing flow, and the carbon flow coming from the volatile matter, $C_{vol}$. The carbon content of the volatiles is directly calculated using the elementary and proximate analyses of both the coal used and char. $C_{char\,eff}$ is the flow of carbon contained in the introduced effective char and was calculated as the carbon flow in the effective coal minus the carbon flow coming from the volatile matter.

The combustion efficiency, $\eta_{comb}$, is a measure of gas conversion and represents the extent of oxidation of volatiles and gasification products by the oxygen-carrier. The combustion efficiency in the fuel-reactor is calculated as the fraction of the oxygen demanded by the volatile matter and gasification products that is supplied by the oxygen-carrier in the fuel-reactor. It is therefore dependent on the reaction rate of ilmenite with the gaseous fuels and on the amount of gases generated. The oxygen supplied by ilmenite in the fuel-reactor is calculated through the oxygen containing species in the fuel-reactor product gas. The sum of volatile matter and gasified char is calculated as the effective coal introduced minus the char flowing towards the air-reactor, $F_{CO_2,AR}$. For a carbon stripper with 100% separation efficiency, no $CO_2$ would go to the air-reactor and the here defined combustion efficiency would correspond to the efficiency of combustion of the effective coal. Therefore, the combustion efficiency was calculated as:

$$\eta_{comb} = \frac{0.5 \cdot (F_{H_2O,FR\,out} - F_{H_2O,in}) + F_{CO_2,FR} + 0.5 \cdot F_{CO,FR} - 0.5 \cdot O_{coal,eff}}{O_{2\,demand\,coal,eff} - F_{CO_2,AR}} \quad (10)$$

$F_{H_2O,FR_{out}}$, $F_{CO_2,FR}$ and $F_{CO,FR}$ being, respectively, the fuel-reactor outlet flows of water, $CO_2$ and CO. $O_{coal,eff}$ is the flow of oxygen contained in the effective coal introduced. $O_{2\,demand\,coal,eff}$ or the oxygen demand of the effective coal flow is the molar oxygen flow as $O_2$ needed to burn the fuel completely and is calculated with the volatile matter in the coal feed and the effective char flow.

An total oxygen demand for the fuel-reactor gases, $\Omega_T$, was defined, as the fraction of oxygen lacking to achieve a complete combustion of the fuel-reactor product gas in comparison to the oxygen demand of the effective introduced coal, $O_{2\,demand\,coal,eff}$. This parameter is the most adequate to evaluate the performance of the combustion process in this facility, since it is the demand of the coal actually involved in the conversion process in the fuel-reactor.

$$\Omega_T = \frac{O_{2\,demand\,gases\,FR}}{O_{2\,demand\,coal,eff}} = \frac{2 \cdot F_{CH_4,FR} + 0.5 \cdot F_{H_2,FR} + 0.5 \cdot F_{CO,FR}}{O_{2\,demand\,coal,eff}} \quad (11)$$

The residence time of char and ilmenite particles were calculated assuming perfect mixing of ilmenite in the fuel reactor. Assuming that char and ash present in the bed are low, the mean residence time of ilmenite, $t_{m,ilm}$, is calculated by Eq. (12).

$$t_{m,ilm} = \frac{m_{ilm,FR}}{F_{ilm}} \quad (12)$$

$m_{ilm,FR}$ being the fuel-reactor bed mass or solid hold-up in the fuel-reactor, and $F_{ilm}$ the solids circulation rate. The mean residence time for ilmenite was calculated to be about 24 min in all experiments.

The elutriation of char particles affect to the residence time of these particles in the reactor. The residence time of ilmenite and char would be the same, but since there is char elutriation, the mean residence time of char, $t_{m,char}$, should be lower than the residence time for ilmenite particles. It was calculated as the mass of char in the fuel-reactor, $m_{char,FR}$, divided by the char flow that exits the fuel-reactor, sum of the carbon flow from the elutriated

char, $C_{\text{char elutr}}$, and the carbon flow from the char to the air-reactor, $C_{\text{char,AR}}$.

$$t_{\text{m,char}} = \frac{m_{\text{char,FR}}}{C_{\text{char,AR}} + C_{\text{char elutr}}} = \frac{\%C_{\text{char,FR}} \cdot m_{\text{ilm,FR}}/(100 \cdot M_C)}{C_{\text{char,AR}} + C_{\text{char elutr}}} \quad (13)$$

$\%C_{\text{char,FR}}$ is the carbon concentration from char in the fuel-reactor, which is calculated considering the carbon char flow that exits the fuel-reactor and goes to the air-reactor, $C_{\text{char,AR}}$, divided by the sum of the char and ilmenite flows entering the air-reactor.

$$\%C_{\text{char,FR}} = \frac{C_{\text{char,AR}} \cdot M_C}{C_{\text{char,AR}} \cdot M_C + F_{\text{ilm}}} \cdot 100 \quad (14)$$

For the reactivity analysis by TGA, the conversion level of the ilmenite, $X_{\text{ilm}}$, was calculated for the reduction and oxidation reactions as:

For reduction:

$$X_{\text{ilm}} = \frac{m_{\text{o}} - m}{R_{\text{O,ilm}} \cdot m_{\text{o}}} \quad (15)$$

For oxidation:

$$X_{\text{ilm}} = \frac{m - m_{\text{r}}}{R_{\text{O,ilm}} \cdot m_{\text{o}}} \quad (16)$$

where $m$ is the instantaneous mass, and $m_{\text{o}}$ and $m_{\text{r}}$ are the mass of fully oxidized and reduced ilmenite at the reacting condition, respectively. The oxygen transport capacity for ilmenite, $R_{\text{O,ilm}}$, was defined as the mass fraction of the oxygen-carrier that is used in the oxygen transfer, calculated as:

$$R_{\text{O,ilm}} = \frac{m_{\text{o}} - m_{\text{r}}}{m_{\text{o}}} \quad (17)$$

The initial oxygen transport capacity of this ilmenite, $R_{\text{O,ilm}}$, was 4.0 wt.%, being $Fe_2TiO_5$ and $Fe_2O_3$ the oxidized species and $FeTiO_3$ and $Fe_3O_4$ the final reduced species in a CLC process.

## 4. Results and discussion

To determine the behavior of ilmenite as oxygen-carrier during coal combustion, several tests were carried out at different temperatures and for different particle sizes of coal. In addition, to evaluate the volatile matter combustion, as well as the char gasification itself in the continuous testing, experiments with char coal feed were also done. Furthermore, the effect of the oxygen-carrier in gasification and combustion of coal was assessed by carrying out experiments with an inert bed material.

The CLC prototype was easy to operate and control, and the steady state for each operating condition was maintained for at least 30 min. The experiments have been carried out when ilmenite was already activated for reduction, so that the reactivity of ilmenite was maximum and constant and did not affect the evaluation of other parameters. Nevertheless, the activation process during the first hours of operation will be later analyzed.

As representative of the gas distributions obtained in this study, the evolution with time of temperature and gas concentration from the air and fuel-reactors is shown in Fig. 3 for experimental tests with the coal particle size of +125–200 μm for different fuel-reactor temperatures when it was increased from 820 to 950 °C. The concentrations in fuel-reactor are in dry basis and $N_2$ free. Steady state after any parameter change was fast reached and all the points were therefore evaluated at stable conditions. The outlet of the fuel-reactor was mainly composed of oxidized $CO_2$, and $H_2$ and CO as not fully oxidized products of devolatilization and char gasification.

### 4.1. Effect of the fuel-reactor temperature on the process

The influence of the fuel-reactor temperature on the main parameters of the CLC process for different coal particle sizes was

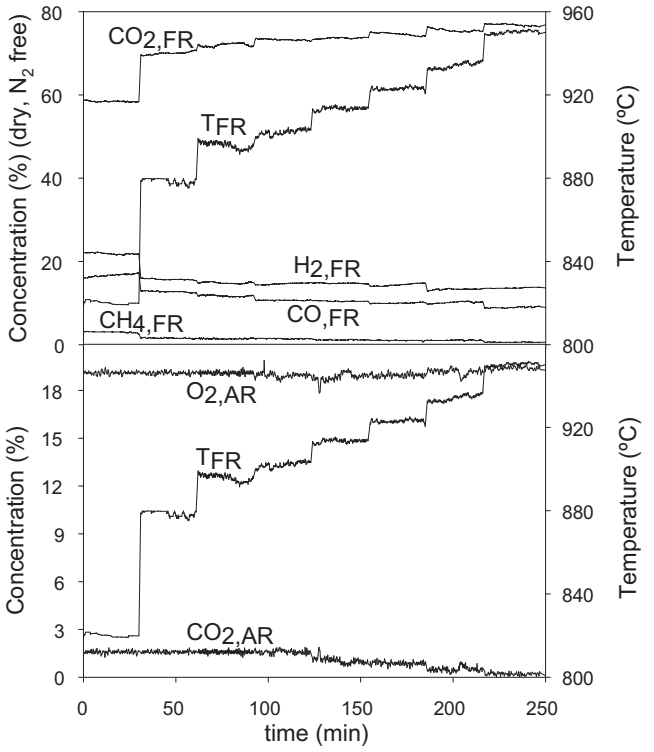


**Fig. 3.** Gas distributions in fuel-reactor (dry basis and $N_2$ free concentrations) and air-reactor for increasing fuel-reactor temperature. Solids circulation flow: 2.1 kg/h. Coal particle size: +125–200 μm.

studied. As seen in Fig. 3, the outlet of the fuel-reactor is mainly composed of oxidized $CO_2$, and $H_2$ and CO as not fully oxidized products of char gasification. It is remarkable to note that the amount of $CH_4$ measured in all experiments was low.

Besides, special experiments were carried out at constant conditions for longer than one hour to determine the presence of higher hydrocarbons. Tar measurements in the fuel-reactor were done using tar protocol. The results showed that there were no tars in the fuel-reactor outlet flow. Later GC measurements proved also that there were no $C_2$–$C_4$ volatiles in the fuel-reactor. It was therefore considered for the calculations that all hydrocarbons from the pyrolysis of the introduced coal heavier than $CH_4$ were reformed or partially or fully oxidized in the fuel-reactor by ilmenite and came out in the fuel-reactor product gas. On the whole, the product gas was only composed by $CH_4$, $CO_2$, CO, $H_2$ and $H_2O$. Furthermore, $CH_4$ concentration was always below 3% in dry and $N_2$ free basis.

There was some char elutriation from the fuel-reactor during the experiments. Black solid particles, which were analyzed to be char particles, were recovered in the first liquid container of the tar condensation train. An estimation of the elutriated char flow was done, by filtering, drying and weighting the amount of char that was collected in the mentioned container during one hour of continuous stable operation. The measured elutriated char flow by this method was similar to the elutriated char flow calculated as the difference between the fed coal carbon and the measured carbon in the fuel-reactor and air-reactor outlet gas flows. Thus, the so-called effective coal that was really fed into the system is the sum between the volatile matter and the char flow that was not elutriated.

Fig. 4 shows the variation with the temperature of concentrations of $CO_2$, CO and $H_2$ at the outlet of the fuel-reactor in dry and free $N_2$ basis for the different particle sizes. On the one hand, the gasification rate is faster at higher temperatures and higher amount of gasification products are generated. On the other hand, combustion reactions are also promoted with increasing temperatures, and

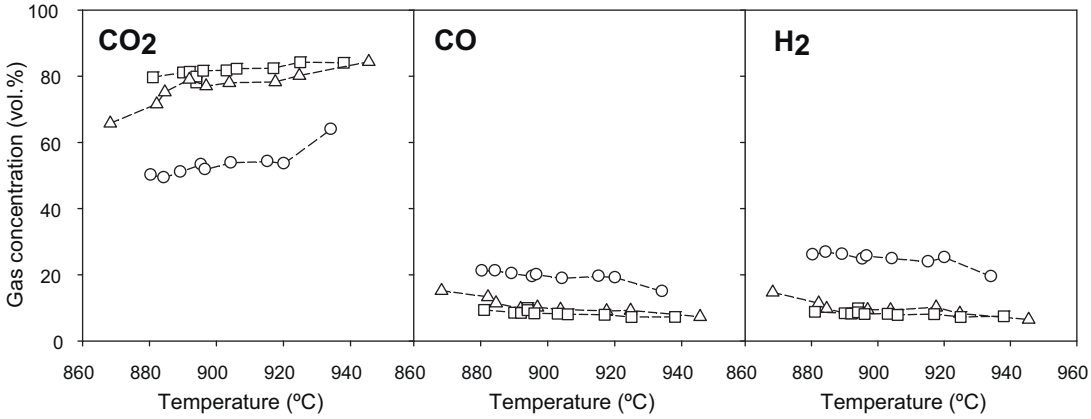


**Fig. 4.** $CO_2$, CO and $H_2$ concentration in the fuel-reactor (dry free $N_2$ basis) at different fuel-reactor temperatures for different coal particle size. Particle size: (○) 74–125 μm; (△) 125–200 μm; (□) 200–300 μm.

therefore more $CO_2$ and $H_2O$ as products of combustion are generated. This has a positive effect on the char conversion, because the oxidation of CO and $H_2$ leads to a lower amount of these gasification inhibitors in the fuel-reactor. The gas composition was similar for coal particle sizes of +125–200 μm and +200–300 μm. However, a lower amount of carbon was detected for the lower particle size (+74–125 μm) because a relevant fraction of char was elutriated from the bed. This issue will be analyzed in the next section.

Fig. 5 represents the char conversion and carbon capture and combustion efficiencies as a function of the reactor temperature for different coal particle sizes. As it was presumable, the results show that there is a continuous increase of efficiency with the temperature for all coal particle sizes. Char conversion changed from 15% at 870 °C to 82% at 950 °C as extreme cases. For the middle and bigger particle sizes, the combustion efficiency varied from 70% at 870 °C to 95% at 950 °C. It is likely that the combustion efficiencies observed for the smaller particle size were lower because more char particles are elutriated and do not get in contact with the oxygen-carrier. This is later further discussed. The carbon capture at 870 °C had a value of 35% and increased up to 86% at 950 °C. The calculated char concentration in the fuel-reactor bed for all the experiments was about 0.35%. If a carbon separation system was implemented, the carbon capture efficiency should be higher, as well as the char concentration in the fuel-reactor should increase until the new steady state was reached.

At the lower temperature the carbon capture efficiency is close to the volatile matter content of the coal, see Table 1. This means that most of carbon in the gases comes from the volatiles, and few amounts of char are being gasified. Note that in this rig and most notably below 920 °C, carbon capture presents low values. This is because the gasification rate at these temperatures is slow and thus a relatively high amount of char goes to the air-reactor.

The increase in the carbon capture efficiency with the temperature is due to more carbon in char is being gasified in the reactor. If the trends are extrapolated, it could be expected that all efficiencies would reach a value close to 100% at 1000 °C, which means that most of carbon in the coal would exit with the fuel-reactor flue gases. This trend is in concordance with the results found at high temperatures by Berguerand and Lyngfelt (2009b). At 950 °C they obtained carbon capture efficiency of 82–96% for South African coal (Berguerand and Lyngfelt, 2009a) and between 60% and 75% for petroleum coke (Berguerand and Lyngfelt, 2008b).

Fig. 6 shows the oxygen demand due to the unburnt gases present in fuel-reactor, $\Omega_T$, at the different temperatures and the coal particle sizes used. Regarding the temperature, it can be seen that $\Omega_T$ decreases because of the increase in ilmenite reaction rate with the temperature. However, the $\Omega_T$ drop is slight. This can be explained through the raise of the gasification rate: there is more production of the gasification products, $H_2$ and CO, which must react with ilmenite. This fact suggests that the increase in the oxygen-carrier reactivity with the temperature is comparable to the increase of the gasification rate. For the medium and bigger coal particle size tested, the oxygen demand was within the values 5–10% for the temperature range 820–950 °C. Higher oxygen demand was determined for the smallest particle size.

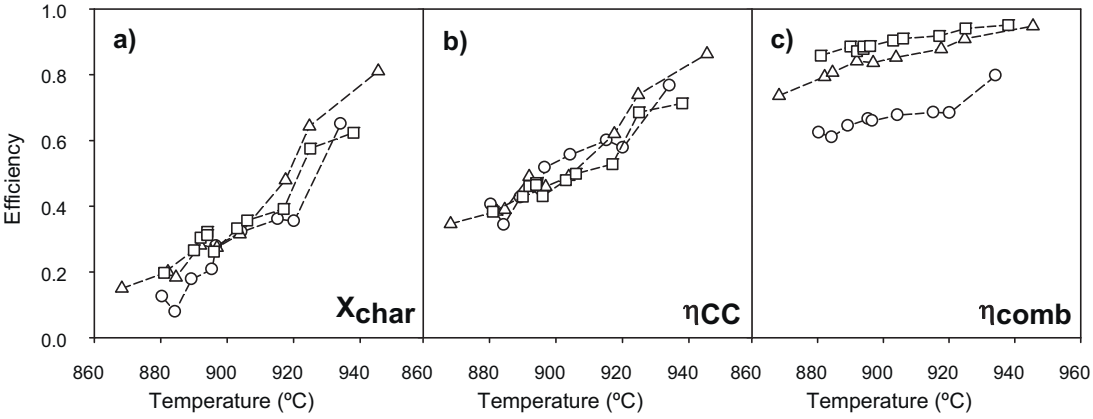


**Fig. 5.** (a) Char conversion, (b) carbon capture and (c) combustion efficiency variation with fuel-reactor temperature for various coal particle sizes. Particle size: (○) 74–125 μm; (△) 125–200 μm; (□) 200–300 μm.

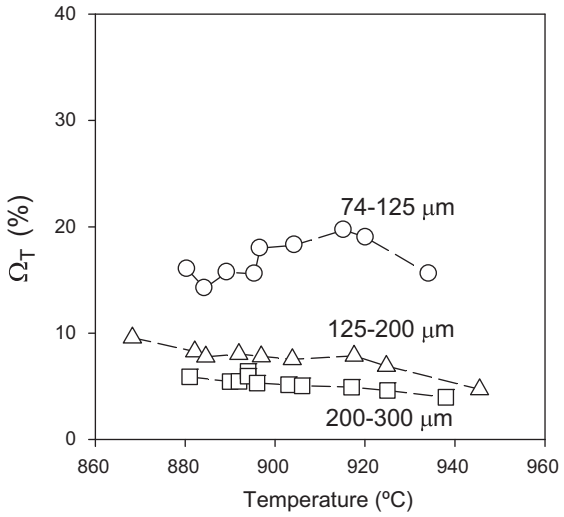


**Fig. 6.** Oxygen demand variation with the fuel-reactor temperature for different coal particle sizes.

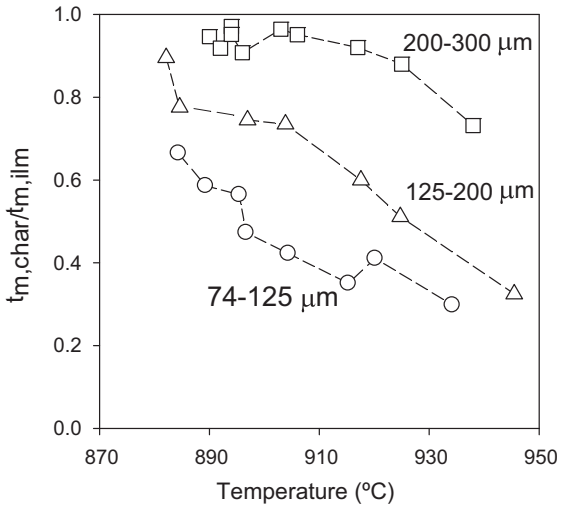


**Fig. 8.** Ratio between char and ilmenite mean residence times at different fuel-reactor temperatures and for different coal particle sizes. $t_{m,ilm}$ = 24 min.

### 4.2. Effect of the coal particle size

The effect of the coal particle size on the process performance was investigated because it is a key parameter in the operation of fluidized-bed reactors. As it can be seen in Fig. 5, minor differences were found for the char conversion and carbon capture with different particle size. However, a more detailed analysis shows that the oxygen demand depended on the particle size. Fig. 6 showed that the total oxygen demand, $\Omega_T$, increased as the particle size was decreasing. This behavior can be related to different flow of char elutriated from the bed for different particle size. Fig. 7 shows the calculated fraction of elutriated char for the different experiments made at different temperatures and coal particle sizes. As expected, smaller particles are more easily elutriated than bigger particles. For particle sizes of +74–125 μm about 35% of the introduced char had been elutriated, whereas lower values than 5% were found in most cases for bigger particles.

The lower values calculated for the combustion efficiency or higher oxygen demands for the smaller particles in this unit were related to the relatively high amounts of CO and $H_2$ in the gas product from fuel-reactor, showed in Fig. 4. Unconverted gaseous products, i.e., CO, $H_2$ and $CH_4$, can come from a partial oxidation of the gases in the fuel-reactor, as well as char gasification in the fuel-reactor freeboard. The high values obtained for elutriated char with the lower coal particle size caused a higher fraction of char in the freeboard for smaller particles. The result was therefore that gasified fuel particles in the freeboard had not been in contact with the ilmenite particles that remain at the bottom bed and thus production of CO and $H_2$ was higher for the smaller coal size. Thus, the combustion efficiency decreased for the particle size of +74–125 μm (see Fig. 5) because the gasification products in the freeboard were not burnt, although the char conversion was rather constant. Indeed, the total oxygen demand, $\Omega_T$, increased when the particle size decreased (see Fig. 6).

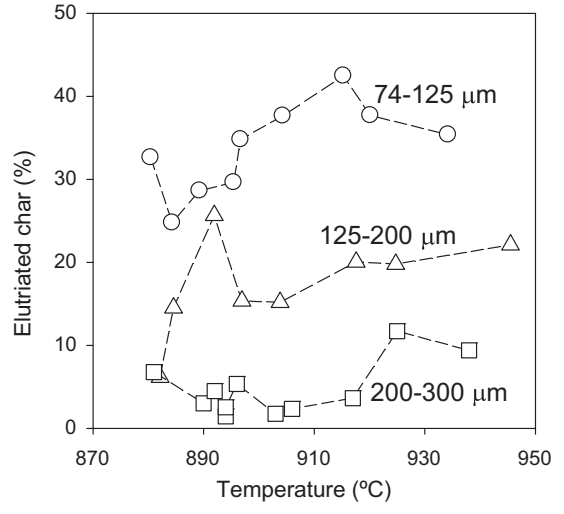


**Fig. 7.** Elutriated char fraction variation with the fuel-reactor temperature for different coal particle sizes.

The average mean residence time of ilmenite in the above described experiments was 10 min. However, as there was char elutriation, the residence time of char particles should be lower than it was for ilmenite. Fig. 8 represents the ratio between the calculated mean residence time of char particles and mean residence time of ilmenite particles for different temperatures and coal particle sizes. Residence times of char, $t_{m,char}$, were always lower than ilmenite residence times, $t_{m,ilm}$. This difference was a consequence of the char elutriation. For the bigger coal particle size the ratio between the residence time of char and ilmenite particles was very close to the unity and the $t_{m,char}/t_{m,ilm}$ ratio was lower for smaller particles because the fraction of elutriated particles was higher. At about 900 °C the residence time of char was 23 min for +200–300 μm, 18 min for +125–200 μm and decreased to 11 min for +74–125 μm. Smaller particles had lower time for gasification in the reactor than coarse particles. However, the char conversion is barely affected by the particle size because both the numerator and denominator of Eq. (9) decrease with the coal particle size. The amount of char gasified in the fuel-reactor was therefore lower for smaller particle sizes as well as the effective char introduced. Furthermore, the difference between $t_{m,char}$ and $t_{m,ilm}$ was greater for higher temperatures. This decrease of $t_{m,char}$ with the temperature could be because at higher temperatures char gasification is promoted, being the smaller or more porous resulting char particles easier elutriated.

If a simplified model is used, an approximation to the char gasification rates for the experiments performed at different temperatures with the coal particle sizes tested can be obtained. The fuel-reactor is considered to follow a continuous stirred-tank reactor (CSTR) model. It is also assumed that the solid fuel reacts at a rate which is proportional to the mass. The carbon char lost exiting the fuel-reactor that enters the air-reactor, $C_{char,AR}$, can be expressed

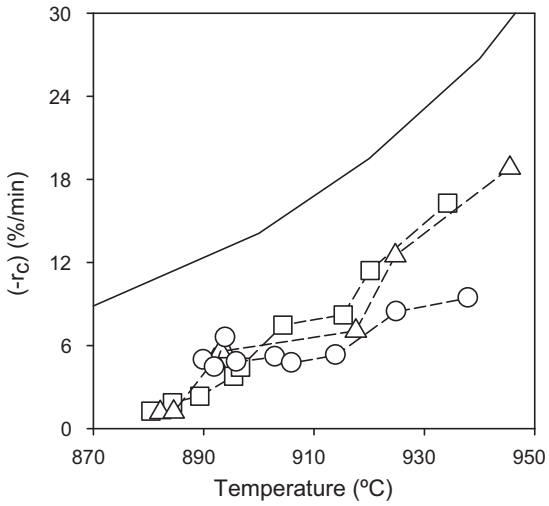


**Fig. 9.** Calculated gasification rate considering the fuel-reactor as a CSTR for different fuel-reactor temperatures. Coal particle size: (○) 74–125 μm; (△) 125–200 μm; (□) 200–300 μm. (—) Theoretical gasification rate as for the results by Linderholm et al. (2011).

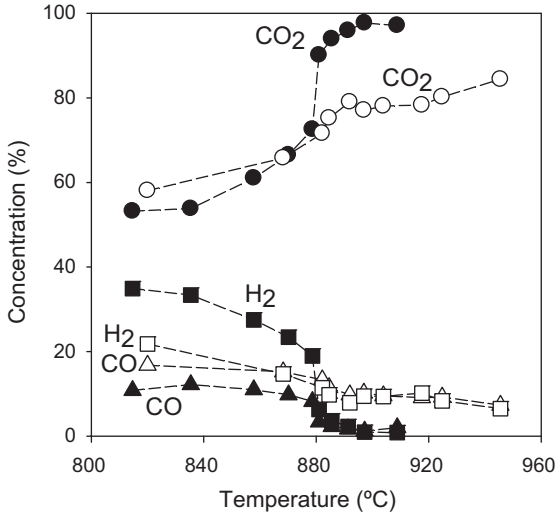


**Fig. 10.** $CO_2$, CO and $H_2$ concentration in the fuel-reactor (dry free $N_2$ basis) at different fuel-reactor temperatures for +125–200 μm char (filled symbol plots) and +125–200 μm coal (void symbol plots).

as a function of the effective carbon char introduced in the CLC system, $C_{char,eff}$, and $(-r_C)\cdot t_{m,char}$, where $(-r_C)$ is the rate of char coal conversion and $t_{m,char}$ is the char mean residence time:

$$\frac{C_{char\,AR}}{C_{char\,eff}} = \frac{1}{(-r_C)\cdot t_{m,char} + 1} \quad (18)$$

Fig. 9 shows the calculated char gasification rates with this simplified model for experiments performed at a temperature range and for the three particle sizes tested. The gasification rate increased with the temperature for every particle size.

The gasification rates at different temperatures using steam as gasification agent for El Cerrejón coal was obtained also by Linderholm et al. (2011). For a comparison purpose, Fig. 9 also represents the theoretical gasification rate as a function of the temperature that would be expected as for these mentioned results. The values for char gasification obtained in this continuous performance are close to the previous results from batch testing by Linderholm et al. (2011), but somewhat lower. However, the gasification rates here obtained were higher than the corresponding found with TGA analysis (Cuadrat et al., 2011).

As it was stated before with the char conversions, it can be seen that in general the gasification rate does not depend on the particle size, as the values are similar at a given temperature for the coal particle size tested. Nevertheless, for the smaller particle size the values were lower at higher temperatures. This was because for the +74–125 μm particles there was some gasification taking place in the freeboard and lower gasification rates in the bed were obtained, which is in line with what was already seen.

### 4.3. Char gasification

10 experiments were done using char coal previously produced in FB fluidized with $N_2$ in which the temperature in the fuel-reactor was varied from 815 to 910 °C. The ultimate analysis of the char is shown in Table 3. The fuel feed was 60.5 g/h, which corresponds to a thermal power of 370 $W_{th}$. The char particle size used was +125–200 μm. For further comparison, the results obtained are analyzed together with the results of the +125–200 μm coal tests, for which 10 experiments with $T_{FR}$ variation were done.

Fig. 10 shows the free $N_2$ basis $CO_2$, CO and $H_2$ dry concentrations obtained in the fuel-reactor at different fuel-reactor temperatures for all experiments tested when feeding +125–200 μm char and when introducing +125–200 μm coal as fuel. The oxidation with ilmenite of the gasification products increases with the temperature, which causes the decrease of CO and $H_2$ and fast increase in the $CO_2$ concentration with $T_{FR}$ when using char as fuel. Above 890 °C the fuel-reactor exit flow is practically composed only by $CO_2$ in dry basis. This trend can be also seen in the tests with coal, but smoother, since the combustion behavior of volatile matter is different.

For char as fuel, the carbon capture and the defined char conversion are coincident. The char conversion using char as fuel increased with the temperature from 5% at 820 °C to 23% at 910 °C. The char residence times were calculated to be 3–5 min. As it can be seen in Fig. 11, for coal experiments higher char conversions were obtained. This was because the char residence time in these tests was higher: 7–22 min. Higher char fraction was elutriated when using char as fuel, about 25%, whereas for the coal tests used as reference was 10–20%.

The oxygen demand for char particles at temperatures higher than 890 °C was near to zero (see Fig. 12), that is, although not all

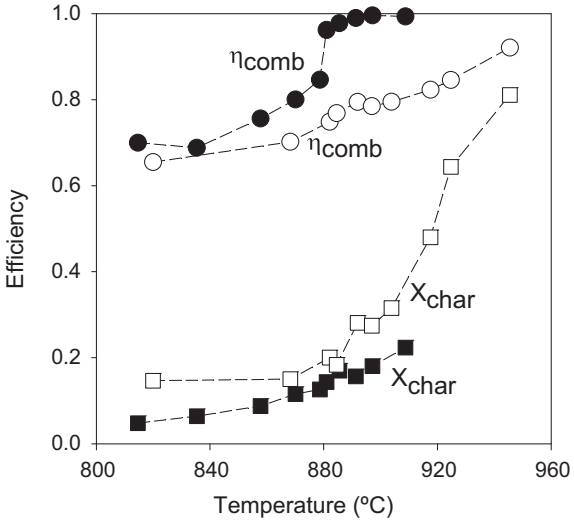


**Fig. 11.** Char conversion and combustion efficiencies at different fuel-reactor temperatures for +125–200 μm char (filled symbol plots) and +125–200 μm coal (void symbol plots).

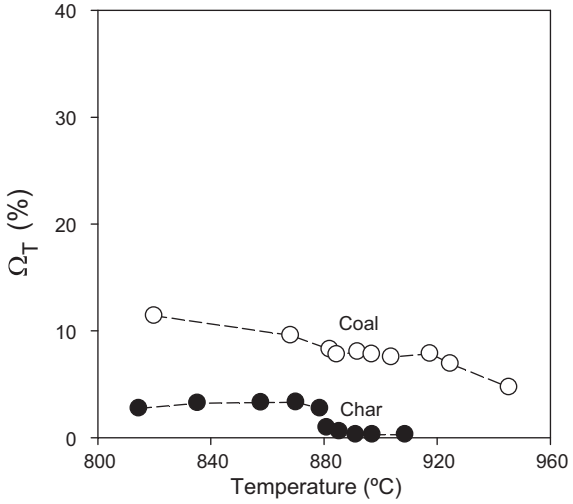


**Fig. 12.** Oxygen demand at different fuel-reactor temperatures for +125–200 μm char (filled symbol plots) and +125–200 μm coal (void symbol plots).

the char was gasified, the produced gases were burnt by ilmenite, which corresponded to a combustion efficiency close to 100% (see Fig. 11). This confirmed that the gasification is the limiting step of this process. Since in the large scale the CLC process will be performed at high temperatures and for enough oxygen-carrier bed mass, it is expected that the combustion efficiency of the gasification products reached high values. Thus, the outgoing unburnt gases seen in the fuel-reactor when using coal as fuel were part of the volatile matter that had not been fully oxidized by ilmenite, and the oxygen demand observed at higher temperatures was mainly due to some unburnt volatile matter. In addition, other possible problems that could cause unburnt gases in the fuel-reactor, would be caused by the later gasification of elutriated char particles in the fuel-reactor freeboard that would not be in contact with ilmenite particles, or insufficient residence time in contact with ilmenite of part of the gasification products.

Thus, in order to avoid unreacted fuel gases in offgas a subsequent oxygen polishing step can be implemented, as already proposed by Berguerand and Lyngfelt (2008a). To reduce the oxygen requirements in this polishing step, an improved design of the fuel-reactor could be done in order to get better contact between the volatile matter and the oxygen-carrier particles.

### 4.4. Volatile matter combustion

A key aspect of the process is the oxidation of the gasification products by ilmenite, as well as the released volatile matter, and possible tars formed. In order to evaluate to what extent ilmenite oxidizes the volatile matter, an experiment with sand as inert bed material was done with coal as fuel at 915 °C and steam as gasification agent in the fuel-reactor. The total sand bed mass in the system was 1.8 kg and the solid bed mass in the fuel-reactor was 0.38 kg sand.

The results obtained were compared to the experiments performed at the same temperature with ilmenite as bed material with coal as fuel and with char as fuel. GC analysis of the outgoing fuel-reactor gases was done to measure possible hydrocarbons, and possible tar formation was also measured following the tar protocol. The fed coal flow was 75 g/h. The particle size used was +125–200 μm and it is here compared with the test performed at 915 °C with +125–200 μm coal and ilmenite as bed material, for which the coal flow was 48 g/h.

For sand as bed material, the GC measurement showed that the fuel-reactor product gas had compositions of 0.13vol.% $C_2H_6$ and 0.04vol.% $C_3H_8$. Besides, the tar content in the fuel-reactor was measured to be 0.895 g/Nm$^3$ dry gas, following the tar protocol. Although the quantities measured of both tars and higher hydrocarbons for this fuel were quite low in absence of an oxygen-carrier, ilmenite has shown to help with the decomposition and later oxidation of those species, since no tars either higher hydrocarbons than $CH_4$ were formed when using ilmenite.

A summary with the main results of both continuous tests using sand and ilmenite are gathered in Tables 4–6. From the ultimate and proximate analysis, the carbon corresponding to the volatile matter, and consequently, the carbon coming from char gasification were calculated. Table 4 shows the fractions from the fuel-reactor product gas that correspond to both volatile matter and gasification products. 88.5% of the carbon contained released gases with sand as bed material came from released volatile matter. But when using ilmenite, the relevance of volatile matter decreased because more gases were released as char was being faster gasified. Table 5 shows the ratio of the carbon containing gases from the volatile matter. For sand as bed material, 36.7% of the carbon from volatile matter exited in form of CO, and 10.2% in form of $CH_4$. When using ilmenite, all the CO, $CH_4$ and $H_2$ measured came from unburnt released volatile matter, as the tests with coal char showed that the gasification products were fully oxidized. For the tests with ilmenite, some CO was oxidized and 23.7% of carbon from the volatile matter exited as CO, the $CH_4$ fraction decreased to 6.3% and the $CO_2$ fraction increased to 70%. From the comparison between both tests, it turned out that at 915°C the gas conversion of the released volatiles by the reaction with ilmenite was 38.3% for $CH_4$, 35.3% for CO and 79.0% for $H_2$. The reaction differences between gases are due to the reaction rates of ilmenite, since it reacts faster with $H_2$ and slower $CH_4$ (Abad et al., 2011). In addition, more oxygen transfer is needed to oxidize

**Table 4**
Relative fraction of the carbon from volatile matter and carbon from gasified char in comparison to the total carbon outgoing with the fuel-reactor product gas. Tests with sand and ilmenite as bed material. $T_{FR}$ = 915 °C.

| | Coal + Sand | Coal + Ilmenite |
|---|---|---|
| $\frac{C_{vol}}{(F_{CH_4}+F_{CO}+F_{CO_2})}$ | 88.5% | 42.6% |
| $\frac{C_{gasif\,char}}{(F_{CH_4}+F_{CO}+F_{CO_2})}$ | 11.5% | 57.4% |

**Table 5**
Flows of the generated gases, i.e., $CH_4$, CO and $CO_2$, released from the devolatilization in comparison to the total carbon contained in the fed volatile matter. Tests with sand and ilmenite as bed material. $T_{FR}$ = 915 °C.

| | Coal + Sand | Coal + Ilmenite |
|---|---|---|
| $\left(\frac{F_{CH_4,FR}}{C_{FR}}\right)_{vol}$ | 10.2% | 6.3% |
| $\left(\frac{F_{CO,FR}}{C_{FR}}\right)_{vol}$ | 36.7% | 23.7% |
| $\left(\frac{F_{CO_2,FR}}{C_{FR}}\right)_{vol}$ | 53.1% | 70.0% |

**Table 6**
Efficiencies and mean residence times for char and the bed materials: sand and ilmenite. Tests with sand and ilmenite as bed material. $T_{FR}$ = 915 °C.

| | $X_{char}$ | $\eta_{CC}$ | $\eta_{comb}$ | $t_{m,char}$ | $t_{m,bed\ material}$ |
|---|---|---|---|---|---|
| Coal + Sand | 0.052 | 0.322 | 0 | 6.2 min | 9.4 min |
| Coal + Ilmenite | 0.481 | 0.617 | 0.810 | 5.7 min | 9 min |

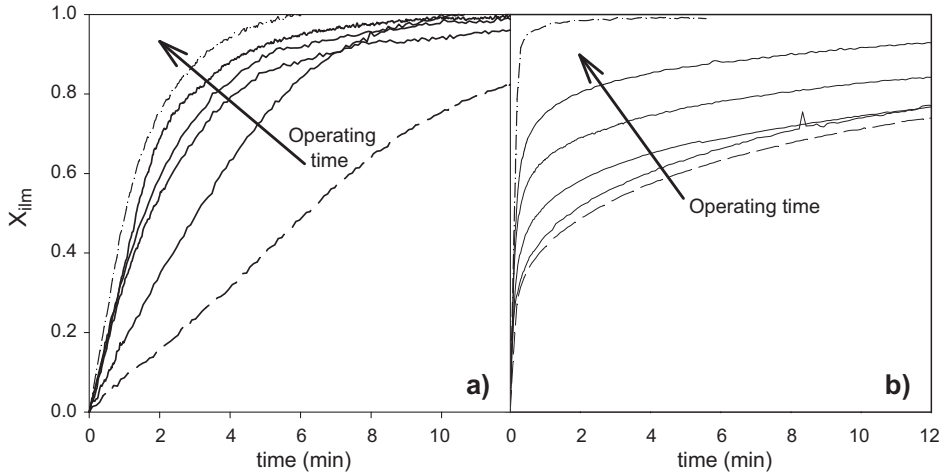


**Fig. 13.** Ilmenite conversion vs. time for (a) reduction and (b) oxidation for calcined ilmenite and for ilmenite samples after 1, 3, 15 and 35 h of continuous operation. Comparison with the reduction and oxidation conversions of calcined ilmenite (– – –) and a fully activated ilmenite sample (– · – · –).

$CH_4$. Thus, 63.0% of the oxygen demanded to fully burn the volatile matter fraction was supplied by ilmenite.

Besides, Table 6 shows all the calculated efficiencies and mean residence times for char and the bed material. Char conversion increased from 5.2% to 48.1%. This can be explained through the inhibition effect that causes the presence of high amounts of $H_2$ and CO in the fuel-reactor, as they do not react with the oxygen-carrier. Obviously, the combustion efficiency was almost zero, as sand is no oxygen-carrier.

### 4.5. Activation of ilmenite in the continuous rig

Solids samples were extracted during the continuous experiments at several operating times. Since the initial material is calcined ilmenite, an activation process is expected to happen with the number of the red-ox cycles, as it was previously seen from batch experiments (Cuadrat et al., submitted for publication-b). A sample taken from the air-reactor after the experiments was analyzed by XRD. $Fe_2TiO_5$, $Fe_2O_3$ and $TiO_2$ were found to be the major components. A semi-quantitative analysis done by XRD showed that the ratio between the weight compositions of the main active species for the oxygen transfer $Fe_2TiO_5$:$Fe_2O_3$ of milled particles was 82:18. That is, as for the XRD analysis there were no major changes in the composition of the particles, compared to the composition of the initial material (Adánez et al., 2010). Furthermore, another sample taken from the fuel-reactor was analyzed by XRD and it was proven to be mainly composed by a mixture of $Fe_2TiO_5$, $Fe_2O_3$, $Fe_3O_4$, $FeTiO_3$ and $TiO_2$.

Reactivity of ilmenite samples taken after 1, 3, 15 and 35 h of operation was determined by TGA at 900°C with 5% $H_2$ + 40% $H_2O$ mixtures, and afterwards to oxidation conditions in air. Fig. 13 shows the conversion, $X_{ilm}$, vs. time curves obtained for the reduction and oxidation for the different samples. To compare and observe the activation process undergone by ilmenite (Adánez et al., 2010), the reduction and oxidation conversions for calcined and a fully activated ilmenite sample are also represented. The activation undergone by ilmenite with the number of hours can be seen. It can be considered that ilmenite is already active after 3 h for the reduction reaction, although the reactivity increases further in minor extension after 15 h.

Nevertheless, ilmenite is not completely activated for oxidation reaction after 35 hours operation yet. As it can be seen in Fig. 12, the oxidation takes place in two steps and the change to the second phase occurs at higher conversions for samples taken after more hours of operation. Abad et al. (2011) concluded that the oxidation reaction for ilmenite follows a changing grain size model with two steps, being the first one faster and determined by the chemical reaction control and the second one is slower and controlled by the diffusion in the solid product. That is, an increase in the porosity decreases the relative importance of the second step. Calcined ilmenite had a porosity of 1.2%, after 15 h the porosity increased to 9.7% and after 35 cycles the measured porosity was 12.3%. The fully activated ilmenite sample is the same shown by Adánez et al. (2010) and it was activated after 100 redox cycles in TGA using $H_2$ as reducing agent, which had a porosity of 35%. The activation process was promoted by high variation of solids conversion in successive redox cycles. The average change in ilmenite conversion in the experiments was low, $\Delta X_{ilm} = 0.23$, and therefore a higher porosity development and full activation could not happen yet.

Besides, there is one further factor affecting the ilmenite properties during the redox cycles. In a previous work it was observed that ilmenite undergoes a migration phenomenon of the iron oxide present towards the external part of the particle while the core gets titanium enriched. That segregation leads to a gradual decrease in the oxygen transport capacity of the oxygen-carrier (Adánez et al., 2010). The oxygen transport capacity of ilmenite for samples taken at different operation times was determined by TGA and it was seen that it was maintained roughly constant with the operation time. A slight decrease from 4.0wt.% for calcined ilmenite to 3.9wt.% for particles used during 35 h in the unit was observed. In previous work (Cuadrat et al., submitted for publication-b) faster decrease in the oxygen transport capacity was measured and need of higher inventories in real CLC continuous systems was foreseen. After undergoing 100 redox cycles in 56 h with a syngas mixture as reducing agent, the oxygen transport capacity decreased from 4.0 to 2.1wt.%. The oxygen-carrier was however in those experiments further reduced, as $X_{ilm}$ was about 0.65 (considering $R_{O,ilm} = 4.0$wt.%). Thus, a low value of $\Delta \underline{X}_{ilm}$ allows maintaining the initial $R_{O,ilm}$ roughly constant during long time. In fact, SEM microphotographs of samples extracted from the CLC reactor do not show iron migration towards the outer part of the particle.

## 5. Conclusions

The capability of ilmenite as oxygen-carrier to burn coal as fuel in a 500 $W_{th}$ unit has been analyzed by obtaining the carbon capture

and combustion efficiencies of the fuel-reactor at a temperature range and with several particle sizes of coal. A bituminous Colombian coal "El Cerrejón" was used as fuel. At higher fuel-reactor temperatures, gasification and combustion reactions are faster and promoted. Carbon capture and combustion efficiencies grow with the temperature, with a faster increase above $T > 910\,^{\circ}C$. Little $CH_4$ was measured in all experiments and there were no tars in the fuel-reactor outlet flow. From 870 °C the char conversion was 15% and reached a value of 82% at 950 °C. The combustion efficiency varied from 70% at 870 °C to 95% at 950 °C. Although the carbon capture efficiency in this rig is not representative for the CLC technology, since it does not have a carbon stripper, high carbon capture efficiencies are expected to be obtained, as well as high combustion efficiency, specially at temperatures higher than 950 °C. Values for the total oxygen demand from 5% to 15% were found in all the experimental work, mainly due to unconverted CO and $H_2$. Thus, oxygen polishing need was quite low.

The experiments performed with char coal as fuel confirmed that the gasification is the limiting step of this process. However, the outgoing unburnt gases in the fuel-reactor measured when using coal as fuel, that is, $CH_4$, CO and $H_2$, came from volatile matter that had not been fully oxidized by ilmenite.

At 915 °C the gas conversion of the released volatiles by the reaction with ilmenite was 38.3% for $CH_4$, 35.3% for CO and 79.0% for $H_2$. The reaction differences between gases were due to the reaction rates of ilmenite, since it reacts faster with $H_2$ and slower $CH_4$. 63.0% of the oxygen demanded to fully burn volatile matter is supplied by ilmenite. Besides, char gasification was promoted by the presence of the oxygen-carrier, as ilmenite reacts with $H_2$ and CO, which are gasification inhibitors.

Minor effect on the char conversion can be expected when the coal particle size is varied. However, it is presumable that gasification continues in the fuel-reactor freeboard, this being more relevant for smaller particles. Thus, it is expected that the oxygen demand would increase as the coal particle size decreases.

Activation of ilmenite with the operating time in the unit was observed. For the reduction it can be considered that ilmenite is already active after 3 h. On the other hand, the oxidation reaction is not fully activated after 35 h operation yet. A decrease on the oxygen transport capacity of ilmenite was not observed.

## Acknowledgments

This work was partially supported by the European Commission, under the RFCS program (ECLAIR Project, Contract RFCP-CT-2008-0008), from Alstom Power Boilers and by the Spanish Ministry of Science and Innovation (Project ENE2010-19550). A. Cuadrat thanks CSIC for the JAE Pre. fellowship. Alberto Abad thanks to the Ministerio de Ciencia e Innovación for the financial support in the course of the I3 Program.

## References

Abad, A., Adánez, J., Cuadrat, A., García-Labiano, F., Gayán, P., de Diego, L.F., 2011. Reaction kinetics of ilmenite for Chemical-looping Combustion. Chemical Engineering Science 66 (4), 689–702.

Adánez, J., de Diego, L.F., García-Labiano, F., Gayán, P., Abad, A., Palacios, J.M., 2004. Selection of oxygen-carriers for chemical-looping combustion. Energy & Fuels 18, 371–377.

Adánez, J., Cuadrat, A., Abad, A., Gayán, P., de Diego, L.F., García-Labiano, F., 2010. Ilmenite activation during consecutive redox cycles in chemical-looping combustion. Energy & Fuels 24, 1402–1413.

Adánez, J., Abad, A., García-Labiano, F., Gayán, P., de Diego, L.F., 2011. Progress in Chemical-Looping Combustion and Reforming Technologies. Progress in Energy and Combustion Science, doi:10.1016/j.pecs.2011.09.001.

Berguerand, N., Lyngfelt, A., 2008a. Design and operation of a 10 kWth chemical-looping combustor for solid fuels—testing with South African coal. Fuel 87, 2713–2726.

Berguerand, N., Lyngfelt, A., 2008b. The use of petroleum coke as fuel in a 10 kWth Chemical-Looping Combustor. International Journal of Greenhouse Gas Control 2, 169–179.

Berguerand, N., Lyngfelt, A., 2009a. Operation in a 10 kWth chemical-looping combustor for solid fuel—testing with a Mexican petroleum coke. Energy Procedia 1 (1), 407–414.

Berguerand, N., Lyngfelt, A., 2009b. Chemical-looping combustion of petroleum coke using ilmenite in a 10 kWth unit-high-temperature operation. Energy & Fuels 23 (10), 5257–5268.

Bidwe, A.R., Mayer, F., Hawthorne, C., Charitos, A., Schuster, A., Scheffknecht, G., 2011. Use of ilmenite as an oxygen-carrier in chemical looping combustion-batch and continuous dual fluidized bed investigation. Energy Procedia 4, 433–440.

Cao, Y., Pan, W.P., 2006. Investigation of Chemical Looping Combustion by solid fuels. 1. Process analysis. Energy & Fuels 20, 1836–1844.

Cuadrat, A., Abad, A., Adánez, J., de Diego, L.F., García-Labiano, F., Gayán, P. Design considerations for Chemical-Looping Combustion of coal—Part 1. Experimental tests, submitted for publication-a.

Cuadrat, A., Abad, A., Adánez, J., de Diego, L.F., García-Labiano, F., Gayán, P. Behaviour of ilmenite as oxygen carrier in Chemical-Looping Combustion, submitted for publication-b.

Cuadrat, A., Abad, A., Gayán, P., de Diego, L.F., García-Labiano, F., Adánez, J., 2011. Modeling and optimization of Chemical Looping Combustion for solid fuels with ilmenite as oxygen carrier. International Conference on Coal Science & Technology (ICCS&T), October 2011.

Eide, L.I., Anheden, M., Lyngfelt, A., Abanades, C., Younes, M., Clodic, D., 2005. Novel capture processes. Oil Gas Science Technology 60, 497–508.

Fossdal, A., Bakken, E., Øye, B.A., Schøning, C., Kaus, I., Mokkelbost, T., Larring, Y., 2011. Study of inexpensive oxygen carriers for chemical looping combustion. International Journal of Greenhouse Gas Control 5 (3), 483–488.

Gu, H.M., Wu, J.H., Hao, J.G., Shen, L.H., Xiao, J., 2010. Experiments on chemical looping combustion of coal in interconnected fluidized bed using hematite as oxygen-carrier. Proceedings of the Chinese Society of Electrical Engineering 30 (17), 51–56.

Intergovernmental Panel of Climate Change, 2005. Special Report on Carbon Dioxide Capture and Storage. Cambridge University Press, Cambridge, UK (available at www.ipcc.ch).

Intergovernmental Panel of Climate Change, 2007. In: Solomon, S., Qin, D., Manning, M., Marquis, M., Averyt, K., Tignor, M.M.B., et al. (Eds.), The Physical Science Basis. Working Group I Contribution to the Fourth Assessment Report of the International Panel on Climate Change. Cambridge, United Kingdom, New York, NY, USA: Cambridge University Press.

Kerr, H.R., 2005. Capture and separation technologies gaps and priority research needs. In: Thomas, D., Benson, S. (Eds.), Carbon Dioxide Capture for Storage in Deep Geologic Formations—Results from the $CO_2$ Capture Project, vol. 1 (38). Elsevier Ltd., Oxford, UK.

Leion, H., Lyngfelt, A., Johansson, M., Jerndal, E., Mattisson, T., 2008a. The use of ilmenite as an oxygen-carrier in chemical-looping combustion. Chemical Engineering Research and Design 86, 1017–1026.

Leion, H., Mattisson, T., Lyngfelt, A., 2008b. Solid fuels in chemical-looping combustion. International Journal of Greenhouse Gas Control 2 (2), 180–193.

Leion, H., Mattissson, T., Lyngfelt, A., 2009. Use of ores and industrial products as oxygen carriers in chemical-looping combustion. Energy & Fuels 23, 2307–2315.

Linderholm, C., Cuadrat, A., Lyngfelt, A., 2011. Chemical-looping combustion of solid fuels in a 10 kWth pilot—batch tests with five fuels. Energy Procedia 4, 385–392.

Markström, P., Berguerand, N., Lyngfelt, A., 2010. The application of a multistage-bed model for residence-time analysis in chemical-looping combustion of solid fuel. Chemical Engineering Science 65, 5055–5066.

Ortiz, M., Gayán, P., de Diego, L.F., García-Labiano, F., Abad, A., Pans, M.A., Adánez, J., 2011. Hydrogen production with CO2 capture by coupling steam reforming of methane and chemical-looping combustion: use of an iron-based waste product as oxygen-carrier burning a PSA tail gas. Journal of Power Sources 196 (9), 4370–4381.

Pröll, T., Mayer, K., Bolhàr-Nordenkampf, J., Kolbitsch, P., Mattisson, T., Lyngfelt, A., Hofbauer, H., 2009. Natural minerals as oxygen-carriers for chemical looping combustion in a dual circulating fluidized bed system. Energy Procedia 1, 27–34.

Shen, L., Wu, J., Xiao, J., 2009a. Experiments on chemical looping combustion of coal with a NiO based oxygen-carrier. Combustion and Flame 156 (3), 721–728.

Shen, L., Wu, J., Gao, Z., Xiao, J., 2009b. Reactivity deterioration of NiO/Al2O3 oxygen-carrier for chemical looping combustion of coal in a 10 kWth reactor. Combustion and Flame 156 (7), 1377–1385.

Shen, L., Wu, J., Gao, Z., Xiao, J., 2010. Characterization of chemical looping combustion of coal in a 1 kWth reactor with a nickel-based oxygen-carrier. Combustion and Flame 157 (5), 934–942.

Simell, P., Stahlberg, P., Kurkela, E., Albretch, J., Deutch, S., Sjostrom, K., 2000. Provisional protocol for the sampling and anlaysis of tar and particulates in the gas from large-scale biomass gasifiers. Version 1998. Biomass and Bioenergy 18, 19–38.

Song, Q., Xiao, R., Deng, Z., Shen, L., Xiao, J., Zhang, M., 2008. Effect of temperature on reduction of CaSO4 of simulated coal gas in a fluidized bed reactor. Industrial Engineering Chemistry Research 47, 8148–8159.

Wang, J., Anthony, E.J., 2008. Clean combustion of solid fuels. Applied Energy 85, 73–79.

# Paper VI

International Journal of Greenhouse Gas Control xxx (2011) xxx–xxx

Contents lists available at SciVerse ScienceDirect

International Journal of Greenhouse Gas Control

journal homepage: www.elsevier.com/locate/ijggc

# Effect of operating conditions in Chemical-Looping Combustion of coal in a 500 $W_{th}$ unit

A. Cuadrat, A. Abad*, F. García-Labiano, P. Gayán, L.F. de Diego, J. Adánez

*Instituto de Carboquímica (CSIC), Department of Energy & Environment, Miguel Luesma Castán 4, 50018 Zaragoza, Spain*

ARTICLE INFO

*Article history:*
Received 10 June 2011
Received in revised form
26 September 2011
Accepted 31 October 2011
Available online xxx

*Keywords:*
Chemical-Looping Combustion
Oxygen-carrier
Ilmenite
$CO_2$ capture
Coal

ABSTRACT

Chemical-Looping Combustion, CLC, is one of the most promising processes to capture $CO_2$ at low cost. It is based on transferring the oxygen from air to the fuel by using a solid oxygen-carrier that circulates between two interconnected fluidized-bed reactors: the fuel- and the air-reactor.

In this work, CLC with coal was investigated in a continuous 500 $W_{th}$ rig using ilmenite as oxygen-carrier and Colombian bituminous coal as fuel. In the fuel-reactor the oxygen-carrier is reduced by the volatile matter and coal gasification products.

The effect of operating conditions such as the solids circulation rate and oxygen-carrier residence time, the coal flow feed and the steam flow as gasification agent were investigated on the combustion efficiency and extent of gasification. The influence of using $CO_2$ as gasification agent was assessed by doing experiments with different $CO_2$–$H_2O$ mixtures.

The results obtained are valid for the scale-up of a CLC process with coal. They indicate that it is feasible to decrease the gasification agent flow to lower values than the corresponding stoichiometric for the gasification, and that some of the steam as gasification agent can be replaced by $CO_2$ recirculated from the fuel-reactor outlet. Low circulation rate of solids improved coal conversion.



## 1. Introduction

It is generally accepted that a reduction in the greenhouse gases emissions is necessary as soon as possible to restrain the effects of climate change. Up to now, the technological options for reducing net $CO_2$ emissions to the atmosphere have been focused on (IPCC, 2005): (1) reducing energy consumption, by increasing the efficiency of energy conversion and/or utilization; (2) switching to less carbon intensive fuels; (3) increasing the use of renewable energy sources (biofuel, wind power, etc.) or nuclear energy, and (4) sequestering $CO_2$. Carbon capture and sequestration or storage, CCS, has attracted interest as a measure for mitigating global climate change because large amounts of $CO_2$ emitted from fossil fuel use are potentially available to be captured and stored underground or prevented from reaching the atmosphere. Furthermore, large industrial sources of $CO_2$, such as electricity-generating plants, are likely initial candidates for CCS because they are predominantly stationary, single-point sources.

In this context, Chemical-Looping Combustion (CLC) is one of the most promising technologies to carry out $CO_2$ capture at a low cost (Eide et al., 2005). CLC is based on the transfer of the oxygen from air to the fuel by means of a solid oxygen-carrier that circulates between two interconnected fluidized beds: the fuel- and the air-reactor. In the fuel-reactor the oxygen-carrier is reduced through oxidation of the fuel, thus obtaining a gas stream composed by $CO_2$ and $H_2O$. The oxygen-carrier is afterwards directed to the air-reactor, where it is re-oxidized with air and regenerated to start a new cycle. The net chemical reaction is the same as at usual combustion with the same combustion heat released, but with the advantage of the intrinsic $CO_2$ separation in the process without an additional step.

Using CLC with solid fuels is very interesting, regarding the intensive use of solid fuels as energy source. One of the options for CLC with solid fuels is directly to introduce coal in the fuel-reactor, where it is mixed with the oxygen-carrier and being the fuel-reactor fluidized by a gasification agent, i.e. $H_2O$ or $CO_2$ (Cao and Pan, 2006). Thereby, the solid fuel gasification takes place as for reactions (1)–(3), and simultaneously the oxidized oxygen-carrier, $Me_xO_y$, reacts with the gaseous products of coal devolatilization and gasification, with $H_2$ and CO as main components, according to reaction (4). The reduced oxygen-carrier from the fuel-reactor, $Me_xO_{y-1}$, is subsequently oxidized with air in the air-reactor following reaction (5):

$$\text{Coal} \rightarrow \text{volatilematter} + \text{char} \quad (1)$$

$$\text{Char} + H_2O \rightarrow H_2 + CO \quad (2)$$

* Corresponding author. Tel.: +34 976 733 977; fax: +34 976 733 318.
*E-mail address:* abad@icb.csic.es (A. Abad).

1750-5836/$ – see front matter © 2011 Published by Elsevier Ltd.
doi:10.1016/j.ijggc.2011.10.013

**Nomenclature**

| | |
|---|---|
| $F_{C\ char\ AR}$ | carbon flow from the char that goes to the air-reactor (mol/s) |
| $F_{C\ char\ elutr}$ | carbon flow from the elutriated char (mol/s) |
| $F_{C\ vol}$ | carbon flow coming from the volatile matter fed (mol/s) |
| $F_i$ | flow in the fuel-reactor of the corresponding gas $i$ (mol/s) |
| $F_{ilm}$ | solids circulation rate (kg/s) |
| $H_2O/C$ | steam to fixed carbon ratio (mol $H_2O$/mol C) |
| $M_C$ | carbon atomic mass (kg/mol) |
| $\dot{m}_{C,coal\ eff}$ | effective carbon in the coal feeding flow rate (kg/s) |
| $m_{char,FR}$ | mass of char in the fuel-reactor (kg) |
| $m_{ilm,FR}$ | fuel-reactor bed mass or solid hold-up in the fuel-reactor (kg) |
| $M_{O_2}$ | oxygen molecular mass (kg/mol) |
| $O_{2\ demand\ coal,eff}$ | oxygen demand of the effective coal fed (mol $O_2$/s) |
| $O_{coal,eff}$ | flow of oxygen contained in the effective coal introduced (mol O/s) |
| $(-r_O)$ | rate of oxygen transferred by the oxygen-carrier (kg $O_2$/s kg OC) |
| $R_{O,ilm}$ | oxygen transport capacity of ilmenite |
| $T_{FR}$ | temperature in the fuel-reactor (°C) |
| $t_{m,char}$ | mean residence time of char (s) |
| $t_{m,ilm}$ | mean residence time of ilmenite (s) |
| $X_{char}$ | char conversion |
| $x_{char,FR}$ | carbon concentration from char in the fuel-reactor |
| $\eta_{CC}$ | carbon capture efficiency |
| $\eta_{comb\ FR}$ | combustion efficiency of the fuel-reactor |
| $\Omega_T$ | oxygen demand |
| $\phi$ | oxygen-carrier to fuel ratio |

$$\text{Char} + CO_2 \rightarrow 2CO \quad (3)$$

$$H_2, CO, \text{volatilematter} + n\text{Me}_x\text{O}_y \rightarrow CO_2 + H_2O + n\text{Me}_x\text{O}_{y-1} \quad (4)$$

$$\text{Me}_x\text{O}_{y-1} + 1/2O_2 \rightarrow \text{Me}_x\text{O}_y \quad (5)$$

Although ideally the $CO_2$ capture is inherent to this process, as the air does not get mixed with the fuel, the $CO_2$ capture efficiency when using solid fuels decreases if non-gasified char particles are by-passed to the air-reactor. The gasification process has been identified as the controlling step in this process (Cuadrat et al., submitted for publication-a; Dennis and Scott, 2010). Char gasification is usually a slow process, and the solids stream exiting from the fuel-reactor could contain some unconverted char together with the oxygen-carrier. Therefore, enough high residence time in the fuel-reactor is needed so that char particles are gasified.

To increase the residence time of char particles in the fuel-reactor, without excessive increase of the reactor size, an option is to separate the char exiting the fuel-reactor from the oxygen-carrier particles and recirculate the char to the fuel-reactor. Thereby, the amount of carbon transferred from the fuel- to the air-reactor is reduced. Based on the different fluidizing properties of remaining char and oxygen-carrier particles, a carbon stripper has been proposed as a promising equipment to carry out the separation of char (Cao and Pan, 2006; Morin et al., 2010). The critical role of the carbon stripper has been pointed out in numerous previous studies (Ströhle et al., 2010; Kramp et al., 2011; Cuadrat et al., submitted for publication-a, submitted for publication-c). In previous CLC experiments with solid fuels performed to date, full oxidation of the outlet fuel-reactor stream could not be achieved (Berguerand and Lyngfelt, 2008a,b, 2009; Cuadrat et al., in press; Shen et al., 2009a,b,c). Therefore, in order to oxidize completely unburnt compounds to $CO_2$ and $H_2O$, an "oxygen polishing" step downstream was proposed, that is, injection of pure oxygen to the gas flow after the fuel-reactor cyclone (Berguerand and Lyngfelt, 2008a,b), which is usually called oxygen demand.

To use an oxygen-carrier with adequate behavior and properties is fundamental to reach high performance of the CLC process. As for this option of CLC with solid fuels, the fuel is physically mixed with the oxygen-carrier, being predictable a partial loss of oxygen-carrier particles together with the draining stream of coal ashes to avoid their accumulation in the system. In this context, the use of low cost materials such as natural minerals or industrial waste products as oxygen-carriers turns out to be very interesting. Ilmenite is a low cost natural mineral which is promising for its large scale industrial use as oxygen-carrier with solid fuels. Performance of ilmenite has been proven to be acceptable as oxygen-carrier for CLC in recent studies made at different scales (Adánez et al., 2010; Abad et al., 2011). Comparing the performance of several natural iron ores and industrial products, Norwegian ilmenite was ranged among the materials which showed higher reactivity as for gaseous fuel as for solid fuels (Leion et al., 2009a,b). Although ilmenite particles have initially a rather low reactivity, it undergoes an activation process after several redox cycles, being its reactivity remarkably increased for $H_2$, CO and $CH_4$ as reacting gases (Adánez et al., 2010). The gas conversion showed by activated ilmenite was even similar to one synthetic $Fe_2O_3/MgAl_2O_4$ material selected from previous works (Leion et al., 2008). Ilmenite has high conversion of CO and $H_2$ for syngas applications, but moderate conversion of $CH_4$ for the use of natural gas as fuel (Adánez et al., 2010). On the whole, ilmenite has adequate values of reactivity and oxygen transport capacity for its use in the CLC technology with solid fuels, which is confirmed by the results from the continuous CLC experiments done to date. Additionally, ilmenite showed good mechanical stability and good fluidizing properties (Cuadrat et al., submitted for publication-b).

The feasibility of the process has been proven during continuous operation in CLC units ranging from 500 $W_{th}$ to 10 $kW_{th}$. As mentioned, ilmenite was the most common oxygen-carrier used. Continuous operation using solid fuels showed that the concentration of CO and $H_2$ in the flue gases due to unconverted gasification products are in the range 0.7–1.5 vol%, corresponding to an oxygen demand in the fuel-reactor of 5–9% (Berguerand et al., 2009). Besides, unconverted gases from volatiles in the fuel-reactor outlet were detected when using ilmenite (Cuadrat et al., in press). The extent of unburt volatiles was the same as if a highly Ni-based oxygen-carrier was used (Shen et al., 2009a,b, 2010). Indeed, the unconverted gases from volatiles were higher than those originated in char gasification. Experiments in a 500 $W_{th}$ CLC unit showed that unburnt tars or hydrocarbons were not present in the fuel-reactor outlet, except $CH_4$ which was found at low concentration (Cuadrat et al., in press). Gasification products were near fully converted to $CO_2$ and $H_2O$ but unconverted CO and $H_2$ proceeding from coal devolatilization were outgoing from the fuel-reactor. In the bigger scale and with other type of fuels, ilmenite was also successfully tested in a 10 $kW_{th}$ chemical-looping combustor using South African coal and petroleum coke as solid fuels by Berguerand and Lyngfelt (2008a,b). They analyzed the combustion process focusing on char conversion. From results showed in these studies the temperature is the main parameter of influence in the performance of the system, being higher efficiencies reached at high temperatures. Temperatures above 1000 °C were tested in some cases (Berguerand and Lyngfelt, 2009). Combustion efficiencies from 85 to 95% and average carbon capture efficiencies of 80% were obtained in all the experimental works at high temperatures in CLC with solids fuels using ilmenite. Likewise, ilmenite as an oxygen-carrier was investigated by Bidwe et al. (2011) on a 10 $kW_{th}$ facility using

Please cite this article in press as: Cuadrat, A., et al., Effect of operating conditions in Chemical-Looping Combustion of coal in a 500 $W_{th}$ unit. Int. J. Greenhouse Gas Control (2011), doi:10.1016/j.ijggc.2011.10.013

batch, semi batch and continuous mode experiments. The rate of gasification was seen to approximately double when increasing the temperature from 900 to 950 °C. Furthermore, an equalmolar CO–$H_2$ syngas was combusted at 900 °C resulting in a steady-state conversion of circa 90%.

The combustion efficiency in the fuel-reactor, the efficiency of char separation in the carbon stripper, and the separation of ashes from the oxygen-carrier are key factors for the development of this process. The coal combustion efficiency depends on the char conversion in the reactor and on the reactivity of the oxygen-carrier with the volatiles and gasification gases.

Biomass as solid fuel was evaluated by Shen et al. (2009c) in a continuous 10 $kW_{th}$ CLC combustor using an oxygen-carrier prepared from iron oxide and $CO_2$ as gasification medium. The CO concentration of the fuel-reactor flue gas increased with the fuel-reactor temperature, since biomass gasification with $CO_2$ was more temperature dependent than CO oxidation with iron oxide. Gu et al. (2011) also proved the feasibility of using CLC for both biomass and a biomass/coal mixture as solid fuels in a continuous 1 $kW_{th}$ CLC facility and using an Australian iron ore as oxygen carrier. Since the CLC process of biomass has potential problems derived from the existence of alkali metals in biomass ash, they proposed to blend biomass with coal to reduce the alkali metal content in the fuel thus decreasing alkalinity, or to add some materials such as $SiO_2$ and kaoline to convert alkali metals to compounds with a high melting point.

The effect of the gasification agent has been assessed in batch experiments. Previous research using bituminous Colombian coal show that the conversion rate of char using $CO_2$ as fluidizing agent is about 5 times lower than using $H_2O$ instead (Cuadrat et al., submitted for publication-a). The $CO_2$ concentration in the fluidizing gas would be limited to 20% in order to maintain a high gasification rate with that bituminous coal (Cuadrat et al., submitted for publication-a). In this case, whereas the steam gasification proceeds in minutes, the $CO_2$ gasification time is of the order of hours. As for the gasification agent, most studies have used steam. If $CO_2$ was used, the energy required for steam production is avoided. $CO_2$ can be re-circulated from the flue gases. The use of $CO_2$ has been proposed for highly reactive solid fuels, such as low-rank coals or biomass (Brown et al., 2010). Sub-bituminous and lignite coal char have shown gasification rates using $CO_2$ as high as for $H_2O$ (Johnson, 1981). Dennis et al. (2006) tested the feasibility of using pure iron oxide and a lignite fuel gasified by $CO_2$ in a batch fluidized-bed reactor. They stated that although the oxygen-carrier used (pure $Fe_2O_3$) was not optimized, it was still able to burn most of the CO produced by the gasification of the carbon. Using these types of coal could be advantageous because recirculated $CO_2$ could be used as fluidizing agent. Besides, dry gasification of a lignite (Scott et al., 2006) was found to be as fast as the steam gasification of bituminous coal (Leion et al., 2009c) using Fe-based oxygen-carriers. In continuous testing, Shen et al. (2009a,c) extracted a small part of the flue gas, which was enriched in $H_2O + CO_2$, and circulated it into its bottom, to use it as the fluidization medium and coal gasification agent. On the whole, the $CO_2$ recirculation can be an interesting option when highly reactive solid fuels, that is, sub-bituminous coal, solid waste or biomass, or high-sulfur coals are used.

The effect of the solids circulation rate and the resulting mean residence time of the oxygen-carrier particles has been to date only tested experimentally for continuous CLC with gaseous fuels (Adánez et al., 2009; Dueso et al., 2009; Forero et al., 2009). Markström et al. (2010) developed a model for solid fuels that determined the circulation mass flow, the residence time and residence-time distribution of particles in the fuel-reactor for a number of operational cases previously done in a 10 $kW_{th}$ rig for solid fuels with different particle circulation. With the model and experimental results they established a relation between the system performance versus residence time using data of batch and continuous tests feeding pet coke and a South African coal at fuel-rector temperature of 950 °C.

**Table 1**
Properties of the used pre-treated Colombian coal.

| | | | |
|---|---|---|---|
| C | 65.8% | Moisture | 2.3% |
| H | 3.3% | Volatile matter | 33.0% |
| N | 1.6% | Fixed carbon | 55.9% |
| S | 0.6% | Ash | 8.8% |
| O | 17.6% | | |

Low heating value: 21,899 kJ/kg.

In this work, the CLC technology with a Colombian bituminous coal was investigated in a continuous 500 $W_{th}$ rig using ilmenite as oxygen-carrier. The aim of this work was to study the conversion of coal in the fuel-reactor under different operating conditions, which has been not tested to date in a continuous facility. The effect of operating conditions such as the solids circulation rate, the coal flow feed and the gasification agent flow were investigated on the combustion efficiency and the extent of gasification in the fuel-reactor. The fluidizing gas, which also acts as gasification agent, was steam. Besides, the influence of using $CO_2$ as gasification agent was assessed by doing experiments with different $CO_2$:$H_2O$ mixtures. The results obtained are analyzed and discussed in order to be useful for the scale-up of a CLC process fuelled with coal.

## 2. Experimental

### 2.1. Bed material and fuel

Norwegian ilmenite has been the most used material for Chemical-Looping coal Combustion. The bed material in this study was ilmenite with particle size of +150–300 μm. Ilmenite is a common mineral found in metamorphic and igneous rocks. The ilmenite used is a concentrate from a natural ore. It is mainly composed of $FeTiO_3$ ($FeO{\cdot}TiO_2$) and some free $Fe_2O_3$, where iron oxide is the active phase that behaves as the oxygen-carrier. A semi-quantitative analysis performed by XRD of an oxidized sample showed that the used ilmenite was composed by 11.7% $Fe_2O_3$, 53.2% $Fe_2TiO_5$ and 29.5% $TiO_2$. More details about the physical properties of the ilmenite particles used and their behavior can be found elsewhere (Adánez et al., 2010; Abad et al., 2011). Ilmenite undergoes an activation process during continuous operation in the plant and reaches a maximum reactivity, which is studied in previous work (Abad et al., 2011). The experiments have been carried out with activated ilmenite, so the reactivity was maximum and constant and did not affect in the evaluation of other parameters. The porosity of the initial sample was 12.3%. The oxygen transport capacity, which is the mass fraction of oxygen that can be used in the oxygen transfer, was measured to be 3.9% for this CLC process with solid fuels.

The fuel used was a bituminous Colombian coal "El Cerrejón". The coal was subjected to a thermal pre-treatment for pre-oxidation in order to avoid bed agglomeration problems or pipes clogging, as El Cerrejón coal had shown high swelling behavior. Hence, coal was placed in trays in layers of about 3 mm height and exposed to heating at 180 °C in air atmosphere for 28 h. Ultimate and proximate analyses of the used pre-treated coal are shown in Table 1. Three different coal particle sizes were used: +74–125, +125–200 and +200–300 μm.

### 2.2. 500 $W_{th}$ CLC facility for solid fuels

A schematic view of the plant is shown in Fig. 1. The set-up was basically composed of two interconnected fluidized-bed reactors

Please cite this article in press as: Cuadrat, A., et al., Effect of operating conditions in Chemical-Looping Combustion of coal in a 500 $W_{th}$ unit. Int. J. Greenhouse Gas Control (2011), doi:10.1016/j.ijggc.2011.10.013

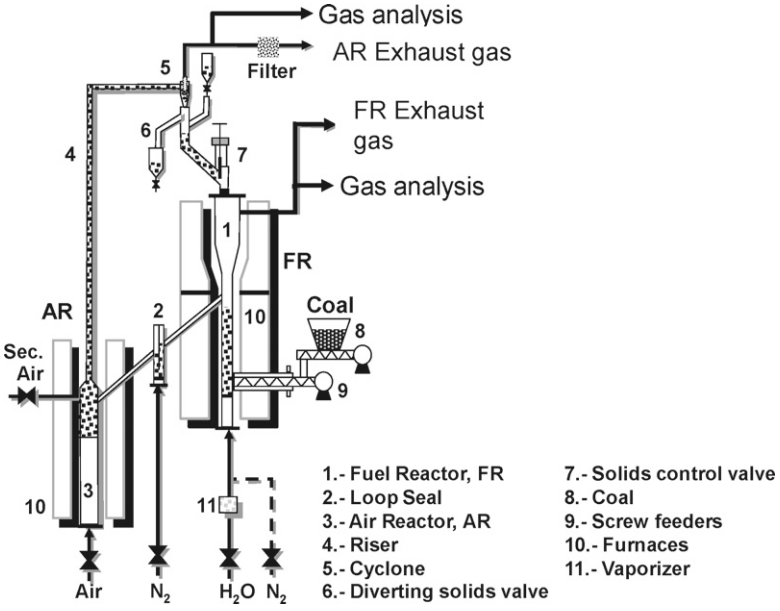


**Fig. 1.** Schematic diagram of the coal-fuelled CLC facility.

joined by a loop seal, a riser for solids transport from the air-reactor to the fuel-reactor, a cyclone and a solids valve to control the flow rate of solids fed to the fuel-reactor. This design allowed the variation and control of the solids circulation flow rate between both reactors.

The fuel-reactor consisted of a bubbling fluidized bed with 5 cm of inner diameter and 20 cm bed height. The fluidizing gas was $H_2O$ or $CO_2$, which are also gasifying agents. Coal is fed by a screw feeder at the bottom of the bed above the fuel-reactor distribution plate in order to maximize the time that the fuel and volatile matter is in contact with the bed material. The screw feeder has two steps: the first one with variable speed to control the coal flow rate, and the second has high rotating velocity to avoid coal pyrolysis inside the screw. A small $N_2$ flow is fed in the beginning of the screw to avoid possible volatile reverse flow or entrance of steam. In the fuel-reactor the oxygen-carrier is reduced by the volatile matter and gasification products of coal. Reduced oxygen-carrier particles overflowed into the air-reactor through a U-shaped fluidized bed loop seal with an inner diameter of 50 mm, to avoid gas mixing between fuel- and air-reactors. The oxidation of the carrier took place in the air-reactor, consisting of a bubbling fluidized bed with 8 cm of inner diameter and 10 cm bed height, and followed by a riser. Secondary air was introduced at the top of the bubbling bed to help particle entrainment. $N_2$ and unreacted $O_2$ left the air-reactor and went through a high-efficiency cyclone and a filter before the stack. The oxidized solid particles recovered by the cyclone were sent to a solids reservoir, which acts as a loop seal, setting the oxygen-carrier ready to start a new cycle. The regenerated oxygen-carrier particles returned to the fuel-reactor by gravity from the solids reservoir through a solids valve which controlled the flow rates of solids entering the fuel-reactor. A diverting solids valve located below the cyclone allowed the measurement of the solids flow rates at any time. The total ilmenite inventory in the system was 3.5 kg and the solids inventory in the fuel-reactor was 0.8 kg ilmenite.

Because of its small size, the system is not auto-thermal and is heated up with various ovens to get independent temperature control of the air-reactor, fuel-reactor, and fuel-reactor freeboard, which is kept constant at about 900 °C in all the experiments. During operation, temperatures in the bed and freeboard of the fuel-reactor, air-reactor bed and riser were monitored as well as the pressure drops in important locations of the system, such as the fuel-reactor bed, the air-reactor bed and the loop seal.

CO, $CO_2$, $H_2$, $CH_4$, and $O_2$ were continuously analyzed in the exit streams from the fuel-reactor and from the air-reactor. In some selected experiments the tar amount present in fuel-reactor product gases was determined following the tar protocol. Some samples of the fuel-reactor outlet stream were taken and analyzed by gas chromatography in order to measure hydrocarbons.

The gas flows introduced in the air-reactor were 400 $L_N$/h as primary air and 2100 $L_N$/h as secondary air, corresponding to a total gas velocity in the air-reactor of 0.6 m/s. The loop-seal was fluidized with 75 $L_N$/h of $N_2$ and a flow of 18 $L_N$/h $N_2$ was introduced in the screw-feeder. The minimum gasification agent flow fluidizing the fuel-reactor tested was 110 $L_N$/h and the maximum was 190 $L_N$/h. For these flows, the gas velocities at 900 °C in the fuel-reactor were, respectively, 0.07 and 0.12 m/s. The minimum fluidization velocity for the ilmenite particles used at 900 °C was 0.022 m/s. Most experiments were done with steam as fluidization agent in the fuel-reactor, and $H_2O$–$CO_2$ mixtures were also used as fluidization agents in a series of tests. At least every condition was maintained stable during 30 min. A total of 30 h of continuous operation feeding fuel and 36 h of continuous fluidization were made. Table 2 shows the conditions for the series of experiments carried out. The temperature in the air-reactor was maintained at around 950 °C and the fuel-reactor temperature was kept at around 890 °C for some experiments and about 940 °C for other tests. In the series of experiments A the coal flow rate was varied from 33 to 83 g/h, corresponding to a thermal power variation between 200 and 505 $W_{th}$; in the series of experiments B the solids circulation flow rate was varied from 1.0 to 11.6 kg/h for 3 different coal particle sizes; in the series of experiments C the gasification agent flow was varied from 110 to 190 $L_N$/h and in the series of experiments D several $H_2O$:$CO_2$ mixtures were used as gasification agent. Tests C and D were done with low solids circulation rate in order to work at high fuel-reactor temperatures.

## 3. Data evaluation

The evaluation of the fuel-reactor performance is carried out by the analysis of two main parameters: the carbon capture efficiency and the combustion efficiency. The purpose of the data

Please cite this article in press as: Cuadrat, A., et al., Effect of operating conditions in Chemical-Looping Combustion of coal in a 500 $W_{th}$ unit. Int. J. Greenhouse Gas Control (2011), doi:10.1016/j.ijggc.2011.10.013

**Table 2**
Conditions for the series of experiments. (A) Variation of coal flow rate; (B) solids circulation flow rate variation for different coal particle sizes; (C) variation of the gasification agent flow; (D) variation of the gasification agent type ($H_2O$:$CO_2$ mixtures).

| Exp. type | Coal particle size, μm | $T_{FR}$, °C | Coal feed, g/h | Solids circ. flow rate, kg/h | Gasification agent flow, $L_N$/h | $H_2O$, % | $CO_2$, % |
|---|---|---|---|---|---|---|---|
| A | 74–125 | 890 | 33–83 | 8.4 | 190 | 100 | 0 |
| B1 | 74–125 | | 41.1 | 1.2–11.6 | | | |
| B2 | 125–200 | 890 | 46.7 | 1.0–3.6 | 190 | 100 | 0 |
| B3 | 200–300 | | 38.5 | 1.6–11.3 | | | |
| C | 125–200 | 940 | 161 | 2.5 | 110–190 | 100 | 0 |
| D | 125–200 | 935 | 72 | 3.3 | 190 | 100–0 | 0–100 |

evaluation is to assess the performance of the process in the different experiments, using the measured values of the gas concentrations, temperature and solids circulation rates. The absence of a carbon stripper facilitates the interpretation of the effect of these operational conditions on the results obtained, specially the effect of the mean residence time.

The efficiencies that indicate the performance of the process are defined as follows. The carbon capture is the physical removal of carbon dioxide that would otherwise be emitted into the atmosphere. Getting high carbon capture during energy generation is the motivation of this technology. The carbon capture efficiency, $\eta_{CC}$, is here defined as the fraction of the carbon introduced that is converted to gas in the fuel-reactor.

$$\eta_{CC} = \frac{[F_{CO_2,FR} + F_{CO,FR} + F_{CH_4,FR}]_{out} - [F_{CO_2,FR}]_{in}}{[F_{CO_2,FR} + F_{CO,FR} + F_{CH_4,FR} + F_{CO_2,AR}]_{out} - [F_{CO_2,FR}]_{in}} \quad (6)$$

$F_{CO_2,FR}$, $F_{CH_4,FR}$ and $F_{CO,FR}$ being the flows in the fuel-reactor of $CO_2$, $CH_4$, and CO, respectively. The carbon of the unreacted char flowing towards the air-reactor is the $CO_2$ gas flow in the air-reactor, $F_{CO_2,AR}$. For the experiments using $CO_2$ as fluidization agent, the inlet $CO_2$ flow must be subtracted. The carbon captured in the system is the carbon contained in the volatiles plus the carbon in the char that is gasified. Thus, the carbon capture efficiency depends on the fraction of char that has been gasified. The gas flows of every component were calculated by multiplying the corresponding gas fraction and the outlet gas flow, i.e. $F_{FR}$ in the case of the fuel-reactor, and $F_{AR}$ for the air-reactor. The dry basis product gas flow, $F_{FR}$, was calculated by using the $N_2$ flow $F_{N_2,FR}$ that is introduced in the fuel-reactor coming from the loop seal. Preliminary results showed that about 65% of the $N_2$ introduced to fluidize the loop seal went to the fuel-reactor and the rest to the air-reactor (Cuadrat et al., in press). The outlet air-reactor gas flow, $F_{AR}$, was calculated though the introduced $N_2$, $F_{N_2,AR}$, which is sum of the $N_2$ present in the air introduced in the air-reactor and the $N_2$ coming from the loop seal:

$$F_{FR} = \frac{F_{N_2,FR}}{1 - (y_{CH_4,FR} + y_{CO_2,FR} + y_{CO,FR} + y_{H_2,FR})} \quad (7)$$

$$F_{AR} = \frac{F_{N_2,AR}}{1 - (y_{CO_2,AR} + y_{O_2,AR})} \quad (8)$$

To do a deeper study of the system behavior, the gasification and combustion steps should be assessed. The char conversion, $X_{char}$, is defined as the fraction of carbon in the effective char fed to the fuel-reactor which is released to the fuel-reactor outgoing gas stream:

$$X_{char} = \frac{[F_{CO_2,FR} + F_{CO,FR} + F_{CH_4,FR} - F_{C\ vol}]_{out} - [F_{CO_2,FR}]_{in}}{[F_{CO_2,FR} + F_{CO,FR} + F_{CH_4,FR} + F_{CO_2,AR} - F_{C\,vol}]_{out} - [F_{CO_2,FR}]_{in}} \quad (9)$$

The gasified char in the fuel-reactor was calculated as difference of the carbon in gases in the fuel-reactor outgoing flow, and the carbon flow coming from the volatile matter, $F_{C\,vol}$. The carbon content of the volatiles is directly calculated using the ultimate and proximate analyses of both the coal used and char (Tables 1 and 3). The carbon in the volatile matter was calculated as the total carbon in coal minus the carbon in char. The yield of char in coal was considered to be the sum of both the ash content and fixed carbon.

The carbon measured in the gases coming from the fuel-reactor and the air-reactor is less than the carbon present in the introduced coal, because there is elutriation of char. However, in case of an industrial plant the possible elutriated char will be collected in a cyclone and reintroduced in the fuel-reactor. The elutriated char flow was calculated as the difference between the fed coal carbon and the measured carbon in the fuel-reactor and air-reactor outlet gas flows. The effective char was calculated as the fed char that had not been elutriated from the fuel-reactor.

The combustion efficiency of the fuel-reactor, $\eta_{comb\ FR}$, is a measure of gas conversion in the fuel-reactor and represents the extent of oxidation of volatiles and gasification products by the oxygen-carrier. It is defined as the fraction of the oxygen demanded by the volatile matter and gasification products that is supplied by the oxygen-carrier in the fuel-reactor. It is therefore dependent on the reaction rate of ilmenite with the gaseous fuels and on the amount of gases generated in the fuel-reactor from coal. The oxygen supplied by ilmenite in the fuel-reactor is calculated through the oxygen containing species in the fuel-reactor product gas. The sum of volatile matter and gasified char is calculated as the effective coal introduced minus the char flowing towards the air-reactor, $F_{CO_2,AR}$. The combustion efficiency was calculated as:

$$\eta_{comb\ FR} = \frac{[0.5F_{H_2O,FR} + F_{CO_2,FR} + 0.5F_{CO,FR}]_{out} - [0.5F_{H_2O,FR} + F_{CO_2,FR} + 0.5O_{coal,eff}]_{in}}{O_{2\,demand\,coal,eff} - F_{CO_2,AR}} \quad (10)$$

$O_{coal,eff}$ is the flow of oxygen contained in the effective coal introduced. The oxygen introduced by the gasification agent, i.e. $H_2O$ and/or $CO_2$, must be removed in the analysis. $O_{2\ demand\ coal,eff}$ or the oxygen demand of the effective coal flow is the oxygen flow needed to burn the fuel completely and is calculated with the volatile matter in the coal feeding flow and the effective char flow.

A total oxygen demand for the fuel-reactor gases, $\Omega_T$, was defined, as the fraction of oxygen lacking to achieve a complete combustion of the fuel-reactor product gas in comparison to the oxygen demand of the coal introduced, $O_{2\ demand\ coal}$. This parameter is the most adequate to evaluate the performance of the

**Table 3**
Ultimate analysis of the used pre-treated Colombian char coal.

| | |
|---|---|
| C | 79.8% |
| H | 0.7% |
| N | 1.3% |
| S | 0.6% |
| O | 4.0% |

Please cite this article in press as: Cuadrat, A., et al., Effect of operating conditions in Chemical-Looping Combustion of coal in a 500 $W_{th}$ unit. Int. J. Greenhouse Gas Control (2011), doi:10.1016/j.ijggc.2011.10.013

combustion process in this facility, since it is the demand of the coal actually involved in the conversion process in the fuel-reactor.

$$\Omega_T = \frac{O_{2\,\text{demand gases FR}}}{O_{2\,\text{demand coal}}} = \frac{2F_{CH_4,FR} + 0.5F_{H_2,FR} + 0.5F_{CO,FR}}{O_{2\,\text{demand coal}}} \quad (11)$$

To evaluate the char conversion in the fuel-reactor, the mean residence time of char particles was calculated. Considering perfect mixing of the solids in the fuel-reactor, the residence time of ilmenite and char would be the same, but since there is char elutriation, the mean residence time of char, $t_{m,char}$, should be lower than the residence time for ilmenite particles. So, the mean residence time of ilmenite, $t_{m,ilm}$, is calculated by Eq. (12):

$$t_{m,ilm} = \frac{m_{ilm,FR}}{F_{ilm}} \quad (12)$$

$m_{ilm,FR}$ being the fuel-reactor bed mass or solid hold-up in the fuel-reactor, and $F_{ilm}$ the solids circulation rate. However, the residence time for char particles was calculated as the mass of char in the fuel-reactor, $m_{char,FR}$, divided by the char flow that exits the fuel-reactor, sum of the carbon flow from the elutriated char, $F_{C\,char\,elutr}$, and the carbon flow from the char to the air-reactor, $F_{C\,char,AR}$.

$$t_{m,char} = \frac{m_{char,FR}}{(F_{C\,char,AR} + F_{C\,char\,elutr}) \cdot M_C} = \frac{(x_{char,FR}/(1 - x_{char,FR})) \cdot m_{ilm,FR}}{(F_{C\,char,AR} + F_{C\,char\,elutr}) \cdot M_C} \quad (13)$$

$x_{char,FR}$ is the carbon concentration from char in the fuel-reactor, which is calculated considering the carbon flow in the air-reactor exiting gases. $M_C$ is the atomic mass of carbon.

The oxygen-carrier to fuel ratio, $\phi$, is a measure of how much oxygen can be supplied by the circulating oxygen-carrier compared to the oxygen needed to burn the fuel fed. In stoichiometric conditions the ratio $\phi$ is equal to one, when the oxygen-carrier is fully oxidized. It is defined as follows:

$$\phi = \frac{F_{ilm} \cdot R_{O,ilm}}{M_{O_2} \cdot O_{2\,\text{demand coal,eff}}} \quad (14)$$

$R_{O,ilm}$ is the transport capacity of ilmenite and $M_{O_2}$ is the oxygen molecular mass.

The rate of oxygen transferred by ilmenite, $(-r_O)$ is a measure of how much and how fast oxygen is transferred from ilmenite to the fuel and is calculated as the flow of the generated oxygen containing species of the fuel-reactor that were generated due to the oxygen transferred by ilmenite, i.e., the generated CO, $CO_2$ and $H_2O$, divided by the ilmenite hold-up:

$$(-r_O) = \frac{([0.5F_{H_2O,FR} + F_{CO_2,FR} + 0.5F_{CO,FR}]_{out} - [0.5F_{H_2O,FR} + F_{CO_2,FR} + 0.5O_{coal,eff}]_{in}) \cdot M_{O_2}}{m_{ilm}} \quad (15)$$

## 4. Results and discussion

The influence of varying different operation parameters on the CLC process with solid fuels was determined. In a previous study it was determined that the temperature in the fuel-reactor had a great influence on coal conversion (Cuadrat et al., in press), which agreed with the results showed by other works (Berguerand and Lyngfelt, 2009; Shen et al., 2010). All continuous experiments of CLC with solid fuels to date are focused on the influence of the fuel-reactor temperature as operational variable. In this work, a wide range of operation conditions was reached, by changing several different operational variables such as the coal feeding rate, the solids circulation flow rate with different particle sizes of coal, the gasification agent flow and the composition of the gasification agent, as several $CO_2$:$H_2O$ mixtures were introduced to fluidize the fuel-reactor.

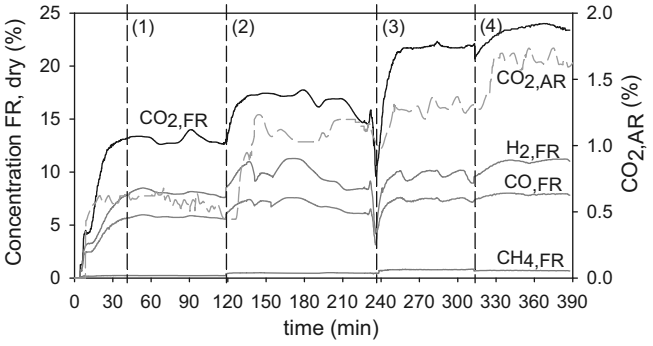


**Fig. 2.** Gas distributions in fuel-reactor (FR) (dry basis concentrations, $N_2$ to balance) and $CO_2$ concentration in the air-reactor for rising coal feeding rate. The dotted lines indicate increase in the fuel feed flow. Coal feed flows tested: (1) 33 g/h, (2) 45 g/h, (3) 62 g/h, and (4) 83 g/h. $T_{FR}$ = 890 °C. Solids circulation flow = 4.8 kg/h. Coal particle size +74–125 μm.

As representative of the gas distributions obtained in this study, the evolution with time of the gas concentrations from the fuel-reactor and the $CO_2$ concentration in the air-reactor as result of ungasified char escaping to that reactor is shown in Fig. 2 for the experiments with increasing coal feeding rate, that is, the series of experiments A. Four coal feed flows were tested and the dotted lines indicate the moments where the coal feeding was raised. The initial period before introducing coal and the transitory period until the stationary state was reached are also represented. Concentrations in fuel-reactor are in dry basis. Steady state after any parameter change was fast reached and all the points were therefore evaluated at stable conditions. The CLC prototype was easy to operate and control, and the steady state for each operating condition was maintained for at least 60 min.

The outlet of the fuel-reactor was mainly composed of oxidized $CO_2$, and $H_2$ and CO and some $CH_4$ as not fully oxidized products of char gasification and volatile matter. The gas chromatography analyses of the samples taken and the tars measurements revealed there were neither hydrocarbons heavier than $CH_4$ nor tars in the fuel-reactor outlet flow.

### 4.1. Effect of the coal feeding rate

The effect of the coal feeding rate on the process performance was studied. Coal feeding flow rate was changed from 33 to 83 g/h, corresponding to a thermal power of 200 $W_{th}$ to 505 $W_{th}$. In these experiments the fuel-reactor temperature was maintained constant at about 890 °C and the solids circulation rate at 8.4 kg/h. This study was carried out using coal with particle size +74–125 μm.

Fig. 2 gives a first idea of how the system behaves when more coal was introduced. All concentrations increased, that is, more gases were being released. Since the residence time of ilmenite was approximately kept constant and higher amount of coal was being introduced, higher flow of char escaped to the air-reactor, where higher quantity of $CO_2$ was generated. Besides, the yield to $CO_2$ in the fuel-reactor increased. The corresponding flows from all products increased with the coal feeding flow because there was more fuel to devolatilize, gasify and burn. Fig. 3 shows the $CO_2$, CO and $H_2$ average concentrations from the fuel-reactor at each resulting effective carbon flow. They are represented $H_2O$ and $N_2$ free to see better the yield of each released specie and the real trend. The $CO_2$ fraction in the air-reactor outlet is also represented. The ratio of oxygen-carrier to fuel decreased from 7 to 2.3 and in all cases the ratio steam to fixed carbon was over 2.9. At these conditions, there is oxygen as well as steam excess and the reactions are not limited by those reactants.

Please cite this article in press as: Cuadrat, A., et al., Effect of operating conditions in Chemical-Looping Combustion of coal in a 500 $W_{th}$ unit. Int. J. Greenhouse Gas Control (2011), doi:10.1016/j.ijggc.2011.10.013

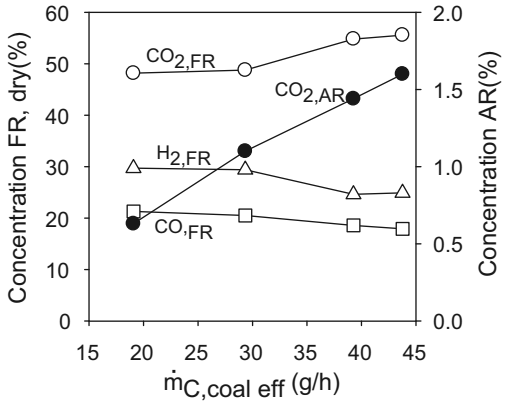


**Fig. 3.** $CO_2$, CO and $H_2$ concentrations from the fuel-reactor, FR, in dry basis and $N_2$ free, and $CO_2$ resulting concentration from the air-reactor for increasing effective carbon in the coal feeding flow rate, $\dot{m}_{C,coal\,eff}$. $T_{FR}$ = 890 °C. Average solids circulation rate = 8.4 kg/h. Particle size +74–125 μm.

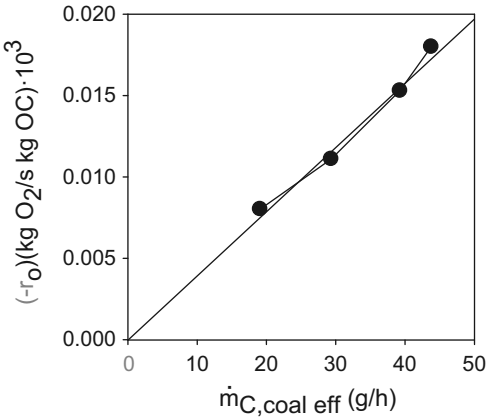


**Fig. 5.** Rate of oxygen transferred by ilmenite for rising effective carbon in the coal feeding flow rate, $\dot{m}_{C,coal\,eff}$. $T_{FR}$ = 890 °C. Average solids circulation rate = 8.4 kg/h. Particle size +74–125 μm.

Fig. 4 shows the gasification and combustion efficiencies as a function of the effective carbon in the coal feeding flow. The resulting combustion efficiency for increasing coal feeding rate increased slightly. This fact was because it turned out that there was lower char elutriation when higher coal flows were fed. If lower char is elutriated, the fraction of carbon in the fuel-reactor that comes from char increases. Since char gasification products are better burnt than the released volatile matter (Cuadrat et al., in press), the resulting combustion efficiency slightly increases. The circulation rate and the temperature were kept constant and there was oxygen and steam excess in all cases. Char residence time was calculated to be within the range 2.7–6 min. The char conversion was not really influenced by an increase in the coal feed. As there was no major increase in the residence time, but higher amount of char was being introduced, the resulting percentage of gasified char had a minor drop. Nevertheless and obviously, the char mass concentration in the fuel-reactor bed was calculated to increase from 0.16% with the coal feeding flow of 33 g/h up to 0.38% when feeding 83 g/h of coal.

Fig. 5 shows the rate of oxygen transferred by ilmenite for the tests preformed. When more coal was introduced in the system, the variation of ilmenite conversion and therefore the oxygen transferred increased proportionally to the coal feeding rate increase. This confirms the statement made that in this system the combustion efficiency is not limited by the reaction rate of ilmenite, but for the gasification step.

### 4.2. Effect of the solids circulation rate

The effect of the solids circulation rate on the process performance was studied. For a CLC system based on two interconnected fluidized beds the circulation rate between them must be high enough to transfer the oxygen necessary for the fuel combustion and the heat necessary to maintain the heat balance in the system, if necessary.

Solids circulation flow rates from 1.0 to 11.6 kg/h for three ranges of coal particle sizes at an average fuel-reactor temperature of 890 °C were used. This range corresponded to an ilmenite residence time range of 4.2–48 min, considering the fuel-reactor inventory. The oxygen-carrier to fuel ratio $\phi$ was varied from 0.5 to 8.4. Thus, there were cases where the solids recirculation rate was lowered so much that $\phi$ reached values under the unity, which meant that there was not enough oxygen-carrier available to fully oxidize the fuel.

Fig. 6 shows the carbon capture efficiency, obtained as a function of the oxygen to fuel ratio for the different coal particle sizes tested. The carbon capture efficiency decreases for increasing oxygen-carrier to fuel ratio, that is, when the recirculation rate increases. This trend is clear for $\phi$ closer to the unity, and when $\phi$ has higher values the influence is much smaller. This follows the tendency of the solids residence time, that is, the decrease in $\eta_{CC}$ can be explained because coal gasification extent was lower, due to a lower residence time of the solids. Fig. 7 shows the calculated ilmenite residence times for $\phi$ values resulting from the solids circulation

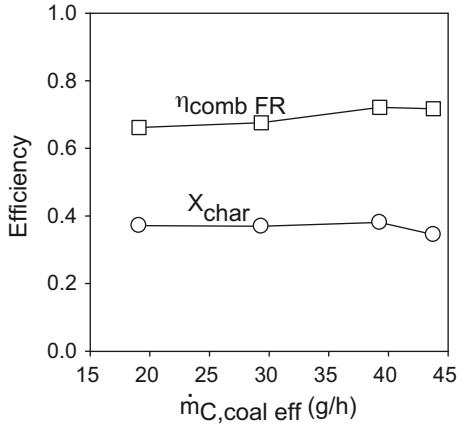


**Fig. 4.** Char conversion and combustion efficiency variation as a function of the effective carbon in the coal feeding flow rate, $\dot{m}_{C,coal\,eff}$. $T_{FR}$ = 890 °C. Average solids circulation rate = 8.4 kg/h. Particle size +74–125 μm.

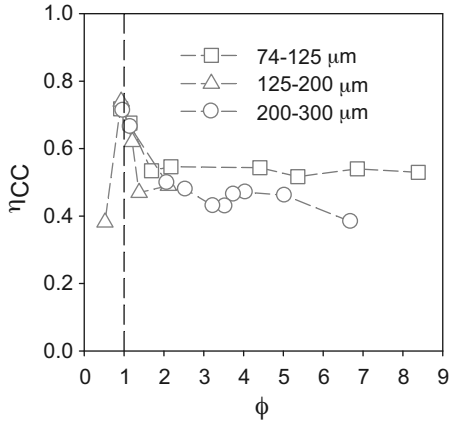


**Fig. 6.** Carbon capture efficiencies with different oxygen-carrier to fuel ratio, $\phi$, and for different coal particle sizes. $T_{FR}$ = 890 °C. Average coal mass flow = 42 g/h.

Please cite this article in press as: Cuadrat, A., et al., Effect of operating conditions in Chemical-Looping Combustion of coal in a 500 $W_{th}$ unit. Int. J. Greenhouse Gas Control (2011), doi:10.1016/j.ijggc.2011.10.013

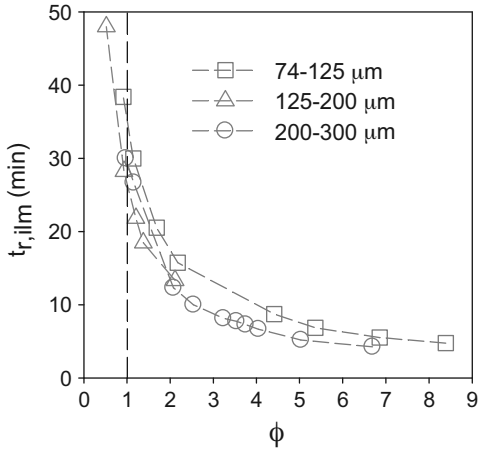


**Fig. 7.** Calculated ilmenite residence times for the oxygen-carrier to fuel ratio, $\phi$, resulting from the solids circulation rates tested for different coal particle sizes. $T_{FR}$ = 890 °C. Average coal mass flow = 42 g/h.

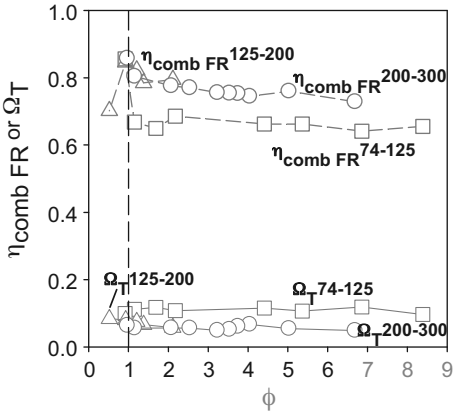


**Fig. 9.** Combustion efficiencies and total oxygen demands with different oxygen-carrier to fuel ratio, $\phi$, and for different coal particle sizes. $T_{FR}$ = 890 °C. Average coal mass flow = 42 g/h.

rates set. The oxygen to fuel ratio increases when increasing the circulation rate for a constant fuel flow. Thus, the resulting ilmenite residence time increased when $\phi$ decreased, as $t_{r,ilm}$ is inversely proportional to the circulation rate. Berguerand and Lyngfelt (2010) obtained the same trend of $CO_2$ capture decrease for increasing circulation rate, but with batch feeding of coal to the CLC reactor. The model developed by Markström et al. (2010) that predicted the carbon capture efficiency versus residence time presented the same trend of increasing $\eta_{CC}$ when the residence time was higher.

Fig. 8 shows the char conversions for increasing ilmenite residence times. One of the main parameters that determine the char conversion is the char residence time – as it was seen for the carbon capture efficiency – which depends on the solids recirculation rate set. For decreasing oxygen to fuel ratio, the solids residence time increased and the char from the fuel had more time to be gasified and the char conversion increased from about 27% with $\phi$ = 8 and an ilmenite residence time $t_{m,ilm}$ of 4.2 min to 63% with $\phi$ = 1.1 and $t_{m,ilm}$ = 30 min. For the range of coal particle size used in these experiments, i.e. 74–300 μm, the char conversion is independent of the coal size used.

Fig. 9 shows that the combustion efficiency had some increase for lower $\phi$ and resulting higher residence times: from 75% with $\phi$ = 8 to 86% with $\phi$ = 1.1. The explanation of this slight benefit was related to the enhanced gasification due to having a higher residence time (see Fig. 8). In previous work in this facility (Cuadrat et al., in press) it was seen that the combustion of the gasification products has very high efficiencies. Full combustion of gasification products can be reached at high temperatures, whereas the unburnt compounds come uniquely from volatiles. Thus, with lower $\phi$ more gasification products were generated and the percentage of unconverted gases – mainly coming from volatiles – decreased, as the relative importance of the gasification products in the reacting gases increased. Therefore, higher char conversions will lead to enhanced combustion efficiencies.

In other studies, continuous experiments of CLC with solid fuels (Berguerand and Lyngfelt, 2008a,b, 2009) were done at higher oxygen-carrier to fuel ratios, so the effect of $\phi$ getting closer to the unity and even under 1, could not be therefore assessed. On the contrary, in this work a wider range of $\phi$ was obtained.

This conclusion for CLC with solid fuels is opposite to the results and trends found for CLC with gaseous fuels, for which it was found that higher $\phi$ leads to better performance of the system, for Ni-based oxygen-carriers (Adánez et al., 2009; Dueso et al., 2009) as well as for Cu-based oxygen carriers (Forero et al., 2009). For gaseous fuels the determining factor is to have oxygen available to fully oxidize the fuel and as the circulation rate increases, i.e. $\phi$ increases, the average reactivity of the oxygen-carrier increases (Abad et al., 2007; García-Labiano et al., 2004). However, for solid fuels more factors come into consideration. The fact that there must be enough residence time for gasification and that gasification products are better burnt than the volatile matter determine this resulting trend for solid fuels in this facility. However, if the system had a carbon stripper with 100% separation efficiency, the trend followed regarding the oxygen to fuel ratio would be the same as for gaseous fuels and the combustion efficiency would increase for higher $\phi$.

Nevertheless, the oxygen demand, $\Omega_T$, was not greatly influenced by the solids circulation rate, as it is shown in Fig. 9. The oxygen demand of gases from the fuel-reactor remains roughly constant with the solids circulation rate because the amount of volatiles evolved in the fuel-reactor was the same in all cases. This indicates that the combustion performance of the fuel-reactor is actually controlled by the extension of char gasification, although the amount or reactivity of the oxygen-carrier has also some influence in the system.

In Fig. 9 it can be seen that lower combustion efficiencies were obtained for the +74–125 μm particles, which were also seen and evaluated in previous tests (Cuadrat et al., 2001b). It is because for the smaller particles there was higher elutriation and there was some gasification happening in the reactor freeboard where the gasification products did not get in contact with the oxygen-carrier

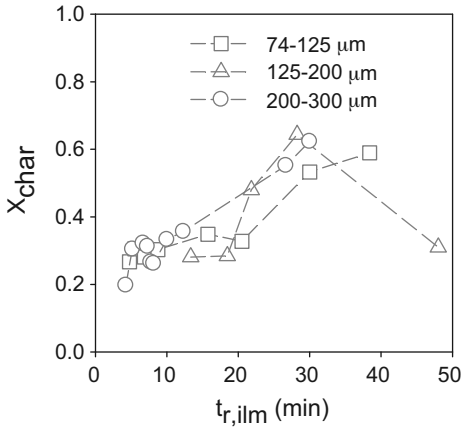


**Fig. 8.** Char conversions for increasing ilmenite residence times for different particle sizes. $T_{FR}$ = 890 °C. Average coal mass flow = 42 g/h.

Please cite this article in press as: Cuadrat, A., et al., Effect of operating conditions in Chemical-Looping Combustion of coal in a 500 $W_{th}$ unit. Int. J. Greenhouse Gas Control (2011), doi:10.1016/j.ijggc.2011.10.013

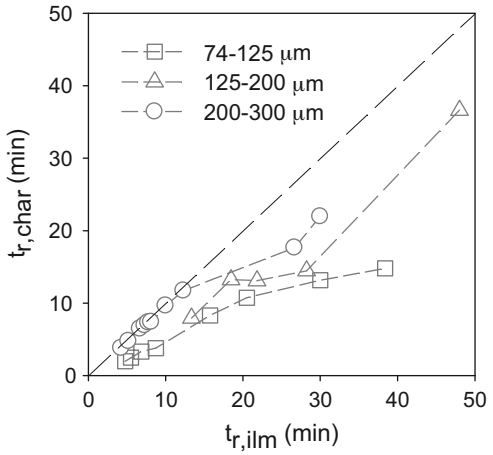


**Fig. 10.** Difference in the residence time of char and ilmenite in the fuel-reactor for different coal particle sizes. $T_{FR}$ = 890 °C. Average coal mass flow = 42 g/h.

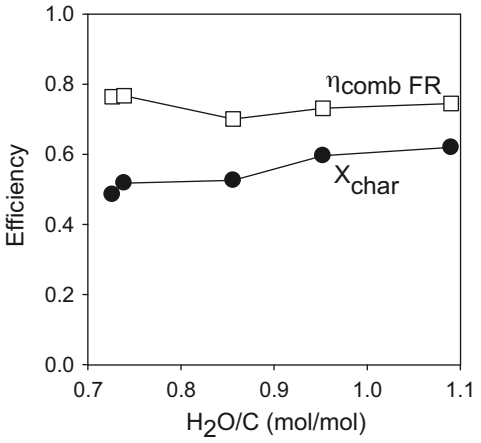


**Fig. 11.** Char conversion and combustion efficiency variation as a function of the $H_2O$/C ratio. $T_{FR}$ = 940 °C. Average solids circulation rate = 2.5 kg/h. Average coal mass flow = 161 g/h. Coal particle size +125–200 μm.

and could not be therefore oxidized. Besides, due to the higher elutriation, the resulting char residence times were lower for the tests with smaller coal particles, see Fig. 10. In previous work it was found that in this facility about 35% of the introduced char was elutriated for particle sizes of +74–125 μm and about 5% for the bigger particles (+200–300 μm) (Cuadrat et al., in press). So, char residence time was closer to the ilmenite residence time for higher particle sizes.

When oxygen-carrier to fuel ratios lower than 1 were obtained, the performance of the system dropped substantially although the residence time was very high. Both gasification and combustion efficiencies decreased when $\phi$ decreased to 0.5 as can be seen in Figs. 8 and 9. The combustion efficiency decreased because there was not enough oxygen available to burn the fuel fed and as a consequence the char conversion also dropped because the reactor got enriched in the generated $H_2$ and CO, which are inhibitors for the gasification.

### 4.3. Effect of the gasification agent flow

The flow of steam feed was varied from 110 to 190 $L_N$/h, corresponding to a gas velocity variation in the fuel-reactor from 0.07 to 0.12 m/s at 900 °C. Steam acts as both fluidization and gasification agent. These experiments were done with a feeding of 161 g/h, equivalent to a thermal power of 980 $W_{th}$. The steam to fixed carbon ratio was varied from 0.72 to 1.09. The coal used in these tests was +125–200 μm and the average fuel-reactor temperature was 940 °C. The circulation rate was around 2.5 kg/h.

In all cases the oxygen-carrier to fuel ratio $\phi$ was under the unity and around 0.5, which indicated that these tests were under stoichiometric conditions. The reason of working in these conditions was that the scope of these experiments was to have low values of $H_2O$/C. To achieve that, the coal feed flow was raised, which caused a decrease in $\phi$. Furthermore, in order to maintain high fuel-reactor temperatures, the solids circulation rate was kept at lower values, which led to work under stoichiometric conditions. However, the results are considered valid to assess the effect of the gasification agent flow, but they are not representative of desirable operation conditions.

In Fig. 11 it can be seen that for the lower steam flows tested, increasing $H_2O$ flow corresponding to a steam to fixed carbon ratio, from 0.72 to 1.09, the increase in the fed steam flow had some beneficial effect on the char conversion. However, for conditions of steam excess, there was no major effect on the char conversion. When the gasification products are burnt by ilmenite, $H_2O$ and $CO_2$ are formed that can further gasify the fuel, so it would not be necessary to have $H_2O$/C over the unity. The change in the gasification agent flow did not influence the combustion efficiency.

Note that since the value of $\phi$ is calculated with all the coal fed to the system, with a $\phi$ of 0.5 combustion efficiencies as high as 0.77 could be obtained. This was because the gasification efficiencies were about 0.6 and the coal in the fuel-reactor that could be burnt in the fuel-reactor was only part of the total fuel fed.

### 4.4. Effect of the gasification agent: $H_2O$–$CO_2$ mixtures

Here, the effect of using a gas mixture of $CO_2$ and $H_2O$ on the gasification step and the whole performance of the process with "El Cerrejón" coal was evaluated. The motivation of using $H_2O$–$CO_2$ mixtures is that $CO_2$ can be fed by recirculating a fraction of the product gas stream. Thus, the steam requirements for the gasification would be decreased in some extension, or even avoided if a pure stream of $CO_2$ was used as fluidizing gas. The coal feeding flow was 72 g/h with a coal particle size of +125–200 μm. The average fuel-reactor temperature was 935 °C. The total gasification agent flow was 190 $L_N$/h. The circulation rate was 3.3 kg/h. The tested $H_2O$:$CO_2$ mixtures tested were 100:0, 90:10, 71:29, 51:49 and 0:100.

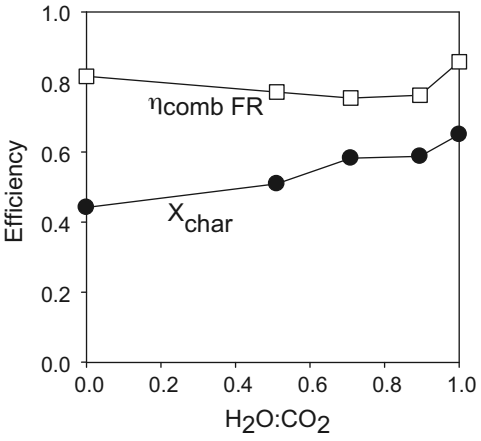


**Fig. 12.** Char conversion and combustion efficiency variation for different $H_2O$:$CO_2$ mixtures as gasification agent. $T_{FR}$ = 935 °C. Average solids circulation rate = 3.3 kg/h. Average coal mass flow = 72 g/h. Coal particle size +125–200 μm.

Please cite this article in press as: Cuadrat, A., et al., Effect of operating conditions in Chemical-Looping Combustion of coal in a 500 $W_{th}$ unit. Int. J. Greenhouse Gas Control (2011), doi:10.1016/j.ijggc.2011.10.013

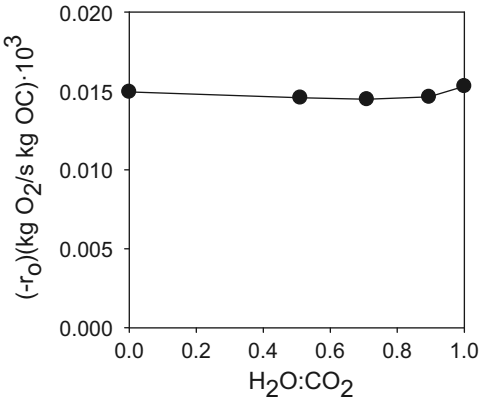


**Fig. 13.** Rate of oxygen transferred by ilmenite for different $H_2O$:$CO_2$ mixtures as gasification agent. $T_{FR}$ = 935 °C. Average solids circulation rate = 3.3 kg/h. Average coal mass flow = 72 g/h. Coal particle size +125–200 μm.

Fig. 12 shows that the char conversion increased for higher fraction of steam in the gasification agent. With this type of fuel, gasification with steam is faster than with $CO_2$ (Cuadrat et al., in press). However, the combustion efficiency was not really influenced by the gasification agent used and the changes seen in $\eta_{comb\ FR}$ could be explained by the slight differences in the oxygen-carrier to fuel ratios and average ilmenite residence times, being higher combustion efficiencies reached for higher ilmenite residence times, which is in concordance with the results showed in Section 4.2. When gasifying with $CO_2$, more CO is generated as when gasifying with steam, where $H_2$ is also generated. Although ilmenite is more reactive with $H_2$ than with CO, the conclusion is that it has enough reactivity to oxidize CO and $H_2$ fast enough, compared to the velocities at which they are generated.

The rates of oxygen transferred by ilmenite for the different $H_2O$:$CO_2$ mixtures tested were calculated (see Fig. 13). The oxygen transferred by ilmenite is fast enough to oxidize the gasification products and the oxygen transferred is slightly higher when more gasification products are generated, that is for higher $H_2O$:$CO_2$ ratios. However it is mainly influenced by the combustion efficiency and it was therefore very similar in all cases for all mixtures tested, as the resulting combustion efficiencies were very similar and independent of the $H_2O$:$CO_2$ ratio used for the gasification agent. Limited use of $CO_2$ in the fluidizing gas would be desirable to maintain high gasification rates for this fuel. This limitation derived from the use of $CO_2$ and the lower gasification rate with this gasification agent than the rate with steam was seen by Cuadrat et al. with a South African coal (Cuadrat et al., submitted for publication-a). However, other types of fuels have higher gasification rates with $CO_2$ (Dennis et al., 2006). On the other hand, the implementation of a carbon stripper that increased the char residence time would offset any possible poorer system performance caused by the slower gasification rate.

## 5. Conclusions

The effect on the fuel-reactor performance of the temperature, the solids circulation rate, the coal feeding rate and the coal particle size were studied in a 500 $W_{th}$ rig based on the CLC technology. Ilmenite was used as oxygen-carrier and the bituminous Colombian coal "El Cerrejón" as fuel. The study in this rig is based on the fuel-reactor performance and the results related to its operation were obtained.

When more coal was introduced in the system, since the circulation rate and the temperature were kept constant and there was oxygen and steam excess in all cases, the resulting combustion efficiency for increasing coal feeding rate did not change substantially. However, the conversion of ilmenite and therefore the oxygen transferred were higher and increased proportionally to the coal feeding rate increase. Thus, the coal conversion is not limited by the reaction rate of ilmenite, but by the char gasification process.

The increase in the recirculation rate and thereby a consequent increase in the oxygen-carrier to fuel ratio and decrease in the mean residence time of solids in the fuel-reactor was assessed. Lower oxygen-carrier to fuel ratios led to enhanced $CO_2$ capture efficiencies. That was because the increase in char residence time led to an increase in the char conversion. Gasification products are more reactive with ilmenite and have better contact with the oxygen-carrier particles than the released volatile matter. Thus, regarding the combustion step, with higher oxygen-carrier to fuel ratio the combustion efficiency increases, as the relative importance of the gasification products in the reacting gases increased.

However, the combustion efficiency decreased if there was not enough oxygen available to burn the fuel fed. Consequently, the char conversion also dropped because the reactor got enriched in $H_2$ and CO, which are gasification inhibitors.

A decrease in the gasification agent to fixed carbon ratio down to 0.7 did not influence the combustion efficiency, although the gasification efficiencies slightly increased for higher gasification agent flows closer to the stoichiometric value for gasification. From the experiments done with steam to fixed carbon ratio over 1 no substantial change in the performance of the process is expected when varying the $H_2O$/C ratio.

The char conversion increased for higher fraction of steam in the gasification agent, although the char conversion with $CO_2$ could be enough high in a CLC system for solid fuels where a carbon stripper is implemented. The combustion efficiency did not seem to be influenced by the gasification agent used. These results indicate that it is feasible to decrease the gasification agent flow lower than the corresponding gasification agent to fixed carbon ratio lower than 1, and that some of the steam as gasification agent can be replaced by $CO_2$ recirculated from the outlet fuel-reactor flow, getting the same system performance. This would lead to energy saving derived from the extra need of evaporating steam, and thereby to enhanced total system efficiency.

## Acknowledgements

This work was partially supported by the European Commission, under the RFCS program (ECLAIR Project, Contract RFCP-CT-2008-0008), from Alstom Power Boilers and by the Spanish Ministry of Science and Innovation (Project ENE2010-19550). A. Cuadrat thanks CSIC for the JAE Pre. fellowship.

## References

Abad, A., Adánez, J., García-Labiano, F., de Diego, L.F., Gayán, P., Celaya, J., 2007. Mapping of the range of operational conditions for Cu–Fe- and Ni-based oxygen carriers in chemical-looping combustion. Chem. Eng. Sci. 62, 533–549.
Abad, A., Adánez, J., Cuadrat, A., García-Labiano, F., Gayán, P., de Diego, L.F., 2011. Reaction kinetics of ilmenite for Chemical-looping Combustion. Chem. Eng. Sci. 66 (4), 689–702.
Adánez, J., Dueso, C., de Diego, L.F., García-Labiano, F., Gayán, P., Abad, A., 2009. Methane combustion in a 500 $W_{th}$ chemical-looping combustion system using an impregnated Ni-based oxygen carrier. Energy Fuels 23, 130–142.
Adánez, J., Cuadrat, A., Abad, A., Gayán, P., de Diego, L.F., García-Labiano, F., 2010. Ilmenite activation during consecutive redox cycles in chemical-looping combustion. Energy Fuels 24, 1402–1413.
Berguerand, N., Lyngfelt, A., 2008a. Design and operation of a 10 $kW_{th}$ chemical-looping combustor for solid fuels – testing with South African coal. Fuel 87, 2713–2726.
Berguerand, N., Lyngfelt, A., 2008b. The use of petroleum coke as fuel in a 10 kW chemical looping combustor. Int. J. Greenhouse Gas Control 2, 169–179.
Berguerand, N., Lyngfelt, A., 2009. Chemical-looping combustion of petroleum coke using ilmenite in a 10 $kW_{th}$ unit-high-temperature operation. Energy Fuels 23 (10), 5257–5268.

Please cite this article in press as: Cuadrat, A., et al., Effect of operating conditions in Chemical-Looping Combustion of coal in a 500 $W_{th}$ unit. Int. J. Greenhouse Gas Control (2011), doi:10.1016/j.ijggc.2011.10.013

Berguerand, N., Lyngfelt, A., 2010. Batch testing of solid fuels with ilmenite in a 10 $kW_{th}$ chemical-looping combustor. Fuel 89, 1749–1762.
Bidwe, A.R., Mayer, F., Hawthorne, C., Charitos, A., Schuster, A., Scheffknecht, G., 2011. Use of ilmenite as an oxygen carrier in chemical looping combustion-batch and continuous dual fluidized bed investigation. Energy Procedia 4, 433–440.
Brown, T.A., Dennis, J.S., Scott, S.A., Davidson, J.F., Hayhurst, A.N., 2010. Gasification and chemical looping combustion of a lignite char in a fluidized bed of iron oxide. Energy Fuels 24, 3034–3048.
Cao, Y., Pan, W-P., 2006. Investigation of chemical looping combustion by solid fuels. 1. Process analysis. Energy Fuels 20, 1836–1844.
Cuadrat, A., Abad, A., Adánez, J., de Diego, L.F., García-Labiano, F., Gayán, P. Design considerations for chemical-looping combustion of coal – Part 1. Experimental tests, submitted for publication-a.
Cuadrat, A., Abad, A., García-Labiano, F., Gayán, P., de Diego, L.F., Adánez, J. The use of ilmenite as oxygen-carrier in a 500 $W_{th}$ Chemical Looping Coal Combustion unit. Int. J. Greenhouse Gas Control, in press.
Cuadrat, A., Abad, A., Adánez, J., de Diego, L.F., García-Labiano, F., Gayán, P. Behavior of ilmenite as oxygen carrier in chemical-looping combustion, submitted for publication-b.
Cuadrat, A., Abad, A., Gayán, P., de Diego, L.F., García-Labiano, F., Adánez, J. Theoretical approach on the CLC performance with solid fuels: optimizing the solids inventory, submitted for publication-c.
Dennis, J.S., Scott, S.A., Hayhurst, A.N., 2006. In situ gasification of coal using steam with chemical looping: a technique for isolating $CO_2$ from burning a solid fuel. J. Energy Inst. 79, 187–190.
Dennis, J.S., Scott, S.A., 2010. In situ gasification of a lignite coal and $CO_2$ separation using chemical looping with a Cu–based oxygen carrier. Fuel 89, 1623–1640.
Dueso, C., García-Labiano, F., Adánez, J., de Diego, L.F., Gayán, P., Abad, A., 2009. Syngas combustion in a chemical-looping combustion system using an impregnated Ni-based oxygen carrier. Fuel 88, 2357–2364.
Eide, L.I., Anheden, M., Lyngfelt, A., Abanades, C., Younes, M., Clodic, D., 2005. Novel capture processes. Oil Gas Sci. Technol. 60, 497–508.
Forero, C.R., Gayán, P., de Diego, L.F., Abad, A., García-Labiano, F., Adánez, J., 2009. Syngas combustion in a 500 $W_{th}$ chemical-looping combustion system using an impregnated Cu-based oxygen carrier. Fuel Proc. Technol. 90, 1471–1479.
García-Labiano, F., de Diego, L.F., Adánez, J., Abad, A., Gayán, P., 2004. Reduction and oxidation kinetics of a copper-based oxygen carrier prepared by impregnation for chemical-looping combustion. Ind. Eng. Chem. Res. 43, 8168–8177.
Gu, H., Shen, L., Xiao, J., Zhang, S., Song, T., 2011. Chemical looping combustion of biomass/coal with natural iron ore as oxygen carrier in a continuous reactor. Energy Fuels 25 (1), 446–455.
Intergovernmental Panel of Climate Change, 2005. Special Report on Carbon Dioxide Capture and Storage. Cambridge University Press, Cambridge, UK, Available at www.ipcc.ch.
Johnson, J.L., 1981. Fundamentals of coal gasification. In: Elliot, M.A. (Ed.), Chemistry of Coal Utilization. Wiley & Sons, New York (Chapter 23).
Kramp, M., Thon, A., Hartge, E.U., Heinrich, S., Werther, J., 2011. Carbon stripping – a critical process step in the chemical looping combustion of solid fuels. In: 2nd International Conference on Energy Process Engineering (ICEPE 2). Efficient Carbon Capture for Coal Power Plants, 2011. ICEPE2, Franfurt, Germany.
Leion, H., Mattisson, T., Lyngfelt, A., 2008. Solid fuels in chemical-looping combustion. Int. J. Greenhouse Gas Control 2, 180–193.
Leion, H., Mattissson, T., Lyngfelt, A., 2009a. Use of ores and industrial products as oxygen carriers in chemical-looping combustion. Energy Fuels 23, 2307–2315.
Leion, H., Jerndal, E., Steenari, B-M., Hermansson, S., Israelsson, M., Jansson, E., Johnsson, M., Thunberg, R., Vadenbo, A., Mattisson, T., Lyngfelt, A., 2009b. Solid fuels in chemical-looping combustion using oxide scale and unprocessed iron ore as oxygen carriers. Fuel 88, 1945–1954.
Leion, H., Lyngfelt, A., Mattisson, T., 2009. Effects of steam and $CO_2$ in the fluidizing gas when using bituminous coal in chemical-looping combustion. In: Proc 20th Int. Conf. on Fluidized Bed Combustion, Xian, China, pp. 608–611.
Markström, P., Berguerand, N., Lyngfelt, A., 2010. The application of a multistage-bed model for residence-time analysis in chemical-looping combustion of solid fuel. Chem. Eng. Sci. 65, 5055–5066.
Morin, J.X., Béal, C., Suraniti, S., 2010. 455 MWe CLC boiler/plant feasibility report and recommendations for the next step. Public Summary Report of ENCAP deliverable D4.2.4. Available at www.encapco2.org.
Scott, A.A., Dennis, J.S., Hayhurst, A.N., Brown, T., 2006. In situ gasification of a solid fuel and $CO_2$ separation using chemical looping. AIChE J. 52, 3325–3328.
Shen, L., Wu, J., Gao, Z., Xiao, J., 2010. Characterization of chemical looping combustion of coal in a 1 $kW_{th}$ reactor with a nickel-based oxygen carrier. Combust. Flame 157, 935–942.
Shen, L., Wu, J., Xiao, J., 2009a. Experiments on chemical looping combustion of coal with a NiO based oxygen carrier. Combust. Flame 156, 721–728.
Shen, L., Wu, J., Gao, Z., Xiao, J., 2009b. Reactivity deterioration of NiO/$Al_2O_3$ oxygen carrier for chemical looping combustion of coal in a 10 $kW_{th}$ reactor. Combust. Flame 156 (7), 1377–1385.
Shen, L., Wu, J., Xiao, J., Song, Q., Xiao, R., 2009c. Chemical-looping combustion of biomass in a 10 kW reactor with iron oxide as an oxygen carrier. Energy Fuels 23, 2498–2505.
Ströhle, J., Orth, M., Epple, B., 2010. Simulation of the fuel reactor of a 1 MWt chemical looping plant for coal. In: En Les Rencontres Scientifiques de l'IFP – 1st International Conference on Chemical Looping, Lyon, France.

Please cite this article in press as: Cuadrat, A., et al., Effect of operating conditions in Chemical-Looping Combustion of coal in a 500 $W_{th}$ unit. Int. J. Greenhouse Gas Control (2011), doi:10.1016/j.ijggc.2011.10.013

# Paper VII

energy&fuels

ARTICLE

pubs.acs.org/EF

# Influence of Limestone Addition in a 10 $kW_{th}$ Chemical-Looping Combustion Unit Operated with Petcoke

Ana Cuadrat,[†] Carl Linderholm,[‡] Alberto Abad,*[,†] Anders Lyngfelt,[‡] and Juan Adánez[†]

[†]Department of Energy and Environment, Instituto de Carboquímica (ICB-CSIC), Miguel Luesma Castán 4, 50018, Zaragoza, Spain

[‡]Department of Energy and Environment, Chalmers University of Technology, S-41296 Göteborg, Sweden

**ABSTRACT:** Ilmenite, a natural mineral composed of $FeTiO_3$, is a low-cost material suitable as an oxygen carrier for chemical-looping combustion (CLC) with solid fuels. One option when using the CLC technology with solid fuels is to introduce the fuel directly into the fuel reactor. Once in there, the fuel is gasified and volatiles and gasification products react with the oxygen carrier. In this study, the influence of limestone addition to ilmenite as an oxygen carrier was tested in a continuous 10 $kW_{th}$ CLC pilot for solid fuels. The fuel fed was a petcoke, and the gasifying agent was steam. Tests with an ilmenite−limestone mixture as the bed material were performed, and also tests using only ilmenite as the bed material were carried out for comparison. Global solid circulation was varied because it is an important operational parameter, which determines the solid fuel residence time. The experiments were made at two fuel-reactor temperatures: 950 and 1000 °C. Generally, a higher residence time of the fuel and a higher temperature increased both gasification and combustion efficiencies. This was seen for both with and without limestone addition. The addition of limestone gave a significant improvement of gas conversion at 950 °C, which could be explained by lime catalyzing the water−gas shift reaction. Moreover, the presence of limestone significantly increased the char conversion at both 950 and 1000 °C.

## INTRODUCTION

It is widely accepted today that carbon dioxide coming from fossil fuel combustion is the most important greenhouse gas contributing to global warming. One of the options to mitigate the anthropogenic greenhouse effect is the development of capture and storage of $CO_2$ emitted from large point sources, such as power plants. Chemical-looping combustion (CLC) is nowadays an attractive option, because it is a combustion process with inherent separation of $CO_2$ that carries out the $CO_2$ capture at a low cost[1,2] without energy losses.[3]

CLC involves the use of an oxygen carrier, which transfers oxygen from air to the fuel, avoiding the direct contact between them. The most typical CLC system consists of two interconnected fluidized-bed reactors, designated as air and fuel reactors. In the fuel reactor, the fuel is oxidized by a metal oxide in its oxidized form ($Me_xO_y$) that is reduced to its reduced form ($Me_xO_{y-1}$). The exit gas from the fuel reactor contains, ideally, only $CO_2$ and $H_2O$. After water condensation, almost pure $CO_2$ can be obtained with little energy lost for component separation. The net chemical reaction is the same as in usual combustion with the same combustion heat released.

One option for the use of CLC with coal as fuel is the direct combustion, where coal is physically mixed with the oxygen carrier in the fuel reactor and the carrier reacts with the gas product of the pyrolysis and gasification of coal. Equations 1−5 express generally the reactions in the fuel reactor. Equations 3−5 are the oxygen-carrier reduction reactions with the main products of coal devolatilization and gasification. The reduced oxide is further transferred into the air reactor, where it is reoxidized with air, following reaction 6.

$$\text{coal} \rightarrow \text{volatiles} + \text{char} \quad (1)$$

$$\text{char} + H_2O \rightarrow CO + H_2 \quad (2)$$

$$CH_4 + 4Me_xO_y \rightarrow CO_2 + 2H_2O + 4Me_xO_{y-1} \quad (3)$$

$$H_2 + Me_xO_y \rightarrow H_2O + Me_xO_{y-1} \quad (4)$$

$$CO + Me_xO_y \rightarrow CO_2 + Me_xO_{y-1} \quad (5)$$

$$Me_xO_{y-1} + \frac{1}{2}O_2 \rightarrow Me_xO_y \quad (6)$$

For the good performance of this process and to achieve high combustion efficiencies, it is essential to obtain intimate contact between the oxygen-carrier particles and the volatile matter and gasification products. Because part of the carrier will be removed together with the removal of solid fuel ashes, optimization of the system must be performed to maximize ash separation and minimize the amount of carrier that will be extracted together with the ash removal. Furthermore, because the gasification process is the limiting step in the fuel reactor,[4] the stream of solids going from the fuel reactor to the air reactor could contain some unconverted char together with the oxygen carrier, which would lower the carbon capture. This could be avoided by a carbon stripper that separates char

**Received:** June 1, 2011
**Revised:** August 22, 2011
**Published:** August 29, 2011

particles, so that they are reintroduced to the fuel reactor, thereby increasing the fuel residence time in the fuel reactor.

Suitable oxygen carriers for a CLC process must have high selectivity toward $CO_2$ and $H_2O$, enough oxygen transport capacity, high reactivity during many reduction and oxidation cycles, high mechanical strength, attrition resistance, and no agglomeration tendency.[5] Besides, an environmentally friendly and low-cost oxygen carrier is preferable for use with solid fuels, because some oxygen carrier will be lost together with coal ash, which has to be removed from the reactor to avoid accumulation of ash in the system. Natural minerals, such as ilmenite, are therefore very interesting. Natural ilmenite is mainly composed of $FeTiO_3$, which corresponds to the most reduced state, when used as an oxygen carrier. As for the reactivity of ilmenite with $H_2$, CO, and $CH_4$, i.e., the main devolatilization and gasification products, ilmenite gave high conversion of CO and $H_2$ but moderate conversion of $CH_4$, similar to synthetic-based oxygen carriers[6] and among the best ores or industrial residues tested.[7,8] In addition, there is a gain in reactivity in reduction as well as in oxidation with the number of cycles, and on the whole, ilmenite has shown to have a good reaction rate and properties.[9,10] Batch testing of ilmenite with coal and coal char showed that the oxygen-carrier presence increases the char gasification rate[11] and that the gasification rate, i.e., the char reactivity, is highly dependent upon the parent fuel.[12] It is also possible to carry out this technology with $CO_2$ as well as steam as fluidizing and gasification agents,[13] although $CO_2$ gasification is much slower. In batch testing, as well as in continuous testing, the gasification as well as combustion efficiencies were shown to be very dependent upon the temperature.[14] To date, continuous testing with ilmenite as an oxygen carrier has been performed with a Mexican petcoke,[15,16] South African coal,[17] and Colombian bituminous coal.[18]

Some catalytic effect seems to occur, as shown in batch reactor tests performed with ilmenite as an oxygen carrier and the addition of calcined and sulfated limestone.[19] In these experiments, it was clear that calcined limestone addition had some beneficial effect on the char conversion rate. More importantly, the conversion of the gas was greatly enhanced, with unconverted CO + $CH_4$ being almost halved. Sulfated limestone particles showed a greater improvement on the char conversion rate during the first cycles, but after a dozen cycles, the benefits disappeared and seemed to stabilize at a level corresponding to ilmenite only. However, the gas conversion when adding sulfated lime was similar to the gas conversion obtained when adding unsulfated limestone, and it was independent of the cycle. Also, it was observed that the beneficial effect on gas conversion was seen already in the very first cycle with unsulfated lime, i.e., before any sulfate could have formed. Thus, it seems that the beneficial effect on gas conversion is largely independent of the degree of sulfation of the lime. Tests with $H_2$, CO, and syngas clearly indicated that the positive effect of lime could be attributed to the water−gas shift (WGS) reaction, which lowers CO and raises $H_2$ concentrations. This improves the gas conversion because $H_2$ is much more reactive than CO.

At high temperatures, limestone ($CaCO_3$) can react with released $SO_2$ and/or $H_2S$, and thereby, $CaSO_4$ and/or CaS are formed.[20,21] Also, calcined lime (CaO) can be the reacting compound depending upon the operating conditions.[22] At reducing conditions, CaS is stable, whereas $CaSO_4$ is stable at oxidizing conditions. CaO is stable in between these regions, and therefore, $SO_2$ may be released during shifts between oxidizing and reducing conditions.[20] At the temperatures of interest for the CLC process, the sulfidation has shown to be relatively fast for both CaO and $CaCO_3$.[21,23,24] The reactions are likely affected by the sorbent characteristics.[25] Furthermore, CaS formed can be expected to be oxidized to $CaSO_4$ in the air reactor. Another interesting factor is that $CaSO_4$ formation could lead to enhanced oxygen transport, because it can act as an oxygen carrier in its reduction to CaS with much higher oxygen-transfer capacity, as compared to other proposed materials.[26,27]

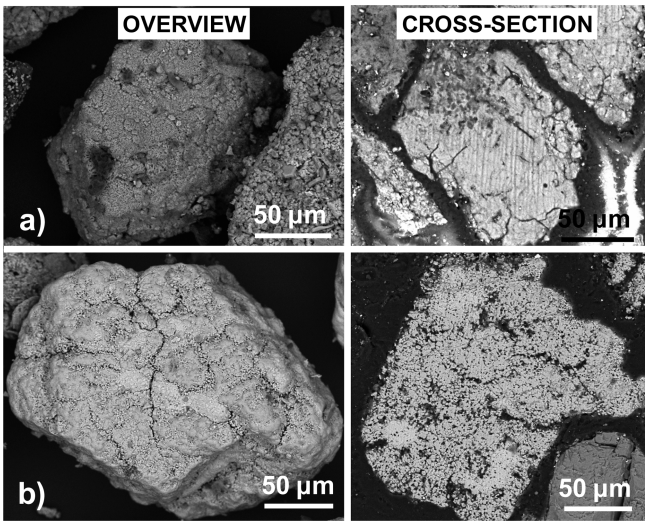


**Figure 1.** SEM images of the general overview of a particle and detail of the cross-section inside the particles for (a) limestone particle and (b) ilmenite.

The aim of this work is to investigate the effect of using limestone particles as an additive to ilmenite as an oxygen carrier in solid fuel CLC based on the positive effect of limestone addition seen in batch experiments on the CLC performance. Both the catalytic effect and possible oxygen transport capacity of $CaSO_4$ formed from limestone were analyzed in a 10 $kW_{th}$ CLC pilot plant.

## EXPERIMENTAL SECTION

**Bed Material.** A mixture of limestone−ilmenite was used as the bed material, but first, experiments were performed with 100% ilmenite as an oxygen carrier to have a base case for comparison. In this base case, the total inventory in the system was 15 kg of ilmenite and the fuel-reactor inventory was about 6 kg. A total of 4 kg of limestone was later added to the CLC system.

Ilmenite is a common mineral found in metamorphic and igneous rocks. It is a cheap material, which is an advantage for its use in CLC with solid fuels, because fuel ash may significantly reduce the lifetime of the oxygen carrier. Ilmenite used in this work is a concentrate from a natural ore from Norway with a purity of 94.3%. In the fully oxidized ilmenite, iron is in the form of $Fe^{3+}$, as either pseudo-brookite ($Fe_2TiO_5$) or free hematite ($Fe_2O_3$). In the CLC process, $Fe_2TiO_5$ and $Fe_2O_3$ are reduced to ilmenite ($FeTiO_3$) and magnetite ($Fe_3O_4$), respectively. Thus, the oxygen transport capacity of ilmenite, $R_{O,ilm}$, defined as the oxygen transport capacity useful for CLC, is calculated as

$$R_{O,\,ilm} = \frac{m_o - m_r}{m_o} \tag{7}$$

where $m_o$ is the mass of the most oxidized form of the oxygen carrier and $m_r$ is the mass in the reduced form. For this CLC process with solid fuels, the oxygen transport capacity of ilmenite was measured to be 3.9% by thermogravimetric analysis (TGA), with $FeTiO_3$ and $Fe_3O_4$ being the reduced species. The theoretical maximum if all $Fe^{3+}$ was reduced to $Fe^{2+}$ is 5%. The porosity was measured to be 13.5% through Hg intrusion with

**Table 1. Composition of the Mexican Petcoke Used**

| | | | |
|---|---|---|---|
| C (%) | 81.3 | moisture (%) | 8.0 |
| H (%) | 2.9 | volatile matter (%) | 9.9 |
| N (%) | 0.9 | fixed carbon (%) | 81.6 |
| S (%) | 6.0 | ash (%) | 0.5 |
| O (%) | 0.4 | lower heating value (kJ/kg) | 31750 |

a Quantachrome PoreMaster 33 porosimeter. The bulk density was about 2100 kg/m$^3$. The particle size for ilmenite was 90−250 $\mu$m.

After several redox cycles, ilmenite undergoes an activation process.[7] Ilmenite in this study had previously been investigated in continuous operation and batch testing with solid fuels.[12,14−18,28,29] TGA of a sample after the tests of this study was performed to check the reactivity, and ilmenite was shown to have the same reaction rate as a fully activated ilmenite sample.[10]

To 15 kg of ilmenite, 4 kg of a Mexican limestone, which is used in the Tamuin Power Plant, was added. The density was about 1900 kg/m$^3$, and the particle size was 90−200 $\mu$m. Figure 1 shows scanning electron microscopy (SEM) images of the general overview of a particle and detail of the cross-section inside the particles for the used limestone and ilmenite particles.

**Solid Fuel.** The fuel used in these experiments was Mexican petcoke. The proximate and ultimate analyses are given in Table 1.

This fuel has previously been tested in this plant. Prior experience from continuous and batch tests has shown that a drawback of this plant is that the fuel feed is performed by means of a fuel chute that introduces the fuel above the bed and a rather high fraction of the reducing gases escapes the fuel reactor unconverted because they do not come in contact with the oxygen carrier. These gases are mainly volatiles but can also be syngas, i.e., products from the char gasification. Because volatile content of petcoke is small, this problem is reduced. Moreover, the sulfur fraction in petcoke is quite high compared to normal coals. This low-volatile and high-sulfur fuel was chosen to be able to better see the fate of sulfur and any possible interaction with limestone. This fuel is not so reactive,[11] with a low char gasification rate.[12]

**Experimental Setup.** The 10 kW$_{th}$ unit used is designed for CLC with solid fuels and located at Chalmers University of Technology. Figure 2 shows a scheme of the whole pilot plant. The reactor system consists of two interconnected fluidized beds: (a) the fuel reactor (FR), where the fuel is gasified with steam and volatile matter and gasification products are oxidized by the oxygen carrier, and (b) the air reactor (AR), where the oxygen-carrier particles are oxidized. The regenerated oxidized particles are led through (c) a riser above the air reactor, which ends up in (d) a cyclone that brings the solid flow back to the fuel reactor. The gas velocity in the air reactor and riser provides the driving force for particle circulation. There are also two loop seals fluidized by nitrogen placed after (d) the cyclone and in the connection leading from the fuel to air reactor. The task of these upper and lower loop seals is to eliminate gas leakages between the reactors. Represented in Figure 2 is also the particle filters, as well as the fuel feeding, steam production unit and a water seal used to collect condensate and balance the pressure in the fuel reactor. Because of its small size, the system is not self-supporting in energy and is therefore enclosed in an oven that keeps and controls the temperature.

Figure 3 shows the layout of the fuel reactor, which has three main sections: (1) a low-velocity section, which is operated as a bubbling bed (this chamber is divided into two parts separated by a wall with an opening at the bottom, through which the particles are forced), (2) a carbon stripper with the purpose to separate char particles from the solid flow going from the fuel reactor to the air reactor, and (3) a high-velocity section that gives the opportunity to increase the flow in the internal loop by increasing the elutriation of the oxygen carrier into the riser. This option was not used in these tests.

The low-velocity section is fluidized with steam, and in this bed, all reactions related to char are expected to take place, that is, fuel gasification and reaction of the gasification products with the oxygen carrier. However, as noted above, most of the volatiles are released above the bed and have little contact with the oxygen carrier. The solid inventory in the low-velocity section is around 6 kg. A detailed description of the 10 kW pilot is given elsewhere.[17]

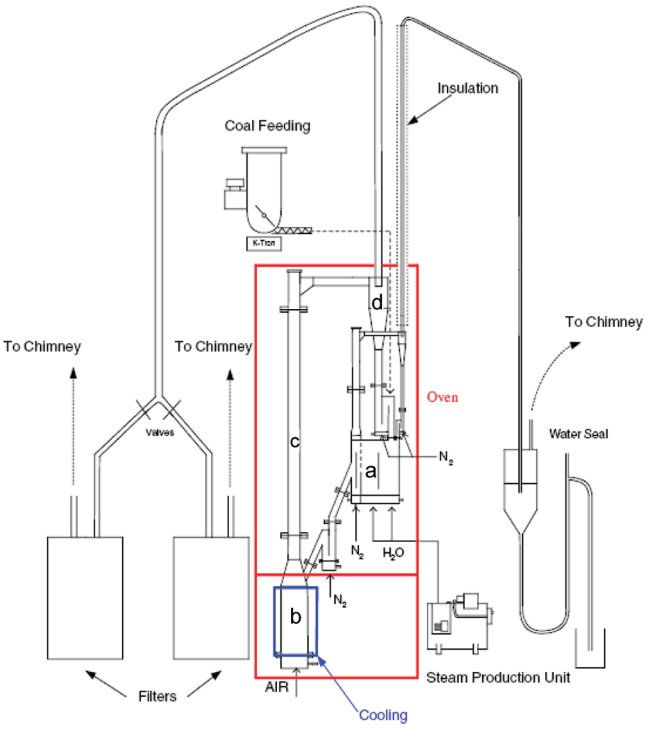


**Figure 2.** Pilot plant system: (a) fuel reactor, (b) air reactor, (c) riser, and (d) cyclone.

This 10 kW$_{th}$ pilot has already been used for approximately 90 h of continuous operation with various solid fuels and ilmenite as an oxygen carrier.[14−17]

The pilot is equipped with 40 pressure transducers to monitor the pressures. The temperatures in the air reactor, fuel reactor, and air-reactor cyclone are also measured. Gas-sampling outlets are located on both chimneys. At the air-reactor outlet, concentrations of CO, $CO_2$, and $O_2$ are measured online, and at the fuel-reactor outlet, concentrations of CO, $CO_2$, $O_2$, $CH_4$, and $SO_2$ are measured online with Sick Maihak Sidor analyzers and registered. The $H_2$ concentration could also be measured online with a Rosemount NGA2000 analyzer. Bag samples of the product gas flow from the fuel reactor were also taken and analyzed with a gas chromatograph Varian Micro-GC CP4900; this was used to confirm the results from the other analyzers. The fluidizing gas flows are controlled and monitored by mass-flow controllers. The steam flow to the low-velocity section is controlled by a steam generator.

The flows for the fuel reactor and the loop seals were kept constant during all experiments and are shown in Table 2. $F_{LOVEL}$ is the steam flow in the low-velocity section in the fuel reactor with a value of 21 $L_N$/min, which corresponds to a gas stay time in the bed of 2.9−3.0 s at the temperatures tested. $F_{CS}$ is the $N_2$ flow in the carbon stripper. $F_{HIVEL}$ is the $N_2$ flow in the high-velocity section in the fuel reactor. $F_{HILS}$ is the $N_2$ flow in the higher loop seal. $F_{LOLS}$ is the $N_2$ flow in the lower loop seal. $F_{FRLS}$ is the $N_2$ flow in the small fuel-reactor loop seal.

## DATA EVALUATION

The purpose of the data evaluation is to assess the performance of the process. Because not all of the fuel fed is converted

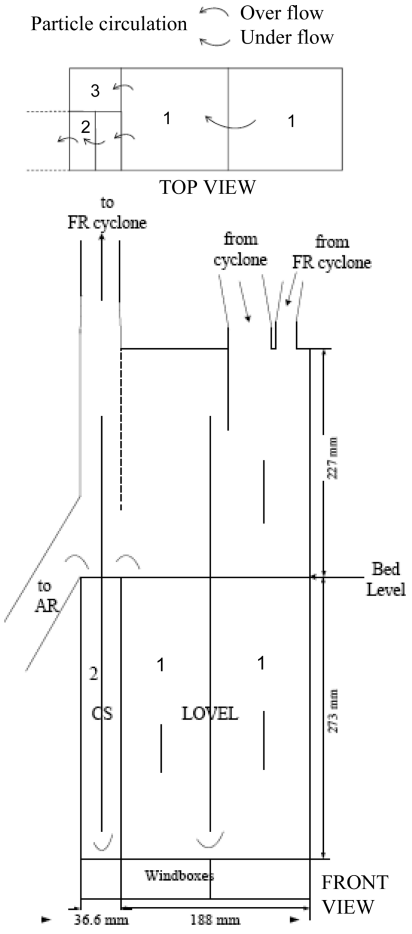


**Figure 3.** Main layout of the fuel reactor, top view and front view, with the particle circulation directions: (1) low-velocity part, (2) carbon stripper, and (3) high-velocity part.

to gaseous compounds, all calculations are made with the fuel fraction that is actually measured to be converted to gas. This fraction is expressed by the solid fuel conversion, $\eta_{SF}$. The carbon flow of the introduced effective coal is calculated as the sum of all carbon-containing flows exiting in the system. $F_{CO_2,FR}$, $F_{CO,FR}$, and $F_{CH_4,FR}$ are the flows of $CO_2$, CO, and $CH_4$, respectively, in the fuel-reactor product gas, and $F_{CO_2,AR}$ is the $CO_2$ flow from the air reactor. $F_{C,fuel,in}$ is the carbon flow contained in the fuel feeding, $\dot{m}_{fuel,in}$, and $[C]_{fuel}$ is the mass-based carbon content in fuel given by the ultimate analysis.

$$\eta_{SF} = \frac{F_{C,\,fuel,\,eff}}{F_{C,\,fuel,\,in}} = \frac{F_{CO_2,\,FR} + F_{CO,\,FR} + F_{CH_4,\,FR} + F_{CO_2,\,AR}}{\dot{m}_{fuel,\,in}[C]_{fuel}1000/12} \tag{8}$$

The flow of each species in the fuel and air reactor is calculated as a product of the fraction in the outgoing gas and the total fuel- and air-reactor flow, both on a dry basis. Sulfur-containing species and higher hydrocarbons are omitted. The total $N_2$ flow introduced in the fuel reactor is the sum of the flows to the high-velocity section of the fuel reactor and small fuel-reactor loop seal and about 50% of the fluidizing $N_2$ to the upper and lower loop seals. $N_2$ to the air reactor is the sum of $N_2$ in the air flow introduced in the air reactor and half of $N_2$ fluidizing the upper and lower loop seals.

**Table 2. Flows for the Fuel Reactor and the Loop Seals, in $L_N$/min**

| $F_{LOVEL}(H_2O)$ | $F_{CS}(N_2)$ | $F_{HIVEL}(N_2)$ | $F_{HILS}(N_2)$ | $F_{LOLS}(N_2)$ | $F_{FRLS}(N_2)$ |
|---|---|---|---|---|---|
| 21 | 6 | 2 | 4 | 4 | 2 |

In every combustion process, ensuring enough oxygen availability is fundamental for the good performance of the process. In the particular case of this technology, this availability can be evaluated by means of the oxygen carrier to fuel ratio, OC/fuel, which is the amount of oxygen that can be supplied by the oxygen carrier divided by the oxygen demand of the effective fuel feed. It depends upon the oxygen-carrier circulation rate, which is given by the operation conditions and configuration of the riser in a circulating fluidized-bed system. For the OC/fuel calculation, only ilmenite is taken into account as the oxygen carrier.

$$\mathrm{OC/fuel} = \frac{O_{2\ \text{supplied by OC}}}{O_{2\ \text{demand, fuel in FR}}} = \frac{F_{OC}R_{O,\,ilm}1000/32}{\Phi_O(F_{CH_4,\,FR} + F_{CO,\,FR} + F_{CO_2,\,FR} + F_{CO_2,\,AR})} \tag{9}$$

$\Phi_O$ is the oxygen carbon ratio, that is, moles of $O_2$ needed to fully oxidize a mass of fuel containing 1 mol of carbon. For this fuel, $\Phi_O$ is 1.13 mol of $O_2$/mol of C. $F_{OC}$ is the solid circulation rate, which can be expressed as the oxygen-carrier inventory in the fuel reactor, $m_{oc}$, which was around 6 kg in this pilot for ilmenite, divided by the mean oxygen-carrier residence time, $t_{r,OC}$.

$$F_{OC} = m_{OC}/t_{r,\,OC} \tag{10}$$

Although $t_{r,OC}$ is not measured in this plant, it is approximately calculated using the correlations established for this plant by Markström et al.[30] that use the pressure drop registered in the riser, the air-reactor total exit flow, and the air-reactor temperature.

The efficiencies that indicate the performance of the process, in gasification as well for the combustion reactions, are defined as follows. The carbon-capture efficiency, $\eta_{CC}$, is the ratio of the carbon that is converted to gas in the fuel reactor to the effective carbon flow. This efficiency reflects unconverted char reaching the air reactor and being burnt to $CO_2$.

$$\eta_{CC} = \frac{F_{CO_2,\,FR} + F_{CO,\,FR} + F_{CH_4,\,FR}}{F_{CO_2,\,FR} + F_{CO,\,FR} + F_{CH_4,\,FR} + F_{CO_2,\,AR}} \tag{11}$$

A parameter that can also be used to evaluate the carbon-capture efficiency via analysis of the air reactor is the oxide oxygen fraction, $\eta_{OO}$, defined as the amount of oxygen used to reoxidize the oxygen carrier in the air reactor divided by the total amount of oxygen consumed in the air reactor, which is the oxygen to oxidize the oxygen carrier and the unreacted char coming from the fuel reactor. $F_{AR\ in}$ is the air flow introduced in the air reactor, and $y_{CO_2,AR}$ and $y_{O_2,AR}$ are the $CO_2$ and $O_2$ fractions in the air reactor.

$$\eta_{OO} = \frac{F_{AR\ in}0.21 - F_{AR}(y_{CO_2,\,AR} + y_{O_2,\,AR})}{F_{AR\ in}0.21 - F_{AR}y_{O_2,\,AR}} \tag{12}$$

For $\Phi_O$ equal to 1, $\eta_{CC}$ should be equal to $\eta_{OO}$ under steady state. In practice, the actual value of the $O_2$/C ratio, $\Phi_{O,act}$, is considerably lower than the theoretical value of 1.13, because of the incomplete oxidation in the fuel reactor. Therefore, $\eta_{OO}$

should also be lower than $\eta_{CC}$. $\eta_{OO}$ has one important advantage because it can be calculated using only gas concentration measurements and does not include any uncertainties arising from the calculation of the gas flows.

To evaluate the performance of the system toward combustion, the parameter oxygen demand, $\Omega_{OD}$, is used. It evaluates the need of a later oxygen-polishing step, and it is the fraction of $O_2$ lacking to achieve full combustion of the fuel-reactor-produced gas (see eq 13). The advantage of $\Omega_{OD}$ is that it does not include any flows; thus, it is only dependent upon gas concentrations and not flows.

$$\Omega_{OD} = \frac{O_{2\ \text{demand gases FR}}}{O_{2\ \text{demand, fuel in FR}}} = \frac{2F_{CH_4,FR} + 0.5F_{H_2,FR} + 0.5F_{CO,FR}}{\Phi_O(F_{CH_4,FR} + F_{CO,FR} + F_{CO_2,FR})} = \frac{2y_{CH_4,FR} + 0.5y_{H_2,FR} + 0.5y_{CO,FR}}{\Phi_O(y_{CH_4,FR} + y_{CO,FR} + y_{CO_2,FR})} \quad (13)$$

The reaction rate of the materials used in the reduction reaction was evaluated with TGA by means of the mass-based conversion degree, $\omega$, defined as

$$\omega = \frac{m}{m_o} \quad (14)$$

with $m$ being the instantaneous mass of the material acting as an oxygen carrier and $m_o$ being the initial mass of fully oxidized material.

## RESULTS AND DISCUSSION

The experiments were performed at two temperatures of the fuel reactor: 950 and 1000 °C. The temperature in the air reactor was within the range of 820−980 °C. The fuel flow was either 479 or 1053 g/h, which corresponds to a fuel power of 4.2 and 9.3 $kW_{th}$, respectively. The particle recirculation between reactors was controlled by the air flow to the air reactor, which was varied from 155 to 190 $L_N$/min. Operation under various conditions was performed for 8 h, of which 4 h with the mixture of ilmenite and limestone and 4 h with only ilmenite. All of the conditions tested were maintained for 30−60 min.

**Continuous Testing with Ilmenite Only. Base Case.** To evaluate the influence of adding limestone on the performance of the CLC process, experiments using only ilmenite as the base case were performed. Initially in the whole plant, there was about a 15 kg inventory of ilmenite with a particle size of 90−250 $\mu$m. The fuel-reactor inventory was about 6 kg.

At each tested temperature, two different air flows were used for the ilmenite tests to change the solid circulation rate and, therefore, the residence time. Conditions were stable, and the coal feeding rate, $\dot{m}_{fuel,in}$, was 479 g/h. Table 3 gathers the averages of gas concentrations for the experiments using only ilmenite as an oxygen carrier at the fuel-reactor temperatures and introduced air flows to the air reactor tested.

Figures 4 and 5 show a comparison of the main parameters that indicate the system performance. At 950 °C, the experiment with a higher circulation rate and OC/fuel ratio (Figure 4a) had a lower carbon-capture and oxide oxygen fraction compared to the test with a lower OC/fuel (Figure 4b). That was due to the increase in the time to gasify the char fuel. Thus, $\eta_{CC}$ increased from 0.7 to 0.83 when the residence time rose from 8.1 to 13.5 min. The same improvement in the gasification efficiency could be seen at 1000 °C. $\eta_{CC}$ increased from 0.59 to 0.77 when the residence time rose from 4.9 to 9.2 min. The oxygen demand is not substantially influenced by the residence time within the resulting range of residence times of the tests. In all cases, the OC/fuel ratio was above 1. At 950 °C, the oxygen demand was 0.33, and at 1000 °C, the oxygen demand was 0.28 and 0.29. However, there was no significant effect of the solid residence time on the oxygen demand. Thus, both gasification efficiency and gas conversion efficiency increased at higher temperatures. An increased performance for higher temperatures when using only ilmenite was already seen by Cuadrat et al.[13] and Berguerand et al.[14]

**Table 3. Gas Concentration Averages (Dry Basis) for the Experiments Performed with Ilmenite, with $N_2$ to Balance**

| temperature (°C) | $F_{AR\ in}$ ($L_N$/h) | $CO_2$ | $H_2$ | CO | $CH_4$ |
|---|---|---|---|---|---|
| 950 | 190 | 14.8 | 5.9 | 2.2 | 1.2 |
| 950 | 155 | 19.4 | 7.7 | 3.4 | 1.3 |
| 1000 | 190 | 15.2 | 5.7 | 2.4 | 1.3 |
| 1000 | 155 | 16.6 | 6.1 | 2.8 | 1.2 |

A high fuel feed test with ilmenite was also performed to compare it to the experiment at high fuel feeding after limestone addition. The petcoke feed flow was 958 g/h, and the average main results obtained will be presented in the section summarizing the results.

**Continuous Testing with Ilmenite and Limestone Mixture. Effect of the Limestone Addition.** After operation of the base case, 4 kg of limestone with a particle size of 90−200 $\mu$m was added, corresponding to 2.2 kg of burnt lime, CaO. The mass fraction of limestone in the fuel reactor was later measured to be about 12%. Because of the fluidization properties of both types of particles, the mass fraction of limestone in the fuel reactor was higher than in the air reactor.

*Effect of the Temperature.* In this section, a series of experiments performed with the mixture of ilmenite and limestone as the bed material with fuel-reactor temperature variation is evaluated. Figure 6 shows the measured gas concentrations in the fuel and air reactor for a 150 min period. Conditions were stable, and the fuel feed was 479 g/h. After 62 min, the fuel-reactor temperature, $T_{FR}$, was raised from 950 to 1000 °C. After 125 min, the temperature was lowered back to 950 °C. Similar values as previously at 950 °C were obtained, indicating the reproducibility of the results.

At 1000 °C, higher amounts of $H_2$, CO, and $CO_2$ are being generated in comparison to the conditions reached at 950 °C, which, however, had a better $CO_2$/CO ratio. The amount of $CH_4$ released was similar and slightly lower at 1000 °C. $CO_2$ from the air reactor was measured, indicating char escaping to the air reactor. $CO_2$ in the air reactor was lower at 1000 °C.

The calculated OC/fuel ratio and mean residence time of the tests shown in Figure 6 are represented in Figure 7. Note the definition of OC/fuel, i.e., the oxygen available from the oxygen carrier based on mass circulation over the oxygen needed by the fuel actually converted in the fuel reactor. Thus, this ratio may decrease from a reduced circulation or an increased fuel conversion rate.

The estimated average oxygen-carrier residence time, $t_{r,OC}$, was in the range of 9−13 min, corresponding to solid circulation rates of 40−28 kg/h. Because the gasification rate for this fuel was found to be quite low, about 20 wt %/min at this temperature

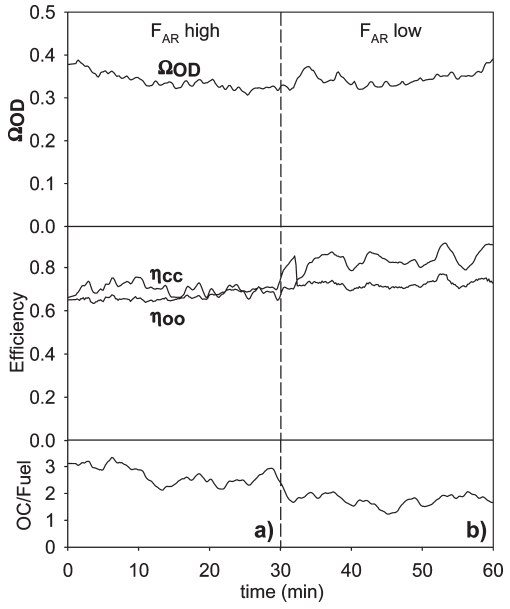


**Figure 4.** Comparison between the oxygen demand, $\Omega_{OD}$, the carbon-capture efficiency, $\eta_{CC}$, the oxide oxygen fraction, $\eta_{OO}$, and the OC/fuel ratio for experiments at $T_{FR}$ = 950 °C using ilmenite as the bed material. $\dot{m}_{fuel,in}$ = 479 g/h. The dashed line shows when the air-reactor flow, $F_{AR}$, was lowered. (a) $F_{AR}$ = 190 $L_N$/h. (b) $F_{AR}$ = 155 $L_N$/h.

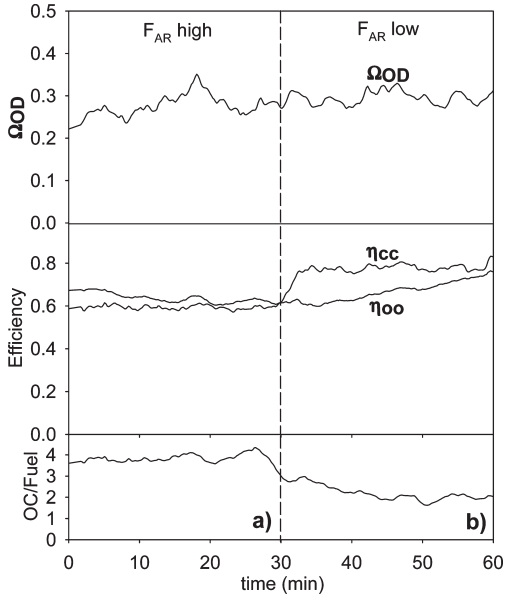


**Figure 5.** Comparison between the oxygen demand, $\Omega_{OD}$, the carbon-capture efficiency, $\eta_{CC}$, the oxide oxygen fraction, $\eta_{OO}$, and the OC/fuel ratio for experiments at $T_{FR}$ = 1000 °C using ilmenite as the bed material. $\dot{m}_{fuel,in}$ = 479 g/h. The dashed line shows when the air-reactor flow, $F_{AR}$, was lowered. (a) $F_{AR}$ = 190 $L_N$/h. (b) $F_{AR}$ = 155 $L_N$/h.

range with ilmenite as an oxygen carrier,[12] and assuming that the residence time for the fuel is the same as for the oxygen carrier, the mean residence time is insufficient to fully gasify the char. The OC/fuel ratio was between 1.2 and 2. When the oxygen carrier is highly converted, the reactivity decreases rapidly. Considering the reaction rate for the reduction of activated ilmenite,[10] the lower conversion rate could start at about a reduction conversion of 0.7−0.8, which corresponds to

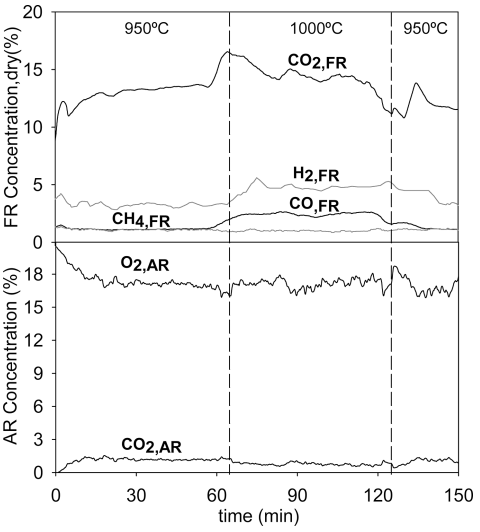


**Figure 6.** Measured product gas distributions in the fuel (dry basis) and air reactor for experiments performed with the mixture of ilmenite and limestone as the bed material with fuel-reactor temperature variation: $T_{FR}$ = 950 and 1000 °C. $\dot{m}_{fuel,in}$ = 479 g/h.

OC/fuel below 1.3−1.4. This is in line with the study made by Markström et al.,[30] who concluded that poorer conversion in this unit was obtained when the mass-based conversion degree variation was around 2.8%, which would correspond to an OC/fuel of 1.4.

Figure 8a shows the corresponding $\eta_{CC}$ and $\eta_{OO}$ when using the mixture ilmenite and limestone as the bed material at $T_{FR}$ of 950 and 1000 °C. At 950 °C, $\eta_{CC}$ is about 79% and $\eta_{OO}$ is about 70%. For 1000 °C, the values are 86 and 81%. That is, the gasification rate is clearly improved by the temperature.

However, the oxygen demand at 950 °C was 24%, which was lower than the oxygen demand at 1000 °C, 28%. This is in contrast to the results with only ilmenite, where the gas conversion was improved by higher temperatures.

*Effect of the Fuel Feed.* A test period where the fuel feed was increased to an effective value of 1053 g/h was performed. The fuel-reactor temperature was 950 °C. The resulting values of the most important parameters are represented in Figure 9.

In the test performed with a higher fuel flow, the resulting OC/fuel ratio dropped to 0.7 and is not fully comparable to the other tests (tests operated with ratios over 1), because the system was operating in sub-stoichiometric conditions. Note that the OC/fuel ratio should be over 1 to ensure that the circulating OC can supply enough oxygen to fully oxidize the introduced fuel.

*Effect of Limestone Addition.* The experiments with only ilmenite chosen for the comparison are those with more similar OC/fuel ratios. Figure 10 shows the process efficiencies before and after limestone addition at a fuel-reactor temperature of 950 °C. The gas conversion was higher at 950 °C, because $\Omega_{OD}$ decreased from 0.33 to 0.24. $\eta_{CC}$ is higher for ilmenite only in Figure 10, but this could be explained by the shorter residence time. Two tests with different residence times were made with ilmenite only (see Figure 4). By interpolation of these two tests, it can be seen that $\eta_{CC}$ is somewhat lower for ilmenite only, 0.76, as compared to ilmenite and limestone, 0.79, which is a slight improvement.

At 1000 °C (Figure 11), there was no significant difference in the gas conversion, because $\Omega_{OD}$ was quite similar after limestone

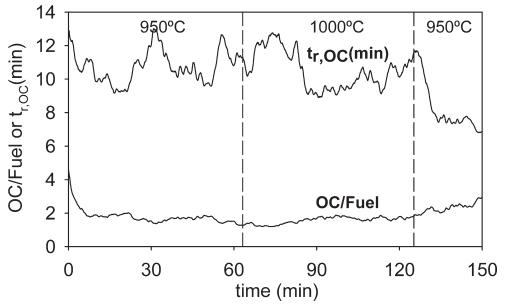


**Figure 7.** OC/fuel ratio and mean residence time in the fuel reactor for the test shown in Figure 6.

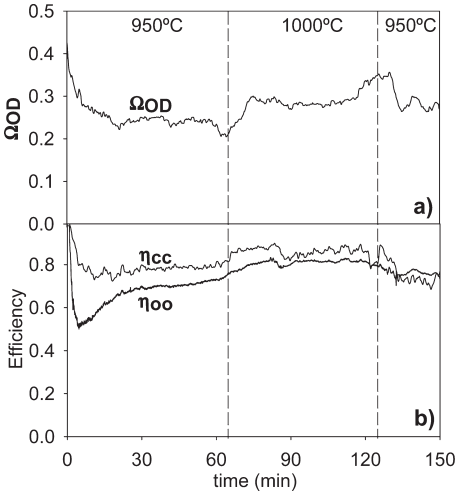


**Figure 8.** (a) Oxygen demand, $\Omega_{OD}$, (b) carbon-capture efficiency, $\eta_{CC}$, and oxide oxygen fraction, $\eta_{OO}$, for experiments with ilmenite and limestone shown in Figures 6 and 7.

addition. However, the efficiencies related to char conversion were improved by the presence of limestone. $\eta_{OO}$ increased from 0.66 to 0.81, and $\eta_{CC}$ increased from 0.77 to 0.86. The improvement of the char conversion was also seen by the higher CO plus $CO_2$ flows from the fuel reactor.

*Operational Overview.* Table 4 shows a summary of the average values for the main experiments performed: the carbon-capture efficiency, $\eta_{CC}$, the oxide oxygen fraction, $\eta_{OO}$, the oxygen demand, $\Omega_{OD}$, the OC/fuel ratio, the oxygen-carrier average residence time in the fuel reactor, $t_{r,OC}$, the sum of the CO and $CO_2$ flows from the fuel reactor, $F_{CO} + F_{CO_2}$, and the total carbon flow in the effective coal fed, $F_{C,fuel,eff}$. The most interesting observations are related to the effect of the limestone: (1) At 950 °C, there is a very clear reduction in the oxygen demand, whereas no clear difference is seen at 1000 °C. (2) In all of the cases compared, there is more rapid conversion of the char in the presence of limestone, as seen in the increased flow of CO plus $CO_2$. Generally, the results shown in Table 4 follow expectations and previous experiences. Thus, (1) char conversion is faster at higher temperatures, and (2) a shorter residence time reduces char conversion in the fuel reactor, i.e., gasification efficiency, as seen by the lower flow of CO plus $CO_2$.

*Operational Problems.* When operating with the mixture of ilmenite−limestone, a substantial fraction of limestone was elutriated and left the reactor system together with the product gas. That caused some operational problems, because some $Ca(OH)_2$ was formed at the end of the outlet pipe of the fuel reactor leading the water seal (see Figure 2). This led to partial blockage of the pipe and risk of overpressure and disturbance of the pressure balance in the system. Therefore, the pipe had to be cleaned regularly. Despite these complications, the unit could be continuously operated and stable conditions and values were eventually obtained. In the beginning of the tests after limestone addition, $CaCO_3$ in the limestone was calcined, CaO was formed with consequent $CO_2$ release, and higher amounts of lime were lost.

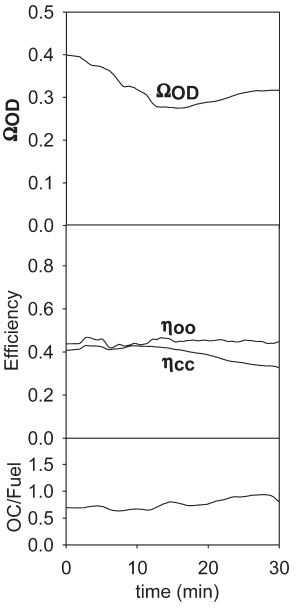


**Figure 9.** Oxygen demand, $\Omega_{OD}$, carbon-capture efficiency, $\eta_{CC}$, oxide oxygen fraction, $\eta_{OO}$, and OC/fuel ratio using ilmenite and limestone and a high fuel feeding rate. $\dot{m}_{fuel,in}$ = 1053 g/h. $T_{FR}$ = 950 °C.

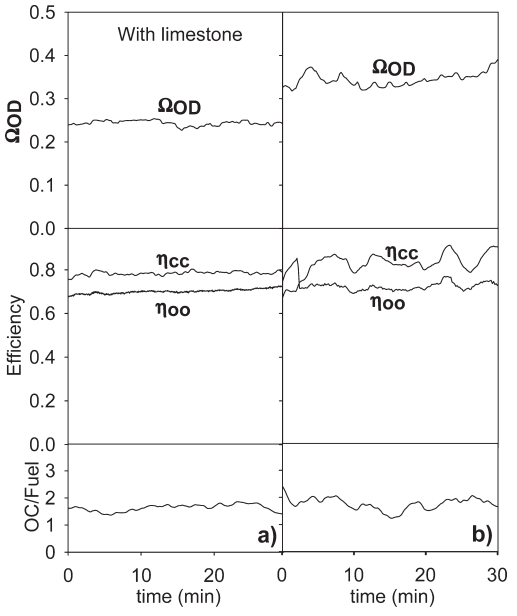


**Figure 10.** Comparison between the oxygen demand, $\Omega_{OD}$, the carbon-capture efficiency, $\eta_{CC}$, the oxide oxygen fraction, $\eta_{OO}$, and the OC/fuel ratio for experiments at $T_{FR}$ = 950 °C using (a) mixture of ilmenite−limestone and (b) ilmenite as the bed material. $\dot{m}_{fuel,in}$ = 479 g/h.


dx.doi.org/10.1021/ef200806q |*Energy Fuels* 2011, 25, 4818–4828

*Discussion of Mechanisms.* To assess the possible oxygen-carrier properties of the limestone particles used in the process, a sample taken from the fuel reactor was reduced in TGA to evaluate whether it transferred oxygen. The sample was reduced with 5% $H_2$ and, subsequently, oxidized in TGA. There was some loss of weight and, hence, oxygen transfer, but it is small. Additionally, to this low oxygen transport capacity of the sample, the reaction rates are much slower than the corresponding rates with ilmenite, as seen in Figure 12. The lower reactivity of $CaSO_4$ as an oxygen carrier with reducing gases ($H_2$, CO, and $CH_4$) compared to ilmenite as an oxygen carrier has been previously seen.[31−34] Thus, it is unlikely that the effect seen in the gas conversion caused by limestone addition is due to its performance as an oxygen carrier. This is also consistent with the previously mentioned laboratory study by Teyssié et al.,[19] where the positive effect of adding CaO to ilmenite was seen already in the first cycle with fuel, i.e., before any formation of $CaSO_4$ is possible. Moreover, this study showed that the positive effect of using highly sulfated limestone was only seen in the first cycles and together with high $SO_2$ release. Thus, the absence of $SO_2$ release in the present tests is an additional indication that $CaSO_4$ did not significantly contribute as an oxygen carrier.

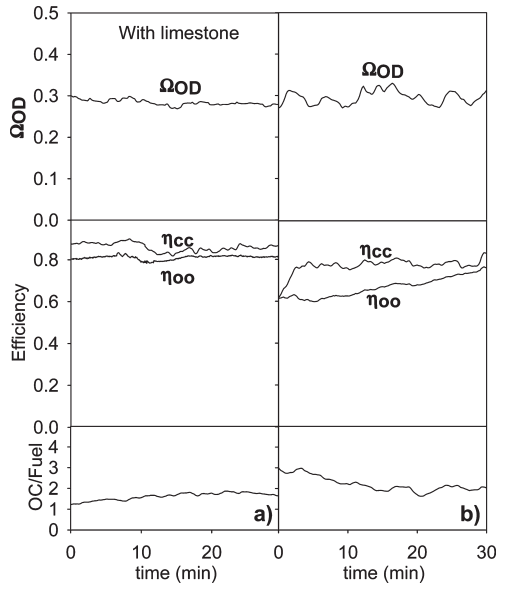


**Figure 11.** Comparison between the oxygen demand, $\Omega_{OD}$, the carbon-capture efficiency, $\eta_{CC}$, the oxide oxygen fraction, $\eta_{OO}$, and the OC/fuel ratio for experiments at $T_{FR}$ = 1000 °C using (a) mixture of ilmenite−limestone and (b) ilmenite as the bed material. $\dot{m}_{fuel,in}$ = 479 g/h.

The study by Teyssié et al.[19] also indicated that the beneficial effect of limestone addition can be explained by means of its influence on the WGS reaction (see eq 15).

$$CO + H_2O \leftrightarrow CO_2 + H_2 \quad (15)$$

To evaluate how far from the WGS equilibrium the fuel-reactor components in the product gas are, the fraction $(F_{H_2,FR}F_{CO_2,FR})/(F_{H_2O,FR\ out}F_{CO,FR})$ is calculated in each point for every experiment performed. It is compared afterward to the WGS constant, $k_{WGS}$, at the corresponding $T_{FR}$. Figure 13 shows the fraction $(F_{H_2,FR}F_{CO_2,FR})/(F_{H_2O,FR\ out}F_{CO,FR})$ obtained for experiments with the ilmenite−limestone mixture and for tests performed with ilmenite only at 950 and 1000 °C. The equilibrium constant $k_{WGS}$ at the temperature considered is also represented. At both temperatures, the exiting gaseous flows with limestone addition were closer to the WGS equilibrium, i.e.,

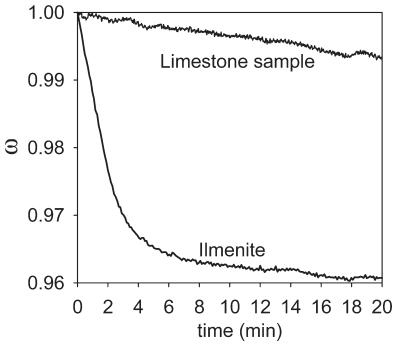


**Figure 12.** Mass-based conversion degree, $\omega$, of ilmenite and limestone samples as a function of time. Reduction in TGA with 5% $H_2$ + 40% $H_2O$ for ilmenite and 5% $H_2$ for limestone. $T$ = 900 °C.

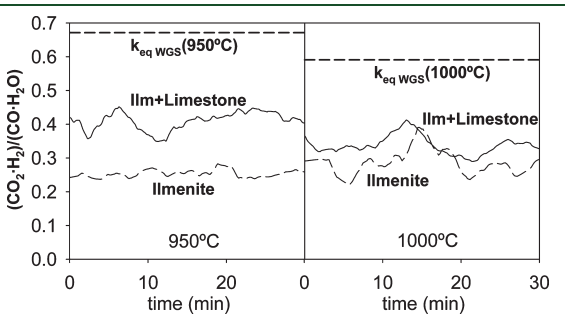


**Figure 13.** Fraction $(F_{H_2,FR}F_{CO_2,FR})/(F_{H_2O,FR\ out}F_{CO,FR})$ for experiments with the ilmenite−limestone mixture and with ilmenite as the bed material at 950 and 1000 °C.

**Table 4. Summary of the Average Values Obtained**

| | $\eta_{CC}$ | $\eta_{OO}$ | $\Omega_{OD}$ | OC/fuel | $t_{r,OC}$ (min) | $F_{CO} + F_{CO_2}$ ($L_N$/h) | $F_{C,fuel,eff}$ (g C/h) | $\dot{m}_{fuel,in}$ (g/h) |
|---|---|---|---|---|---|---|---|---|
| 950 °C, mixture | 0.79 | 0.7 | 0.24 | 1.8 | 10.7 | 360 | 270 | 479 |
| 950 °C, ilmenite | 0.7 | 0.67 | 0.33 | 2.6 | 8.1 | 230 | 210 | 479 |
| 950 °C, ilmenite | 0.83 | 0.73 | 0.33 | 1.8 | 13.5 | 300 | 210 | 479 |
| 1000 °C, mixture | 0.86 | 0.81 | 0.28 | 1.6 | 10.8 | 445 | 290 | 479 |
| 1000 °C, ilmenite | 0.58 | 0.64 | 0.28 | 3.7 | 4.9 | 255 | 250 | 479 |
| 1000 °C, ilmenite | 0.77 | 0.66 | 0.29 | 2.2 | 9.2 | 350 | 260 | 479 |
| 950 °C, ↑ feed, mixture | 0.42 | 0.45 | 0.33 | 0.7 | 8 | 640 | 870 | 1053 |
| 950 °C, ↑ feed, ilmenite | 0.54 | 0.66 | 0.33 | 1.1 | 8.4 | 420 | 440 | 958 |


dx.doi.org/10.1021/ef200806q |*Energy Fuels* 2011, 25, 4818–4828

to higher $H_2 + CO_2$ formation, although the difference was much more pronounced at 950 °C.

Thus, limestone addition causes CO and $H_2O$ to react to give $CO_2$ and $H_2$; i.e., Ca-based compounds could act as a catalyst for the WGS reaction. This happens in the presence of an oxygen carrier, ilmenite, which reacts faster with $H_2$ than with CO. Consequently, the oxidation of the gas should proceed faster, giving higher gas conversion and lower oxygen demand. This effect is clearly seen at 950 °C (see Figure 10), although at a temperature of 1000 °C, the improvement regarding the gas conversion was residual when CaO was present in the solid mixture (see Figure 11). From results shown in Figure 13, it seems that the WGS reaction itself is fast enough at 1000 °C to happen at similar extension with and without limestone addition.

The mechanism for improved char conversion is less clear. The effect seen here is different from that found in the literature,[35,36] for which calcium is known to have catalytic effects on steam gasification of coal. To obtain good catalytic activity, calcium must be atomically dispersed throughout the char, which is not the case in this process.

In comparison to the addition of unsulfated limestone, batch experiments with the addition of sulfated limestone to an ilmenite bed at 970 °C showed more rapid char conversion in the initial redox cycles and together with high $SO_2$ release, but the benefits as well as the $SO_2$ release disappeared after a dozen cycles.[19] It is known that $SO_2$ enhances char conversion,[4] and this is also the likely explanation for faster char conversion in the cycles where $SO_2$ is released from $CaSO_4$ decomposition. The present tests showed no $SO_2$ release from the fuel reactor, and consequently, the mechanism of $SO_2$ release would not explain the enhanced char conversion rate. Thus, the explanation for the beneficial effect on the char conversion should be found in the presence of CaO and not $CaSO_4$.

Furthermore, the effect of the WGS equilibrium on char conversion is not clear. The general effect is to lower CO and raise $H_2$. Because $H_2$ is a known inhibitor of steam gasification, this would be expected to lower char conversion, but possibly the lowered CO could compensate for this, with CO also being an inhibitor of gasification.

**Effect of Limestone Addition. Fate of Sulfur.** Sulfur contained in the fuel is released mainly in the form of $H_2S$ under the reducing conditions in the reactor. Previous experience with petcoke feed and ilmenite as an oxygen carrier showed that also some $SO_2$ can be formed when oxygen-carrier circulation is high enough.[15]

$SO_2$ in the fuel reactor was continuously measured online in all experiments. For the experiments performed using only ilmenite, the amount of $SO_2$ released in the fuel reactor depended upon the oxidation conditions in the reactor. Thus, higher OC/fuel ratios meant that more sulfur from the fuel was oxidized to $SO_2$. At 950 °C with an OC/fuel ratio of about 1.6, about 2% of sulfur from the fuel feed was oxidized to $SO_2$. For a higher OC/fuel ratio of 2.5, about 3.5% of the sulfur feed was released as $SO_2$. At 1000 °C, 2 and 9% of the sulfur feed, correspondingly, were oxidized to $SO_2$, as seen in Figure 14. The higher value of 9% is explained by a high OC/fuel ratio. It was not possible to see any clear influence of the temperature.

Thermodynamic simulations showed that, under these conditions, the rest of the sulfur coming from the fuel reactor should be $H_2S$. The simulations confirmed that $SO_2$ formed in the fuel reactor was close to the thermodynamic equilibrium for $SO_2$ regarding both the $CO/CO_2$ and $H_2/H_2O$ ratios for each test.

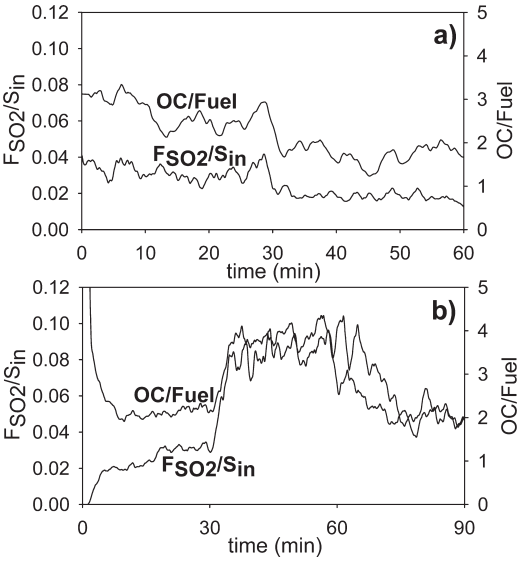


**Figure 14.** $F_{SO_2}/S_{in}$ ratio and OC/fuel ratio for experiments with ilmenite as the bed material at (a) 950 °C and (b) 1000 °C.

In the experiments with the mixture of ilmenite−limestone, the $SO_2$ measurement showed that there was no $SO_2$ generated during the 4 h of testing.

The $SO_2$ analyzer was connected for some minutes to the air reactor during experiments at 950 °C and an OC/fuel ratio of 1.3, and it turned out that about 13% of the sulfur feed was being released in the air reactor. This sulfur was presumably coming from the combustion of char that was flowing into the air reactor, because the carbon capture in that moment was about 62%. Considering that 38% of the effective fuel feed is converted in the air reactor and assuming that S released from petcoke is proportional to the carbon release, about 66% of sulfur that would have been released in the air reactor was being retained by limestone. Thus, $SO_2$ coming from the air reactor was smaller than the expected release of sulfur from the fuel burning.

Sulfur and calcium mapping of a sample of limestone cross-cut particles taken from the fuel reactor was performed by SEM analysis. Sulfur was seen to be homogeneously distributed throughout the particle (see Figure 15). The mass fraction of sulfur in the particles was 4−5%.

An additional TGA analysis was performed as an approximate measurement of the calcium species present in the used limestone after these tests. A limestone sample taken from the fuel reactor was heated from room temperature to 900 °C in a $N_2$ atmosphere and lost about 25% of the initial weight. This corresponded to the decomposition of $Ca(OH)_2$ that would have been formed from humidity uptake by the used limestone from the fuel reactor. Afterward, the sample was reduced with 5% $H_2$, and the sample lost about 3.6% mass, compared to the initial weight. This corresponded to the reduction of $CaSO_4$ contained in the sample. It is presumable that there is also CaS as the other main sulfur-containing compound. The main component in the used limestone taken from the fuel reactor was therefore CaO.

In total, 95 g of sulfur were fed during the hours of tests with petcoke. In the fuel reactor, about 0.8 kg of limestone was recovered. Considering the measured sulfur content of 4−5%, the limestone extracted from the fuel reactor contained 32−40 g of sulfur. Because there is also some limestone in the air reactor and in the loop seals, as well as some $SO_2$ release from the char

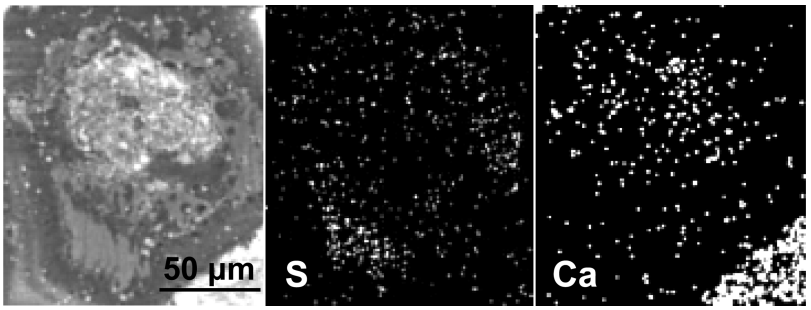


**Figure 15.** Image of a cross-cut particle and sulfur and calcium mapping performed by SEM analysis of a sample of limestone taken from the fuel reactor.

burnt in the air reactor, it is likely that a major part of all sulfur released in the fuel reactor was taken up by limestone; that is, both $H_2S$ and $SO_2$ released in the fuel reactor were reacting with limestone to form CaS.

In conclusion, most of the sulfur released seems to have been captured by the lime. Moreover, a steady state with respect to sulfur was likely not reached during the 4 h of operation.

## CONCLUSION

In this paper, the effect of limestone addition in a 10 $kW_{th}$ continuous CLC system fed with Mexican petcoke as fuel and a mixture of ilmenite−limestone and ilmenite as an oxygen carrier was assessed. The limestone content in the fuel-reactor bed at the conclusion of the experiments was weighed to be about 12%, and the rest was ilmenite. The tests showed good agreement with previous tests and with what should be expected. (1) When the residence time was higher, the gasification efficiency increased, as shown by, e.g., the higher release of CO plus $CO_2$ from the fuel reactor. (2) The fuel-reactor temperature was also provn to be one of the determining variables for the performance of the process, with an increase of the temperature being very positive to increase the efficiency of gasification and, thus, the carbon capture.

The more interesting conclusions are related to the effect of limestone addition: (1) At 950 °C, limestone addition led to improved gas conversion, with the oxygen demand being lowered from 0.33 to 0.24. At 1000 °C, however, no improvement in gas conversion could be seen for lime addition. The improvement in gas conversion can be explained by lime catalyzing the WGS equilibrium and the subsequent faster reaction of $H_2$ with ilmenite. (2) The oxygen transfer by sulfated limestone seems to be small, and the improvement in gas conversion is probably explained mostly by the effect of limestone on the WGS reaction. (3) The char gasification rate was also improved by the addition of limestone, at both 950 °C and 1000 °C, although the mechanism has not been fully clarified. (4) Before limestone addition, there was $SO_2$ and $H_2S$ release in the fuel reactor, and the amount of $SO_2$ released was higher when the oxygen carrier to fuel ratio was higher. After limestone addition, no $SO_2$ was measured in the fuel reactor. $SO_2$ was measured in the air reactor, coming from the unconverted char from the fuel reactor. (5) There was sulfur retention by limestone, but more hours of continuous operation would be necessary to ensure that limestone uptake and release of sulfur stabilized with a constant sulfur concentration in the particles. Although not apparent in the present test, the beneficial effects of $CaSO_4$/CaS as an oxygen carrier could be different under other conditions. First, the tests did not reach steady state, and second, the sulfur concentrations were much lower than would have been the case in a real unit, i.e., with less dilution of gases in $H_2O$. (6) For the solid fuel CLC, it is not recommended to use limestone for sulfur removal because the extraction of the used limestone would likely cause the loss of high amounts of oxygen carrier. (7) The use of some limestone in the process as an additive because of its effect in the WGS equilibrium has been shown to be advantageous for the efficiency improvement, gasification, and gas conversion.

## AUTHOR INFORMATION

### Corresponding Author

*Telephone: +34-976-733977. Fax: +34-976-733318. E-mail: abad@icb.csic.es.

## ACKNOWLEDGMENT

This work was partially supported by the European Commission, under the RFCS Program (ECLAIR Project, Contract RFCP-CT-2008-0008), and from Alstom Power Boilers. Ana Cuadrat thanks CSIC for the JAE Predoctoral Fellowship.

## NOMENCLATURE

AR = air reactor
FR = fuel reactor
CLC = chemical-looping combustion
$[C]_{fuel}$ = mass-based carbon content in fuel
$[O]_{fuel}$ = mass-based oxygen content in fuel
$F_{AR,in}$ = air flow introduced in the air reactor (mol/s)
$F_{AR}$ = outlet air-reactor gas flow (mol/s)
$F_{C,fuel,eff}$ = carbon flow in the effective coal fed (mol/s)
$F_{C,fuel,in}$ = carbon flow in the coal feed introduced (mol/s)
$F_{CO_2,AR}$ = $CO_2$ flow from the air reactor (mol/s)
$F_{CO_2,FR}$, $F_{CO,FR}$, $F_{CH_4,FR}$, $F_{H_2O,FR\ out}$, and $F_{SO_2}$ = flows of $CO_2$, CO, $CH_4$, $H_2O$, and $SO_2$, respectively, in the fuel-reactor product gas (mol/s)
$F_{CS}$ = flow in the carbon stripper (mol/s)
$F_{FR}$ = dry basis product gas flow (mol/s)
$F_{FRLS}$ = flow in the small fuel-reactor loop seal (mol/s)
$F_{H_2O,in}$ = water steam inlet flow in the fuel reactor (mol/s)
$F_{HILS}$ = flow in the higher loop seal (mol/s)
$F_{HIVEL}$ = flow in the high-velocity section in the fuel reactor (mol/s)
$F_{LOLS}$ = flow in the lower loop seal (mol/s)
$F_{LOVEL}$ = flow in the low-velocity section in the fuel reactor (mol/s)

$F_{N_2,AR}$ = $N_2$ inlet flow in the air reactor (mol/s)
$F_{N_2,FR}$ = $N_2$ inlet flow in the fuel reactor (mol/s)
$F_{OC}$ = solid circulation rate (kg/s)
$Me_xO_y$ = oxidized oxygen carrier
$Me_xO_{y-1}$ = reduced oxygen carrier
$m$ = instantaneous mass of the oxygen carrier (kg)
$m_o$ = mass of the oxidized form of the oxygen carrier (kg)
$m_{oc}$ = oxygen-carrier inventory in the fuel reactor (kg)
$m_r$ = mass of the reduced form of the oxygen carrier (kg)
$\dot{m}_{fuel,in}$ = fuel feeding flow (kg/s)
OC = oxygen carrier
$R_{O,ilm}$ = oxygen transport capacity of ilmenite
$S_{in}$ = sulfur flow contained in the fuel feeding (mol/s)
$T$ = temperature (°C)
$T_{FR}$ = temperature in the fuel reactor (°C)
$t_{r,OC}$ = mean residence time of the oxygen carrier (s)
WGS = water−gas shift
$y_{O_2,AR}$ and $y_{CO_2,AR}$ = fractions in the air-reactor outlet flow of $O_2$ and $CO_2$
$y_{CH_4,FR}$, $y_{CO_2,FR}$, $y_{CO,FR}$, and $y_{H_2,FR}$ = dry basis fractions in the fuel-reactor product gas of $CH_4$, $CO_2$, CO, and $H_2$, respectively
$\eta_{CC}$ = carbon-capture efficiency
$\eta_{OO}$ = oxide oxygen fraction
$\eta_{SF}$ = solid fuel conversion
$\omega$ = mass-based conversion degree
$\Omega_{OD}$ = oxygen demand
$\Phi_O$ = $O_2$/C ratio for the fuel (mol of $O_2$/mol of C)
$\Phi_{O,act}$ = actual $O_2$/C ratio for the fuel (mol of $O_2$/mol of C)

## REFERENCES


(1) Eide, L. I.; Anheden, M.; Lyngfelt, A.; Abanades, C.; Younes, M.; Clodic, D. *Oil Gas Sci. Technol.* **2005**, *60*, 497–508.
(2) Hossain, M. M.; de Lasa, H. I. *Chem. Eng. Sci.* **2008**, *63*, 4433–4451.
(3) Kerr, H. R. Capture and separation technologies gaps and priority research needs. In *Carbon Dioxide Capture for Storage in Deep Geologic Formations—Results from the $CO_2$ Capture Project*; Thomas, D., Benson, S., Eds.; Elsevier, Ltd.: Amsterdam, The Netherlands, 2005; Vol. 1, Chapter 38.
(4) Leion, H.; Mattisson, T.; Lyngfelt, A. *Fuel* **2007**, *86*, 1947–1958.
(5) Adánez, J.; Abad, A.; Garcia-Labiano, F.; Gayán, P.; de Diego, L. F. Manuscript submitted for publication.
(6) Leion, H.; Lyngfelt, A.; Johansson, M.; Jerndal, E.; Mattisson, T. *Chem. Eng. Res. Des.* **2008**, *86*, 1017–1026.
(7) Leion, H.; Mattisson, T.; Lyngfelt, A. *Energy Fuels* **2009**, *23*, 2307–2315.
(8) Leion, H.; Jerndal, E.; Steenari, B. M.; Hermansson, S.; Israelsson, M.; Jansson, E.; Johnsson, M.; Thunberg, R.; Vadenbo, A.; Mattisson, T.; Lyngfelt, A. *Fuel* **2009**, *88*, 1945–1954.
(9) Adánez, J.; Cuadrat, A.; Abad, A.; Gayán, P.; de Diego, L. F.; García-Labiano, F. *Energy Fuels* **2010**, *24*, 1402–1413.
(10) Abad, A.; Adánez, J.; Cuadrat, A.; García-Labiano, F.; Gayán, P.; de Diego, L. F. *Chem. Eng. Sci.* **2011**, *66* (4), 689–702.
(11) Leion, H.; Mattisson, T.; Lyngfelt, A. *Int. J. Greenhouse Gas Control* **2008**, *2*, 180–193.
(12) Linderholm, C.; Cuadrat, A.; Lyngfelt, A. *Energy Procedia* **2011**, *4*, 385–392.
(13) Cuadrat, A.; Abad, A.; Adánez, J.; de Diego, L. F.; García-Labiano, F.; Gayán, P. Design considerations for chemical-looping combustion of coal—Part 1. Experimental tests. Manuscript submitted for publication.
(14) Berguerand, N.; Lyngfelt, A. *Energy Fuels* **2009**, *23* (10), 5257–5268.
(15) Berguerand, N.; Lyngfelt, A. *Int. J. Greenhouse Gas Control* **2008**, *2*, 169–179.
(16) Berguerand, N.; Lyngfelt, A. *Energy Procedia* **2009**, *1* (1), 407–414.
(17) Berguerand, N.; Lyngfelt, A. *Fuel* **2008**, *87*, 2713–2726.
(18) Cuadrat, A.; Abad, A.; García-Labiano, F.; Gayán, P.; de Diego, L. F.; Adánez, J. The use of ilmenite as oxygen carrier in a 500 $W_{th}$ chemical looping coal combustion unit. Manuscript submitted for publication.
(19) Teyssié, G.; Leion, H.; Schwebel, G.; Lyngfelt, A.; Mattisson, T. Influence of limestone addition to ilmenite in chemical-looping combustion (CLC) with solid fuels. Manuscript submitted for publication.
(20) Mattisson, T.; Lyngfelt, A. *Thermochim. Acta* **1999**, *325*, 59–67.
(21) de Diego, L. F.; Abad, A.; García-Labiano, F.; Adánez, J.; Gayán, P. *Ind. Eng. Chem. Res.* **2004**, *43*, 3261–3269.
(22) García-Labiano, F.; Abad, A.; de Diego, L. F.; Gayán, P.; Adánez, J. *Chem. Eng. Sci.* **2002**, *57*, 2381–2393.
(23) García-Labiano, F.; Adánez, J.; Abad, A.; de Diego, L. F.; Gayán, P. *Energy Fuels* **2004**, *18*, 761–769.
(24) Adánez, J.; Abad, A.; de Diego, L. F.; García-Labiano, F.; Gayan, P. *Ind. Eng. Chem. Res.* **2004**, *43*, 4132–4139.
(25) Abad, A; Adánez, J.; García-Labiano, F.; de Diego, L. F.; Gayán, P. *Energy Fuels* **2004**, *18*, 1543–1554.
(26) Tian, H.; Guo, Q. *Ind. Eng. Chem. Res.* **2009**, *48*, 5624–5632.
(27) Song, Q; Xiao, R; Deng, Z; Shen, L; Zhang, M. *Korean J. Chem. Eng.* **2009**, *23*, 592–602.
(28) Cuadrat, A.; Abad, A.; García-Labiano, F.; Gayán, P.; de Diego, L. F.; Adánez, J. Effect of operating conditions in chemical-looping combustion of coal in a 500 $W_{th}$ unit. Manuscript submitted for publication.
(29) Berguerand, N.; Lyngfelt, A. *Fuel* **2010**, *89* (8), 1749–1762.
(30) Markström, P.; Berguerand, N.; Lyngfelt, A. *Chem. Eng. Sci.* **2010**, *65*, 5055–5066.
(31) Xiao, R; Song, Q.; Zheng, W. G.; Deng, Z. Y.; Shen, L. H.; Zhang, M. Y. Reduction kinetics of a $CaSO_4$-based oxygen carrier for chemical-looping combustion. *Proceedings of the 20th International Conference on Fluidized Bed Combustion*; Xian, China, 2009; pp 519–526.
(32) Song, Q.; Xiao, R.; Deng, Z.; Shen, L.; Xiao, J.; Zhang, M. *Ind. Eng. Chem. Res.* **2008**, *47*, 8148–8159.
(33) Song, Q.; Xiao, R.; Deng, Z.; Zhang, H.; Shen, L.; Xiao, J.; Zhang, M. *Energy Convers. Manage.* **2008**, *49*, 3178–3187.
(34) Song, Q.; Xiao, R.; Deng, Z.; Zheng, W.; Shen, L.; Xiao, J. *Energy Fuels* **2008**, *22*, 3661–3672.
(35) Timpe, R. C.; Sears, R. E. Anion effects on calcium catalysis of low-rank coal char steam gasification; *Proceedings of the Symposium on Fuels Chemistry*; Boston, MA, April, 1990.
(36) Lang, R. J.; Neavel, R. C. *Fuel* **1982**, *61*, 620–626.

# Paper VIII

# Theoretical approach on the CLC performance with solid fuels: optimizing the solids inventory

*Ana Cuadrat, Alberto Abad*[*], *Pilar Gayán, Luis F. de Diego, Francisco García-Labiano, Juan Adánez*

Instituto de Carboquímica (ICB-CSIC), Dept. of Energy & Environment, Miguel Luesma Castán, 4, Zaragoza, 50018, Spain

[*] Corresponding author: Tel: (+34) 976 733 977. Fax: (+34) 976 733 318. E-mail address: abad@icb.csic.es (A. Abad)

## Abstract

Chemical-Looping Combustion (CLC) is a combustion technology with inherent separation of the greenhouse gas $CO_2$. CLC is considered to be an option with low energy penalty and low cost for $CO_2$ capture. An option for use CLC with solid fuels is the in-situ Gasification-CLC (iG-CLC), where the solid fuel gasification and the oxidation of gaseous products, i.e. volatile matter and gasification products, simultaneously take place in the fuel reactor of the CLC system.

The objective of this work was to optimize the operating conditions for direct CLC with solid fuels using ilmenite as oxygen carrier. A simplified model for the fuel reactor has been developed, which describes the complex processes happening in the fuel reactor. Thus, the effect of the main operating variables in the iG-CLC process can be analyzed in a simpler way than using a detailed model. The model includes the possibility of using a carbon separation system to recirculate unreacted char particles exiting from the fuel reactor, reducing the by-pass of carbon to the air reactor. Also, the gasification kinetics of a bituminous coal for both $H_2O$ and $CO_2$ as gasification agents and the kinetics of the reduction reaction of ilmenite with $H_2$, CO and $CH_4$ are incorporated to the model. First, the simulated results have been compared to experimental results from tests performed in a continuous 500$W_{th}$ CLC plant. Later, model simulations were performed to evaluate the effect of the main operating variables of the fuel reactor (e.g. temperature, solids inventory, efficiency of the carbon separation system, oxygen carrier to fuel ratio, or flow and type of gasification agent) on the combustion and carbon

capture efficiencies. The carbon capture was directly related to the extent of gasification, which is promoted by increasing the temperature or the residence time of char particles in the fuel reactor. It is highly beneficial to increase the solids inventory up to 1000 kg/$MW_{th}$, but further increase does not give a relevant improvement in the carbon capture and it is better to increase the carbon separation efficiency than the solids inventory. With an inventory of 1000 kg/$MW_{th}$, at 1000ºC and a carbon separation efficiency of 90% the carbon capture predicted was 86.0%.

## 1. Introduction

Chemical-Looping Combustion (CLC) is a novel combustion technology with inherent separation of the greenhouse gas $CO_2$ that involves the use of an oxygen carrier, that transfers oxygen from air to the fuel avoiding the direct contact between them. Commonly, the CLC system is made of two interconnected reactors, designated as air and fuel reactors. In the fuel reactor, the fuel is oxidized to $CO_2$ and $H_2O$ by an oxygen carrier that is reduced. The reduced oxygen carrier is further transferred into the air reactor where it is oxidized with air, and the material regenerated is ready to start a new cycle. The flue gas leaving the air reactor contains $N_2$ and unreacted $O_2$. The exit gas from the fuel reactor contains only $CO_2$ and $H_2O$. After water condensation, almost pure $CO_2$ can be obtained with little energy lost and low cost [1,2].

The CLC process has been widely developed for gaseous fuels [3]. However, it could be advantageous if the CLC process could be adapted to the use of solid fuels. One of the options to use the CLC technology with solid fuels is the so-called in-situ gasification Chemical-Looping Combustion (iG-CLC) [3]. In this technology the solid fuel is introduced directly in the CLC system and thereby coal gasification and reaction of the released volatile matter and gasification products with the oxygen carrier take place simultaneously in the fuel reactor. In the iG-CLC process the fuel reactor is fluidized by a gasifying agent, e.g., $H_2O$ or $CO_2$, as proposed by Cao et al. [4]. Thereby, the solid fuel devolatilization and gasification takes place in the fuel reactor first and the resulting gases and volatiles are oxidized through reduction of the oxidized oxygen carrier, $Me_xO_y$. The oxygen carrier reduced in the fuel reactor, $Me_xO_{y-1}$, is subsequently led to the air reactor where it is re-oxidized with air. The net chemical reaction as well as the heat involved in the global process is the same as for usual combustion.

Fig. 1 shows the simplified reactor scheme of the CLC process with direct introduction of solid fuels, which is composed by an air and a fuel reactor and the oxygen carrier that circulates between them. Experimentally it was found that working at high temperatures is required to reach high gasification rates [5]. The gasification process was found to be the most relevant step to achieve high carbon capture as the solids stream going out from the fuel reactor can contain certain fraction of unconverted char [6]. Thus, the implementation of a carbon separation system is fundamental to ensure high gasification extent and thus high carbon capture. Simple calculations done in a previous work have shown that a carbon separation system is a critical component in order to have high carbon capture efficiency [7]. A carbon stripper has been proposed in the literature as the carbon separation system [4]. The carbon stripper increases the residence time of char in the fuel reactor by separating and reintroducing ungasified char particles exiting the fuel reactor [4,6].

To use an oxygen carrier with adequate behavior and properties is fundamental to reach high performance in the CLC process. As for this option of CLC with solid fuels, the fuel is physically mixed with the oxygen carrier, being predictable a partial loss of oxygen carrier particles together with the draining stream of coal ashes to avoid their accumulation in the system. In this context, the use of low cost materials such as natural minerals or industrial waste products as oxygen carriers turns out to be very interesting [6-12]. Among them, ilmenite is a low cost natural mineral which is promising for its large scale industrial use as oxygen carrier with solid fuels. Performance of ilmenite has been proven to be acceptable as oxygen carrier for CLC in recent studies made at different scales [13,14]. Comparing the performance of several natural iron ores and industrial products, Norwegian ilmenite was ranked among the materials which showed higher reactivity for both gaseous and solid fuels [9,10]. Although ilmenite particles initially have a rather low reactivity, it undergoes an activation process after several redox cycles, where its reactivity remarkably increases for $H_2$, CO and $CH_4$ as reacting gases [14]. The gas conversion showed by activated ilmenite was even similar to one synthetic $Fe_2O_3/MgAl_2O_4$ material selected from previous works [15]. Ilmenite has high conversion of CO and $H_2$ for syngas applications, but moderate conversion of $CH_4$ for the use of natural gas as fuel [14]. On the whole, ilmenite has adequate values of reactivity and oxygen transport capacity for its use in the CLC technology with solid fuels, which is confirmed by the results from the continuous CLC experiments done to

date. Additionally, ilmenite showed good mechanical stability and good fluidizing properties [16].

In order to optimize the iG-CLC system the modeling of the process is needed. A summary of the mechanisms to date used for the modeling of CLC with solid fuels can be found in Adánez et al. [3]. There is little modeling work done in CLC with solid fuels. Mahalatkar et al. [17] simulated the behavior of a small batch fluidized bed for coal conversion using a Fe-based oxygen carrier. They used the gasification kinetics and the reduction kinetics of the oxygen carrier with pyrolysis and gasification products. The theoretical results agreed to the experimental results. The combustion efficiency depends on the char conversion in the fuel reactor and on the reactivity of the oxygen carrier with the volatiles and gasification gases [5]. In addition, Ströhle et al. [18] presented a simulation of 1 $MW_{th}$ iG-CLC unit. They showed the need of a carbon separation system in order to reach high values of char conversion in the fuel reactor because of the slow gasification reaction.

The objective of this work was to determine the operating conditions that optimize the carbon capture and combustion efficiencies in a CLC system fuelled with coal. For that, a simplified model based on mass balances of a CLC system, including chemical reactions and flow patterns, has been developed. Ilmenite was selected as oxygen carrier and a bituminous Colombian coal "El Cerrejón" as solid fuel. In order to prove the validity of the model, the results predicted with this model were compared to experimental tests done in a 500 $W_{th}$ unit with this type of fuel and this oxygen carrier. Later, the effect of the main operating parameters on the combustion and carbon capture efficiency of the CLC system was analyzed. The parameters considered were the solids inventory, the fuel reactor temperature, the efficiency of the carbon separation system, the oxygen carrier to fuel ratio, the reduction degree of the oxygen carrier, the type and flow of gasification agent, the fraction of oxygen carrier in contact with the volatile matter, and the oxygen carrier reaction rate.

## 2. Reacting scheme in the fuel reactor

A theoretical model is a very useful tool to understand the operation of the system in a general way, as well as to predict the influence of the different variables and optimize their values. In this section a theoretical model for the fuel reactor has been developed based on a simple reacting scheme. The model was as simple as possible, but describing

with accuracy the complex chemical processes happening in the fuel reactor. Thus, the effect of the main operating variables in the iG-CLC process can be analyzed in a simpler way than using a more complete description of the gas and solids flow pattern in the reactor.

The flow patterns of gas and solids here assumed were based on results obtained in a continuously operated CLC unit [5,12]. In these experimental works, it was found that the unconverted $CH_4$, CO and $H_2$ from the fuel reactor were mainly coming from unconverted volatile matter. However, neither tars nor other hydrocarbons than $CH_4$ were found. Also, gasification products were highly converted to $CO_2$ and $H_2O$. A bad contact between volatile matter and oxygen carrier particles was proposed as the main reason for incomplete combustion.

Based on these results, a model of the system was developed to predict and optimize the combustion and carbon capture efficiencies of the CLC process as a function of various operational parameters. Thus, two different gaseous flows in the reactor are considered independently and in plug flow: one for the gasification products in the dense phase and another for the volatile matter released in plume. Fig. 2 shows a scheme of this flow pattern. To simulate the different contact between the released gaseous fuels, the oxygen carrier bed in the fuel reactor was considered to be divided into two separated zones: one zone is in contact with the volatiles and the other zone reacts with the generated gasification products. It is considered that there is perfect mixing of the solids and no constrictions for the gas-solid reactions. Thus, this model assumes that there is no gas exchange between the generated flow of gasification products in the dense bed and volatile plume. Also, the model assumes that the only reducing species in the dense bed are $H_2$ and CO, whereas $CH_4$ also appears in the flow coming from the volatile plume.

The model was developed and applied to ilmenite as oxygen carrier and El Cerrejón coal as fuel. Calculations were made on the basis of 1 $MW_{th}$ of corresponding fuel power. The ultimate and proximate analyses and the heating value of the fuel are gathered in Table 1. The simulations with variation of different parameters were done using the properties of the fresh coal. However, the first simulations were done using the pre-treated coal as fuel, since their results were used to compare and validate the model with experimental results which were done with coal that was pre-treated to eliminate some agglomeration problems that were observed in this coal [5]. Neither sulfur nor nitrogen present in the fuel were considered in this model.

For the development of the model, it is necessary to know (1) the reaction scheme to be considered in the mass balance; (2) the content and composition of the volatile matter in coal, (3) the kinetics of char gasification with the gasification agent used; and (4) the kinetics of the subsequent reaction of the gasification products with the oxygen carrier together with the kinetics of the later reaction of the volatile matter with the oxygen carrier are also required.

### 2.1. Differential mass balances in the fuel reactor

The mass flow changes in a differential mass of the reactor have been considered in the model. To carry out differential mass balances of reactants and products during reaction, the bed is divided into differential elements, both for (1) the gas flow in the dense phase, where gasification takes place, and (2) the flow of volatile matter. Both flows go in parallel and it was assumed that there is no exchange of gases among them. $F_{i,g,1}$ and $F_{i,g,2}$ are the gas flows of the gasification product $i$ at the inlet and outlet of the compartment in the dense phase, respectively; and $F_{i,v,1}$ and $F_{i,v,2}$ are the gas flows of the released gas $i$ in the volatiles at the inlet and outlet of the inventory differential mass, respectively.

The mass balance in a differential mass is defined according to the following scheme of reactions happening simultaneously in the fuel reactor:

$$\text{Coal} \rightarrow a\,CO + b\,H_2 + c\,CH_4 + d\,H_2O + e\,CO_2 + f\,C\,(\text{Char}) \quad (1)$$

$$C\,(\text{Char}) + H_2O \rightarrow CO + H_2 \quad (2)$$

$$C\,(\text{Char}) + CO_2 \rightarrow 2\,CO \quad (3)$$

$$Me_xO_y + CH_4 \rightarrow Me_xO_{y-1} + CO + 2\,H_2 \quad (4)$$

$$Me_xO_y + H_2 \rightarrow Me_xO_{y-1} + H_2O \quad (5)$$

$$Me_xO_y + CO \rightarrow Me_xO_{y-1} + CO_2 \quad (6)$$

$$2\,Me_xO_y + C\,(\text{Char}) \rightarrow 2\,Me_xO_{y-1} + CO_2 \quad (7)$$

$$CO + H_2O \leftrightarrow CO_2 + H_2 \quad (8)$$

Eq. (1) represents the coal devolatilization. Coefficients *a* to *e* depend on the distribution of gases generated during the devolatilization in steam-$CO_2$ mixtures, whose correlation used in this model will be described in section 2.2. Eqs. (2) and (3) show the char gasification with steam and $CO_2$, and Eqs. (4) to (6) represent the

oxidation of the products of coal devolatilization and gasification by the oxygen carrier, i.e. only $H_2$, CO and $CH_4$ are considered as reducing species. The reduction of ilmenite with solid carbon through a true solid-solid reaction is represented in Eq. (7). However, results obtained in fluidized-bed reactors showed that the reduction by gasification products, i.e. $H_2$ and CO, had a higher relevance than the direct solid-solid reaction [7,20,21]. Therefore, the solid-solid reaction was not included in the model.

Eq. (7) corresponds to the Water-Gas Shift reaction. The fulfillment of it could modify the CO, $H_2$, $H_2O$ and $CO_2$ final concentrations. However, previous CLC experiments performed with solid fuels show that the outlet concentrations are not in equilibrium and that the Water-Gas Shift has no important influence on the gas product composition [16].

Because of the different contact with the oxygen carrier and location of generation, the reaction of the volatile matter species and char gasification products are considered separately in this simplified model. Therefore, the mass balances for the $H_2$ and CO generated in the dense bed from char gasification are expressed by Eq. (9) and (10), respectively. For the volatile matter released reducing species, i.e., $CH_4$, $H_2$ and CO, the mass balances are Eqs. (13), (14) and (15). These equations show the variation of the molar flows of $H_2$, CO and $CH_4$ - $F_{H_2}$, $F_{CO}$ and $F_{CH_4}$, respectively-, for the gasification and devolatilization products in a bed differential mass inventory $dm_{OC}$.

Mass balances in dense bed:

$$\frac{\partial F_{H_2}}{\partial m_{OC}} + \left[ \frac{1}{2d \cdot M_O} (-r_{ilm,H_2})(1-\chi_{OC,v}) - \frac{f_C}{1-f_C} (r_{gasif})_{H_2O} \frac{1}{M_C} \right] = 0 \quad (9)$$

$$\frac{\partial F_{CO}}{\partial m_{OC}} + \left[ \frac{1}{2d \cdot M_O} (-r_{ilm,CO})(1-\chi_{OC,v}) - \frac{f_C}{1-f_C} (r_{gasif})_{H_2O} \frac{1}{M_C} - 2\frac{f_C}{1-f_C} (r_{gasif})_{CO_2} \frac{1}{M_C} \right] = 0 \quad (10)$$

$$\frac{\partial F_{H_2O}}{\partial m_{OC}} + \left[ -\frac{1}{2d \cdot M_O} (-r_{ilm,H_2})(1-\chi_{OC,v}) + \frac{f_C}{1-f_C} (r_{gasif})_{H_2O} \frac{1}{M_C} \right] = 0 \quad (11)$$

$$\frac{\partial F_{CO_2}}{\partial m_{OC}} + \left[ -\frac{1}{2d \cdot M_O} (-r_{ilm,CO})(1-\chi_{OC,v}) + \frac{f_C}{1-f_C} (r_{gasif})_{CO_2} \frac{1}{M_C} \right] = 0 \quad (12)$$

Mass balances in volatile plume:

$$\frac{\partial F_{CH_4}}{\partial m_{OC}} + \frac{1}{2d \cdot M_O} (-r_{ilm,CH_4}) \cdot \chi_{OC,v} = 0 \quad (13)$$

$$\frac{\partial F_{H_2}}{\partial m_{OC}} + \frac{1}{2d \cdot M_O}(-r_{ilm,H_2}) \cdot \chi_{OC,v} + 2\frac{\partial F_{CH_4}}{\partial m_{OC}} = 0 \quad (14)$$

$$\frac{\partial F_{CO}}{\partial m_{OC}} + \frac{1}{2d \cdot M_O}(-r_{ilm,CO}) \cdot \chi_{OC,v} + \frac{\partial F_{CH_4}}{\partial m_{OC}} = 0 \quad (15)$$

$$\frac{\partial F_{H_2O}}{\partial m_{OC}} - \frac{1}{2d \cdot M_O}(-r_{ilm,H_2}) \cdot \chi_{OC,v} = 0 \quad (16)$$

$$\frac{\partial F_{CO_2}}{\partial m_{OC}} - \frac{1}{2d \cdot M_O}(-r_{ilm,CO}) \cdot \chi_{OC,v} = 0 \quad (17)$$

It was assumed that the coal devolatilization takes place instantaneously at the coal feeding level. The contour conditions for the dense bed and plume phase are described by Eqs. (18) and (19), respectively, which are defined at $m_{OC} = 0$, that is, at the bottom of the fuel reactor:

$$F_j = F_{j,gas}^0 \quad (18)$$

$$F_k = F_{k,vol}^0 \quad (19)$$

where $F_j$ is the flow of the gas component $j$ in the dense bed and $F_{j,gas}^0$ is the flow of the gas $j$ introduced as gasification agent -usually $H_2O$ or $CO_2$. $F_k$ is the flow of the gas component $k$ in the plume, i.e., $CH_4$, $H_2$, CO, $H_2O$ and $CO_2$, and $F_{k,vol}^0$ is the flow of the gas component $k$ that is released when coal is devolatilized at the bottom of the fuel reactor.

Char is assumed to be uniformly distributed throughout the bed in perfect mixing. Thus, the carbon concentration in the bed, $f_C$, has a constant value throughout the reactor. The gasification rate, $r_{gasif}$, is based per mass of carbon in char. But the mass balances in the dense bed are formulated per mass of oxygen carrier; see Eqs (9-12). Thus, the term $f_C/(1-f_C)$ in these equations is necessary to express the gasification rate per mass of oxygen carrier in a differential element, being congruent with the formulation of the equations. The gasification takes place simultaneously with the reaction of the released volatile matter and gasification products with ilmenite. $(-r_{ilm,H_2})$, $(-r_{ilm,CO})$ and $(-r_{ilm,CH_4})$ are the reaction rates of ilmenite with $H_2$, CO and $CH_4$, respectively. The gasification products are generated in the dense bed and they have good contact with the

oxygen carrier particles and are considered to react separately from the volatiles. The volatiles are released in a plume and they get in poorer contact with the oxygen carrier. To take this into account, the oxygen carrier bed is considered to be separated in two zones and the parameter $\chi_{OC,v}$ is introduced as the fraction of the oxygen carrier bed that is in contact with the volatile matter.

The global balance to the whole reactor is done by integrating the differential equations over the total bed mass inventory. To solve the system of simultaneous differential equations, the Runge–Kutta–Merson method was used. To find the solution of the mathematical system, a value of ilmenite conversion variation $\Delta X$ and of carbon fraction in the bed $f_C$ are initially assumed and the system is solved in two interconnected loops. In the internal loop, with the assumed value of $f_C$ the system of differential equations is integrated and with these data the outlet gaseous flows are obtained, as well as the carbon flow that returns from the carbon separation system and that leaves the fuel-reactor. With the last carbon flow $f_C$ is recalculated, until the convergence is reached after successive approaches. Once the carbon balance has converged, the oxygen balance that would give the value of $\Delta X$ for the fixed ilmenite circulation rate must be accomplished. With this new value the calculations are repeated until the simultaneous convergence for both $f_C$ and $\Delta X$ is reached.

From experimental results obtained in continuously operated units [5,12] it was concluded that the implementation of a carbon separation system seemed to be essential to obtain high carbon capture in an iG-CLC process. The carbon separation system separates un-gasified char from oxygen carrier particles exiting from the fuel reactor, to be later reintroduced to the fuel reactor. Thereby the fraction of carbon by-passed to the air reactor, which will be burnt and not captured, is reduced. The use of a highly efficient carbon separation system ensures high extent of gasification, and thereby high carbon capture, by increasing char residence time in the fuel reactor. In Fig. 3 a scheme of carbon flows involved in the fuel reactor and carbon separation system is represented. The efficiency of the carbon separation system, $\eta_{CS}$, on the carbon capture efficiency has been evaluated in this work. $\eta_{CS}$ is defined as the fraction of carbon in char that is separated and recirculated back to the fuel reactor with respect to the carbon in the char that exits the fuel reactor together with the flow of oxygen carrier particles.

$$\eta_{CS} = 1 - \frac{F_{CO_2,AR}}{\left(F_{C,char}\right)_{out}} \quad (20)$$

$\left(F_{C,char}\right)_{out}$ is the molar flow of carbon in char exiting the fuel reactor:

$$\left(F_{C,char}\right)_{out} = \frac{\dot{m}_{OC} \cdot f_C / M_C}{(1 - f_C)} \quad (21)$$

$\dot{m}_{OC}$ is the solids recirculation rate, which is the oxygen carrier flow in the fuel reactor. Thus, the calculated carbon capture efficiency will depend on the solids circulation rate. In addition, the carbon not separated by the carbon separation system enters in the air reactor where it gets oxidized to $CO_2$. This carbon flow, $F_{CO_2,AR}$, is calculated from the mass balance expressed by Eq (22).

$$F_{CO_2,AR} = [C]_{fuel} \cdot \dot{m}_{fuel,in} / M_C - \left[\left(F_{CO_2} + F_{CO} + F_{CH_4}\right)_{out} - \left(F_{CO_2}\right)_{in}\right] \quad (22)$$

The simulation results are obtained after adjusting the carbon fraction in the fuel reactor bed so that the flow of gasification products accomplishes the following mass balances:

$$\left(F_{C,char}\right)_{in} = \left(F_{C,char}\right)_{out} + \left(F_C\right)_{gp} \quad (23)$$

$$\left(F_C\right)_{gp} + \left(F_C\right)_{vol} = \left(F_{CO_2} + F_{CO} + F_{CH_4}\right)_{out} - \left(F_{CO_2}\right)_{in} \quad (24)$$

$\left(F_{C,char}\right)_{in}$ is the carbon flow in char entering the fuel reactor, which is sum of the char in the coal feed and the char recirculated by the carbon separation system; $\left(F_{C,char}\right)_{out}$ is the carbon flow of ungasified char that exits the fuel reactor; $\left(F_C\right)_{gp}$ is the flow of carbon contained in the products of char gasification; and $\left(F_C\right)_{vol}$ is the flow of carbon in volatiles.

Taking into account for the calculation of the carbon flow exiting the fuel reactor, see Eq (21), if the solids circulation rate is increased, the fraction of carbon from char in the fuel reactor, $f_C$, must decrease to fulfill the carbon balance expressed in Eq. (23). This fact is also considered in the carbon balance in the fuel reactor, expressed in Eqs. (9-12), affecting to the carbon being gasified.

### 2.2. Solid fuel devolatilization

In this simplified model it was assumed that the devolatilization was instantaneous for the range of coal particle size used and it took place in the bottom part of the bed, since models predict devolatilization times in the order of less than one second under these conditions [22]. All volatile matter was considered to be converted into gaseous species. The composition of volatiles was experimentally obtained from devolatilization of El Cerrejón coal in a fluidized bed using silica sand as bed material and $H_2O$ or $CO_2$ as fluidizing gas [5]. In all cases the volatile matter was released in form of $H_2$, CO, $CH_4$, $H_2O$ and $CO_2$ as gaseous species. Also small amounts of light hydrocarbons and tars were found. Table 2 gathers the mass of the main gaseous species found in volatile matter generated from 100 g of El Cerrejón coal for the three different $H_2O$-$CO_2$ mixtures. The difference between the released devolatilized species for different fluidizing gas composition is because there is some $CH_4$ reforming taking place with $H_2O$ and $CO_2$. Note also that, in some cases of the compositions given the values of $H_2O$ or $CO_2$ have negative values, because some $H_2O$ and $CO_2$ was taken from the gasification agent flow for the partial $CH_4$ reforming.

### 2.3. Char gasification

In char gasification, whose main component is carbon, the most common gasification agents are steam and $CO_2$, through which $H_2$ and CO are generated as for the following reactions (2) and (3).

Kinetics of the gasification reactions for the El Cerrejón coal were obtained by TGA analysis. For kinetics determination, conversion vs. time curves at different temperatures (900-1050ºC), gasification agent concentrations (i.e. 20-80 vol.% $H_2O$ or $CO_2$) and gas product concentrations (i.e. 0-40 vol.% $H_2$ or CO) were obtained. A similar procedure was used to those found in [23]. As an example, Fig. 4 shows the char conversion versus time curves for the gasification reactions with $H_2O$ of El Cerrejón coal at different temperatures and different $H_2$ fractions as inhibitory agent obtained by TGA.

It was assumed that char gasifies according to the homogeneous reaction model with control by chemical reaction. The surface reaction follows a Langmuir-Hinshelwood reaction model [23] and the reaction rate is constant with the char conversion. The gasification rate $r_{gasif}$ is defined by Eq. 32.

$$r_{gasif} = \frac{1}{(1-X_{char})}\frac{dX_{char}}{dt} = \frac{k_1 p_{react}}{1+k_2 p_{react}+k_3 p_{prod}} \quad (25)$$

where $X_{char}$ is the char conversion, $p_{react}$ is the partial pressure of the gaseous reactants, i.e. $H_2O$ or $CO_2$, $p_{prod}$ is the partial pressure of the gasification products, i.e. $H_2$ or CO, and $k_1$, $k_2$ and $k_3$ are the kinetic constants.

Thus, the gasification kinetic parameters were obtained when using $H_2O$ and $CO_2$ as gasification agents and taking into account the inhibitory effect of $H_2$ and CO. The gasification kinetic constants obtained are gathered in Table 3 in case of using $H_2O$ or $CO_2$ as gasification agent.

### 2.4. Reaction of ilmenite with devolatilization and gasification products

The oxygen carrier considered in this work is ilmenite. Physical and chemical properties of this material can be found elsewhere [14]. The oxidized ilmenite is a mixture of $Fe_2TiO_5$ and $Fe_2O_3$ as the main reacting compounds. The reduced compounds were considered to be $FeTiO_3$ and $Fe_3O_4$, respectively. The corresponding oxygen transport capacity of ilmenite, $R_{O,ilm}$, was 4 wt.%, which was stated to be invariant in tests in a 500 $W_{th}$ facility [5].

Ilmenite undergoes an activation process and reaches a maximum and stable reaction rate. This activation was seen to occur fast in continuous operation with coal as fuel [5]. Thus, the kinetics for activated ilmenite with $H_2$, CO and $CH_4$ has been used for modeling purposes in this work, which were obtained in a previous work by Abad et al. [13].

A changing grain size model, with uniform reaction in the particle and chemical reaction control was assumed. The main equations that describe this model are the following:

$$t/\tau_i = 1-\left(1-X_{s,i}\right)^{1/3} \quad (26)$$

$$\tau_i = \frac{\rho_m r_{grain}}{\overline{b}\cdot k_{s0}\cdot e^{(-E_a/RT)}\cdot C_{g,i}^n} \quad (27)$$

$\tau_i$ being the time for complete solid conversion of the oxygen carrier for the reduction reaction considered. Table 4 summarizes the kinetic parameters used for the calculation of the reaction of ilmenite with $H_2$, CO and $CH_4$, coming from the devolatilization and char gasification. In this case, the reaction of $CH_4$ with the oxygen carrier is considered to take place by means of a partial oxidation with CO and $H_2$ as intermediate products, see Eq. (11), as it has been observed in other studies [24-26]. Thus, the stoichiometric parameter $\bar{b}$ takes the correspondent value for the stoichiometry of reaction (4) with ilmenite, where $Fe_2TiO_5$ and $Fe_2O_3$ are reduced to $FeTiO_3$ and $Fe_3O_4$, respectively.

The reaction rate of ilmenite for a given reaction *i*, $(-r_{ilm,i})$, is calculated as:

$$(-r_{ilm,i}) = \frac{\Phi}{3} R_{O,ilm} \frac{dX_{s,i}}{dt} \tag{28}$$

$X_{s,i}$ being the conversion of ilmenite by the reaction *i* and $\Phi$ the characteristic reactivity in the reactor. The parameter $\Phi$ takes into account the residence time distribution of particles in the reactor and the reacting time until complete conversion of particles. Assuming perfect mixing of solids in the reactor and reaction of particles following a shrinking core model with spherical geometry, the characteristic reactivity can be calculated as [27]:

$$\Phi = 3\left[1-\bar{X}_{s,in}^{2/3}\exp\left(-\frac{\left(1-\bar{X}_{s,in}^{1/3}\right)}{\Delta X_s}\Phi_j\right)\right]-\frac{6\Delta X_s}{\Phi}\left[1-\bar{X}_{s,in}^{1/3}\exp\left(-\frac{\left(1-\bar{X}_{s,in}^{1/3}\right)}{\Delta X_s}\Phi\right)\right] + \frac{6\Delta X_s^2}{\Phi^2}\left[1-\exp\left(-\frac{\left(1-\bar{X}_{s,in}^{1/3}\right)}{\Delta X_s}\Phi\right)\right] \tag{29}$$

$\Delta X_s$ being the variation of solids conversion in the reactor and $X_{s,in}$ the conversion of solids at the reactor inlet. As starting point, the calculations for the model consider that ilmenite is fully oxidized in the air reactor, i.e. the conversion for the reduction reaction is 0.

The variation of the solids conversion in the reactor, $\Delta X_s$, is the oxygen transferred by the oxygen carrier in the fuel reactor to oxidize the fuel divided by the oxygen that can be supplied by the circulating oxygen carrier. So $\Delta X_s$, is calculated as:

$$\Delta X_s = M_O \frac{\left[2F_{CO_2} + F_{CO} + F_{H_2O}\right]_{out} - \left[2F_{CO_2} + F_{H_2O}\right]_{in}}{R_{O,ilm} G_s} \quad (30)$$

$G_s$ being the solids circulation flow rate.

## 3. Performance evaluation

One of the main parameters to evaluate the performance of a CLC system is the carbon capture efficiency, $\eta_{CC}$. This efficiency takes into consideration the physical removal of carbon dioxide that would otherwise be emitted into the atmosphere and it is defined as the fraction of the carbon introduced that is converted to gas in the fuel reactor.

$$\eta_{CC} = M_C \frac{\left(F_{CO_2} + F_{CO} + F_{CH_4}\right)_{out} - \left(F_{CO_2}\right)_{in}}{[C]_{fuel} \cdot \dot{m}_{fuel,in}} \quad (31)$$

$\dot{m}_{fuel,in}$ being the coal feeding flow and $[C]_{fuel}$ the carbon fraction in the fuel. Note that in this technology the char that has not been gasified is by-passed to the air reactor, where is burnt to $CO_2$ which is not captured.

All the volatiles get out through the fuel reactor, so $\eta_{CC}$ depends on the gasification efficiency or char conversion, $X_{char}$, which is the fraction of the carbon in char introduced the fuel reactor, $(F_{C,char})_{in}$, that has been gasified. It is calculated as:

$$X_{char} = \frac{(F_{C,char})_{in} - F_{CO_2,AR}}{(F_{C,char})_{in}} \quad (32)$$

As CLC is a combustion technology, it is fundamental to get high combustion efficiency in the fuel reactor, $\eta_{comb\ FR}$. The combustion efficiency in the fuel reactor is defined as the fraction of the oxygen demanded by the volatile matter and gasification products that is supplied by the oxygen carrier in the fuel-reactor.

$$\eta_{comb\,FR} = \frac{(F_{H_2O} + 2F_{CO_2} + F_{CO})_{out} - (F_{H_2O} + 2F_{CO_2} + F_{CO})_{in}}{\Omega_{coal} - 2F_{CO_2,AR}} \quad (33)$$

Thus, the combustion efficiency in the fuel reactor only considers the combustion of compounds that can be oxidized in the reactor, i.e. gases from volatiles or char gasification. The oxygen supplied by the oxygen carrier, numerator in Eq. (33), is calculated from an oxygen balance to gaseous compounds entering to and exiting from the reactor. The oxygen demanded by gaseous compounds evolved in the fuel reactor, denominator in Eq. (33), is calculated as the oxygen demanded by coal to be fully oxidized, $\Omega_{coal}$, minus the oxygen demanded by carbon not emitted in the fuel reactor, i.e. $F_{CO_2,AR}$. The oxygen demanded by coal is defined as:

$$\Omega_{coal} = M_O(2[C]_{fuel}/M_C + 0.5[H]_{fuel}/M_H - [O]_{fuel}/M_O)\cdot\dot{m}_{fuel,in} \quad (34)$$

$[C]_{fuel}$, $[H]_{fuel}$ and $[O]_{fuel}$ being the carbon, hydrogen and oxygen fractions in the fuel, whose values are obtained from the proximate analysis.

To evaluate the extent that coal is burned to $CO_2$ and $H_2O$ in the CLC system, not only in the fuel reactor but also in the air reactor, the oxygen demand is defined. In this case, the oxygen demand is referred here as the oxygen required to fully oxidize the unconverted gases exiting the fuel reactor to $CO_2$ and $H_2O$ with respect the total oxygen demand of the fuel.

$$\Omega_T = \frac{(F_{H_2} + F_{CO} + 4F_{CH_4})_{out}}{\Omega_{coal}} \quad (35)$$

The performance of the iG-CLC process was evaluated by analyzing these parameters as a function of the residence time of particles in the fuel reactor, which depends on the solids inventory and the solids circulation flow rate. Evaluation of the solids circulation flow rate was done by the use of the oxygen carrier to fuel ratio, $\phi$, defined as the availability of oxygen in the flow of oxygen carrier divided by the oxygen required to fully convert the fuel to $CO_2$ and $H_2O$:

$$\phi = \frac{R_{O,ilm}\dot{m}_{OC}}{\Omega_{coal}} \quad (36)$$

So, $\phi$ = 1 corresponds to the stoichiometric flow of oxygen carrier needed for a full conversion of the fuel to $CO_2$ and $H_2O$.

## 4. Results and discussion

A model has been developed to predict both the carbon capture and combustion efficiencies of the iG-CLC process as a function of various operational parameters with ilmenite as oxygen carrier and a bituminous coal "El Cerrejón" as fuel. The gasification kinetics of this type of coal including the inhibitory effect of the gasification products, and the reaction kinetics of ilmenite obtained by Abad et al. [13] were included in the model. In addition, the effect of the presence of a carbon separation system is analyzed. The model calculates the gas flow for $CO_2$, CO, $H_2$, $H_2O$ and $CH_4$ exiting from the fuel reactor, as well as the fraction of unconverted char passing to the air reactor. Thus, the carbon capture and combustion efficiency can be evaluated. Firstly, the predictions of the model were checked with experimental results in a 500 $W_{th}$ CLC plant. After that, simulations were performed using the model in order to evaluate the effect of operational parameters on the performance of iG-CLC systems. The operational parameters analyzed were the fuel reactor temperature, the solids inventory, the efficiency of the carbon separation system, the type and flow of gasification agent, the oxygen carrier to fuel ratio, the reduction degree of the oxygen carrier at the inlet of the fuel reactor, the oxygen carrier reaction rate and the fraction of oxygen carrier bed that is in contact with the volatile matter. All simulations performed were made for a corresponding thermal power of 1 $MW_{th}$, which is a feeding rate of El Cerrejón fresh coal of 0.0386 kg/s.

### 4.1. Comparison with experimental results

The model results simulated were compared to the experimental results obtained in continuous operation in the 500$W_{th}$ CLC unit placed at the Instituto de Carboquímica operated with pre-treated El Cerrejón bituminous coal and using ilmenite as oxygen carrier. The facility has no carbon separation system. Thus, calculations were done by setting the parameter $\eta_{CS}$ = 0. The experiments were done at $T_{FR}$ of 900ºC, the corresponding oxygen carrier to fuel ratio $\phi$ was around 2, steam was used as gasification agent with steam to fixed carbon ratio $H_2O/C$ = 0.7 and the inventory was

3100 kg/$MW_{th}$. In addition, ilmenite enters in the fuel reactor fully oxidized, i.e. $X_{s,i} = 0$ [5].

Preliminary results were obtained considering that the whole oxygen carrier bed got in contact with the volatile matter and the gasification products in the dense bed. The first simulations predicted full combustion of the products of devolatilization and gasification. However, the experimental results showed some incomplete combustion, which was found to be due to $H_2$, CO and $CH_4$ coming from the volatile matter. As mentioned, the volatile matter was not fully burnt due to poor contact with the oxygen carrier particles, whereas char gasification products were found to be fully burnt at temperatures above 890ºC, as for the results obtained from experiments fuelled with char from the same coal [5]. Therefore, it was considered that only part of the oxygen carrier bed was in contact with the volatile matter. Thus, a fraction of oxygen carrier in the fuel reactor that is in contact with the volatile matter, $\chi_{OC,v}$, was introduced to predict the experimental fuel reactor combustion efficiencies obtained. Simulations varying $\chi_{OC,v}$ were performed. It was obtained that the $\chi_{OC,v}$ that predicts the combustion efficiencies obtained experimentally at different temperatures is 0.53%. $\chi_{OC,v} = 0.53\%$ is a rather low value, that is, the volatile matter released in the plume in the experimental facility had indeed bad contact with the oxygen carrier. Fig. 5 shows a comparison between predicted and experimental fuel reactor combustion efficiencies, considering $\chi_{OC,v} = 0.53\%$. It can be seen that there is a good agreement between the predicted and measured values.

As an example, experimentally at 900ºC the following efficiencies were obtained: $\eta_{CC} = 51.0\%$, $X_{char} = 32.0\%$ and $\eta_{comb\ FR} = 90.0\%$ in the 500$W_{th}$ plant. Two simulations with the same operating conditions were done to compare with experimental results. The first one considered that the whole oxygen carrier bed is in contact with both volatile matter and gasification products. With this simulation a combustion efficiency of 100% was obtained. The second simulation considered that only a fraction of the oxygen carrier of $\chi_{OC,v} = 0.53\%$ is in contact with the volatile matter. It turned out that the predictions obtained with the model generally agreed with the experimental results, since the resulting $\eta_{comb\ FR}$ obtained was 89.9%. In both simulations the char conversion and carbon capture efficiency simulated were close to the values obtained experimentally. Note that the introduction of $\chi_{OC,v}$ affects the combustion efficiency, being its effect on $\eta_{CC}$ and $X_{char}$ of very low relevance. In the simulation made

considering $\chi_{OC,v}$=0.53%, the mass fraction of char in the fuel reactor, $f_C$, had a value of 0.34% and the calculated ilmenite conversion variation $\Delta X_s$ was 24.7%.

Fig. 6 represents the evolution of $CH_4$, $H_2$, CO, $CO_2$ and $H_2O$ molar flows within the fuel reactor bed, expressed as mass fraction of the bed, $m_{OC}/m_{OC,tot}$, for a total solids inventory of 3100 kg/$MW_{th}$. Fig. 6a) shows the flows in the dense bed, that is, derived from the gasification; Fig. 6b) represents the evolution of the volatile matter species released in the plume; and the total sum of the flows of both phases is shown in Fig. 6c). In the dense bed all the gasification products, i.e., $H_2$ and CO, are fully oxidized by the oxygen carrier and the dense bed is only composed by increasing $CO_2$ from char oxidation and the $H_2O$ as gasification agent. In the plume both $CH_4$ and $H_2$ decrease with the reactor mass. $CH_4$ comes only as part of the released volatile matter species and it is gradually consumed by its oxidation with the oxygen carrier. $H_2$ and CO come from volatile matter release and as intermediates of $CH_4$ oxidation. $H_2$ disappears continuously along the bed mass as it is quickly oxidized by ilmenite, while the CO profile has a maximum because there is competition between the CO generation and its reaction with the oxygen carrier.

After seeing that the model predicts the experimental results with a determined $\chi_{OC,v}$, simulation and process optimization proceed and thereby solutions for the modeling and scale-up to a pilot plant or an industrial power plant can be performed. The effect of the main variables in CLC with solid fuels is analyzed. In each evaluated case, the solids inventory was taken as independent variable.

### 4.2. Influence of the fuel reactor temperature

Temperature was evaluated as one of the main operating variables in a CLC system [5,19,28]. These and all the following simulations were done using fresh El Cerrejón coal as fuel. Fig. 7 shows the obtained $\eta_{CC}$, $X_{char}$ and $\eta_{comb\ FR}$ with increasing solids inventory in the fuel reactor for fuel reactor temperatures of 900, 950 and 1000ºC and considering a system without carbon separation system. Gasification and combustion reactions are promoted with the temperature, and thus $X_{char}$, $\eta_{CC}$ and $\eta_{comb\ FR}$, increased at higher temperatures. This was also seen experimentally by Cuadrat et al. with El Cerrejón coal [5] and Berguerand et al. [28] with pet coke.

It is clear that the fuel reactor needs to have enough oxygen carrier inventory to oxidize the fuel and to enhance the extent of gasification, since the residence time increases.

Besides, the presence of an oxygen carrier increases the gasification rate because the CO and $H_2$ concentrations decrease and thus their inhibitory effect, as it has been experimentally tested [7,15]. For all the temperatures simulated and up to a solids inventory of 2000 kg/$MW_{th}$ all efficiencies increase substantially. For higher inventories the beneficial effect is not so intense. With an inventory of 2000 kg/$MW_{th}$, $\eta_{comb\ FR}$ is 89% and it increases up to 98.7% with 5000 kg/$MW_{th}$, so it is not worth it to increase so much the solids inventory, as well as the size and investment of such big facility. At 950ºC as reference temperature, and with an inventory of 2000 kg/$MW_{th}$, values obtained for char conversion and carbon capture efficiency were $X_{char}$ = 33.4% and $\eta_{CC}$ = 52.5%. However, not even with an inventory of 10000 kg/$MW_{th}$ full carbon capture could be obtained.

In order to get higher extent of gasification, it was proposed to separate the char that has not been gasified and recirculate it back to the fuel reactor, in order to increase the residence time of char particles and thereby raise the carbon capture efficiency. This can be made by means of a carbon stripper, whose beneficial effect has been experimentally confirmed [8]. The critical role of the carbon stripper has been pointed out in various previous studies [18,29]. Thus, the subsequent studies of the influence of several parameters are done considering that the iG-CLC system accounts with a carbon separation system.

Fig. 8 shows the concentrations of $H_2$, CO and $CH_4$ at the fuel reactor outlet when changing the fuel reactor temperature for increasing solids inventory in an iG-CLC system with a carbon stripper of 90% efficiency. 90% can be considered as a very high and extreme value of efficiency for a carbon separation system, but in this study it is taken to assess how much the CLC performance can be improved with such a good separation system and better see the influence of other parameters if carbon was highly separated and recirculated. The simulated outgoing unburnt $H_2$, CO and $CH_4$ decrease as the temperature rises because both gasification and oxidation reactions are faster. For inventories lower than 1000 kg/$MW_{th}$, the CO concentration at higher temperatures is higher. This is attributed to a more important improvement in the gasification rate and reaction of $CH_4$ –as CO is an intermediate product of $CH_4$ oxidation–, compared to the increase in the oxidation rate of CO.

Fig. 9 represents the carbon capture and char conversion in the process, where it can be seen that to get high performance of the process, an inventory between 1000 and 2000

kg/$MW_{th}$ seem to be necessary and reasonable at all temperatures tested. To get high gasification and oxidation rates, it is necessary to work at high temperatures. As an example, with an inventory of 2000 kg/$MW_{th}$ and $\eta_{CS}$ = 90%, predictions of $\eta_{CC}$ of 79.3% at 900ºC and 90.7% at 1000ºC were obtained. Note the important increase in the carbon capture and the char conversion when using the carbon separation system. All the values of $\eta_{CC}$ obtained with $\eta_{CS}$ = 0%, i.e. for a system with no carbon separation system, were lower. Therefore, the presence of a carbon stripper is confirmed to be fundamental in order to increase the coal fed into the fuel reactor.

The simulated performance of the process regarding the oxidation of volatiles and gasification products is shown in Fig. 10. In Fig. 10a) it can be seen that the fuel reactor combustion efficiency grows with the temperature because of the increase in the oxidation reaction of ilmenite with the products of gasification and devolatilization. Above 900ºC, the minimum solids inventory needed to obtain $\eta_{comb\ FR}$ above 85% is 1000 kg/$MW_{th}$. As an example, with a solids inventory of 2000 kg/$MW_{th}$, the simulated resulting $\eta_{comb\ FR}$ was 86.0% at 900ºC, 90.7% at 950ºC and 94.2% at 1000ºC. As there is some $H_2$, CO and $CH_4$ at the fuel reactor outlet, there must be a subsequent oxidation step to fully burn the fuel reactor stream. Fig. 10b) plots the simulated total oxygen demand, defined as the fraction of the oxygen demanded by the coal fed that is necessary to burn the fuel reactor outlet gases to $CO_2$ and $H_2O$. This is the oxygen that should be supplied in a later polishing step to ensure final full combustion of the fuel. The oxygen demand in the polishing step decreases with an increase of the fuel reactor temperature. It is rather high at low inventories and decreases a lot at higher inventories up to 2000 kg/$MW_{th}$. For instance with an inventory of 2000 kg/$MW_{th}$ the total oxygen demand is 5.3% at 1000ºC. For an optimum performance of the iG-CLC system, it would be best to operate at temperatures above 950ºC.

### 4.3. Influence of carbon stripper efficiency, $\eta_{CS}$

Fig. 11 shows the concentrations of $H_2$, CO and $CH_4$ at the fuel reactor outlet predicted with increasing solids inventory for $\eta_{CS}$ = 0%, 80%, 90% and 100% at a fuel reactor temperature of 950ºC. As expected, for all $\eta_{CS}$ tested, for higher solids inventories, the amount of released gaseous fuels that are not fully burnt is lower, i.e., $H_2$, CO and $CH_4$ mainly because the corresponding increase in the residence time of char particles in the reactor. In a lower relevance, there is more oxygen carrier available to react and its

average reactivity is slightly higher. In all cases this improvement in the oxidation and the corresponding decrease in the $H_2$, CO and $CH_4$ concentrations is sharper from inventories up to 2000 kg/$MW_{th}$.

$H_2$ and $CH_4$ concentrations at the fuel reactor outlet decrease somewhat when $\eta_{CS}$ increases. That is because more gasification products are being generated and as they are better oxidized, more $CO_2$ and $H_2O$ are generated and the concentration of the unburnt gaseous species decrease. The combustion of the gasification products is better because they are generated in the dense bed of the fluidized-bed and they get in more intimate contact with the oxygen carrier particles, whereas the bubbles of volatile matter formed have worse contact with the oxygen carrier. The concentration of CO at the fuel reactor outlet has maximum values for inventories of around 500 kg/$MW_{th}$ with $\eta_{CS}$ = 0% to 90%. Char recirculation causes an increase of char concentration in the bed. Thus, the increase in the CO generation rate from gasification leads to those maximum values. Compared with other values of $\eta_{CS}$, in case of having a carbon separation system with 100% efficiency, the CO concentration is higher for low inventories, as there is a lot of CO being generated from char gasification, which ilmenite is less effective to convert to $CO_2$ when the solids inventory is lower than 400 kg/$MW_{th}$.

Fig. 12 shows the simulated char conversion, carbon capture and combustion efficiencies with a wide range of oxygen carrier inventory if the system has a carbon stripper of efficiency 0%, 80%, 90% and 100%. Higher $\eta_{CS}$ leads to higher $\eta_{CC}$, which is essential in this process. For example, with 1000 kg/$MW_{th}$ at 950ºC the resulting simulated $\eta_{CC}$ increase from 45.2% with $\eta_{CS}$ = 0% to 79.8% with $\eta_{CS}$ = 90%. That is, this process needs a char recirculation system to achieve satisfactory values of $\eta_{CC}$. Obviously, $\eta_{CS}$ = 100% means that both char conversion and carbon capture efficiencies are 100%, since there is no char transferred to the air reactor. The char concentration in the bed is increased with the carbon stripper efficiency: with 1000 kg/$MW_{th}$ at 950ºC $f_C$ was 0.36% with $\eta_{CS}$ = 0% and raised to 1.32% with $\eta_{CS}$ = 90%. This fact was advanced in a theoretical analysis of the results obtained in a batch fluidized bed reactor [7].

As it could be foreseen from the outlet concentrations, the process performance for all $\eta_{CS}$ simulated has the higher differences and improvements up to oxygen carrier inventories of 1000-2000 kg/$MW_{th}$. Furthermore, from an inventory of 2000 kg/$MW_{th}$ an increase in $\eta_{CS}$ scarcely influences the combustion efficiency. For adequate values of inventory and with the presence of a carbon separation system, there are still some

unburnt gases at the fuel reactor outlet. Cuadrat et al. [5] saw experimentally that the unburnt species come from released volatile matter because they leave the bed reactor with insufficient contact with the oxygen carrier. That is, although the operation was done at high temperature, with high oxygen carrier inventory and high $\eta_{CS}$, there would be still some unburnt volatile matter and a subsequent oxygen polishing step would be necessary to fully oxidize the unburnt gases in the outlet stream from the fuel reactor.

### 4.4. Influence of the steam to fixed carbon ratio, $H_2O/C$

The motivation of evaluating the influence of steam to fixed carbon ratio, here represented as $H_2O/C$, is to assess if the requirements of steam as fluidizing and gasification agent are enough for the process. A ratio equal to 1 means that the amount of steam introduced is the stoichiometric flow to gasify all the carbon in char from coal fed. Fig. 13 shows predicted char conversion, carbon capture and combustion efficiency variation obtained with increasing oxygen carrier inventories with this simplified model for different $H_2O/C$ ratios from 0.4 to 4. The calculations are made for a wide range of inventories. Possible changes in the fluid dynamics of the system derived from varying the fluidization velocity are not taken into account in the results presented here.

It can be seen that this ratio has negligible influence on the combustion efficiency. On the other hand, higher $H_2O/C$ ratio leads to enhanced char conversion and thus carbon capture efficiency. However the effect is of low relevance for $H_2O/C > 0.7$ and no further improvement for ratios above 2 was found. The reason for this is that $H_2O$ is only an intermediate compound in coal conversion, i.e. $H_2O$ is consumed by char gasification but is regenerated by oxidation of $H_2$ produced during gasification. Both reactions happen inside the fuel reactor.

Although a $H_2O/C$ ratio of 0.4 could be insufficient to ensure high gasification extent, with a $H_2O/C$ ratio of 0.7 similar $X_{char}$ values to the maximum are obtained. Thus, the ratio $H_2O/C$ has very little influence on the process performance and it seems reasonable to work with a $H_2O/C$ ratio of 0.7, as high values of $\eta_{CC}$ would be obtained and some additional energy for steam evaporation would be saved. The same gasification promotion trends and the independence of the oxidation reaction when increasing the $H_2O/C$ ratio was experimentally seen in tests in a continuous 500 $W_{th}$ CLC facility that used this type of fuel and ilmenite as oxygen carrier [12].

### 4.5. Influence of the gasification agent type: $H_2O$:$CO_2$ mixtures

The motivation of using $CO_2$ is that $CO_2$ is a gasification agent and that the recirculation of part of the fuel reactor outlet stream will lead to savings of energy that are needed for steam generation and therefore increase the efficiency of the whole process. Fig. 14 shows that the carbon capture and char gasification extent increase when there is higher steam fraction in the gasification agent, being this less noticeable for higher $\eta_{CS}$. This is because for this fuel the gasification rate by steam is faster than gasification by $CO_2$, as it was assessed during kinetics determination. However, the influence of the type of gasification agent in the combustion efficiency is not very relevant. Although steam gasification generates $H_2$ which is faster oxidized by ilmenite than CO, the reaction rate of ilmenite with the gases generated is faster than their generation rate. Thus, the slight increase in $\eta_{comb\ FR}$ with higher $H_2O$ fraction that can be seen in Fig. 14c) can be only partially explained by the enhanced gasification. The generation of a higher flow of gasification products -which are better burnt because they have better contact with the oxygen carrier- leads to higher combustion efficiency of the gases in the fuel reactor. To maintain high gasification rates a carbon separation system should be implemented and some $CO_2$ could be recirculated, finding a balance between the increase in the energy efficiency of the whole system and the decrease in the carbon capture. For higher efficiencies of the carbon separation system, the influence of the type of gasification agent and the corresponding gasification rate are lower. Nevertheless, the char concentration in the fuel reactor bed increases as the char gasification rate decreases, as it is the case of using more $CO_2$ in the gas mixture. This fact will affect the design of the carbon separation system, because the load of char will be higher if $CO_2$ is used as gasification agent.

### 4.6. Influence of the oxygen carrier to fuel ratio, $\phi$

One important variable in the CLC process is the oxygen carrier to fuel ratio, $\phi$. This ratio indicates the oxygen that can be supplied by the circulating ilmenite compared to the oxygen needed to burn the fuel fed. In stoichiometric conditions the $\phi$ ratio is equal to one. Fig. 15 shows the carbon capture and combustion efficiencies for increasing fuel reactor inventories and for oxygen carrier to fuel ratios from 1.1 to 3.3.

The carbon capture efficiency clearly decreases for higher $\phi$. High oxygen carrier to fuel ratio means high solids recirculation rate and thereby low residence time. The lower

residence time leads to lower extent of gasification and thereby lower $\eta_{CC}$. Moreover, and increase in the solids circulation rate entails a decrease in the char concentration in the bed. For higher solids recirculation rates and higher $\phi$, $f_C$ decreases correspondingly: with 1000 kg/$MW_{th}$ at 950ºC $f_C$ was 1.70% with $\phi$ = 1.1 and decreased to 1.05% with $\phi$ = 3.3.

Fig. 16 plots the resulting combustion efficiency with increasing $\phi$ for set inventories from 200 to 5000 kg/$MW_{th}$. Complementary to Fig. 15b), it shows that for high inventories the combustion efficiency increases for higher $\phi$ because higher amount of oxygen carrier is recirculated between reactors. When more ilmenite is recirculated, it is less converted. Thus, the oxygen carrier average reactivity is higher and it is more capable to convert faster the released gaseous fuels. On the other hand, for inventories below 500 kg/$MW_{th}$ $\eta_{comb\ FR}$ has a slight decrease with increasing $\phi$ because there is competition between the lower average reactivity and oxygen availability with the higher generation of gasification products which are better oxidized. The trend of increasing $\eta_{comb\ FR}$ for higher $\phi$ was experimentally seen for gaseous fuels [30,31]. The increase of char conversion and carbon capture efficiency and decrease of $\eta_{comb\ FR}$ with rising $\phi$ were observed with this type of fuel and oxygen carrier by Cuadrat et al. during CLC fuelled with coal in a continuous unit [12].

The negative influence of the gasification step as $\phi$ increases has higher relevance as $\eta_{CS}$ decreases. However, $\eta_{comb\ FR}$ in CLC with solid fuels, as well as with gaseous fuels, would increase with the oxygen carrier to fuel ratio if high $\eta_{CC}$ were reached, that is, when the gasification step did not influence the system performance.

### 4.7. Influence of the reduction degree of the oxygen carrier, $X_{s,in}$

The reduction degree of the oxygen carrier at the air reactor outlet, $X_{s,in}$, establishes that the minimum stoichiometric oxygen carrier to fuel ratio is $1/X_{s,in}$. It also determines the oxygen carrier average reactivity. For the fuel reactor, when the oxygen carrier is more oxidized, the average reactivity and the combustion efficiency are higher. However, when the need of reoxidation is higher, the inventory needed in the air reactor is greater. The optimum value that minimizes the total inventory in both reactors is therefore an intermediate conversion that depends on the reduction and oxidation kinetics [27]. As a reference default value, the previous simulations have been performed with an oxygen carrier reduction degree in the air reactor $X_{s,in}$ of 0. Fig. 17 represents the combustion

efficiency variation for increasing $X_{s,in}$ when $\phi = 2$. From 0 and up to $X_{s,in}$=0.4, $\eta_{comb\ FR}$ is scarcely influenced. From 0.4 the average reactivity decreases too much. The theoretical minimum value for $X_{s,in}$ is 0.5 when $\phi = 2$ in order to transport the required oxygen from the air reactor to full oxidize the fuel fed. However, since the resulting $\eta_{CC}$ is lower than 100%, for this simulation $X_{s,in}$ could be decreased to 0.7 to have enough oxygen in the recirculated ilmenite to burn the carbon that is converted in the fuel reactor. However, in that case the resulting $\eta_{comb\ FR}$ was only 60%. Thus, as first approach and without a more complete study that included the air reactor, it can be assumed that the optimum $X_{s,in}$ is within the range 0-0.4.

### 4.8. Influence of increasing the oxygen carrier reaction rate

An appropriate oxygen carrier in a CLC process should have enough reactivity with the fuel. In CLC with gaseous fuels higher oxygen carrier reactivity leads directly to an improvement of the process efficiency for the same inventory and it will be able to work with lower inventories. In case of CLC with solid fuels, another factor must be taken into account, which is the gasification, as it is the limiting step of this process. Fig. 18 shows the resulting carbon capture, char conversion and combustion efficiencies predicted when increasing the oxygen carrier reaction rates. In these simulations, reaction rate of ilmenite with all the gases -that is, $H_2$, CO and $CH_4$- is considered to be multiplied by a factor represented by $(-r)/(-r_{ilm})$, being $(-r_{ilm})$ the ilmenite reaction rate. The results show that although the final combustion efficiency increases with an enhancement in the oxygen carrier reaction rate, the influence on both char conversion and carbon capture efficiency is negligible. This has been calculated for a system without carbon separation system and considering that the process accounts with a carbon stripper with 90% efficiency. Thus, the use of an oxygen carrier with high reactivity is important in order to reach high combustion efficiencies in the fuel reactor, but is not the key factor in iG-CLC to get high $\eta_{CC}$.

### 4.9. Improvement of the volatile matter oxidation

The volatile matter is released in a plume and the fraction of the oxygen carrier which is in contact with the volatile matter resulted to be quite small. Thus, there are a poor contact between volatiles and oxygen carrier particles which led to low value of the combustion efficiency. However, note that the bed is a bubbling fluidized bed and the

height in the simulated facility is only 20 cm. The contact efficiency of volatiles with solid particles can be improved in larger circulating fluidized beds. Besides, the contact of volatile matter with the oxygen carrier in a fluidized bed combustor could be improved by enhancing their dispersion along the bed surface, as by means of an increase of the coal feeding points [32]. Any change in the contact efficiency of volatiles can be simulated by the model by varying the parameter $\chi_{OC,v.}$ Fig. 19 shows the effect of $\chi_{OC,v}$ on the combustion efficiency for different oxygen carrier inventories in the fuel reactor. The char conversion and carbon capture for this case are not affected, as the combustion efficiency lower than 1 was due to unburnt volatile matter and the gasification products were completely oxidized in all cases. So it was not possible to improve the char conversion due to decrease in the gasification inhibition. The $\chi_{OC,v}$ obtained from experimental results in the continuous unit was 0.53%. As can be observed there is a big effect of $\chi_{OC,v}$ on the combustion efficiency and $\eta_{comb\ FR}$ can be increased from 80.8% to 99% if $\chi_{OC,v}$ increased from 0.53% to 3% with an inventory of 1000 kg/$MW_{th}$.

A second option to fully burn the volatile matter is to implement a second step in the fuel reactor (FR2), whose fuel would be the outlet gaseous stream of the solid fuelled fuel reactor (FR1). The idea of installing a second stage for the complete combustion of volatiles was first brought up by Lewis and Gilliland [33]. It is also an alternative to the oxygen polishing step. As the fuel is gaseous, this second reactor would not be limited by the gasification step and the contact with the oxygen carrier would be much better, since the fuel would be introduced at the bottom of the reactor and not released in a plume. Fig. 20 shows the minimum ilmenite inventory that would be required in the second fuel reactor step to fully burn the outlet stream coming from the first fuel reactor for different inventories in the first fuel reactor, for the case of using a carbon separation system with 90% efficiency and working at 950ºC. In FR2 it is considered that the whole oxygen carrier bed is in contact with both volatiles and gasification products.

Values obtained for the second step fuel reactor are small: the maximum is 45 kg/$MW_{th}$. Note that although for increasing inventory in FR1, the quantities of unconverted gases are lower, but they are more diluted because the total flows are higher as more $H_2O$ and $CO_2$ are generated. This trade-off between the dilution and the amount of gaseous fuels introduced in the second reactor explains the first increase in the resulting inventory needed for the second fuel reactor.

This seems a very promising option, as with an inventory of 1000 kg/$MW_{th}$ in the first fuel reactor, only additional 44 kg/$MW_{th}$ in the second step of the fuel reactor FR2 would be needed to fully oxidize the fuel. For 2000 kg/$MW_{th}$ in FR1, the second fuel reactor would need 40 kg/$MW_{th}$. It is necessary to have an efficient carbon separation system, as well as to have enough inventory in the first step of the fuel reactor to achieve high carbon capture and combustion efficiency. However, the inventory of the first step of the fuel reactor could be decreased as the outlet gases can be completely burnt in the second fuel reactor, which is much smaller.

## 5. Conclusions

In this work a simplified model for in situ gasification Chemical-Looping Combustion (iG-CLC) with solid fuels has been developed, based on the differential mass balances with reaction of the fuel reactor for the gasification products evolved in the dense bed and volatile matter in form of a plume. The model includes the kinetics of coal char gasification and reaction of gasification and devolatilization products with the oxygen carrier. The model results were compared with experimental results from tests performed in a 500$W_{th}$ facility fuelled with "El Cerrejón" bituminous coal and ilmenite as oxygen carrier. The limitation to obtain full combustion in the fuel reactor was assigned to poor contact of the volatile matter with the oxygen carrier. A division of the oxygen carrier bed in the fuel reactor was done and it was calculated that the fraction of oxygen carrier in contact with the volatiles was 0.53% for the simulated facility. After that, the operating conditions for iG-CLC were optimized by analyzing the effect of relevant operating conditions on the performance of the system.

It was seen that it is essential that the fuel reactor has enough inventory to oxidize the fuel and to enhance the extent of carbon capture, since the residence time increases. The carbon capture was directly related to the extent of gasification, which is promoted by increasing the temperature or the residence time of char particles in the fuel reactor. It is highly beneficial to increase the solids inventory up to 1000 kg/$MW_{th}$, but further increase does not give a relevant improvement in the carbon capture. With inventory in the fuel reactor of 1000 kg/$MW_{th}$, at 1000ºC and an efficiency of the carbon separation system of 90%, the carbon capture obtained is 86.0%. To further enhance the carbon capture, to increase the efficiency of the carbon separation system is preferred rather than increasing the solids inventory.

As there is some $H_2$, CO and $CH_4$ at the fuel reactor outlet, there must be a subsequent oxidation step to fully burn the fuel reactor stream. The corresponding calculated oxygen demand of this subsequent oxygen polishing step was 5.3% at 1000ºC.

High oxygen carrier to fuel ratio means high solids recirculation rate and thereby lower residence time, which leads a decrease in carbon capture efficiency. The negative influence of the gasification step as the oxygen carrier to fuel ratio increases had lower relevance as the efficiency of the carbon separation system increased.

To have a high reactive oxygen carrier is important to reach high combustion efficiencies, but is not the key factor to get high performance of the process. Lower influence on the iG-CLC performance was observed for the gasification agent to fixed carbon ratio; the type of gasification agent in case of different $H_2O$:$CO_2$ mixtures, being the influence of the gasification agent type of less importance for higher efficiencies of the carbon separation system; and the reduction degree of the oxygen carrier in the air reactor outlet.

Improvement in the contact of the volatile matter with the oxygen carrier is necessary to get high combustion efficiency. Some design solutions can be applied to increase the contact. An improvement in the volatile matter dispersion along the bed would increase the contact efficiency of volatiles. Full combustion can be also reached by implementing a second fuel reactor step, whose fuel would be the outlet gaseous stream of the first fuel reactor. The inventories needed in this second fuel reactor are very small: 45 kg/$MW_{th}$ as maximum value.

The simulation of a wide range of conditions showed that an optimized iG-CLC system for solid fuels with ilmenite as oxygen carrier should have a carbon separation system with high efficiency above 90% and the fuel reactor temperature should be above 950ºC. A gasification agent to fixed carbon ratio of 0.7 would be enough and some $CO_2$ from the outlet fuel reactor could be recirculated and used as gasification agent. The optimum reduction degree in the air reactor outlet would be within the range 0-0.4. The contact of the volatile matter with the oxygen carrier should be improved with some design solutions or the implementation of a second fuel reactor is proposed as a very promising option to fully burn the volatile matter and besides avoid another oxygen polishing step. With these measures and range of values of the parameters and with an inventory around 1000 kg/$MW_{th}$, carbon capture efficiency higher than 90% and full combustion will be reached.

**Notation**

$\bar{b}$ = average stoichiometric coefficient for reaction of solid with reacting gas

$[C]_{fuel}$, $[H]_{fuel}$, $[O]_{fuel}$ fraction of carbon, hydrogen and oxygen, respectively, in the fuel

$C_g$ = reacting gas concentration (mol/m$^3$)

CLC Chemical Looping Combustion

$d$ = stoichiometric factor in the fuel combustion reaction with oxygen (mol $O_2$ per mol of fuel)

$E_a$ activation energy (kJ/mol)

$f_C$ carbon concentration in the fuel reactor bed

$F_{C,char}$ carbon flow from the char introduced with the fuel (mol/s)

$(F_{C,char})_{in}$ carbon flow from char entering the fuel reactor (mol/s)

$(F_{C,char})_{out}$ carbon flow of ungasified char that exits the fuel reactor (mol/s)

$(F_C)_{gp}$ flow of carbon contained in the products of char gasification (mol/s)

$(F_C)_{vol}$ flow of carbon contained in the volatile matter (mol/s)

$(F_{CO_2})_{in}$ flow of introduced $CO_2$ as gasification agent (mol/s)

$F_{CO_2,AR}$ molar flow of carbon that is oxidized in the air reactor (mol/s)

$F_{i,e,1}$, $F_{i,e,2}$ gas flows of the gasification product $i$ in the dense bed at the inlet and outlet of an inventory differential mass (mol/s)

$F_{i,v,1}$, $F_{i,v,2}$ gas flows of the released gas $i$ in the volatiles at the inlet and outlet of an inventory differential mass (mol/s)

$F_j$ flow of the gas component $j$ in the dense bed (mol/s)

$F_k$ flow of the gas component $k$ in the plume (mol/s)

$F_{H_2}$, $F_{CO}$, $F_{CH_4}$, $F_{CO_2}$, $F_{H_2O}$ molar flows of $H_2$, CO, $CH_4$, $CO_2$ and $H_2O$, respectively

$F^0_{k,vol}$ flow of the gas component $k$ that is released when coal is devolatilized (mol/s)

$F^0_{j,gas}$ flow of gas $j$ introduced as gasification agent (mol/s)

FR1 solid fuelled fuel reactor

FR2 second fuel reactor proposed

$G_S$ solids circulation rate (kg/s)

$H_2O$/C gasification agent to fixed carbon ratio

iG-CLC in situ Gasification-Chemical Looping Combustion

$k_1$, $k_2$ kinetic constants in the gasification rate ($s^{-1}bar^{-1}$)

$k_3$ kinetic constants in the gasification rate ($s^{-1}$)

$k_{s0}$ = pre-exponential factor for chemical kinetic constant ($mol^{1-n}\ m^{3n-2}\ s^{-1}$)

$Me_xO_y$ oxygen carrier in its oxidized form

$Me_xO_{y-1}$ oxygen carrier in its reduced form

$\dot{m}_{fuel,in}$ coal feeding flow (kg/s)

$M_C$ molecular weight of carbon (kg/mol)

$M_O$ molecular weight of oxygen (kg/mol)

$\dot{m}_{OC}$ solids circulation rate per $MW_{th}$ of fuel (kg/s per $MW_{th}$)

$m_{OC}$ solids inventory (kg per $MW_{th}$)

$n$ reaction order

$p_{prod}$ partial pressure of the gasification products (bar)

$p_{react}$ partial pressure of the gaseous reactants (bar)

$(-r_{ilm,i})$ reaction rate of ilmenite for a given reaction $i$ ($s^{-1}$)

(-r) oxygen carrier reaction rate ($s^{-1}$)

($-r_{ilm}$) ilmenite reaction rate ($s^{-1}$)

$r_{gasif}$ gasification rate ($s^{-1}$)

$(r_{gasif})_{H_2O}$, $(r_{gasif})_{CO_2}$ char gasification rates with $H_2O$ and $CO_2$, respectively ($s^{-1}$)

$(-r_{ilm,H_2})$, $(-r_{ilm,CO})$, $(-r_{ilm,CH_4})$ reaction rates of ilmenite with $H_2$, CO and $CH_4$, respectively ($s^{-1}$)

$r_{grain}$ grain radius (m)

$R_{O,ilm}$ oxygen transport capacity of ilmenite (kg oxygen/kg oxygen carrier)

t time (s)

$T_{FR}$ fuel reactor temperature (ºC)

$X_{char}$ char conversion

$X_{s,i}$ conversion of the oxygen carrier of reaction i

$X_{s,in}$ conversion of solids at the fuel reactor inlet

$\Delta X_s$ variation of the solids conversion in the reactor

$\Phi$ characteristic reactivity of the oxygen carrier

$\Omega_T$ oxygen demand (%)

$\Omega_{coal}$ oxygen demanded by the coal feeding flow (mol O/s)

$\phi$ oxygen carrier to fuel ratio

$\eta_{CC}$ carbon capture efficiency

$\eta_{CS}$ carbon stripper efficiency

$\eta_{comb\ FR}$ fuel reactor combustion efficiency

$\chi_{OC,v}$ fraction of oxygen carrier in bed that is in contact with the volatile matter

$\rho_m$= molar density (mol/$m^3$)

$\tau$ time for complete solid conversion of the oxygen carrier for the reduction reaction considered (s)

**Acknowledgments**

This work was partially supported by the Spanish Ministry of Science and Innovation (Project ENE2010-19550). A. Cuadrat thanks CSIC for the JAE Pre. fellowship. Alberto Abad thanks to the Ministerio de Ciencia e Innovación for the financial support in the course of the I3 Program.

## References

[1] Kerr HR. Capture and separation technology gaps and priority research needs. In: Thomas DC, Benson SM, editors. Carbon dioxide capture for storage in deep geologic formations– Results from the CO2 capture project, Oxford, UK: Elsevier; 2005, vol. 1, Chapter 38.

[2] Thambimuthu K, Soltanieh M, Abanades JC. Capture of CO2. In: Metz B, Davidson O, de Coninck HC, Loos M, Meyer LA, editors. IPCC special report on carbon dioxide capture and storage, Cambridge. UK: Cambridge University Press; 2005, chapter 3.

[3] Adánez J, Abad A, Garcia-Labiano F, Gayán P, de Diego LF. Progress in Chemical-Looping Combustion and Reforming technologies. Progress Energy Combustion Science 2012;38:215-282.

[4] Cao Y, Pan WP. Investigation of chemical looping combustion by solid fuels. 1. Process analysis. Energy & Fuels 2006;20:1836-1844.

[5] Cuadrat A, Abad A, García-Labiano F, Gayán P, de Diego LF, Adánez J. The use of ilmenite as oxygen carrier in a 500 Wth Chemical Looping Coal Combustion unit. Int J Greenhouse Gas Control 2011;5:1630–42.

[6] Berguerand N, Lyngfelt A. Design and operation of a 10 kWth chemical-looping combustor for solid fuels – Testing with South African coal. Fuel 2008;87:2713-2726.

[7] Cuadrat A, Abad A, de Diego LF, García-Labiano F, Gayán P , Adánez J. Prompt Considerations on the Design of Chemical-Looping Combustion of Coal from Experimental Tests. Fuel 2012; in press.

[8] Berguerand N, Lyngfelt A. The use of petroleum coke as fuel in a 10 kW chemical looping combustor. Int J Greenhouse Gas Control 2008;2:169-79.

[9] Leion H, Mattissson T, Lyngfelt A. Use of ores and industrial products as oxygen carriers in chemical-looping combustion. Energy Fuels 2009;23:2307-15.

[10] Leion H, Jerndal E, Steenari BM, Hermansson S, Israelsson M, Jansson E, Johnsson M, Thunberg R, Vadenbo A, Mattisson T, Lyngfelt A. Solid fuels in chemical–looping combustion using oxide scale and unprocessed iron ore as oxygen carriers. Fuel 2009;88:1945-1954.

[11] Jerndal E, Leion H, Mattisson T, Lyngfelt A. Using low–cost iron–based materials as oxygen carriers for chemical–looping combustion. Oil & Gas Science and Technology 2011;66(2):235-248.

[12] Cuadrat A, Abad A, García-Labiano F, Gayán P, de Diego LF, Adánez J. Effect of operating conditions in Chemical-Looping Combustion of coal in a 500 $W_{th}$ unit. Int J Greenhouse Gas Control 2012;6:153-163.

[13] Abad A, Adánez J, Cuadrat A, García-Labiano F, Gayán P, de Diego LF. Reaction kinetics of ilmenite for Chemical-looping Combustion. Chemical Engineering Science 2011;66(4):689-702.

[14] Adánez J, Cuadrat A, Abad A, Gayán P, de Diego LF, García-Labiano F. Ilmenite Activation during Consecutive Redox Cycles in Chemical-Looping Combustion. Energy & Fuels 2010;24:1402-1413.

[15] Leion H, Mattisson T, Lyngfelt A. Solid fuels in chemical-looping combustion. Int J Greenhouse Gas Control 2008;2:180-193.

[16] Cuadrat A, Abad A, Adánez J, de Diego LF, García-Labiano F, Gayán P. Behavior of Ilmenite as Oxygen Carrier in Chemical-Looping Combustion. Fuel Proc Tech 2012;94(1):101-112.

[17] Mahalatkar K, O'Brien T, Huckaby ED, Kuhlman J. Computational fluid dynamic simulation of the fuel reactor of a coal–fired chemical looping combustor. Proc 1st Int Conf on Chemical Looping. Lyon, France; 2010.

[18] Ströhle J, Orth M, Epple B. Simulation of the fuel reactor of a 1 MWth chemical looping plant for coal. Proc 1st Int Conf on Chemical Looping. Lyon, France; 2010.

[19] Kolbitsch P, Pröll T, Hofbauer H. Modeling of a 120 kW chemical looping combustion reactor system using a Ni-based oxygen carrier. Chemical Engineering Science 2009;64:99-108.

[20] Brown TA, Dennis JS, Scott SA, Davidson JF, Hayhurst AN. Gasification and chemical looping combustion of a lignite char in a fluidized bed of iron oxide. Energy Fuels 2010;24:3034-48.

[21] Leion H, Mattisson T, Lyngfelt A. The use of petroleum coke as fuel in chemical looping combustion. Fuel 2007;86:1947-58.

[22] Agarwal PK, Genetti WA, Lee YY. Model for devolatilization of coal particles in fluidized beds. Fuel 1984; 63; 1157–1165.

[23] Adánez J, Miranda JL, Gavilán JM. Kinetics of a lignite-char gasification by $CO_2$. Fuel 1985;64(6):801-804.

[24] Abad A, Mattisson T, Lyngfelt A, Johansson M. The use of iron oxide as oxygen carrier in a chemical-looping reactor. Fuel 2007;86:1021-35.

[25] Pröll T, Mayer K, Bolhàr-Nordenkampf J, Kolbitsch P, Mattisson T, Lyngfelt A, Hofbauer H. Natural minerals as oxygen carriers for chemical looping combustion in a dual circulating fluidized bed system. Energy Procedia 2009;1:27-34.

[26] Abad A, Adánez J, García-Labiano F, de Diego LF, Gayán P. Modeling of the chemical-looping combustion of methane using a Cu-based oxygen carrier. Combustion and Flame 2010;157(3):602-615.

[27] Abad A, Adánez J, García-Labiano F, de Diego LF, Gayán P, Celaya J. Mapping of the range of operational conditions for Cu-, Fe-, and Ni-based oxygen carriers in chemical-looping combustion. Chemical Engineering Science 2007;62:533-549.

[28] Berguerand N, Lyngfelt A. Chemical-looping combustion of petroleum coke using ilmenite in a 10 $kW_{th}$ unit-high-temperature operation. Energy & Fuels 2009;23(10):5257-5268.

[29] Kramp, M., Thon A, Hartge EU, Heinrich S, Werther J.. Carbon Stripping - A Critical Process Step in the Chemical Looping Combustion of Solid Fuels, in: 2nd International Conference on Energy Process Engineering (ICEPE 2). Efficient Carbon Capture for Coal Power Plants. ICEPE2. 2011. Franfurt, Germany.

[30] Dueso C, García-Labiano F, Adánez J, de Diego LF, Gayán P, Abad A. Syngas combustion in a chemical-looping combustion system using an impregnated Ni-based oxygen carrier. Fuel 2009;88:2357-2364.

[31] Forero CR, Gayán P, de Diego LF, Abad A, García-Labiano F, Adánez J. Syngas combustion in a 500 Wth chemical-looping combustion system using an impregnated Cu-based oxygen carrier. Fuel Proc Technol 2009;90:1471-1479.

[32] Park D, Levenspiel O, Fitzgerald TJ. Plume model for large particle fluidized-bed combustors. Fuel 1981;60(4):295-306.

[33] Lewis WK, Gilliland ER. Production of pure carbon dioxide. Patent US 2665971 1954.

Theoretical approach on the CLC performance with solid fuels: optimizing the solids inventory

Ana Cuadrat, Alberto Abad*, Pilar Gayán, Luis F. de Diego, Francisco García-Labiano, Juan Adánez

**Tables**

**Table 1.** Proximate and ultimate analyses and lower heating value of fresh and pre-treated El Cerrejón coal.

**Table 2.** Mass (g) of the different gaseous species generated from the release of the volatile matter of 100 g of El Cerrejón coal after $CH_4$ reforming, for different $H_2O$-$CO_2$ mixtures as gasification agent.

**Table 3.** Gasification kinetic constants for char from pre-treated El Cerrejón coal. Gasification agents: $H_2O/H_2$ and $CO_2/CO$.

**Table 4.** Main parameters for ilmenite reduction kinetics with $H_2$, CO and $CH_4$ at 950ºC. P=1atm.

Theoretical approach on the CLC performance with solid fuels: optimizing the solids inventory

Ana Cuadrat, Alberto Abad*, Pilar Gayán, Luis F. de Diego, Francisco García-Labiano, Juan Adánez

**Table 1.** Proximate and ultimate analyses and lower heating value of fresh and pre-treated El Cerrejón coal.

| Fresh Colombian coal | | | |
|---|---|---|---|
| C | 68.0 % | Moisture | 6.2 % |
| H | 4.2 % | Volatile matter | 33.4 % |
| N | 1.6 % | Fixed carbon | 48.5 % |
| S | 0.6 % | Ash | 11.9 % |
| | Lower Heating Value: 25878 kJ/kg | | |
| Pre-treated Colombian coal | | | |
| C | 65.8 % | Moisture | 2.3 % |
| H | 3.3 % | Volatile matter | 33.0 % |
| N | 1.6 % | Fixed carbon | 55.9 % |
| S | 0.6 % | Ash | 8.8 % |
| | Lower Heating Value: 21899 kJ/kg | | |

**Table 2.** Mass (g) of the different gaseous species generated from the release of the volatile matter of 100 g of El Cerrejón coal after $CH_4$ reforming, for different $H_2O$-$CO_2$ mixtures as gasification agent.

| Gasification agent | CO | $CO_2$ | $CH_4$ | $H_2O$ | $H_2$ |
|---|---|---|---|---|---|
| 100% $H_2O$ | 5.7 | 42.8 | 7.1 | -27.8 | 5.5 |
| 50% $H_2O$ + 50% $CO_2$ | 23.1 | 12.7 | 8.8 | -14.7 | 3.4 |
| 100% $CO_2$ | 46.5 | -29.1 | 9.9 | 4.8 | 1.2 |

**Table 3.** Gasification kinetic constants for char from pre-treated El Cerrejón coal. Gasification agents: $H_2O/H_2$ and $CO_2/CO$.

| | $H_2O$ | | | $CO_2$ | | |
|---|---|---|---|---|---|---|
| | $k_{1,H2O}$ ($s^{-1}bar^{-1}$) | $k_{2,H2O}$ ($s^{-1}bar^{-1}$) | $k_{3,H2O}$ ($s^{-1}$) | $k_{1,CO2}$ ($s^{-1}bar^{-1}$) | $k_{2,CO2}$ ($s^{-1}bar^{-1}$) | $k_{3,CO2}$ ($s^{-1}$) |
| $k_o$ | 52.6 | $2.81 \cdot 10^{-6}$ | $8.1 \cdot 10^{-9}$ | $4.53 \cdot 10^{3}$ | $3.28 \cdot 10^{-7}$ | $1.84 \cdot 10^{-6}$ |
| $E_a$ (kJ/mol) | 95.1 | -135.1 | -218.5 | 160.1 | -158.5 | -157.6 |

Ana Cuadrat, Alberto Abad*, Pilar Gayán, Luis F. de Diego, Francisco García-Labiano, Juan Adánez

**Table 4.** Main parameters for ilmenite reduction kinetics with $H_2$, CO and $CH_4$ at 950ºC. P=1atm.

| | $H_2$ | CO | $CH_4$ |
|---|---|---|---|
| *d* | 0.5 | 0.5 | 2 |
| $\rho_m$ (mol/m$^3$) | 13589 | 13589 | 13589 |
| $r_{grain}$ (m) | $1.25 \cdot 10^{-6}$ | $1.25 \cdot 10^{-6}$ | $1.25 \cdot 10^{-6}$ |
| $\bar{b}$ | 1.45 | 1.45 | 1.45 |
| $k_{so}$ | 0.062 | 0.1 | 42 |
| $E_a$ (kJ/mol) | 65 | 80.7 | 135.9 |
| n | 1 | 0.8 | 1 |

Theoretical approach on the CLC performance with solid fuels: optimizing the solids inventory

Ana Cuadrat, Alberto Abad*, Pilar Gayán, Luis F. de Diego, Francisco García-Labiano, Juan Adánez

**Captions of figures**

**Fig. 1.** Reactor scheme of the CLC process using solid fuels (- - - optional stream).

**Fig. 2.** Mass flows changes of the gases involved in the process –products of gasification and devolatilization- for a fuel reactor differential mass inventory, d$m_{OC}$.

**Fig. 3.** Scheme of carbon flows involved in the fuel reactor and carbon separation system.

**Fig. 4.** Char conversion versus time curves for the gasification reactions with $H_2O$ of El Cerrejón coal obtained by TGA a) at different temperatures: 900ºC, 950ºC, 1000ºC and 1050ºC, using 20% $H_2O$ + 0% $H_2$; and b) with 40% $H_2O$ and different $H_2$ fractions: 0%, 10% 20% and 30% $H_2$ at 1000ºC.

**Fig. 5.** Fuel reactor combustion efficiencies obtained experimentally and theoretically with the model, considering $\chi_{OC,v}$ = 0.53%, at different fuel reactor temperatures. Solids inventory = 3100 kg/$MW_{th}$. $H_2O$/C=0.7. $\phi$=2. $\eta_{CS}$=0. $X_{s,in}$=0. Fuel: pre-treated El Cerrejón coal.

**Fig. 6.** Evolution of the a) in the dense bed b) in the plume and c) total $CH_4$, $H_2$, CO, $CO_2$ and $H_2O$ molar flows within the fuel reactor bed, for a solids inventory of 3100 kg/$MW_{th}$. $T_{FR}$=900ºC. $H_2O$/C=0.7. $\phi$=2. $\eta_{CS}$=0. $X_{s,in}$=0. $\chi_{OC,v}$=0.53%. Fuel: pre-treated El Cerrejón coal.

**Fig. 7.** Variation of a) carbon capture, b) char conversion and c) combustion efficiency with increasing solids inventory for several fuel reactor temperatures. ── 900ºC, ---- 950ºC and ·-·-·- 1000ºC. $H_2O/C$=0.7. $\phi$=2. $\eta_{CS}$=0. $X_{s,in}$=0. $\chi_{OC,v}$=0.53%.

**Fig. 8.** Variation of $H_2$, CO and $CH_4$ concentrations at the fuel reactor outlet with increasing solids inventory for several fuel reactor temperatures. ── 900ºC, ---- 950ºC and ·-·-·- 1000ºC. $H_2O/C$=0.7. $\phi$=2. $\eta_{CS}$=90%. $X_{s,in}$=0. $\chi_{OC,v}$=0.53%.

**Fig. 9.** Variation of a) carbon capture and b) char conversion with increasing solids inventory for several fuel reactor temperatures. ── 900ºC, ---- 950ºC and ·-·-·- 1000ºC. $H_2O/C$=0.7. $\phi$=2. $\eta_{CS}$=90%. $X_{s,in}$=0. $\chi_{OC,v}$=0.53%.

**Fig. 10.** Variation of a) combustion efficiency and b) total oxygen demand with increasing solids inventory for several fuel reactor temperatures. ── 900ºC, ---- 950ºC and ·-·-·- 1000ºC. $H_2O/C$=0.7. $\phi$=2. $\eta_{CS}$=90%. $X_{s,in}$=0. $\chi_{OC,v}$=0.53%.

**Fig. 11.** Variation of $H_2$, CO and $CH_4$ concentrations at the fuel reactor outlet with increasing solids inventory for $\eta_{CS}$=0%, 80%, 90% and 100%. $T_{FR}$=950ºC. $H_2O/C$=0.7. $\phi$=2. $X_{s,in}$=0. $\chi_{OC,v}$=0.53%.

**Fig. 12.** Variation of a) carbon capture, b) char conversion and c) combustion efficiency with increasing solids inventory for $\eta_{CS}$=0, 80%, 90% and 100%. $T_{FR}$=950ºC. $H_2O/C$=0.7. $\phi$=2. $X_{s,in}$=0. $\chi_{OC,v}$=0.53%.

**Fig. 13.** Variation of a) carbon capture, b) char conversion and c) combustion efficiencies with increasing solids inventory for $H_2O/C$ ratios of 0.4, 0.7, 2 and 4. $T_{FR}$=950ºC. $\phi$=2. $\eta_{CS}$=90%. $X_{s,in}$=0. $\chi_{OC,v}$=0.53%.

**Fig. 14.** Variation of a) carbon capture, b) char conversion and c) combustion efficiencies with different $H_2O$:$CO_2$ mixtures as gasification agent and for several $\eta_{CS}$: 0%, 80%, 90%, 95% and 98%. Inventory= 1000 kg/$MW_{th}$. $T_{FR}$=950ºC. $(H_2O+CO_2)/C$=0.7. $\phi$=2. $X_{s,in}$=0. $\chi_{OC,v}$=0.53%.

**Fig. 15.** Variation of a) carbon capture and b) combustion efficiencies with increasing solids inventory for oxygen carrier to fuel ratios, $\phi$, of 1.1, 1.2, 1.5, 2 and 3.33. $T_{FR}$=950ºC. $H_2O/C$=0.7. $\eta_{CS}$=90%. $X_{s,in}$=0. $\chi_{OC,v}$=0.53%.

**Fig. 16.** Resulting combustion efficiency with increasing $\phi$ for inventories of 200, 500, 1000 and 5000 kg/$MW_{th}$. $T_{FR}$=950ºC. $H_2O/C$=0.7. $\eta_{CS}$=90%. $X_{s,in}$=0. $\chi_{OC,v}$=0.53%.

**Fig. 17.** Combustion efficiency variation with increasing $X_{s,in}$. Inventory = 1000 kg/$MW_{th}$. $T_{FR}$=950ºC. $H_2O/C$=0.7. $\phi$=2. $\eta_{CS}$=90%. $\chi_{OC,v}$=0.53%.

**Fig. 18.** Variation of a) carbon capture, b) char conversion and c) combustion efficiency with increasing oxygen carrier reaction rate, for carbon stripper efficiencies of 0% and 90%. Inventory=500 kg/$MW_{th}$. $T_{FR}$=950ºC. $H_2O/C$=0.7. $\phi$=2. $X_{s,in}$=0.

**Fig. 19.** Combustion efficiency variation with increasing $\chi_{OC,v}$ for several inventories: —— 200 kg/$MW_{th}$, - - - - 500 kg/$MW_{th}$ and ····· 1000 kg/$MW_{th}$. $T_{FR}$=950ºC. $H_2O/C$=0.7. $\phi$=2. $\eta_{CS}$=90%. $X_{s,in}$=0.

**Fig. 20.** Minimum ilmenite inventory in the second fuel reactor to completely oxidize the fuel for different inventories in the first fuel reactor. $T_{FR}$=950ºC. Conditions in the first fuel reactor: $H_2O/C$=0.7. $\phi$=2. $\eta_{CS}$=90%. $X_{s,in}$=0. $\chi_{OC,v}$=0.53%.

Theoretical approach on the CLC performance with solid fuels: optimizing the solids inventory

Ana Cuadrat, Alberto Abad*, Pilar Gayán, Luis F. de Diego, Francisco García-Labiano, Juan Adánez

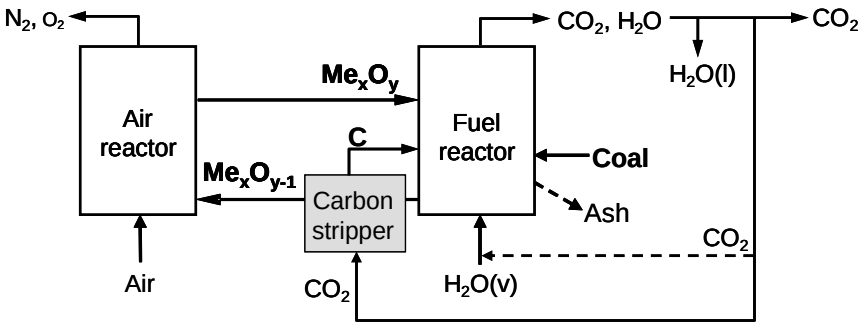


**Fig. 1.** Reactor scheme of the CLC process using solid fuels (- - - optional stream).

Ana Cuadrat, Alberto Abad*, Pilar Gayán, Luis F. de Diego, Francisco García-Labiano, Juan Adánez

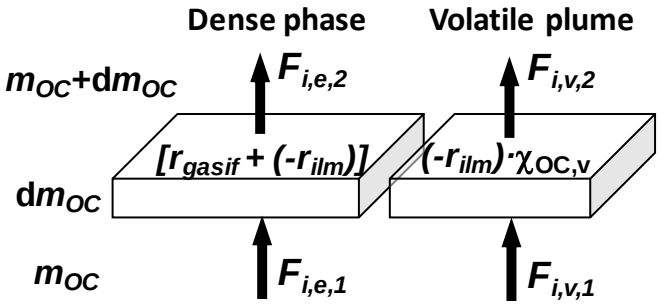


**Fig. 2.** Mass flows changes of the gases involved in the process –products of gasification and devolatilization- for a fuel reactor differential mass inventory, d$m_{OC}$.

Theoretical approach on the CLC performance with solid fuels: optimizing the solids inventory

Ana Cuadrat, Alberto Abad*, Pilar Gayán, Luis F. de Diego, Francisco García-Labiano, Juan Adánez

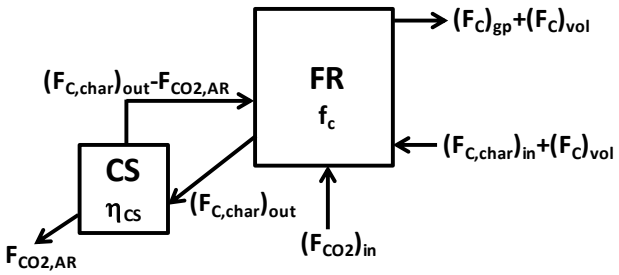


**Fig. 3.** Scheme of carbon flows involved in the fuel reactor and carbon separation system.

Theoretical approach on the CLC performance with solid fuels: optimizing the solids inventory

Ana Cuadrat, Alberto Abad*, Pilar Gayán, Luis F. de Diego, Francisco García-Labiano, Juan Adánez

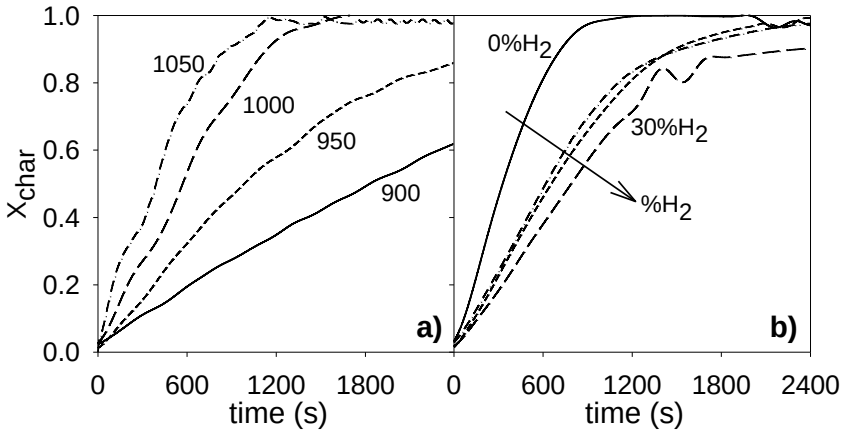


**Fig. 4.** Char conversion versus time curves for the gasification reactions with $H_2O$ of El Cerrejón coal obtained by TGA a) at different temperatures: 900ºC, 950ºC, 1000ºC and 1050ºC, using 20% $H_2O$ + 0% $H_2$; and b) with 40% $H_2O$ and different $H_2$ fractions: 0%, 10% 20% and 30% $H_2$ at 1000ºC.

Theoretical approach on the CLC performance with solid fuels: optimizing the solids inventory

Ana Cuadrat, Alberto Abad*, Pilar Gayán, Luis F. de Diego, Francisco García-Labiano, Juan Adánez

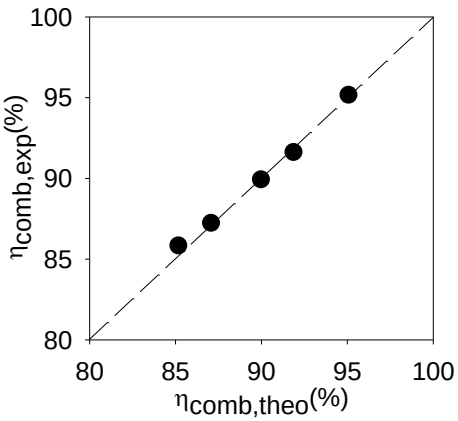


**Fig. 5.** Fuel reactor combustion efficiencies obtained experimentally and theoretically with the model, considering $\chi_{OC,v}$ = 0.53%, at fuel reactor temperatures in the range 880-940ºC. Solids inventory = 3100 kg/$MW_{th}$. $H_2O$/C=0.7. $\phi$=2. $\eta_{CS}$=0. $X_{s,in}$= 0. Fuel: pre-treated El Cerrejón coal.

Theoretical approach on the CLC performance with solid fuels: optimizing the solids inventory

Ana Cuadrat, Alberto Abad*, Pilar Gayán, Luis F. de Diego, Francisco García-Labiano, Juan Adánez

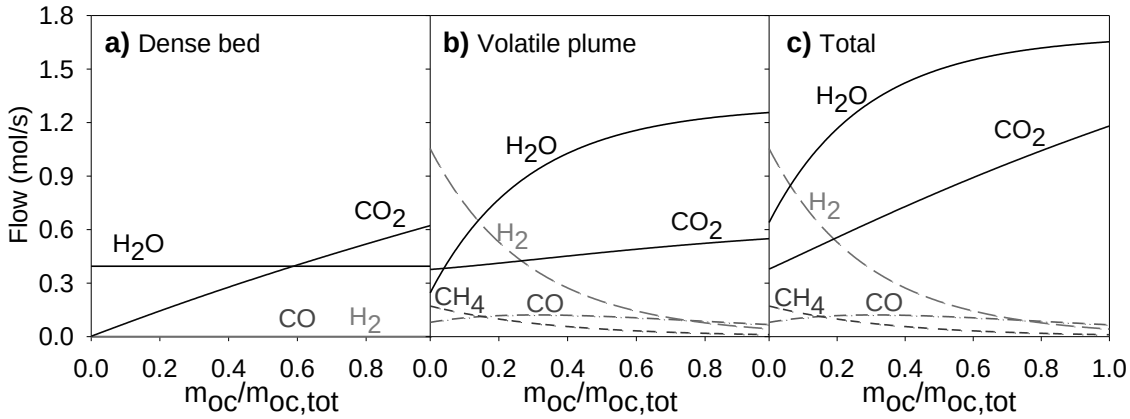


**Fig. 6.** Evolution of the a) in the dense bed b) in the plume and c) total $CH_4$, $H_2$, CO, $CO_2$ and $H_2O$ molar flows within the fuel reactor bed, for a solids inventory of 3100 kg/$MW_{th}$. $T_{FR}$=900ºC. $H_2O$/C=0.7. $\phi$=2. $\eta_{CS}$=0. $X_{s,in}$= 0. $\chi_{OC,v}$=0.53%. Fuel: pre-treated El Cerrejón coal.

Theoretical approach on the CLC performance with solid fuels: optimizing the solids inventory

Ana Cuadrat, Alberto Abad*, Pilar Gayán, Luis F. de Diego, Francisco García-Labiano, Juan Adánez

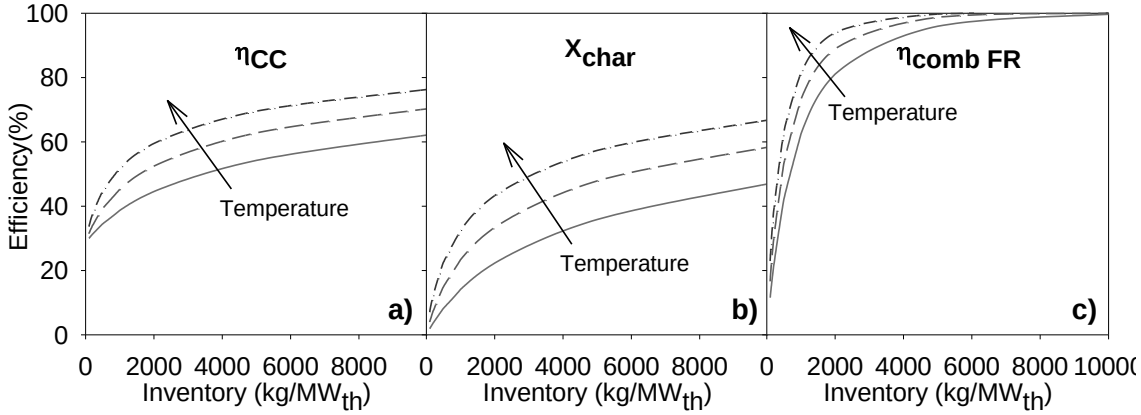


**Fig. 7.** Variation of a) carbon capture, b) char conversion and c) combustion efficiency with increasing solids inventory for several fuel reactor temperatures. —— 900ºC, - - - - 950ºC and ····· 1000ºC. $H_2O/C$=0.7. $\phi$=2. $\eta_{CS}$=0. $X_{s,in}$= 0. $\chi_{OC,v}$=0.53%.

Theoretical approach on the CLC performance with solid fuels: optimizing the solids inventory

Ana Cuadrat, Alberto Abad*, Pilar Gayán, Luis F. de Diego, Francisco García-Labiano, Juan Adánez

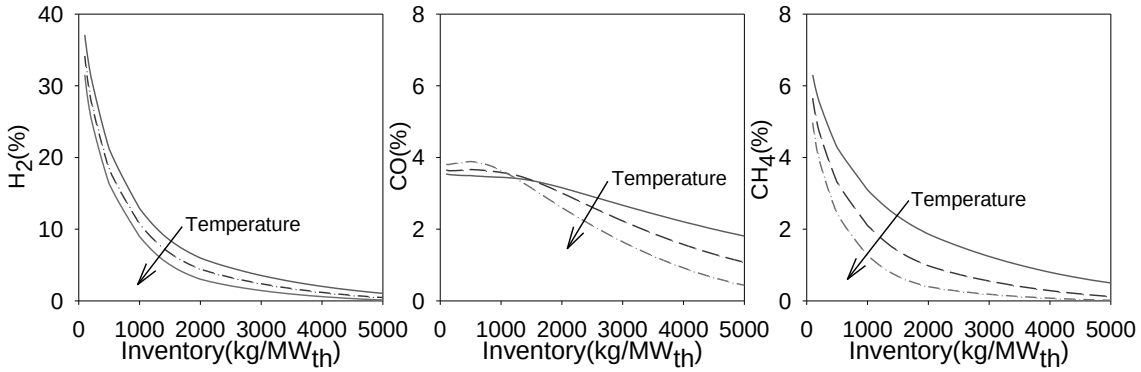


**Fig. 8.** Variation of $H_2$, CO and $CH_4$ concentrations at the fuel reactor outlet with increasing solids inventory for several fuel reactor temperatures. —— 900ºC, - - - - 950ºC and ····· 1000ºC. $H_2O/C$=0.7. $\phi$=2. $\eta_{CS}$=90%. $X_{s,in}$= 0. $\chi_{OC,v}$=0.53%.

Theoretical approach on the CLC performance with solid fuels: optimizing the solids inventory

Ana Cuadrat, Alberto Abad*, Pilar Gayán, Luis F. de Diego, Francisco García-Labiano, Juan Adánez

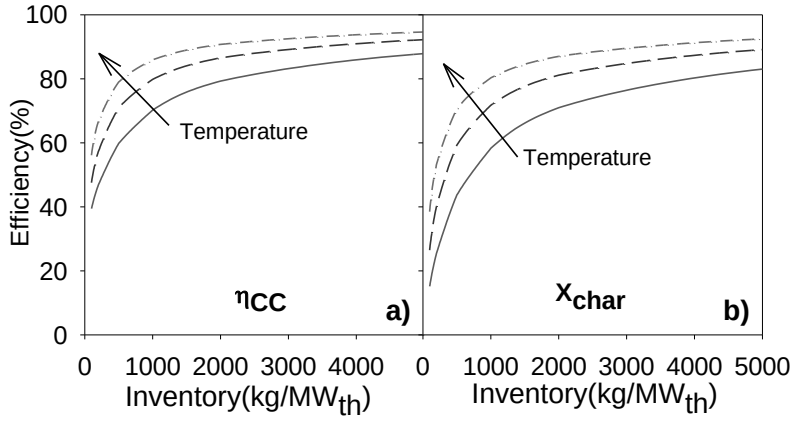


**Fig. 9.** Variation of a) carbon capture and b) char conversion with increasing solids inventory for several fuel reactor temperatures. —— 900ºC, - - - - 950ºC and ····· 1000ºC. $H_2O/C$=0.7. $\phi$=2. $\eta_{CS}$=90%. $X_{s,in}$= 0. $\chi_{OC,v}$=0.53%.

Theoretical approach on the CLC performance with solid fuels: optimizing the solids inventory

Ana Cuadrat, Alberto Abad*, Pilar Gayán, Luis F. de Diego, Francisco García-Labiano, Juan Adánez

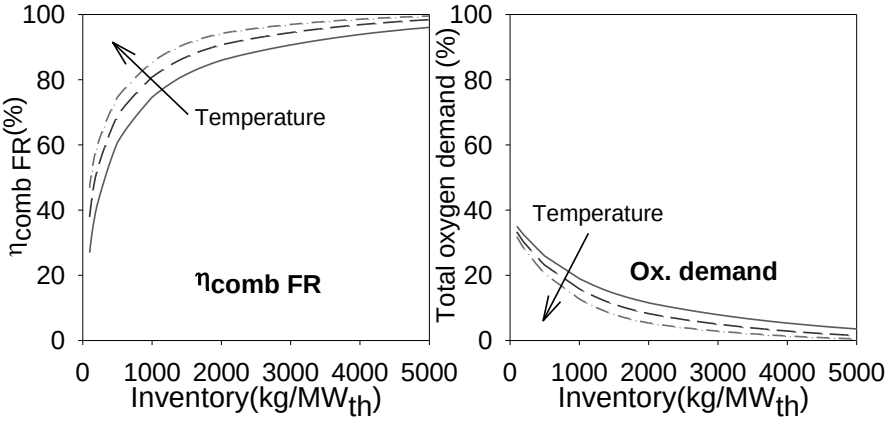


**Fig. 10.** Variation of a) combustion efficiency and b) total oxygen demand with increasing solids inventory for several fuel reactor temperatures. —— 900ºC, - - - - 950ºC and ····· 1000ºC. $H_2O/C$=0.7. $\phi$=2. $\eta_{CS}$=90%. $X_{s,in}$= 0. $\chi_{OC,v}$=0.53%.

Theoretical approach on the CLC performance with solid fuels: optimizing the solids inventory

Ana Cuadrat, Alberto Abad*, Pilar Gayán, Luis F. de Diego, Francisco García-Labiano, Juan Adánez

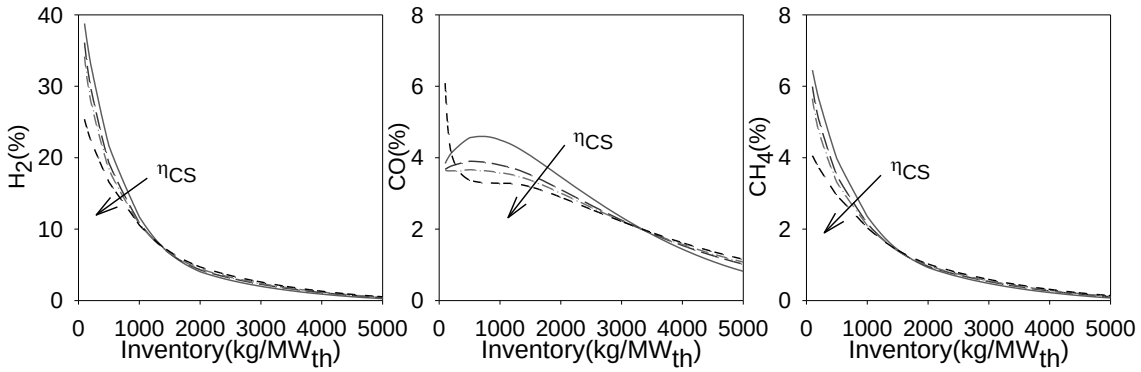


**Fig. 11.** Variation of $H_2$, CO and $CH_4$ concentrations at the fuel reactor outlet with increasing solids inventory for $\eta_{CS}$=0%, 80%, 90% and 100%. $T_{FR}$=950ºC. $H_2O/C$=0.7. $\phi$=2. $X_{s,in}$= 0. $\chi_{OC,v}$=0.53%.

Theoretical approach on the CLC performance with solid fuels: optimizing the solids inventory

Ana Cuadrat, Alberto Abad*, Pilar Gayán, Luis F. de Diego, Francisco García-Labiano, Juan Adánez

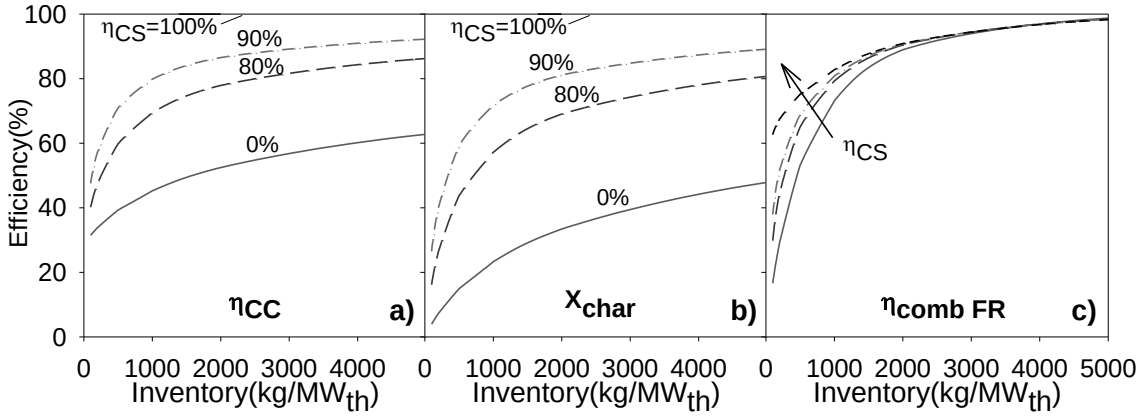


**Fig. 12.** Variation of a) carbon capture, b) char conversion and c) combustion efficiency with increasing solids inventory for $\eta_{CS}$=0, 80%, 90% and 100%. $T_{FR}$=950ºC. $H_2O/C$=0.7. $\phi$=2. $X_{s,in}$= 0. $\chi_{OC,v}$=0.53%.

Theoretical approach on the CLC performance with solid fuels: optimizing the solids inventory

Ana Cuadrat, Alberto Abad*, Pilar Gayán, Luis F. de Diego, Francisco García-Labiano, Juan Adánez

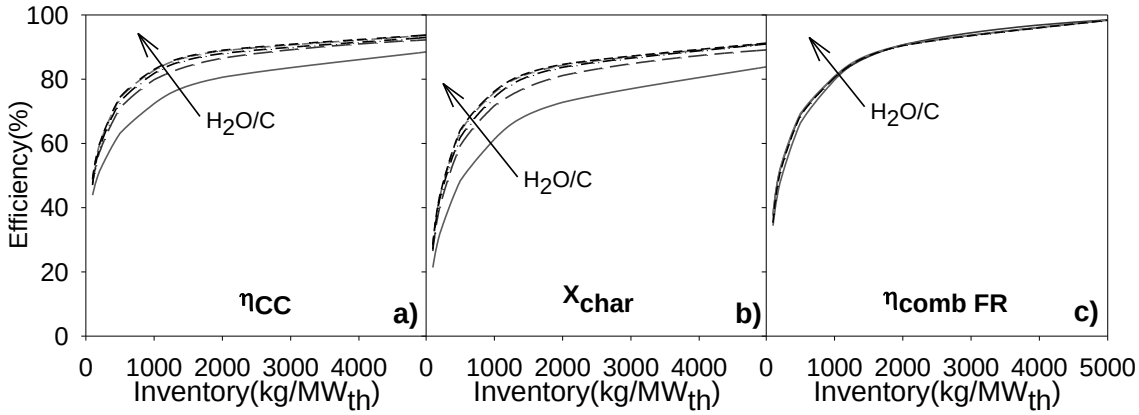


**Fig. 13.** Variation of a) carbon capture, b) char conversion and c) combustion efficiencies with increasing solids inventory for $H_2O/C$ ratios of 0.4, 0.7, 2 and 4. $T_{FR}$=950ºC. $\phi$=2. $\eta_{CS}$=90%. $X_{s,in}$= 0. $\chi_{OC,v}$=0.53%.

Theoretical approach on the CLC performance with solid fuels: optimizing the solids inventory

Ana Cuadrat, Alberto Abad*, Pilar Gayán, Luis F. de Diego, Francisco García-Labiano, Juan Adánez

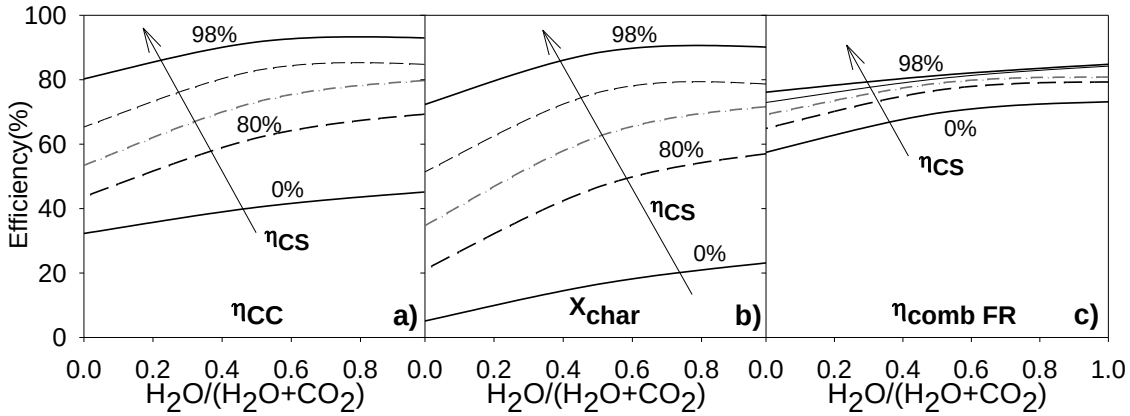


**Fig. 14.** Variation of a) carbon capture, b) char conversion and c) combustion efficiencies with different $H_2O$:$CO_2$ mixtures as gasification agent and for several $\eta_{CS}$: 0%, 80%, 90%, 95% and 98%. Inventory= 1000 kg/$MW_{th}$. $T_{FR}$=950ºC. ($H_2O$+$CO_2$)/C=0.7. $\phi$=2. $X_{s,in}$= 0. $\chi_{OC,v}$=0.53%.

Theoretical approach on the CLC performance with solid fuels: optimizing the solids inventory

Ana Cuadrat, Alberto Abad*, Pilar Gayán, Luis F. de Diego, Francisco García-Labiano, Juan Adánez

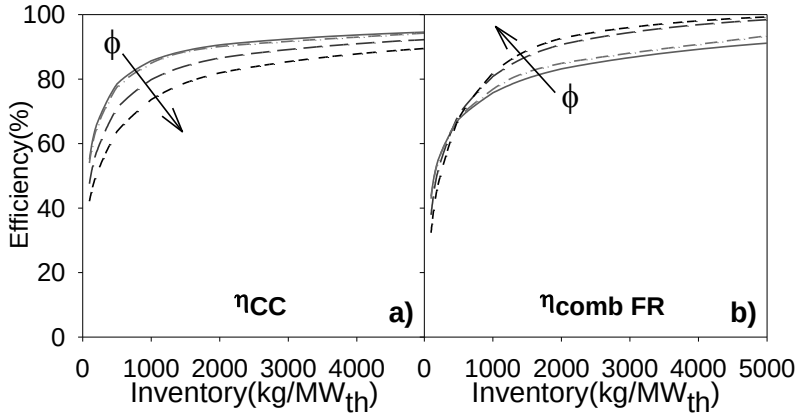


**Fig. 15.** Variation of a) carbon capture and b) combustion efficiencies with increasing solids inventory for oxygen carrier to fuel ratios, ϕ, of 1.1, 1.2, 1.5, 2 and 3.33. $T_{FR}$=950ºC. $H_2O/C$=0.7. $\eta_{CS}$=90%. $X_{s,in}$= 0. $\chi_{OC,v}$=0.53%.

Theoretical approach on the CLC performance with solid fuels: optimizing the solids inventory

Ana Cuadrat, Alberto Abad*, Pilar Gayán, Luis F. de Diego, Francisco García-Labiano, Juan Adánez

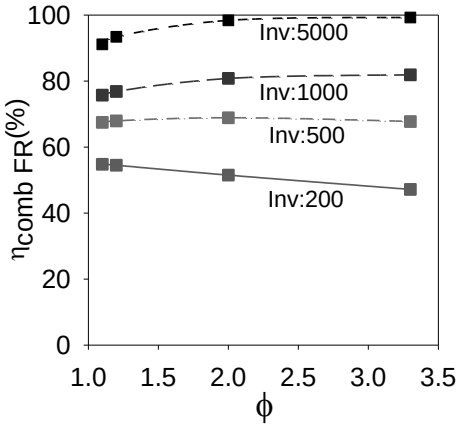


**Fig. 16.** Resulting combustion efficiency with increasing ϕ for inventories of 200, 500, 1000 and 5000 kg/$MW_{th}$. $T_{FR}$=950ºC. $H_2O$/C=0.7. $\eta_{CS}$=90%. $X_{s,in}$= 0. $\chi_{OC,v}$=0.53%.

Theoretical approach on the CLC performance with solid fuels: optimizing the solids inventory

Ana Cuadrat, Alberto Abad*, Pilar Gayán, Luis F. de Diego, Francisco García-Labiano, Juan Adánez

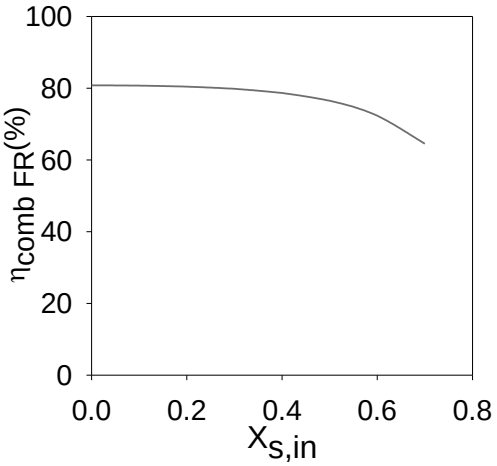


**Fig. 17.** Combustion efficiency variation with increasing $X_{s,in}$. Inventory = 1000 kg/$MW_{th}$. $T_{FR}$=950ºC. $H_2O$/C=0.7. $\phi$=2. $\eta_{CS}$=90%. $\chi_{OC,v}$=0.53%.

Theoretical approach on the CLC performance with solid fuels: optimizing the solids inventory

Theoretical approach on the CLC performance with solid fuels: optimizing the solids inventory

Ana Cuadrat, Alberto Abad*, Pilar Gayán, Luis F. de Diego, Francisco García-Labiano, Juan Adánez

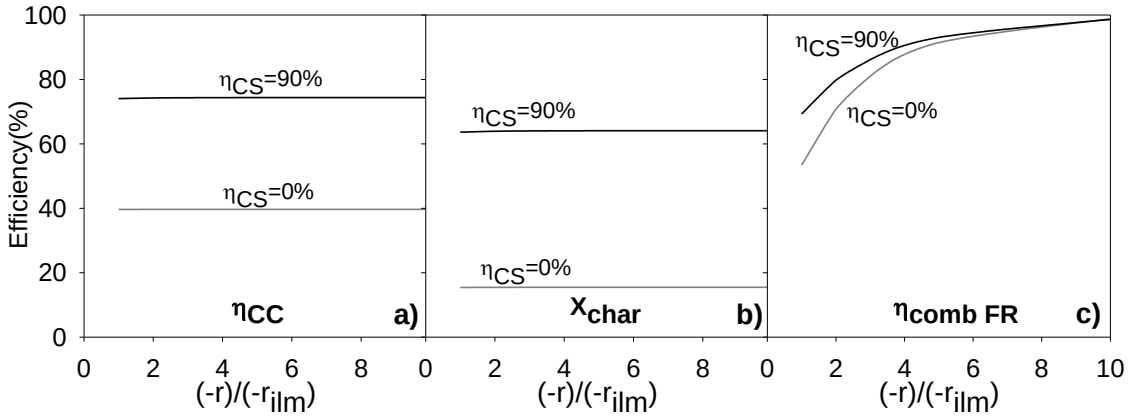


**Fig. 18.** Variation of a) carbon capture, b) char conversion and c) combustion efficiency with increasing oxygen carrier reaction rate, for carbon stripper efficiencies of 0% and 90%. Inventory=500 kg/$MW_{th}$. $T_{FR}$=950ºC. $H_2O$/C=0.7. $\phi$=2. $X_{s,in}$= 0.

Theoretical approach on the CLC performance with solid fuels: optimizing the solids inventory

Ana Cuadrat, Alberto Abad*, Pilar Gayán, Luis F. de Diego, Francisco García-Labiano, Juan Adánez

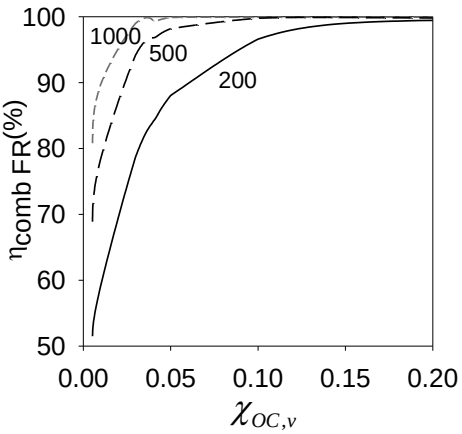


**Fig. 19.** Combustion efficiency variation with increasing $\chi_{OC,v}$ for several inventories: —— 200 kg/$MW_{th}$, ---- 500 kg/$MW_{th}$ and ····· 1000 kg/$MW_{th}$. $T_{FR}$=950ºC. $H_2O$/C=0.7. $\phi$=2. $\eta_{CS}$=90%. $X_{s,in}$= 0.

Theoretical approach on the CLC performance with solid fuels: optimizing the solids inventory

Ana Cuadrat, Alberto Abad*, Pilar Gayán, Luis F. de Diego, Francisco García-Labiano, Juan Adánez

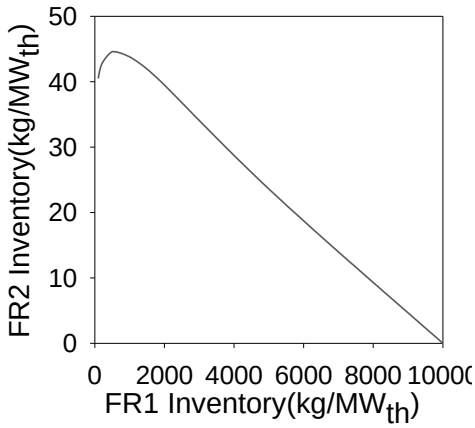


**Fig. 20.** Minimum ilmenite inventory in the second fuel reactor to completely oxidize the fuel for different inventories in the first fuel reactor. $T_{FR}$=950ºC. Conditions in the first fuel reactor: $H_2O$/C=0.7. $\phi$=2. $\eta_{CS}$=90%. $X_{s,in}$= 0. $\chi_{OC,v}$=0.53%.

# Paper IX

# Effect of the coal rank in the performance of in-situ Gasification Chemical-Looping Combustion

**A. Cuadrat, A. Abad*, F. García-Labiano, P. Gayán, L.F. de Diego, J. Adánez**

Instituto de Carboquímica (ICB-CSIC), Dept. of Energy & Environment, Miguel Luesma Castán 4, 50018-Zaragoza, Spain

* Corresponding author: Tel: (+34) 976 733 977. Fax: (+34) 976 733 318. E-mail address: abad@icb.csic.es (A. Abad)

**Abstract**

Chemical-Looping Combustion, CLC, is among the most promising technologies to capture $CO_2$ at low cost in power plants that use fossil fuels. In CLC the oxygen from air is transferred to the fuel by a solid oxygen-carrier that circulates between two interconnected fluidized-beds: the air- and the fuel-reactor.

In this work the CLC process for solid fuels using ilmenite as oxygen-carrier was evaluated in a continuous CLC unit. In this process, gasification of solid fuel happens in the fuel-reactor which is fluidized by a gasifying agent, i.e, $H_2O$. This process has been referred as in-situ Gasification CLC, iG-CLC. Different types of fuels were used to evaluate the feasibility of using fuels ranging from lignite to anthracite and the effect of the coal rank on the process performance. The temperature as one of the main process parameters was analyzed and a temperature increase was proven to be advantageous to reach high efficiencies for all the fuels

tested. All the parameters of influence were analyzed in the char conversion and combustion efficiency. The carbon capture efficiency followed the trend of the coal rank, as it was higher for lignite, then for the bituminous coals and it was lower for anthracite. Special attention was put on the combustion of the volatile matter of the different fuels. In all cases oxygen demands lower than 10% were found, and for anthracite the oxygen demand values were 3.5% because of the lower volatile content of this fuel. The feasibility of using $H_2O$:$CO_2$ mixtures as gasification agent with each type of fuel was also assessed and it was seen that depending on the type of fuel, some of the steam as gasification agent can be replaced by $CO_2$, as in case of bituminous coals and lignite.

**Keywords**: Chemical-looping combustion, Oxygen-carrier, Ilmenite, $CO_2$ capture, Coal.

## 1. Introduction

$CO_2$ is considered the gas making the largest contribution to the global warming. Its concentration in the atmosphere has increased strongly over the few past decades as a result of the dependency on fossil fuels for energy production. The global atmospheric concentration of $CO_2$ increased from a pre-industrial value of about 280 ppm to 390 ppm in 2010 [1]. The abatement of greenhouse gas emissions can be achieved through a wide portfolio of measures in the energy, industry, agricultural and forest sectors. According to the analysis made by the IPCC and IEA [2,3], Carbon Capture and Storage could contribute 15–55% to the cumulative mitigation effort worldwide until 2100, to stabilize climate change at a reasonable cost.

In this context, Chemical-Looping Combustion (CLC) is one of the most promising technologies to carry out $CO_2$ capture at a low cost [4]. CLC is based on the transfer of the oxygen from air to the fuel by means of a solid oxygen-carrier. Different configurations have been proposed for CLC: interconnected fluidized beds [5] and fixed alternating beds [6,7]. The most used for coal combustion is the two interconnected fluidized beds configuration [8-

17], for which the two reactors are the fuel- and the air-reactor). In the fuel-reactor the oxygen-carrier is reduced through oxidation of the fuel, thus obtaining a gas stream composed by $CO_2$ and $H_2O$. The oxygen-carrier is afterwards directed to the air-reactor, where it is re-oxidized with air and regenerated to start a new cycle. The net chemical reaction is the same as at usual combustion with the same combustion heat released, but with the advantage of the intrinsic $CO_2$ separation in the process without an additional step.

The development of clean coal conversion processes is of great interest regarding the intensive use of coal as energy source. In this sense, the use of CLC with solid fuels is very interesting when the capture of $CO_2$ is considered for a clean coal conversion process. One of the options for CLC with solid fuels is the in-situ Gasification CLC, iG-CLC, see scheme in Fig. 1.

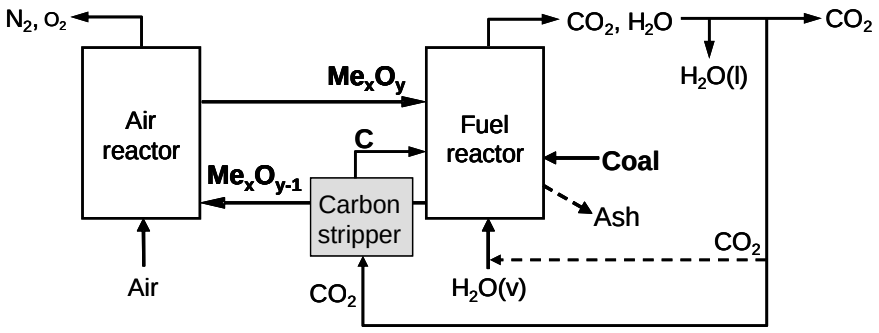


**Fig. 1.** Reactor scheme of the CLC with solid fuels process using solid fuels. ( optional stream).

In this process the solid fuel is directly introduced in the fuel-reactor, where it is mixed with the oxygen-carrier and being gasified by the fluidizing gas, i.e. $H_2O$ or $CO_2$ [18]. Thereby, the solid fuel devolatilizes and the char gets gasified following reactions (1-3). The oxidized oxygen-carrier, $Me_xO_y$, reacts simultaneously with the gaseous products of coal devolatilization and gasification, with $H_2$ and CO as main components to give the combustion

products, $CO_2$ and $H_2O$ (see Eq. 4). Then the reduced oxygen-carrier, $Me_xO_{y-1}$, exits the fuel-reactor and is oxidized with air in the air-reactor according to reaction (5).

$$\text{Coal} \rightarrow \text{Volatile matter} + \text{Char} \quad (1)$$

$$\text{Char} + H_2O \rightarrow H_2 + CO \quad (2)$$

$$\text{Char} + CO_2 \rightarrow 2\ CO \quad (3)$$

$$H_2, CO, \text{Volatile matter} + n\ Me_xO_y \rightarrow CO_2 + H_2O + n\ Me_xO_{y-1} \quad (4)$$

$$Me_xO_{y-1} + ½\ O_2 \rightarrow Me_xO_y \quad (5)$$

To find suitable oxygen-carriers is a key factor for the development of the CLC technology. An oxygen-carrier should have, during many cycles, high selectivity towards $CO_2$ and $H_2O$, enough oxygen transport capacity, high reactivity in reduction and oxidation, mechanical resistance, low attrition rate and show no agglomeration problems. For the use of CLC with solid fuels, since part of the oxygen-carrier is expected to be removed mixed with fuel ashes, it would be desirable that the oxygen-carrier was environmentally friendly and of low cost. Therefore natural minerals [17, 19], industrial residues [20, 21] or synthetic carriers made with low-cost raw materials [22,23] are of great interest, being ilmenite an appropriate material, as it has shown to be suitable for its use in CLC with solid fuels [8-11]. Ilmenite is a relatively cheap and abundantly occurring mineral mainly consisting of $FeTiO_3$.

In previous CLC experiments with solid fuels performed to date, full oxidation of the outlet fuel-reactor stream could not be achieved [8-17]. Furthermore, the extent of unburt gases was similar as if a highly Ni-based oxygen-carrier was used [14-16]. Therefore, in order to oxidize completely unburnt compounds to $CO_2$ and $H_2O$ and enhance combustion, an oxygen polishing step downstream was proposed, that is, injection of pure oxygen to the gas flow after the fuel-reactor cyclone [8,9], with the corresponding oxygen demand.

The gasification process has been identified as the controlling step in this process [24-27]. Leion et al. [28] saw in a batch fluidized-bed reactor with various bituminous coals and

petcoke that the oxygen-carrier enhances the gasification rate of coal because the presence of oxygen-carrier particles reduces the fraction of $H_2$ in the bed, which has an inhibitory effect on the gasification. This fact has been observed as much for steam gasification as for $CO_2$ gasification using different oxygen-carrier materials, for solid fuels such as bituminous coals o lignites [27-30]. Char gasification is usually a slow process and the solids stream exiting from the fuel-reactor could contain some unconverted char together with the oxygen-carrier [12,13]. Thus, total $CO_2$ capture efficiency cannot be reached when using solid fuels if there is by-pass of non-gasified char particles to the air-reactor. The use of a carbon separation system, for instance a carbon stripper, has been proposed to carry out the separation of char from the oxygen-carrier and later to be re-introduced to the fuel-reactor, thus reducing the amount of carbon transferred from the fuel- to the air-reactor [18]. Berguerand et al. designed and built a 10 $kW_{th}$ CLC plant that included a carbon stripper [9].

Char conversion was seen to be related to the reactivity of solid fuel particles [28], being the nature of the oxygen-carrier of lower relevance [25]. TGA tests done with a synthetic Cu-based oxygen-carrier and a sub-bituminous coal, wood and a low-density polyethylene as fuels showed the feasibility of using solid fuels with higher reactivity, that is, higher volatile matter, for this technology [18]. Linderholm et al. [31] studied the fuel conversion in a batch fluidized bed reactor for five fuels using ilmenite as oxygen-carrier and found that in all cases the fuel conversions were promoted with the temperature, with an increase from 1.6 to 3.2 times when the temperature raised from 970 to 1030ºC. They also found that three bituminous coals had similar char conversion rates, and it was much slower for a petroleum coke, followed by a metallurgical coke. Dennis et al. also found differences in the conversion of char, depending on the type of fuel when lignite or bituminous coals were used as fuels [29,30].

As for continuous operation, Berguerand and Lyngfelt [8-11] used a 10 $kW_{th}$ chemical-looping combustor with ilmenite as oxygen-carrier and South African coal and petroleum coke as solid fuels. They analyzed the combustion process focusing on char conversion and the conversion of gases from steam gasification (CO and $H_2$) was analyzed. A $CO_2$ capture within the range 65-82% was obtained for South African coal as fuel at 900-950ºC. The incomplete gas conversion resulted into the presence of unconverted gases in the fuel-reactor outlet stream (CO, $H_2$ and $CH_4$) that demanded 29-30% of the total oxygen needed to fully burn coal to $H_2O$ and $CO_2$. They analyzed mainly the temperature as one of the main process parameters affecting the system performance, being higher efficiencies reached at high temperatures. Temperatures above 1000 ºC were tested in some cases [10], for which oxygen demands of 27-36% were found, where 5-9% corresponded to the oxygen demand for char combustion. Average carbon capture efficiencies of 80% were obtained in all the experimental works at high temperatures with petcoke, which is a fuel with low volatile content.

Biomass as solid fuel was evaluated by Shen et al. [32] in a continuous 10 $kW_{th}$ CLC combustor using an oxygen-carrier prepared from iron oxide and $CO_2$ as gasification medium. Gu et al. [33] also proved the feasibility of using CLC for both biomass and a biomass/coal mixture as solid fuels in a continuous 1 $kW_{th}$ CLC facility and using an Australian iron ore as oxygen carrier. They found that the difference in the carbon capture efficiency between the biomass and the biomass/coal mixture, was caused by the combustible carbonaceous gases in the fuel reactor. It was 98% above 800ºC for biomass and 93-98% at 900-985ºC for the biomass/coal mixture. The blend of biomass with coal was proposed as an effective measure to reduce the potential negative influence of the alkali metals of biomass ash on the performance of oxygen-carriers.

In this work the feasibility of the iG-CLC process for different types of solid fuels using ilmenite as oxygen-carrier was evaluated in a continuous CLC unit. Fuels ranging from lignite to anthracite were used. The effect of the coal rank on the process performance was assessed. The temperature as one of the main parameters of influence was analyzed for all the fuels tested. The feasibility of using $H_2O$:$CO_2$ mixtures as gasification agent with each type of fuel was also studied. The effect of the main process parameters on char conversion and combustion efficiency was analyzed. Special attention was put on the combustion of the volatile matter of the different fuels, since to date no research has been done on the combustion of devolatilization products.

## 2. Experimental section

### 2.1. Bed material and fuel

Ilmenite has been one of the most used materials for combustion of coal in iG-CLC [8-13,34]. The bed material in this study was a Norwegian ilmenite with particle size of +150-300 μm. Ilmenite is a common mineral found in metamorphic and igneous rocks. The ilmenite used is a concentrate from a natural ore. $Fe_2O_3$ and $Fe_2TiO_5$ are the active phases that behave as the oxygen-carrier. Ilmenite undergoes an activation process which was deeply studied in previous works [35,36]. The batch of ilmenite used in these experiments which had a particle size of +150-300 μm was previously used in continuous tests using Colombian coal as fuel and it was fully activated [12,13]. Thereby, ilmenite particles showed constant reactivity during experimental tests. Table 1 shows the main physical and chemical properties of as received fresh ilmenite and the ilmenite used in these experiments, which was already activated. The procedure to obtain the physic-chemical characteristics has been described previously [12].

**Table 1.** Main properties of fresh and activated ilmenite particles.

| | Fresh ilmenite | Activated ilmenite |
|---|---|---|
| XRD phases | $FeTiO_3$, $Fe_2O_3$, $TiO_2$ | $Fe_2TiO_5$, $Fe_2O_3$, $TiO_2$ |
| Crushing strength (N) | 2.4 | 2.0 |
| Oxygen transport capacity(%) | 4.0 | 3.9 |
| True density ($kg/m^3$) | 4580 | 4200 |
| Porosity (%) | 0 | 18 |
| BET Surface ($m^2/g$) | 0.6 | 0.4 |

The oxygen transport capacity, which is the mass fraction of oxygen that can be used in the oxygen transfer, was measured to be 3.9% for this CLC process with solid fuels. Note that the oxygen transport capacity and crushing strength barely changed after a total of 98 hours of operation. In this process the oxidized species $Fe_2TiO_5$ and $Fe_2O_3$ transfer oxygen by getting reduced to $FeTiO_3$ and $Fe_3O_4$, respectively. The ilmenite used was composed by 11.7% $Fe_2O_3$, 53.2% $Fe_2TiO_5$ and 29.5% $TiO_2$.

A range of coals with different rank was used as fuels: a Spanish anthracite, a Spanish lignite and two bituminous coals from Colombia and South Africa. Following the ASTM characterization, South African coal is a medium volatile (MV) bituminous coal, whereas Colombian coal is a high volatile (HV) bituminous coal. The coal particle size for all coals tested was +200-300 μm. Ultimate and proximate analyses and low heating values of the used coals are gathered in Table 2. The high volatile bituminous Colombian coal used had been subjected to a thermal treatment at 180ºC that eliminated the swelling properties seen in this fuel. Due to this pre-treatment the coal gets somewhat pre-oxidized, which can lead to some reactivity change of the fuel [12].

**Table 2.** Proximate and ultimate analysis and low heating value, LHV, of coals used in this work.

| | Lignite | HV Bit. Colombian | MV Bit. S.African | Anthracite |
|---|---|---|---|---|
| Moisture,%wt. | 12.5 | 2.3 | 4.2 | 1 |
| Volatile matter,%wt. | 28.7 | 33 | 25.5 | 7.6 |
| Fixed carbon,%wt. | 33.6 | 55.9 | 56 | 59.9 |
| Ash,%wt. | 25.2 | 8.8 | 14.3 | 31.5 |
| LHV,kJ/kg | 16250 | 21900 | 26435 | 21880 |
| C,%wt. | 45.4 | 65.8 | 69.3 | 60.7 |
| H,%wt. | 2.5 | 3.3 | 3.5 | 2 |
| N,%wt. | 0.5 | 1.6 | 2 | 0.9 |
| S,%wt. | 5.2 | 0.6 | 1 | 1.3 |
| O,%wt. | 8.6 | 17.6 | 5.7 | 2.4 |

### 2.2. ICB-CSIC-s1 facility for CLC with solid fuels

A schematic view of the plant is shown in Fig. 2. The set-up was basically composed of two interconnected fluidized-bed reactors joined by a loop seal, a riser for solids transport from the air-reactor to the fuel-reactor, a cyclone and a solids valve to control the flow rate of solids fed to the fuel-reactor. This design allowed the measure and the control of the solid circulation flow rate between both reactors. The total ilmenite inventory in the system was 3.5 kg and the solids inventory in the fuel-reactor was 0.8 kg ilmenite. This facility has been used in continuous operation in previous studies with El Cerrejón bituminous Colombian coal as fuel [12,13].

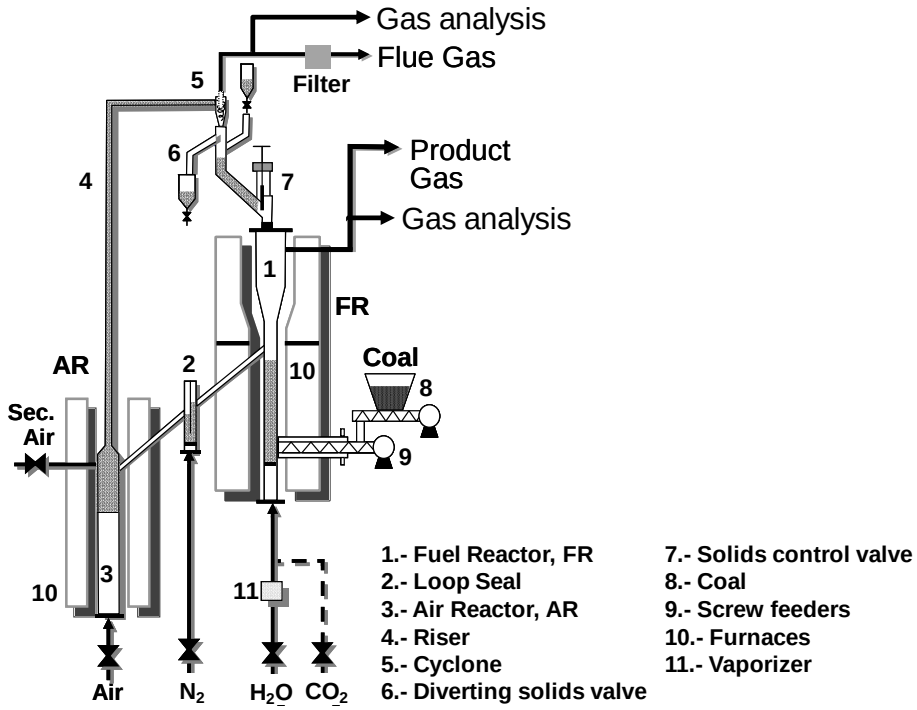


**Fig. 2.** Schematic diagram of the ICB-CSIC-s1 facility for coal-fuelled CLC.

The fuel-reactor consisted of a bubbling fluidized bed with 5 cm of inner diameter and 20 cm bed height. The fluidizing gas was composed of $H_2O$:$CO_2$ mixtures, which acts also as gasifying agent. The gasification agent flow was 190 $L_N$/h. Coal is fed by a screw feeder placed just above the fuel-reactor distributor plate in order to maximize the time that the fuel and volatile matter are in contact with the bed material. The screw feeder has two steps: the first one with variable speed to control the coal flow rate, and the second has high rotating velocity to avoid coal pyrolysis inside the screw. A small $N_2$ flow of 18 $L_N$/h is fed at the beginning of the screw-feeder to avoid possible volatile reverse flow or entrance of steam. In the fuel-reactor the oxygen-carrier is reduced by the volatile matter and gasification products of coal. Reduced oxygen-carrier particles overflowed into the air-reactor through a U-shaped fluidized bed loop seal with an inner diameter of 50 mm. The loop-seal was fluidized with 90 $L_N$/h of $N_2$. Thus, gas mixing between fuel- and air-reactors was avoided. The oxidation of the carrier took place in the air-reactor, consisting of a bubbling fluidized bed with 8 cm of inner

diameter and 10 cm bed height, and followed by a riser of 3 cm inner diameter. The gas flows introduced in the air-reactor were 2100 $L_N$/h as primary air and 400 $L_N$/h of secondary air at the top of the bubbling bed to help particle entrainment. $N_2$ and unreacted $O_2$ left the air-reactor and went through a high-efficiency cyclone and a filter before the stack. The oxidized solid particles recovered by the cyclone were sent to a solids reservoir, which acts as a loop seal, setting the oxygen-carrier ready to start a new cycle. The regenerated oxygen-carrier particles returned to the fuel-reactor by gravity from the solids reservoir through a solids valve which controlled the flow rates of solids entering the fuel-reactor. A diverting solids valve located below the cyclone allowed the measurement of the solids flow rates at any time.

Because of its small size, the system is not auto-thermal and is heated up with various ovens to get independent temperature control of the air-reactor, fuel-reactor, and fuel-reactor freeboard. During operation, temperatures in the bed and freeboard of the fuel-reactor, air-reactor bed and riser were monitored as well as the pressure drops in important locations of the system, such as the fuel-reactor bed, the air-reactor bed and the loop seal.

$CH_4$, CO and $CO_2$ concentrations in the fuel-reactor stream were continuously measured by nondispersive infrared (NDIR) analyzers (Maihak S710/UNOR, Siemens Ultramat/Oxymat 6) and $H_2$ concentration by a thermal conductivity detector (Maihak S710/THERMOR). CO, $CO_2$ and $O_2$ concentrations in the fuel-reactor were determined by a combined NDIR-paramagnetic analyzer (Siemens Ultramat/Oxymat 6). All data were collected by means of a data logger connected to a computer.

In some selected experiments, GC analysis of the outgoing fuel-reactor gases was done to measure possible hydrocarbons, and possible tar formation was also measured following the tar protocol [37].

Table 3 shows the conditions for the series of experiments carried out. During all the experiments, the temperature in the air-reactor was kept at around 930ºC and in the fuel-

reactor freeboard at about 900ºC. The fuel-reactor temperature was varied within the range 860-930 ºC. Most experiments were done with steam as fluidization agent in the fuel-reactor, and $H_2O$:$CO_2$ mixtures were also used as fluidization agents in a series of tests. The gas velocity in the fuel-reactor was 0.12 m/s at 900ºC, which corresponded to around 5 times the minimum fluidization velocity of the particles. However, a previous study showed that the effect of the gasification agent flow was negligible for ratios steam to fixed carbon over 1 [13]. The gas velocity in the air-reactor was 0.1 m/s and the velocity in the air-reactor riser was 4.3 m/s at a temperature of 900 ºC. The average solids circulation flow was 3.0 kg/h for all fuels tested. At least every condition was maintained stable during 30 minutes. Coal was fed for 13 hours using lignite, 7 hours using bituminous South African coal and 11 hours using anthracite. In total, 44 hours of continuous operation of hot conditions were carried out. An experiment previously performed with Colombian bituminous coal "El Cerrejón" which was done with similar solids residence time and solids inventory is also included. A deeper study on "El Cerrejón" coal as fuel used in iG-CLC can be found elsewhere [12,13].

**Table 3.** Conditions for the series of experiments with variation of the fuel-reactor temperature and variation of the gasification agent type ($H_2O$:$CO_2$ mixtures) with the different types of coals tested, i.e, lignite, bituminous South African coal and anthracite. The conditions of a previous test done with Colombian bituminous coal is also included [13].

Effect of the temperature

| Coal type | $T_{FR}$,ºC | Coal feed, g/h | $\frac{\text{Gasif.agent}}{\text{Fixed C}}$ | Gasification mixture,%$H_2O$ | Thermal output, $W_{th}$ |
|---|---|---|---|---|---|
| Lignite | 870-920 | 100 | 3.0 | 100 | 450 |
| MV Bit. S.African | 850-915 | 79 | 2.3 | 100 | 580 |
| Anthracite | 870-930 | 94 | 1.8 | 100 | 570 |

| | | | | | |
|---|---|---|---|---|---|
| HV Bit. Colombian | 890 | 83 | 2.2 | 100 | 505 |

Effect of the gasification mixture $H_2O$:$CO_2$

| Coal type | $T_{FR}$,ºC | Coal feed, g/h | Gasif.agent / Fixed C | Gasification mixture,%$H_2O$ | Thermal output, $W_{th}$ |
|---|---|---|---|---|---|
| Lignite | 920 | 100 | 3.0 | 100;60;0 | 450 |
| MV Bit. S.African | 910 | 79 | 2.3 | 100;58;0 | 580 |
| Anthracite | 925 | 94 | 1.8 | 100;48;0 | 570 |

To do a more complete study on the gasification rates for the different coals under well defined conditions, the char conversions reached with time were measured by TGA at 950ºC. The samples were heated up to the desired temperature in $N_2$ and when the volatiles had been released and the weight of the sample was stable, the remaining char was gasified with steam with a 50%$H_2O$+50%$N_2$ mixture.

## 3. Data evaluation

The evaluation of the fuel-reactor performance is carried out by the analysis of two main parameters: the carbon capture efficiency and the combustion efficiency in the fuel-reactor. The purpose of the data evaluation is to assess the performance of the process in the different experiments, using the measured values of the gas concentrations, temperature and solid circulation rates. The absence of a carbon separation system facilitates the interpretation of the effect of the operational conditions on the results obtained, as the solids mean residence time can be easily calculated in this facility. Otherwise, the presence of a carbon separation system would increase the mean residence time of char particles to an unknown value.

As it was seen in previous experiments [12], there is some elutriation of char in this facility with coal. Thus, the sum of carbon measured in the gases coming from the fuel-reactor and

the air-reactor is less than the carbon in the coal feeding flow. However, in case of an industrial plant the possible elutriated char will be collected by a cyclone and reintroduced in the fuel-reactor. The total effective carbon introduced in the facility for particle size of +200-300μm was 89% for lignite, 94% for Colombian coal, 77% for South African and 87% for anthracite. All calculations and analyses in this study are made considering only the effective char, that is, the introduced char that had not been elutriated from the fuel-reactor. Thus, the balance to carbon atoms was done by considering the carbon exiting the fuel-reactor as gases ($CO_2$, CO and $CH_4$) and the carbon in char exiting together with ilmenite. In the last case, carbon will be burnt in the air-reactor and detected as $CO_2$.

The efficiencies that indicate the performance of the process are defined as follows. The carbon capture is the physical removal of carbon dioxide that would otherwise be emitted into the atmosphere. Getting high carbon capture during energy generation is the motivation of this technology. The carbon capture efficiency, $\eta_{CC}$, is here defined as the fraction of the carbon introduced that is converted to gas in the fuel-reactor.

$$\eta_{CC} = \frac{[F_{CO2,FR} + F_{CO,FR} + F_{CH4,FR}]_{out} - [F_{CO2,FR}]_{in}}{[F_{CO2,FR} + F_{CO,FR} + F_{CH4,FR} + F_{CO2,AR}]_{out} - [F_{CO2,FR}]_{in}} \quad (6)$$

$F_{CO2,FR}$, $F_{CH4,FR}$ and $F_{CO,FR}$ being the flows in the fuel-reactor of $CO_2$, $CH_4$, and CO. The carbon of the unreacted char flowing towards the air-reactor is the $CO_2$ gas flow in the air-reactor, $F_{CO2,AR}$. The gaseous flows are calculated by a balance of the $N_2$ flows introduced in the system. Previous fluidization measurement and tests showed that about 65% of this $N_2$ flow goes to the fuel-reactor and the rest goes to the air-reactor. For the experiments using $CO_2$ as fluidization agent, the inlet $CO_2$ flow must be subtracted. The carbon captured in the system is the carbon contained in the volatiles plus the carbon in the char that is gasified. Thus, the carbon capture efficiency depends on the fraction of char that has been gasified.

To do a deeper study of the carbon capture behavior, the gasification step should be assessed. The conversion of carbon in char, $X_{char}$, is defined as the fraction of carbon in the effective char fed to the fuel-reactor which is gasified and thus released to the fuel-reactor outgoing gas stream:

$$X_{char} = \frac{[F_{CO2,FR} + F_{CO,FR} + F_{CH4,FR} - F_{C,vol}]_{out} - [F_{CO2,FR}]_{in}}{[F_{CO2,FR} + F_{CO,FR} + F_{CH4,FR} + F_{CO2,AR} - F_{C,vol}]_{out} - [F_{CO2,FR}]_{in}} = \frac{F_{C,char\ eff} - F_{CO2,AR}}{F_{C,char\ eff}} \quad (7)$$

The gasified char in the fuel-reactor was calculated as difference between the carbon in gases in the fuel-reactor outgoing flow, and the carbon flow coming from the volatile matter. The carbon content in the volatiles is directly calculated using the ultimate and proximate analysis of coal. $F_{C,char\ eff}$ is the carbon in the effective char flow introduced in the CLC system.

An approximation to the char gasification rates can be obtained, if a simplified model is used. The fuel-reactor is considered to follow a continuous stirred-tank reactor (CSTR) model. The char is assumed to be in perfect mixing with the solids in the fuel-reactor and to react at a rate $(-r_C)$ which is proportional to the mass. With these considerations, $(-r_C)$ is calculated from a carbon balance in the fuel-reactor:

$$(-r_C) = \frac{1}{m_{char}} \frac{dm_{char}}{dt} = k \quad \Rightarrow \quad (-r_C) = \frac{X_{char} \cdot F_{C,char\ eff} \cdot M_C}{m_{char,FR}} \quad (8)$$

being $M_C$ the carbon molar weight and $m_{char,FR}$ the mass of carbon in char in the fuel-reactor, which can be calculated with the mass of ilmenite in the fuel-reactor $m_{ilm,FR}$, and the solids circulation rate $F_{ilm}$:

$$\frac{m_{char,FR}}{m_{ilm,FR}} = \frac{F_{CO2,AR}}{F_{ilm}} \quad (9)$$

Besides, the mean residence time of ilmenite, $t_{m,ilm}$, is calculated by Eq. (10).

$$t_{m,ilm} = \frac{m_{ilm,FR}}{F_{ilm}} \quad (10)$$

The combustion efficiency in the fuel-reactor, $\eta_{comb\ FR}$, is a measure of gas conversion in the fuel-reactor. It is defined as the fraction of the oxygen demanded by the volatile matter and gasification products that is supplied by the oxygen-carrier in the fuel-reactor. It depends on the reaction rate of ilmenite with the gaseous fuels and on the amount of the reducing gases released by coal in the fuel-reactor. The combustion efficiency was calculated as:

$$\eta_{comb\ FR} = \frac{[0.5 \cdot F_{H2O,FR} + F_{CO2,FR} + 0.5 \cdot F_{CO,FR}]_{out} - [0.5 \cdot F_{H2O,FR} + F_{CO2,FR} + 0.5 \cdot O_{coal,eff}]_{in}}{O_{2\ demand\ coal,eff} - F_{CO2,AR}} \quad (11)$$

$O_{coal,eff}$ is the flow of oxygen contained in the effective coal introduced. $O_{2\ demand\ coal,eff}$ or the oxygen demand of the effective coal flow is the oxygen flow needed to fully burn the fuel.

The oxygen demand, $\Omega_T$, has been also used as an adequate parameter to evaluate the performance of the whole combustion process. It is defined as the fraction of oxygen lacking to achieve a complete combustion to $CO_2$ and $H_2O$ of the fuel-reactor product gas in comparison to the oxygen demand of the effective introduced coal. It is the only fraction of oxygen required in the iG-CLC process to reach full combustion of the fuel that must be supplied in a subsequent polishing step as pure $O_2$.

$$\Omega_T = \frac{O_{2\ demand\ gases\ FR}}{O_{2\ demand\ coal,eff}} = \frac{2 \cdot F_{CH4,FR} + 0.5 \cdot F_{H2,FR} + 0.5 \cdot F_{CO,FR}}{O_{2\ demand\ coal,eff}} \quad (12)$$

The rate of oxygen transferred by ilmenite, $(-r_O)$, is a measure of how much and how fast oxygen is transferred from ilmenite to the fuel. $(-r_O)$ is calculated as the increased flow of oxygen in the oxygen-containing gases (CO, $CO_2$ and $H_2O$), divided by the ilmenite hold-up:

$$(-r_O) = \frac{([0.5 \cdot F_{H2O,FR} + F_{CO2,FR} + 0.5 \cdot F_{CO,FR}]_{out} - [0.5 \cdot F_{H2O,FR} + F_{CO2,FR} + 0.5 \cdot O_{coal,eff}]_{in}) \cdot M_{O_2}}{m_{ilm,FR}} \quad (13)$$

## 4. Results and discussion

The feasibility of using the CLC technology with different fuels was tested, and influence of the type of fuel on the continuous performance was determined. In the literature it was found

that the temperature in the fuel-reactor is one of the parameters with most influence on coal conversion [10,12,16] because of its effect on the gasification rate. Indeed, the gasification step has high influence on the performance of this process [24-27]. In this work an evaluation of the iG-CLC process performance with different coals was made for increasing fuel-reactor temperature. Also different $H_2O$:$CO_2$ mixtures as gasification agent for all fuels were tested.

Previous experiments done to evaluate the influence of different operational parameters showed that in this process to operate at lower recirculation rates led to an increase in the char conversion and to an enhancement of the system performance [12] because of an increase in the residence times of solids in the fuel-reactor. Therefore, the recirculation rates in all these experiments were set at low values. In these conditions, the resulting oxygen-carrier to fuel ratio for all fuels tested was about 1.0-1.1. The oxygen-carrier to fuel ratio is a measure of how much oxygen can be supplied by the circulating oxygen-carrier compared to the oxygen needed to burn the fuel fed in. In stoichiometric conditions this ratio is equal to one.

As representative of the gas distributions obtained in this study, the evolution with time of the gas concentrations from the fuel-reactor is shown in Fig. 3 for the experiments using anthracite as fuel with increasing fuel-reactor temperature, $T_{FR}$. The initial period before introducing coal and the transitory period until the steady state was reached are also represented. Concentrations in fuel-reactor are in dry basis. Steady state after changing the temperature was fast reached and all the points were therefore evaluated at stable conditions. Similar behavior of the transient period was observed when the type of gasifying gas was changed. The CLC prototype was easy to operate and control with all kinds of fuels, and the steady state for each operating condition was maintained for at least 30 min. Thus, the feasibility of using coals of different rank in an *in-situ* gasification CLC system was proven with this study. The performance of the system according to the characteristics of each fuel is later assessed.

The outlet of the fuel-reactor was mainly composed of oxidized $CO_2$, and $H_2$ and CO and some $CH_4$ as not fully oxidized products of char gasification and volatile matter. Gas chromatography analyses and tars measurements showed that there were neither hydrocarbons heavier than $CH_4$ nor tars in the fuel-reactor outlet flow. Thus, these species were converted in the fuel-reactor. The char that was not gasified in the fuel-reactor entered into the air-reactor and was there burnt with a consequent $CO_2$ release. The $CO_2$ concentration in the air-reactor is also shown in Fig. 3.

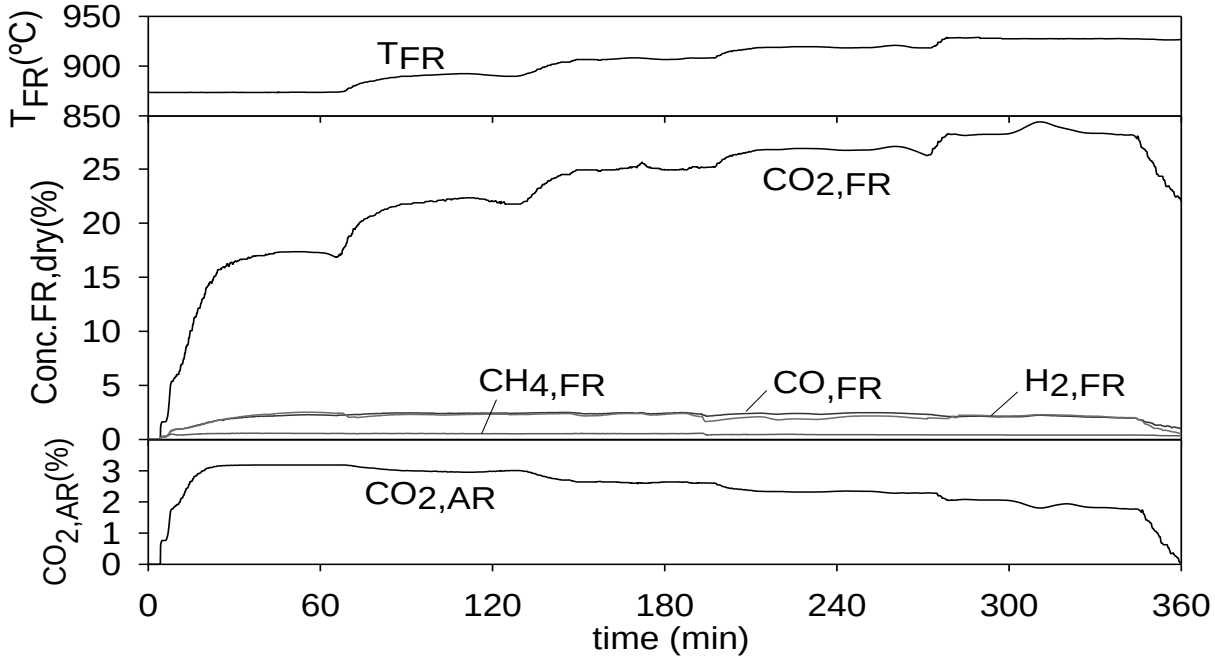


**Fig. 3.** Evolution with time of the gas concentrations from the fuel-reactor and $CO_2$ from the air-reactor for the experiments using anthracite as fuel with increasing fuel-reactor temperature, $T_{FR}$.

### 4.1. Effect of the temperature on the iG-CLC performance

Continuous tests were done at different temperatures with each fuel. In this section, results obtained with Spanish lignite within the temperature interval 870-920ºC, with MV bituminous South African coal within the temperature interval 850-915ºC and a third series of

experiments with Spanish anthracite within the temperature interval 870-930ºC were done. The coal feeding flows, average temperatures and solids circulation flow rates used are gathered in Table 3. In all cases steam was used as gasification agent.

Fig. 4 shows the concentrations of $CO_2$, CO, $H_2$ and $CH_4$ in the fuel-reactor outlet for the series of experiments performed at different temperatures and for the fuels tested in this work, that is, Spanish lignite, MV bituminous South African coal and Spanish anthracite. The concentrations are given in dry and $N_2$ free basis. $CO_2$ comes mainly from the oxidation of the products of gasification and devolatilization. In case of anthracite, the fraction of $CH_4$ in the fuel-reactor outlet is low because this fuel has low fraction of volatiles. The fraction of $CH_4$ for South African coal is higher as this fuel has higher fraction of volatile matter. For lignite the $CO_2$ fraction is quite high compared to the other gases, which indicates that the combustion efficiency with this fuel will be high. As for the effect of the temperature, the trends are the same for all the fuels tested: both gasification and oxidation reactions are promoted with the temperature. Thus the generated $CO_2$ flow and therefore $CO_2$ fraction increases with the temperature, whereas the $H_2$, CO and $CH_4$ fractions decrease.

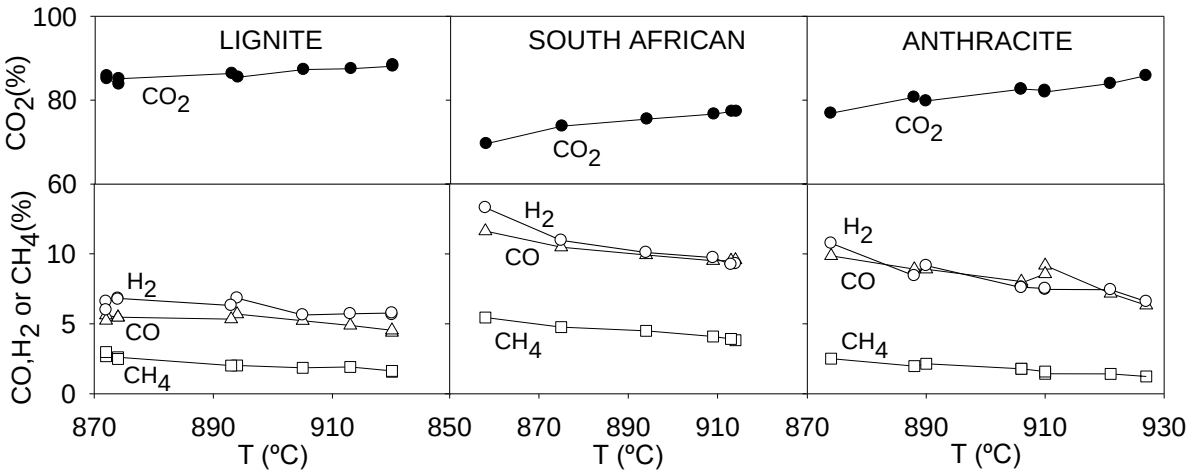

**Fig. 4.** $CO_2$, CO, $H_2$ and $CH_4$ concentrations in the fuel-reactor (dry and free $N_2$ basis) at different fuel-reactor temperatures with lignite, MV bituminous South African coal and anthracite. –●– $CO_2$, –■– CO, –○– $H_2$ and –□– $CH_4$.

One experiment done at 890ºC with HV bituminous Colombian coal is here also considered. The results with Colombian coal are comparable with the values of this study, as it has similar values of inventory and residence time. With this coal the relative gaseous fractions at 890ºC were $CH_4$: 3.6%, $H_2$: 11.4%, CO: 13.3%, and $CO_2$: 71.6%. That is, $CH_4$ in the product gas was lower and $H_2$ and CO concentrations were higher than the corresponding for the MV bituminous South African coal. CO, $H_2$ and $CH_4$ were higher compared to the distributions obtained for lignite and anthracite. It is necessary to indicate that this coal was previously pre-oxidized to eliminate its agglomeration trend. This process modifies its composition and reactivity of the used coal.

#### 4.1.1. Carbon capture and char gasification

Fig. 5 shows the carbon capture obtained for different temperatures for the coals tested. As well, at similar experimental conditions the value obtained for HV bituminous Colombian coal in a previous study is shown. $\eta_{CC}$ was dependent on coal rank because of the gasification reactivity of the coal chars. Lignite reached the highest values of $\eta_{CC}$, followed by HV bituminous Colombian, MV bituminous South African coal and it was lower for anthracite. Note that this facility has no carbon separation system and higher values could be obtained in a unit if a carbon separation system was incorporated. A theoretical approach supports this statement [38]. Nevertheless, the results obtained in this facility are valuable to evaluate the performance of the iG-CLC technology with different types of coals.

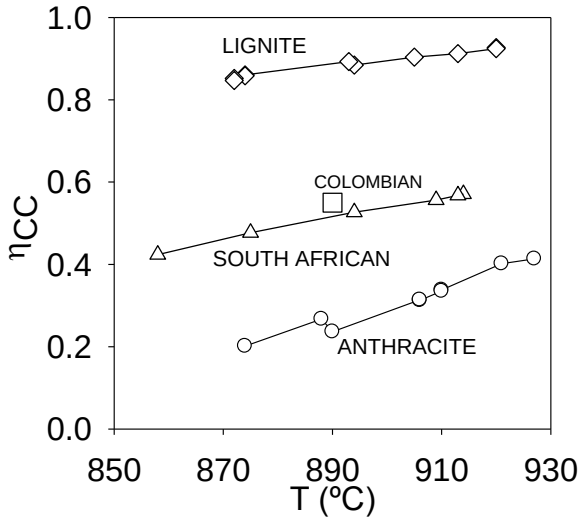


**Fig. 5.** Carbon capture efficiency variation with the fuel-reactor temperature for ⊸◇⊸ lignite, ⊸□⊸ HV bituminous Colombian coal, ⊸△⊸ MV bituminous South African coal, ⊸○⊸ anthracite. Coal particle size: +200-300 μm.

Since the carbon from the volatiles exits with the fuel-reactor outlet stream, that fraction of carbon is always captured. Thus, the carbon capture depends on the char conversion and on the ratio between the flow of carbon in the volatile matter, $F_{C,vol}$ and flow of carbon in the introduced char, $F_{C,char\ eff}$:

$$\eta_{CC} = \frac{X_{char} \cdot F_{C,char\ eff} + F_{C,vol}}{F_{C,char\ eff} + F_{C,vol}} \tag{14}$$

That is, the char conversion attained and the different content of volatiles in the fuels, or more precisely, the ratio $F_{C,vol}/F_{C,char\ eff}$ of the coal considered, determine the carbon capture achieved. Only the effective carbon fed is considered in the analysis. Thus, the char elutriated is not taken into account because it is not really involved in the process. The average $F_{C,vol}/F_{C,char\ eff}$ ratios were 0.57 for lignite, 0.35 for Colombian bituminous coal, 0.43 for South African bituminous coal and 0.01 for anthracite.

Fig. 6 represents the char conversions reached at different temperatures for the coals studied. The comparable result for HV bituminous Colombian coal is also shown. Lignite had much

higher char conversion than the rest. The char conversion obtained for the other coals are closer, indicating that they have more similar gasification rates, but lower that the gasification rate of lignite [25,28-31].

Both char conversions and carbon capture for anthracite were similar because the volatile matter fraction is low, whereas for the other coals the values of carbon capture were higher than values of $X_{char}$. HV bituminous Colombian and MV bituminous South African coal have similar $F_{C,vol}/F_{C,char\ eff}$ ratios and char conversions reached, so their increase in $\eta_{CC}$ compared to $X_{char}$ is similar. Nevertheless, for lignite $X_{char}$ and $\eta_{CC}$ are similar.

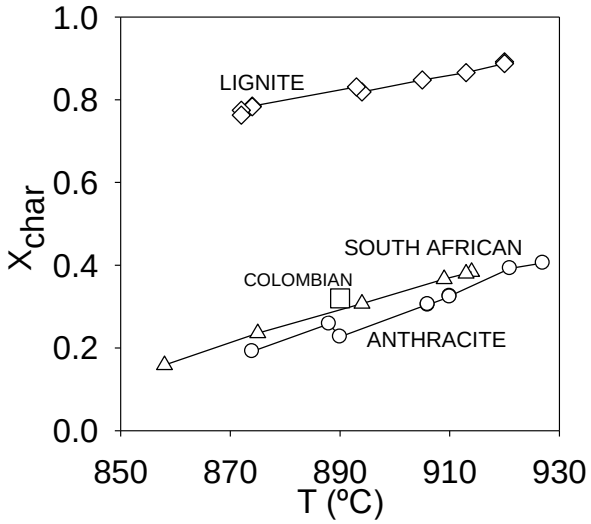


**Fig. 6.** Char conversion variation with the fuel-reactor temperature for ⟡ lignite, ⊟ HV bituminous Colombian coal, △ MV bituminous South African coal, ○ anthracite. Coal particle size: +200-300 μm.

The mean residence time of char particles in the fuel-reactor is a key factor affecting the char conversion [13]. The mean residence time of ilmenite gives an idea of the time that char had to gasify. The resulting mean residence times of ilmenite were 15.5 minutes for lignite, 15.0 minutes for MV bituminous South African coal and 16.6 minutes for anthracite. For the experiment done with HV bituminous Colombian coal it was 14.5 minutes. That is, all

experiments with different coals had similar mean residence time of solids. The char conversion reached for anthracite was somewhat lower, which indicates that the gasification rate of anthracite is lower than the rest.

Fig. 7 shows the char conversion rates calculated for all the coals tested at different temperatures, calculated with Eq. 8. As it could be anticipated from the resulting char conversions, at all temperatures anthracite has the lowest char conversion rate, both bituminous coals have similar ($-r_C$), although for HV Colombian is higher, and lignite shows much higher conversion rates compared to the rest. As an example, at 900ºC, ($-r_C$) was 31.0%/min for lignite, 4.5%/min for HV bituminous Colombian coal, 3.1%/min for MV bituminous South African coal, 2.2%/min for anthracite. This is also in line with the trend expected from the rank of the coals tested [39].

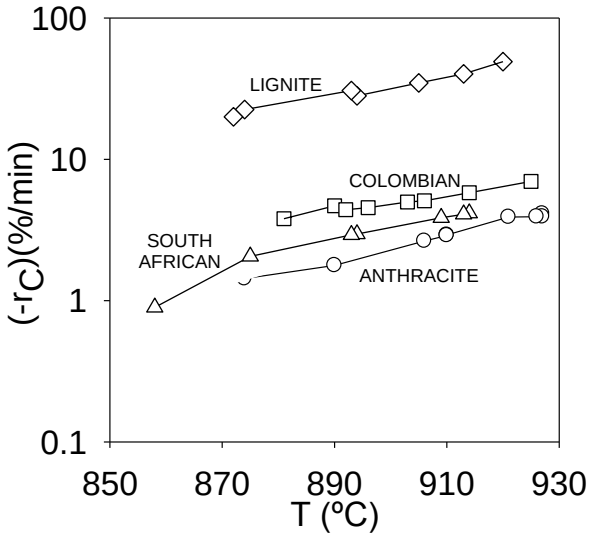


**Fig. 7.** Rates of char conversion at different fuel-reactor temperatures for ◇ lignite, □ HV bituminous Colombian coal, △ MV bituminous South African coal, ○ anthracite. Coal particle size: +200-300 μm.

Additional tests in TGA were done to evaluate the conversion of char under well-defined conditions. Fig. 8 shows the variation of char conversion with time reached at 950ºC in TGA

for the coals used in this study. As it would be expected from the coal ranks, char from lignite has the fastest gasification rate, followed by bituminous Colombian coal char, then bituminous South African coal char and char from anthracite has the slowest gasification rate. In case of the bituminous Colombian coal, the experiments were done with a thermal pre-treated coal instead of fresh, in order to avoid the swelling properties showed by this coal. This resulting char was somewhat more reactive compared to fresh coal, as it can be seen in Fig. 8. However, this enhancement in the gasification rate was not substantial.

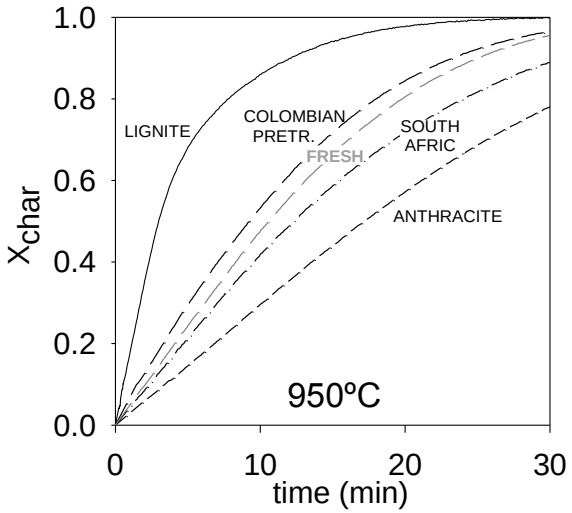


**Fig. 8.** Char conversion vs. time using a mixture 50%$H_2O$+50%$N_2$ as gasification agent done in TGA of char from —— lignite, – – – pretreated and – – – fresh HV bituminous Colombian coal, - - - - MV bituminous South African coal and ------ anthracite at 950ºC.

Note that the values of char conversion rate obtained in continuous testing are lower than the values obtained in batch fluidized bed experiments [27] or from the above TGA tests. That is because for the continuous tests the supposition that there is perfect mixing was made and the char mass in the fuel-reactor considered is probably higher than the real value due to some char segregation at the upper part of the bed. Furthermore, for the calculation of ($-r_C$) in the continuous tests no inhibition effect is considered.

From these results, it can be concluded that the gasification rates follow the order expected from the rank of the different coals: it is faster for lignite, then HV bituminous coal, MV bituminous coal and it is slower for anthracite.

### 4.1.2. Combustion efficiency and oxygen demand

The fuel-reactor combustion efficiency, $\eta_{comb\ FR}$, indicates the extent of conversion of the gases released in the fuel-reactor, that is, the devolatilization and gasification products, due to the oxidation by ilmenite. Fig. 9 shows $\eta_{comb\ FR}$ for all fuels tested at the different temperatures. For all the fuels tested, the combustion efficiencies obtained grow slightly with the temperature because the reaction rate of ilmenite increases with the temperature. The temperature influences the $\eta_{comb\ FR}$ of all types of coals in a similar way as the slopes of the curves are similar. The activation energy of the reaction of $CH_4$ with ilmenite is higher than with $H_2$ and CO [40], and a coal with high volatile content could be slightly more influenced by the temperature, but the differences are not relevant.

For all the temperatures tested, $\eta_{comb\ FR}$ was higher for anthracite, followed by lignite and MV bituminous South African coal. The test with HV bituminous Colombian coal gave a value of $\eta_{comb\ FR}$ slightly higher than with MV bituminous South African coal. In previous experiments it was seen that the released volatiles have worse contact with the oxygen-carrier particles and are therefore less converted. On the contrary, gasification products are highly oxidized [12]. This explains the higher $\eta_{comb\ FR}$ for anthracite, since the volatile fraction is lower. Lignite has higher fraction of volatile matter compared to South African coal, which could indicate lower $\eta_{comb\ FR}$ for lignite. However, the resulting $\eta_{comb\ FR}$ for lignite was slightly higher because the relative fraction of gasification products compared to volatiles was higher due to the fast char gasification rate of lignite. To reach high values of combustion efficiency, it is necessary to have enough solids inventory in the fuel-reactor [38]. The solids inventories used were 1770

kg/$MW_{th}$ for lignite, 1580 kg/$MW_{th}$ for Colombian coal, 1380 kg/$MW_{th}$ for South African coal and 1400 kg/$MW_{th}$ for anthracite.

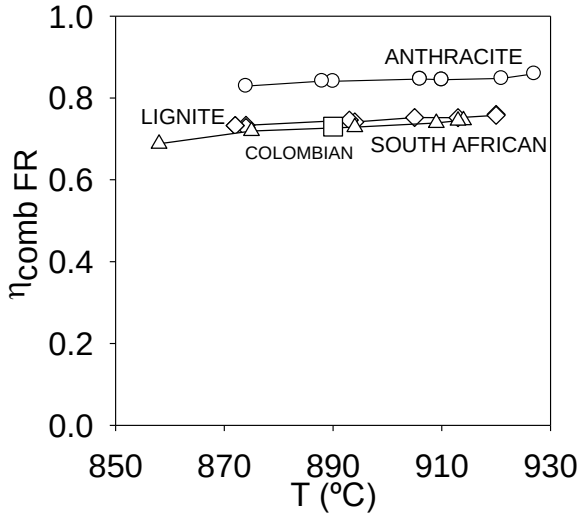


**Fig. 9.** Fuel-reactor combustion efficiency variation with the fuel-reactor temperature for ⊣◇⊢ lignite, ⊣□⊢ HV bituminous Colombian coal, ⊣△⊢ MV bituminous South African coal, ⊣○⊢ anthracite. Coal particle size: +200-300 μm.

From previous experiments with a HV bituminous Colombian coal, it was concluded that the unconverted $H_2$, CO and $CH_4$ in the fuel-reactor outlet come from unconverted volatile matter due to its poorer contact with the oxygen-carrier particles, whereas gasification products reached full oxidation. If complete combustion of the gasification products is assumed, a combustion efficiency of the volatile matter, $\eta_{comb\ vol}$, can be calculated, as for Eq. (15).

$$\eta_{comb\ vol} = \frac{O_{2\ demand\ gases\ FR}}{O_{2\ demand\ volatiles}} = \frac{2 \cdot F_{CH4,FR} + 0.5 \cdot F_{H2,FR} + 0.5 \cdot F_{CO,FR}}{O_{2\ demand\ coal} - O_{2\ demand\ char}} \quad (15)$$

This parameter can give an idea of how much the volatiles of each type of fuel are oxidized since they have poorer contact with the oxygen-carrier bed [12]. As it can be seen in Fig. 10, the volatile matter of each type of fuel reached different combustion efficiency: it was lower for anthracite and higher for lignite and very similar for both bituminous coals. This could be

explained by means of the composition of volatiles of each type of fuel: the oxygen demanded by the volatiles of anthracite is higher than for lignite, then for South African and then for bituminous Colombian coal. The lower combustion efficiency of volatiles from anthracite could be also explained because volatiles from this coal are more refractory against combustion. Since this combustion efficiency seems to depend mainly on the contact between the released volatile matter and oxygen-carrier bed and the composition of these gases, it did not show any remarkable trend with the temperature. The average of combustion efficiency of volatiles was around 52% for lignite, 61% for HV bituminous Colombian coal, 58% for MV bituminous South African coal, 42% for anthracite.

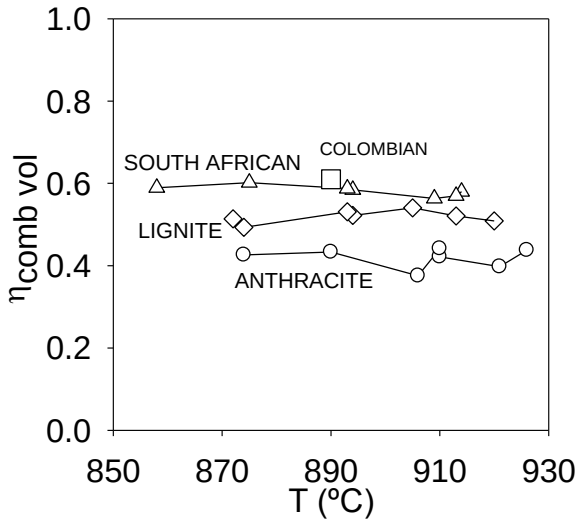


**Fig. 10.** Combustion efficiency of volatile matter at several fuel-reactor temperatures for ⊣◇⊢ lignite, ⊣□⊢ HV bituminous Colombian coal, ⊣△⊢ MV bituminous South African coal, ⊣○⊢ anthracite. Coal particle size: +200-300 μm.

The additional oxygen that would be needed to fully oxidize the outlet gas stream compared to the total oxygen demanded by the fuel fed is the oxygen demand, $\Omega_T$. It represents an extra cost for the process, since an oxygen polishing step would be necessary to fulfill this demand. Fig. 11 shows the oxygen demand of all fuels tested at different temperatures, which turned

out to be quite low: it was below 10% in all cases. As mentioned, the oxygen demand is caused by unconverted volatiles at the fuel-reactor outlet. The slight decrease of the oxygen demand with the temperature is explained because the oxidation reactions are promoted with the temperature. $\Omega_T$ was especially low for anthracite, as it was around 3.5%, because the volatile fraction in this fuel is low. Bituminous coals have the higher volatile fraction and thereby higher oxygen demand.

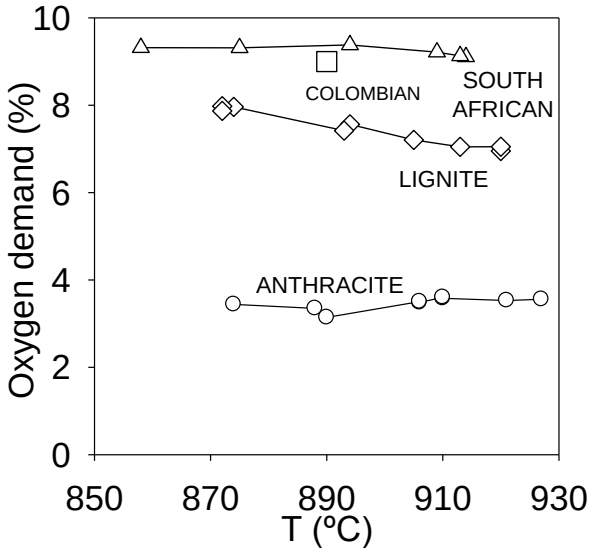


**Fig. 11.** Oxygen demand variation with the fuel-reactor temperature for ◇ lignite, ⊟ HV bituminous Colombian coal, △ MV bituminous South African coal, ○ anthracite. Coal particle size: +200-300 μm.

Fig. 12 shows the rate of oxygen transferred by ilmenite, ($-r_O$), for all the fuels tested with increasing temperature. It can be seen that more oxygen was transferred to oxidize the volatiles and the gasification products for increasing temperature for all fuels tested. The transfer of oxygen is limited by the extent of char gasification and the contact of the volatile matter with the oxygen-carrier. Nevertheless, the intrinsic reactivity of ilmenite particles is higher than the values showed in Fig. 12 [40]. Thus, the reaction rate of ilmenite increases

with the temperature, but the resulting increased oxygen transfer was mainly because char was further gasified at higher temperatures and there were more gasification products which were oxidized. The rate of oxygen transferred in case of lignite was higher because lignite char was further gasified compared to char from other coals and there was therefore higher amount of gases released that could react with ilmenite. The rate of oxygen transferred for anthracite was lower because its volatiles content is low and lower amount of gasification products were released due to its slower gasification rate. The oxygen transferred for both bituminous coals were similar due to the similar char conversions and combustion efficiencies reached.

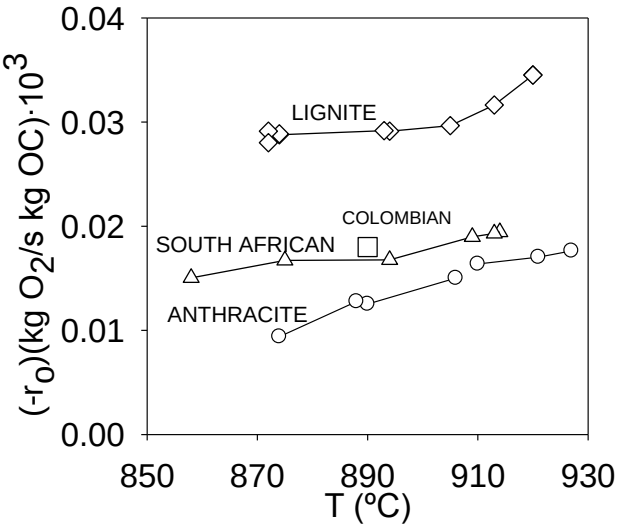


**Fig. 12.** Oxygen transfer rate variation with the fuel-reactor temperature for ⟡ lignite, □ HV bituminous Colombian coal, △ MV bituminous South African coal, ○ anthracite. Coal particle size: +200-300 μm.

### 4.2. Effect of the gasification agent type

Since the rate of gasification of the fuel in this process is a determining factor, the effect of using a gas mixture of $CO_2$ and $H_2O$ on the gasification step and the whole performance of the process with all the fuels considered was evaluated. The motivation of using $H_2O$-$CO_2$

mixtures as fluidizing gas is that $CO_2$ can be fed by recirculating a fraction of the product gas stream. Thus, the steam requirements for the gasification would be decreased in some extension, or even avoided if a pure stream of $CO_2$ was used as fluidizing gas. The coal feeding flows used for the different solid fuels tested, as well as the corresponding average temperatures and solids circulation flow rates are gathered in Table 3. The gasification agent tested for the different fuels were composed by pure steam, pure $CO_2$ and a $CO_2$:$H_2O$ mixture around 50:50.

#### 4.2.1. Carbon capture and char gasification

Fig. 13 shows the carbon capture and char conversion obtained for the experiments done with different $H_2O$:$CO_2$ mixtures as gasification agent. For all fuels tested, the extension of char gasified and carbon capture decrease for higher $CO_2$ fraction in the gasification flow. That is because for all the fuels here used the gasification rate is faster with steam than with $CO_2$. Note that there are some fuels whose gasification rate with $CO_2$ is fast enough so that it is feasible to use $CO_2$ as gasification agent [25,29,30]. The decrease in the reached char conversion and $\eta_{CC}$ when gasifying with higher fraction of $CO_2$ compared to using pure steam is less pronounced for lignite and higher for anthracite. That is because the char gasification rate with $CO_2$ is closer to the corresponding rate with steam in case of lignite, and the decrease in the gasification rate is higher in case of anthracite.

When using iG-CLC with some fuels it can be beneficial to use recirculated $CO_2$ as fluidizing agent in the fuel-reactor, as it is the case of lignite. For other fuels to have some $CO_2$ recirculation can be interesting, as it can be the case of MV bituminous South African coal, which agrees with the results obtained with this fuel in a batch fluidized bed reactor [27]. Similar results were found for HV bituminous Colombian coal [12].

In the experiments with different $H_2O$:$CO_2$ mixtures with anthracite the fuel-reactor temperature was about 925 ºC and with mean solids residence time of 16.6 minutes, whereas

with bituminous South African coal they were 910 ºC and 15.0 minutes, respectively. This explains that, although char gasification rate with steam is higher for South African coal, the in Fig. 13 represented $X_{char}$ with anthracite and bituminous coal had similar values with $CO_2$ or $H_2O$:$CO_2$ mixtures, or even slightly lower for bituminous coal in case of gasifying with steam. On the other hand, the implementation of an efficient carbon separation system that increased the char residence time would offset any possible disadvantage caused by the slower gasification rate with $CO_2$.

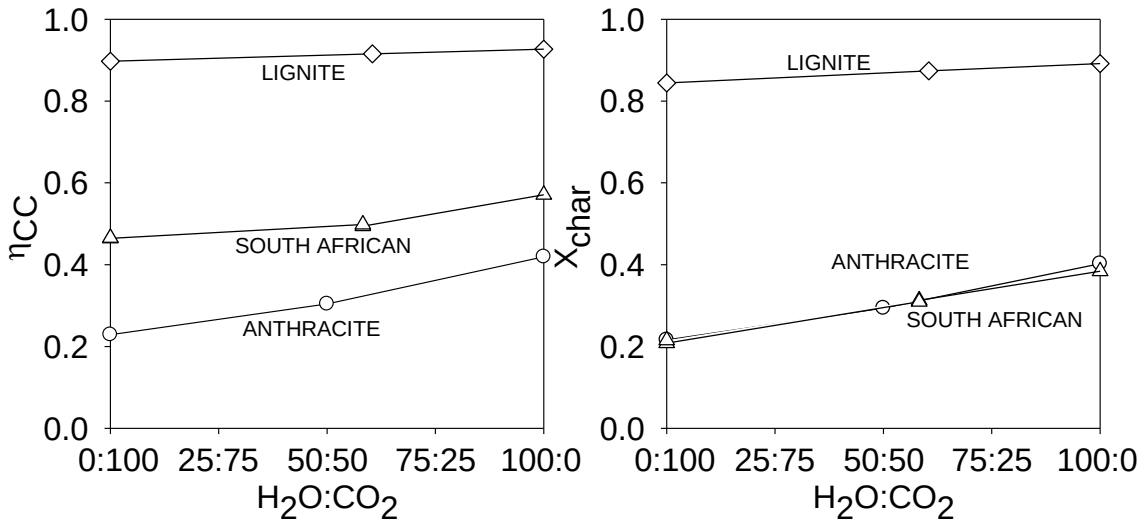


**Fig. 13.** a) Carbon capture efficiency and b) Char conversion variation for different $H_2O$:$CO_2$ mixtures as gasification agent for ⟡ lignite, △ MV bituminous South African coal, ○ anthracite. Coal particle size: +200-300 μm. Conditions of experiments: see Table 3.

### 4.2.2. Combustion efficiency and oxygen demand

Fig. 14 shows the resulting fuel-reactor combustion efficiencies and oxygen demands for the experiments done with different $H_2O$:$CO_2$ mixtures as gasification agent. It can be seen that both the fuel-reactor combustion efficiency and oxygen demand are scarcely influenced by the composition of the gasification agent. When gasifying with higher fraction of $CO_2$ only CO is produced, whereas when gasifying with $H_2O$, $H_2$ is also generated. Although ilmenite

reacts faster with $H_2$ than with CO, the reaction rate of ilmenite is fast enough and the resulting $\eta_{comb\ FR}$ or $\Omega_T$ have no substantial change if the gasification products are enriched in $H_2$ or CO. As it was calculated by Abad et al. [40], an inventory of 189 kg/$MW_{th}$ would be enough to fully oxidize the generated CO at 900ºC, and for $H_2$ the inventory needed would be even lower: 66 kg/$MW_{th}$. However, in these experiments the solids inventories about 1500 kg/$MW_{th}$ are used. As the poor contact between volatiles and oxygen-carrier particles is the reason for incomplete combustion even with high solids inventory, the effect of the reactivity of the gas, i.e., $H_2$ or CO, is of low relevance.

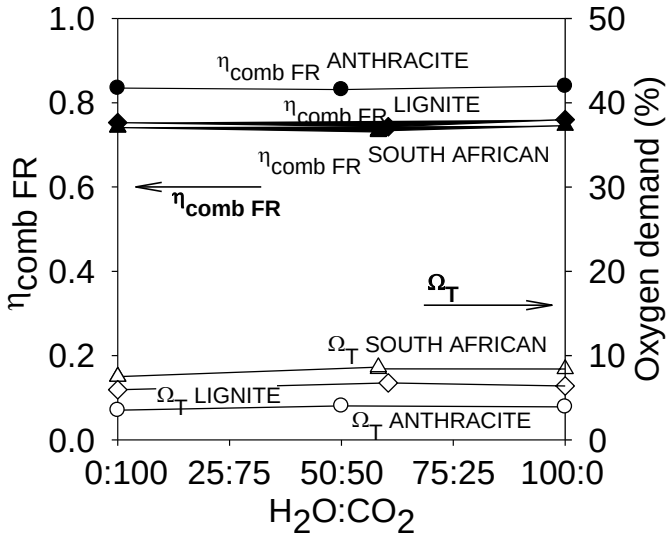


**Fig. 14.** Fuel-reactor combustion efficiency (filled symbols) and oxygen demand (void symbols) variation for different $H_2O$:$CO_2$ mixtures as gasification agent for –◇– lignite, –△– MV bituminous South African coal, –○– anthracite. Coal particle size: +200-300 μm. Conditions of experiments: see Table 3.

## 5. Conclusions

The feasibility of using different types of solid fuels with the *in-situ* gasification CLC and the variations in the performance of the process was assessed in a CLC rig for solid fuels when

the fuel-reactor temperature or the fluidizing gas were changed. The oxygen-carrier utilized was ilmenite and a lignite, a high volatile bituminous coal, a medium volatile bituminous coal and a anthracite were used as solid fuels. The study in this rig is based on the fuel-reactor performance and the results related to its operation were obtained. The effect on the performance of the characteristics of each fuel was evaluated.

An increase in the temperature has a beneficial effect on the system performance for all types of solid fuels. The carbon capture reached is higher for the solid fuels with faster char gasification rates and also when the volatile content in the fuel is higher. High values of carbon capture, even higher than 90%, can be obtained, but it is essential to have a highly efficient carbon separation system that reintroduced unconverted char particles back to the fuel-reactor, especially in case of solid fuels with slow gasification rates such as anthracites. Carbon capture as high as 93% at 920ºC was obtained even without a carbon separation system with lignite, which has a fast char gasification rate.

The combustion efficiency is higher for higher solids inventory and for solid fuels with lower volatile content and for coals with faster gasification rate. The combustion efficiency in the fuel-reactor was seen not to be limited by the reaction rate of ilmenite but it is limited by the low conversion of volatile matter. The combustion efficiency of the volatiles seems to depend on the composition of the released volatiles of each type of fuel. The average of combustion efficiency of volatiles was around 52% for lignite, 61% for HV bituminous Colombian coal, 58% for MV bituminous South African coal, 42% for anthracite. Furthermore, in all cases oxygen demands lower than 10% were found, and for anthracite the oxygen demand values were 3.5% because of the lower volatile content of this fuel.

Depending on the type of fuel, some of the steam used as gasification agent can be replaced by $CO_2$ recirculated from the outlet fuel-reactor flow, getting similar system performance and thereby saving energy derived from steam generation. In case of lignite, there is no change in

the process performance when gasifying with $CO_2$. On the other hand, for anthracite the lower gasification rate of char with $CO_2$ leads to a substantial drop in the performance.

The results show that this technology has the potential to be used to carry out combustion with inherent $CO_2$ separation using highly reactive solid fuels.

**Acknowledgments**

This work was partially supported by the Spanish Ministry of Science and Innovation (Project ENE2010-19550). A. Cuadrat thanks CSIC for the JAE Pre. fellowship.

**Nomenclature**

$F_{C,char,eff}$ carbon flow in the effective char fed (mol/s)

$F_{CO2\ AR}$ carbon flow from the char that goes to the air-reactor (mol/s)

$F_{C\ vol}$ carbon flow coming from the volatile matter fed (mol/s)

$F_{i,FR}$ flow in the fuel-reactor of the corresponding gas i (mol/s)

$F_{ilm}$ solids circulation rate (kg/s)

k constant value of the char gasification rate ($s^{-1}$)

$M_C$ carbon molar weight (kg/mol)

$m_{char,FR}$ mass of char in the fuel-reactor (kg)

$m_{ilm,FR}$ fuel-reactor bed mass or solid hold-up in the fuel-reactor (kg)

$M_{O_2}$ oxygen molecular weight (kg/mol)

$O_{coal,eff}$ flow of oxygen contained in the effective coal introduced (moles O/s)

$O_{2\ demand\ coal,eff}$ oxygen demand of the effective coal fed (moles $O_2$/s)

$(-r_C)$ char gasification rate ($s^{-1}$)

$(-r_O)$ rate of oxygen transferred by the oxygen-carrier (kg $O_2$/s kg OC)

$T_{FR}$ temperature in the fuel-reactor (ºC)

$t_{m,char}$ mean residence time of char (s)

$t_{m,ilm}$ mean residence time of ilmenite (s)

$\eta_{CC}$ carbon capture efficiency

$\eta_{comb\ FR}$ fuel-reactor combustion efficiency

$\eta_{comb\ vol}$ combustion efficiency of the volatile matter

$X_{char}$ char conversion

$\Omega_T$ total oxygen demand

**References**

[1] NOAA-ESRL, 2010. National Oceanic and Atmospheric Administration in the US. Average concentration of $CO_2$ in the atmosphere (Mauna Loa Observatory) for 2010 was posted September 8, 2011.

[2] IPCC special report on carbon dioxide capture and storage, Cambridge, UK: Cambridge University Press. 2005.

[3] International Energy Agency (IEA). Energy technology perspectives: Scenarios and strategies to 2050. Paris, France: OECD/IEA. 2006.

[4] L.I. Eide, M. Anheden, A. Lyngfelt, C. Abanades, M. Younes, D. Clodic. Novel Capture Processes. Oil Gas Sci. Technol., 60 (2005), pp. 497-508.

[5] A. Lyngfelt, B. Leckner, T. Mattisson. A fluidized-bed combustion process with inherent $CO_2$ separation; Application of chemical-looping combustion. Chem. Eng. Sci. 56 (2001), pp. 3101-3113.

[6] S. Noorman, F. Gallucci, M. van Sint Annaland, J.A.M. Kuipers, A theoretical investigation of CLC in packed beds. Part 1: Particle model. Chem. Eng. J., 167 (2011), pp. 297-307.

[7] S. Noorman, F. Gallucci, M. van Sint Annaland, J.A.M. Kuipers, A theoretical investigation of CLC in packed beds. Part 2: Reactor model. Chem. Eng. J., 167 (2011), pp. 369-376.

[8] N. Berguerand, A. Lyngfelt. The use of petroleum coke as fuel in a 10 kWth chemical-looping combustor. Int. J. Greenhouse Gas Control, 2 (2008), pp. 169-179.

[9] N. Berguerand, A. Lyngfelt. Design and operation of a 10 kWth chemical-looping combustor for solid fuels – Testing with South African coal. Fuel, 87 (2008), pp. 2713-2726.

[10] N. Berguerand, A. Lyngfelt. Chemical-Looping combustion of petroleum coke using ilmenite in a 10 kWth unit-high-temperature operation. Energy Fuels, 23 (2009), pp. 5257-5268.

[11] N. Berguerand, A. Lyngfelt. Operation in a 10 kWth chemical-looping combustor for solid fuel—Testing with a Mexican petroleum coke. Energy Procedia, 1(2009), pp. 407-414.

[12] A. Cuadrat, A. Abad, F. García-Labiano, P. Gayán, L.F. de Diego, J. Adánez. The use of ilmenite as oxygen-carrier in a 500 Wth Chemical-Looping Coal Combustion unit. Int. J. Greenhouse Gas Control, 5 (2011), pp. 1630-1642.

[13] A. Cuadrat, A. Abad, F. García-Labiano, P. Gayán, L.F. de Diego, J. Adánez. Effect of operating conditions in Chemical-Looping Combustion of coal in a 500 Wth unit. Int. J. Greenhouse Gas Control. doi:10.1016/j.ijggc.2011.10.013.

[14] L. Shen, J. Wu, J. Xiao. Experiments on chemical looping combustion of coal with a NiO based oxygen carrier. Combust. Flame, 156 (2009), pp. 721-728.

[15] L. Shen, J. Wu, Z. Gao, J. Xiao. Reactivity deterioration of $NiO/Al_2O_3$ oxygen carrier for chemical looping combustion of coal in a 10 kWth reactor. Combust Flame, 156 (2009), pp. 1377-1385.

[16] L. Shen, J. Wu, Z. Gao, J. Xiao. Characterization of chemical looping combustion of coal in a 1 kWth reactor with a nickel-based oxygen carrier. Combust Flame, 157 (2010), pp. 934-942.

[17] J. Wu, L. Shen, J. Hao, H. Gu. Chemical looping combustion of coal in a 1 kWth reactor with iron ore as an oxygen carrier. Proc 1st Int Conf on Chemical Looping. Lyon, France; 2010.

[18] Y. Cao, B. Casenas, W.P. Pan. Investigation of Chemical-Looping Combustion by Solid Fuels. 2. Redox Reaction Kinetics and Product Characterization with Coal, Biomass, and Solid Waste as Solid Fuels and CuO as an Oxygen-carrier. Energy Fuels, 20 (2006), pp. 1845-1854.

[19] H. Leion, A. Lyngfelt, M. Johansson, E. Jerndal, T. Mattisson. The use of ilmenite as an oxygen-carrier in chemical-looping combustion. Chem. Eng. Res. Des., 86 (2008), pp. 1017-1026.

[20] T.Mendiara, A. Abad, L.F. de Diego, F. García-Labiano, P. Gayán, J. Adánez. Use of a Fe-based residue from alumina production as oxygen carrier in chemical-looping combustion. Energy Fuels (2011), doi: 10.1021/ef201458v.

[21] H. Leion, E. Jerndal, B.M. Steenari, S. Hermansson, M. Israelsson, E. Jansson, M. Johnsson, R. Thunberg, A. Vadenbo, T. Mattisson, A. Lyngfelt. Solid fuels in chemical-looping combustion using oxide scale and unprocessed iron ore as oxygen carriers. Fuel, 88 (2009), pp. 1945-1954.

[22] N. Ding, Y. Zheng, C. Luo, Q. Wu, P. Fu, C. Zheng. Development and performance of binder-supported CaSO4 oxygen carriers for chemical looping combustion. Chem. Eng. J., 171 (2011), pp. 1018-1026.

[23] M.M. Azis, E. Jerndal, H. Leion, T. Mattisson, A. Lyngfelt. On the evaluation of synthetic and natural ilmenite using syngas as fuel in chemical-looping combustion (CLC). Chem. Eng. Des. Res., 88 (2010), pp. 1505–1514.

[24] J.S. Dennis, S.A. Scott, A.N. Hayhurst. In situ gasification of coal using steam with chemical looping: a technique for isolating $CO_2$ from burning a solid fuel. J. Energy Inst., 79 (2006), pp. 187-190.

[25] S.A. Scott, J.S. Dennis, A.N. Hayhurst, T. Brown. In situ gasification of a solid fuel and $CO_2$ separation using chemical looping. AIChE J, 52 (2006), pp. 3325-3328.

[26] H. Leion, T. Mattisson, A. Lyngfelt. The use of petroleum coke as fuel in chemical-looping combustion. Fuel, 86 (2007), pp. 1947-1958.

[27] A. Cuadrat, A. Abad, J. Adánez, L.F. de Diego, F. García-Labiano, P. Gayán. Design Considerations for Chemical-Looping Combustion of coal – Part 1. Experimental Tests. Fuel. *Submitted to publish.*

[28] H. Leion, T. Mattisson, A. Lyngfelt. Solid fuels in chemical-looping combustion. Int. J. Greenhouse Gas Control, 2 (2008), pp. 180-193.

[29] J.S. Dennis, S.A. Scott. In situ gasification of a lignite coal and $CO_2$ separation using chemical looping with a Cu-based oxygen carrier. Fuel, 89 (2010), pp. 1623-1640.

[30] J.S. Dennis, C.R. Müller, S.A. Scott. In situ gasification and $CO_2$ separation using chemical looping with a Cu-based oxygen carrier: Performance with bituminous coals. Fuel, 89 (2010), pp. 2353-64.

[31] C. Linderholm, A. Cuadrat, A. Lyngfelt. Chemical-Looping combustion of solid fuels in a 10 kWth pilot – batch tests with five fuels. Energy Procedia, 4 (2011), pp. 385-92.

[32] L. Shen, J. Wu, J. Xiao, Q. Song, R. Xiao. Chemical-Looping Combustion of Biomass in a 10 kWth Reactor with Iron Oxide as an Oxygen-carrier. Energy Fuels, 23 (2009), pp. 2498-2505.

[33] H. Gu, L. Shen, J. Xiao, S. Zhang, T. Song. Chemical Looping Combustion of Biomass/Coal with Natural Iron Ore as Oxygen Carrier in a Continuous Reactor. Energy Fuels, 25(2011), pp. 446–455.

[34] A.R. Bidwe, F. Mayer, C. Hawthorne, A. Charitos, A. Schuster, G. Scheffknecht. Use of ilmenite as an oxygen-carrier in Chemical-Looping Combustion – Batch and continuous dual fluidized bed investigation. Energy Procedia, 2011, 4, 433-440.

[35] A. Cuadrat, A. Abad, J. Adánez, L.F. de Diego, F. García-Labiano, P. Gayán. Behavior of Ilmenite as Oxygen-carrier in Chemical-Looping Combustion. Fuel Proc. Tech. 94 (2012), pp. 101-112.

[36] J. Adánez, A. Cuadrat, A. Abad, P. Gayán, L.F. de Diego, F. García-Labiano. Ilmenite Activation during Consecutive Redox Cycles in Chemical-Looping Combustion. Energy Fuels, 24 (2010), pp. 1402-1413.

[37] P.Simell, P. Stahlberg, E. Kurkela, J. Albretch, S. Deutch, K. Sjostrom. Provisional protocol for the sampling and anlaysis of tar and particulates in the gas from large-scale biomass gasifiers. Version 1998. Biomass and Bioenergy, 18(2000), pp. 19-38.

[38] A. Cuadrat, A. Abad, P. Gayán, L.F. de Diego, F. García-Labiano, J. Adánez. Theoretical approach on the CLC performance with solid fuels: optimizing the solids inventory. Fuel. *Submitted to publish.*

[39] J.L. Johnson. Fundamentals of Coal Gasification. In Chemistry of coal utilization. 2$^{nd}$ supplementary volume. Chapter 23. Ed. M.A. Elliott. Wiley-Interscience Publication, New York, 1981.

[40] A. Abad, J. Adánez, A. Cuadrat, F. García-Labiano, P. Gayán, L.F. de Diego. Reaction kinetics of ilmenite for Chemical-Looping Combustion. Chem. Eng. Sci., 66 (2011), pp. 689-702.